ADVANCES IN SCIENCE AND MATHEMATICS

EDITOR
ASSOC. PROF. AYKUT DEMIRCALI, PH.D.

DOI:10.5281/zenodo.14576277

Advances in Science and Mathematics

EDITOR

Assoc. Prof. Aykut Demirçalı, Ph.D.

Publisher
Platanus Publishing®

Editor in Chief
Assoc. Prof. Aykut Demirçalı, Ph.D.

Cover & Interior Design
Platanus Publishing®

Editorial Coordinator
Arzu Betül Çuhacıoğlu

The First Edition
December, 2024

Publisher's Certificate No
45813

ISBN
978-625-6636-52-9

Platanus Publishing®
Address: Natoyolu Cad. Fahri Korutürk Mah. 157/B, 06480, Mamak, Ankara, Turkey.
Phone: +90 312 390 1 118
web: www.platanuskitap.com
e-mail: platanuskitap@gmail.com

PLATANUS PUBLISHING®

CONTENTS

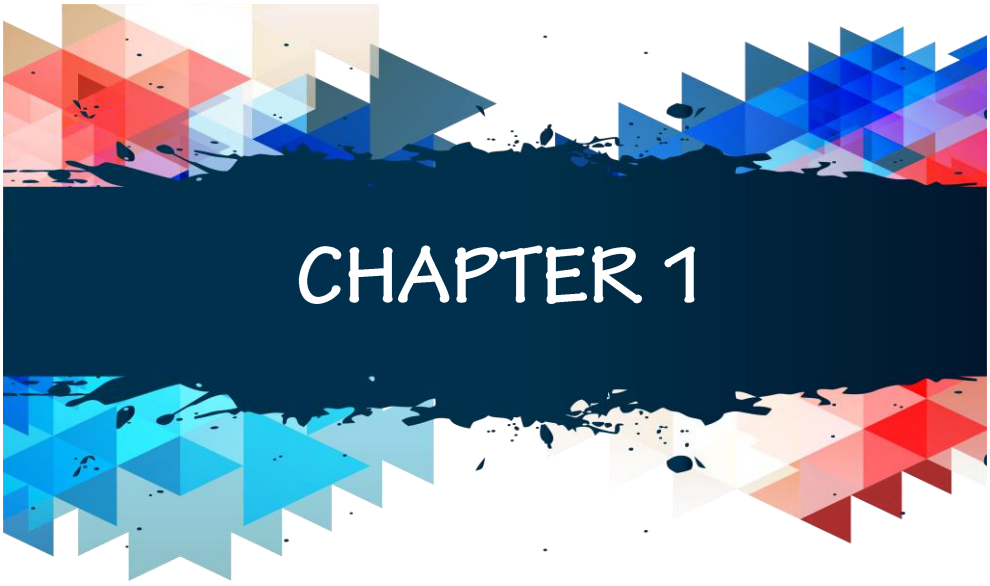

Mathematical Modeling of Some Factors Effecting of Co_2 Emission

Bahatdin Daşbaşı[1] & Teslima Daşbaşı[2]

1 Kayseri University, Faculty of Engineering, Architecture and Design, Department of Engineering Basic Sciences, Kayseri, Turkey, https://orcid.org/0000-0001-8201-7495
2 Kayseri University, Bünyan Vocational School, Kayseri, Turkey, https://orcid.org/0000-0002-8546-612X,

1. INTRODUCTION

The atmosphere consists of various gases. Sun rays pass through the atmosphere and heat the earth. Gases such as CO_2, CH_4, N_2O, O_3, CFC (chlorofluorocarbon) in the atmosphere hold some of the heat coming from the sun to the earth, allowing the earth to remain at a certain temperature. The heat-holding feature of the atmosphere prevents the seas and oceans from freezing. This heating and heat-holding feature of the atmosphere is called the greenhouse effect [1].

Energy is defined as the power that exists in the structure of matter and is released in various ways. Humanity has started to benefit from energy sources since its existence. The need for energy increased rapidly with the Industrial Revolution and this increase continues today. Factors such as population growth, urbanization, industrialization, technological development and increasing welfare levels increase the demand for energy. With the increase in energy consumption, the negative effects of energy on the environment also increase. When fossil energy sources such as oil, natural gas and coal, which are exhaustible and non-renewable, are used, they release more pollutants and greenhouse gases into the environment compared to renewable energy sources [2]. Greenhouse gases are gaseous components of the atmosphere, both natural and anthropogenic, that absorb and emit radiation of specific wavelengths within the infrared radiation spectrum emitted by the Earth's surface, atmosphere, and clouds. Because of these properties, they contribute to the greenhouse effect. The most abundant greenhouse gases in the Earth's atmosphere are:

Water steam (H_2O)

Carbon dioxide (CO_2)

- Methane (CH_4)
- Nitrous Oxide (N_2O)
- Ozone (O_3)
- Chlorofluorocarbons (CFC's)
- Hydrofluorocarbons (HCFC's and HFC's)

[3]. Greenhouse gas emissions are examined by sector as Energy, Industrial processes and product use, Agriculture and Waste. The vast majority (71.6%) of global greenhouse gas emissions were CO_2 from the combustion of fossil fuels in

2022. CH_4 contributed 21%, while the rest of the emissions were made up of N_2O (4.8%) and fluorinated gases (F-gases) (2.6%) [4].

In this study, the change in the amount of CO_2 (Million tons) for Turkey was analyzed mathematically. For this purpose, the data was obtained through TSI (Turkish Statistical Institute) for the years 1990-2022. For this purpose, the Energy (Million tons), Industrial processes and product use (Million tons), Agriculture (Million tons), Waste (Million tons) sectors and the total population of Turkey, which affect greenhouse gas emissions, were taken into account. Thus, their effects on the amount of CO_2 (Million tons) were tried to be explained mathematically with various optimization methods. Therefore, the amount of CO_2 (Million tons) was investigated with the ANN (Artificial Neural Network) activation function according to the above 5 input variables. On the other hand, the time-dependent change of these 6 variables was estimated based on the real values throughout the linear differential equation system. Finally, the performances of the ANN and differential equation system were compared according to the real values of CO_2.

The literature is quite rich in studying carbon dioxide emission. Some recently published research results claim to predict, understand and control the emission behavior of carbon dioxide [5]. To predict carbon dioxide emission, one can refer to references [6, 7, 8, 9] for some studies applying artificial neural network (ANN) and to references [10, 11, 12, 13, 14] for some studies applying dynamical systems.

2. METHODOLOGY

Within the scope of this study, greenhouse gas CO_2 (Million tons) data obtained from the Turkish Statistical Institute for the years 1990-2022 for Turkey were analyzed. First of all, the data were normalized. For this analysis, mathematically presented and analyzed ANN activation functions and differential equation system were used. The process begins with compiling data from TSI and augmenting the data with a linear differential equation system since the data for 33 years is not sufficient for ANN modeling. Since Ordinary Differential Equation (ODE) system and ANN performances are compared at the end of the study, the augmented data are again intermediate values belonging to the same time interval. The augmented data were used only in the training processes of ANN models and only the original data obtained from TSI were used in both linear ODE system model analysis and testing processes. The training processes of the ANN model, whose activation function was given as the Tangent hyperbolic (tanh) function, were carried out with normalized data and the

parameter determination of the tanh activation function was carried out as explained in detail in this section. After this process, the ANN model and linear ODE system were proposed using the normalized original data. With the data obtained as a result of the estimation, separate MSE values were calculated for each model. Thus, the process of revealing the model that estimates the amount of greenhouse gas CO_2 (Million tons) with the lowest error rate was carried out with comparative analysis.

2.1. Dataset

Let t denote the independent variable and time. For Turkey, the expression and definition of the variables used in this study are given in Table 1.

Table 1. State variables used in the analysis

$x(t)$	Energy (Million tonnes)
$y(t)$	Industrial processes and product use (Million tonnes)
$z(t)$	Agriculture (Million tonnes)
$u(t)$	Waste (Million tonnes)
$v(t)$	Population (Million)
$w(t)$	CO_2 (Million tonnes)

The values obtained from TSI for the variables mentioned in Table 1 are presented in Table 2.

Table 2. Dataset [15, 16]

t	$x(t)$	$y(t)$	$z(t)$	$u(t)$	$v(t)$	$w(t)$
1990	143,1470198	22,69117693	51,84783085	10,31588698	56,473035	154,1
1991	147,4541682	24,42877822	52,8621757	10,65379753	57,6061242	160,6
1992	153,9982627	24,13442927	52,69559779	10,98331549	58,7392134	166,7
1993	160,4067916	24,64187372	52,76736551	11,32623989	59,8723026	173,8
1994	156,7515581	23,98810976	50,34591778	11,6832472	61,0053918	170,1
1995	169,9785309	25,37116631	49,03032854	12,11431094	62,138481	184,1
1996	187,7794439	26,00640277	49,54534753	12,52105373	63,2715702	202,5
1997	199,9309327	26,85137401	46,81719519	13,13865528	64,4046594	214,9
1998	199,7204595	27,163362	47,74664776	13,50765488	65,5377486	215,0
1999	197,7817881	25,64145515	48,16938119	14,0404225	66,6708378	210,7
2000	219,7641586	26,05411781	46,03286861	14,53716466	67,803927	232,4
2001	203,1022157	25,70502522	43,69093496	15,05664373	68,20140257	216,3

2002	209,5558562	26,6596083	40,70851159	15,54118485	68,59887814	223,7
2003	223,9211451	28,00141174	44,24284818	15,97342265	68,99635371	239,2
2004	229,6736623	30,55885829	44,951295	16,50593765	69,39382929	247,2
2005	247,6651078	33,95962373	46,2659057	16,89157733	69,79130486	267,0
2006	263,8615262	36,41442319	47,5672221	17,38648827	70,18878043	284,6
2007	294,9183709	39,30366712	47,15090012	17,65508293	70,586256	315,6
2008	291,0458025	41,31472744	44,77562411	17,78742419	71,5171	311,7
2009	295,6532509	42,71914171	45,12103106	17,82330598	72,561312	317,5
2010	290,9384803	48,57480914	47,67840969	18,07754258	73,722988	317,6
2011	312,6251708	53,44300143	50,2683312	18,43424878	74,724269	343,0
2012	324,9455635	55,67909687	56,2577966	18,2822058	75,627384	357,4
2013	311,9269943	58,73633244	59,35978415	17,28440023	76,667864	349,2
2014	330,3501739	59,43405514	59,49789435	17,09760664	77,695904	365,7
2015	343,9851134	59,15990776	59,20755088	17,72202112	78,741053	386,3
2016	361,8714153	63,20276487	61,68992958	17,32484193	79,814871	404,6
2017	381,8283581	66,07692275	66,32944112	16,87281174	80,810525	429,4
2018	374,7233109	67,14831961	68,91004941	17,2974934	82,003882	422,1
2019	368,9375248	58,3549989	71,51693774	16,77275527	83,154997	404,3
2020	369,5212557	67,24087805	76,43694186	16,97632961	83,614362	414,4
2021	406,4722862	74,71520609	75,37638779	15,42386321	84,680273	455,2
2022	400,5858487	69,90821383	71,51154995	16,26486932	85,279553	441,4

2.2. Data Augmentation with ODE System Model

Since there are 33 rows of data in Table 2, it will be increased with linear ODE to reach 123 data. However, the increased 90 rows of data were again obtained between 1990-2022. In the estimation process, their performance will be measured with real data. However, before performing this operation, the data will be normalized.

Table 2 shows sample data related to data estimations made. $x(t), y(t), z(t), u(t)$ and $v(t)$ represent the attributes given as input to ANN, and $w(t)$ represents the value taken as output. Augmentation process was performed with linear ODE system. This data set including original and estimated data was analyzed with ANN and model given as differential equation system within the scope of this study and CO_2 emission amount was estimated. In the last stage, analysis results were compared with original and real measurement data and error values were compared.

Here, the purpose of doing this is to make analyses with smaller error values. At the end of the analysis process, the normalized data will be denormalized and estimates will be made. A common technique for normalizing vectors is L2 normalization, also known as Euclidean normalization or unit vector normalization. In this method, each element of the vector is divided by its Euclidean norm, which is calculated as the square root of the sum of the squares of all components of the vector. Let $\omega = \omega_{original} = (\omega_1, \omega_2, \dots, \omega_n)$ be the elements of the data matrix such that $n \in Z^+$. In this case, the normalized data is given as $\omega_{normalized} = (\frac{\omega_1}{\|\omega\|_2}, \frac{\omega_2}{\|\omega\|_2}, \dots, \frac{\omega_n}{\|\omega\|_2})$, where $\|\omega\|_2$ is the Euclidean norm in R^n such that $\|\omega\|_2 = \sqrt{(\omega_1^2 + \omega_2^2 + \cdots + \omega_n^2}$. The norm of each variable listed in Table 2 is obtained as $\|t\| = 11523{,}72$ $\|x(t)\| = 1598{,}132$ $\|y(t)\| = 260{,}1944$ $\|z(t)\| = 314{,}3251$ $\|u(t)\| = 89{,}79774$ $\|v(t)\| = 411{,}7463$ $\|w(t)\| = 1755{,}528$. Thus, the normalized values of the Table 2 values are given in Table 3.

Table 3. Normalised Dataset

$\bar{t} = \frac{t}{\|t\|}$	$\bar{x} = \frac{x}{\|x\|}$	$\bar{y} = \frac{y}{\|y\|}$	$\bar{z} = \frac{z}{\|z\|}$	$\bar{u} = \frac{u}{\|u\|}$	$\bar{v} = \frac{v}{\|v\|}$	$\bar{w} = \frac{w}{\|w\|}$
0,1726872546	0,0895714624	0,0872085523	0,1649497185	0,1148791330	0,1371549214	0,0878030190
0,1727740322	0,0922665767	0,0938866410	0,1681767754	0,1186421512	0,1399068323	0,0914659760
0,1728608097	0,0963614165	0,0927553755	0,1676468211	0,1223117084	0,1426587432	0,0949596563
0,1729475872	0,1003714287	0,0947056267	0,1678751444	0,1261305616	0,1454106541	0,0989846816
0,1730343647	0,0980842375	0,0921930286	0,1601715025	0,1301062440	0,1481625650	0,0968794553
0,1731211422	0,1063607584	0,0975085025	0,1559860607	0,1349066289	0,1509144759	0,1048871556
0,1732079197	0,1174993334	0,0999498943	0,1576245524	0,1394361725	0,1536663868	0,1153699988
0,1732946972	0,1251028911	0,1031973556	0,1489451544	0,1463138681	0,1564182977	0,1224314534
0,1733814747	0,1249711915	0,1043964128	0,1519021332	0,1504230983	0,1591702086	0,1224696810
0,1734682523	0,1237581056	0,0985472983	0,1532470257	0,1563560716	0,1619221195	0,1200084325
0,1735550298	0,1375131463	0,1001332765	0,1464498822	0,1618878604	0,1646740303	0,1323540549
0,1736418073	0,1270872597	0,0987916159	0,1389992080	0,1676728507	0,1656393713	0,1232070854
0,1737285848	0,1311254997	0,1024603462	0,1295108671	0,1730687670	0,1666047122	0,1274399503
0,1738153623	0,1401142997	0,1076172728	0,1407550757	0,1778822265	0,1675700531	0,1362744792
0,1739021398	0,1437138254	0,1174462567	0,1430089424	0,1838123865	0,1685353940	0,1408024559

0,1739889174	0,1549716223	0,1305163514	0,1471912710	0,1881069230	0,1695007349	0,1520856779
0,1740756949	0,1651062160	0,1399508337	0,1513313048	0,1936183191	0,1704660758	0,1621333123
0,1741624724	0,1845394323	0,1510550078	0,1500068098	0,1966094261	0,1714314167	0,1797832485
0,1742492499	0,1821162480	0,1587840762	0,1424500596	0,1980831966	0,1736921387	0,1775388735
0,1743360274	0,1849992692	0,1641816339	0,1435489441	0,1984827811	0,1762281954	0,1808640444
0,1744228049	0,1820490932	0,1866866049	0,1516850393	0,2013139948	0,1790495345	0,1808886661
0,1745095825	0,1956191178	0,2053964322	0,1599246670	0,2052863240	0,1814813254	0,1953613825
0,1745963600	0,2033283638	0,2139903736	0,1789796711	0,2035931525	0,1836747026	0,2036096512
0,1746831375	0,1951822474	0,2257401867	0,1888483959	0,1924814527	0,1862016954	0,1989111166
0,1747699150	0,2067101936	0,2284217306	0,1892877824	0,1904012936	0,1886984754	0,2082858090
0,1748566925	0,2152419917	0,2273681054	0,1883640780	0,1973548590	0,1912368077	0,2200600633
0,1749434700	0,2264339971	0,2429059383	0,1962615669	0,1929318170	0,1938447679	0,2304992591
0,1750302475	0,2389216658	0,2539521325	0,2110218010	0,1878979468	0,1962628927	0,2445704165
0,1751170251	0,2344758207	0,2580698109	0,2192317994	0,1926272601	0,1991611747	0,2404668269
0,1752038026	0,2308554776	0,2242746151	0,2275254057	0,1867837042	0,2019568645	0,2303015686
0,1752905801	0,2312207359	0,2584255389	0,2431780045	0,1890507360	0,2030725150	0,2360416759
0,1753773576	0,2543421243	0,2871514763	0,2398039367	0,1717622571	0,2056612716	0,2593227187
0,1754641351	0,2506588005	0,2686768579	0,2275082649	0,1811278166	0,2071167308	0,2514472699

The linear ODE mathematical model, where t denotes the time parameter and the independent variable, is as follows:

$$
\begin{aligned}
\frac{d\bar{x}}{d\bar{t}} &= \delta_1 + \delta_2\bar{x} + \delta_3\bar{y} + \delta_4\bar{z} + \delta_5\bar{u} + \delta_6\bar{v} + \delta_7\bar{w} \\
\frac{d\bar{y}}{d\bar{t}} &= \delta_8 + \delta_9\bar{x} + \delta_{10}\bar{y} + \delta_{11}\bar{z} + \delta_{12}\bar{u} + \delta_{13}\bar{v} + \delta_{14}\bar{w} \\
\frac{d\bar{z}}{d\bar{t}} &= \delta_{15} + \delta_{16}\bar{x} + \delta_{17}\bar{y} + \delta_{18}\bar{z} + \delta_{19}\bar{u} + \delta_{20}\bar{v} + \delta_{21}\bar{w} \\
\frac{d\bar{u}}{d\bar{t}} &= \delta_{22} + \delta_{23}\bar{x} + \delta_{24}\bar{y} + \delta_{25}\bar{z} + \delta_{26}\bar{u} + \delta_{27}\bar{v} + \delta_{28}\bar{w} \\
\frac{d\bar{v}}{d\bar{t}} &= \delta_{29} + \delta_{30}\bar{x} + \delta_{31}\bar{y} + \delta_{32}\bar{z} + \delta_{33}\bar{u} + \delta_{34}\bar{v} + \delta_{35}\bar{w} \\
\frac{d\bar{w}}{d\bar{t}} &= \delta_{36} + \delta_{37}\bar{x} + \delta_{38}\bar{y} + \delta_{39}\bar{z} + \delta_{40}\bar{u} + \delta_{41}\bar{v} + \delta_{42}\bar{w}
\end{aligned}
\qquad (1)
$$

Here, it is $\bar{x} \equiv \bar{x}(\bar{t})$, $\bar{y} \equiv \bar{y}(\bar{t})$, $\bar{z} \equiv z(\bar{t})$, $\bar{u} \equiv \bar{u}(\bar{t})$, $\bar{v} \equiv \bar{v}(\bar{t})$ and $\bar{w} \equiv \bar{w}(\bar{t})$ and the system (1) has to be finished with positive initial conditions $\bar{x}(\bar{t}_0) = \bar{x}_0$, $\bar{y}(\bar{t}_0) = \bar{y}_0$, $\bar{z}(\bar{t}_0) = \bar{z}_0$, $\bar{u}(\bar{t}_0) = \bar{u}_0$, $\bar{v}(\bar{t}_0) = \bar{v}_0$ and $\bar{w}(\bar{t}_0) = \bar{w}_0$ for $\bar{t} \geq \bar{t}_0$.

The ODE model in (6) was solved with the Matlab R2023a program rungekutta45, and then the parameter values closest to the values in Table 1 (giving the minimum error) were found by using the lsqcurvefit function. In this context, the approach in [17] was used. Thus, the parameters δ_i for $i = 1,2,\ldots,42$ are presented in Table 4.

Table 4. Rate constants of system (1)

$\delta_1 = 34{,}22850$	$\delta_{10} = 0{,}0258$	$\delta_{19} = 232{,}12172$	$\delta_{27} = 377{,}19179$	$\delta_{35} = -46{,}84580$
$\delta_2 = 72{,}05751$	$\delta_{11} = -826{,}67744$	$\delta_{20} = -589{,}00570$	$\delta_{28} = -8{,}82243$	$\delta_{36} = 49{,}32834$
$\delta_3 = -61{,}83530$	$\delta_{12} = 1041{,}55237$	$\delta_{21} = 1{,}99028$	$\delta_{29} = 43{,}6812$	$\delta_{37} = 28{,}3092$
$\delta_4 = -316{,}54553$	$\delta_{13} = -272{,}18342$	$\delta_{22} = 71{,}22702$	$\delta_{30} = -68{,}17511$	$\delta_{38} = 73{,}8331$
$\delta_5 = 334{,}15619$	$\delta_{14} = 281{,}47523$	$\delta_{23} = 79{,}05189$	$\delta_{31} = 130{,}44490$	$\delta_{39} = -430{,}315$
$\delta_6 = 45{,}12734$	$\delta_{15} = -18{,}19352$	$\delta_{24} = -717{,}15390$	$\delta_{32} = 106{,}58835$	$\delta_{40} = 437{,}941$
$\delta_7 = 53{,}68125$	$\delta_{16} = -105{,}27466$	$\delta_{25} = -309{,}47579$	$\delta_{33} = -110{,}689$	$\delta_{41} = -79{,}58219$
$\delta_8 = -12{,}90362$	$\delta_{17} = 954{,}5494$	$\delta_{26} = 223{,}37558$	$\delta_{34} = -105{,}50130$	$\delta_{42} = 26{,}15628$
$\delta_9 = 241{,}94701$	$\delta_{18} = -145{,}87196$			

When the values of Table 2 are compared with Eqs. (1), Figure 1-6 are found.

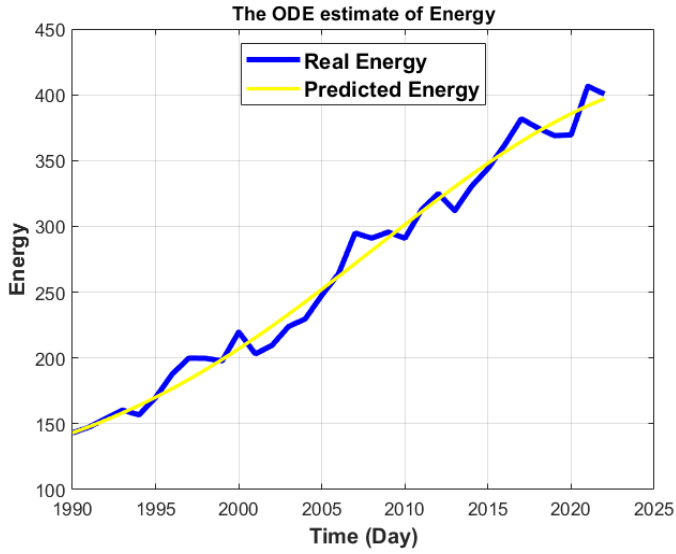

Figure 1. Graphical representation for $x(t)$ of the proposed ODE system

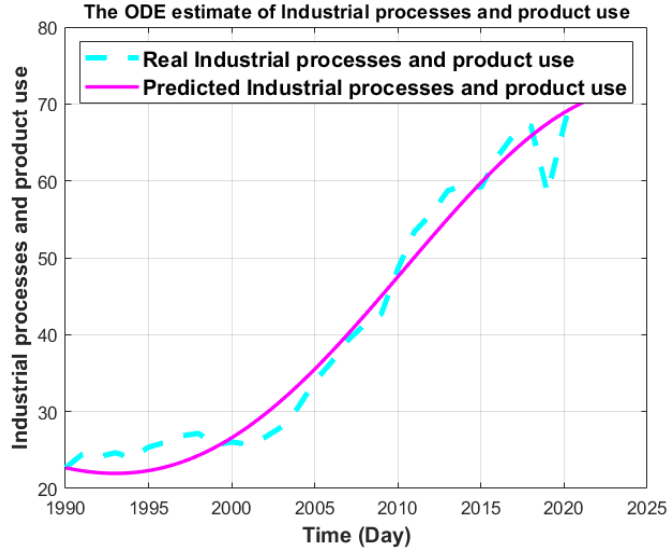

Figure 2. Graphical representation for $y(t)$ of the proposed ODE system

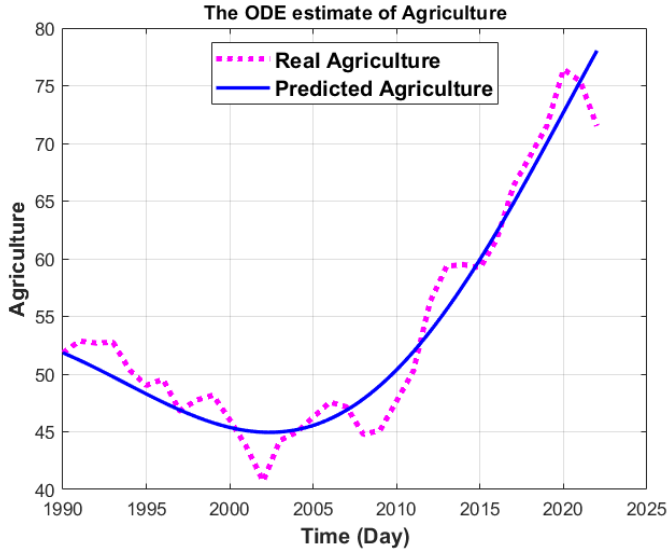

Figure 3. Graphical representation for $z(t)$ of the proposed ODE system

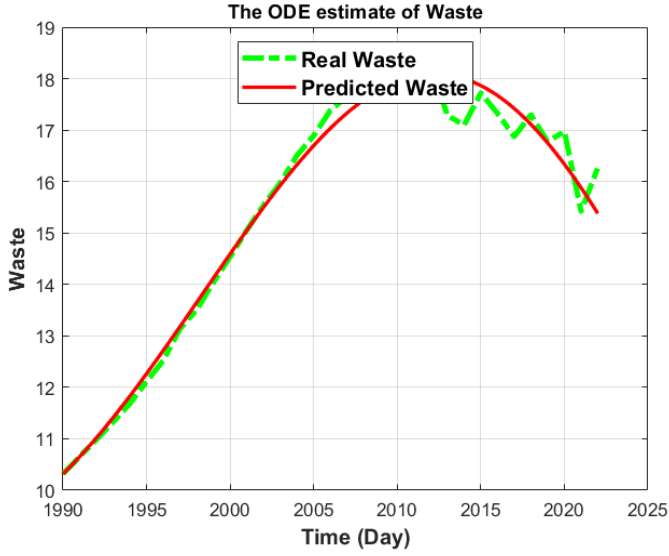

Figure 4. Graphical representation for $u(t)$ of the proposed ODE system

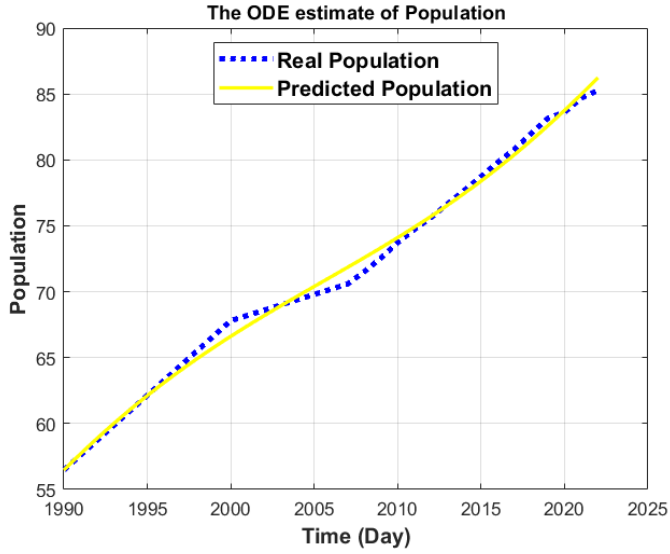

Figure 5. Graphical representation for $v(t)$ of the proposed ODE system

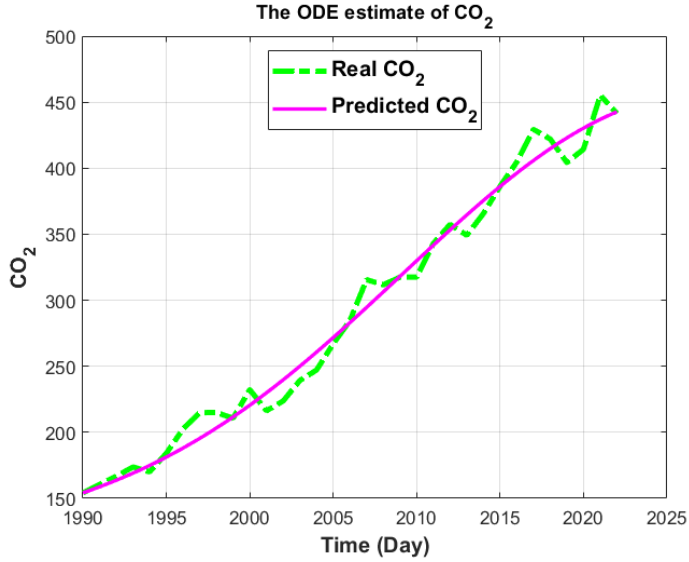

Figure 6. Graphical representation for $w(t)$ of the proposed ODE system

Data were estimated with the ODE system and the augmented data set from which the estimated results were obtained is shown in Table 5. In this table, the augmented data is shown in green.

Table 5. Dataset augmented through ODE

t	$x(t)$	$y(t)$	$z(t)$	$u(t)$	$v(t)$	$w(t)$	t	$x(t)$	$y(t)$	$z(t)$	$u(t)$	$v(t)$	$w(t)$
1990	143,147	22,69118	51,84783	10,31589	56,47304	154,1	2006	263,8615	36,41442	47,56722	17,38649	70,18878	284,6
1990,3	144,6154	22,5482	51,6468	10,4216	56,8772	155,587	2006,2	263,4824	38,1346	46,2265	17,086	71,2393	284,9206
1990,6	146,1194	22,4197	51,4387	10,5306	57,2759	157,0695	2006,5	266,6522	38,8857	46,4615	17,1846	71,4742	288,6412
1991	147,4542	24,42878	52,86218	10,6538	57,60612	160,6	2006,8	269,8317	39,6469	46,7174	17,2787	71,7096	292,3823
1991,3	149,2371	22,2079	51,004	10,7579	58,0568	160,1493	2007	294,9184	39,30367	47,15509	17,65508	70,58626	315,6
1991,6	150,8523	22,1257	50,7786	10,876	58,4391	161,7495	2007,1	273,019	40,4177	46,9943	17,3684	71,9458	296,1414
1991,9	152,5059	22,0598	50,5488	10,9971	58,8159	163,3918	2007,5	276,2125	41,1971	47,2923	17,4534	72,1829	299,9163
1992	153,9983	24,13443	52,6956	10,98332	58,73921	166,7	2007,8	279,4103	41,9843	47,6115	17,5336	72,4211	303,7045
1992,3	154,1984	22,0107	50,3152	11,1209	59,1872	165,0773	2008	291,0458	41,31473	44,77562	17,78742	71,5171	311,7
1992,6	155,9305	21,9789	50,0784	11,2474	59,5532	166,8075	2008,1	282,6106	42,7787	47,9518	17,609	72,6606	307,5035
1992,9	157,7027	21,9646	49,8392	11,3765	59,9138	168,5834	2008,4	285,8116	43,5793	48,3133	17,6792	72,9017	311,3108
1993	160,4068	24,64187	52,76737	11,32624	59,8723	173,8	2008,7	289,0114	44,3853	48,6959	17,7443	73,1444	315,1238
1993,2	159,5153	21,9684	49,5983	11,5081	60,2691	170,4062	2009	295,6533	42,71914	45,12103	17,82331	72,56131	317,5
1993,6	161,3688	21,9905	49,3563	11,642	60,6191	172,277	2009,1	292,2081	45,1959	49,0995	17,8042	73,389	318,9398
1993,9	163,2636	22,0313	49,114	11,7782	60,9639	174,1967	2009,4	295,3999	46,0102	49,5242	17,8586	73,6356	322,7562
1994	156,7516	23,98811	50,34592	11,68325	61,00539	170,1	2009,7	298,5849	46,8273	49,9697	17,9075	73,8844	326,5703
1994,2	165,1999	22,0912	48,872	11,9165	61,3035	176,1663	2010	290,9385	48,57481	47,67841	18,07754	73,72299	317,6
1994,5	167,1779	22,1703	48,631	12,0568	61,638	178,1865	2010,4	304,9268	48,4664	50,9226	17,9885	74,3894	334,1807
1994,8	169,1979	22,2691	48,3918	12,1989	61,9675	180,2582	2010,7	308,0799	49,2865	51,4296	18,0203	74,6459	337,9714
1995	169,9785	25,37117	49,03033	12,11431	62,13848	184,1	2011	312,6252	53,443	50,26833	18,43425	74,72427	343
1995,2	171,2599	22,3876	48,155	12,3428	62,292	182,382	2011,3	314,341	50,9235	52,5032	18,0664	75,1676	345,5099
1995,5	173,364	22,5261	47,9214	12,4882	62,6116	184,5584	2011,7	317,4451	51,7384	53,0694	18,0805	75,4332	349,252
1995,8	175,5102	22,6848	47,6917	12,6351	62,9265	186,7881	2012	324,9456	55,6791	56,2578	18,28221	75,62738	357,4
1996	187,7794	26,0064	49,54535	12,52105	63,27157	202,5	2012,3	323,5912	53,3565	54,2584	18,0905	75,9745	356,6678
1996,1	177,6985	22,864	47,4665	12,7832	63,2366	189,0715	2012,6	326,6293	54,1578	54,8806	18,0863	76,2506	360,3356
1996,5	179,9288	23,0636	47,2466	12,9324	63,5422	191,4089	2012,9	329,6417	54,9526	55,5206	18,076	76,5304	363,973
1996,8	182,2009	23,2839	47,0327	13,0827	63,8432	193,8007	2013	311,927	58,73633	59,35978	17,2844	76,66786	349,2
1997	199,9309	26,85137	46,8172	13,13866	64,40466	214,9	2013,3	332,6266	55,74	56,178	18,0594	76,814	367,577
1997,1	184,5146	23,5249	46,8255	13,2337	64,1399	196,2471	2013,6	335,582	56,519	56,8522	18,0366	77,1017	371,1449
1997,4	186,8697	23,7867	46,6257	13,3854	64,4322	198,7481	2013,9	338,5063	57,2887	57,5428	18,0075	77,3936	374,6737
1997,8	189,2657	24,0692	46,4339	13,5375	64,7204	201,3037	2014	330,3502	59,43406	59,49789	17,09761	77,6959	365,7
1998	199,7205	27,16336	47,74665	13,50765	65,53775	215	2014,2	341,3978	58,0483	58,2492	17,9722	77,6896	378,1608

1998,1	191,7023	24,3726	46,2509	13,69	65,0046	203,914	2014,6	344,2545	58,7966	58,9708	17,9307	77,99	381,6032
1998,4	194,179	24,6968	46,0772	13,8426	65,2849	206,5786	2014,9	347,075	59,5329	59,7069	17,8829	78,2948	384,9984
1998,7	196,6954	25,0417	45,9136	13,9952	65,5613	209,2975	2015	343,9851	59,15991	59,20755	17,72202	78,74105	386,3
1999	197,7818	25,64146	48,16938	14,04042	66,67084	210,7	2015,2	349,8574	60,2562	60,457	17,8289	78,6042	388,3434
1999,1	199,2507	25,4072	45,7607	14,1476	65,8342	212,0702	2015,5	352,6002	60,9655	61,2204	17,7687	78,9182	391,6355
1999,4	201,8445	25,7932	45,6191	14,2996	66,1035	214,8963	2015,9	355,3017	61,66	61,9963	17,7024	79,2369	394,8721
1999,7	204,476	26,1997	45,4895	14,451	66,3695	217,7754	2016	361,8714	63,20276	61,68993	17,32484	79,81487	404,6
2000	219,7642	26,05412	46,03287	14,53716	67,80393	232,4	2016,2	357,9604	62,3388	62,7841	17,63	79,5603	398,0506
2000,3	209,8491	27,0729	45,2686	14,7516	66,892	223,69	2016,5	360,5748	63,001	63,583	17,5515	79,8886	401,1682
2000,7	212,5891	27,5394	45,1785	14,9003	67,1488	226,7241	2016,8	363,1434	63,6457	64,3923	17,467	80,2218	404,2226
2001	203,1022	25,70503	43,69093	15,05664	68,2014	216,3	2017	381,8284	66,07692	66,32944	16,87281	80,81053	429,4
2001,3	218,1712	28,5305	45,0419	15,1936	67,6544	232,9413	2017,2	365,6648	64,2721	65,2111	17,3766	80,5599	407,2113
2001,6	221,0114	29,0547	44,9964	15,338	67,9035	236,1225	2017,5	368,1377	64,8794	66,0386	17,2803	80,903	410,1318
2002	209,5559	26,65961	40,70851	15,54118	68,59888	223,7	2017,8	370,5608	65,4668	66,8741	17,1783	81,2511	412,9818
2002,3	226,7846	30,1582	44,9537	15,621	68,3952	242,6243	2018	374,7233	67,14832	68,91005	17,29749	82,00388	422,1
2002,6	229,7153	30,7369	44,9574	15,7593	68,6382	245,9425	2018,1	372,9328	66,0335	67,7166	17,0706	81,6042	415,7589
2002,9	232,6737	31,3329	44,9785	15,8952	68,8795	249,3037	2018,4	375,2526	66,5786	68,5653	16,9573	81,9624	418,461
2003	223,9211	28,00141	44,24285	15,97342	68,99635	239,2	2018,8	377,5189	67,1015	69,4193	16,8386	82,3256	421,0857
2003,3	235,6587	31,9458	45,0174	16,0286	69,1192	252,7064	2019	368,9375	58,355	71,51694	16,77276	83,155	404,3
2003,6	238,6688	32,5752	45,0744	16,1593	69,3576	256,1492	2019,1	379,7307	67,6014	70,2777	16,7145	82,6939	423,6311
2003,9	241,7028	33,2205	45,1501	16,287	69,5949	259,6304	2019,4	381,887	68,0777	71,1395	16,5852	83,0672	426,095
2004	229,6737	30,55886	44,9513	16,50594	69,39383	247,2	2019,7	383,9868	68,5295	72,0038	16,4509	83,4456	428,4756
2004,2	244,7591	33,8811	45,2446	16,4117	69,8312	263,1482	2020	369,5213	67,24088	76,43694	16,97633	83,61436	414,4
2004,5	247,8363	34,5566	45,3584	16,5332	70,0667	266,7009	2020,1	386,0293	68,9564	72,8698	16,3115	83,829	430,7711
2004,9	250,933	35,2463	45,4918	16,6512	70,3016	270,2867	2020,4	388,0137	69,3576	73,7363	16,1674	84,2174	432,9796
2005	247,6651	33,95962	46,26591	16,89158	69,7913	267	2020,7	389,9393	69,7326	74,6024	16,0186	84,6107	435,0996
2005,2	254,0475	35,9496	45,6451	16,7657	70,5362	273,9036	2021	406,4723	74,71521	75,37639	15,42386	84,68027	455,2
2005,5	257,1784	36,6658	45,8184	16,8764	70,7705	277,5496	2021,4	393,6115	70,4017	76,3297	15,7078	85,412	439,0677
2005,8	260,3239	37,3944	46,0122	16,9833	71,0048	281,2227	2021,7	395,3569	70,6948	77,1888	15,5461	85,8198	440,9129
							2022	400,5858	69,90821	71,51155	16,26487	85,27955	441,4

2.3. Design of ANN Prediction Model and its Results

Before the ANN analysis, the data were subjected to L2 normalization in a similar manner. For this, the new norms of the variables are $\|t\| = 22247{,}85411$, $\|x(t)\| = 3076{,}86$, $\|y(t)\| = 497{,}7367$, $\|z(t)\| = 600{,}5575$, $\|u(t)\| = 174{,}0908$, $\|v(t)\| = 794{,}653$ and $\|w(t)\| = 3377{,}249$. Thus, the normalized data set is given in Table 6.

Table 6. Normalised augmented dataset

$\bar{x} = \frac{x}{\|x\|}$	$\bar{y} = \frac{y}{\|y\|}$	$\bar{z} = \frac{z}{\|z\|}$	$\bar{u} = \frac{u}{\|u\|}$	$\bar{v} = \frac{v}{\|v\|}$	$\bar{w} = \frac{w}{\|w\|}$	$\bar{x} = \frac{x}{\|x\|}$	$\bar{y} = \frac{y}{\|y\|}$	$\bar{z} = \frac{z}{\|z\|}$	$\bar{u} = \frac{u}{\|u\|}$	$\bar{v} = \frac{v}{\|v\|}$	$\bar{w} = \frac{w}{\|w\|}$
0,046524	0,045589	0,086333	0,059256	0,071066	0,045641	0,085634	0,076616	0,076973	0,098144	0,089648	0,084365
0,047001	0,045301	0,085998	0,059863	0,071575	0,046069	0,086664	0,078125	0,077364	0,098711	0,089944	0,085466
0,04749	0,045043	0,085652	0,060489	0,072077	0,046508	0,087697	0,079654	0,07779	0,099251	0,09024	0,086574
0,047924	0,04908	0,088022	0,061197	0,072492	0,047545	0,09585	0,078965	0,078512	0,101413	0,088827	0,093453
0,048503	0,044618	0,084928	0,061795	0,073059	0,04742	0,088733	0,081203	0,078251	0,099766	0,090537	0,087687
0,049028	0,044453	0,084552	0,062473	0,073054	0,047894	0,089771	0,082769	0,078747	0,100255	0,090836	0,088805
0,049565	0,04432	0,084017	0,063169	0,074015	0,04838	0,09081	0,084035	0,079279	0,100715	0,091136	0,089927
0,05005	0,048488	0,087744	0,06309	0,073918	0,049361	0,094592	0,083005	0,074557	0,102173	0,089998	0,092286
0,050116	0,044222	0,083781	0,06388	0,074482	0,048879	0,09185	0,085946	0,079845	0,101148	0,091437	0,091051
0,050678	0,044158	0,083387	0,064607	0,074942	0,049392	0,092891	0,087555	0,080447	0,101552	0,09174	0,092179
0,051254	0,044129	0,082988	0,065348	0,075396	0,049917	0,093931	0,089174	0,081084	0,101926	0,092046	0,093308
0,052133	0,049508	0,087864	0,065059	0,075344	0,051453	0,096089	0,085827	0,075132	0,102379	0,091312	0,094015
0,051844	0,044137	0,082587	0,066104	0,075843	0,050457	0,09497	0,090803	0,081757	0,10227	0,092354	0,094438
0,052446	0,044181	0,082184	0,066873	0,076284	0,051011	0,096007	0,092439	0,082464	0,102582	0,092664	0,095568
0,053062	0,044263	0,081781	0,067655	0,076718	0,051579	0,097042	0,09408	0,083206	0,102863	0,092977	0,096697
0,050945	0,048194	0,083832	0,06711	0,07677	0,050359	0,094557	0,097591	0,07939	0,10384	0,092774	0,094028
0,053691	0,044383	0,081378	0,06845	0,077145	0,052163	0,099103	0,097374	0,084792	0,103328	0,093612	0,098951
0,054334	0,044542	0,080976	0,069256	0,077566	0,052761	0,100128	0,099021	0,085636	0,103511	0,093935	0,100073
0,05499	0,044741	0,080578	0,070072	0,077981	0,053374	0,101605	0,107372	0,083703	0,105889	0,094034	0,101551
0,055244	0,050973	0,081641	0,069586	0,078196	0,054521	0,102163	0,10231	0,087424	0,103776	0,094592	0,102305
0,055661	0,044979	0,080184	0,070899	0,078389	0,054003	0,103172	0,103947	0,088367	0,103857	0,094926	0,103413
0,056344	0,045257	0,079795	0,071734	0,078791	0,054648	0,105609	0,111865	0,093676	0,105015	0,09517	0,105838
0,057042	0,045576	0,079412	0,072578	0,079187	0,055308	0,105169	0,107198	0,090347	0,103914	0,095607	0,105609
0,06103	0,052249	0,082499	0,071923	0,079622	0,05997	0,106157	0,108808	0,091383	0,10389	0,095955	0,106695
0,057753	0,045936	0,079037	0,073428	0,079578	0,055984	0,107136	0,110405	0,092448	0,103831	0,096307	0,107772

0,058 478	0,046 337	0,078 671	0,074 285	0,079 962	0,0566 76	0,101 378	0,118 007	0,098 841	0,099 284	0,096 48	0,103 396
0,059 217	0,046 78	0,078 315	0,075 149	0,080 341	0,0573 84	0,108 106	0,111 987	0,093 543	0,103 736	0,096 664	0,108 839
0,064 979	0,053 947	0,077 956	0,075 47	0,081 048	0,0636 41	0,109 066	0,113 552	0,094 666	0,103 605	0,097 026	0,109 896
0,059 968	0,047 264	0,077 97	0,076 016	0,080 714	0,0581 09	0,110 017	0,115 098	0,095 816	0,103 437	0,097 393	0,110 94
0,060 734	0,047 79	0,077 637	0,076 887	0,081 082	0,0588 49	0,107 366	0,119 409	0,099 071	0,098 211	0,097 773	0,108 269
0,061 513	0,048 357	0,077 318	0,077 761	0,081 445	0,0596 06	0,110 957	0,116 625	0,096 992	0,103 235	0,097 765	0,111 973
0,064 91	0,054 574	0,079 504	0,077 59	0,082 473	0,0636 61	0,111 885	0,118 128	0,098 193	0,102 996	0,098 143	0,112 992
0,062 305	0,048 967	0,077 013	0,078 637	0,081 802	0,0603 79	0,112 802	0,119 607	0,099 419	0,102 722	0,098 527	0,113 998
0,063 109	0,049 618	0,076 724	0,079 514	0,082 155	0,0611 68	0,111 797	0,118 858	0,098 588	0,101 798	0,099 089	0,114 389
0,063 927	0,050 311	0,076 452	0,080 39	0,082 503	0,0619 73	0,113 706	0,121 06	0,100 668	0,102 412	0,098 916	0,114 988
0,064 28	0,051 516	0,080 208	0,080 65	0,083 899	0,0623 82	0,114 597	0,122 485	0,101 939	0,102 066	0,099 312	0,115 963
0,064 758	0,051 045	0,076 197	0,081 266	0,082 846	0,0627 94	0,115 475	0,123 881	0,103 231	0,101 685	0,099 713	0,116 921
0,065 601	0,051 821	0,075 961	0,082 139	0,083 185	0,0636 31	0,117 611	0,126 98	0,102 721	0,099 516	0,100 44	0,119 816
0,066 456	0,052 638	0,075 745	0,083 008	0,083 52	0,0644 83	0,116 34	0,125 245	0,104 543	0,101 269	0,100 12	0,117 862
0,071 425	0,052 345	0,076 65	0,083 503	0,085 325	0,0687 99	0,117 189	0,126 575	0,105 873	0,100 818	0,100 533	0,118 785
0,068 202	0,054 392	0,075 378	0,084 735	0,084 178	0,0662 34	0,118 024	0,127 87	0,107 221	0,100 333	0,100 952	0,119 69
0,069 093	0,055 329	0,075 228	0,085 589	0,084 501	0,0671 33	0,124 097	0,132 755	0,110 446	0,096 92	0,101 693	0,127 13
0,066 01	0,051 644	0,072 751	0,086 487	0,085 825	0,0640 44	0,118 843	0,129 129	0,108 584	0,099 813	0,101 377	0,120 575
0,070 907	0,057 32	0,075	0,087 274	0,085 137	0,0689 74	0,119 647	0,130 349	0,109 962	0,099 26	0,101 809	0,121 44
0,071 83	0,058 374	0,074 924	0,088 103	0,085 451	0,0699 16	0,120 435	0,131 529	0,111 353	0,098 674	0,102 247	0,122 283
0,068 107	0,053 562	0,067 785	0,089 271	0,086 326	0,0662 45	0,121 788	0,134 907	0,114 743	0,099 359	0,103 195	0,124 997
0,073 707	0,060 591	0,074 853	0,089 729	0,086 069	0,0718 41	0,121 206	0,132 668	0,112 756	0,098 056	0,102 692	0,123 106
0,074 659	0,061 753	0,074 859	0,090 523	0,086 375	0,0728 23	0,121 96	0,133 763	0,114 169	0,097 405	0,103 142	0,123 906
0,075 621	0,062 951	0,074 895	0,091 304	0,086 679	0,0738 19	0,122 696	0,134 813	0,115 591	0,096 723	0,103 599	0,124 683
0,072 776	0,056 257	0,073 67	0,091 753	0,086 826	0,0708 37	0,119 907	0,117 241	0,119 084	0,096 345	0,104 643	0,119 713
0,076 591	0,064 182	0,074 959	0,092 07	0,086 98	0,0748 26	0,123 415	0,135 818	0,117 021	0,096 01	0,104 063	0,125 437
0,077 569	0,065 447	0,075 054	0,092 821	0,087 28	0,0758 46	0,124 116	0,136 775	0,118 456	0,095 268	0,104 533	0,126 166
0,078 555	0,066 743	0,075 18	0,093 555	0,087 579	0,0768 76	0,124 798	0,137 682	0,119 895	0,094 496	0,105 009	0,126 871
0,074 645	0,061 396	0,074 849	0,094 812	0,087 326	0,0731 91	0,120 097	0,135 093	0,127 277	0,097 514	0,105 221	0,122 697
0,079 548	0,068 07	0,075 338	0,094 271	0,087 876	0,0779 18	0,125 462	0,138 54	0,121 337	0,093 695	0,105 491	0,127 551
0,080 548	0,069 427	0,075 527	0,094 969	0,088 173	0,0789 7	0,126 107	0,139 346	0,122 78	0,092 868	0,105 98	0,128 205
0,081 555	0,070 813	0,075 749	0,095 647	0,088 468	0,0800 32	0,126 733	0,140 099	0,124 222	0,092 013	0,106 475	0,128 833
0,080 493	0,068 228	0,077 038	0,097 027	0,087 826	0,0790 56	0,132 106	0,150 11	0,125 511	0,088 597	0,106 563	0,134 799
0,082 567	0,072 226	0,076 005	0,096 304	0,088 764	0,0811 03	0,127 926	0,141 444	0,127 098	0,090 228	0,107 483	0,130 007

0,083 585	0,073 665	0,076 293	0,096 94	0,089 058	0,0821 82	0,128 494	0,142 033	0,128 529	0,089 299	0,107 997	0,130 554
0,084 607	0,075 129	0,076 616	0,097 554	0,089 353	0,0832 7	0,130 193	0,140 452	0,119 075	0,093 428	0,107 317	0,130 705
0,085 757	0,073 16	0,079 205	0,099 87	0,088 326	0,0842 79						

Artificial Neural Networks (ANN) are a versatile technique used in many disciplines and industrial applications. Artificial Neural Networks are frequently used in many areas of science. For some of them, see the following references: [18, 19, 20, 21]. ANNs can be used to predict output by training the network on past data that relates input features to corresponding output values. In an ANN, an activation function refers to a mathematical operation applied to the output of each neuron in a layer of the network.

The ANN model proposed in this study, whose schematic is given in Figure 7, was used to estimate CO_2 emissions using five different input parameters. The selection of activation functions is critical in the design of the nonlinear network and facilitates the discovery and learning of complex patterns and relationships found in the data by applying them to the output of each neuron.

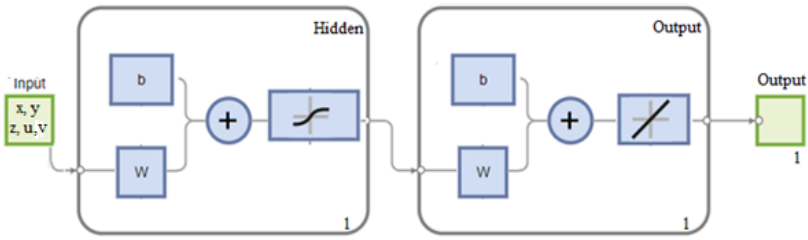

Figure 7. ANN architecture

The variable w(t) (CO_2 emission) in Table 6 was estimated using the other five inputs. For the estimation, the training and testing processes were performed using the data in Table 7. The hyperbolic tangent transfer function was used as the activation function. In addition, the percentages of the data used for the training, validation and testing stages are as follows: 70%, 15% and 15%, respectively. Then, the data were denormalized.

Some parameters for ANN analysis are explained in Table 7. The model was determined by considering the parameter selections and the situations where good results were obtained.

Table 7. Training progress

Unit	Initial Value	Stopped Value	Target Value
Epoch	0	10000	10000
Elapsed Time	-	00:00:09	-
Performance	0.491	1.14e-07	1e-16
Gradient	1.23	5.65e-09	0
Mu	0.001	1e-10	1e+10
Validation Checks	0	9.93e+03	1.11e+06

The outcoming model by activation functions of ANN is written as in Equation (2). Therefore, we have

$$w(t) = w = b_2 + LW \tanh\left(b_1 + IW \begin{pmatrix} x \\ y \\ z \\ u \\ v \end{pmatrix}\right) \tag{2}$$

where

$$b_1 = (0{,}4745), b_2 = (0{,}2312), LW = (-0{,}5240),$$
$$IW = (-1{,}7997 \quad -0{,}2413 \quad 0{,}0070 \quad -0{,}0386 \quad -0{,}1170). \tag{3}$$

3. COMPARISON of ANN and ODE MODELS

In this section, the ANN and ODE model estimation results for the original values between 1990-2022 are shown in Table 8. The 33 rows of data given in Table 2 are taken as basis here.

Table 8. Estimation performances of the proposed models according to the values in Table 2

CO_2	ANN prediction of CO_2	ODE prediction of CO_2	**CO_2**	ANN prediction of CO_2	ODE prediction of CO_2	**CO_2**	ANN prediction of CO_2	ODE prediction of CO_2
154,1	154,8939	154,1407	216,3	216,729	229,8082	357,4	359,3946	352,9723
160,6	160,462	158,5898	223,7	223,795	239,3506	349,2	348,9997	364,874
166,7	166,5654	163,8132	239,2	238,4507	250,1544	365,7	367,7275	375,8361
173,8	173,1689	169,191	247,2	246,1151	260,803	386,3	381,3699	386,1134

170,1	169,7673	174,8532	267,0	265,9688	271,4923	404,6	402,3597	395,9316
184,1	183,3442	181,3201	284,6	283,545	283,0717	429,4	424,4731	405,717
202,5	200,6089	188,3104	315,6	315,8108	294,8884	422,1	418,7104	414,8332
214,9	213,0432	195,4316	311,7	314,0058	306,2372	404,3	405,8024	422,7826
215,0	213,4657	203,0439	317,5	319,8292	317,9858	414,4	413,7635	430,1972
210,7	210,9398	211,377	317,6	320,29	330,3794	455,2	456,419	437,1295
232,4	232,2198	220,7069	343,0	345,5336	341,7487	441,4	447,101	442,6639

The performance indicators of both models are presented in Table 9 by comparing them with the actual values in Table 2. According to these results, it is seen in Table 9 that both the linear ODE system model and the ANN model are successful in predicting CO_2 emissions, but the ANN model is more successful.

Table 9. Performances of ODE and ANN estimation results

	The ANN prediction of *w*	The ODE prediction of *w*
Total Absolute Error	51,79381617	299,3497677
MAD	1,569509581	9,07120508
MSE	4,552812915	129,8321319
RMSE	2,133732156	11,39439037
MAPE	0,004925816	0,032107884
R-Squared	0,999488465	0,985402435

4. RESULT and DISCUSSIONS

In this study, the ANN model and linear ODE system model were compared to estimate the amount of CO_2 emissions between 1990-2022. The factors affecting the amount of CO_2 emissions are the population of Turkey obtained from TSI and the distribution of this amount of emissions by sectors. The comparison of these two optimization methods was made according to the real values found between 1990-2022. The result of this comparison is shown in Table 9. Here, it was seen that the ANN method gave more successful results. However, when the mathematical modeling of the instantaneous change of a variable depending on time is considered, differential equations first come to mind. With

this method, the change of the variable depending on time can be predicted in the future. When compared with the real values, the ODE model achieved a not bad success. In the ANN method, the instantaneous states of the input variables find the value of the output variable w(t). This shows that the current values of the inputs must be known in order to make predictions. However, in mathematical modeling with ODE, using the parameter values obtained in this study, forward-looking estimates can be made only with the starting point data. The amount of carbon dioxide emissions from 1990 to 2080 is shown graphically in Figure 8.

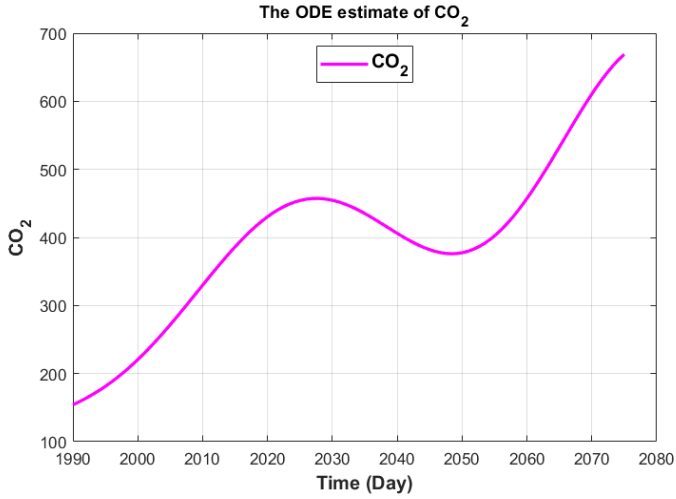

Figure 8. Prediction curve for CO_2 emissions of the ODE model in the years 1990-2080

Table 10 shows the estimate of the amount of CO_2 emissions until 2075. Here, it is seen that towards the end of 2027, CO_2 emissions will reach 458 million tons. This point is the local maximum point. It is observed that CO_2 emissions will tend to decrease from 2028 to 2050 and will decrease to 378 million tons. However, our prediction is that there will be an increase from 2050 to 2075 and CO_2 emissions will reach 669 million tons in 2075.

Table 10. ODE model CO_2 forecast for 2023-2075

Year	CO_2 (ODE)	Year	CO_2 (ODE)	Year	CO_2 (ODE)	Year	CO_2 (ODE)	Year	CO_2 (ODE)
2022,6	445,833	2033,8	441,2221	2044,9	382,1288	2056,1	412,0661	2067,3	569,1969

2023,5	449,52	2034,6	436,9639	2045,8	379,5752	2057	420,6263	2068,1	582,6838
2024,3	452,5015	2035,5	432,3822	2046,7	377,6694	2057,8	430,0295	2069	595,8341
2025,2	454,7689	2036,4	427,5477	2047,5	376,4687	2058,7	440,2281	2069,8	608,5267
2026,1	456,3211	2037,2	422,5376	2048,4	376,0344	2059,5	451,1639	2070,7	620,6543
2026,9	457,1643	2038,1	417,426	2049,2	376,4181	2060,4	462,7681	2071,6	632,1026
2027,8	457,312	2038,9	412,283	2050,1	377,6621	2061,3	474,9611	2072,4	642,7618
2028,6	456,7854	2039,8	407,1908	2051	379,7994	2062,1	487,6613	2073,3	652,5287
2029,5	455,6114	2040,7	402,2301	2051,8	382,8536	2063	500,7825	2074,1	661,3067
2030,4	453,8181	2041,5	397,4803	2052,7	386,8387	2063,8	514,2286	2075	669,0061
2031,2	451,4394	2042,4	393,0194	2053,5	391,7595	2064,7	527,8993		
2032,1	448,5153	2043,2	388,9239	2054,4	397,6117	2065,6	541,6905		
2032,9	445,0921	2044,1	385,2692	2055,3	404,3858	2066,4	555,4937		

REFERENCES

[1] G. Akın, «Küresel isınma, nedenleri ve sonuçları,» *Ankara Üniversitesi Dil ve Tarih-Coğrafya Fakültesi Dergisi,* cilt 46, no. 2, pp. 29-43, 2006.

[2] S. Erdoğan, «Enerji, çevre ve sera gazları,» *Çankırı Karatekin Üniversitesi İktisadi ve İdari Bilimler Fakültesi Dergisi,* cilt 10, no. 1, pp. 277-303, 2020.

[3] Wikipedia, «Sera Gazları,» [Çevrimiçi]. Available: https://tr.wikipedia.org/wiki/Sera_gazlar%C4%B1#:~:text=S%C4%B1ras%C4%B1yla%2C%20D%C3%BCnya%20atmosferinde%20en%20bol,Metan%20(CH4). [Accessed: 15 October 2024].

[4] Ş. v. İ. D. B. T.C. Çevre, «Çevresel Göstergeler, Sektörlere Göre Toplam Seragazı Emisyonları,» [Çevrimiçi]. Available: https://cevreselgostergeler.csb.gov.tr/sektorlere-gore-toplam-seragazi-emisyonlari-i-101864. [Accessed: 15 October 2024].

[5] R. Kafle, K. Pokhrel, N. Khanal ve C. Tsokos, «Differential equation model of carbon dioxide emission using functional linear regression,» *Journal of Applied Statistics,* cilt 46, no. 7, pp. 1246-1259, 2019.

[6] Z. Chen, X. Ye ve P. Huang, «Estimating carbon dioxide (CO2) emissions from reservoirs using artificial neural networks,» *Water,* cilt 10, no. 1, 2018.

[7] A. Nanda, S. Gupta, A. Saleth ve S. Kiran, «Multi-layer perceptron's neural network with optimization algorithm for greenhouse gas forecasting systems,» *Environmental Challenges,* cilt 11, no. 100708, 2023.

[8] S. Altikat, «Prediction of CO2 emission from greenhouse to atmosphere with artificial neural networks and deep learning neural networks,» *International Journal of Environmental Science and Technology,* cilt 18, no. 10, pp. 3169-3178, 2021.

[9] M. Mutascu, «CO2 emissions in the USA: new insights based on ANN approach,» *Environmental Science and Pollution Research,* cilt 29, no. 45, pp. 68332-68356, 2022.

[10] C. Tsokos ve Y. Xu, «Modeling carbon dioxide emissions with a system of differential equations,» *Nonlinear Analysis: Theory, Methods & Applications,* cilt 71, no. 12, pp. e1182-e1197, 2009.

[11] M. Caetano, D. Gherardi ve T. Yoneyama, «Optimal resource management control for CO2 emission and reduction of the greenhouse effect,» *Ecological Modelling,* cilt 213, no. 1, pp. 119-126, 2008.

[12] R. Kafle, K. Pokhrel, N. Khanal ve C. Tsokos, «Differential equation model of carbon dioxide emission using functional linear regression,» *Journal of Applied Statistics,* cilt 46, no. 7, pp. 1246-1259, 2019.

[13] R. Braddock, J. Filar, R. Zapert, J. Rotmans ve M. d. Elzen, «The IMAGE greenhouse model as a mathematical system,» *Applied Mathematical Modelling,* cilt 18, no. 5, pp. 234-254, 1994.

[14] F. Wirl, «International greenhouse gas emissions when global warming is a stochastic process,» *Applied Stochastic Models in Business and Industry,* cilt 20, no. 2, pp. 95-114, 2004.

[15] TUIK, «Sera Gazı Emisyon İstatistikleri, 1990-2022,» 2024. [Çevrimiçi]. Available: https://data.tuik.gov.tr/Bulten/Index?p=Sera-Gazi-Emisyon-Istatistikleri-1990-2022-53701. [Accessed: 15 October 2024].

[16] TUIK, «Nüfus ve Demografi,» 2024. [Çevrimiçi]. Available: https://data.tuik.gov.tr/Kategori/GetKategori?p=Nufus-ve-Demografi-109. [Accessed: 15 October 2024].

[17] E. Işık ve B. Daşbaşı, «A compartmental fractional-order mobbing model and the determination of its parameters,» *Bulletin of Biomathematics,* cilt 1, no. 2, pp. 153-176, 2023.

[18] A. Baliyan, K. Gaurav ve S. K. Mishra, «A review of short term load forecasting using artificial neural network models,» *Procedia Computer Science ,* p. 121–125, 2015.

[19] S. Agatonovic-Kustrin ve R. Beresford, «Basic concepts of artificial neural network (ANN) modeling and its application in pharmaceutical research,» *Journal of pharmaceutical and biomedical analysis,* p. 717–727, 2000.

[20] F. Amato, A. López, E. M. Peña-Méndez, P. Vanhara, A. Hampl ve J. Havel, «Artificial neural networks in medical diagnosis,» *Journal of applied biomedicine,* pp. 47-58, 2013.

[21] R. Shaw ve B.K. Patra, «Classifying students based on cognitive state in flipped learning pedagogy,» *Future Generation Computer Systems,* p. 305–317, 2022.

CHAPTER 2

Synthesis and Characterization of Curcumin-Modified Amorphous TiO_2 For Adsorption of Pb(II) Ions From Aqueous Solution

Fırat Ünal[1] & Hatice Çağlar Yılmaz[2] & Emine Mete[3] & Sema Erdemoğlu[4]

[1] İnönü University, Faculty of Science and Arts, Department of Chemistry, Malatya, TURKEY
ORCID 0000-0002-3798-4651
[2] Dr., Malatya Turgut Özal University, Technology Transfer Office, Malatya, TURKEY
ORCID 0000-0002-9730-9930
[3] İnönü University, Faculty of Science and Arts, Department of Chemistry, Malatya, TURKEY,
ORCID 0000-0003-3846-5471
[4] Prof. Dr., İnönü University, Faculty of Science and Arts, Department of Chemistry, Malatya, TURKEY,
ORCID 0000-0002-0119-1596

1. Introduction

Pollution of the air, soil, and water, in short, the ecological system in which all living things take place as a result of the increase in human and industrial activities with rapidly increasing population and developing industrialization, and accordingly increasing environmental pollution is still one of the biggest problems of the whole world (Novikau & Lujaniene 2022). It is possible to find heavy metals in many areas of today's world due to increasing pollution sources. Although some of these metals are involved in biochemical and physiological activities in living organisms at trace concentrations, their toxic effects occur when threshold concentration values are exceeded. Some properties of heavy metals such as not being degradable like organic pollutants, transforming into hydrated ions that show more toxic effects in water, accumulation in living organisms in aquatic environments, and durability cause great difficulties in their removal from wastewater. (Shrestha et al., 2021; Akpor et al., 2014). In recent years, a large number of researches have been carried out for the removal of organic and inorganic-based pollutants from the ecological system and their quantitative determination (Kumar et al., 2017).

Heavy metal ions pose a great risk as environmental pollutants. Pb is among the most common pollutants in industrial wastewater. Today, lead is used in many industrial areas. Pb is used in the production of industrial products such as lead-acid batteries in cars, computer screen pages for radiation protection, ammunition, and bullets, cable coating, sports equipment, weight belts for divers, drums for corrosive liquids, roofing in buildings, stained glass windows, lead pipes. In addition, battery production, paints, and electroplating processes are among the industrial areas where lead is used. Such intensive use of lead in industrial areas has led to the development of strategies to eliminate the damage to the environment (Carolin et al., 2017; Briffa et al., 2020). Beacuse its presence in the human body can cause serious danger to the normal functioning of the kidneys, liver, nervous system and neuronal cells. The World Health Organization has identified lead as one of the 10 harmful chemicals that threaten public health. Due to its toxic properties, the allowable lead ion concentration in drinking water and surface water is below 0.015 mg/L (Kunquan et al., 2010). Restrictions have been imposed especially on the use of lead in paints. There is no known safe blood lead concentration; even blood lead concentrations as low as 3.5 μg/dL may be associated with decreased intelligence in children, behavioural difficulties and learning problems (https://www.cdc.gov/lead-prevention/php/news-features/updates-blood-lead-reference value.html).

Various methods are used for the safe treatment of wastewater polluted by various sources. These include ion exchange, chemical precipitation, reverse osmosis, membrane separation, electrochemical methods, coagulation/flocculation, ultrafiltration, and adsorption. The choice of which technique to use depends on the type and concentration of both the available supporting materials and the adsorbent used, as well as their costs (Burakov et al., 2018; Dabrowski 2001). These methods used in the removal of heavy metals have some disadvantages such as insufficient removal, requiring high energy and cost, limited reusability, and requiring sensitive operation. To overcome these disadvantages, the adsorption method is generally preferred to remove toxic metal ions from the aqueous environment. Adsorption has many important advantages compared to other water treatment methods, such as ease of application, high degree of purification, high profitability and reusability. Additionally, no secondary toxic byproducts are formed when adsorption methods are used (Soliman & Moustafa 2020).

Activated carbon, natural and synthetic zeolites, ion exchange resins and some biopolymers such as chitosan, gelatin, cellulose and lignin are used as traditional adsorbent materials in water purification. Recently, materials such as carbon nanotubes, nanofibers, graphene and graphene oxide have been studied extensively due to their high adsorption efficiency. However, the widespread use of carbon nanomaterials in real water purification systems is limited due to problems such as high production costs, environmentally unsafe production methods, granulation and regeneration. Biopolymers show high adsorption capacity due to their mesoporous structure and hydroxyl and carboxyl functional groups. However, they have low chemical and mechanical stability.

Nanomaterials are candidates for being good adsorbent materials due to their nanosizes, high surface areas, huge surface-to-volume ratios, good dispersion in water and excellent surface reactions (Hornyak 2008). There are many studies on the effective separation of heavy metal ions from aqueous media with nano TiO_2. Additionally, TiO_2-based nanocomposite materials and immobilization of TiO_2 on support materialshave been investigated to enhance the adsorption capacity of nano TiO_2.

In most studies in the literature, crystalline nano TiO_2 (anatase or rutile) has been used alone or by preparing composite materials (carbon nitride, hydroxide ethyl aniline, etc.) for adsorption of heavy metal ions. In this study, amorphous TiO_2 was prepared instead of crystalline TiO_2 and its adsorption capacity for Pb(II) ions was investigated by modifying it with curcumin, a natural functional group. Curcumin, often called diferuloylmethane or 1,7-bis(4-hydroxy-3-

methoxyphenyl)-1,6-heptadiene-3,5-dione, is a hydrophobic polyphenol extracted from the root of the Curcuma longa plant (turmeric). Turmeric has traditionally been used for many ailments due to its wide range of pharmacological activities. However, recent studies have shown that curcumin exhibits antioxidant, anti-inflammatory, antimicrobial, anticarcinogenic, and many other pharmacological activities. Turmeric contains three important derivatives, curcumin, demethoxycurcumin (DMC), and bis-demethoxycurcumin (BDMC). The three compounds, called curcuminoids, differ in the methoxy bonding on the aromatic ring (Anand et al., 2008; Simon et al., 1997). The analytical application of curcumin complexes is related to the spectroscopic analysis of trace amounts of metals in many areas such as food, plants, wastewater, and nuclear technological wastes. In particular, the spectroscopic determination of boron in very trace amounts is among the first analytical applications (Wanninger et al., 2015). Although most of the literature demonstrates the remarkable antioxidant and antibacterial performance of curcumin, applications of curcumin for heavy metal ion removal and membrane applications have not been sufficiently investigated to date (Naushad et al., 2019; Priyadarsini 2014).

The amorphous phase is mainly characterized by partial loss and disordered formation of TiO_2 octahedral coordination. Amorphous TiO_2 is thought to have weak photocatalytic activity due to its irregular structure. However, compared to crystalline TiO_2, it has advantages such as easier synthesis conditions, larger surface area, and more favorable surface modification. This has increased the adsorption properties of amorphous TiO_2. In addition, due to its large specific surface area, it is possible to increase its photocatalytic activity and heavy metal adsorption capacity by doping with highly conductive metals or substances containing functional groups (Sun et al., 2019; Modvi et al., 2023).

The objective of this study was to investigate, after synthesis and characterization of curcumin modified amorphous-TiO_2, (curcumin/a-TiO_2) for enhanced adsorption capacity and its utility for the removal of Pb2+ ions, from aqueous media by adsorption. The adsorption conditions (pH, contact time, amount of adsorbent, Pb2+ concentration, etc.) in batch mode experiments were optimized. Additionally, adsorption isotherm and kinetics were determined. According to our research, no studies have been found in literature on the adsorption of Pb ions by curcumin-modified TiO_2.

2. Experimental

2.1 Reagents and solution

Titanium-iso-propoxide ($Ti(OPri)_4$, 97%), curcumin ($[HOC_6H_3(OCH_3)CH=CHCO]_2CH_2$, 99%), 2-propanol ($C_3H_8O_9$) and tannic acid (C76H52O48) were purchased from Alfa Aesar) and Sigma-Aldrich (German). Hydrochloric acid (HCl, 37%), lead(II) nitrate $Pb(NO)_2$ solution (1000 mg L^{-1}), sodium hydroxide (NaOH), ethanol (C_2H_5OH), sulfuric acid (H_2SO_4), nitric acid (HNO_3), sodium dihydrogen phosphate (H_2NaPO_4), magnesium chloride hexahydrate (MgCl2.6H2O), dimethyl sulfoxide (CH_3)2SO were purchased from Merck (German). All chemicals were analytical grade. Millipore Milli-Q Direct 16 ultrapure water (18.2 MΩ cm resistivity, Millipore, USA) was used for the preparation of all aqueous solutions.

2.2 Instrumentation

X-ray diffraction (XRD) patterns obtained with a Rigaku Geigerflex D Max/B model diffractometer using Cu Kα radiation (λ = 0.15418 nm). The analysis was carried out at a scanning range of 10-80° and a scanning degree of 2 min^{-1}. Fourier transform infrared spectroscopy (FT-IR) (Perkin Elmer Spectrum One) spectra of the synthesized materials were characterized at 4000-500 cm-1 wavelength and 4.0 cm^{-1} resolution. Digital LEO-EVO 40 scanning electron microscope (SEM) was used to determine the surface morphology. SEM and SEM-EDX analyses were performed with a microscope with an accelerating voltage of 30 kV, a detector with 3 nm separation power (secondary electron), and a BSD (Back Scattering Detector) with 4.5 nm separation power in XVP mode, an accelerating voltage range of 0.2-30 kV. The imaged material was coated with a gold coating to obtain better images and ensure conductivity. Micromeritics Instrument Corp.Gemini VII 3.03, serial 679 surface area measurement device (BET). A Malvern Zeta-sizer Nano series Nano-ZS instrument was used to measure the surface charge and hydrodynamic diameters. The concentrations of the ions remaining in the aqueous medium after all adsorption studies were determined by Thermo iCE-3000 Series flame atomic absorption spectrophotometer (FAAS).

2.3 Synthesis of curc/a-TiO_2

The synthesis was carried out in two stages. In the first step, 2-PrOH/$Ti(OPri)_4$ (n/n) was taken in a ratio of 23.07 and $H_2O/Ti(OPri)_4$ (n/n) 3.26 for amorphous TiO_2 (a-TiO_2) synthesis by sol-gel method. $Ti(OPri)_4$ was added to 2-PrOH and dispersed for 30 min and after homogenization, water was added dropwise at the determined ratio and stirred at the lowest speed (250 rpm) for 4 hours at room

temperature. After evaporation of alcohol by centrifugation at 9000 rpm and then the material was dried in a vacuum oven at 105ºC for 1 night.

In the second step, curcumin was modified to amorphous TiO_2 by wet impregnation. 1.000 g of curcumin was dissolved homogeneously in 70 ml MetOH in an ultrasonic bath. 2.000 g a-TiO_2 was dispersed in 2.5 mL DMSO and added to the curcumin dissolved in methanol and stirred in a reflux system at 250 rpm for 8 hours at room conditions. Then, the supernatant obtained after centrifugation at 9000 rpm for 15 minutes was washed several times in DMSO and MeOH separately to remove impurities. It was then dried in a vacuum oven at 70 ºC for 7 hours.

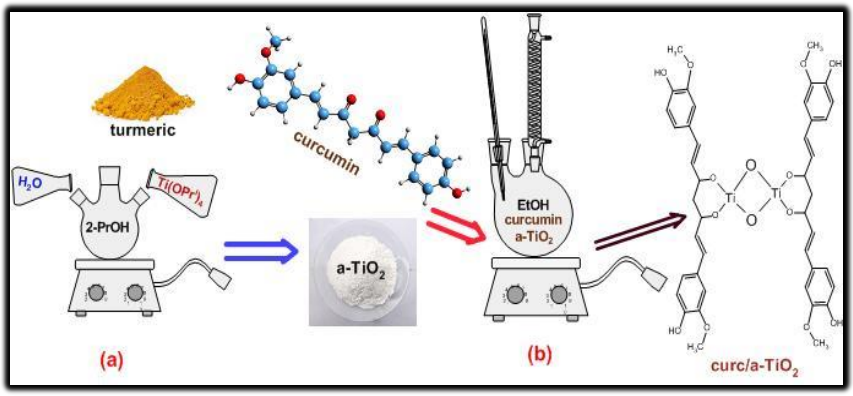

Figure 1. Synthesis of a-TiO_2 by sol-gel process (a), modification of curcumin to a-TiO_2 by wet impregnation technique (b).

2.4 Adsorption studies

Adsorption studies of lead ions using curc/a-TiO_2 were performed by batch method procedure. In the adsorption studies performed by batch technique, initially, different ratios of curcumin were modified to amorphous TiO_2, and the effect of curcumin ratio on the adsorption of Pb^{2+} ions was investigated. After determining the optimum curcumin ratio, the effects of time (5-120 min), pH (2-8), adsorbent amount (0.025-0.4 % w/v), initial concentration (50-700 mg L^{-1}), pollutant volume (25-200 ml), organic matrix (10-30 mg L^{-1}) optimum parameter values in batch adsorption studies were investigated operating under room conditions. The adsorption capacity of lead ions on curc/a-TiO_2 (mg g^{-1}) was calculated as equation (1).

$$q_e = (c_0 - c_e).\frac{V}{m} \quad (1)$$

In the equation, qe is the adsorption capacity, Co is the initial concentration of Pb^{2+} ions, C is the concentration at equilibrium, V is the volume, and m is the amount of adsorbent. Pb^{2+} concentrations in all adsorption studies were determined by FAAS.

3. RESULT AND DISCUSSION

3.1. Characterization of the synthesised materials

XRD patterns

XRD was used to determine the phase analyses and crystallite size of the synthesized materials and XRD diffraction patterns were given in Figure 3. The average crystallite sizes of the materials were calculated from the Scherrer equation.

$$D = Kx\lambda/\beta x cos\ \theta \quad (2)$$

In the equation, D is the average crystal size in nanometres, K is the crystal form factor (0.94), λ is the wavelength of the X-ray beam (0.1548 nm for CuKα radiation), β is the width at half height of the maximum scattering peak and θ is the peak point (Bragg angle). XRD patterns are shown in Figure 3.

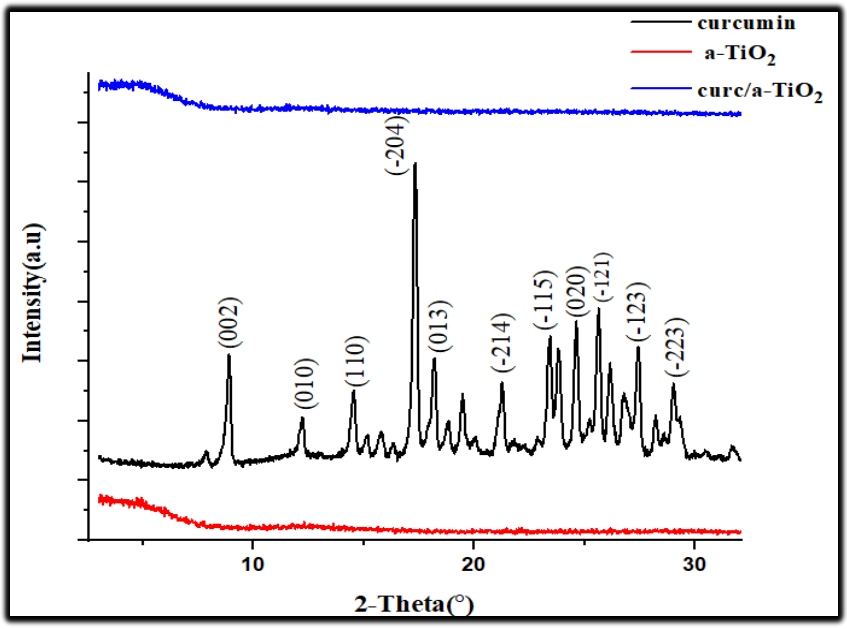

Figure 2. XRD powder diffraction patterns of the synthesized materials.

Many peaks with 2θ diffraction angles between 7-30º are observed, confirming the crystal structure of curcumin. The observed XRD diffraction patterns were analyzed using the ICDD PDF-4 2021 (ICDD Card No. 00-066-1420) database library, with $C_{21}H_{20}O_6$ as the reference model of curcumin. The values corresponding to the angles 2θ=9.08°, 14.78°, 17.61°, 19.07°, 23.81°, 24.20°, 25.97°, 26.51, 26.62°, 27.14°, 27.32°, and 28.95° are (002), (010), (110), (-204), (013), (-214), (-115), (020), (-121), (-123), (-223), respectively (Paranthaman et al., 2021). The crystal size corresponding to the peaks in the XRD pattern of curcumin was calculated using the Debye-Scherrer equation. The crystal size of curcumin calculated according to this equation is 267 nm. As seen XRD pattern in Figure 3 curcumin-modified amorphous-TiO_2 was observed that there were no distinct peaks and a diffraction pattern similar to amorphous-TiO_2 was formed. This indicates that the crystallinity of curcumin on amorphous-TiO_2 is lost and the synthesis material is amorphous.

FT-IR

FT-IR spectrum of curcumin, a-TiO_2, and curc/a-TiO_2 were characterized at a wavelength of 4000-500 cm^{-1} and resolution of 4.0 cm^{-1}. The spectra of these materials are shown in Figure 4. As seen from the FT-IR spectrum OH stretching at 3505 cm^{-1}, C=C and C=O stretching in the chain at 1627 cm^{-1}, C-C and C-C=O in-plane bending at 1510 cm^{-1}, C-C, C-H, and C-OH out-of-plane bending in the aromatic ring at 1430 cm^{-1}, at 1281 cm^{-1}, C-CH and C-OH in-plane bending and stretching in the aromatic ring in curcumin in the enol structure, and CH in-plane bending vibrations in the aromatic ring at 963 cm^{-1} and 856 cm^{-1} is observed. In addition, no peak is observed at wavelengths 1800-1650 cm^{-1}, which is the carbonyl region. This indicates that curcumin has a keto-enol tautomeric structure (Derong et al., 2022). When the FT-IR spectra of curcumin-modified a-TiO_2 were examined, the OH groups at 3505 cm^{-1} in curcumin disappeared. In addition, the spectrum caused by C-OH and CCH in-plane bending vibrations in the enol structure of curcumin at 1153 cm^{-1} is not seen in the curc/a-TiO_2 particle. The disappearance of the OH groups and the spectra in the enolic structure despite staying at stable pH and temperature indicates that curcumin forms a coordination bond with a-TiO_2 via OH groups.

The spectra at 1585.38 cm^{-1} and 1497.28 cm^{-1} are due to the aromatic skeleton structure. However, the shift from 1627 cm^{-1} to 1585 cm^{-1}, from 856 cm^{-1} to 822.19 cm^{-1}, and the decrease in peak intensity indicate that curc/a-TiO_2 is amorphous.

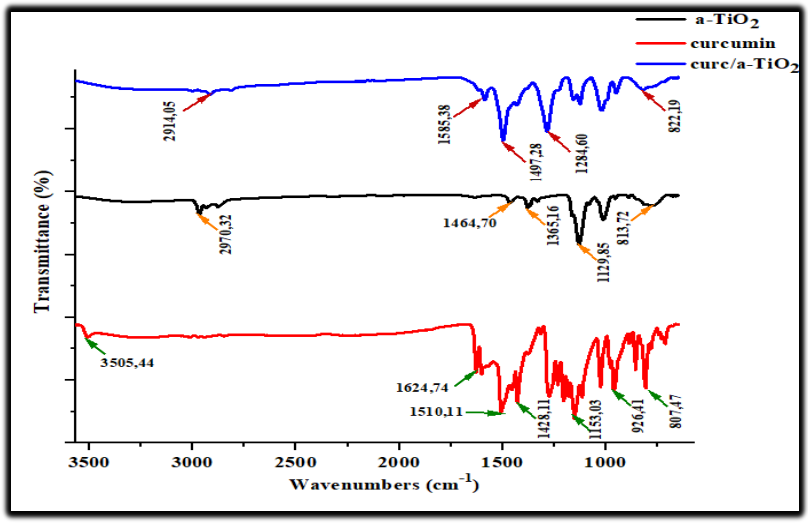

Figure 3. FT-IR spectra of the synthesized materials.

SEM and SEM-EDX

a-TiO_2, and curc/a-TiO_2 was determined by SEM-EDX images shown in Figure 5. When the scanning electron microscopy (SEM) images of both a-TiO_2 and curc/a-TiO_2 were analyzed, large particles were formed as a result of aggregation in both materials. Although the particle size of a-TiO_2 was between 393.12 nm and 698.52 nm, the particle size of curc/a-TiO_2 ranged between 386.58 nm and 895.39 nm. In this case, curc/a-TiO_2 and the particle sizes increased. As seen in Figure 5, EDX analysis shows that the C by mass ratio in curcumin is higher than that in curc/a-TiO_2. In addition, the Ti content in the a-TiO_2 is approximately the same as in the curc/a-TiO_2 material. Both of these cases show that curcumin is modified to a-TiO_2 at room conditions. However, while the S element was not observed in curcumin, the S element was found in curc/a-TiO_2. This is because TiO_2 was modified with curcumin after being dispersed in DMSO during the synthesis. This shows that S in the structure of DMSO after modification could not be removed by methanol washing and remained in the amorphous structure.

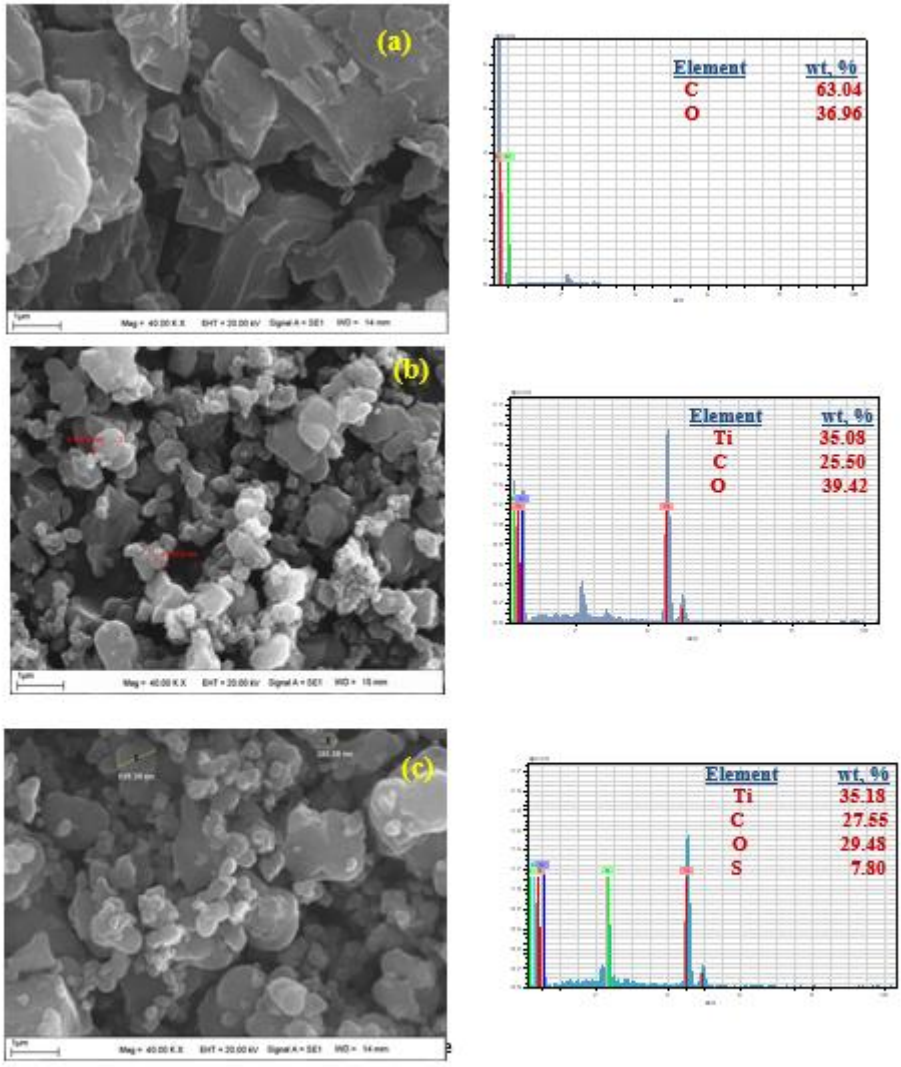

Figure 5. SEM images and EDX spectra of curcumin (a), a-TiO_2 (b) and curc/a-TiO_2 (c).

Zeta Potential

A Malvern Zetasizer was used to measure the surface charge and hydrodynamic diameters of the synthesized materials. The size distributions of particles in colloidal suspensions are measured by dynamic light scattering (DLS) and given as hydrodynamic diameter. Surface charges (zeta potential) were determined by laser doppler electrophoresis (LDE). When the particle size distribution graphs were analyzed, it was observed that the hydrodynamic

diameter of amorphous TiO_2 increased as a result of the modification of curcumin to the amorphous structure. As can be seen from Figure 8 and Figure 9, a-TiO_2 shows a zeta potential close to +30 mV in the pH 4-5 range, while the surface is charged at -27 mV in this pH range by modifying the structure with curcumin. The change in surface charge with curcumin modification indicates that curcumin enters the structure of a-TiO_2. In addition, the fact that these values are close to ±30 mV is also important in terms of showing that stable dispersions are formed in aqueous media. As shown in Table 4, the pH_{ISEP} value of the synthesized curc/a-TiO_2 was similar to that of curcumin. The zeta potentials of a-TiO_2 and curcumin show similar behavior. In adsorption studies using a-TiO_2, maximum adsorption was observed at pH:6, while Pb^{2+} ions were adsorbed at pH:5 at the zeta potential value of -26.8 mV of curc/a-TiO_2.

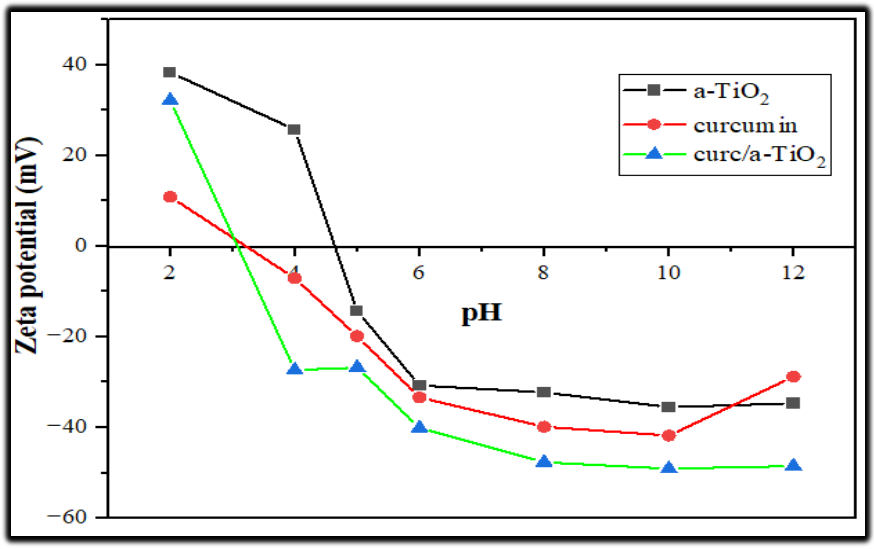

Figure 4. Zeta potential of the synthesized materials.

Table 1. Isoelectric points of the synthesized materials.

Materials	Isoelectric point, pH_{ISEP}
a-TiO_2	4.64
curcumin	3.23
curc/ a-TiO_2	3.08

Temperature (°C):	25,0			**Duration Used (s):**	60
Count Rate (kcps):	268,1			**Measurement Position (mm):**	4,65
Cell Description:	Disposable sizing cuvette			**Attenuator:**	10
			Size (d.nm):	**% Intensity:**	**St Dev (d.nm):**
Z-Average (d.nm):	2036	**Peak 1:**	1372	100,0	180,7
PdI:	0,025	**Peak 2:**	0,000	0,0	0,000
Intercept:	0,824	**Peak 3:**	0,000	0,0	0,000
Result quality :	Refer to quality report				

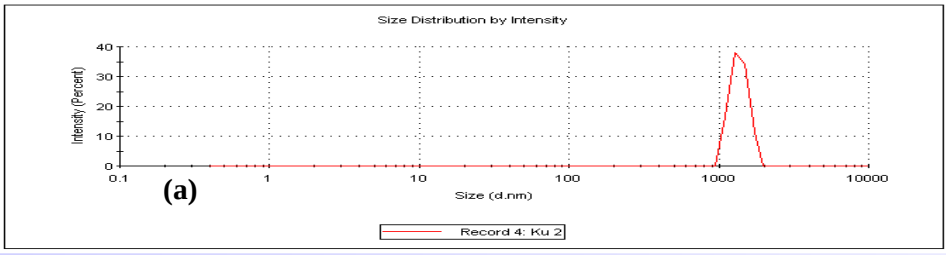

(a)

Temperature (°C):	25,0			**Duration Used (s):**	60
Count Rate (kcps):	213,3			**Measurement Position (mm):**	4,65
Cell Description:	Disposable sizing cuvette			**Attenuator:**	8
			Size (d.nm):	**% Intensity:**	**St Dev (d.nm):**
Z-Average (d.nm):	740,3	**Peak 1:**	554,0	100,0	74,01
PdI:	0,753	**Peak 2:**	0,000	0,0	0,000
Intercept:	0,892	**Peak 3:**	0,000	0,0	0,000
Result quality :	Refer to quality report				

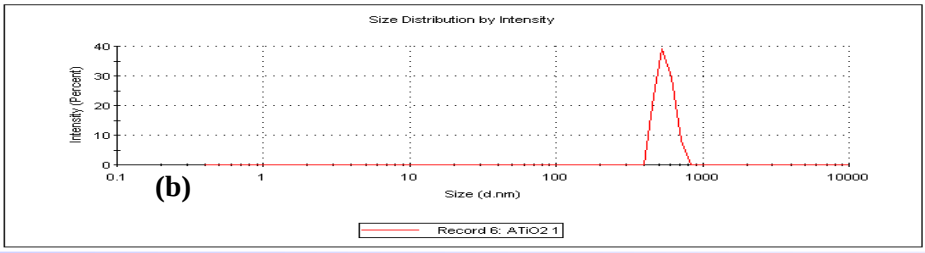

(b)

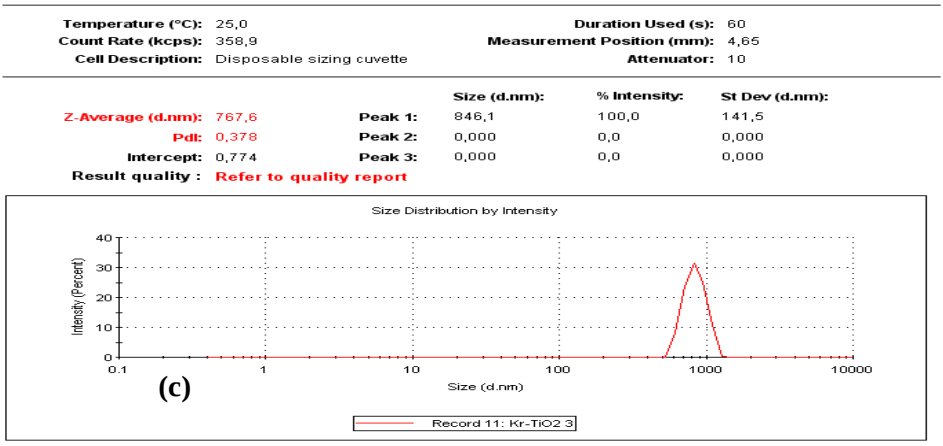

Figure 5. DLS analysis of synthesis curcumin (a), a-TiO_2 (b), curc/a-TiO_2 (c).

S*BET* Surface Area

The synthesized curc/a-TiO_2 has a surface area of 336 m^2 g^{-1}, pore volume of 0.1866 cm^3 g^{-1}, pore size of 10.27 Å.

3.2 Adsorption of Pb^{2+} ions

Determination of modified curcumin amount

To compare the adsorption of Pb^{2+} ions on a-TiO_2 with the adsorption of Pb^{2+} ions on amorphous TiO_2 synthesis material modified with curcumin, the adsorption capacity and Pb^{2+} removal % ratios of the synthesis materials were compared by modifying different ratios of curcumin on a-TiO_2. Considering the chelation of metal ions with diketone groups in curcumin, the adsorption performance of curc/a-TiO_2 synthesis material is expected to increase compared to a-TiO_2 This situation is examined at optimum conditions and given in Table 2. When the mole ratios of curcumin and a-TiO_2 modification are analyzed in Table 2, the most suitable curc/a-TiO_2 (n/n)*100; 10.84 was determined and an adsorption study was performed with this synthesis material.

Table 2. Effect of the amount of curcumin modified to a-TiO_2 on Pb^{2+} adsorption adsorption (adsorbent amount; 0.1 % w/v, adsorption time: 30 min and pollutant volume 25 mL Pb^{2+} concentration: 400 mg L^{-1}) (X_{ort}±s for n=3).

curc/a-TiO_2 ratio (n/n)*100 (mg g^{-1})	**Adsorption,%**	**Adsorption capacity**
2.71	87.51±0.52	350.4±1.14
5.4	89.90±0.47	359.6±0.87
10.84	99.81±0.34	399.2±0.03
21.68	92.67±0.94	370.6±1.94

Effect of pH solution

The most important variable in adsorption parameters is the pH of the aqueous solution. The ionic equilibrium of the analyte changes at different pH values, while the surface charge of the adsorbent material also changes. Pb^{2+} ions are hydrolyzed up to pH: 6. It starts to complex in a neutral and alkaline environment. These complexes are $PbOH^-$, $Pb_3(OH)_4^{2+}$, and $Pb(OH)_3^-$ hydroxide complexes. Lead forms precipitate in the form of Pb^{2+} at pH≤6 and $Pb(OH)_2$ at pH 8-12. In a highly alkaline environment, $Pb(OH)_3^-$ complex is observed. In addition, curcumin shows enol tautomerism in an acidic medium and keto tautomerism in an alkaline medium. Therefore, pH was determined as the most important priority in the adsorption study (Kaur et al., 2018; Duan et al., 2015). The results of the study from pH:2 to pH:8 in acidic medium are shown in Figure 10. The highest removal percentage and adsorption capacity were determined as pH:5 in the adsorption study and the adsorption study was continued at this pH value.

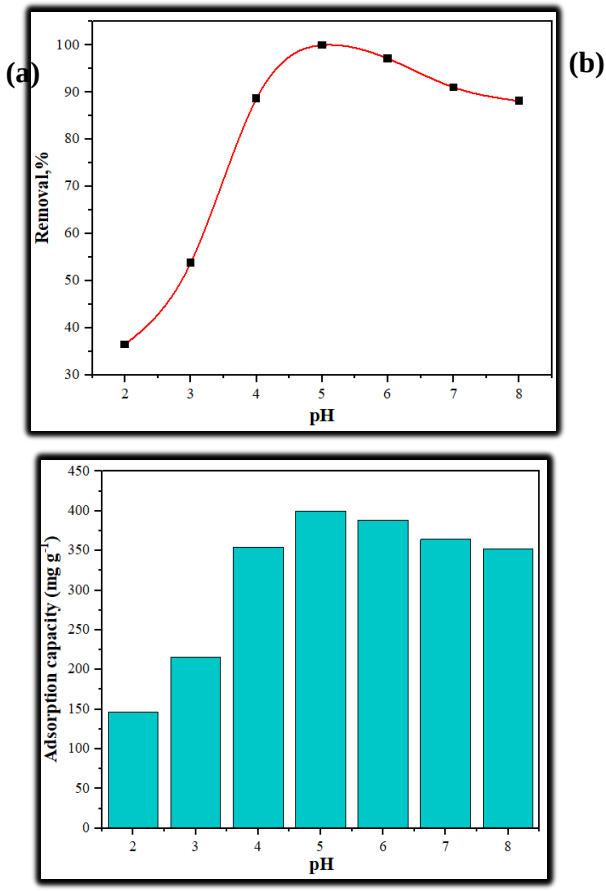

Figure 6. Effect of pH on Pb^{2+} removal (a), adsorption capacity (b).

Effect of adsorbent dosage and initial lead concentration

Pb^{2+} removal percentage efficiency and adsorption capacity of different adsorbent ratios at optimum conditions are shown in Figure 11(a). In this case, it is seen that the adsorption capacity increased up to 1220.96 mg g^{-1} at 0.025% w/v adsorbent amount. However, the adsorption capacity decreased to 399.81 mg g^{-1} at 0.1% w/v where Pb^{2+} removal percentage was obtained with 99.96% efficiency. Therefore, the study was continued at this rate.

In the adsorption study, the initial concentration is an important variable that affects the binding mechanism of the analyte to the adsorbent and determines the adsorption equilibrium performance of the adsorbent. Therefore, to investigate the effect of Pb^{2+} ions on curc/a-TiO_2, an adsorption study was carried out in aqueous media containing concentrations of 50-700 mg L^{-1}, and adsorption %

rates are shown in Figure 11(b). As the initial concentration increased, the adsorption capacity increased relatively, while the adsorption percentage of Pb^{2+} ions decreased. Adsorption equilibrium was established after the initial concentration was 600 mg L^{-1}. Based on these data, the initial concentration of Pb^{2+} ion in aqueous media was determined as 400 mg L^{-1}.

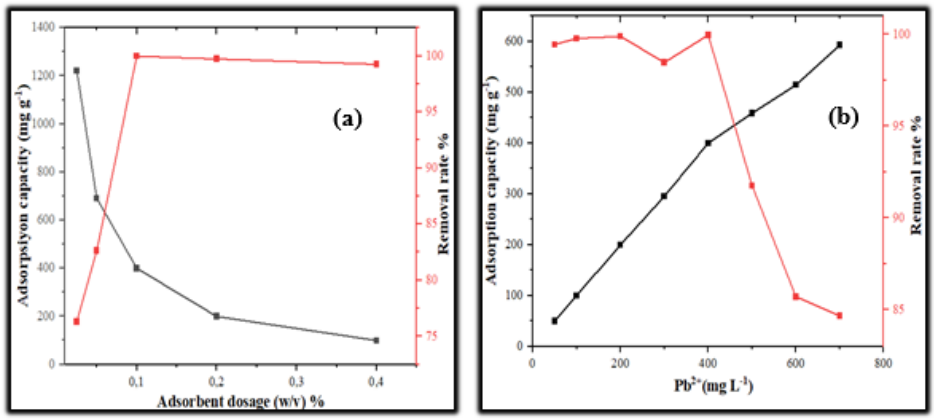

Figure 7. *Adsorption of Pb^{2+} ions by curc/a-TiO_2 effect of; adsorbent dosage (a), initial Pb^{2+} concentration (b).*

Kinetics of Adsorption

The effect of contact time on adsorption is a significant parameter in terms of equilibrium isotherms and the kinetic performance of the adsorbent. The contact time of up to 120 min under the determined adsorption parameters was studied to determine the performance of curc/a-TiO_2 adsorbent. In Figure 10 (a) and Figure 10 (b), the effect of contact time of Pb^{2+} ions on curc/a-TiO_2 adsorbent is shown. The time-dependent removal of Pb^{2+} ions on curc/a-TiO_2 was realized at a high rate in a short time. The adsorption rate is high in the first moments. Because of this reason, the removal of Pb^{2+} ions reached 90% in the very first 10 minutes. But over time, as a result of the decrease of functional groups and the rapid binding of Pb^{2+} ions to the amorphous structure, adsorption equilibrium occurred. Because the removal of Pb^{2+} ions reached the highest value in 30 minutes, it was optimized the contact time effect of the adsorption study was 30 minutes. The adsorption kinetics of Pb^{2+} ions on curc/a-TiO_2 was calculated using the pseudo-first-order, pseudo-second-order equations. The values shown in Table 3 and Figure 10 (c) and Figure 10 (d) were generated from the adsorption kinetics of

400 mg L^{-1} Pb^{2+} ions on curc/a-TiO_2 at 0-120 min adsorption time and initial concentration (c_0). When the rate kinetics were analyzed, the adsorption of Pb^{2+} ions on curc/a-TiO_2 fits the pseudo-second-order rate kinetics very well. According to the pseudo-second-order rate kinetics, the calculated q_e (mg g^{-1}) of 396.82 is very close to the experimentally determined adsorption capacity of 399.81 (mg g^{-1}).

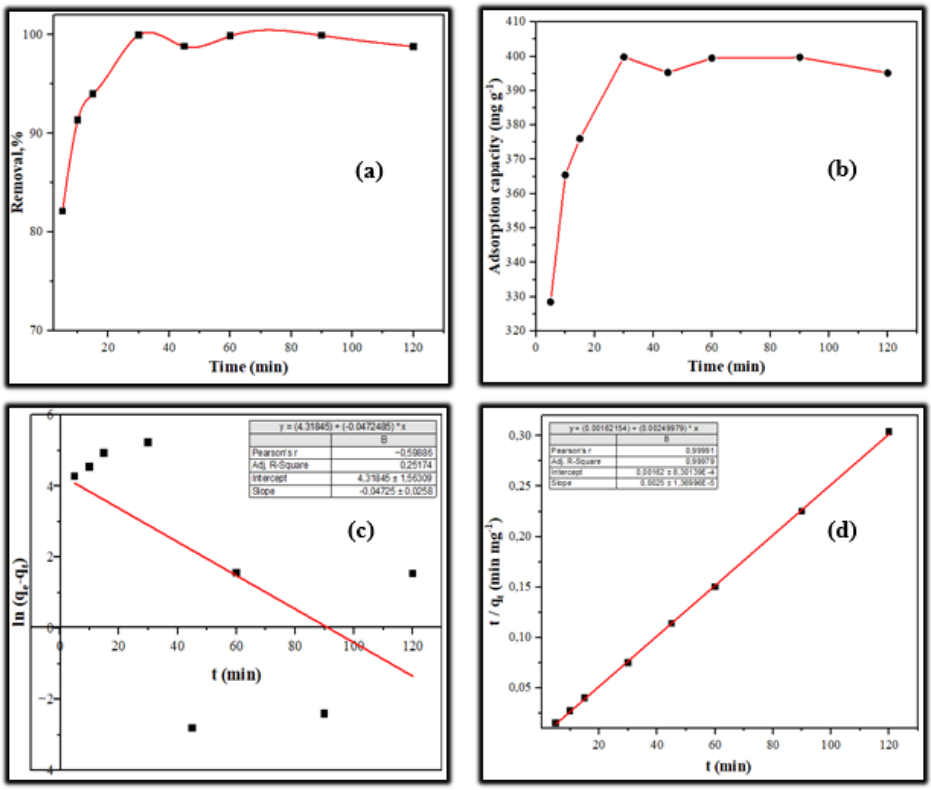

Figure 8. *Effect of contact time of lead ions on curc/a-TiO_2; removal percentage (a), adsorption capacity (b) and adsorption kinetics; pseudo first order (c), pseudo second order (d) models.*

Table 3. Adsorption kinetics parameters of Pb^{2+} on curc/a-TiO_2, (adsorbent amount: 0.1% w/v, pH: 5; 25 ml, 400 mg L^{-1} Pb^{2+} , contact time: 5-120 min).

pseudo-first-order	**q_e (mg g^{-1})**	**k_1 (dk^{-1})**	**R^2**
	2.6164	0.000068	0.25136
pseudo-second-order	**q_e (mg g^{-1})**	**k_2 (mg g^{-1} dk^{-1})**	**R^2**
	396.82	4.8342	0,9998

Isotherm of Adsorption

In determining the adsorption capacity of Pb^{2+} ions on curc/a-TiO_2 at room conditions, adsorption isotherm values of 50-700 mg L^{-1} Pb^{2+} ion concentrations at optimum conditions were linearly plotted according to Langmuir and Freundlich isotherms. These calculations were made according to (Equation 3) and (Equation 4). The constants determined according to the linear graph and the adsorption capacities calculated according to the isotherm graphs are shown in Table 4. Furthermore, linear adsorption isotherm graphs are shown in Figure 11 (a) and Figure 11 (b).

$$\frac{c_e}{q_e} = \frac{1}{q_m . b} + \frac{c_e}{q_m} \qquad (3)$$

Langmuir linear isotherm ce versus ce/qe values were plotted. Langmuir isotherm constant (K_L) and maximum Langmuir adsorption amount (q_{max}) with 1/slope (1/n) were calculated. Freundlich adsorption model is the isotherm in which multilayer adsorption equations are determined based on the assumption that the interface, adsorption sites, and energy are heterogeneous. Freundlich adsorption isotherm is given by the following equation.

$$log\, q_e = log\, K_f + \frac{1}{n} log C_e \qquad (4)$$

For the linear isotherm of Freundlich adsorption, a linear plot of logqe versus logce was constructed to find K_f and n values. The 1/n value was calculated as the slope of the graph and the K_f value was calculated so that 1/n value was equal to logK_f value. As shown in Table 4, according to Langmuir and Freundlich linear adsorption isotherms plotted at Pb^{2+} ion concentrations of 50-700 mg L^{-1} on curc/a-TiO_2 under optimum conditions, the isotherm of the adsorption study was in accordance with Langmuir isotherm ($R^2 > 0.99$). The q_{max}= 564.97 mg g^{-1} value calculated according to Langmuir isotherm shows that the adsorption capacity of Pb^{2+} on curc/a-TiO_2 adsorbent is quite high. Moreover, the n_f value determined by Freundlich isotherm is greater than 1 indicating that the adsorption is chemisorption.

Table 4. Parameters of Langmuir and Freundlich isotherm linear graphs for the adsorption of Pb^{2+} with curc/a-TiO_2 (pH: 5 at 25 ºC, adsorbent amount: 0.1 % (w/v), contact time 30 min, Pb^{2+} initial concentrations: 400 mg L^{-1}, volume: 25 mL).

Langmuir	**q_m (mg g^{-1})**	**K_L**	**R^2**
	564.97	0.3484	0.9951
Freundlich	**K_f (mg g^{-1})(mg L^{-1})$^{1/n}$**	**n_f**	**R^2**
	199.75	4.5871	0.5135

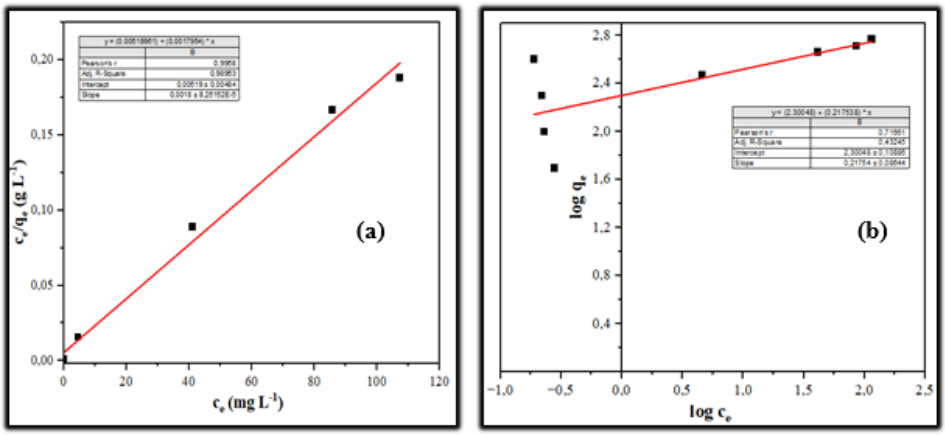

Figure 9. *Adsorption isotherms for removal Pb^{2+} by curc/a-TiO_2: linear; Langmuir (a), Freundlich models.*

Effect of inorganic matrix and ionic strenght

Besides the pollutant analyte, organic or inorganic matrix components may also be present in real samples. Therefore, to determine the adsorption performance of the synthesized curc/a-TiO_2 material, the removal of Pb^{2+} ions and adsorption capacity of Pb^{2+} ions from the sample aqueous medium containing cationic (Ca^{2+}, Mg^{2+}, Na^{+}) and anionic (PO_4^{3-}, Cl^{-}, SO_4^{2-}, NO_3^{-}) strength, which are present in high concentrations in wastewater, as well as tannic acid and gallic acid, which are organic matrices, were investigated under optimum adsorption conditions. The organic matrix effect has not much effect on the adsorption of Pb^{2+} ions, while the adsorption rate decreases by 8.2% and the adsorption capacity decreases by about 4% depending on the ion strength of the medium (Table 6).

Table 5. Concentrations of cations and anions added to the solution

cations	concentration, mg L^{-1}	anions	concentration, mg L^{-1}
Na^{+}	30.00	SO_4^{2-}	24.00
Mg^{2+}	10.00	PO_4^{3-}	13.77
Ca^{2+}	20.00	Cl^{-}	47.36
		CO_3^{2-}	26.08

Table 6. Effect of inorganic matrix on Pb^{2+} adsorption from curc/a-TiO_2 (400 mg L^{-1}, 200 mL Pb^{2+}, pH: 5, adsorbent amount: 0.1 % w/v, time: 30 min) (X_{ort}±s for n=3).

Adsorption medium	Adsorption, %	Adsorption capacity, mg g^{-1}
Inorganic matrix none, Pb^{2+}	98.22±1.16	3143.04±12.29
Inorganic matrix presence, Pb^{2+}	90.16±1.08	3021.00±11.71

Desorption of Pb^{2+} ions

Primarily suitable solution and then suitable solution concentration was determined for the desorption of Pb^{2+} ions via curc/a-TiO_2. The recovery percentages at different Pb^{2+} ion concentrations and solution volumes were calculated by taking HCl acid solution in the concentration range of 1-2.5 mol L^{-1} for elution. For the desorption study, HCl was selected from acidic eluents. The acidic eluent HNO_3 was excluded due to the possibility of conversion of the organic structure of curcumin bound to a-TiO_2 into metabolites and disruption of its structure. Alkaline eluents were not used due to the possibility of complexing with Pb^{2+} ions at high pH. The eluent selection and desorption rates related to the desorption studies are consistent with the studies in the literature (Xiangbing et al., 2007; Naushad et al., 2015). Desorption conditions were determined as a desorption time of 120 minutes and 25 mL desorption solution, static stirring at 200 rpm. Desorption results of Pb^{2+} ions adsorbed at different concentrations and elution solutions are shown in Figure 14.

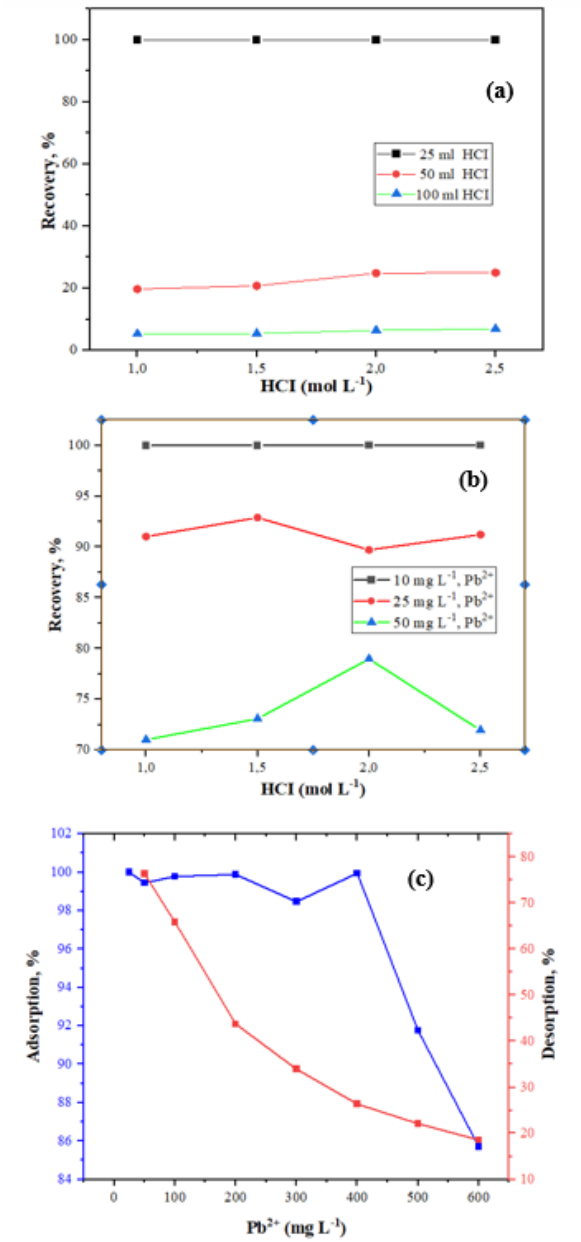

Figure 10. Effect of desorption of Pb^{2+} from curc/a-TiO_2 at different eluent volumes (a) and different initial Pb^{2+} concentrations (b), adsorption-desorption percentages (c), (desorption contact time: 120 min).

Adsorption of lead ions comparison with other adsorbent materials

The comparison of the maximum adsorption capacity of Pb^{2+} on curc/a-TiO_2 with other adsorbent materials is shown in Table 7. It is shown that curc/a-TiO_2 has higher monolayer, equally active sites and homogeneous energy, as well as no interaction between adsorbed molecules and has an outstanding adsorption capacity. Therefore, curc/a-TiO_2 was found to be highly effective for the adsorption of Pb^{2+} ions in water.

Table 7: Comparison of maximum adsorption capacity of Pb^{2+} between curc/a-TiO_2 and those reported in the literatüre.

Absorbent	Sample matrices	q_m (mg g^{-1})	References
Fe_3O_4@SiO_2@NH_2@SH	Model wastewater containing organic and Pb^{2+} contamination	23.92	Esrafili et al., 2019
MCC -g-poly(AA-co-)hydrogels	Model wastewater containing Pb^{2+} and Cd^{2+} contamination	393.3	Zhao et al., 2019
Cell-g-NIPAM-co-AAc	Pb^{2+}, Ni^{2+} and Cu^{2+} contaminated model wastewater	118.13	Kumar & Sharma 2019
CCN-Alg	Model wastewater containing Pb^{2+} pollution	0.95	Hu et al., 2018
PEI-BC	Pb^{2+}, Cu^{2+} containing wastewater	148	Jin et al., 2017
Gu-MC	Model wastewater	52.0	Kenawy et al., 2018
MCS-ITMB	Pb^{2+}, Cd^{2+} containing wastewater	134.10	Shahraki et al., 2019
m-PSAC	Model wastewater containing Pb^{2+} pollution	80.65	Parlayıcı & Pehlivan 2017.
PHEA/TiO_2	Model wastewater containing Pb^{2+} pollution	26.05	Yousefzadeh et al., 2018

chitosan/TiO_2 hybrid film	Model wastewater containing Pb^{2+} pollution	145.53	Tao et al., 2009
GPTMS/nano-TiO_2	Model wastewater containing Pb^{2+} pollution	22.7	Chunxiang et al., 2009
curc/a-TiO_2	**Model wastewater containing Pb^{2+} pollution**	**564.97**	**This study**

Reusability of Adsorbent

In this study, the recovery of Pb^{2+} was evaluated in 5 adsorption-elution cycles to determine the adsorption capacity and stability of the synthesis material. The results of the study are shown in Table 9. In the reusability study, over 95% recovery was observed as a result of 5 repetitions. In terms of reusability, the material was determined to be stable for up to 5 cycles.

Table 8. Reusability of curc/a-TiO_2 (adsorbent amount: 0.1% w/v, pH: 5; 25 ml, 50 mg L^{-1} Pb^{2+} , contact time:30 min).

Operation cycle	Pb^{2+} Recovery, %
1.	98.70±0.26
2.	97.16±0.32
3.	97.79±0.38
4.	95.15±0.34
5.	94.61±0.32

4. CONCLUSIONS

In this study, amorphous TiO_2 synthesized by the sol-gel process was modified with curcumin by wet impregnation. The synthesized curc/a-TiO_2 has a surface area of 336 m^2 g^{-1}, pore volume of 0.1866 cm^3 g^{-1}, pore size of 10.27 ºA, and particle size ranging from 386 to 895.39 nm. FT-IR showed that the carbonyl and methoxy functional groups from curcumin. The amorphous structure of TiO_2 increased the adsorption capacity. a-TiO_2 has a hydrodynamic diameter of 554 d.nm, while curc/a-TiO_2 has a hydrodynamic diameter of 846 dnm, indicating that the hydrodynamic diameter increases with the modification of curcumin. According to the zeta potential results, the surface charge of curc/a-TiO_2 is close to -30 mV, indicating that stable dispersions are formed in aqueous media.

The synthesized curc/a-TiO_2 was used as an adsorbent and Pb^{2+} ions were succesfully removed from aqueous media by adsorption method. Curcumin/a-TiO_2 showed a very high adsorption capacity of 564.97 mg g^{-1} for the removal of Pb^{2+} ions from the aqueous medium. Moreover, the adsorption rate was found to be over 90% even after 5 reuses. The experimental data show that monolayer adsorption occurs by confirming the Langmuir model, is compatible with pseudo-second-order (PSO) adsorption kinetics, and has a very high adsorption capacity. Thus, an eco-friendly adsorbent with high affinity for the adsorption of heavy metals such as Pb^{2+} was synthesized.

REFERENCES

Akpor, O., Ohiobor, G., & Olaolu, D. (2014). Heavy metal pollutants in wastewater effluents: sources, effects and remediation. *Advances in Bioscience and Bioengineering*, pp. 37-43.

Anand, P., Thomas, S., Kunnumakkara, A., Sundaram, C., Harikumar, K., Sung, B., . . . Aggarwal, B. (2008, December 1). Biological activities of curcumin and its analogues (Congeners) made by man and Mother Nature. *Biochemical Pharmacology*, s. 1590-1611.

Beshare, H., Zohrabi, P., & Shamsipur, M. (2018). Recent developments and applications of different sorbents for SPE and SPME from biological samples. *Talanta, 187*, pp. 337-347.

Briffa, J., Sinagra, E., & Blundell, R. (2020, September). Heavy metal pollution in the environment and their toxicological effects on humans. *Heliyon, 6*(9), p. e04691.

Burakov, A., Galunin, E., Burakova, I., Kucherova, A., Agarwal, S., & Tkachev, A. (2018, February). Adsorption of heavy metals on conventional and nanostructured materials for wastewater treatment purposes: A review. *Ecotoxicology and Environmental Safety, 148*, pp. 702-712.

Carolin, C., Kumar, P., Saravanan, A., Janet Joshiba, G., & Naushad, M. (2017, June). Efficient techniques for the removal of toxic heavy metals from aquatic environment: A review. *Journal of Environmental Chemical Engineering, 5*(3), pp. 2782-2799.

CDC updates blood lead reference value. Atlanta: US Centers for Disease Control and Prevention; 2024 (https://www.cdc.gov/lead-prevention/php/news-features/updates-blood-lead-reference-value.html).

Dabrowski, A. (2001). Adsorption — from theory to practice. *Advances in Colloid and Interface Science, 93*(1-3), pp. 135-224.

Derong, L., Lijuan, X., Wen, Q., Douglas, A., Zhijun, W., Hong, C., & Qing, Z. (2022). Preparation, characterization and antioxidant properties of curcumin encapsulated chitosan/lignosulfonate micelles. *Carbohydrate Polymers, 281*, s. 119080.

Duan, S., Tang, R., Xue, Z., Zhang, X., Zhao, Y., Zhang, W., . . . Sun, D. (2015, March 01). Effective removal of Pb(II) using magnetic Co0.6Fe2.4O4 micro-particles as the adsorbent: Synthesis and study on the kinetic and thermodynamic behaviors for its adsorption(Article). *Colloids and Surfaces A: Physicochemical and Engineering Aspects, 469*, pp. 211-223.

Kaur, R., Singh, N., Khullar, P., Gupta, A., Mahal, P., Ahluwalia, G., & Bakshi, M. (2018, October 25). Keto–Enol Tautomerism of Temperature and pH Sensitive Hydrated Curcumin Nanoparticles: Their Role as Nanoreactors and

Compatibility with Blood Cells. *Journal of Agricultural and Food Chemistry, 66*(45), pp. 11974–11980.

Kumar, P., Kim, K.-H., Bansal, V., Lazarides, T., & Kumar, N. (2017). Progress in the sensing techniques for heavy metal ions using nanomaterials. *Journal of Industrial and Engineering Chemistry, 54*, pp. 30-43.

Naushad, M., Ahamad, T., Alothman, Z., & Al-Muhtaseb, A. (2019). reen and eco-friendly nanocomposite for the removal of toxic Hg(II) metal ion from aqueous environment: Adsorption kinetics & isotherm modelling,. *Journal of Molecular Liquids, 279*, pp. 1-8.

Paranthaman, R., Moses, J., & Anandharamakrishnan, C. (2022). C. Powder X-ray diffraction conditions for screening curcumin in turmeric powder. *Food Measure, 16*, s. 1105–1113.

Priyadarsini, K. I. (2014, December 1). The chemistry of curcumin: from extraction to therapeutic agent.Rewiev. *Molecules, 19*(12), pp. 20091-20112.

Shrestha, R., Ban, S., Devkota, S., Sharma, S., Joshi, R., Tiwari, A., . . . Joshi, M. (2021). Technological trends in heavy metals removal from industrial wastewater: A review. *Journal of Environmental Chemical Engineering, 9*(4), p. 105688.

Simon, A., Allais, D., Duroux, J., Basly, J., Durand-Fontanier, S., & Delage, C. (1997, June 23). Inhibitory effect of curcuminoids on MCF-7 cell proliferationand structure–activity relationships. *Cancer Letters*, pp. 111-116.

Soliman, N., & Moustafa, A. (2020). Industrial solid waste for heavy metals adsorption features and challenges; a review. *Journal of Materials Research and Technology, 9*(5), pp. 10235-10253.

Sun, S., Song, P., Cui, J., & Liang, S. (2019). Amorphous TiO2 nanostructures: synthesis,fundamental properties and photocatalytic applications: Minireview. *Catalysis Science & Technology, 9*, pp. 4198-4215.

Wanninger, S., Lorenz, V., Subhan, A., & Edelmann, F. T. (2015, January 30). Metal complexes of curcumin – synthetic strategies, structures and medicinal applications. *Chem.Soc.Rev, 44*, p. 4986.

Xiangbing, Z., Xijun, C., Yuemei, C., Xiaojun, Z., Dong, Y., & Zheng, H. (2007). Solid-phase extraction of trace Cu(II) Fe(III) and Zn(II) with silica gel modified with curcumin from biological and natural water samples by ICP-OES. *Microchemical Journal, 86*(2), pp. 189-194.

CHAPTER 3

A Research on the Anatomical and Micromorphological Characteristics of the Species *Tragopogon* Pratensis L. (Asteraceae)

Sibel Ulcay[1] & Gülcan Şenel[2]

1 Assoc. Prof, Kırşehir Ahi Evran University, Faculty of Agriculture, Department of Field Crops, Kırşehir, Orcid ID: 0000-0002-2878-1721
2 Prof., Ondokuz Mayis University, Faculty of Sciences, Department of Biology, Samsun
Orcid ID: 0000-0002-8967-7290

Introduction

The Asteraceae family is the largest family of flowering plants, known for its extensive diversity and distribution (Cheek et al., 2020). It is represented by approximately 1100 genera and 25000 species worldwide (Seçmen et al., 2000). In Türkiye, the family includes a total of 1438 taxa, consisting of 152 genera, 1230 species, 133 subspecies, and 75 varieties (Yıldırımlı, 1999). In addition to its high number of individuals, this family also holds significant medicinal, economic, and ecological importance (Demir, 2020a; Demir, 2013). Many members of this family are utilized for food, medicinal, and fodder purposes in various parts of the world (Kaval et al., 2014; Kawarty, 2020; Demir, 2020b). Most members of the Asteraceae family have therapeutic applications and a long history in traditional medicine, with some species cultivated for edible and medicinal purposes for over 3000 years. In arid and semi-arid regions, certain taxa from this family are cultivated and farmed (Demir, 2020c; Demir, 2021). Members of the Asteraceae family exhibit a wide range of activities, including anti-inflammatory, antimicrobial, antioxidant, and hepatoprotective effects (Rolnik and Olas, 2021).

Tragopogon L. is represented by 18 species in Türkiye, with the number rising to 25 when including doubtfully recorded and recently described taxa (Coşkunçelebi and Gültepe 2012). Seven of these taxa are endemic to Türkiye, resulting in an endemism rate of 33%.

Tragopogon (Asteraceae) includes nearly 150 species primarily found in Europe and Asia (Bremer 1994; Soltis et al. 2004). It is one of the largest genera in the subtribe Scorzonerinae Dumort. (Mavrodiev et al. 2004) and is characterized by entire, parallel-veined leaves, a single row of involucral bracts, and beaked achenes. Correctly identifying *Tragopogon* taxa is nearly impossible without a thorough understanding of mature achenes and the color of the ligules (Borisova 1964; Matthews 1975).

Tragopogon pratensis L. commonly known as Goat's beard, is an annual or perennial plant that grows up to 0.6 meters. This species is considered a beneficial remedy for liver and gallbladder issues, exhibiting detoxifying properties that may stimulate appetite and digestion. Its high inulin content makes it a valuable food source for diabetics. The root is recognized for its astringent, depurative, diuretic, expectorant, nutritive, and stomachic properties. Experimental studies on methanol extracts of *T. pratensis* have demonstrated that phenolic compounds possess antiproliferative and tumor-arresting effects (Mitic et al. 2014). This study aims to reveal the anatomical and micromorphological features of *T.*

pratensis, a plant of economic and medicinal importance. The results obtained will serve as a foundation for future research on this species.

MATERIAL AND METHODS

The research material, *T. pratensis*, was collected from Tokat and its surroundings between April and August, when it was flowering. Some of the samples were preserved as herbarium specimens. The work "Flora of Turkey" was used to identify the species (Davis, 1982). To determine its anatomical features, first the parts of the plant such as roots, stems and leaves were divided into small pieces. Sections were taken manually and glycerin was used as the examination medium. The preparations were sealed with paraffin and turned into semi-permanent preparations (Vardar 1987). Photographs were taken with a Zeiss AxioLab A1 microscope and a Zeiss Axiocam 105 imaging system. Measurements were taken from cells in different tissues from the prepared preparations and the averages were obtained over 30 measurements. The fruit, seed and leaf surface micromorphologies of the species were examined in detail. The upper and lower epidermis of the leaves and stoma cells were determined, and the surface shapes and general appearance of the fruits and seeds were analyzed. Samples were fixed on stubs for electron microscope shooting using double-sided carbon tape and then coated with 12.5-15 nm gold-palladium (SEM coating system, SC7620). Examinations and shootings were carried out on a JEOL JMS-7001F Scanning Electron Microscope (SEM) in the voltage range of 5-15 KV.

RESULTS

Anatomical Results

Root

The periderm consists of 1-2 layers. The cells of the periderm measure 21.33±6.61 mm by 18.94±4.17 mm. Spaces have been reported between the cortical parenchyma cells located just beneath the periderm. The cortical parenchyma cells average 18.34±4.00 mm in size. Just below the cortex layer, an endodermis measuring 16.37±3.95 mm has been identified. In the vascular elements, the phloem and xylem are arranged radially. The tracheid in the xylem have a diameter of 33.34±6.01 mm. Secondary pith rays consist of 3-5 layers. The core region is covered with xylem elements (Figure 1).

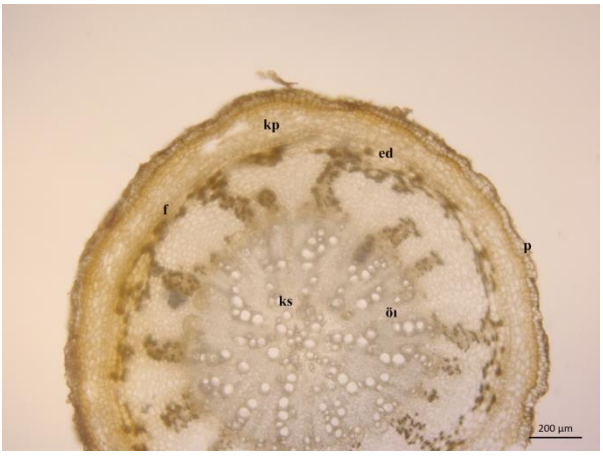

Figure 1. *Tragopogon pratensis* root transverse section. p: periderm, kp: cortical parenchyma, f: phloem, ks xylem, ed: endodermis, öi: pith ray.

Stem

The outermost part of the stem has epidermis cells with an average size of 9.12±2.16 x 13.18±2.5171 µm. Immediately below the epidermis are 3-4 rows of collenchyma cells with an average diameter of 12.85±2.95 µm. The cortex is narrow. Vascular bundles are arranged in a circular shape. Phloem is very prominent. Xylem elements are surrounded from the bottom and sides by sclerenchyma cells with an average diameter of 6.93±1.21 µm, forming a perivascular ring. The thallus has an average diameter of 17.99±3.44 µm. The upper part of the phloem cells contains red colored substances as in the root and leaf. The pith region is very large. It is filled with parenchyma cells with a diameter of 34.49±8.55 µm (Figure 2.)

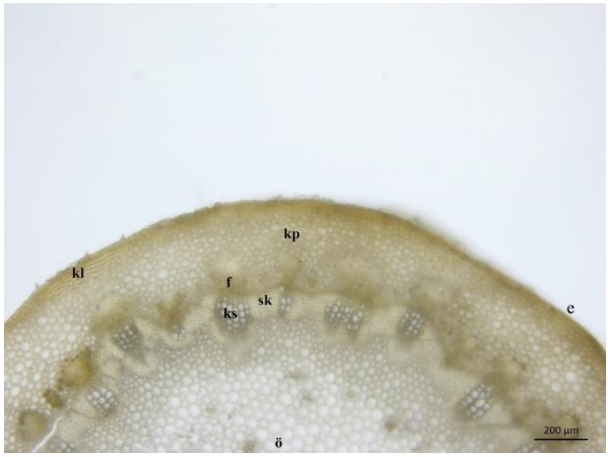

Figure 2. *Tragopogon pratensis* stem transverse section. e: epidermis, kp: cortical parenchyma, f: phloem, ks: xylem, sk: sclerenchyma, kl: collenchyma, ö: pith.

Leaf

In leaf cross sections, lower epidermis cells with an average size of 18.66±4.49 x 35.65±10.24 µm and upper epidermis cells with an average size of 25.82±3.40 x 25.21±4.01 µm are observed. The central vascular region is wide. As it matures, this part becomes hollow and only the vascular bundle remains. The mesophyll is differentiated in leaf parts other than the mid-vein. There are two rows of palisade parenchyma cells with an average size of 24.41±5.17 x 30.58±5.42 µm and spongy parenchyma cells with an average size of 23.77±5.91 x 27.75±7.57 µm (Figure 3). The surface of the leaf is covered by a cuticle layer with an average thickness of 8.07±3.84 µm. Tetracytic stomatal cells are seen on the upper and lower surface sections (Figure 4).

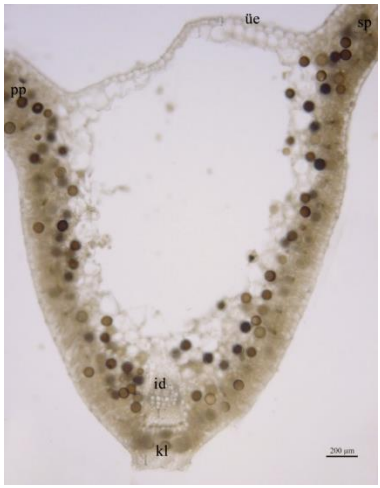

Figure 3. *Tragopogon pratensis* leaf cross-section. üe: upper epidermis, sp: spongy parenchyma, pp: palisade parenchyma, kl: collenchyma....

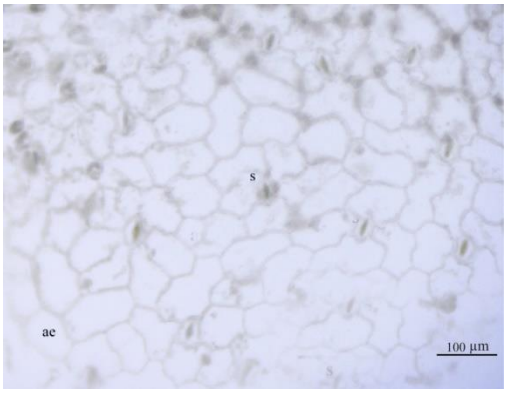

Figure 4. Lower surface superficial sections of *Tragopogon pratensis*. ae: lower epidermis, s: stoma. Scale: 100 µm

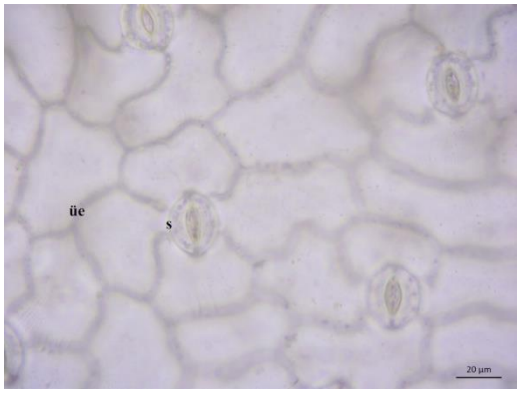

Figure 5 Upper surface superficial sections of *Tragopogon pratensis* leaf. ue: upper epidermis, s: stomata.

Micromorphological Results

The epidermal cells of the fruit are square, rectangular or polygonal. The general patterning is ribbed. Papillae can be seen on the surface close to the pappus. The ornamentation in this region is sulcate (Figure 6). The cells on the pappus are elongated rectangular. Sulcate ornamentation is observed. Hairs are seen on the surface towards the pappus. The tip of the beak with the seed is wavy, forked or straight. The surface cells of the seed are square, rectangular or polygonal. The patterning type is reticulate-striated (Figure 7).

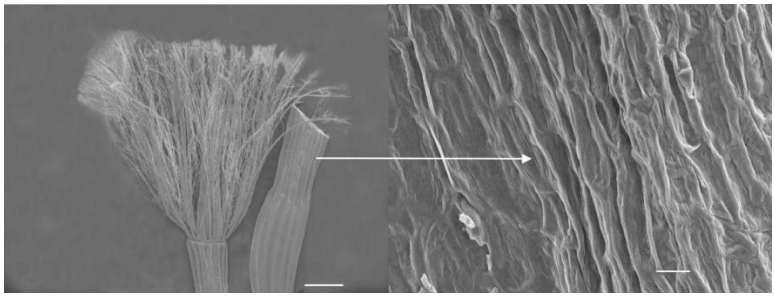

Figure 6. Fruit surface micromorphology of *T. pratensis* Scala 10 µm

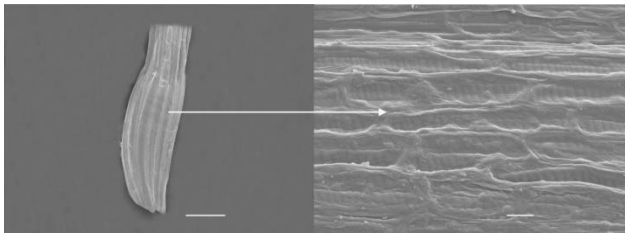

Figure 7. Seed surface micromorphology of *T. pratensis*. Scala 10 µm

The anatomical and micromorphological features of *T. pratensis* belonging to the Astereceae family have been studied in detail. The species carries the features of the Asteraceae family. Metcalfe and Chalk (1950) have revealed the anatomical features of the family. its stem contains a narrow cortex and a wide phloem. Sclerenchyma surrounds the vascular bundles from below and continues in the interveinal spaces. The leaf of *T. pratensis* is also quite characteristic in terms of shape. As the plant continues to grow, the parenchyma cells in the mid-vein region of the leaf decrease and only the vascular bundle and sclerenchyma cells remain. Anomocytic and tetracytic stomata are found on the lower surface, and tetracytic stomata are found on the upper surface. *Tragopogon latifolius* Boiss. its stomata are anomocytic and anisocytic (Akçin 2007). *Tragopogon gracilis* D. Don. Tetracytic stomata are mentioned in Mem.Wern. (Qureshi et al. 2008).

REFERENCES

Akçin, Ö. E. (2007). Morphological and anatomical characteristics of Cichorium intybus L., Tragopogon latifolius Boiss. and Tussilago farfara L.(Asteraceae).

Bremer K. 1994. Asteraceae. Cladistics and classification. Portland (OR): Timber Press.

Borisova AG. 1964. Tragopogon. In: Shishkin BK, editor.Flora of the USSR. vol 29. Moscow: Nauka; p. 115–196.

Cheek, M., Nic Lughadha, E., Kirk, P., Lindon, H., Carretero, J., Looney, B., ... & Niskanen, T. (2020). New scientific discoveries: Plants and fungi. Plants, People, Planet, 2(5), 371-388.

Coşkunçelebi K, Gültepe M. 2012. *Tragopogon* L. In: Güner A, editor. A checklist of the flora of Turkey (Vascular Plants). Istanbul: Nezahat Gökyiğit Botanical Garden and Flora Research Association Publication; p. 211–212.

Demir, İ. (2020a). Inter and intra row competition effects on growth and yield components of sunflower (Helianthus annuus L.) Under rainfed conditions. JAPS: Journal of Animal & Plant Sciences, 30(1).

Demir, İ. (2020b). Comparing the performances of sunflower hybrids in semi-arid condition. Turkish Journal of Agriculture and Natural Sciences, 7(4), 1108-1115.

Demir, I. (2020c). Improving seed and oil yield of sunflower (*Helianthus annuus* L.) by using different inter and intra row space combinations. J. Glob. Innov. Agric. Soc. Sci, 8, 147-153.

Demir, I (2013) Oilseed crop cultivation in TR71 region and effects of climate change. Turkish Journal of Agriculture-Food Science and Technology 1, 73–78.

Demir, I. (2021). The evaluation of confectionery sunflower (Helianthus annuus L.) cultivars and populations for yield and yield components. International Journal of Agriculture, Environment and Bioresearch, 6(01), 179-186.

Davis PH, editor 1982. Flora of Turkey and the east Aegean Islands. Edinburgh; Edinburgh University Press. VII.

Kawarty, A. M. A., Behçet, L., & Çakilcioğlu, U. (2020). An ethnobotanical survey of medicinal plants in Ballakayati (Erbil, North Iraq). Turkish Journal of Botany, 44(3), 345-357.

Metcalfe CR, Chalk L (1950). Anatomy of the Dicotyledons: Leaves, Stem, and Wood in Relation to Taxonomy with Notes on Economic uses. V.2. - Claredon Press, Oxford. Matthews VA. 1975. Tragopogon L. In: Davis PH, editor. Flora of Turkey and the East Aegean Islands. vol 5. Edinburgh: Edinburgh University Press; p. 657–668.

Mavrodiev EV, Edwards CE, Albach DC, Gitzendanner MA, Soltis PS, Soltis DE. 2004. Phylogenetic relationships in subtribe Scorzonerineae (Asteraceae, Cichorioideae, Cichorioieae) based on ITS sequence data. Taxon. 53(3):699–712.

Mitic, V. D., Stankov-Jovanovic, V. P., Ilic, M. D., Vasiljevic, P. J., Zabar, A. L., & Stojanovic, G. S. (2014). The antioxidant, hemolytic and cholinesterase inhibition properties of Galium verum L. and *Tragopogon pratensis* subsp. *pratensis*. Bulgarian Chem Commun, 46(2), 269-276.

Qureshi, S. J., Khan, M. A., & Ahmad, M. (2008). Comparative morphology, palynology and anatomy of five astraceous species from Pakistan. African Journal of Agricultural Research, 3(9), 622-632.

Rolnik, A., & Olas, B. (2021). The plants of the Asteraceae family as agents in the protection of human health. International journal of molecular sciences, 22(6), 3009.

Seçmen, Ö., Gemici, Y., Görk, G., Bekat, L., & Leblebici, E. (2000). Systematics of seed plants. Ege University Faculty of Science Book Series, 116, 394.

Soltis, D. E., Soltis, P. S., Pires, J. C., Kovarik, A., Tate, J. A., & Mavrodiev, E. (2004). Recent and recurrent polyploidy in Tragopogon (Asteraceae): cytogenetic, genomic and genetic comparisons. Biological Journal of the Linnean Society, 82(4), 485-501.

Vardar, Y. (1987). Preparation Techniques in Botany. Ege University Faculty of Science Press, Izmir, No 1.

Yıldırımlı, Ş. (1999). The chorology of the Turkish species of Asteraceae family. Journal of Systematic Botany. 6(2), 75-123.

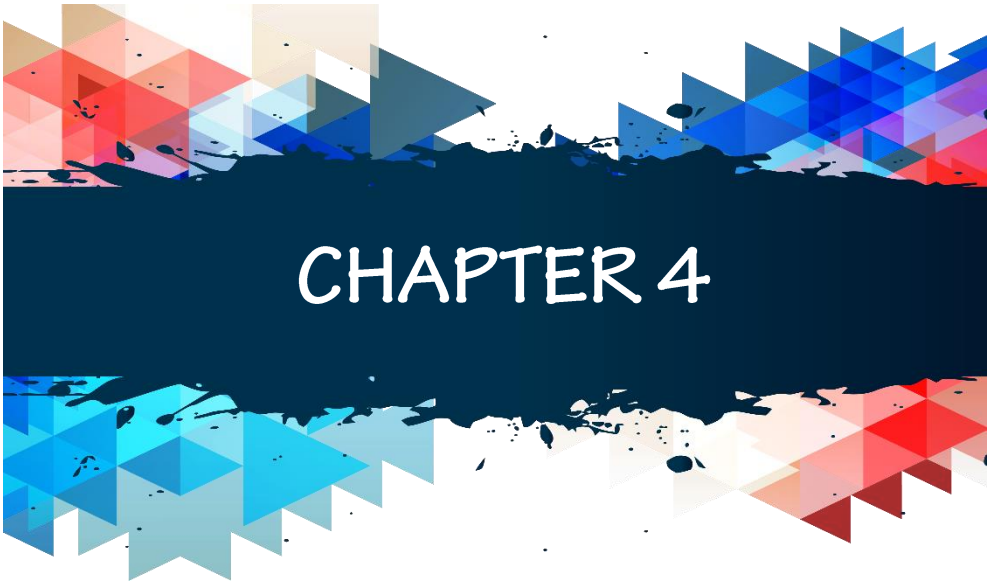

Gibonacci 3-Parameter Generalized Quaternions

Göksal Bilgici [1]

1 Kastamonu University, ORCID: 0000-0001-9964-5578

1. INTRODUCTION

Fibonacci numbers is the most famous sequence among integer sequences. These numbers are defined by the recurrence relation

$$F_n = F_{n-1} + F_{n-2}$$

where initial conditions $F_0 = 0$ and $F_1 = 1$. The Lucas numbers satisfy the same recurrence relation except initial conditions $L_0 = 2$ and $L_1 = 1$. There are a number of generalization of the Fibonacci sequence. We can give the Gibonacci numbers as an example of them. Gibonacci numbers are defined by the same recurrence relation

$$G_n = G_{n-1} + G_{n-2}$$

except the initial conditions $G_1 = m$ and $G_2 = n$ where m and n are arbitrary real numbers. The Binet-like formula for the Gibonacci numbers is

$$G_r = \frac{\alpha^{\#}\alpha^r - \beta^{\#}\beta^r}{\alpha - \beta}$$

where $\alpha = \frac{1+\sqrt{5}}{2}$, $\beta = \frac{1-\sqrt{5}}{2}$, $\alpha^{\#} = m + (m-n)\beta$ and $\beta^{\#} = m + (m-n)\alpha$. Here, α and β are roots of the equation $q^2 - q - 1 = 0$. More information and application of Gibonacci numbers can be found in (Koshy, 2019).

Quaternions are introduced by Sir Rowan Hamilton to extend complex numbers to hyper-complex numbers. After his definition, some generalizations of quaternions were introduced by some researchers. Recently, a new generalization given by Senturk and Unal (2022), namely 3-parameter generalized quaternions. Let *r* be a 3-parameter generalized quaternions. Then *r* is in the form of $a_0 + a_1 i + a_2 j + a_3 k$ where a_0, a_1, a_2 and a_3 are any real numbers and the versors $\{i, j, k\}$ satisfy the following multiplication relations.

	i	j	k
i	$-\theta_1\theta_2$	$\theta_1 k$	$-\theta_2 j$
j	$-\theta_1 k$	$-\theta_1\lambda_3$	$\theta_3 i$
k	$\theta_2 j$	$-\theta_3 i$	$-\theta_2\theta_3$

Table 1 Multiplication rules of $\{i, j, k\}$

The set of 3-parameter quaternions is

$$\mathbb{Q} = \{r_0 + ir_1 + jr_2 + kr_3 : r_0, r_1, r_2, r_3 \in \mathbb{R}\}.$$

Let $q_1 = r_0 + ir_1 + jr_2 + kr_3$ and $q_2 = s_0 + is_1 + js_2 + ks_3$ be two any 3-parameter generalized quaternions. Table 1 gives product of q_1 and q_2 as follows

$$\begin{aligned} q_1 q_2 = {} & r_0 s_0 - r_1 s_1 \theta_1 \theta_2 - r_2 s_2 \theta_1 \theta_3 - r_3 s_3 \theta_2 \theta_3 \\ & + i(r_0 s_1 + r_1 s_0 + r_2 s_3 \theta_3 - r_3 s_2 \theta_3) \\ & + j(r_0 s_2 + r_2 s_0 - r_1 s_3 \theta_2 + r_3 s_1 \theta_2) \\ & + k(r_0 s_3 + r_3 s_0 + r_1 s_2 \theta_1 - r_2 s_1 \theta_1). \end{aligned}$$

After Horadam (1963) introduced Fibonacci quaternions, many authors studied Fibonacci quaternions (Iyer, 1969; Swamy, 1973; Halici 2012; Akyigit, Kosal and Tosun, 2013; Nukan and Guven, 2015; Tan, Yilmaz and Sahin, 2016; Yuce and Aydin, 2016; Polatli, Kizilates and Kesim, 2016; Polatli, 2016; Ipek, 2017; Bilgici, Tokeser and Unal, 2017; Aydin, 2018; Kizilates and Kone, 2021; Gul, 2022; Dasdemir and Bilgici, 2021). Bilgici studied 3-parameter generalized quaternions whose coefficients are Fibonacci numbers and present study may be regard as a generalization of that study.

Definition 1.1. For $r \in \mathbb{Z}^+$, the *n*th Gibonacci 3-parameter generalized quaternion is

$$\Lambda_r = G_r + iG_{r+1} + jG_{r+2} + kG_{r+3}.$$

By this definition and the recurrence relation of Gibonacci numbers, for $r \geq 2$, we have

$$\Lambda_r = \Lambda_{r-1} + \Lambda_{r-2}. \tag{1.1}$$

Koshy (2019) gives the identity $G_r = mF_{r-2} + nF_{r-1}$. Together with this identity and the well-known identity $F_{-r} = (-1)^{r+1}F_r$ give

$$\Lambda_{-r} = (-1)^r[-mF_{r+2} + nF_{r+1}]. \tag{1.2}$$

2. BINET-LIKE FORMULA AND GENERATING FUNCTION

The following theorem gives the Binet-like formula for the Gibonacci 3-parameter generalized quaternions.

Theorem 2.1. For any integer r, the rth Gibonacci 3-parameter generalized quaternion is

$$\Lambda_r = \frac{\alpha_G \alpha^{\#} \alpha^r - \beta_G \beta^{\#} \beta^r}{\alpha - \beta}$$

where $\alpha_G = 1 + i\alpha + j\alpha^2 + k\alpha^3$ and $\beta^{/} = 1 + i\beta + j\beta^2 + k\beta^3$.

Proof. Binet-like formula for the Gibonacci numbers gives

$$\begin{aligned}\Lambda_r &= G_r + iG_{r+1} + jG_{r+2} + kG_{r+3} \\ &= \frac{1}{\alpha-\beta}[\alpha^{\#}\alpha^r - \beta^{\#}\beta^r + i(\alpha^{\#}\alpha^{r+1} - \beta^{\#}\beta^{r+1}) \\ &\qquad + j(\alpha^{\#}\alpha^{r+2} - \beta^{\#}\beta^{r+2}) + k(\alpha^{\#}\alpha^{r+3} - \beta^{\#}\beta^{r+3})] \\ &= \frac{1}{\alpha-\beta}[\alpha^{\#}\alpha^r(1 + i\alpha + j\alpha^2 + k\alpha^3) \\ &\qquad - \beta^{\#}\beta^r(1 + i\beta + j\beta^2 + k\beta^3)].\end{aligned}$$

Final equation proves the theorem. ■

We use the following results in next proofs of theorems.

Corollary 2.2. We have

$$\alpha_G\beta_G = C + D\sqrt{5}$$

and

$$\beta_G\alpha_G = C - D\sqrt{5}$$

where

$$C = 1 + i + 3j + 4k + \theta_1\theta_2 - \theta_2\theta_3 + \theta_1\theta_3$$

and

$$D = -i\theta_1 - j\theta_2 + k\theta_3.$$

Proof. By using the Table 1, the proofs are straightforward. ■

Theorem 2.3. The generating function for the sequence $\{\Lambda_r\}_{r=0}^{\infty}$ is

$$\sum_{r=0}^{\infty}\Lambda_r q^r = \frac{-m + n + im + jn + k(m+n) + [2m - n + i(-m+n) + jm + kn]}{1 - q - q\text{^}2}.$$

Proof. Let $\Lambda(q)$ be the generating function for the sequence $\{\Lambda_r\}_{r=0}^{\infty}$. Then we have

$$\Lambda(q) = \Lambda_0 + \Lambda_1 q + \sum_{r=2}^{\infty}\Lambda_r q^r. \qquad (2.1)$$

By multiplying both hand sides of Eq. (2.1) by $-q$, we obtain

$$-q\Lambda(q) = -\Lambda_0 q - \sum_{r=2}^{\infty} \Lambda_{r-1} q^r. \tag{2.2}$$

Multiplying both hand sides of Eq. (2.1) by $-q^2$ gives

$$-q^2\Lambda(q) = -\sum_{r=2}^{\infty} \Lambda_{r-2} q^r. \tag{2.3}$$

If we add Eqs. (2.1), (2.2) and (2.3) side by side, we get

$$(1 - q - q^2)\Lambda(q) = \Lambda_0 + (\Lambda_1 - \Lambda_0)q.$$

Last equation proves the theorem. ■

3. RESULTS

Vajda's identity can be found in next theorem.

Theorem 3.1. For any integers r, s and t, the following holds

$$\Lambda_{r+s}\Lambda_{r+t} - \Lambda_r\Lambda_{r+s+t} = (m^2 + mn - n^2)(-1)^r F_s(CF_t - DL_t).$$

Proof. Theorem 2.1 gives

$$\begin{aligned}
&\Lambda_{r+s}\Lambda_{r+t} - \Lambda_r\Lambda_{r+s+t} \\
&= \frac{1}{(\alpha-\beta)^2}[(\alpha_G\alpha^{\#}\alpha^{r+s} - \beta_G\beta^{\#}\beta^{r+s})(\alpha_G\alpha^{\#}\alpha^{r+t} - \beta_G\beta^{\#}\beta^{r+t}) \\
&\qquad - (\alpha_G\alpha^{\#}\alpha^{r} - \beta_G\beta^{\#}\beta^{r})(\alpha_G\alpha^{\#}\alpha^{r+s+t} - \beta_G\beta^{\#}\beta^{r+s+t})] \\
&= \frac{1}{(\alpha-\beta)^2}[-\alpha_G\beta_G\alpha^{\#}\beta^{\#}\alpha^{r+s}\beta^{r+t} + \alpha_G\beta_G\alpha^{\#}\beta^{\#}\alpha^{r}\beta^{r+s+t} \\
&\qquad - \beta_G\alpha_G\alpha^{\#}\beta^{\#}\alpha^{r+t}\beta^{r+s} + \beta_G\alpha_G\alpha^{\#}\beta^{\#}\alpha^{r+s+t}\beta^{r}] \\
&= \frac{\alpha^{\#}\beta^{\#}}{(\alpha-\beta)^2}[\alpha_G\beta_G(\alpha^{r}\beta^{r+s+t} - \alpha^{r+s}\beta^{r+t}) \\
&\qquad + \beta_G\alpha_G(\alpha^{r+s+t}\beta^{r} - \alpha^{r+t}\beta^{r+s})] \\
&= \frac{(m^2+mn-n^2)(-1)^r}{(\alpha-\beta)^2}[\alpha_G\beta_G(\beta^{s+t} - \alpha^{s}\beta^{t}) + \beta_G\alpha_G(\alpha^{s+t} - \alpha^{t}\beta^{s})] \\
&= \frac{(m^2+mn-n^2)(-1)^{r+1}}{(\alpha-\beta)^2}[\alpha_G\beta_G\beta^{t}(\alpha^{s} - \beta^{s}) - \beta_G\alpha_G\alpha^{t}(\alpha^{s} - \beta^{s})]
\end{aligned}$$

$$= \frac{(m^2+mn-n^2)(-1)^{r+1}F_s}{(\alpha-\beta)^2}\left[\left(C+D\sqrt{5}\right)\beta^t-\left(C-D\sqrt{5}\right)\alpha^t\right]$$

$$= \frac{(m^2+mn-n^2)(-1)^{r+1}F_s}{(\alpha-\beta)^2}\left[-C(\alpha^t-\beta^t)+D\sqrt{5}(\alpha^t+\beta^t)\right].$$

The last equation with Binet formulas prove the theorem. ■

For $(m,n)=(1,1)$ and $(1,3)$, we obtain the Vajda's identities for Fibonacci and Lucas 3-parameter generalized quaternions as follows

$$\Lambda_{r+s}\Lambda_{r+t}-\Lambda_r\Lambda_{r+s+t}=(-1)^r F_s(CF_t-DL_t)$$

and

$$\Lambda_{r+s}\Lambda_{r+t}-\Lambda_r\Lambda_{r+s+t}=5(-1)^{r+1}F_s(CF_t-DL_t).$$

For $t\to -s$, Vajda's identity and the identity $F_{2s}=F_sL_s$ give the Catalan's identity as follows

$$\Lambda_{r+s}\Lambda_{r-s}-\Lambda_r^2=(m^2+mn-n^2)(-1)^{r+s+1}(CF_s^2+DF_{2s}).$$

For $(m,n)=(1,1)$ and $(1,3)$, we obtain the Catalan's identities for Fibonacci and Lucas 3-parameter generalized quaternions as follows

$$\Lambda_{r+s}\Lambda_{r-s}-\Lambda_r^2=(-1)^{r+s+1}(CF_s^2+DF_{2s})$$

and

$$\Lambda_{r+s}\Lambda_{r-s}-\Lambda_r^2=5(-1)^{r+s}(CF_s^2+DF_{2s}).$$

For $s\to 1$, Catalan's identity gives the Cassini's identity as follows

$$\Lambda_{r+1}\Lambda_{r-1}-\Lambda_r^2=(m^2+mn-n^2)(-1)^r(C+D).$$

For $(m,n)=(1,1)$ and $(1,3)$, we obtain the Cassini's identities for Fibonacci and Lucas 3-parameter generalized quaternions as follows

$$\Lambda_{r+1}\Lambda_{r-1}-\Lambda_r^2=(-1)^r(C+D)$$

and

$$\Lambda_{r+1}\Lambda_{r-1}-\Lambda_r^2=5(-1)^{r+1}(C+D)$$

D'Ocagne's identity for the Gibonacci 3-parameter generalized quaternions is in the next theorem.

Theorem 3.2. For any integers r and s, the following equation holds

$$\Lambda_r\Lambda_{s+1} - \Lambda_{r+1}\Lambda_s = (m^2 + mn - n^2)(-1)^s(CF_{r-s} + DL_{r-s}).$$

Proof. From Theorem 2.1, we have

$$\begin{aligned}
&\Lambda_r\Lambda_{s+1} - \Lambda_{r+1}\Lambda_s \\
&= \frac{1}{(\alpha-\beta)^2}\big[\big(\alpha_G\alpha^{\#}\alpha^r - \beta_G\beta^{\#}\beta^r\big)\big(\alpha_G\alpha^{\#}\alpha^{s+1} - \beta_G\beta^{\#}\beta^{s+1}\big) \\
&\qquad - \big(\alpha_G\alpha^{\#}\alpha^{r+1} - \beta_G\beta^{\#}\beta^{r+1}\big)\big(\alpha_G\alpha^{\#}\alpha^s - \beta_G\beta^{\#}\beta^s\big)\big] \\
&= \frac{\alpha^{\#}\beta^{\#}}{(\alpha-\beta)^2}[-\alpha_G\beta_G\alpha^r\beta^{s+1} + \alpha_G\beta_G\alpha^{r+1}\beta^s - \beta_G\alpha_G\alpha^{s+1}\beta^r + \beta_G\alpha_G\alpha^s\beta^{r+1}] \\
&= \frac{(m^2 + mn - n^2)(-1)^s}{(\alpha-\beta)^2}[\alpha_G\beta_G\alpha^{r-s}(\alpha-\beta) - \beta_G\alpha_G\beta^{r-s}(\alpha-\beta)] \\
&= \frac{(m^2 + mn - n^2)(-1)^s}{\alpha-\beta}\big[(C + D\sqrt{5})\alpha^{r-s} - (C - D\sqrt{5})\beta^{r-s}\big] \\
&= \frac{(m^2 + mn - n^2)(-1)^s}{\alpha-\beta}\big[C(\alpha^{r-s} - \beta^{r-s}) + D\sqrt{5}(\alpha^{r-s} + \beta^{r-s})\big].
\end{aligned}$$

The last equation and the Binet formulas for the Fibonacci and Lucas numbers proves the theorem. ■

For $(m, n) = (1,1)$ and $(1,3)$, we obtain the d'Ocagne's identities for Fibonacci and Lucas 3-parameter generalized quaternions as follows

$$\Lambda_r\Lambda_{s+1} - \Lambda_{r+1}\Lambda_s = (-1)^s(CF_{r-s} + DL_{r-s})$$

and

$$\Lambda_r\Lambda_{s+1} - \Lambda_{r+1}\Lambda_s = 5(-1)^{s+1}(CF_{r-s} + DL_{r-s}).$$

Another interesting results between Gibonacci 3-parameter generalized quaternions given in the following theorem.

Theorem 3.3. For any integers r and s, the following equation s hold

$$\Lambda_r\Lambda_s - \Lambda_s\Lambda_r = 2(-1)^r(m^2 + mn - n^2)DF_{s-r}.$$

Proof. Theorem 2.1 gives

$$\Lambda_r\Lambda_s - \Lambda_s\Lambda_r$$

$$= \frac{1}{(\alpha-\beta)^2}\big[\big(\alpha_G\alpha^{\#}\alpha^r - \beta_G\beta^{\#}\beta^r\big)\big(\alpha_G\alpha^{\#}\alpha^s - \beta_G\beta^{\#}\beta^s\big) - \big(\alpha_G\alpha^{\#}\alpha^s - \beta_G\beta^{\#}\beta^s\big)\big(\alpha_G\alpha^{\#}\alpha^r - \beta_G\beta^{\#}\beta^r\big)\big]$$

$$= \frac{\alpha^{\#}\beta^{\#}}{(\alpha-\beta)^2}[-\alpha_G\beta_G\alpha^r\beta^s + \alpha_G\beta_G\alpha^s\beta^r - \beta_G\alpha_G\alpha^s\beta^r + \beta_G\alpha_G\alpha^r\beta^s]$$

$$= \frac{(m^2+mn-n^2)}{(\alpha-\beta)^2}[\alpha^r\beta^s(-\alpha_G\beta_G + \beta_G\alpha_G) + \alpha^s\beta^r(\alpha_G\beta_G - \beta_G\alpha_G)]$$

$$= \frac{(m^2+mn-n^2)2D}{\alpha-\beta}(-\alpha^r\beta^s + \alpha^s\beta^r)$$

$$= \frac{(m^2+mn-n^2)2D(-1)^r}{\alpha-\beta}(\alpha^{s-r} - \beta^{s-r}).$$

The last equation proves the theorem. ■

REFERENCES

Akyigit, M., Kosal, H. H., & Tosun, M. (2013). Split Fibonacci quaternions. Advances in Applied Clifford Algebras, 23, 535-545.

Akyigit, M., Kosal, H. H., & Tosun, M. (2014). Fibonacci generalized quaternions. Advances in Applied Clifford Algebras, 24, 631-641.

Aydin, F. T. (2018). Bicomplex Fibonacci quaternions. Chaos, Solitons & Fractals, 106, 147-153.

Bilgici, G. (2022). Fibonacci 3-Parameter Generalized Quaternions. European Journal of Science and Technology, 41, 357-361.

Bilgici, G., Tokeser, U. & Unal, Z. (2017). k-Fibonacci and k-Lucas generalized quaternıons. Konuralp Journal of Mathematics, 5(2), 102-113

Dasdemir, A., & Bilgici, G. (2021). Unrestricted Fibonacci and Lucas quaternions. Fundamental Journal of Mathematics and Applications, 4(1), 1-9.

Falcon, S. (2011). On the k-Lucas numbers. International Journal of Contemporary Mathematical Sciences, 6(21), 1039-1050.

Falcon, S., & Plaza, A. (2007). On the Fibonacci k-numbers. Chaos, Solitons & Fractals, 32(5), 1615-1624.

Gul, K. (2022). Generalized k-order Fibonacci hybrid quaternions. Erzincan University Journal of Science and Technology, 15(2), 670-683.

Halici, S. (2012). On Fibonacci quaternions. Advances in Applied Clifford Algebras, 22(2), 321-327.

Horadam, A. F. (1963). Complex Fibonacci numbers and Fibonacci quaternions. The American Mathematical Monthly, 70(3), 289-291.

Ipek, A. (2017). On (p, q)-Fibonacci quaternions and their Binet formulas, generating functions and certain binomial sums. Advances in Applied Clifford Algebras, 27, 1343-1351.

Kizilates, C., & Kone, T. (2021). On higher order Fibonacci quaternions. The Journal of Analysis, 1-12.

Koshy, T. (2019). Fibonacci and Lucas Numbers with Applications. John Wiley & Sons.

Nurkan, S. K., & Guven, I. A. (2015). Dual Fibonacci quaternions. Advances in Applied Clifford Algebras, 25, 403-414.

Polatlı, E. (2016). A generalization of Fibonacci and Lucas Quaternions. Advances in Applied Clifford Algebras, 26, 719-730.

Sentürk, T. D., & Unal, Z. (2022). 3-parameter generalized quaternions. Computational Methods and Function Theory, 22(3), 575-608.

Swamy, M. N. S. (1973). On generalized Fibonacci quarternions. The Fibonacci Quarterly, 11(5), 547-549.

Tan, E., Yilmaz, S., & Sahin, M. (2016). On a new generalization of Fibonacci quaternions. Chaos, Solitons & Fractals, 82, 1-4.

Yuce, S., & Aydin, F. T. (2016). A new aspect of dual Fibonacci quaternions. Advances in Applied Clifford Algebras, 26, 873-884.

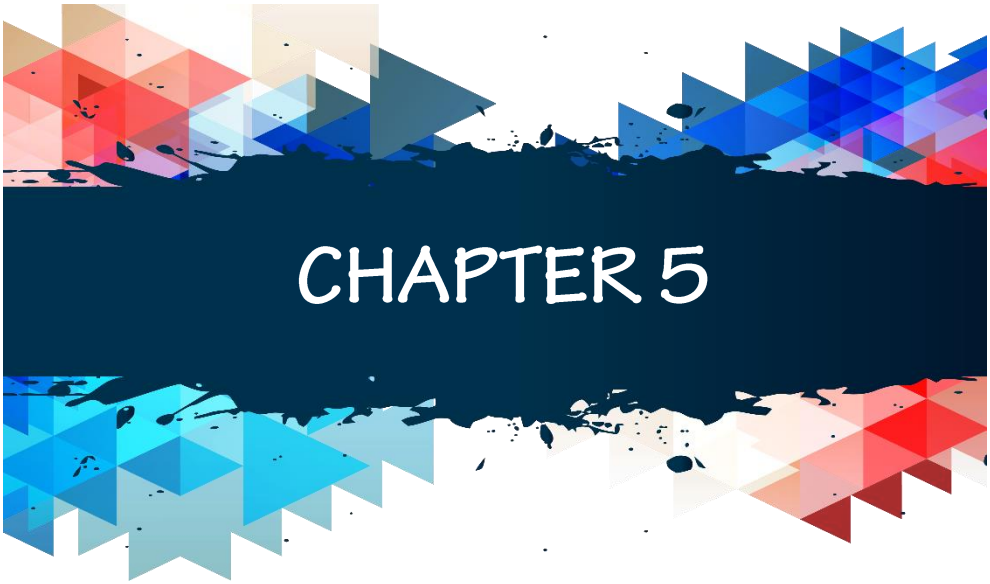

The Role of Fungal Chitinases in Biological Control

Tülin Aşkun[1] & Aylin Er[2] & Pınar Güner[3] & Muhammet Deniz[4]

1 Prof. Dr., Department of Biology, Faculty of Sciences and Arts, University of Balikesir, Turkey
0000-0002-2700-1965
[2] Prof. Dr., Department of Biology, Faculty of Sciences and Arts, University of Balikesir, Turkey,
0000-0002-8108-8950
[3] Dr., Department of Biology, Faculty of Sciences and Arts, University of Balikesir, Turkey,
0000-0001-6922-7009
[4] Department of Biology, Faculty of Sciences and Arts, University of Balikesir, Turkey
0000-0003-0501-9766

1. INTRODUCTION

Chitinases, the enzymes responsible for the biodegradation of chitin, have been identified in a wide range of organisms, from bacteria to higher plants and animals (Vega and Kalkum, 2012). These enzymes are related to various physiological processes, including nutrition, parasitism, morphogenesis, and immunity. Additionally, several organisms have evolved to produce chitinase-like lectins that lack enzymatic activity but play a regulatory role. Various organisms, including bacteria, fungi, insects, plants and animals, produce chitinolytic enzymes for various purposes, such as nutrition, morphogenesis and defence against chitin-containing pathogens (Adrangi et al., 2010). Notably, many of these organisms possess genes that encode enzymes capable of degrading chitin. These enzymes are related to various physiological processes, including nutrition, parasitism, morphogenesis, and immunity. Additionally, several organisms have evolved to produce chitinase-like lectins that lack enzymatic activity but play a regulatory role. Most filamentous fungi possess between 10 and 20 distinct chitinolytic genes, while mycoparasitic species may have 30 or more such genes (Hartl et al., 2012). These enzymes work synergistically or sequentially to break down chitin (Patil et al., 2000). Furthermore, studies have demonstrated that higher organisms possess many chitinolytic genes (Hossain et al., 2010). However, it is known that not all of the genes mentioned above encode active enzymes. Hossain et al. (2010) and Vega and Kalkum (2012), many organisms, including plants, invertebrates and higher animals, express genes encoding so-called chitinase-like lectins that are devoid of chitinolytic activity due to the presence of substitutions in their vital catalytic residues. Notwithstanding the absence of catalytic activity, these proteins retain the capacity to bind chitin. Given their pervasive presence and multifaceted biological roles, chitinolytic enzymes have been harnessed for various applications such the production of single-cell proteins, isolation of fungal protoplasts, estimation of fungal biomass, development of three-dimensional cell culture scaffolds, biocontrol of plant-pathogenic fungi and insect vectors, and the production of chitooligosaccharides, glucosamine, GlcNAc, neoglycoproteins and artificial polysaccharides (Li et al., 2008; Adrangi et al.,2010; Ortiz-Rodriguez et al., 2010; Tajdini et al., 2010; Jamialahmadi et al., 2011; Zakariassen et al., 2011). Recent studies of chitinolytic enzymes have demonstrated that their diversity and physiological roles are far more extensive than previously recognised.

1.1 Fungal Chitinases

The production of chitinase fungi has received far less research attention than chitinolytic bacteria. The glycoside hydrolase 18 (GH18 fungal chitinases) are categorized into A, B, C, and D subfamilies according to sequence similarity and domain arrangement, demonstrating significant amino acid homology with class III plant chitinases (Junges et al., 2014). Fungal chitinase genes comprise five domains, which encompass the chitin-binding domain, catalytic domain, N-terminal signal peptide region, serine/threonine-rich domain, and C-terminal extension region (Hamid et al., 2013). Chitinase genes are prevalent in fungal genomes, pre-dominantly falling within GH18 family, except for *Nosema bombycis*, which harbours the first documented the glycoside hydrolase (GH19) chitinase in fungi (Han et al., 2016). The genomes of filamentous fungi typically encompass a range of 10 to 25 chitinases that fulfil various physio-logical roles, encompassing chitin degradation within cell walls, remodelling during hyphal growth, branching, hyphal fusion, autolysis, and defence against other fungi occupying the same ecological niche (Adams, 2004). Like their bacterial counterparts, fungal chitinases exhibit a range of functions, playing essential roles in morphogenesis, nutrition, and various fungal developmental processes. Chitin, as a primary component of fungal cell walls, makes fungal chitinases essential for various functions, including degradation, cell division, morphogenesis, autolysis, and chitin acquisition (Rathore and Gupta, 2015; Langner and Göhre, 2016). Filamentous fungi harbour larger chitinase gene families (seven groups) than yeast. However, the functions of individual chitinases have remained obscure due to difficulties in knocking down multiple genes to characterize phenotypic alterations. The only commercial application of chitinases obtained from fungi is *Trichoderma harzianum*. *Penicillium janthinellum* has been employed to produce chitinases in vitro (Laein and Mohammadi, 2018). Entomopathogenic fungi (EPF) like *Verticillium lecanii*, *Metarhizium anisopliae*, and *Beauveria bassiana*, when cultivated in liquid cultures supplemented with locust cuticle as the exclusive carbon source, produce a range of hydrolytic enzymes that target the primary constituents of insect cuticles, including protein, chitin, and lipid (Leger et al., 1986). Collaborating with proteases, chitinases aid in the breakdown of insect cuticles (Leger et al., 1986) and play roles in multiple phases of EPF, including germination, hyphal growth, morphogenesis, nutrition, and defence against rivals (Adams, 2004). Throughout the infection process, *Penicillium citrinum* produces and releases extracellular enzymes, including proteases, chitinases, and lipases, to break down cuticle components such as proteins, lipids, and chitin. Subsequently, conidia attach to the insect cuticle,

germinate, and form spores within the host bodies, ultimately leading to insect death (Ibrahim et al., 2016; Dhawan and Joshi, 2017; Mannino et al., 2019). A core protein located on the outer surface of the conidia possesses a hydrophobic rodlet layer that binds to the insect's epicuticle. (Pedrini, 2018). The unique hydrophobins in *P. citrinum* are es-sential for its sporulation, growth, development, pathogenesis, and thermotolerance. Additionally, environmental factors impact the virulence of *P. citrinum* (Jiang et al., 2020; Shahriari et al., 2021). Enzymes that break down insect cuticles are essential virulence factors for EPF, showing a correlation between pathogenicity and enzyme production (Ownley et al., 2008).

1.2 Correlation Between Pathogenicity and Enzyme Production of Entomopathogenic Fungi

The epicuticle consists of an intricate blend of non-polar lipids, whereas the primary constituents of the insect cuticle are chitin and chitin protein. Lipids within the epicuticle contribute to chemical signalling pathways (Blomquist and Vogt, 2003). As the primary defence mechanism against microbial assaults, the waterproof epicuticle constitutes an outer layer of the insect's exoskeleton. It constitutes a heterogeneous blend of a varied combination of lipids, extended-chain alkenes, fatty acids, and esters. The essential role of lipases in the degradation of ester bonds within lipoproteins, waxes, and fats embedded within the insect exoskeleton interior is widely recognised (Ali et al., 2009). Lipases are crucial in enabling cuticle penetration and the initial release of nutrients. In the absence of lipases and lipoxygenases, certain structures within the fats, lipoproteins, and waxy layers of the insect epicuticle exhibit antifungal properties. Lord et al. (2002) presented evidence indicating that saturated fatty acid chains can impair the proliferation of EPF strains. They clarified how the lipoxygenase pathway contributes to the cellular immune response mediated by eicosanoids of *B. bassiana*. Moreover, James et al. (2003) confirmed the influence of cuticular lipids from silverleaf whitefly (*Bemisia argentifolii*) on conidia germination from *Paecilomyces fumosoroseus* and *B. bassiana*. Whitefly nymphs hinder spore germination through the extensive deposition of long-chain wax esters. EPFs are distinguished by their pathogenicity and virulence; pathogenicity denotes the microorganism's capacity to induce disease, while virulence signifies the level of pathogenicity utilized to eliminate the host under controlled circumstances. Protease production, deemed essential in the infectious process, is closely linked to these characteristics (Mustafa and Kaur, 2009). Some fungi, *Nomuraea rileyi*, *Beauveria brongniartii*, *B. bassiana*, *Lagenidium giganteum*, *Erynia* spp., *Evenus coronata*, *Aschersonia aleyrodis*, *V. lecanii*, and

M. anisopliae, were characterized as the producers of protein-degrading enzyme such as proteases, collagenases (Sheng et al., 2006). Similarly, Freimoser et al. (2005) witnessed intersecting gene responses displaying diverse expression patterns when exposed to cuticles from *Popilla japonica, Blaberus giganteus*, and *Lymantria dispar*. After lipases enzymatically break down the epicuticle, the fungus generates notable quantities of Pr1 protease. This protease kickstarts the dissolution process of proteinaceous material. The decomposition process persists until exopeptidases and amino peptidases into amino acids fragment the dissolved proteins. These amino acids are then utilized as nourishment by EPF (Wang et al., 2012). The subtilisin-like serine protease Pr1 and the protease Pr2, which exhibit trypsin-like characteristics, have been extensively researched. Eleven identified and cloned isoforms of the Pr1 protein gene and a metalloprotease have been documented. (St Leger et al., 1994). At the cuticle initiation stage, these proteases are secreted and participate in a signal transduction process that requires protein kinase A (PKA) activation, which is mediated through AMPc (Fang et al., 2009). Sun and Liu (2006) reported that the crucial involvement of the protease Pr1 in cuticle penetration has been firmly established, and the infective process cannot advance in its absence. Chitinases are used to disrupt chitin-containing structures, such as the cuticle and peritrophic matrix (PM), which are essential for the growth, development, and survival of insects (Figure 1) (Zhu et al., 2008). As sources of fungal chitinase, some of the most researched EPFs, such as *Pochonia* spp., *Arthrobotrys* spp., and *Paecilomyces* spp., can be used as biological control agents. Entomopathogenic microorganisms offer a significant advantage over chemical insecticides, as they can perform various activities simultaneously. Therefore, metabolites from entomopathogenic organisms can be used as biological pesticides. Collaborating with proteases, chitinases aid in the breakdown of insect cuticles (Leger et al., 1986) and play roles in multiple phases of EPF, including germination, hyphal growth, morphogenesis, nutrition, and defence against rivals (Adams, 2004). Enzymes that break down insect cuticles are essential virulence factors for EPF, showing a correlation between pathogenicity and enzyme production (Ownley et al.,2008). It has been determined that important EPFs (*M. anisopliae*, *Metarhizium flavoviride*, and *B. bassiana*) produce chitinolytic enzymes, N-acetyl-β-D-glucosaminidases, and endochitinases in culture media prepared using insect cuticle (St Leger et al., 1996).

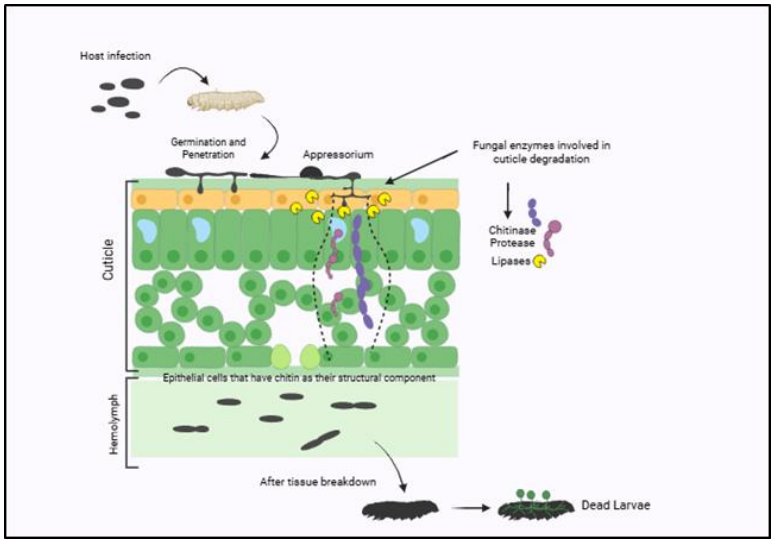

Figure 1: Fungal enzymes involved in cuticle degradation.

1.3 Uses of Fungal Chitinases as Biological Control Agents

Recognising the precise substrates on which chitinases act is vital, providing insights into how their specificity relates to physiological roles and facilitating the efficient transformation of chitin into novel and industrially valuable items. (Matsumiya et al., 2008). Microorganisms, especially *Firmicutes*, *Actinobacteria*, and specific *Proteobacteria*, are recognised for their production and activity of chitinolytic enzymes (Liu et al., 2010; Beier and Bertilsson, 2013). Chitinolytic enzymes synthesised by microorganisms exhibit antifungal, antibacterial, nematocidal, or insecticidal activity by breaking down or weakening the cell walls of pests and pathogens. Using chitinases produced by microorganisms against synthetic pesticides and fungicides is essential for protecting the environment and human health (Edreva, 2005). The growing interest in chitinase enzymes has occurred due to their use in agriculture for the biological control of phytopathogenic fungi and pests (Lu et al., 2005). Enzymes responsible for degrading the insect cuticle serve as pivotal virulence factors for EPF. A relationship between pathogenicity and enzyme production exists, suggesting potential applications in inducing the weakening or thinning of cuticular structures (Kaur and Padmaja, 2009). If these enzymes reach the larval intestine, they can cause significant damage to the peritrophic membrane, disrupting the insect's ability to feed and ultimately leading to its death (Binod et al., 2007). The revelation has presented fresh opportunities for employing enzymes as biocontrol agents against insects and has held promise for

applications targeting specific plant diseases caused by phytopathogenic fungi (Ownley et al., 2008).

EPF, particularly those belonging to the Zygomycota and Deuteromycota classes, demonstrate substantial promise for the biological management of insect pests harmful to plants. Numerous endeavours have been undertaken to utilise fungi like *Beauveria* spp., *Metarhizium anisopliae*, *A. aleyrodis*, *N. rileyi*, and *V. lecanii* in insect control applications. Enzymes that degrade the cuticle, notably proteases and chitinases, have been identified as critical factors influencing virulence in these fungi. (Ortiz-Urquiza et al., 2015). EPFs overcome the physicochemical barriers formed by insects peritrophic membrane and exoskeleton by secreting numerous extracellular enzymes, such as chitinolytic and proteolytic enzymes, that aid cuticle penetration and infection (St Leger et al., 1994). In their study, Tu et al. (2010) discovered and evaluated the chitinase-producing *Serratia marcescens* GEI strain, isolated from the gut of Chinese honeybee workers, for its effectiveness in managing the insect parasite *Varroa destructor* in western honeybees. The results showed that the mortality rate for the mites was 100% within 5 days. This underscores the potential of enzymes as biocontrol agents, not only for insects but also for combatting specific plant diseases triggered by phytopathogenic fungi (Ownley et al., 2008). Enzymes have proven effective against the cotton aphid (*Aphis gossyppii* Glover), with chitinases notably contributing to their insecticidal properties (Kim et al., 2010). The application of enzymes to *Plutella xylostella* larvae has a significant impact on their growth and metamorphosis (Ali et al., 2010). Chitinases play a role in the penetration of the host cuticle by EPF. Entomopathogens such as *V. lecanii*, *M. anisopliae*, and *B. bassiana* secrete β-N-acetylglucosaminidases and chitinases when cultivated on insect cuticles (St Leger, 1996). During cuticle penetration, virulent isolates of *N. rileyi* demonstrate more significant chitinase activity than avirulent strains (El-Sayed et al., 1989). It is hypothesised that chitinase gene expression in EPF is regulated by a system involving repressors and inducers, with chitin or its degradation products acting as inducers. Due to the presence of chitin and exoskeleton, *Aspergillus fumigatus* displays insecticidal activity against *Callosobruchus maculates* through the induction of chitinolytic/insecticidal en-zymes (Pereira et al., 2006). Chitinases have demonstrated efficacy as biological control agents, exhibiting antifungal activity against *Fusarium equiseti* and functioning as bioinsecticides in the diamond-back moth (*P. xylostella*), thereby reducing time to mortality (Prasanna et al., 2013). Reports indicate that *Trichoderma viride* can generate a range of compounds or molecules with different effects against various insects' feeding activities.

Chitinases frequently lead to a significant reduction in the feeding behaviour of lepidopteran larvae by impacting their peritrophic membrane. Research studies have reported a 50% mortality rate within 7 days for rice moth (*Corcyra cephalonic*a) (Vijayakumar and Alagar, 2017), cotton bollworm (*Helicoverpa armigera*) (Chin-naperumal et al., 2018), and silkworm (*Bombyx mori*) (Berini et al., 2016). Kim et al. (2010) partially purified the chitinase enzyme obtained from the culture supernatant of *B. bassiana* SFB 205 isolate using the ammonium sulfate precipitation method. They mixed it with isotridecyl ether and measured its effectiveness against cotton aphids. The study concluded that the partially purified enzyme caused significant mortality in aphids compared to the control group treated with Tween 80. Binod et al. (2007) purified the chitinase enzyme obtained from *Penicillium ochrochloron* using column chromatography. They tested its effectiveness on *H. armigera* through spraying and dipping methods at various concentrations. The highest mortality rate was observed at 2000 U mL−1 chitinase activity. They demonstrated that the enzyme adversely affected larval growth and metamorphosis (Binod et al.,2007). Chitinase enzyme isolated from *Paecilomyces javanicus* has been tested against the cotton root nematode *Meloidogyne incognita*, causing thinning of the chitin layer in nematode eggshells and showing adverse effects on the development of larvae (Chan et al., 2010). Fungal chitinase enzymes synthesised from *Monacrosporium thaumasium* and *Duddingtonia flagrans* fungi have demonstrated nematocidal effects (Soares et al., 2015; Brago et al., 2015). According to the studies, bacterial and fungal chitinases have proven effective as biological control agents against fungi and insect infections harmful to agriculture. Considering these studies, chitinase is anticipated to be developed as a commercially formulated biological control agent against agricultural pests in the coming years. Chitinase-producing fungi and those associated with insects are presented in Table 1.

Table 1. Chitinase production and insect infection.

Fungi	The insect species that are infected	References
A.aleyrodis	*Bemisia tabaci, Diaphorina citri*	Wang et al., (2012); Zhang et al., (2017); Singh et al., (2021)
A.fumigatus	-	Laein and Mohammadi, (2018)
Aspergillus niger	*Galleria mellonella*	Stączek et al., (2020; Abdel Wahab et al., (2023)
B. bassiana	*D. citri, Trialeurodes vaporariorum, Frankliniella occidentalis, Thrips tabaci, Rhynchophorus ferrugineus, Ips typographus, Polyphylla fullo, Ips avulsus, Oryzaephilus surinamensis, Sitophilus granarius, Tribolium castaneum, Teretrius nigrescens, Thaumastocoris peregrinus, Ceratitis rosa, Dendrolimus punctatus, Spodoptera litura, Spodoptera exigua, H. armigera, Maruca vitrata, Ostrinia furnacalis, Phaseolus vulgaris, P. xylostella, Spodoptera frugiperda, A. gossypii*	(Fang et al., 2005; Zhang et al., 2015a; Dannon et al., 2020)
Candida guilliermondii	----	(Yu et al., 2008)
Candida oleophila	-----	(Yu et al., 2008)
Choanephora cucurbitar	----	(Laein and Mohammadi, 2018)
Clonostachys rogersonia		(Laein and Mohammadi, 2018)
Isaria fumosorosea	*B. tabaci, Aleurodicus dispersus, Cameraria ohridella, A.gossypi, Leptopharsa gibbicarina, Scirtothrips dorsalis, Em-*	(Zimmermann, 2008; Montemayor et al., 2016; Bugti et al., 2018)

	poasca decipiens, Microtheca ochroloma, Sitophilus oryzae, S. granarius	
Lecanicillium muscarium	*S. granarius, S. oryzae, T. vaporariorum, A. gossypii, Aphis fabae, Tuta absoluta, Tetranychus urticae*	(Fenice et al., 2012; Mohammed and Hatcher, 2017; Mohammed, 2018; Ak, 2019; Chouikhi et al.,2022)
M. anisopliae	*Gryllotalpa gryllotalpa, Ixodes ricinus, Rhipicephalus microplus, S. litura, Haemaphysalis qinghaiensis, Aedes aegypti, Aedes albopictus, Culex quinquefasciatus, Haemaphysalis qinghaiensis, Hyalomma excavatum, I. ricinus, Glossina fuscipes, Rhipicephalus sanguineus*	(Fang et al., 2005; Sönmez et al., 2016; Aw and Hue, 2017; Wamiti et al., 2018)
Neurospora crassa	----	(Laein and Mohammadi, 2018)
Penicillium aculeatum	---	(Binod et al., 2007)
P. citrinum	*S. litura P. xylostella*	(Sharma et al., 2021; Nguyen et al., 2023)
Penicillium chrysogenum	*Anopheles stephensi*	(Patidar et al., 2005; Fouda et al., 2021)
Penicillium digitatum	---	(Liu et al., 2022)
Penicillium funiculosum	-----	(Binod et al., 2007)
Penicillium pinophilum	----	(Binod et al., 2007)
Phascolomyces articulos	-----	(Laein and Mohammadi, 2018)
Pichia membranifaciens	----	(Yu et al., 2008)
Piromyces communis	----	(Laein and Mohammadi, 2018)
Saccharomyces cerevisia	-----	(Yu et al., 2008)
Talaromyces emersonii	-----	(Laein and Mohammadi, 2018)
Thermomyces lanuginosu	*Eldana saccharina*	(Zhang et al., 2015b; Okongo et al., 2019)
Trichoderma asperellum	*Callosobruchus maculatus, A. aegypti, Zophobas morio, O. furnacalis,*	(Loc et al., 2020; Batool et al., 2020; da Silveira et al., 2021; Poveda, 2021;

	T. urticae, *T. tabaci*, *Liriomyza huidobrensis*, *Xylosandrus germanus*	Sebumpan et al., 2022; Ozdemir,2023)
Trichoderma atroviride	*S. frugiperda*, *Drosophila melanogaster*, *Xylotrechus arvicol Xylosandrus germanus*, *T. tabaci*, *Spodoptera littoralis*, *Macrosiphum euphorbiae*	(Contreras-Cornejo et al., 2018; Poveda, 2021)
Trichoderma brevicompa	*Acanthoscelides obtectus*	(Laein and Mohammadi, 2018; Rodríguez-González et al., 2021)
Trichoderma harzianum	*Odontotermes formosanus*, *Cimex hemipterus*, *Periplaneta americana*, *Diuraphis noxia*, *Schizaphis graminum*, *A.aegypti*, *S. oryzae*, *Tenebrio molitor*, *T.castaneum*, *Xylotrechus arvicola*, *Earias insulana*, *Pectinophora gossypiella*, *B. tabaci*, *Hellula undalis*	(Zhang et al., 2015b; de Souza Maia Filho et al., 2017; Poveda, 2021)
Trichoderma longibrachi	*B. tabaci*, *M. euphorbiae*, *C. hemipterus*	Zhang et al.,(2015b) de Souza Maia Filho et al., (2017) Poveda, (2021)
Trichoderma virens	-----	Zhang et al., (2015b) de Souza Maia Filho., (2017)
Trichoderma viride	*O. formosanus*, *C. quinquefasciatus*, *B. mori*, *C. cephalonica*, *H. armigera*, *T. tabaci*, *Cassida rubiginosa*	Zhang et al., (2015b) de Souza Maia Filho et al., (2017) Poveda, (2021)

V. lecanii	*B. tabaci*, *B.argentifolii*	Liu et al., (2003) Wang et al., (2004)

4. CONCLUSION

This review provides a perspective on the mechanisms of action of chitinases synthesized by entomopathogenic fungi (EPF) and chitinase-producing fungi and their applications in biological control. There is a growing interest in environmentally friendly research, which encourages investigating combined strategies using natural products, microorganisms and their metabolites for pest control in agricultural products, both pre-harvest and post-harvest. In the coming years, it is expected that research on the use of enzymes obtained from phytopathogenic fungi as biological control agents targeting specific insects and plant diseases will be further developed with molecular biology techniques and interdisciplinary approaches.

Acknowledgements

We would like to thank TUBITAK-1001 The Scientific and Tecnological Research Projects Funding Program (122O398).

REFERENCES

Abdel Wahab, W. A., El-Dein, A. N., Hussein, M., Mostafa, F. A., & Saleh, S. A. (2023). Kinetic, thermodynamic and bio-applicable studies on *Aspergillus niger* Mk981235 Chitinase. *Catalysis Letters*, 153(4), 1089-1095. https://doi.org/10.1007/s10562-022-04045-9

Adams, D. J. (2004). Fungal cell wall chitinases and glucanases. *Microbiology*, *150*(7), 2029-2035. https://doi.org/10.1099/mic.0.26980-0

Adrangi, S., Faramarzi, M.A., Shahverdi, A.R. ,Sepehrizadeh, Z. (2010). Purification and characterization of two extracellular endochitinases from Massiliatimonae. *Carbohydrate Research*, 345: 402–7

Ak, K. (2019). Efficacy of entomopathogenic fungi against the stored-grain pests, *Sitophilus granarius* L. and *Sitophilus oryzae* L.(Coleoptera: Curculionidae). *Egyptian Journal of Biological Pest Control*, *29*, 1-7. https://doi.org/10.1186/s41938-019-0115-y

Ali, S., Huang, Z., & Ren, S. (2010). Production of cuticle degrading enzymes by *Isaria fumosorosea* and their evaluation as a biocontrol agent against diamondback moth. *Journal of Pest Science*, *83*, 361-370. https://doi.org/10.1007/s10340-010-0305-6

Ali, S., Huang, Z., & Ren, S. X. (2009). Production and extraction of extracellular lipase from the entomopathogenic fungus *Isaria fumosoroseus* (Cordycipitaceae; Hypocreales). *Biocontrol Science and Technology*, *19*(1), 81-89. https://doi.org/10.1080/09583150802588524

Aw, K. M. S., & Hue, S. M. (2017). Mode of infection of Metarhizium spp. fungus and their potential as biological control agents. *Journal of fungi*, *3*(2), 30. https://doi.org/10.3390/jof3020030

Batool, R., Umer, M. J., Wang, Y., He, K., Zhang, T., Bai, S., ... & Wang, Z. (2020). Synergistic effect of *Beauveria bassiana* and *Trichoderma asperellum* to induce maize (*Zea mays* L.) defense against the Asian corn borer, *Ostrinia furnacalis* (Lepidoptera, Crambidae) and larval immune response. *International journal of molecular sciences*, *21*(21), 8215. https://doi.org/10.3390/ijms21218215

Beier, S., & Bertilsson, S. (2013). Bacterial chitin degradation—mechanisms and ecophysiological strategies. *Frontiers in microbiology*, *4*, 52995. https://doi.org/10.3389/fmicb.2013.00149

Berini, F., Caccia, S., Franzetti, E., Congiu, T., Marinelli, F., Casartelli, M., & Tettamanti, G. (2016). Effects of *Trichoderma viride* chitinases on the peritrophic matrix of Lepidoptera. *Pest Management Science*, *72*(5), 980-989. https://doi.org/10.1002/ps.4078

Binod, P., Sukumaran, R. K., Shirke, S. V., Rajput, J. C., & Pandey, A. (2007). Evaluation of fungal culture filtrate containing chitinase as a biocontrol agent against

Helicoverpa armigera. *Journal of applied microbiology*, *103*(5), 1845-1852. https://doi.org/10.1111/j.1365-2672.2007.03428.x

Blomquist, G. J., & Vogt, R. G. (2003). Biosynthesis and detection of pheromones and plant volatiles—introduction and overview. In *Insect pheromone biochemistry and molecular biology* (pp. 3-18). Academic Press. https://doi.org/10.1016/B978-012107151-6/50003-7

Braga, F. R., Soares, F. E. F., Giuberti, T. Z., Lopes, A. D. C. G., Lacerda, T., de Hollanda Ayupe, T., ... & Araújo, J. V. (2015). Nematocidal activity of extracellular enzymes produced by the nematophagous fungus Duddingtonia flagrans on cyathostomin infective larvae. *Veterinary parasitology*, *212*(3-4), 214-218. https://doi.org/10.1016/j.vetpar.2015.08.018

Bugti, G. A., Na, C., Bin, W., & Feng, L. H. (2018). Control of plant sap-sucking insects using entomopathogenic fungi *Isaria fumosorosea* strain (Ifu13a). *Plant Protection Science*, 54, 258-264. https://doi.org/10.17221/118/2017-PPS

Chan, Y. L., Cai, D., Taylor, P. W. J., Chan, M. T., & Yeh, K. W. (2010). Adverse effect of the chitinolytic enzyme PjCHI-1 in transgenic tomato on egg mass production and embryonic development of *Meloidogyne incognita*. *Plant pathology*, *59*(5), 922-930. https://doi.org/10.1111/j.1365-3059.2010.02314.x

Charnley, A. K. (2003). Fungal pathogens of insects: cuticle degrading enzymes and toxins. *Advances in Botanical Research*, *40*, 241-321. https://doi.org/10.1016/S0065-2296(05)40006-3

Charnley, A. K., & Collins, S. A. (2007). 10 entomopathogenic fungi and their role in pest control. *Environmental and microbial relationships*, *4*, 159. https://doi.org/10.1007/978-3-540-71840-6

Chen, Y., Wang, T., Zhang, X., Zhang, F., & Linhardt, R. J. (2021). Structural and immunological studies on the polysaccharide from spores of a medicinal entomogenous fungus *Paecilomyces cicadae*. *Carbohydrate polymers*, *254*, 117462. https://doi.org/10.1016/j.carbpol.2020.117462

Cheong, P., Glare, T. R., Rostás, M., & Haines, S. R. (2016). Measuring chitinase and protease activity in cultures of fungal entomopathogens. *Microbial-Based Biopesticides: Methods and Protocols*, 177-189. https://doi.org/10.1007/978-1-4939-6367-6_14

Chinnaperumal, K., Govindasamy, B., Paramasivam, D., Dilipkumar, A., Dhayalan, A., Vadivel, A., ... & Pachiappan, P. (2018). Bio-pesticidal effects of *Trichoderma viride* formulated titanium dioxide nanoparticle and their physiological and biochemical changes on *Helicoverpa armigera* (Hub.). *Pesticide biochemistry and physiology*, *149*, 26-36. https://doi.org/10.1016/j.pestbp.2018.05.005

Chouikhi, S., Assadi, B. H., Lebdi, K., & Belkadhi, M. S. (2022). Efficacy of the entomopathogenic fungi *Beauveria bassiana* and *Lecanicillium muscarium* in the

control of the tomato leaf miner, *Tuta absoluta* (Meyrick)(Lepidoptera: Gelechiidae). *Egyptian Journal of Biological Pest Control*, *32*(1), 139. https://doi.org/10.1186/s41938-022-00640-5

Contreras-Cornejo, H. A., Del-Val, E. K., Macías-Rodríguez, L., Alarcón, A., González-Esquivel, C. E., & Larsen, J. (2018). *Trichoderma atroviride*, a maize root associated fungus, increases the parasitism rate of the fall armyworm *Spodoptera frugiperda* by its natural enemy *Campoletis sonorensis*. *Soil Biology and Biochemistry*, *122*, 196-202. https://doi.org/10.1016/j.soilbio.2018.04.013

da Silveira, A. A., Andrade, J. S. P., Guissoni, A. C. P., da Costa, A. C., de Carvalho e Silva, A., da Silva, H. G., ... & Fernandes, K. F. (2021). Larvicidal potential of cell wall degrading enzymes from *Trichoderma asperellum* against *Aedes aegypti* (Diptera: Culicidae). *Biotechnology Progress*, *37*(5), e3182. https://doi.org/ 10.1002/btpr.3182

Dannon, H. F., Dannon, A. E., Douro-Kpindou, O. K., Zinsou, A. V., Houndete, A. T., Toffa-Mehinto, J., ... & Tamò, M. (2020). Toward the efficient use of *Beauveria bassiana* in integrated cotton insect pest management. *Journal of Cotton Research*, *3*, 1-21. https://doi.org/10.1186/s42397-020-00061-5

de Faria, M. R., & Wraight, S. P. (2007). Mycoinsecticides and mycoacaricides: a comprehensive list with worldwide coverage and international classification of formulation types. *Biological control*, *43*(3), 237-256. https://doi.org/10.1016/j.biocontrol.2007.08.001

de Souza Maia Filho, F., da Silva Fonseca, A. O., Persici, B. M., de Souza Silveira, J., Braga, C. Q., Pötter, L., ... & Pereira, D. I. B. (2017). *Trichoderma virens* as a biocontrol of *Toxocara canis*: In vivo evaluation. *Revista iberoamericana de micologia*, *34*(1), 32-35. https://doi.org/10.1016/j.riam.2016.06.004

Dhawan, M., & Joshi, N. (2017). Enzymatic comparison and mortality of *Beauveria bassiana* against cabbage caterpillar *Pieris brassicae* LINN. *Brazilian journal of microbiology*, *48*, 522-529. https://doi.org/10.1016/j.bjm.2016.08.004

Edreva, A. (2005). Pathogenesis-related proteins: research progress in the last 15 years. Gen Appl Plant Physiol, 31(1-2), 105-24.

El-Sayed, G. N., Coudron, T. A., Ignoffo, C. M., & Riba, G. (1989). Chitinolytic activity and virulence associated with native and mutant isolates of an entomopathogenic fungus, *Nomuraea rileyi*. *Journal of Invertebrate Pathology*, *54*(3), 394-403. https://doi.org/10.1016/0022-2011(89)90124-9

Fang, W., Leng, B., Xiao, Y., Jin, K., Ma, J., Fan, Y., ... & Pei, Y. (2005). Cloning of *Beauveria bassiana* chitinase gene Bbchit1 and its application to improve fungal strain virulence. *Applied and environmental microbiology*, *71*(1), 363-370. https://doi.org/ 10.1128/AEM.71.1.363–370.2005

Fang, W., Pava-Ripoll, M., Wang, S., & Leger, R. S. (2009). Protein kinase A regulates production of virulence determinants by the entomopathogenic fungus, *Metarhizium anisopliae*. *Fungal Genetics and Biology*, *46*(3), 277-285. https://doi.org/10.1016/j.fgb.2008.12.001

Fenice, M., Barghini, P., Selbmann, L., & Federici, F. (2012). Combined effects of agitation and aeration on the chitinolytic enzymes production by the Antarctic fungus *Lecanicillium muscarium* CCFEE 5003. *Microbial cell factories*, *11*, 1-11. https://doi.org/10.1186/1475-2859-11-12

Fouda, A., Awad, M. A., Eid, A. M., Saied, E., Barghoth, M. G., Hamza, M. F., ... & Hassan, S. E. D. (2021). An eco-friendly approach to the control of pathogenic microbes and *Anopheles stephensi* malarial vector using magnesium oxide nanoparticles (Mg-nps) fabricated by *Penicillium chrysogenum*. *International Journal of Molecular Sciences*, *22*(10), 5096. https://doi.org/10.3390/ijms22105096

Freimoser, F. M., Hu, G., & Leger, R. J. S. (2005). Variation in gene expression patterns as the insect pathogen *Metarhizium anisopliae* adapts to different host cuticles or nutrient deprivation in vitro. *Microbiology*, *151*(2), 361-371. https://doi.org/10.1099/mic.0.27560-0

Hamid, R., Khan, M. A., Ahmad, M., Ahmad, M. M., Abdin, M. Z., Musarrat, J., & Javed, S. (2013). Chitinases: an update. *Journal of Pharmacy and Bioallied Sciences*, *5*(1), 21-29. https://doi.org/10.4103/0975-7406.106559

Han, B., Zhou, K., Li, Z., Sun, B., Ni, Q., Meng, X., ... & Zhou, Z. (2016). Characterization of the first fungal glycosyl hydrolase family 19 chitinase (NbchiA) from *Nosema bombycis* (Nb). *Journal of eukaryotic microbiology*, *63*(1), 37-45. https://doi.org/10.1111/jeu.12246

Hartl, L., Zach, S., SeidlSeiboth, V. (2012). Fungal chitinases:diversity,mechanisticpropertiesand biotechnologicalpotential. *Applied Microbiology and Biotechnology*, 93:533–43.

Hossain, M.A., Noh, H.N., Kim, K.I., Koh, E.J., Wi, S.G. ,Bae, H.J., et al. (2010).Mutation of the chitinase-like protein-encoding AtCTL2 gene enhances lignin accumulation indark-grownArabidopsis seedlings. *Journal of Plant Physiology*, 167:650–8.

Ibrahim, A. A., Mohamed, H. F., El-Naggar, S. E. M., Swelim, M. A., & Elkhawaga, O. E. (2016). Isolation and selection of entomopathogenic fungi as biocontrol agent against the greater wax moth, *Galleria mellonella* L.(Lepidoptera: Pyralidae). *Egyptian Journal of Biological Pest Control*, 26(2), 249-253.

James, R. R., Buckner, J. S., & Freeman, T. P. (2003). Cuticular lipids and silverleaf whitefly stage affect conidial germination of *Beauveria bassiana* and *Paecilomyces fumosoroseus*. *Journal of Invertebrate Pathology*, *84*(2), 67-74. https://doi.org/10.1016/j.jip.2003.08.006

Jamialahmadi, K., Behravan, J.,Najafi, M.F., Yazdi, M.T., Shahverdi, A.R., Faramarzi, M.A. (2011). Enzymatic productionof N-acetyl-D glucosamine from chitinusing crude enzyme preparation of Aeromonassp. PTCC1691.*Biotechnology*, 10:292–7.

Jiang, Z. Y., Ligoxygakis, P., & Xia, Y. X. (2020). HYD3, a conidial hydrophobin of the fungal entomopathogen *Metarhizium acridum* induces the immunity of its specialist host locust. *International Journal of Biological Macromolecules*, *165*, 1303-1311. https://doi.org/10.1016/j.ijbiomac.2020.09.222

Junges, Â., Boldo, J. T., Souza, B. K., Guedes, R. L. M., Sbaraini, N., Kmetzsch, L., ... & Schrank, A. (2014). Genomic analyses and transcriptional profiles of the glycoside hydrolase family 18 genes of the entomopathogenic fungus *Metarhizium anisopliae*. *PLoS One*, *9*(9), e107864.https://doi.org/10.1371/journal.pone.0107864

Kasprzewska, A. N. N. A. (2003). Plant chitinases-regulation and function. *Cellular and Molecular Biology Letters*, *8*(3), 809-824.

Kaur, G., & Padmaja, V. (2009). Relationships among activities of extracellular enzyme production and virulence against *Helicoverpa armigera* in *Beauveria bassiana*. *Journal of Basic Microbiology*, *49*(3), 264-274. https://doi.org/10.1002/jobm.200800156

Khachatourians G and Qazi S. (2008). Entomopathogenic Fungi: Biochemistry and Molecular Biology. *Human and Animal Relationships*, 33-61. https://doi.org/10.1007/978-3-540-79307-6_3

Kim, J. S., Roh, J. Y., Choi, J. Y., Wang, Y., Shim, H. J., & Je, Y. H. (2010). Correlation of the aphicidal activity of *Beauveria bassiana* SFB-205 supernatant with enzymes. *Fungal biology*, *114*(1), 120-128. https://doi.org/10.1016/j.mycres.2009.10.011

Laein, M. A., & Mohammadi, A. (2018). Chitinolytic fungi from the birjand plain of southern khorasan province in eastern Iran. *Acta mycologica*, *53*(1). https://doi.org/10.5586/am.1107

Langner, T., & Göhre, V. (2016). Fungal chitinases: function, regulation, and potential roles in plant/pathogen interactions. *Current genetics*, *62*, 243-254. https://doi.org/10.1007/s00294-015-0530-x

Leger, R.J., Charnley, A.K., & Cooper, R.M. (1986). Cuticle-degrading enzymes of entomopathogenic fungi: Synthesis in culture on cuticle. *Journal of Invertebrate Pathology*, 48, 85-95. https://doi.org/ 10.1016/0022-2011(86)90146-1

Li C, HuangW,Wang LX. Chemoenzymatic synthesis of N-linkedneoglycoproteins throughachitinase-catalyzedtransglycosylation.BioorgMed-Chem2008;16:8366–72.

Liu, B. L., Kao, P. M., Tzeng, Y. M., & Feng, K. C. (2003). Production of chitinase from *Verticillium lecanii* F091 using submerged fermentation. *Enzyme and Microbial Technology*, *33*(4), 410-415. https://doi.org/10.1016/S0141-0229(03)00138-8

Liu, D., Cai, J., Xie, C. C., Liu, C., & Chen, Y. H. (2010). Purification and partial characterization of a 36-kDa chitinase from *Bacillus thuringiensis* subsp. colmeri, and its biocontrol potential. *Enzyme and Microbial Technology*, *46*(3-4), 252-256. https://doi.org/10.1016/j.enzmictec.2009.10.007

Liu, S., Du, Y., Zhang, D., Yang, F., He, X., & Long, C. (2022). Aluminum sulfate inhibits green mold by inducing chitinase activity of *Penicillium digitatum* and enzyme activity of citrus fruit. *Food Control*, *136*, 108854. https://doi.org/10.1016/j.foodcont.2022.108854

Loc, N. H., Huy, N. D., Quang, H. T., Lan, T. T., & Thu Ha, T. T. (2020). Characterisation and antifungal activity of extracellular chitinase from a biocontrol fungus, *Trichoderma asperellum* PQ34. *Mycology*, *11*(1), 38-48. https://doi.org/10.1080/21501203.2019.1703839

Lord, J. C., Anderson, S., & Stanley, D. W. (2002). Eicosanoids mediate *Manduca sexta* cellular response to the fungal pathogen *Beauveria bassiana*: a role for the lipoxygenase pathway. *Archives of Insect Biochemistry and Physiology: Published in Collaboration with the Entomological Society of America*, *51*(1), 46-54. https://doi.org/10.1002/arch.10049

Lu, Z. X., Laroche, A., & Huang, H. C. (2005). Isolation and characterization of chitinases from *Verticillium lecanii*. *Canadian Journal of Microbiology*, 51(12), 1045-1055. https://doi.org/10.1139/w05-088

Mahboub, H. H. (2021). Mycological and histopathological identification of potential fish pathogens in *Nile tilapia*. *Aquaculture*, 530, 735849. https://doi.org/10.1016/j.aquaculture.2020.735849

Mannino, M. C., Huarte-Bonnet, C., Davyt-Colo, B., & Pedrini, N. (2019). Is the insect cuticle the only entry gate for fungal infection? Insights into alternative modes of action of entomopathogenic fungi. *Journal of Fungi*, 5(2), 33. https://doi.org/10.3390/jof5020033

Matsumiya, M., Karasuda, S., Miyauchi, K., & Mochizuki, A. (2008). Substrate specificity and partial amino acid sequence of a Chitinase from the stomach of coelacanth *Latimeria chalumnae*. *Fisheries Science*, 74, 1360-1362. https://doi.org/10.1111/j.1444-2906.2008.01669.x

Mohammed, A. A. (2018). *Lecanicillium muscarium* and *Adalia bipunctata* combination for the control of black bean aphid, *Aphis fabae*. *BioControl*, 63(2), 277-287. https://doi.org/ 10.1007/s10526-018-9868-6

Mohammed, A. A., & Hatcher, P. E. (2017). Combining entomopathogenic fungi and parasitoids to control the green peach aphid *Myzus persicae*. *Biological Control*, 110, 44-55. https://doi.org/ 10.1016/j.biocontrol.2017.03.012

Montemayor, C. O., Avery, P. B., & Cave, R. D. (2016). Infection and mortality of *Microtheca ochroloma* (Coleoptera: Chrysomelidae) by *Isaria fumosorosea* (Hypocreales: Cordycipitaceae) under laboratory conditions. *Biocontrol Science and Technology*, 26(5), 605-616. https://doi.org/ 10.1080/09583157.2015.1126222

Mustafa, U., & Kaur, G. (2009). Extracellular enzyme production in *Metarhizium anisopliae* isolates. *Folia Microbiologica*, 54, 499-504. https://doi.org/ 10.1007/s12223-009-0071-0

Nguyen, H. C., Lin, K. H., Nguyen, T. P., Le, H. S., Ngo, K. N., Pham, D. C., ... & Barrow, C. J. (2023). Isolation and Cultivation of *Penicillium citrinum* for Biological Control of *Spodoptera litura* and *Plutella xylostella*. *Fermentation*, 9(5), 438. https://doi.org/ 10.3390/fermentation9050438

Okongo, R. N., Puri, A. K., Wang, Z., Singh, S., & Permaul, K. (2019). Comparative biocontrol ability of chitinases from bacteria and recombinant chitinases from the thermophilic fungus *Thermomyces lanuginosus*. *Journal of Bioscience and Bioengineering*, 127(6), 663-671. https://doi.org/ 10.1016/j.jbiosc.2018.11.007

Ortiz-Rodriguez, T., delaFuente-Salcido, N., Bideshi, D..K, Salcedo-Hernandez, R., Barboza Corona, J.E. (2010). Generation of chitin-derived oligosaccharides toxic to pathogenic bacteria usingChiA74, an endochitinase native to *Bacillus thuringiensis*. *Letters in Applied Microbiology* ,51:184–90.

Ortiz-Urquiza, A., Luo, Z., & Keyhani, N. O. (2015). Improving mycoinsecticides for insect biological control. *Applied Microbiology and Biotechnology*, 99, 1057-1068. https://doi.org/ 10.1007/s00253-014-6270-x

Ownley, B. H., Griffin, M. R., Klingeman, W. E., Gwinn, K. D., Moulton, J. K., & Pereira, R. M. (2008). *Beauveria bassiana*: endophytic colonization and plant disease control. *Journal of Invertebrate Pathology*, 98(3), 267-270. https://doi.org/ 10.1016/j.jip.2008.01.010

Ozdemir, I. O. (2023). Efficacy of diatomaceous earth, and entomopathogenic fungi, *Beauveria bassiana*, and *Trichoderma asperellum* in combination and separately, against *Callosobruchus maculatus* (F.)(Coleoptera: Chrysomelidae). *Egyptian Journal of Biological Pest Control*, 33(1), 48. https://doi.org/ 10.1186/s41938-023-00699-8

Patidar, P., Agrawal, D., Banerjee, T., & Patil, S. (2005). Optimisation of process parameters for chitinase production by soil isolates of *Penicillium chrysogenum* under solid substrate fermentation. *Process Biochemistry*, 40(9), 2962-2967. https://doi.org/ 10.1016/j.procbio.2005.01.013

Patil, N. S., & Jadhav, J. P. (2015). Significance of *Penicillium ochrochloron* chitinase as a biocontrol agent against pest *Helicoverpa armigera*. *Chemosphere*, 128, 231-235. https://doi.org/ 10.1016/j.chemosphere.2015.01.038

Patil, R.S., Ghormade, V.V., Deshpande, M.V. (2000). Chitinolytic enzymes:an exploration. *Enzyme and Microbial Technology*, 26:473–83.

Pedrini, N. (2018). Molecular interactions between entomopathogenic fungi (Hypocreales) and their insect host: Perspectives from stressful cuticle and hemolymph battlefields and the potential of dual RNA sequencing for future studies. *Fungal Biology*, 122(6), 538-545. https://doi.org/ 10.1016/j.funbio.2017.10.003

Pedrini, N., Crespo, R., & Juárez, M. P. (2007). Biochemistry of insect epicuticle degradation by entomopathogenic fungi. *Comparative Biochemistry and Physiology Part C: Toxicology & Pharmacology*, 146(1-2), 124-137. https://doi.org/ 10.1016/j.cbpc.2006.08.003

Pereira, J. L., Franco, O. L., & Noronha, E. F. (2006). Production and biochemical characterization of insecticidal enzymes from Aspergillus fumigatus toward *Callosobruchus maculatus*. *Current Microbiology*, 52, 430-434. https://doi.org/ 10.1007/s00284-005-0192-x

Poveda, J. (2021). Trichoderma as biocontrol agent against pests: New uses for amycoparasite. *Biological Control*, 159, 104634. https://doi.org/ 10.1016/j.biocontrol.2021.104634

Prasanna, L., Eijsink, V. G., Meadow, R., & Gåseidnes, S. (2013). A novel strain of *Brevibacillus laterosporus* produces chitinases that contribute to its biocontrol potential. *Applied Microbiology and Biotechnology*, 97, 1601-1611. https://doi.org/ 10.1371/journal.pone.0090124

Rathore, A. S., & Gupta, R. D. (2015). Chitinases from bacteria to human: properties, applications, and future perspectives. *Enzyme Research*, 2015:791907. https://doi.org/ 10.1155/2015/791907

Rodríguez-González, Á., Guerra, M., Ramírez-Lozano, D., Casquero, P. A., & Gutiérrez, S. (2021). Germination and Agronomic Traits of *Phaseolus vulgaris* L. Beans Sprayed with *Trichoderma* Strains and Attacked by *Acanthoscelides obtectus*. *Agronomy*, 11(11), 2130. https://doi.org/ 10.3390/agronomy11112130

Sebumpan, R., Guiritan, K. R., Suan, M., Abapo, C. J., Bhat, A. H., Machado, R. A., ... & Sumaya, N. H. (2022). Morphological and molecular identification of *Trichoderma asperellum* isolated from a dragon fruit farm in the southern Philippines and its pathogenicity against the larvae of the super worm, *Zophobas morio* (Fabricius, 1776) (Coleoptera: Tenebrionidae). *Egyptian Journal of Biological Pest Control*, 32(1), 1-7. https://doi.org/ 10.1186/s41938-022-00548-0

Shahriari, M., Zibaee, A., Khodaparast, S.A., Fazeli-Dinan, M. (2021). Screening and virulence of the entomopathogenic fungi associated with *Chilo suppressalis* Walker. *Journal of Fungi*, 7, 34. https://doi.org/ 10.3390/jof7010034

Sharma, H., Rai, A. K., Chettri, R., & Nigam, P. S. (2021). Bioactivites of *Penicillium citrinum* isolated from a medicinal plant *Swertia chirayita*. *Archives of Microbiology*, 203, 5173-5182. https://doi.org/ 10.1007/s00203-021-02498-x

Sheng, J., An, K., Deng, C., Li, W., Bao, X., & Qiu, D. (2006). Cloning a cuticle-degrading serine protease gene with biologic control function from *Beauveria*

brongniartii and its expression in *Escherichia coli*. *Current Microbiology*, 53, 124-128. https://doi.org/ 10.1007/s00284-005-5336-5

Singh, S., Ramanujam, B., Sandhu, R. K., Kandan, A., Poornesha, B., & Kundu, R. (2021). Natural occurrence of entomopathogenic fungus, *Aschersonia aleyrodis* on citrus whitefly, *Dialeurodes citri* (Ashmead) in Kinnow mandarin in Punjab, India. *Journal of Biological Control*, 181-186. https://doi.org/ 10.18311/jbc/2021/29506

Soares, A. M. D. S., Araújo, S. A. D., Lopes, S. G., Junior, C., & Martins, L. (2015). Anthelmintic activity of *Leucaena leucocephala* protein extracts on *Haemonchus contortus*. *Revista Brasileira de Parasitologia Veterinária*, 24(4), 396-401, https://doi.org/10.1590/S1984-29612015072

Song, Y., Liu, X., Feng, S., Zhao, K., Qi, Z., Wu, W., ... & Qin, B. (2023). Discovery, Identification, and Insecticidal Activity of an *Aspergillus flavus* Strain Isolated from a Saline–Alkali Soil Sample. *Microorganisms*, 11(11), 2788. https://doi.org/ 10.3390/microorganisms11112788

Sönmez, E., Sevim, A., Demirbağ, Z., & Demir, I. (2016). Isolation, characterization, and virulence of entomopathogenic fungi from *Gryllotalpa gryllotalpa* (Orthoptera: Gryllotalpidae). *Applied Entomology and Zoology*, 51, 213-223. https://doi.org/ 10.1007/s13355-015-0390-3

St Leger, R. J., Bidochka, M. J., & Roberts, D. W. (1994). Isoforms of the cuticle-degrading Pr1 proteinase and production of a metalloproteinase by *Metarhizium anisopliae*. *Archives of Biochemistry and Biophysics*, 313(1), 1-7. https://doi.org/10.1006/abbi.1994.1350

St Leger, R., Joshi, L., Bidochka, M.J., Roberts, D.W. (1996). Construction of an improved mycoinsecticide overexpressing a toxic protease. *Proceedings of the National Academy of Sciences*, 93(13):6349-54. https://doi.org/ 10.1073/pnas.93.13.6349.

Stączek, S., Zdybicka-Barabas, A., Wiater, A., Pleszczyńska, M., & Cytryńska, M. (2020). Activation of cellular immune response in insect model host *Galleria mellonella* by fungal α-1, 3-glucan. *Pathogens and Disease*, 78(9), ftaa062. https://doi.org/10.1093/femspd/ftaa062

Sun, M., & Liu, X. (2006). Carbon requirements of some nematophagous, entomopathogenic and mycoparasitic hyphomycetes as fungal biocontrol agents. *Mycopathologia*, 161, 295-305. https://doi.org/10.1007/s11046-006-0249-9

Tajdini, F., Amini, M.A., Nafissi-Varcheh, N., Faramarzi, M.A. (2010). Production, physiochemical and antimicrobial properties of fungal chitosan from *Rhizomu cormiehei* and *Mucor racemosus*. *International Journal of Biological Macromolecules*, 47:180–3.

Tu, S., Qiu, X., Cao, L., Han, R., Zhang, Y., & Liu, X. (2010). Expression and characterization of the chitinases from *Serratia marcescens* GEI strain for the control

of *Varroa destructor*, a honeybee parasite. *Journal of Invertebrate Pathology*, 104(2), 75-82. https://doi.org/10.1016/j.jip.2010.02.002.

Vega, K., Kalkum, M. (2012). Chitin, chitinase responses, and invasive fungal infections. *International Journal of Microbiology*, 2012:920459.

Vijayakumar, N., & Alagar, S. (2017). Consequence of chitinase from *Trichoderma viride* integrated feed on digestive enzymes in *Corcyra cephalonica* (Stainton) and antimicrobial potential. *Biosciences Biotechnology Research Asia*, 14(2), 513. https://doi.org/ 10.13005/bbra/2473

Wamiti, L. G., Khamis, F. M., Abd-Alla, A. M., Ombura, F. L., Akutse, K. S., Subramanian, S., ... & Maniania, N. K. (2018). *Metarhizium anisopliae* infection reduces *Trypanosoma congolense* reproduction in *Glossina fuscipes* and its ability to acquire or transmit the parasite. *BMC Microbiology*, 18, 271-278. https://doi.org/ 10.1186/s12866-018-1277-6

Wang, L., Huang, J., You, M., & Liu, B. (2004). Time-dose-mortality modelling and virulence indices for six strains of *Verticillium lecanii* against sweetpotato whitefly, *Bemisia tabaci* (Gennadius). *Journal of Applied Entomology*, 128(7), 494-500. https://doi.org/ 10.1111/j.1439-0418.2004.00879.x

Wang, Z., Ali, S., Huang, Z., & Ren, S. (2012). Production and regulation of extracellular chitinase by *Aschersonia aleyrodis* (Cordycipitaceae: Hypocreales). *Pakistan Journal of Zoology*, 44(5). https://doi.org/ 10.1590/S1517-838220090003000026

Yu, T., Wang, L., Yin, Y., Wang, Y., & Zheng, X. (2008). Effect of chitin on the antagonistic activity of *Cryptococcus laurentii* against *Penicillium expansum* in pear fruit. *International Journal of Food Microbiology*, 122(1-2), 44-48. https://doi.org/ 10.1016/j.ijfoodmicro.2007.11.059

Zakariassen, H., Hansen, M.C., Joranli, M., Eijsink, V.G., Sqrlie,M. (2011). Mutational effects on transglycosylating activity of family 18 chitinases and constructionof a hyper trans glycosylating mutant. *Biochemitry*, 50:5693–703.

Zhang, C., Ali, S., Musa, P. D., Wang, X. M., & Qiu, B. L. (2017). Evaluation of the pathogenicity of *Aschersonia aleyrodis* on *Bemisia tabaci* in the laboratory and greenhouse. *Biocontrol Science and Technology*, 27(2), 210-221. https://doi.org/ 10.1080/09583157.2016.1274878

Zhang, M., Puri, A. K., Govender, A., Wang, Z., Singh, S., & Permaul, K. (2015b). The multi-chitinolytic enzyme system of the compost-dwelling thermophilic fungus *Thermomyces lanuginosus*. *Process Biochemistry*, 50(2), 237-244. https://doi.org/ 10.1016/j.procbio.2014.11.008

Zhang, Y. X., Sun, L., Lin, G. Y., Lin, J. Z., Chen, X., Ji, J., ... & Saito, Y. (2015a). A novel use of predatory mites for dissemination of fungal pathogen for insect biocontrol: The case of *Amblyseius swirskii* and *Neoseiulus cucumeris* (Phytoseiidae) as vectors of *Beauveria bassiana* against *Diaphorina citri* (Psyllidae).

Systematic and Applied Acarology, 20(2), 177-187. https://doi.org/10.11158/saa.20.2.4

Zimmermann, G. (2008). The entomopathogenic fungi *Isaria farinosa* (formerly *Paecilomyces farinosus*) and the *Isaria fumosorosea* species complex (formerly *Paecilomyces fumosoroseus*): biology, ecology and use in biological control. *Biocontrol Science and Technology*, 18, 865-901. https://doi.org/10.1080/09583150802471812

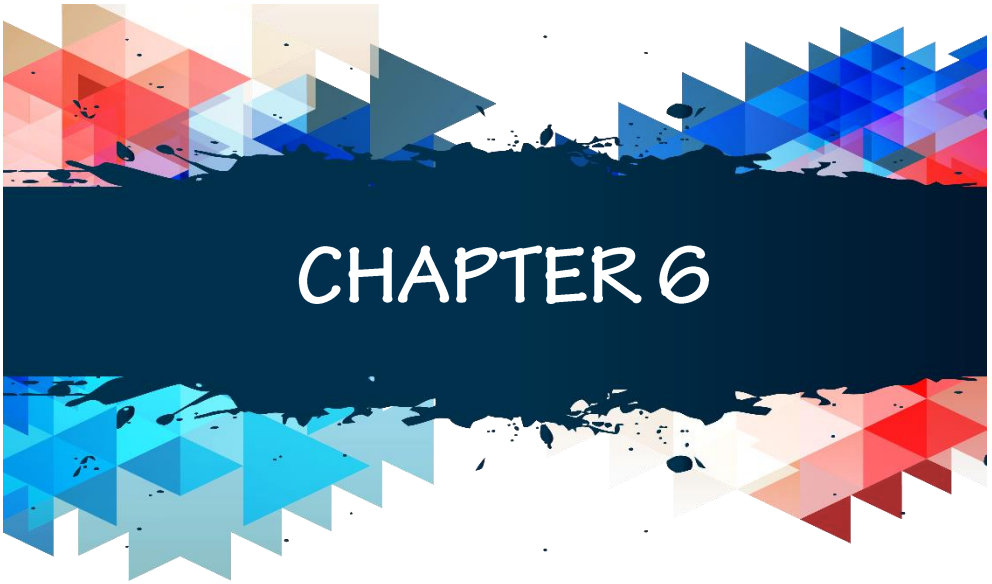

A Strong Approximation for Singularly Perturbed Delay Volterra Integro Differential Equation

***Derya Arslan*[1]**

1 Assoc. Prof. Dr., Bitlis Eren University, ORCID: 0000-0001-6138-0607

Introduction

Many natural events in the world can show sudden chages depending on different variables. Especially in science and mathematics disciplines, such sudden changes are called small deviation analysis (singular and regular perturbation). This theory first emerged with Prandtl's study on the existence of boundary layers presented at the 3rd International Mathematics Congress held in Heidelberg in 1904 and has a deep-rooted history extending to the present day with the contributions of Lindstedt and Poincare. Singular Perturbation problems express that the coefficients of the terms of the highest order derivatives are quite small, that is, a constant parameter between zero and one. The exact and approximate solutions of such problems show very fast and scattered changes in the sensitive transition regions called the extreme (boundary) layer of the definition set, while they show slow and rhythmic changes in other places. As a result of such scattering, infinite derivatives occur in the solution. This situation is especially visible in the boundary layers and increases the complex structure of the solution even more. Thus, very serious problems occur in the mechanism of problems with singular perturbation properties.

These problems especially manifest themselves in the process of analyzing the sudden and irregular changes occurring in the boundary layers and determining the effect of these changes on the general solution of the problem. Singular perturbation theory requires special methods and techniques to understand and solve these complex behaviors. These characteristic situations also manifest themselves clearly in numerical solutions. Since known classical numerical methods generally do not give results towards the correct solution, it is necessary to use effective numerical methods that converge regularly with respect to, which is quite small, that is, between zero and one (closer to zero), in solving exactly this type of problems [2,5,13,18,19-21,23,25,26,28].

Differential equations with conditions that connect the values of the unknown solution at the boundary with the values inside are known as nonlocal boundary value problems. Problems with integral nonlocal conditions can be encountered when studying heat transfer problems [1,3,4,9-12,14,15,17,22,21,24].

Volterra integr-differential equations are used in many different areas of science and engineering: Oceanography, fluid mechanics, electromagnetic theory, financial mathematics, plasma physics, population dynamics, artificial neural networks, and biological processes [18,23].

In this study, the solution of delay singularly perturbed Volterra integro-differential equation with integral boundary condition is investigated by the

numerical integration method. The solution of the following problem has a boundary layer at the point $x = b$.

$$-\varepsilon v''(t) + a(t)v'(t) + b(t)v(t) - v(t-\theta) = g(t),$$

$$t \in (a,b), v(a) = K_1,\ t \in [a-\theta, b-\theta], \quad \theta > 0,$$

$$Kv(b) = v(b) - \varepsilon \int_0^b \frac{t}{d} v(t)dt = b,$$

where, $a(t)$, $b(t)$, $g(t)$ are continuous functions; a, b, d, K and K_1 are finite constants.

The Method and Application of the Method

In this section, an example involving the following three difficult cases of nonlocal (integral) boundary condition, delay term and singular perturbation term is solved to demonstrate the approximate solution by the numerical integration method [6-8,16,26,27,29]:

The numerical integration procedure as:

- ✓ Th delay term of the equation is arranged according to the Taylor expansion.
- ✓ The integration is taken according to the left or right boundary layer of the first equation.
- ✓ Some integrations are solved by trapezoid method.
- ✓ Difference derivatives are used and finite difference equation is obtained. It is solved with the Thomas algorithm.

• If the problem has a boundary layer on the right, the numerical integration method will be as follows:

$$-\boldsymbol{\varepsilon v''(t) + a(t)v'(t) + b(t)v(t) - v(t-\theta) = g(t)},$$
$$\boldsymbol{0 < t < 1, \quad \theta > 0}, \qquad (\mathbf{1})$$

$$\boldsymbol{v(0) = K_1, \quad t \in [-\theta, 1-\theta], \quad \theta > 0}, \qquad (\mathbf{2})$$

$$\boldsymbol{Kv(1) = v(1) - \varepsilon \int_0^1 \frac{t}{d} v(t)dt = 1}, \qquad (\mathbf{3})$$

In equation (2.1), $\boldsymbol{a(t) < \gamma < 0}$, $\boldsymbol{\gamma}$ constant indcates the existence of a right boundary layer around the point $\boldsymbol{t = 1}$.
Again, if the $\boldsymbol{v(t-\theta) = v(t) - \theta v'(t)}$ Taylor expansion is written instead of the delay term in the equation (1) [16].

$$\boldsymbol{\varepsilon v''(t) + a(t)v'(t) + b(t)[v(t) - \theta v'(t)] = g(t),} \qquad (\mathbf{4})$$
$$\boldsymbol{\varepsilon v''(t) + [a(t) - \theta b(t)]v'(t) + b(t)v(t) = g(t).} \qquad (\mathbf{5})$$

The equations (4)-(5) are obtained, respectively.
If the interval $[\mathbf{0}, \mathbf{1}]$ is divided into equal parts $\boldsymbol{N}$ for $\boldsymbol{i = 1, 2, \dots, N-1}$, the integral of the equation (1) in the interval $[\boldsymbol{t_{i-1}, t_i}]$ is taken as follows:

$$\int_{t_{i-1}}^{t_i} \boldsymbol{\varepsilon v''(t) + [a(t) - \theta b(t)]v'(t) + b(t)v(t)} = \int_{t_{i-1}}^{t_i} \boldsymbol{g(t)},$$

and

$$\boldsymbol{\varepsilon v'(t_i) - \varepsilon v'(t_{i-1}) + [a_i - \theta b_i]v(t_i) - [a_{i-1} - \theta b_{i-1}]v(t_{i-1})} + \int_{t_{i-1}}^{t_i} \boldsymbol{b(t)v(t)\,dt} = \int_{t_{i-1}}^{t_i} \boldsymbol{g(t)\,dt},$$

is organized in the above equation.
Here, instead of the $\boldsymbol{v'(t_i)}$ and $\boldsymbol{v'(t_{i-1})}$ derivatives $\boldsymbol{v'_{i-1} = \frac{v_i - v_{i-1}}{h}}$ and $\boldsymbol{v'_i = \frac{v_{i+1} - v_i}{h}}$ difference derivatives are used. If the trapezoidal method is applied instead of integrals, the following equation is obtained:

$$\boldsymbol{\varepsilon \frac{v_{i+1} - v_i}{h} - \varepsilon \frac{v_i - v_{i-1}}{h} + [a_i - \theta b_i]v(t_i) - [a_{i-1} - \theta b_{i-1}]v(t_{i-1})} + \frac{\boldsymbol{h}}{\mathbf{2}}\boldsymbol{[b_i v_i + b_{i-1} v_{i-1}]} = \frac{\boldsymbol{h}}{\mathbf{2}}\boldsymbol{[g_i + g_{i-1}]}.$$

Here, after making the necessary arrangements according to $\boldsymbol{v_{i-1}, v_i, v_{i+1}}$ in the previous step

$$v_{i-1}\left(\frac{\varepsilon}{h}-a_{i-1}+\sigma b_{i-1}+h\frac{b_{i-1}}{2}\right)-v_i\left(\frac{2\varepsilon}{h}-a_i+\sigma b_i+h\frac{b_i}{2}\right)+v_{i+1}\left(\frac{\varepsilon}{h}\right)$$
$$=\frac{h}{2}[g_i+g_{i-1}],$$

the differen
ce equation occurs as above. If the boundary conditions are added to this difference equation, the following difference problem is found as.

$$v_{i-1}\left(\frac{\varepsilon}{h}-a_{i-1}+\sigma b_{i-1}+h\frac{b_{i-1}}{2}\right)-v_i\left(\frac{2\varepsilon}{h}-a_i+\sigma b_i+h\frac{b_i}{2}\right)+v_{i+1}\left(\frac{\varepsilon}{h}\right)$$
$$=\frac{h}{2}[g_i+g_{i-1}], \qquad (6)$$
$$v_0=A, \quad v_N=\frac{1}{1-K}\sum_{j=0}^{N-1}ht_jv_j+1. \qquad (7)$$

The difference problem (6)-(7) is solved using the Thomas algorithm given below as [9].

$$A_i=\frac{\varepsilon}{h}-a_{i-1}+\sigma b_{i-1}+h\frac{b_{i-1}}{2}, \quad B_i=\frac{\varepsilon}{h},$$
$$C_i=\frac{2\varepsilon}{h}-a_i+\sigma b_i+h\frac{b_i}{2}, \quad F_i=-\frac{h}{2}[g_i+g_{i-1}].$$

• If the problem has a left boundary layer, the numerical integration method will be as follows:

The equation (2.1) must be a fixed condition $a(t)>\alpha>0$, α for being a left-boundary problem. The steps are very similar to the right-boundary problem, but it has its own unique properties and can be expressed as follows.
First of all, the integral of all terms in equation (1) for $i=0,1,\dots,N-1$ is taken in the interval $\left[t_i,t_{i+1}\right]$ and the trapezoidal method is used. As a result, approximate solution is found with Thomas algorithm as.

$$\alpha_1=0, \quad \beta_1=A,$$
$$\alpha_{i+1}=\frac{B_i}{C_i-\alpha_iA_i}, \quad \beta_{i+1}=\frac{F_i+\beta_iA_i}{C_i-\alpha_iA_i},$$
$$v_i=\alpha_{i+1}v_{i+1}+\beta_{i+1}, \quad i=N-1,\dots,2,1.$$

With the theory given above, delay singularly perturbed Volterra integro-differential equation with integral boundary condition is solved approximately by the numerical integration method. The application of this problem is made for an example given below which has a right boundary layer.

Example 1

The approximate solution of the following delay singularly perturbed Volterra integro-differential equation with integral boundary condition will be obtained by the numerical integral method.
Since the coefficient of the second term of the problem is $-\mathbf{3} < \mathbf{0}$, it is a right boundary layer problem.

$$-\varepsilon \mathbf{v}''(\mathbf{t}) + \mathbf{3}\mathbf{v}'(\mathbf{t}) + \mathbf{v}(\mathbf{t}) - \mathbf{v}(\mathbf{t}-\mathbf{1}) = \mathbf{1}, \mathbf{t} \in (\mathbf{0},\mathbf{1}) \cup (\mathbf{1},\mathbf{2}) \quad (\mathbf{8})$$

$$\mathbf{v}(\mathbf{t}) = \mathbf{1}, \quad \mathbf{t} \in [-\mathbf{1},\mathbf{0}], \quad \theta > \mathbf{0}, \quad (\mathbf{9})$$

$$\mathbf{K}\mathbf{v}(\mathbf{2}) = \mathbf{v}(\mathbf{2}) - \varepsilon \int_{\mathbf{0}}^{\mathbf{2}} \frac{\mathbf{t}}{\mathbf{3}} \mathbf{v}(\mathbf{t})\mathbf{dt} = \mathbf{2}. \quad (\mathbf{10})$$

Here, instead of the delay term $\mathbf{u}(\mathbf{t}-\mathbf{1})$ the following expression is written by

$$\mathbf{v}(\mathbf{t}-\mathbf{1}) = \mathbf{v}(\mathbf{t}) - \mathbf{v}'(\mathbf{t}),$$

$$\varepsilon \mathbf{v}''(\mathbf{t}) - \mathbf{4}\mathbf{v}'(\mathbf{t}) = -\mathbf{1}, \int_{\mathbf{t_{i-1}}}^{\mathbf{t_i}} (\varepsilon \mathbf{v}''(\mathbf{t}) - \mathbf{4}\mathbf{v}'(\mathbf{t}))\, \mathbf{dt} = -\int_{\mathbf{t_{i-1}}}^{\mathbf{t_i}} \mathbf{1}\mathbf{dt},$$

it is found and after the integration operations

$$\varepsilon \mathbf{v}'(\mathbf{t_i}) - \varepsilon \mathbf{v}'(\mathbf{t_{i-1}}) - \mathbf{4}\mathbf{v}(\mathbf{t_i}) + \mathbf{4}(\mathbf{t_{i-1}}) = \int_{\mathbf{t_{i-1}}}^{\mathbf{t_i}} \mathbf{1}\mathbf{dt},$$

is obtained. Here, the trapezoidal method is applied to the integral and the necessary arrangements are made,

$$\varepsilon \mathbf{v}_\mathbf{i}' - \varepsilon \mathbf{v}_{\mathbf{i-1}}' - \mathbf{4}\mathbf{v}_\mathbf{i} + \mathbf{4}\mathbf{v}_{\mathbf{i-1}} = -\mathbf{h},$$

the equation is obtained as follows. However,

$\mathbf{w'_{i+1}} = \frac{\mathbf{w_{i+1}} - \mathbf{w_i}}{\mathbf{h}}$ and $\mathbf{w'_i} = \frac{\mathbf{w_i} - \mathbf{w_{i-1}}}{\mathbf{h}}$, $\mathbf{i = 1, 2, \dots, N - 1}$ the forward and back difference approach is applied as

$$\varepsilon\left(\frac{v_{i+1} - v_i}{h}\right) - \varepsilon\left(\frac{v_i - v_{i-1}}{h}\right) - 4v_i + 4v_{i-1} = -h, \qquad ()$$

difference equation is formed. Then, if the equation is adjusted as follows and the limit values are added

$$\mathbf{v_{i-1}\left(\frac{\varepsilon}{h} + 4\right) - v_i\left(\frac{2\varepsilon}{h} + 4\right) + v_{i+1}\left(\frac{\varepsilon}{h}\right) = -h},$$

$$\mathbf{v_0 = A}, \quad \mathbf{v_N = \frac{1}{1 - K}\sum_{j=0}^{N-1} ht_j v_j + 1}.$$

difference boundary value problem occurs.

The solution for this problem is provided by the Thomas algorithm method explained as for $\mathbf{i = 1, 2, \dots, N - 1}$,

$$\mathbf{A_i = \frac{\varepsilon}{h} + 4, B_i = \frac{\varepsilon}{h}, C_i = \frac{2\varepsilon}{h} + 4, F_i = h}, \qquad \boldsymbol{\alpha_1 = 0}, \ \boldsymbol{\beta_1 = 1},$$

$$\boldsymbol{\alpha_{i+1} = \frac{\frac{\varepsilon}{h}}{\left(\frac{2\varepsilon}{h} + 4\right) - \left(\frac{\varepsilon}{h} + 4\right)\alpha_i}, \beta_{i+1} = \frac{h + \left(\frac{\varepsilon}{h} + 4\right)\beta_i}{\left(\frac{2\varepsilon}{h} + 4\right) - \left(\frac{\varepsilon}{h} + 4\right)\alpha_i}}.$$

By following the steps of the above algorithm, the approximate solution through a suitable mathematical program and numerical results are obtained. It is shown with tables and figures.

Table 1. The approximate solutions for different ε, N

ε/N	16	32	64	128	256
1	0.140000	0.007000	0.0036711	0.0018360	0.0009182
$2^{(-1)}$	0.0194550	0.113640	0.0062494	0.0033030	0.0017025
$2^{(-2)}$	0.0338763	0.0225885	0.0139547	0.0078947	0.0042234
$2^{(-3)}$	0.0400197	0.0373979	0.0249325	0.0155844	0.0088664

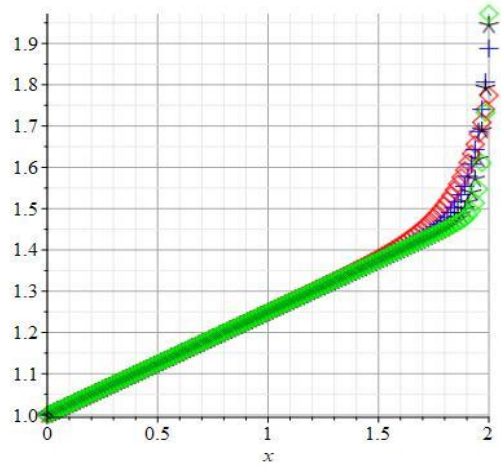

Figure 1. Approximate solutions for $N = 128$, $\varepsilon = 2^{-1}, 2^{-2},\ 2^{-3}, 2^{-4}$

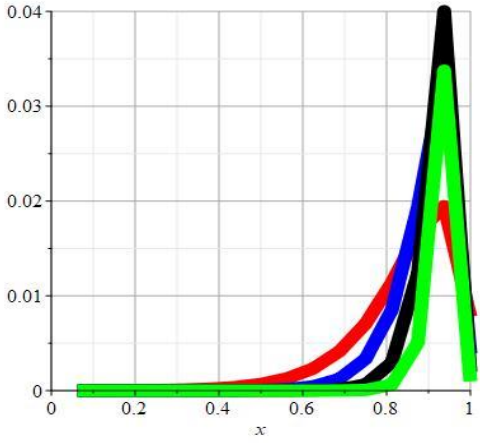

Figure 2. Error distributions for $N = 16$, $\varepsilon = 2^{-1}, 2^{-2},\ 2^{-3}, 2^{-4}$

With the Table 1, the maximum errors are obtained for the values of $\varepsilon = 2^{-1}, 2^{-2}, 2^{-3}, 2^{-4}$ and $N = 16$. Approximate solution and error curves are drawn. The errors are maximum around the $x = 1$ boundary layer. As the values of ε decrease, the approximate solution curves lean touards the axes. With these results, it is seen that the proposed method solves the problem considered in the study stably. Thus, it is presented how suitable, reliable and fast the numerical integral method is for integral boundary layer case problems with delayed singular perturbation.

CONCLUSION

In this study, delay singularly perturbed Volterra integro-differential equation with integral boundary condition was investigated by the numerical integration method. An example application was made. The results of the approximate solution and error were shown uith tables and figures. It was also seen that the solution showed sudden, fast and irregular changes in the sensitive transition region around the point $x = 1$.

As a result, it was seen how easily and quickly the numerical integration method used in this study solved the application example with a suitable mathematical program

For contribution to the literature, approximate solutions of fractional order and fuzzy differential equations with delayed types can be investigated by the numerical integration method.

References

1. Adzic, N. (2000). Spectral approximation and nonlocal boundary value problems. Novi Sad Journal of Mathematics, 30, 1-10.
2. Amiraliyev, G. M. & Amirali, I. (2018). *Nümerik analiz teori ve uygulamalarla*. Ankara: Seçkin Yayınevi.
3. Amiraliyev, G. M., Amiraliyeva, I. G. & Kudu, M., (2007). A numerical treatment for singularly perturbed differential equations with integral boundary condition. Applied Mathematics and Computation, 185, 574-582.
4. Amiraliyev, G. M. & Çakır, M. (2002). Numerical solution of the singularly perturbed problem with nonlocal boundary condition. Applied Mathematics and Mechanics, (English Ed.) 23, 755 764.
5. Amiraliyev, G. M. & Erdoğan, F. (2007). Uniform numerical method for singularly perturbed delay differential equations. Computers & Mathematics Applications, 53, 1251-1259.
6. Andargie, A. & Reddy, Y. N. (2008). Numerical integration method for singular perturbation problems with mixed boundary conditions. Journal of Applied Mathematics & Informatics, 26(5-6), 1273-1287.
7. Arslan, D. (2020). A numerical solution for singularly perturbed multi-point boundary value problems with the numerical integration method. BEU Journal of Science, 9(1), 157-167.
8. Arslan, D. (2022). Approximate solution of singularly perturbed problems with numerical integration method. Yüzüncü Yıl Üniversitesi Fen Bilimleri Enstitüsü Dergisi, *27*(3), 612-618.
9. Arslan, D. (2023). A Robust Numerical Approach for Singularly Perturbed Problem with Integral Boundary Condition. Gazi University Journal of Science, 36(4), 1647-1656.
10. Arslan, D. & Çakır, M. (2022). Numerical simulation for singularly perturbed problem with two nonlocal boundary conditions. Turkish Journal of Mathematics and Computer Science, 14(2), 235-247.
11. Arslan, D. (2023). A Robust numerical approach for singularly perturbed problem with integral boundary condition. Gazi University Journal of Science, 36(4), 1647-1656.
12. Bitsadze, A. V. & Samarskii, A. A. (1969). On some simpler generalization of linear elliptic boundary value problems. Doklady Akademii Nauk SSSR, 185: 739-740.
13. Cakir, M. & Arslan, D. (2015). The Adomian decomposition method and the differential transform method for numerical solution of multi-pantograph delay differential equations. Applied Mathematics, 6, 1332-1343.

14. Cakir, M. & Arslan, D. (2021). A neu numerical approach for a singularly perturbed problem with two integral boundary conditions. Computational & Applied Mathematics, 40(6).

15. Cakir, M. & Amiraliyev, G. M. (2005). A finite difference method for the singularly perturbed problem with nonlocal boundary condition. Applied Mathematics and Computation, 160, 539-549.

16. Cengizci, S. (2017). An asymptotic-numerical hybrid method for solving singularly perturbed linear delay differential equations. International Journal of Differential Equations, 2017(8).

17. Chegis, R. (1988). The Numerical solution of problems uith small parameter at higher derivatives and nonlocal conditions. Lietuvos Matematikos Rinkinys (in Russian), 28, 144-152.

18. Diekmann, O. (1978). Thresholds and travelling waves for the geographical spread of infection. J. Math. Biol., 6, 109-130.

19. Doolan, E. R., Miller, J. J. H. & Schilders, W. H. A. (1980). *Uniform numerical methods for problems with initial and boundary layers*. Dublin: Boole Press.

20. Elango S. & Tamilselvan A. (2018). Singularly perturbed delay differential equations of convection–diffusion type with integral boundary condition. Journal of Applied Mathematics and Computing · doi: 10.1007/s12190-018-1198-4.

21. Farrell, P. A., Hegarty, A. F., Miller, J. J. H., O'Riordan, E. & Shishkin, G. I. (2000). *Robust Computational Techniques for Boundary Layers*. New York: Chapman Hall/CRC.

22. Herceg D. & Surla K. (1991). Solving a nonlocal singularly perturbed nonlocal problem by splines in tension. Univ. u Novom Sadu Zb. Rad. Prirod.-Mat. Fak. Ser. Math., 21 (2), 119- 132.

23. Lakshmikantham, V. (1995). Theory of Integro-differential Equations. CRC press.

24. Ma, R. (1997). Existence theorems for a second order m-point boundary value problem. Journal of Mathematical Analysis and Applications, 211, 545-555.

25. O'Malley, R. E. (1991). *Singular Perturbations Methods for Ordinary Differential Equations.* New York: Springer-Verlag.

26. Ranjan, R. & Prasad, H. S. (2018). An efficient method of numerical integration for a class of singularly perturbed two point boundary value problems. Mathematics, 17, 265-273.

27. Reddy, Y. N. (1990). A Numerical integration method for solving singular perturbation problems. Applied Mathematics and Computation, 37, 83-95.

28. Roos, H. G., Stynes, M. & Tobiska, L. (1996). *Numerical Methods for Singularly Perturbed Differential Equations*. Berlin: Springer-Verlag.

29. Soujanya, G. & Phnaeendra, K. (2015). Numerical intergration method for singular-singularly perturbed two- point boundary value problems. Procedia Engineering, 127, 545-552.

CHAPTER 7

A Brief Comparison of Two Molecular Docking Tools: Cbdock2 vs Seamdock

Can Yılmaz[1] & Metin Konuş[2]

1 Doç. Dr., Van Yüzüncü Yıl Üniversitesi, Fen Fakültesi, Moleküler Biyoloji ve Genetik Bölümü, ORCID: 0000-0002-0028-6614, cyilmaz@yyu.edu.tr (*): Sorumlu yazar
[2] Doç. Dr., Van Yüzüncü Yıl Üniversitesi, Fen Fakültesi, Moleküler Biyoloji ve Genetik Bölümü, ORCID: 0000-0002-9953-1375

A. Introduction

In recent years, molecular docking has emerged as a crucial component of in-silico drug development. This method entails making atomic-level predictions about how a small molecule and a protein will interact. This makes it possible for scientists to examine how tiny compounds behave within a target protein's binding site and comprehend the basic biochemical mechanism underpinning this interaction (Meng et al. 2011). The method is structure-based and necessitates a high-resolution three-dimensional representation of the target protein, which can be acquired using methods such as nuclear magnetic resonance spectroscopy, cryo-electron microscopy, or X-ray crystallography (Agu et al. 2023).

Protein–ligand or protein–protein docking is a crucial technique in contemporary drug development that uses shape and electrostatic interactions to quantify the orientation of the ligand when it is coupled to an enzyme or protein receptor. Along with Coulombic interactions and hydrogen bond formation, van der Waals interactions are also significant. A docking score, which indicates the potentiality of binding, is an approximation of the sum of all these interactions. The ligand is searched in a six-dimensional rotational or translational space to fit in the binding site in the most basic rigid-body systems, which can be used as a lead molecule for drug creation (Ferreira et al. 2015).

The first step is to sample ligand conformations based on the active site of the protein. Second, a scoring system is used to rank the conformations. Theoretically, sampling algorithms should replicate experimental binding modes, and a scoring function should be used to score the confirmed results (Kontoyianni 2017).

The goal of automated molecular docking software is to decipher and predict molecular recognition on two levels: energetically by predicting binding affinity and structurally by identifying likely binding patterns. The dynamic interaction between a small molecule and a target macromolecule is where this computational effort mostly takes place (Zhao, Cao, and Zhang 2020).

For molecular docking approaches, a number of free and commercial computational tools and algorithms are available. Drug research and academic disciplines are currently using these programs and tools that have been developed (Stanzione, Giangreco, and Cole 2021). AutoDock Vina, Discovery Studio, Surflex, AutoDock GOLD, Glide, MCDock, MOE-Dock, FlexX, DOCK, LeDock, rDock, ICM, Cdcker, LigandFit, FRED, and UCSF Dock are among the most widely used docking applications. The top ranked poses with the highest scores were predicted by AutoDock Vina, GOLD, and MOE-Dock out of all these

programs. LeDock and GOLD were successful in determining the proper ligand binding positions. But the others also offer some benefits that are easy to use (Mursal et al. 2024; Pagadala, Syed, and Tuszynski 2017).

In this study, we compared two online molecular docking tools that are not among the most popular molecular docking software available, but are becoming preferred in more and more studies due to their differences in both usage and working principles. After briefly comparing CBDock2 and SeamDock software on criteria such as methodologies, operating principles, advantages and limitations, an application analysis was also carried out in the last section. Acetylcholinesterase, a well-known enzyme, and galantamine, one of the three well-known inhibitors of this enzyme, were subjected to blind docking analysis with CBDock2 and SeamDock software. The results obtained were examined in the best docking position, indicating the bonds and interactions.

The web-based molecular docking programs CBDock2 and SeamDock are both utilised, especially in biomolecular research. By modelling potential interactions between two molecules, these techniques assist researchers in predicting the three-dimensional structures of protein-protein and protein-ligand complexes. Despite having the same objective, they differ greatly in terms of methodology, features, and capacities.

B. A thorough analysis contrasting software

B.1. Overview and Purpose

CBDock2:

CBDock2 is an expansion of the CBDock method, which predicts protein-protein/ligand interactions using a coarse-grained docking approach. It is made especially for blind docking, which is used when the binding location is unknown. CBDock2 performs well for docking both unbound proteins and is very effective at managing huge and complicated docking problems. It chooses the most likely configuration of protein-protein/ligand interaction by ranking various docking poses using a knowledge-based scoring mechanism.

SeamDock:

SeamDock is a more recent tool, focused on high-accuracy protein docking. It predicts docking results by integrating numerous scoring systems using a deep learning-based methodology. SeamDock can be used to dock unbound proteins as well as in situations when the binding sites are known. The program offers comprehensive data, frequently including docking along with the prediction of protein-protein interaction sites.

B.2. Methodology

CBDock2:

Coarse-grained docking: CBDock2 does not explicitly describe every atomic feature during the first search phase because it is a coarse-grained docking simulation. For big systems, this method is quicker and more effective.

Flexible docking: It permits protein structures to be somewhat flexible in order to accommodate conformational changes that occur during docking.

Scoring: CBDock2 ranks the docking poses according to their propensity to establish a stable connection using a knowledge-based scoring function that has been trained on experimental data.

SeamDock:

Deep learning-based: To anticipate docking positions, SeamDock uses machine learning methods. To maximise its predictions, it incorporates training data and several scoring systems.

High accuracy scoring: The tool employs more sophisticated scoring based on statistical learning in addition to more conventional energy-based functions. Predicting possible binding sites on proteins is one area in which SeamDock excels, and this ability can be highly helpful when docking unbound proteins.

Atomic-level resolution: SeamDock typically produces more thorough, physically precise docking predictions since it operates at a greater resolution than CBDock2.

B.3. Performance and Speed

CBDock2:

Speed: CBDock2 is made to dock massive systems quickly. It is frequently chosen when docking relatively large protein complexes or when one or both proteins' structures are unknown (a process known as blind docking).

Efficiency: CBDock2 can handle a large number of docking poses and efficiently search the protein-protein interaction space in a shorter amount of time thanks to the coarse-grained methodology.

Scalability: CBDock2 can handle big datasets or libraries of protein complexes and is scalable for high-throughput docking pose screening.

SeamDock:

Speed: SeamDock can be slower than CBDock2, particularly for big complexes or while blind docking, even though it is more precise thanks to its atomic-level precision and deep learning methods.

Computational resources: In order to process complicated situations in a fair period of time, SeamDock's deep learning-based techniques might be computationally costly and require additional resources (such as GPU acceleration).

Throughput: Because SeamDock prioritises accuracy above speed, it might be slower for large-throughput applications. However, it works incredibly well when a small number of docking predictions require great accuracy.

B.4. Accuracy and Resolution

CBDock2:

Accuracy: For protein-protein and protein/ligand docking, CBDock2 offers a respectably high degree of accuracy, particularly in blind docking scenarios when the binding location is unknown. When fine-grained accuracy is required, it is less accurate than more atomically detailed techniques.

Resolution: The resolution of the final docking poses may be reduced because of the coarse-grained nature of the initial search and docking process. To increase the precision of the anticipated binding interactions, the technique incorporates post-docking tuning.

SeamDock:

Accuracy: SeamDock achieves higher accuracy, particularly for smaller protein complexes or known binding sites, by utilising deep learning approaches and multi-scenario scoring systems. It's frequently regarded as one of the best techniques for high-accuracy docking.

Resolution: In order to comprehend the molecular underpinnings of especially protein interactions, SeamDock often generates docking models with a greater resolution, offering comprehensive, atomic-level interaction information.

B.5. Ease of Use

CBDock2:

Interface: CBDock2's web interface is very user-friendly, with explicit input requirements (such as protein structure files in PDB format) and intuitive options for choosing docking parameters.

Tutorials and Documentation: It offers sufficient tutorials and documentation to assist users in getting started, particularly those who are accustomed to docking operations.

SeamDock:

Interface: SeamDock's interface is also web-based and designed to be easy to use. It requires protein structure inputs in PDB format and offers options for specifying parameters like the number of docking poses to generate.

Documentation: Although SeamDock's documentation is thorough, it may be necessary to have a greater understanding of protein docking and machine learning in order to properly comprehend its more complex features.

B.6. Use Cases

CBDock2:

CBDock2 works well in scenarios that call for large-scale docking or high-throughput screening, or in blind docking when the binding site is unknown. When merely the general interaction and binding affinity—rather than the most exact atomic details—are required for protein-protein docking, it works equally well.

SeamDock:

When you know the binding sites or need to dock smaller complexes with more precise interactions, SeamDock is perfect for high-accuracy docking. It is an excellent option for high-resolution docking where atomic-level precision and comprehension of the molecular intricacies of the interaction are the main goals due to its deep learning-based methodology.

B.7. Limitations

CBDock2:

For small or complicated systems where atomic detail is crucial, the coarse-grained technique could result in reduced accuracy. Some fine-grained details in the anticipated docking poses may be sacrificed for its efficiency.

SeamDock:

For large-scale or high-throughput applications, SeamDock is slower and more computationally costly, especially when dealing with bigger complexes. A significant amount of training data is needed for deep learning-based techniques, and for particular kinds of unique protein complexes, the prediction may not be as accurate if comparable data was not used to train the model.

B.8. Final Verdict: Which One to Choose?

Choose CBDock2 if you:

-require a quick, scalable solution for big protein complexes or blind docking.

-are putting computational speed ahead of atomic-level accuracy.

Choose SeamDock If you:

-need precise and comprehensive results, particularly for smaller, clearly defined docking problems or known binding locations.

-must produce atomic-level accuracy and have a high degree of faithfulness in understanding molecular interactions.

In summary, both CBDock2 and SeamDock have their strengths and weaknesses, depending on the specific needs of your docking study. If speed and large-scale docking are more important, CBDock2 might be the better choice. If you're focused on accuracy and detailed molecular insights, then SeamDock would be more suitable.

C. A practical comparison of software

The chapter concludes with a presentation of the use of the software CBDock2 and SeamDock for the molecular docking analysis of the inhibition of electric eel acetylcholinesterase (PDB ID:1C2O) (AChE) by galantamine (Gal), a common competitive inhibitor of this enzyme.

C.1. SeamDock results

The Gridbox position and the dimensions for the SeamDock:

x , y , z 2 , 7 , -9

x , y , z 25 , 25 , 25

Table 1. The list of interactions and bonds for AChE-Gal docking.

Type of interaction	Ligand atom	Receptor
Hydrophobic contacts	C3	W286(A) CE3
	C3	L289(A) CD1
	C6	I294(A) CG2
	C8	F297(A) CE1
pi-pi stackings	C10	W286(A) NE1
	C10	W286(A) CZ3
Hydrogen bond	O3	F295(A) N
Weak hydrogen bond	C17	Y72(A) OH
	C17	D74(A) OD1
	C2	S293(A) O

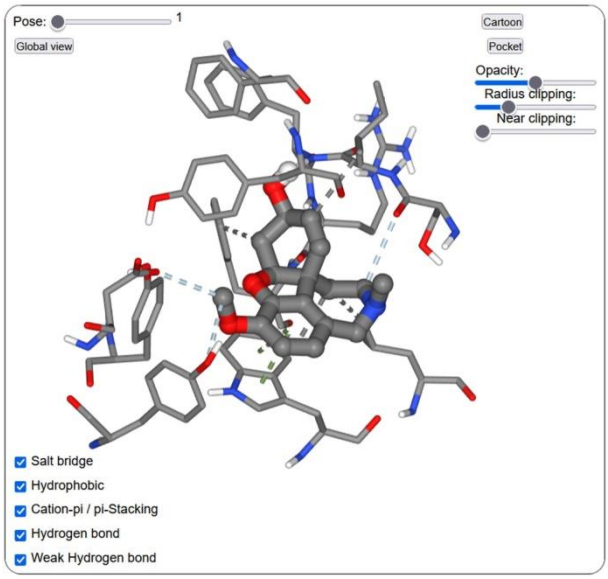

Figure 1. The demonstration of the bonds and interactions at the best docking pose calculated by SeamDock

C.2.CBDock2 results

There are two approaches for the detection of cavities and prediction of ligand-binding poses in CBDock2 molecular docking analysis.

C.2.1. Template-based docking

CBDock2 presented a list of templates and calculated parameters (Table 2).

Table 2. The template's information presented by CBDock2 for the molecular docking of receptor (1C2O) and ligand (Gal).

Template ID	Template Protein	Template Ligand	FP2	Pocket Identity	Pocket RMSD
t1	4ey6	GNT	1.0	1.0	0.37
t2	1w6r	GNT	1.0	0.94	0.41
t3	1w76	GNT	1.0	0.9	0.4
t4	3i6m	G3X	0.97	0.88	0.58
t5	1w4l	GL8	0.89	0.86	0.61

At this table, there are important parameters taken into account for the determination of the best pose. *Template protein* is the PDB ID in RCSB PDB, *Template ligand* is the chemical ID in RCSB PDB, *FP2* is the similarity of template and querry ligand, *Pocket identity* is the sequence identity of template and querry protein in pocket region, *Pocket RMSD* is RMSD (Cα) of template and querry protein in pocket region.

The template associated with the best pose was 3i6m, which was actually the only pose supported the docking criteria. FitPocket ID: F1 (FitDock Score: -5.4)

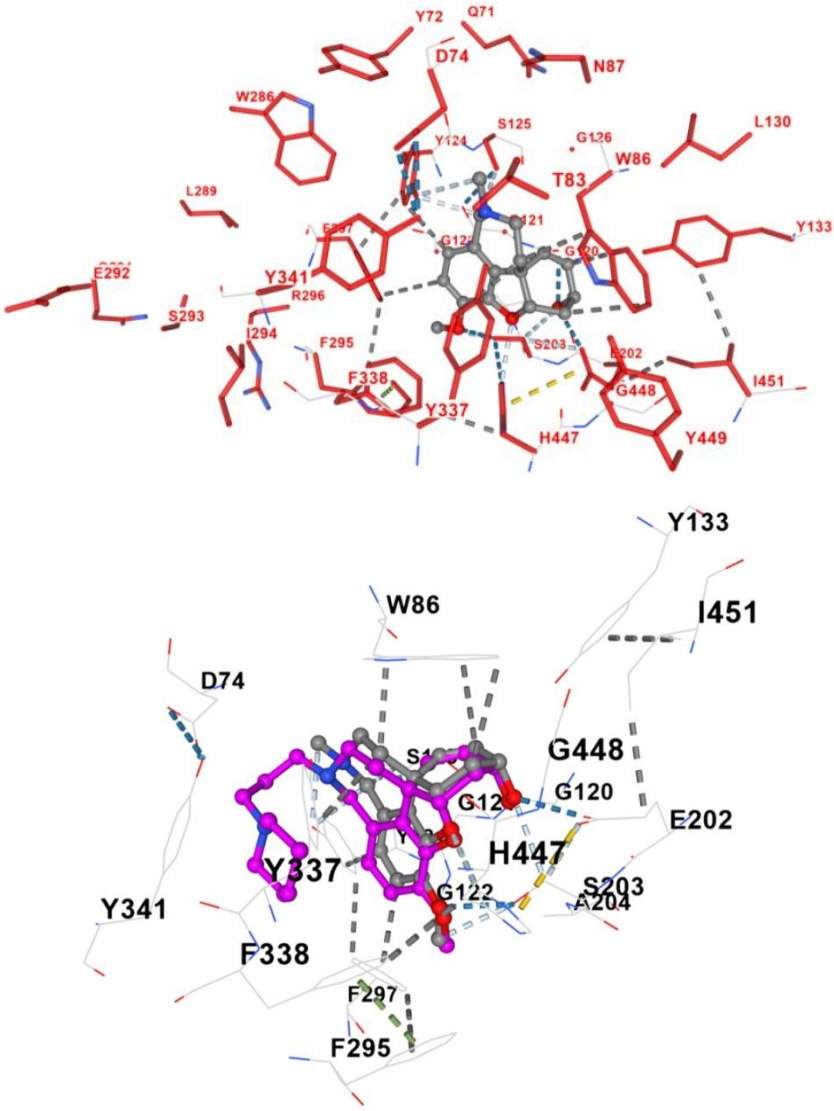

Figure 2. The above figure is the best pose of Gal docked at the active site of the receptor; and the below one is the templated docking of the ligand.

The contact residues: ASP74 TRP86 GLY120 GLY121 GLY122 TYR124 SER125 TYR133 GLU202 SER203 PHE295 PHE297 TYR337 PHE338 HIS447 GLY448 ILE451

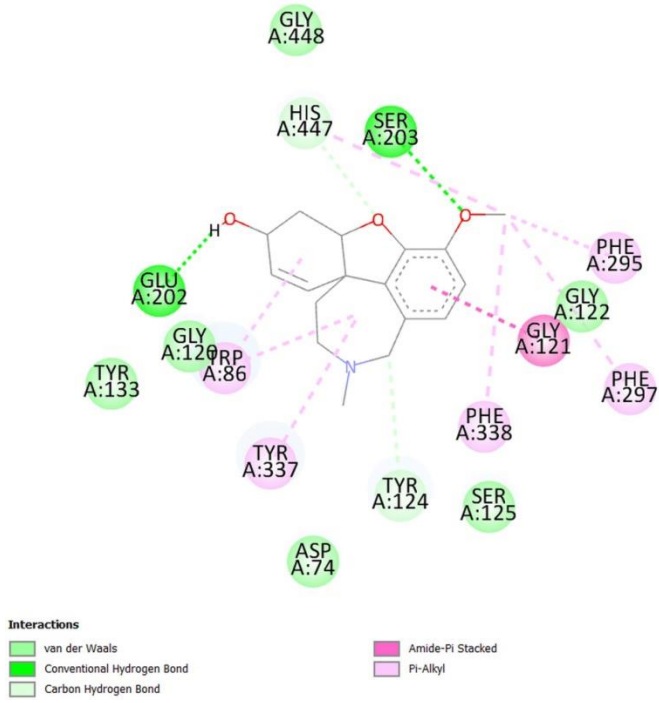

Figure 3. The inteactions and the bonds between ligand and the amino acids at the narrow gorge of the acetylcholinesterase after template-based docking procedure, supported by the illustration of the .pdb file of docked complexes by Discovery Studio 2021 Client.

Table 3. The list of the intearactions and the bonds proposed by the template-based docking of CBDock2 tool.

Amino acid	Type of interaction
TRP86	3 hydrophobic contacts
GLY120	hydrogen bond
TYR124	hydrophobic contact
TYR124	2 weak hydrogen bonds
SER125	weak hydrogen bond
GLU202	hydrogen bond
SER203	2 weak hydrogen bonds
SER203	hydrogen bond
PHE297	hydrophobic contact
TYR337	hydrophobic contact
HIS447	weak hydrogen bond

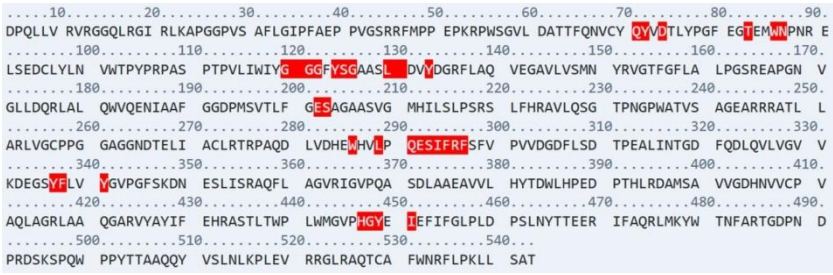

Figure 4. Interacting amino acids, which are highlighted by red color, of the receptor protein (AChE).

C.2.2. Structure-based blind docking

Current Pocket ID: C1 was proposed as the best docking position with a vina score of -7.7 kcal/mol.

Table 4. The results of the blind docking procedure after cavity search. The center and the docking size of the GridBox is, also, stated in the table.

CurPocket ID	Vina score	Cavity volume ($Å^3$)	Center (x, y, z)	Docking size (x, y, z)
C1	-7.7	960	35, 74, -86	19, 27, 19
C2	-6.0	478	36, 58, -93	19, 19, 19
C4	-5.9	369	29, 50, -90	19, 19, 19
C3	-5.6	470	26, 72, -63	19, 19, 19
C5	-5.6	358	15, 92, -78	19, 19, 19

The contact residues: GLN71 TYR72 ASP74 THR75 LEU76 TRP86 ASN87 PRO88 GLY120 GLY121 GLY122 TYR124 SER125 GLY126 LEU130 GLU202 SER203 TRP286 LEU289 GLN291 GLU292 SER293 ILE294 PHE295 ARG296 PHE297 TYR337 PHE338 LEU339 TYR341 GLY342 HIS447 GLY448 ILE451

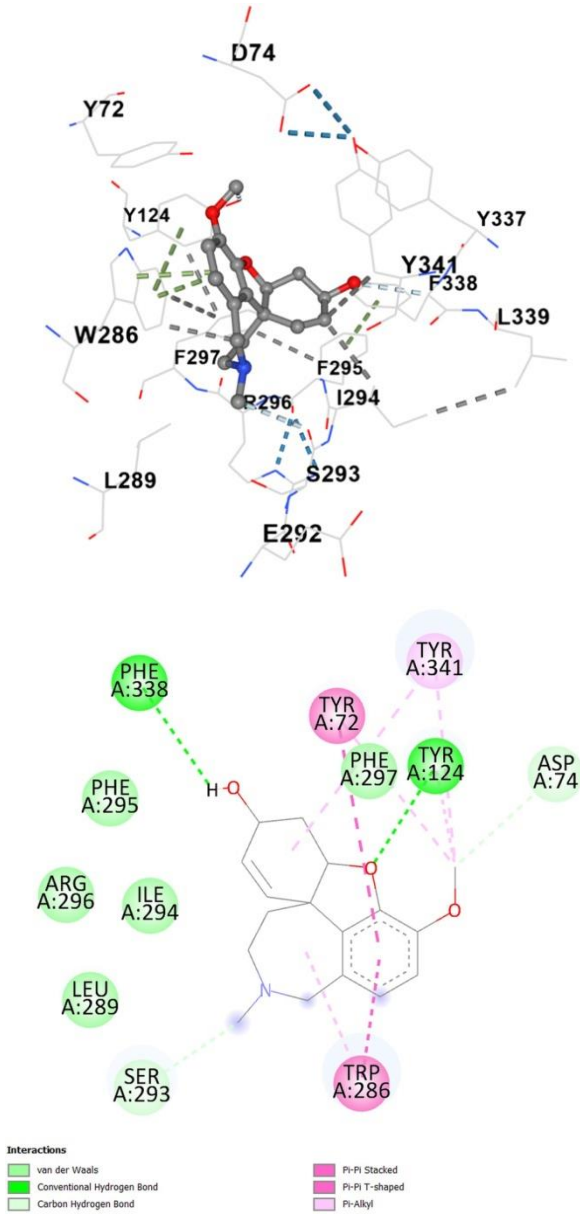

Figure 5. The above figure is the ligand at the best docking pose and the below one shows the inteactions and the bonds between ligand and the amino acids at the narrow gorge of the acetylcholinesterase after blind docking procedure, supported by the illustration of the .pdb file of docked complexes by Discovery Studio 2021 Client.

Table 5. The list of the intearactions and the bonds proposed by the structure-based blind docking performed by CBDock2.

Amino acid	Type of interaction
PHE338	weak hydrogen bond
TYR341	hydrophobic contact
ILE294	hydrophobic contact
TRP286	hydrophobic contact
SER293	weak hydrogen bond
TYR124	weak hydrogen bond
TRP286	2 pi-pi stackings

If we compare the results of the two analyzes performed with the CBDock2 online tool, that is, template-based and blind-docking approaches, it can be said that the template-based one shows a more successful performance compared to blind-docking, with the advantage of having a suitable template for the AChE-Gal relationship. This approach more successfully reported the bonds and interactions that the galantamine molecule, which is also reported in the literature to show an effective inhibition with more bonds, performs, or is very likely to perform, with the active site and surrounding amino acids. On the other hand, when the results of SeamDock analysis and the template-based results of CBDock2 were brought together, only the hydrophobic contact existing with PHE297 could be detected in common. If we compare the interactions listed as a result of CBDock's blind docking analysis with the list provided by SeamDock, we observe many more common results: A hydrophobic contact established separately with amino acids ILE294 and TRP286, a weak hydrogen bond formed with SER293, and finally two different pi-pi stacking relationships with TRP286 were reported jointly. This situation also shows us that deep-learning strategy and blind-docking by structure and energy based approaches reach approximate results, but they may not give the most probable result in docking analyzes that are well-known and have an existing template.

References

Agu, P. C., C. A. Afiukwa, O. U. Orji, E. M. Ezeh, I. H. Ofoke,C. O. Ogbu, E. I. Ugwuja, and P. M. Aja. 2023. "Molecular Docking as a Tool for the Discovery of Molecular Targets of Nutraceuticals in Diseases Management." Scientific Reports 2023 13:1 13(1):1-18. doi: 10.1038/s41598-023-40160-2.

Ferreira, Leonardo G., Ricardo N. Dos Santos, Glaucius Oliva, and Adriano D. Andricopulo. 2015. "Molecular Docking and Structure-Based Drug Design Strategies." Molecules (Basel, Switzerland) 20(7):13384–421. doi: 10.3390/MOLECULES200713384.

Kontoyianni, Maria. 2017. "Docking and Virtual Screening in Drug Discovery." Methods in Molecular Biology (Clifton, N.J.) 1647:255–66. doi: 10.1007/978-1-4939-7201-2_18.

Meng, Xuan-Yu, Hong-Xing Zhang, Mihaly Mezei, and Meng Cui. 2011. "Molecular Docking: A Powerful Approach for Structure-Based Drug Discovery." Current Computer-Aided Drug Design 7(2):146–57. doi: 10.2174/157340911795677602.

Mursal, Mohd, Mohammad Ahmad, Sahil Hussain, Mohemmed Faraz Khan, Mohd Mursal, Mohammad Ahmad, Sahil Hussain, and Mohemmed Faraz Khan. 2024. "Navigating the Computational Seas: A Comprehensive Overview of Molecular Docking Software in Drug Discovery." Unravelling Molecular Docking - From Theory to Practice [Working Title]. doi: 10.5772/INTECHOPEN.1004802.

Pagadala, Nataraj S., Khajamohiddin Syed, and Jack Tuszynski. 2017. "Software for Molecular Docking: A Review." Biophysical Reviews 9(2):91–102. doi: 10.1007/S12551-016-0247-1.

Stanzione, Francesca, Ilenia Giangreco, and Jason C. Cole. 2021. "Use of Molecular Docking Computational Tools in Drug Discovery." Progress in Medicinal Chemistry 60:273–343. doi: 10.1016/BS.PMCH.2021.01.004.

Zhao, Jingtian, Yang Cao, and Le Zhang. 2020. "Exploring the Computational Methods for Protein-Ligand Binding Site Prediction." Computational and Structural Biotechnology Journal 18:417–26. doi: 10.1016/J.CSBJ.2020.02.008.

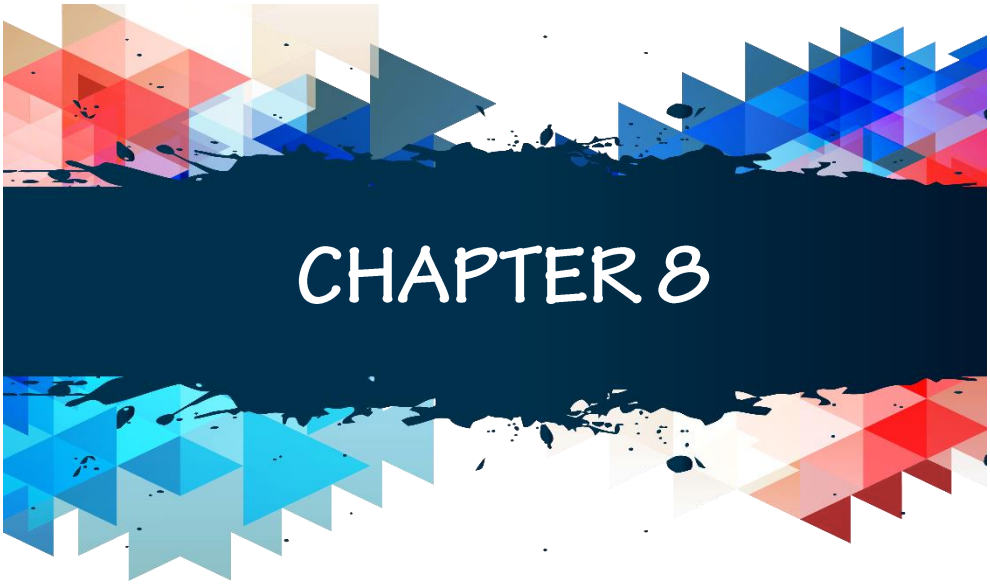

Essential Oils and Health

Ozge Telhuner[1] & Omer Elkiran[2]

1 Sinop Provincial Health Directorate, Public Health Laboratory, Sinop, 57000, Turkey. ORCID: 0009-0002-4234-4605
[2] Department of Medical Services and Techniques, Vocational School of Health Services, Sinop University, Sinop, 57000, Turkey. ORCID: 0000-0003-1933-4003, *Corresponding author

1. Definition of Essential Oils

People have relied on plants for shelter and nutrition for centuries, depending on them for carbohydrates, proteins, and fats. In addition to these primary metabolites, plants are also a significant source of a wide variety of secondary metabolites. In fact, over 80% of nearly 30,000 natural products are derived from plants (Ramachandra and Ravishankar, 2002).

Secondary metabolites are small molecular compounds found in plants, often in low concentrations, that are not essential for the plant's survival. These include phenols, alkaloids, essential oils, glycosides, flavonoids, steroids, saponins, tannins, and pigments. Initially, secondary metabolites were considered waste products with no specific plant function. However, it has since been established that they play important roles and have significant functions (Baydar, 2013).

Essential oils can be extracted from various parts of a plant, including the roots, stems, leaves, fruits, peels, and flowers, using various methods. They are generally colorless or light yellow liquids that are volatile, sometimes solidifying at lower temperatures, and possess strong fragrances. Because they can evaporate when left exposed, they are referred to as "volatile oils." Additionally, due to their ability to evaporate like ether, they are also called "ethereal oils." Their pleasant aromas and use in perfumery lead to the designation "essential oils" (Telhüner, 2024).

1.1. General Properties of Essential Oils

Essential oils provide the characteristic aroma and flavor of the plants they come from and are composed of a wide variety of chemical components. They are lighter than water, which means they do not mix with it and can be carried away by it. Their solubility in aqueous ethanol is one of the key features that distinguish them from fixed oils (Kaya and Ergönül, 2015).

When stored, essential oils can oxidize and undergo hydrolysis if exposed to air and heat for extended periods. To preserve their quality over time, they should be kept in airtight, tightly sealed dark glass bottles or aluminum containers, stored in a cool, dark place (Kaya and Ergönül, 2015).

When examining the chemical structures of essential oils, it is observed that the largest group is terpenes. Additionally, small amounts of other compounds such as alcohols, aldehydes, esters, phenols, and nitrogen- and sulfur-containing compounds are also present. (Linskens and Jackson, 1997a). So far, over 2,000 chemical compounds have been identified in essential oils, with terpenes and

phenylpropanoids being the most significant among them (Çelik and Çelik, 2007).

The most important factor in the quality of essential oils is their composition. The components found in essential oils can vary significantly depending on several factors, including the type of plant from which they are derived, the cultivation methods used, the harvesting techniques, the drying processes after harvest, and the methods of extraction (Franz and Novak, 2020).

Essential oils possess a variety of properties, including antioxidant, digestive stimulant, antifungal, antiseptic, antitoxic, antiviral, antibacterial, antiparasitic, insecticidal, and anti-inflammatory effects (Beyaz, 2014).

1.2. Methods of Extracting Essential Oils

Essential oils are obtained from various parts of plants or from the entire plant using different methods.

1.2.1 Distillation Methods

The distillation process is a separation technique based on the differences in boiling points of two or more liquid components. This method relies on vaporizing the substance with a lower boiling point and then cooling the vapor to condense it back into liquid form (Kaya and Ergönül, 2015).

Distillation methods can be categorized into three types:

1.2.1.1. Water Distillation

Essential oils are commonly extracted using a traditional method known as distillation. This process is carried out using a device called a Clevenger apparatus (Figure 1) (Kılıç, 2008).

This method involves heating the material placed in water, causing the volatile components to evaporate and then condensing them back into liquid form through cooling (Kaya and Ergönül, 2015). In this method, a glass flask containing water and plant material is connected to a condenser and boiled for 2 to 8 hours. During this time, the oil molecules from the plant move with the steam, condensing in the condenser and separating from the water. The best results are typically obtained from powdered plant materials (Linskens and Jackson, 1997b).

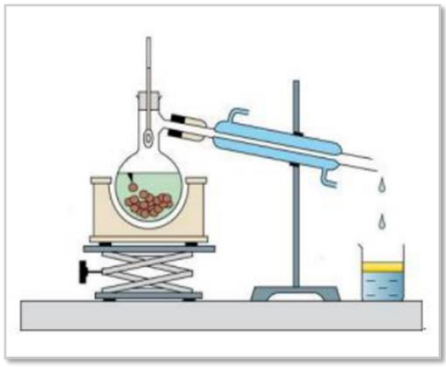

Figure 1. Water Distillation Setup (Türer, 2019).

1.2.1.2. Steam Distillation

In the steam distillation method, fresh plant material is placed in a glass container, and steam is applied under pressure. This steam carries the oil droplets and transports them to a collection chamber, where the oil condenses and separates from the water (Figure 2) (Linskens and Jackson, 1997b).

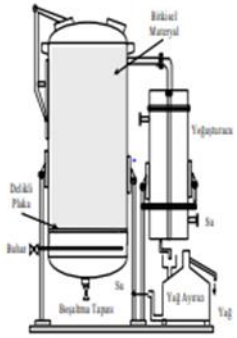

Figure 1. Steam Distillation Unit (Lawrance, 1995).

1.2.1.3. Vacuum Distillation

To obtain certain compounds with high boiling points, it is necessary to lower the pressure instead of increasing the temperature. For these compounds, once the pressure drops below the vapor pressure of the substance, the boiling and distillation processes can commence (Kılıç, 2008).

1.2.2. Extraction Methods

1.2.2.1. Solvent Extraction

This extraction method is a traditional approach. In this method, the plant material can be directly immersed in a solvent or boiled in an organic solvent using a device called a Soxhlet extractor. After the process, the organic solvent is removed using distillation. The remaining oily portion contains volatile compounds (Kılıç, 2008).

1.2.2.2. Supercritical Fluid Extraction (SFE)

This is a method of supercritical fluid extraction. In this technique, supercritical fluids are used as solvents instead of organic solvents (Linskens and Jackson, 1997b). Among the solvents used in supercritical fluid extraction, carbon dioxide (CO_2) is often preferred due to its availability, low cost, ease of use, high purity, and minimal environmental impact (Della Porta et al., 1999).

1.2.2.3. Microwave Extraction

This is an extraction process performed using a small amount of solvent and microwave energy in a short time. During this method, both temperature and duration must be carefully controlled (Kaya and Ergönül, 2015). The advantage of this method is that it requires a short extraction time and a minimal amount of solvent (Beejmohun et al., 2007).

1.2.2.4. Pressurized Solvent Extraction

This method is an alternative developed to classical extraction techniques. Among its advantages are reduced extraction time, lower solvent consumption, higher yield, and repeatability. The use of organic solvents at high pressure and temperature enhances the method's effectiveness. In this process, the solid or semi-solid sample is placed in a steel container with the solvent and heated in an oven at temperatures ranging from 50 to 200 °C. During heating, a pressure of 500 to 3000 psi is applied in the oven. Between the 5th and 10th minutes of the application, fresh solvent is introduced to wash the sample and the container. Nitrogen gas is used to collect the solvent in a bottle from the system (Kaufmann and Christen, 2002).

1.2.2.5. Solid-Phase Microextraction (SPME)

SPME (Solid Phase Microextraction) is a simple device that resembles a modified syringe. It consists of a fiber holder and a group of fibers. The fiber is typically 1-2 cm long and can be moved back and forth. This method applies to samples in either gas or liquid form (Vas and Vekey, 2004).

The duration of SPME extraction ranges from 1 to 20 minutes. Its simplicity, low cost, and ability to obtain clean and concentrated extracts make it an ideal method for use in mass spectrometry (Araujo et al., 2007). Multi-Directional Extraction (SDE)

1.2.2.6. Simultaneous Distillation Extraction (SDE)

According to the method, the material is placed in a water-filled glass flask on the left side of the apparatus and heated. During this process, the volatiles are distilled with the steam and rise through the left column, while the solvent evaporates on the right side of the apparatus. The extraction process occurs through the condensation of water and solvent vapors (Chaintreau, 2001).

1.2.3. Mechanical Method (Pressing)

When the distillation method is applied to the peels of citrus fruits like oranges and lemons, it can lead to the degradation of volatile compounds. Therefore, the peels of such fruits are placed in cloth bags and squeezed using cold hydraulic presses to obtain the essential oils (Kılıç, 2008).

2. Areas of Use for Essential Oils

To date, raw materials obtained from different parts of plants have been used for food, spices, and medicinal purposes. Over time, and with advancements in technology, the applications of plants have expanded, and they have begun to be utilized in various industrial sectors as well (Göktaş and Gıdık, 2019).

2.1. Uses of Essential Oils in Aromatherapy

For aromatherapy to be an effective complementary treatment, it must be applied at the right time and using the appropriate methods. Aromatherapy is highly effective in promoting relaxation for both the mind and body, alleviating pain, and regulating bodily systems. When essential oils are used in the body, they alter the body's chemistry, support bodily systems, and help improve mental and emotional states (Tatlı, 2012).

2.2. Uses of Essential Oils in the Food Industry

Today, plant extracts are increasingly used in the food industry to extend shelf life. Plants rich in essential oils or their extracted oils are utilized in organic food production and marketing, particularly for their antimicrobial properties, due to their natural composition (Cerit, 2008).

When such plants and their essential oils are applied to the contents of prepared foods, they can extend the shelf life of the products due to their antimicrobial effects (Farag et al., 2016).

Essential oils from thyme, oregano, clove, sage, black seed, rosemary, garlic, and onion exhibit significant antimicrobial effects against a wide range of bacteria and molds (Barker, 2019).

2.3. Uses of Essential Oils in the Perfumery and Cosmetics Industry

Perfumes are obtained by mixing essential oils from medicinal and aromatic plants in specific ratios and combining them with alcohol to make them lasting. People have started to move away from synthetic perfumes containing petroleum derivatives, which are known to have harmful effects, and are increasingly opting for natural alternatives. Various parts of plants, including woods, stems and bark, fruit peels, fruits, flowers, roots, rhizomes and bulbs, seeds, leaves, and resins, are used in the production of perfumes (Göktaş and Gıdık, 2019). Some commonly used cosmetic plants and their applications are as follows:

Calendula: Used in shampoos, creams, toothpaste, skincare products, and baby oil.

Elderflower: Soothes skin irritation, softens, tightens, and acts as an antiseptic and skin cleanser.

Echinacea: Known for its anti-aging, moisturizing, and skin irritation-reducing effects.

Licorice Root: Has skin-brightening and spot-reducing properties.

Horsetail: Effective in preventing hair loss (Tanrıkulu, 2014).

2.4. Other Uses of Essential Oils

Rapeseed, flaxseed, sunflower, castor, and jojoba are examples of plants used as biofuels (Göktaş and Gıdık, 2019).

The thyme plant, known for its allelopathic properties, is used in France to protect stored agricultural products from pests (Bozdemir, 2019).

Today, commercially available azadirachtin, a limonoid extracted from neem tree seeds, is effectively used against many insects as a growth and feeding inhibitor. Eucalyptus and clove species have also been found to have a significant repellent effect against mosquitoes (Topuz and Madanlar, 2006).

3. Uses of Essential Oils in Healthcare

Since ancient times, plants have been used for medicinal purposes to treat various diseases (Essawi and Srour, 2000; Özer et al., 2001). Because essential oils are composed of different components, their biological activities can vary. While the effects of essential oils change depending on the active compounds they contain, they generally exhibit antimicrobial, carminative, choleretic, sedative, diuretic, and antispasmodic effects (Maksimović et al., 2005).

Garlic, cinnamon, curry, mustard, basil, ginger, and several other plants have been found to exhibit antimicrobial properties (Marino et al., 1999). Additionally, essential oils from many plants belonging to the Labiatae family have been identified as having antimicrobial activity (Elgayyar et al., 2001). For example, essential oils from basil, bay, clove, thyme, and rosemary have been reported to show bactericidal activity against L. monocytogenes and other pathogens (O'Gara et al., 2000). People use these plants by gathering them from nature or purchasing them for various purposes and in different forms (Baytop, 1999).

Some Medical and Aromatic Plants and Their Health Uses:

Lavender Essential Oil (*Lavandulae aetheroleum*)

The primary active compounds in lavender essential oil are linalool and linalyl acetate. In addition to these, it also contains other components such as limonene, camphor, terpinen-4-ol, lavandulol, lavandulyl acetate, and 1,8-cineole (Tisserand and Young, 2014).

Lavender essential oil exhibits strong antibacterial properties against a wide range of bacterial species. Additionally, it possesses antiviral, antifungal, and anti-inflammatory effects. It also has antiallergic properties, making it useful in the treatment of allergies and asthma. Its antiallergic effects are thought to stem from its ability to reduce histamine release from mast cells (Ueno-Iio et al., 2014).

Lavender essential oil is effective in treating migraine-type headaches (Tisserand and Young, 2014). In women, it is effective when used in massage for premenstrual syndrome, dysmenorrhea, and pain related to childbirth (Yazdkhasti and Pirak, 2016). It has been identified that lavender essential oil has a stimulating effect on the central nervous system, leading to its use as a calming and stress-reducing agent (Güler et al., 2015).

Additionally, lavender essential oil is known to be effective in addressing sleep disorders (Velasco-Rodríguez et al., 2019).

Tea Tree Essential Oil (*Melaleucae alternifolii aetheroleum*)

The active compounds in tea tree essential oil include terpinen-4-ol, α- and γ-terpinene, terpinolene, and 1,8-cineole. The primary component is terpinen-4-ol (Tisserand and Young, 2014).

Tea tree essential oil has been shown to possess antibacterial, antifungal, and antiviral activity against tested strains (Schnitzler et al., 2001). It can accelerate the healing process of wounds and is also used in the treatment of conditions such as acne vulgaris, seborrheic dermatitis, and chronic gingivitis. Research indicates that tea tree essential oil may help prevent melanoma, a type of skin cancer (Sabir et al., 2014).

Medicinal Peppermint Essential Oil (*Menthae piperitae aetheroleum*)

The components of medicinal peppermint essential oil include menthol, menthyl acetate, limonene, isomenthone, mentone, and carvone (Tisserand and Young, 2014). When used topically, peppermint essential oil has antipruritic, astringent, and antiseptic effects. It also possesses a decongestant property and serves as a strong digestive aid (Kennedy et al., 2018).

Studies have shown that peppermint essential oil is effective in reducing nausea and vomiting (Fearrington et al., 2019). Additionally, it is known to be effective for headaches, migraines, and lowering fever (Göbel et al., 1996).

Salvia Essential Oil (*Salvia officinalis*)

The essential oil of sage contains components such as α- and β-thujone, eucalyptol, camphor, borneol, and bornyl acetate. The primary component of sage is cineole. Sage is known for its antiseptic and fungicidal effects, particularly in throat infections and respiratory conditions (Bayraktar et al., 2017). Additionally, sage essential oil has antibacterial properties and is included in herbal deodorants due to its effectiveness against sweating (Güler et al., 2015).

Lemon Essential Oil (*Limonis aetheroleum*)

Lemon essential oil's main component is limonene, along with other significant constituents such as β-pinene, γ-terpinene, sabinene, and geranial (Tisserand and Young, 2014).

Research has shown that lemon essential oil has positive effects on memory by reducing acetylcholinesterase activity and preventing scopolamine-induced amnesia (Fukumoto et al., 2008). It is also reported to have anxiolytic and antidepressant effects, helping to reduce both physical and psychological stress (Lopes Campêlo et al., 2011).

Clove Essential Oil (*Caryophylli flos aetheroleum*)

Clove essential oil changes color from red to brown over time. Its main component is eugenol, with other constituents including β-caryophyllene and acetyl eugenol (Tisserand and Young, 2014).

Clove essential oil has anesthetic properties, making it useful for relieving muscle and joint pain (Chaieb et al., 2007). Additionally, clove essential oil exhibits antipyretic, anti-inflammatory, and antinociceptive effects. Research has shown that it can reduce oxidative stress and has positive effects on memory (Halder et al., 2011).

Medicinal Chamomile Essential Oil (*Matricariae aetheroleum*)

There are two chemotypes of medicinal chamomile essential oil, rich in bisabolol and (-)-α-bisabolol. Both chemotypes contain chamazulene as well (Tisserand and Young, 2014).

Medicinal chamomile essential oil has analgesic properties, making it quite effective for migraine headaches (Zargaran et al., 2014). This essential oil also possesses anxiolytic effects and has been used for insomnia issues for a long time (Srivastava et al., 2010). Due to the presence of (-)-α-Bisabolol and chamazulene, medicinal chamomile essential oil has anti-inflammatory, wound-healing, and antihistaminic effects. It has also been used for many years in treating diaper rash in infants and skin conditions like eczema (Lee et al., 2010).

Linden Essential Oil (*Tilia cordata* Miller)

Linden essential oil contains components such as sineol, linalool, camphor, carvone, geraniol, thymol, carvacrol, anethole, farnesol, and farnesyl acetate. It is reported to have anti-inflammatory, sedative, antidepressant, and antimicrobial effects (Toker, 1995).

Rose Essential Oil (*Rosa damascenae aetheroleum*):

The essential oil contains components such as citronellol, geraniol, nerol, and methyl eugenol (Tisserand and Young, 2014).

It has antibacterial, antiviral, antifungal, antiseptic, antioxidant, analgesic, anti-inflammatory, and wound-healing effects, and it has also been reported to be effective in migraines (Mohebitabari et al., 2017).

It has been found to be effective in reducing pain and anxiety during childbirth and in alleviating premenstrual syndrome in women (Hamdamian et al., 2018).

Fennel Essential Oil (*Foeniculum vulgare*)

The components of fennel essential oil include trans-anethole, estragole (methyl chavicol), fenchone, α-phellandrene, limonene, and α-pinene (Telhüner, 2024).

Studies have reported that fennel essential oil has antimicrobial and antioxidant effects (Karayel, 2019). Due to these properties, it is used like a medicine. It is commonly used in folk medicine for its ability to increase milk production, relieve gas, and soothe the stomach (Kan, 2006).

Thyme Essential Oil (*Origanum spp.*)

Thyme essential oil contains thymol and carvacrol as its main components (Bayar and Çınar, 2020). Due to the compounds it contains, thyme essential oil exhibits strong antimicrobial activity (Santoro et al., 2007). It is also used as a soothing remedy for illnesses such as the common cold and throat infections. Additionally, thyme essential oil is applied in cases of muscle cramps, sprains, and muscle strains, as well as for alleviating rheumatic pain, and in the treatment of coughs, epileptic seizures, and pneumonia (Güler et al., 2015).

4. Economic Values of Essential Oils

The sourcing methods for medicinal and aromatic plants involve either agricultural production or wild collection. In our country, common crops include mint, poppy, lavender, cumin, fennel, chamomile, parsley, and similar plants (Kılıç, 2018).

Due to its geographical location, Turkey has a high level of genetic diversity and endemism. Despite being one of the leading countries in the world for the trade of medicinal and aromatic plants and having a high export potential for these plants, the desired level has not yet been achieved (Bayraktar et al., 2017). In 2016, the export of medicinal plants amounted to 158 million USD, while the import reached 41 million USD. The export-to-import ratio for medicinal and aromatic plants in 2016 was 385%.

The most exported medicinal and aromatic plants from Turkey are bay leaves, anise, cumin, ginger, and thyme (Varlı et al., 2020).

According to research, global trade in medicinal and aromatic plants has shown a steady increase since 2001. The export value rose from 18.3 billion USD in 2001 to 70.7 billion USD in 2019. Notably, the United States, India, and France stand out as key countries in the export of essential oils, with a total export value of 5.6 billion USD (ITC, 2020).

5. Conclusion

Medicinal and aromatic plants are widely used today in the food industry, perfumery, cosmetics, and healthcare. This trend is related to people's growing desire to move away from synthetic drugs and create their treatments, along with increasing awareness. Due to their components, essential oils obtained from these plants have shown various biological activities (such as antioxidant, antimicrobial, antifungal, etc.). Because of this potential, they have become an important alternative in the fight against diseases. As a result of these properties, the transformation of medicinal and aromatic plants, along with their essential oils, into new commercial products is increasing day by day. When these essential oils are converted into products, efforts should be made to increase the amount of active compounds they contain, and new methods should be developed to ensure larger-scale production without causing harm. In conclusion, further research on medicinal and aromatic plants and the essential oils derived from them can enhance their use as alternatives to synthetic drugs, both now and in the future.

References

Araújo, H. C., Lacerda, M. E. G., Lopes, D., Bizzo, H. R., & Kaplan, M. A. C. (2007). Studies on the aroma of maté (Ilex paraguariensis St. Hil.) using headspace solid-phase microextraction. *Phytochemical Analysis: An International Journal of Plant Chemical and Biochemical Techniques*, *18*(6), 469-474.

Barker, A. V. (2008). Natural products from plants. *HortScience*, *43*(2), 581b-582.

Bayar, F. U., & Çınar, O. (2020). Kültür koşullarında yetiştirilen farklı Origanum spp. türlerinin bazı verim ve kalite parametreleri. *Derim*, *37*(1), 10-17.

Bayaz, M. (2014). Esansiyel yağlar: antimikrobiyal, antioksidan ve antimutajenik aktiviteleri. *Akademik Gıda*, *12*(3), 45-53.

Baydar, H. (2013). Tıbbi ve aromatik bitkiler bilimi ve teknolojisi (Genişletilmiş 4. Baskı). *Süleyman Demirel Üniversitesi Yayın*, (51), 303.

Bayraktar, Ö. V., Öztürk, G., & Arslan, D. (2017). Türkiye'de bazı tıbbi ve aromatik bitkilerin üretimi ve pazarlamasındaki gelişmelerin değerlendirilmesi. *Tarla Bitkileri Merkez Araştırma Enstitüsü Dergisi*, *26*(2), 216-229.

Baytop, T. (1984). *Türkiyede bitkiler ile tedavi (geçmişte ve bugün)* (No. 3255). İstanbul Üniversitesi.

Beejmohun, V., Fliniaux, O., Grand, É., Lamblin, F., Bensaddek, L., Christen, P., ... & Mesnard, F. (2007). Microwave-assisted extraction of the main phenolic compounds in flaxseed. *Phytochemical Analysis: An International Journal of Plant Chemical and Biochemical Techniques*, *18*(4), 275-282.

Bozdemir, Ç. (2019). Türkiye'de yetişen kekik türleri, ekonomik önemi ve kullanım alanları. *Yuzuncu Yıl University Journal of Agricultural Sciences*, *29*(3), 583-594.

Cerit, L. S. (2008). *Bazı baharat uçucu yağlarının antimikrobiyal özellikleri* (Master's thesis, Pamukkale Üniversitesi Fen Bilimleri Enstitüsü).

Chaieb, K., Hajlaoui, H., Zmantar, T., Kahla-Nakbi, A. B., Rouabhia, M., Mahdouani, K., & Bakhrouf, A. (2007). The chemical composition and biological activity of clove essential oil, Eugenia caryophyllata (Syzigium aromaticum L. Myrtaceae): a short review. *Phytotherapy Research: An International Journal Devoted to Pharmacological and Toxicological Evaluation of Natural Product Derivatives*, *21*(6), 501-506.

Kılıç, A. (2008). Uçucu yağ elde etme yöntemleri. *Bartın Orman Fakültesi Dergisi*, *10*(13), 37-45.

Çelik, E., & Çelik, G. Y. (2007). Bitki uçucu yağlarının antimikrobiyal özellikleri. *Orlab On-Line Mikrobiyoloji Dergisi*, *5*(2), 1-6.

Della Porta, G., Porcedda, S., Marongiu, B., & Reverchon, E. (1999). Isolation of eucalyptus oil by supercritical fluid extraction. *Flavour and fragrance journal*, *14*(4), 214-218.

Elgayyar, M., Draughon, F. A., Golden, D. A., & Mount, J. R. (2001). Antimicrobial activity of essential oils from plants against selected pathogenic and saprophytic microorganisms. *Journal of food protection*, *64*(7), 1019-1024.

Essawi, T., & Srour, M. (2000). Screening of some Palestinian medicinal plants for antibacterial activity. *Journal of ethnopharmacology*, *70*(3), 343-349.

Farag, R. S., Daw, Z. Y., Hewedi, F. M., & El-Baroty, G. S. A. (1989). Antimicrobial activity of some Egyptian spice essential oils. *Journal of food protection*, *52*(9), 665-667.

Fearrington, M. A., Qualls, B. W., & Carey, M. G. (2019). Essential oils to reduce postoperative nausea and vomiting. *Journal of Perianesthesia Nursing*, *34*(5), 1047-1053.

Franz, C., & Novak, J. (2020). Sources of essential oils. In *Handbook of essential oils* (pp. 41-83). CRC press.

Fukumoto, S., Morishita, A., Furutachi, K., Terashima, T., Nakayama, T., & Yokogoshi, H. (2008). Effect of flavour components in lemon essential oil on physical or psychological stress. *Stress and Health: Journal of the International Society for the Investigation of Stress*, *24*(1), 3-12.

Göbel, H., Heinze, A., Dworschak, M., & Soyka, D. (1996). Effektivität von Oleum menthae piperitae und von Paracetamol in der Therapie des Kopfschmerzes vom Spannungstyp. *Der Nervenarzt*, *67*, 672-681.

Göktaş, Ö., & Gıdık, B. (2019). Tıbbi ve aromatik bitkilerin kullanım alanları. *Bayburt Üniversitesi Fen Bilimleri Dergisi*, *2*(1), 145-151.

Güler, H. K., Dönmez, İ., & Aksoy, S. A. (2015). Tıbbi ve aromatik bitkilerin antibakteriyel aktivitesi ve tekstil sektöründe kullanımı. *Süleyman Demirel University Faculty of Arts and Science Journal of Science*, *10*(2), 27-34.

Halder, S., Mehta, A. K., Kar, R., Mustafa, M., Mediratta, P. K., & Sharma, K. K. (2011). Clove oil reverses learning and memory deficits in scopolamine-treated mice. *Planta Medica*, *77*(08), 830-834.

Hamdamian, S., Nazarpour, S., Simbar, M., Hajian, S., Mojab, F., & Talebi, A. (2018). Effects of aromatherapy with Rosa damascena on nulliparous women's pain and anxiety of labor during first stage of labor. *Journal of integrative medicine*, *16*(2), 120-125.

ITC, (2020). International Trade Center, TradeMap Veri tabanı, https://www.trademap.org/Index.aspx

Kan, Y. (2006). Composition of essential oil of fennel fruits cultivated at different conditions. *Journal of Faculty of Pharmacy of Ankara University*, *35*(2), 95-101.

Karayel, H. B. (2019). Kütahya-Gediz koşullarında yetiştirilen rezene (Foeniculum vulgare Mill.) bitkisinin uçucu yağ bileşenlerinin belirlenmesi. *Avrupa Bilim ve Teknoloji Dergisi*, (16), 131-135.

Kaufmann, B., & Christen, P. (2002). Recent extraction techniques for natural products: microwave-assisted extraction and pressurised solvent extraction. *Phytochemical Analysis: An International Journal of Plant Chemical and Biochemical Techniques*, *13*(2), 105-113.

Kaya, D., & Ergönül, P. G. (2015). Uçucu Yağları Elde Etme Yöntemleri. *Gıda*, *40*(5), 303-312.

Kennedy, D., Okello, E., Chazot, P., Howes, M. J., Ohiomokhare, S., Jackson, P., ... & Wightman, E. (2018). Volatile terpenes and brain function: investigation of the cognitive and mood effects of Mentha× Piperita L. essential oil with in vitro properties relevant to central nervous system function. *Nutrients*, *10*(8), 1029.

Kılıç, A. (2008). Uçucu yağ elde etme yöntemleri. *Bartın Orman Fakültesi Dergisi*, *10*(13), 37-45.

KILIÇ, S. (2018). Aromatik Bitki Ve Yağlarının Mineral Element Miktarlarının Karşılaştırılması. *GIDA*, *43*(4), 617-623.

Lawrence, B. M. (1995). The isolation of aromatic materials from natural plant products. *A manual on the essential oil industry*, 57-154.

Lee, S. H., Heo, Y., & Kim, Y. C. (2010). Effect of German chamomile oil application on alleviating atopic dermatitis-like immune alterations in mice. *Journal of veterinary science*, *11*(1), 35-41.

Linskens, H.F., Jackson, J.F, 1997a Modern Methods of Plant Analysis, Vol. 19: Plant Volatile Analysis, Springer, Germany.

Linskens, H. F., Jackson, J.F, 1997b Modern Methods of Plant Analysis, Vol. 12: Essential Oils and waxes, Springer, Germany.

Lopes Campêlo, L. M., Gonçalves e Sá, C., De Almeida, A. A. C., Pereira da Costa, J., Costa Marques, T. H., Mendes Feitosa, C., ... & Mendes de Freitas, R. (2011). Sedative, anxiolytic and antidepressant activities of Citrus limon (Burn) essential oil in mice. *Die Pharmazie-An International Journal of Pharmaceutical Sciences*, *66*(8), 623-627.

Maksimovic, Z. A., Dordevic, S., & Mraovic, M. (2005). Antimicrobial activity of Chenopodium botrys essential oil. *Fitoterapia*, *76*(1), 112-114.

Marino, M., Bersani, C., & Comi, G. (1999). Antimicrobial activity of the essential oils of Thymus vulgaris L. measured using a bioimpedometric method. *Journal of food protection*, *62*(9), 1017-1023.

Mohebitabar, S., Shirazi, M., Bioos, S., Rahimi, R., Malekshahi, F., & Nejatbakhsh, F. (2017). Therapeutic efficacy of rose oil: A comprehensive review of clinical evidence. *Avicenna journal of phytomedicine*, *7*(3), 206.

O'Gara, E. A., Hill, D. J., & Maslin, D. J. (2000). Activities of garlic oil, garlic powder, and their diallyl constituents against Helicobacter pylori. *Applied and environmental microbiology*, *66*(5), 2269-2273.

Özer, Z., Tursun, N., & Önen, H. (2001). *Yabancı otlarla sağlıklı yaşam:(Gıda ve tedavi)*. 4Renk Yayınları.

Rao, S. R., & Ravishankar, G. A. (2002). Plant cell cultures: chemical factories of secondary metabolites. *Biotechnology advances*, *20*(2), 101-153.

Sabir, S., Arshad, M., Zahara, K., Tabassum, S., & Chaudhari, S. K. (2014). Pharmacological attributes and nutritional benefits of tea tree oil. *Int. J. Biol. Sci*, *5*, 80-91.

Santoro, G. F., das Graças Cardoso, M., Guimarães, L. G. L., Salgado, A. P. S., Menna-Barreto, R. F., & Soares, M. J. (2007). Effect of oregano (Origanum vulgare L.) and thyme (Thymus vulgaris L.) essential oils on Trypanosoma cruzi (Protozoa: Kinetoplastida) growth and ultrastructure. *Parasitology research*, *100*, 783-790.

Schnitzler, P., Schön, K., & Reichling, J. (2001). Antiviral activity of Australian tea tree oil and eucalyptus oil against herpes simplex virus in cell culture. *Die Pharmazie*, *56*(4), 343-347.

Srivastava, J. K., Shankar, E., & Gupta, S. (2010). Chamomile: A herbal medicine of the past with a bright future. *Molecular medicine reports*, *3*(6), 895-901.

Tanrıkulu, N. (2014). Kozmetik Bitkileri Tarımı ve Türkiye Florasının Kozmetik Bitkileri Açısından Önemi, 4. *4. Kozmetik Kimyası, Üretimi, Standardizasyonu Kongresi, Kimyagerler Derneği*.

TATLI, İ. İ. (2012). Doğal Aromaterapötik Yağlar ile Cilt Terapisi. *Turkiye Klinikleri Cosmetic Dermatology-Special Topics*, *5*(4), 46-53.

Telhüner Ö. (2024). Rezene (Foenıculum Vulgare Mill.) Bitkisinin Farklı Organlarının Uçucu Yağlarının Kimyasal Kompozisyonu Biyolojik Aktivitesi ve Çevresel Faktörlerden Etkilenmişlik Düzeyi. Yüksek Lisans, Sinop Üniversitesi Lisansüstü Eğitim Enstitüsü, Sinop. 70 s.

Tisserand R, Young R. 2014. Essential Oils Safety. 2nd ed. London: Churchill Livingstone Elsevier.

Toker, G. (1995). Ihlamur çiçek ve kabuklarının biyolojik aktivitesi ve kullanılışı. *FABAD Journal of Pharmaceutical Sciences*, *20*, 75-79.

Topuz, E., & Madanlar, N. (2006). Bitkisel Kökenli Eterik Yağlar Ve Zararlılara Karşı Kullanim Olanakları. *Derim*, *23*(2), 54-66.

Türer, G. *Pelargonium gravolens L.her. bitkisi yapraklarından uçucu yağların izolasyonu, analizi ve antimikrobiyal aktivitesi* (Master's thesis, Fen Bilimleri Enstitüsü).

Ueno-Iio, T., Shibakura, M., Yokota, K., Aoe, M., Hyoda, T., Shinohata, R., ... & Kataoka, M. (2014). Lavender essential oil inhalation suppresses allergic airway inflammation and mucous cell hyperplasia in a murine model of asthma. *Life sciences*, *108*(2), 109-115.

Varlı, M., Hancı, H., & Kalafat, G. (2020). Tıbbi ve aromatik bitkilerin üretim potansiyeli ve biyoyararlılığı. *Research Journal of Biomedical and Biotechnology, 1*(1), 24-32.

Vas, G., & Vekey, K. (2004). Solid-phase microextraction: a powerful sample preparation tool prior to mass spectrometric analysis. *Journal of mass spectrometry, 39*(3), 233-254.

Velasco-Rodríguez, R., Pérez-Hernández, M. G., Maturano-Melgoza, J. A., Hilerio-López, Á. G., Monroy-Rojas, A., Arana-Gómez, B., & Vásquez, C. (2019). The effect of aromatherapy with lavender (Lavandula angustifolia) on serum melatonin levels. *Complementary therapies in medicine*, *47*, 102208.

Yazdkhasti, M., & Pirak, A. (2016). The effect of aromatherapy with lavender essence on severity of labor pain and duration of labor in primiparous women. *Complementary therapies in clinical practice*, *25*, 81-86.

Zargaran, A., Borhani-Haghighi, A., Faridi, P., Daneshamouz, S., Kordafshari, G., & Mohagheghzadeh, A. (2014). Potential effect and mechanism of action of topical chamomile (Matricaria chammomila L.) oil on migraine headache: A medical hypothesis. *Medical hypotheses*, *83*(5), 566-569.

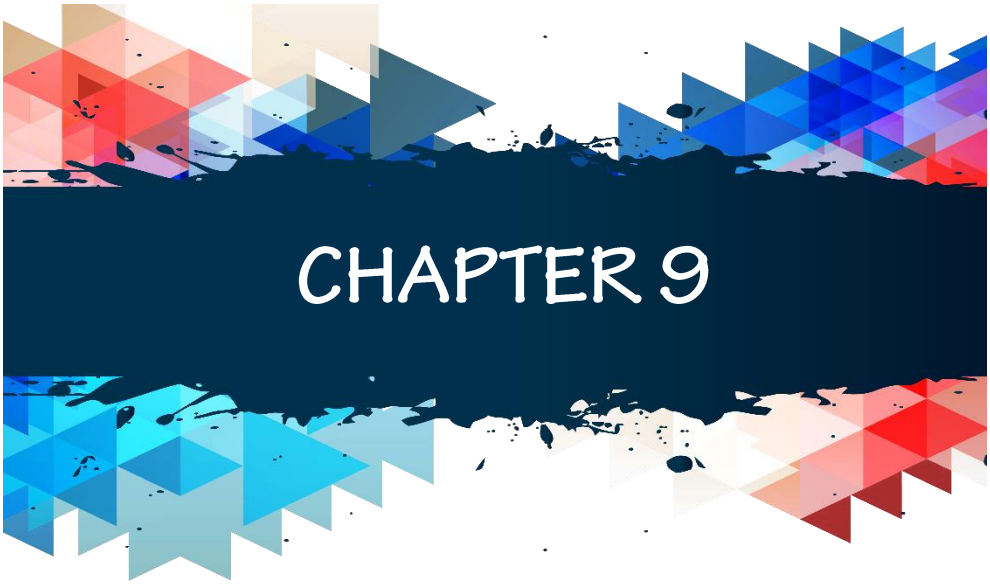

On Submersions of A Submanifold of Generalized Kenmotsu Manifold

Ramazan Sarı[1] & Süleyman Dirik[2]

1 Assoc.Prof., Amasya University, 0000-0002-4618-8243
[2] Assoc.Prof., Amasya University, 0000-0001-9093-1607

1. INTRODUCTION

Riemann submersions were first defined and studied independently by O'Neill and Gray in 1966 and 1967 (O'Neill, 1966), (Gray, 1967). Such transformations were originally defined for the construction of manifolds of negative curvature, but it was later found that such transformations are very useful for comparing manifolds. O'Neill defined two fundamental tensor fields for Riemannian submersions and showed that these tensors correspond to the second fundamental form and shape operator in isometric immersions. These studies have shown that by using submersions, the properties of the underlying manifold can be studied much more easily with the help of a manifold whose geometric properties are known. For this reason, submersion transformations are used and developed in many branches of science, especially in engineering and physics.

In mathematical physics, especially in Kaluza-Klein theory, new methods developed for the general solution of Einstein equations can be expressed by harmonic transformations. Moreover, a class of solutions can be expressed with Riemann submersions. In 2004, Falcitelli et al. computed the solution of additional dimensional spaces taking values in the scalar field using Riemann submersions (Falcitelli, Ianus and Pastore, 2004)

Globally framed metric f-manifolds, which are a generalization of almost contact manifolds, were first introduced by H. Nakagawa (Nakagawa, 1966) and developed by S. I. Goldberg and K. Yano in 1971 (Goldberg and Yano, 1971). In 1972 Vanzura (Vanzura, 1972) defined almost s-contact structures on f-manifolds. Vanli and Sari [7] generalized Kenmotsu manifolds to almost s-contact structures and defined generalized Kenmotsu manifolds. Vanı and Sarı also showed that the generalized Kenmotsu manifold can be written as a warped product of the Kaehler manifold with $\mathbb{R}^s$ and studied invariant and semi-invariant submanifolds of this manifold (Turgut Vanlı and Sarı, 2015), (Turgut Vanlı and Sarı, 2023).

Firstly, Kobayashi defined and studied submersions of submanifold (Kobayashi, 1987). Deshmekh et al. investigated properties curvature of this submersions (Deshmukh, Ali and Husain, 1988). Moreover, Papaghuic and Shahid et al introduced submersion of semi-invariant submanifolds of a Sasakan manifold and a trans-Sasakan manifold, respectively (Papaghiuc, 1989), (Shahid, Al-Solamy, Jun and Ahmad, 2013). Hence many authors studied these subject (Jamali,and Shahid, 2012), (Srivastava and Pandey, 2017).

2. GENERALIZED KENMOTSU MANIFOLD

Let $\bar{N}$ be (2n+s)-dimensional differentiable manifold. Therefore $\bar{N}$ is called almost s-contact manifold by

$$\varphi^2 = -I + \sum_{i=1}^{s} \eta^i \otimes \xi_i \,,\ \eta^i(\xi_j) = \delta_{ij} \qquad (1)$$

$$g(\varphi X, \varphi Y) = g(X,Y) - \sum_{i=1}^{s} \eta^i(X)\eta^i(Y) \qquad (2)$$

where φ is tensor field, g is a Riemannian metric, $\{\xi_1, \dots, \xi_s\}$ and $\{\eta^1, \dots, \eta^s\}$ are vector fields and 1-forms, respectively.

Therefore, Φ is said to be the fundamental 2-form, $\Phi(X,Y) = g(X, \varphi Y)$, for any $X, Y \in \Gamma(T\bar{N})$. An almost s-contact manifold is normal if

$$[\varphi, \varphi] + 2\sum_{i=1}^{s} d\,\eta^i \otimes \xi_i = 0.$$

On the other hand, $\bar{N}$ is called generalized Kenmotsu manifold by

$$(\bar{\nabla}_X \varphi)Y = \sum_{i=1}^{s} \{g(\varphi X, Y)\xi_i + \eta^i(Y)\varphi X\}\,. \qquad (3)$$

Using (3), we obtain that

$$\bar{\nabla}_X \xi_i = -\varphi^2 X. \qquad (4)$$

Definition 1. Let N be submanifold of generalized Kenmotsu manifold $\bar{N}$. Therefore N is said to be semi-invariant sbmanifold if

i. $TN = D \oplus D^{\perp} \oplus Sp\{\xi_1, \dots, \xi_s\}$,

ii. $\varphi D = D$,

iii. $\varphi D^{\perp} \subset TN^{\perp}$

where, $\{D, D^{\perp}\}$ is orthogonal distribution and ξ_i are tangent to $\bar{N}$.

Example 2. Let $(R^{2n+s}, \varphi, \eta^i, \xi_i, g)$ be generalized Kenmotsu manifold with

$$\eta^i = \frac{1}{2}\left(dz_i - \sum_{i=1}^{n} y_i dx_i\right), \xi_i = 2\frac{\partial}{\partial z_i}$$

$$\varphi\left(\sum_{i=1}^{n}(X_i\frac{\partial}{\partial x_i}+Y_i\frac{\partial}{\partial y_i}\right)+\sum_{j=1}^{s}Z_j\frac{\partial}{\partial Z_j})=\sum_{i=1}^{n}(Y_i\frac{\partial}{\partial x_i}-X_i\frac{\partial}{\partial y_i})+$$
$$\sum_{j=1}^{s}\sum_{i=1}^{n}Y_iy_i\frac{\partial}{\partial Z_j}$$

$$g=e^{2\sum_{j=1}^{s}z_j}(\sum_{i=1}^{n}(dx_i\otimes dx_i+dy_i\otimes dy_i)+\sum_{j=1}^{s}\eta^j\otimes\eta^j,$$

$(x_1,\dots,x_n,y_1,\dots,y_n,z_1,\dots,z_s)$ denoting the Cartesian coordinates on R^{2n+s}.
Let N is submanifold of R^8 defined by

$$N=X(s,t,u,v,z_1,z_2)=e^{-2\sum_{j=1}^{2}z_j}(s,0,u,t,v,z_1,z_2)$$

Then local frame of TN

$$E_1=e^{-2\sum_{j=1}^{2}z_j}\frac{\partial}{\partial x_1},\quad E_2=e^{-2\sum_{j=1}^{2}z_j}\frac{\partial}{\partial y_1}$$
$$E_3=e^{-2\sum_{j=1}^{2}z_j}\frac{\partial}{\partial x_3},\quad E_4=e^{-2\sum_{j=1}^{2}z_j}\frac{\partial}{\partial y_2}$$
$$E_5=e^{-2\sum_{j=1}^{2}z_j}\frac{\partial}{\partial z_1},\quad E_2=e^{-2\sum_{j=1}^{2}z_j}\frac{\partial}{\partial z_2}$$

and

$${E_1}^*=\frac{\partial}{\partial x_1},\quad {E_2}^*=\frac{\partial}{\partial y_3}$$

from a basis of $TN^{\perp}$. We determine $D_1=sp\{E_1,E_2\}$ and $D_2=sp\{E_3,E_4\}$, then D_1, D_2 are invariant and anti-invariant distribution. Therefore $TN=D_1\oplus D_2\oplus Sp\{\xi_1,\xi_2\}$ is a semi-invariant submanifold of R^8.

Let $\overline{\nabla}$ be the Levi-Civita connection of $\bar{N}$. Therefore Gauss and Weingarten equations are given by

$$\overline{\nabla}_XY=\nabla^*{}_{\mathrm{X}}\mathrm{Y}-\sigma(\mathrm{X},\mathrm{Y}) \qquad (5)$$

$$\overline{\nabla}_XV=-\mathrm{A_V}\mathrm{X}+\nabla^{*\perp}_{\mathrm{X}}\mathrm{Y}. \qquad (6)$$

Therefore we obtain

$$g(\sigma(X,Y),V)=g(\mathrm{A_V}X,Y)\,. \qquad (7)$$

Let $\bar{R}$ and R be curvature tensors $\bar{N}$ and N, respectively. Therefore we have

$$\bar{R}(X,Y,Z,W) = R(X,Y,Z,W) - g\big(\sigma(Y,Z),\sigma(X,W)\big) + g(\sigma(X,Z),\sigma(Y,W)) \quad (8)$$

Therefore, for all $X \in TN$ we get

$$X = hX + vX + \eta^i(X)\xi_i \quad (9)$$

where h and v are denoted projection of D and $D^{\perp}$, respectively.

On the other hand, we get

$$TN^{\perp} = \varphi D^{\perp} \oplus \mu.$$

For all $K \in TN^{\perp}$, we have

$$K = pK + qK \quad (10)$$

where $pK \in \varphi D^{\perp}$, $qK \in \mu$. Therefore we get

$$\varphi K = \varphi pK + \varphi qK.$$

Now we can define Riemannian submersion. Let ψ: $(N^n, g_N) \to (B^b, g_B)$ be a submersion. Therefore ψ is called Riemannian submersion with

i) ψ_* preserves the lengths of horizontal vector.

ii) ψ has maximal rank

Hence, ψ^{-1} is said to be fibers, which a submanifold of N. Vector fields are called vertical and horizontal if they are tangent and orthogonal, respectively. On the other hand, a vector field X is said to be basic if X is horizontal and $\psi_* X = X'_{\psi_*}$.

Proposition 3. Let X, Y be basic vector fields on N. Therefore

(i) $g_N(X,Y) = g_B(X_*, Y_*) \circ \psi$,

(ii) The component $\sigma([X,Y]) + \eta^i([X,Y])\xi_i$ of $[X,Y]$ is a basic vector field and coresponds to $[X_*, Y_*]$, i.e., $\psi_*(\sigma([X,Y]) + \eta^i([X,Y])\xi_i = [X_*, Y_*]$,

(iii) $[K,X] \in D^{\perp}$ for any $K \in D^{\perp}$,

(iv) $h(\nabla_X Y) + \eta^i(\nabla_X Y)\xi_i$ is a basic vector field corresponding to $\nabla^*_X Y_*$.

Therefore, let X,Y be basic vector fields. For all $X, Y \in (D \oplus \{\xi_i\})$, we can write $\widetilde{\nabla}^*_X Y = h(\nabla_X Y) + \eta^i(\nabla_X Y)\xi_i$, where $\widetilde{\nabla}^*$ corresponding to ∇^*. Then $\widetilde{\nabla}^*_X Y$ is a basic vector field and we obtain

$$\psi_*(\widetilde{\nabla}^*_X Y) = \nabla^*_{X_*} Y_* \,. \qquad (11)$$

Now we determine a tensor field G by

$$\nabla_X Y = \widetilde{\nabla}^*_X Y + G(X,Y), \quad X, Y \in \Gamma(D \oplus sp\{\xi_i\}) \,, \qquad (12)$$

where $G(X,Y)$ is the vertical part of $\nabla_X Y$ and G is defined by

$$G(X,Y) = \frac{1}{2}\nu[X,Y] \,, \quad X, Y \in \Gamma(D \oplus sp\{\xi_i\}) \,.$$

Let R, R^* be curvature tensors of N and B respectively. Therefore we have

$$R(X,Y,Z,W) = R^*(X_*, Y_*, Z_*, W_*) - g\big(G(Y,Z), G(X,W)\big) + g(G(X,Z), G(Y,W) + 2g(G(X,Y), G(Z,W)) \qquad (13)$$

where $X, Y, Z, W \in \Gamma(D \oplus sp\{\xi_i\})$, $\psi_* X = X_*$, $\psi_* Y = Y_*$, $\psi_* Z = Z_*$ and $\psi_* W = W_* \in \Gamma(TB)$.

3. SUBMERSIONS OF SEMI INVARIANT SUBMANIFOLDS

Let $\psi : N \longrightarrow N_1$ is a submersion. We assume that

(i) $D^{\perp} = ker\psi_*$, where $\psi_* : TN \longrightarrow TN_1$ is the tangent mapping to ψ,

(ii) $\psi_*: D_p \oplus sp\{\xi_i\} \longrightarrow T_{\psi(p)}N_1$ is an isometry for each $p \in M$ which satisfies $\psi_* \circ \varphi = \varphi_1 \circ \psi_*$; $\eta^i = {\eta_1}^i \circ \psi_*$; $\psi_*\left({\xi^1}_{i(p)}\right) = {\xi^1}_{i(\psi(p))}$, where $T_{\psi(p)}N_1$ denotes the tangent space of N_1 at $\psi(p)$.

where $(N_1, \varphi_1, {\xi_i}^1, {\eta_1}^i, g_1)$ is an almost s-contact metric manifold.

From now on we will denote a s-contact metric manifold and a semi-invariant submanifold of a generalized Kenmotsu manifold $\overline{N}$ by N_1 and N.

Proposition 4. Let ψ: $(N, g_N) \to (N_1, g_{N_1})$ is a submersion. Therefore we have

$$(\widetilde{\nabla}^*_X \varphi)Y = \sum_{i=1}^{s}\{g(\varphi X, Y)\xi_i + \eta^i(Y)\varphi X\} \,, \qquad (14)$$

$$G(X, \varphi Y) = \varphi\, p\sigma(X,Y) \,, \qquad (15)$$

$$\varphi G(X,Y) = p\sigma(X, \varphi Y) \,, \qquad (16)$$

$$\varphi q\sigma(X,Y) = q\sigma(X,\phi Y) \qquad (17)$$

for any $X, Y \in \Gamma(TN)$.

Proof. For any $X, Y \in \Gamma(TN)$, using (5) and (12) we have

$$\overline{\nabla}_X Y = \widetilde{\nabla}^*_X Y + G(X,Y) + p\sigma(X,Y) + q\sigma(X,Y). \qquad (18)$$

Hence,we get

$$\varphi\overline{\nabla}_X Y = \varphi\widetilde{\nabla}^*_X Y + \varphi G(X,Y) + \varphi p\sigma(X,Y) + \varphi q\sigma(X,Y). \quad (19)$$

Putting $Y = \varphi Y$ in (18), it follows

$$\overline{\nabla}_X \varphi Y = \varphi\widetilde{\nabla}^*_X \varphi Y + G(X,\varphi Y) + p\sigma(X,\varphi Y) + q\sigma(X,\varphi Y). \quad (20)$$

Therefore, we using (3) we get

$$(\overline{\nabla}_X \varphi)Y = \overline{\nabla}_X \varphi Y - \varphi\overline{\nabla}_X Y = \sum_{i=1}^{s}\{g(\varphi X,Y)\xi_i + \eta^i(Y)\varphi X\} \quad (21)$$

Substituting (19) and (20) in (21) we get

$$\widetilde{\nabla}^*_X \varphi Y + G(X,\varphi Y) + p\sigma(X,\varphi Y) + q\sigma(X,\varphi Y) - \varphi\widetilde{\nabla}^*_X Y - \varphi G(X,Y) - \varphi p\sigma(X,Y) - \varphi q\sigma(X,Y) = \sum_{i=1}^{s}\{g(\varphi X,Y)\xi_i + \eta^i(Y)\varphi X\}.$$

We give proof.

Theorem 5. Let ψ: $(N, g_N) \to (N_1, g_{N_1})$ is a submersion. Therefore we have

$$\mathcal{A}_{\varphi X} V = \varphi \mathcal{A}_X V$$

for all $X \in \Gamma(D)$ and $V \in \Gamma(\varphi \mathrm{D}^{\perp})$.

Proof. X is basic vector and for $Y \in \Gamma(D)$ ve $V \in \Gamma(\varphi \mathrm{D}^{\perp})$ we get

$$g\big(\mathcal{A}_{\varphi X} V, Y\big) = g\big(\nabla_{\varphi X} V, Y\big) - g(\mathcal{V}\nabla_{\varphi X} V, Y)$$

Moreover, using $g\big(\mathcal{V}\nabla_{\varphi X} V, Y\big) = 0$ and ∇ lineer connection we get

$$g\big(\mathcal{A}_{\varphi X} V, Y\big) = g(\nabla_V \varphi X, Y).$$

Then for (5) we have

$$g\big(\mathcal{A}_{\varphi X} V, Y\big) = g(\varphi\overline{\nabla}_V X, Y).$$

Moreover, we using (2) and (6) we obtain

$$g\big(\mathcal{A}_{\varphi X} V, Y\big) = -g(\mathcal{A}_X V, \varphi Y)$$

which complate proof.

Theorem 6. Let ψ: $(N, g_N) \to (N_1, g_{N_1})$ is a submersion. Therefore N_1 is also a generalized Kenmotsu manifold.

Proof. For any $X, Y \in \Gamma(TN)$, using (14), we get

$$(\widetilde{\nabla}^*_X \varphi)Y = \sum_{i=1}^{s}\{g_N(\varphi X, Y)\xi_i + \eta^i(Y)\varphi X\}\ .$$

Let's apply ψ_* to the above. Therefore we using (11) and definition of submersion, we obtain

$$\left(\widetilde{\nabla}^*_{X_*}\varphi_1\right)Y_* = \sum_{i=1}^{s}\{g_{N_1}(\varphi_1 X_*, Y_*)\xi_i{}^1 - \eta_1{}^i(Y_*)\varphi_1 X_*\}$$

which complate proof **.**

Theorem 7. Let ψ: $(N, g_N) \to (N_1, g_{N_1})$ is a submersion. Therefore we have

i. $p\sigma(\varphi X, \varphi Y) + p\sigma(\varphi X, Y) = 0$
ii. $p\sigma(\varphi X, \varphi Y) = p\sigma(X, Y)$
iii. $q\sigma(\varphi X, \varphi Y) = -q\sigma(X, Y)$
iv. $G(\varphi X, \varphi Y) = G(X, Y)$
v. $G(X, Y) = -\varphi p\sigma(X, \varphi Y)$

for all $X, Y \in (D \oplus Sp\{\xi_i\})$.

Proof.

Interchanging X and Y in (15) we have

$$\varphi G(Y, X) = p\sigma(Y, \varphi X) = p\sigma(\varphi X, Y).$$

Then, we get

$$\begin{aligned} p\sigma(X, \varphi Y) + p\sigma(\varphi X, Y) &= \varphi G(X, Y) + \varphi G(Y, X) \\ &= \varphi G(X, Y) - \varphi G(X, Y) \\ &= 0. \end{aligned}$$

Putting $X = \varphi X$ in (15), we get

$$p\sigma(\varphi X, \varphi Y) = \varphi G(\phi X, Y) = -\varphi G(Y, \phi X).$$

Using (14) in the above equation, we have

$$p\sigma(\varphi X, \varphi Y) = -\varphi G(Y, \phi X) = -\varphi\big(\varphi p\sigma(Y, X)\big).$$

Then, from (1) we conclude

$$p\sigma(\varphi X,\varphi Y) = p\sigma(Y,X) - \eta^i\big(\sigma(X,Y)\big)\xi_i = p\sigma(Y,X).$$

Putting $X = \varphi X$ in (16) and using again the same equation, we have

$$q\sigma(\varphi X,\varphi Y) = \varphi q\sigma(\varphi X,Y) = \varphi q\sigma(Y,\varphi X) = \varphi^2 q\sigma(Y,X) = -q\sigma(X,Y).$$

Putting $X = \varphi X$ in (14) and then using (15) yields

$$G(\varphi X,\varphi Y) = \varphi p\sigma(\varphi X,Y) = \varphi p\sigma(Y,\varphi X) = \varphi^2 G(Y,X).$$

Therfore from (1) we have

$$G(\varphi X,\varphi Y) = G(Y,X).$$

Finally, Applying φ to equation $\varphi G(X,Y) = ph(X,\varphi Y)$, we have

$$\varphi^2 G(X,Y) = \varphi p\sigma(X,\varphi Y).$$

This gives

$$-G(X,Y) + \eta\big(G(X,Y)\big)\xi = \varphi p\sigma(X,\varphi Y).$$

4. CURVATURE PROPERTIES

Proposition 7. Let $\psi\colon (N,g_N) \to (N_1,g_{N_1})$ is a submersion. Therefore the bisectional curvature of $\bar{N}$ is given

$$\overline{K}(X,Y) = K^1(X_*,Y_*) - 2\,\|p\sigma\,(X,Y)\|^2 - 2\|p\sigma(X,\varphi Y\|^2 - 2g\big(p\sigma(X,X),p\sigma(Y,Y)\big) + 2\|q\sigma(X,Y)\|^2$$

where $X,Y \in (D \oplus Sp\{\xi_i\})$.

Proof. Let $\overline{K}$ be bisectional curvature of $\bar{N}$. Therefore we have

$$\overline{K}(X,Y) = \bar{R}(X,\varphi X,\varphi Y,Y).$$

For all $X,Y \in (D \oplus Sp\{\xi_i\})$ we using equation (7) we arrive at

$$\bar{R}(X,\varphi X,\varphi Y,Y) = R(X,\varphi X,\varphi Y,Y) - g\big(\sigma(X,Y),\sigma(\varphi X,\varphi Y)\big) + g(\sigma(X,\varphi Y),\sigma(\varphi X,Y)).$$

Substituting $h = ph + qh$, we obtain

$$\bar{R}(X,\varphi X,\varphi Y,Y) = R(X,\varphi X,\varphi Y,Y) - \|p\sigma(X,Y)\|^2 + 2\|q\sigma(X,Y)\|^2 - \|p\sigma(X,\varphi Y)\|^2 \qquad (21)$$

On the other hand we using equation (12) we write

$$R(X,\varphi X,\varphi Y,Y) = R^*(X_*,\varphi_1 X_*,\varphi_1 Y_*,Y_*) - g\big(G(\varphi X,\varphi Y),G(X,Y)\big) - g\big(G(X,\varphi Y),G(Y,\varphi X)\big) - 2g(G(X,\varphi X),G(Y,\varphi Y)) \quad (22)$$

Therefore using Theorem 7 in (22), we have

$$R(X,\varphi X,\varphi Y,Y) = R^*(X_*,\varphi_1 X_*,\varphi_1 Y_*,Y_*) - \|p\sigma(X,Y)\|^2 - \|p\sigma(X,\varphi Y)\|^2 - 2g\big(p\sigma(X,X),p\sigma(Y,Y)\big).$$

Therefore we using (21) we get

$$\bar{R}(X,\varphi X,\varphi Y,Y) = R^*(X_*,\varphi_1 X_*,\varphi_1 Y_*,Y_*) - \|p\sigma(X,Y)\|^2 - \|p\sigma(X,\varphi Y)\|^2 - 2g\big(p\sigma(X,X),p\sigma(Y,Y)\big) - \|p\sigma(X,Y)\|^2 + 2\|q\sigma(X,Y)\|^2 - \|p\sigma(X,\varphi Y)\|^2$$

which implies that

$$\overline{K}(X,Y) = K^1(X_*,Y_*) - 2\,\|p\sigma\,(X,Y)\|^2 - 2\|p\sigma(X,\varphi Y)\|^2 - 2g\big(p\sigma(X,X),p\sigma(Y,Y)\big) + 2\|q\sigma(X,Y)\|^2.$$

Corollary 8. Let $\psi\colon (N,g_N)\to(N_1,g_{N_1})$ is a submersion. Therefore the φ-sectional curvature is given

$$\bar{B}(X) = B^1(X_*) - 4\|p\sigma(X,X)\|^2 + 2\|q\sigma(X,X)\|^2,$$

where $X\in(D\oplus Sp\{\xi_i\})$.

Proof. Putting $X=Y$ in the above expression of $\overline{K}(X,Y)$,we have

$$\overline{K}(X,X) = \bar{B}(X) = B^1(X_*) - 2\,\|p\sigma\,(X,X)\|^2 - 2\|p\sigma(X,\varphi X\|^2 - 2g\big(p\sigma(X,X),p\sigma(X,X)\big) + 2\|q\sigma(X,X)\|^2.$$

Then we conclude

$$\bar{B}(X,X) = H'(X_*) - 4\|p\sigma(X,X)\|^2 - 2\|p\sigma(X,\varphi X)\|^2 + 2\|q\sigma(X,X)\|^2.$$

Putting $Y=X$ in equation (15) we have

$$p\sigma(X,\varphi X) = \varphi G(X,X) = 0.$$

Thus we get

$$\bar{H}(X) = H'(X_*) - 4\|p\sigma(X,X)\|^2 + 2\|q\sigma(X,X)\|^2.$$

REFERENCES

Deshmukh, S., Ali, S. & Husain, S.I. (1988). Submersions of CR-submanifolds of a Kaehler manifold, Indian J. Pure Appl. Math., 19(12), 1185–1205.

Falcitelli, M. Ianus, S. & Pastore, A. M. (2004). Riemannian Submersions and Related Topics, World Scientific.

Goldberg, S.I. & Yano, K. (1971). Globally framed f-manifolds, III. J. Math.15, 456-474.

Gray, A. (1967). Pseudo-Riemannian Almost Product Manifolds and Submersions. J. Math. Mech. 16, 715–737.

Kobayashi S. (1987). Submersions of CR submanifolds. Tohoku Math. J., 39(1), 95-100.

Jamali, M. & Shahid, M.H. (2012). Submersion of CR-submanifolds of nearly Trans-Sasakian manifolds, Thai J. Math., 10, 157-165.

Nakagawa, H. (1966). f-structures induced on submanifolds in spaces, almost Hermitian or Kaehlerian, Kodai Math. Sem. Rep. 18, 161-183.

O'Neill, B. (1966). The Fundamental Equations of a Submersion, Michigan Math. J. 13, 459-469.

Papaghiuc, N. (1989). Submersions of semi-invariant submanifolds of a Sasakian manifold, An. Ştiint. Univ. Al. I. Cuza Iaşi Sect. I Mat., 35(3),281-288.

Shahid, M. H., Al-Solamy, F. R. Jun, J. & Ahmad, M. (2013). Submersion of Semi-invariant Submanifolds of Trans-Sasakian Manifold, Bull. Malaysian Math. Sci. Soc., 36(1), 63-71.

Srivastava V. & Pandey,P.N. (2017). Submersion of semi-invariant submanifolds of contact manifolds, Global J. Pure and App. Math., 13(9), 5213-5224.

Turgut Vanlı, A. & Sarı, R. (2015). On Semi-invariant Submanifolds of Generalized Kenmotsu Manifold of Admitting of Semi-Symmetric Non-Metric Connection, Pure and Applied Mathematics Journal, 4(1-2), 14-18.

Turgut Vanlı, A. & Sarı, R. (2016). Generalized Kenmotsu manifolds, Communications in Mathematics and Applications, 7(4), 311-328.

Turgut Vanlı, A. & Sarı, R. (2023). Some submanifolds of Generalized Kenmotsu manifolds, Gulf Journal of Mathematics, 14(1), 114-124.

Vanzura, J., 1972. Almost r-contact structures, Ann. Scuola Norm. Sup. Pisa Sci. Fis. Mat. 26, 97-115.

Pseudo-Slant Submanifolds in Silver Riemannian Manifolds

Süleyman Dirik[1] & Ramazan Sarı[2]

1 .Prof., Amasya University, 0000-0001-9093-1607
[2] Assoc.Prof., Amasya University, 0000-0002-4618-8243

1.INTRODUCTION

Let $\widetilde{M}$ be a smooth n -dimensional manifold, and consider a tensor field of type (s,t) on $\widetilde{M}$, defined as a module over $\varphi(\widetilde{M})$. Here $\varphi(\widetilde{M}) \in C^{\infty}(\widetilde{M})$ denotes the space of diferential functions on $\widetilde{M}$, while the tensör field has s covariant and t contravariant parts. Througout, all manifolds, connections and tensors are assumed to be smooth.

An $f-$ structure on a manifold is a $(1,1)-$ tensor field of constant rank, first intoduced by Yano in (Yano and Kon, 1984). It satisfying the equation $f^3+f=0$, and this concept generalizes both almost contact and almost complex structures. Lather, Goldberg and yano extended this concept by examining a polynomial structure of degree l for a $(1,1)$ tensor field f of constant rank on $\widetilde{M}$ satisfied the equation: (Goldberg and yano,1970).

$$\Theta(f) = f^l + a_l f^{l-1} + a_2 f + a_1 I = 0.$$

Here I is identity tensor of $(1,1)-$ type, and $a_l, \ldots, a_2, a_1$ are real numbers.

In (Hretcanu and Crasmareanu, 2007), Hretcanu introduced the golden structure on $\widetilde{M}$, defined by a type $(1,1)-$ tensor J on $\widetilde{M}$ that satisfies a polynomial eq.:

$$J^2 = J + I$$

This golden structure on manifolds was further explored in (Crasmareanu and Hreţcanu,2008), and more recent studies on the golden structure found in (Bahadır and Uddin, 2018), (Crasmareanu,and Hreţcanu, 2008), (Hretcanu, 2007), (Hretcanu and Crasmareanu, 2009), (Livio, 2008), (Özkan, 2014)

The positive solution to the equation $x^2-2x-1=0$ yields another notable irrational number $\varphi = 1+\sqrt{2}$, which is as interesting as golden ratio and is referred to as the silver mean, silver number or silver ration. In (Chandra and Rani, 2009). Chandra and Rani utulized the silver number in defining fractal geometry, and ozkan (Özkan and Peltek, 2016) introduced the silver structure as a nowel structure on manifolds. Lastly, Isah et.al. stadied On integrability of silver Riemannian structure (Isah, et.al, 2021)

Various researchers have studied pure metrics in relation to these structures in [(Hretcanu and Crasmareanu, 2007), (Gezer et al,. (2013). The silver Riemann manifold is of particular interest because pure Riemann metrics are related to the silver structure. Since the Silver Riemann structure is related to almost product structures, the method of the $\Phi-$ operator, commonly used in the theory of

almost product structure, can also applied to the silver structure. In this paper we aim to explore the polynomial structure $\varphi^2 - 2\varphi - I = 0$ by utilizing its connection tp the almost product structure $\varphi^2 - I = 0$.

In the late 20th century, Chen developed the concept of slant submanifolds within the framework of almost Hermitian manifolds, as detailed in references (Chen,1990) A. Lotta later expanded this idea to contact metric manifolds (Lotta, 1996), and Cabrerizo et al. extended it further to include slant submanifoldss of K-contact and Sasakian manifolds (Cabrerizo et all, 2000). Moreover, semi-slant and slant submanifoldss of metallic Riemann manifolds were examined in (Hretcanu and Blaga, 2018).

The concept of semi-slant submanifoldss within an almost Hermitian manifold was initially introduced by Papagiuc (Papaghuic 2009). Similarly, hemi-slant submanifoldss were first presented by A. Carrizo. These submanifoldss were also described as pseudo-slant submanifoldss. More recently, Dirik and his colleagues have studied pseudo-slant submanifoldss in various manifolds (Dirik et al, 2014), (Dirik et al, 2016).

This paper investigates pseudo-slant submanfolds in the context of Silver Riemann manifolds. Section 2 introduces fundamental definitions and concepts. Section 3 explores key findings regarding submanifoldss in Riemann manifolds endowed with a Silver structure. In Section 4, we provide a detailed characterization of pseudo-slant submanifoldss within Silver Riemann manifolds. The paper concludes with illustrative examples of non-trivial pseudo-slant submanifoldss in these manifolds.

2. PRELIMINERS

In this section, we introduce certain definitions and notations related to Silver Riemann manifolds.

Definition 1. Let $\widetilde{M}$ be a C^{∞} -manifold. A (1,1)- tensor field φ on $\widetilde{M}$ is referred to as a Silver structure if φ satisfies the equation:

$$\varphi^2 = 2\varphi + I \qquad (2.1)$$

where I denotes the identity map (Özkan and Peltek, 2016).

If φ represents a Silver structure on a manifold $\widetilde{M}$, then the expression

$$P = \frac{1}{\sqrt{2}}(\varphi - I)$$

is referred to as an almost pro duct structure on the manifold $\widetilde{M}$. Conversely, any given almost pro duct structure P on $\widetilde{M}$ can define a Silver structure on $\widetilde{M}$ in the following way:

$$\varphi = I + \sqrt{2}P$$

Consider P as an almost product structure on a manifold $\widetilde{M}$, and g as a Riemann metric satisfying:

$$g(PX, PY) = g(X, Y) \qquad (2.2)$$

for any $X, Y \in \Gamma(T\widetilde{M})$.

Alternatively, P can be considered as a g-symmetric tensor, defined as:

$$g(PX, Y) = g(X, PY) \qquad (2.3)$$

for any $X, Y \in \Gamma(T\widetilde{M})$. Here, (g, P) is called a Riemann almost product structure .

φ is referred to as the Silver structure. If the Riemann metric g is φ harmonious, then $(\widetilde{M}, g, \varphi)$ is called a Silver Riemann manifold (Gezer, at al, 2013). For $\varphi -$ harmonious metric, we get

$$g(\varphi X, Y) = g(X, \varphi Y) \qquad (2.4)$$

for any $X, Y \in \Gamma(T\ \widetilde{M})$. If the interchange X and φX in (2.4), then , we have

$$\begin{aligned} g(\varphi X, \varphi Y) &= g(\varphi^2 X, Y) = g(2\varphi X + X, Y) \\ &= 2g(\varphi X, Y) + g(X, Y). \qquad (2.5) \end{aligned}$$

Example 1. Let $\mathbb{R}^4$ denote the Euclidean 4-space with standard coordinates $(\mathrm{u}_1, \mathrm{u}_2, \mathrm{u}_3, \mathrm{u}_4)$. Consider ϕ a (1,1)-tensor field defined on $\mathbb{R}^4$.

$$\varphi(u_1, \mathrm{u}, u_3, u_4) = (\psi u_1, \psi u_2, (2-\psi)u_3, (2-\psi)u_4)$$

for any vector field $(\mathrm{u}_1, \mathrm{u}_2, \mathrm{u}_3, \mathrm{u}_4) \in \mathbb{R}^4$, where $\psi = 1 + \sqrt{2}$ and $2 - \psi = 1 - \sqrt{2}$ are the roots of $x^2 - 2x - 1 = 0$. To understand the structure of this tensor, we can look at its matrix representation. The tensor field φ maps the vector field as follows, corresponding to the matrix B:

$$\mathrm{B}=\begin{pmatrix} \psi & 0 & 0 & 0 \\ 0 & \psi & 0 & 0 \\ 0 & 0 & 2-\psi & 0 \\ 0 & 0 & 0 & 2-\psi \end{pmatrix}$$

The eigenvalues of this matrix are ψ and $2-\psi$. Then we obtain Thus, we have $\varphi^2 - 2\varphi - I = 0$. Moreover, we get

$$\langle \varphi(\mathrm{u}_1, \mathrm{u}_2, \mathrm{u}_3, \mathrm{u}_4), (t_1, t_2, t_3, t_4) = \langle (\psi u_1, \psi u_2, (2-\psi)u_3, (2-\psi)u_4), (t_1, t_2, t_3, t_4) \rangle$$

$$= \psi u_1 t_1 + \psi u_2 t_2 + (2-\psi)u_3 t_3 + (2-\psi)u_4 t_4$$

$$= \psi t_1 u_1 + \psi t_2 u_2 + (2-\psi)t_3 u_3 + (2-\psi)t_4 u_4$$

$$= \langle (\mathrm{u}_1, \mathrm{u}_2, \mathrm{u}_3, \mathrm{u}_4), (\psi t_1, \psi t_2, (2-\psi)t_3, (2-\psi)t_4) \rangle$$

$$= \langle (\mathrm{u}_1, \mathrm{u}_2, \mathrm{u}_3, \mathrm{u}_4), \varphi(t_1, t_2, t_3, t_4) \rangle$$

On the other hand,

$$\langle \varphi X, \varphi Y \rangle = \langle \varphi^2 X, Y \rangle = \langle 2\varphi X + X, Y \rangle$$
$$= \langle 2\varphi(\mathrm{u}_1, \mathrm{u}_2, \mathrm{u}_3, \mathrm{u}_4) + (\mathrm{u}_1, \mathrm{u}_2, \mathrm{u}_3, \mathrm{u}_4), (t_1, t_2, t_3, t_4) \rangle$$
$$= \big\langle \big(2(\psi u_1, \psi u_2, (2-\psi)u_3, (2-\psi)u_4) + (\mathrm{u}_1, \mathrm{u}_2, \mathrm{u}_3, \mathrm{u}_4)\big), (t_1, t_2, t_3, t_4) \big\rangle,$$

$$= \langle (2(\psi u_1, \psi u_2, (2-\psi)u_3, (2-\psi)u_4), (t_1, t_2, t_3, t_4)) \rangle + \langle (\mathrm{u}_1, \mathrm{u}_2, \mathrm{u}_3, \mathrm{u}_4), (t_1, t_2, t_3, t_4) \rangle$$

$$= \langle 2\varphi(\mathrm{u}_1, \mathrm{u}_2, \mathrm{u}_3, \mathrm{u}_4), (t_1, t_2, t_3, t_4) \rangle + \langle (\mathrm{u}_1, \mathrm{u}_2, \mathrm{u}_3, \mathrm{u}_4), (t_1, t_2, t_3, t_4) \rangle$$

$$= \langle 2\varphi X, Y \rangle + \langle X, Y \rangle.$$

for each vector fields $(\mathrm{u}_1, \mathrm{u}_2, \mathrm{u}_3, \mathrm{u}_4), (t_1, t_2, t_3, t_4) \in \mathbb{R}^4$. Hence, $(\mathbb{R}^4, \langle , \rangle, \varphi)$ is a Silver Riemann manifold.

Theorem 1. Let $(\widetilde{\mathrm{M}}, g, \varphi)$ represent a Silver Riemann manifold. The Silver structure φ is said to be integrable $\Leftrightarrow \widetilde{\nabla}\varphi = 0$,

3. SUBMANIFOLDS OFA SILVER RIEMANN MANIFOLD

Submanifoldss of a Silver Riemann manifold are structures that preserve the geometric and metric properties of the manifold, characterized by a special tensor structure related to the Silver ratio.

Let M be a submanifolds of a Silver Riemann manifold $(\widetilde{M}, g, \varphi)$, here g metric on M. Furthermore, let ∇ and $\nabla^{\perp}$ be the connections on TM and $T^{\perp}M$ of M, respectively. In this context, the **Gauss** and **Weingarteen formulas** can be stated as follows:

$$\tilde{\nabla}_X Y = \nabla_X Y + \sigma(X, Y), \qquad (3.1)$$

$$\tilde{\nabla}_X V = -A_V X + \nabla_X^{\perp} V, \tag{3.2}$$

for all $X, Y \in \Gamma(TM)$, $V \in \Gamma(T^{\perp}M)$.

σ and A_V are connected by the following relationship.

$$g(A_V X, Y) = g(V, \sigma(X, Y)) \tag{3.3}$$

for all $X, Y \in \Gamma(TM)$, $V \in \Gamma(T^{\perp}M)$. The mean curvature vector K of M is given by

$$K = \frac{1}{m} \sum_{i=1}^{m} \sigma(e_i, e_i) \tag{3.4}$$

Here m =dim(M), $sp\{e_1, e_2, \ldots, e_m\}$ is a local ortho-normal frame of M.

Let (M, g) be a submanifolds of a Silver Riemann manifold $(\tilde{M}, g, \varphi)$. The submanifolds M is said to be totally umbilical if σ satisfies

$$\sigma(X, Y) = g(X, Y)K, \tag{3.5}$$

for all $X, Y \in \Gamma(TM)$, here K is the mean curvature vector. A submanifolds M is said to be totally geodesic if the second fundamental form $\sigma = 0$, and the manifold M is said to be minimal if $K = 0$.

Let (M, g) be a submanifolds of a Silver Riemann manifold $(\tilde{M}, g, \varphi)$. Then, we get

$$\varphi X = TX + NX, \tag{3.6}$$

In this context, TX represents the **tangential part**, while NX denotes the **normal part** of φX**,** for all $X \in \Gamma(TM)$.

Similary , we get

$$\varphi V = tV + nV, \tag{3.7}$$

In this context, tV represents the **tangential part,** while nV denotes th**e normal part** of φV, for all $V \in \Gamma(T^{\perp}M)$.

Proposition 1. Let M be a submanifolds of a Silver Riemann manifold $(\tilde{M}, g, \varphi)$.Then, we get

$$g(TX, Y) = g(X, TY), \tag{3.8}$$

$$g(nW, V) = g(W, nV), \tag{3.9}$$

$$g(NX, V) = g(X, tV)$$

for any $X, Y \in \Gamma(TM)$ and for W, $V \in \Gamma(TM)^{\perp}$.

From (2.5) , we easily see that

$g(TX,TY)+g(NX,NY)=g(X,Y)+2g(TX,Y)$.(3.10)

Thus by using (2.1), (3.6) and (3.7), we obtain

$T^2X=2TX+X-tNX,\ 2NX=\ NTX+nNX$ (3.11)

and

$2tV=TtV+tnV,\ n^2V=2nV\ +V-NtV.$ (3.12)

If M is $\varphi-$ invariant, thus $N=0$. so, from (3.11) and (3.12), we obtain

$T^2=2T+I,\ n^2=2n+I.$ (3.13)

Therefore, (T,g) and (n,g) forms a Silver structure on M.

Here, the covariant derivatives of T, N, t and n are defined as follows:

$(\nabla_X T)Y=\nabla_X TY-T\nabla_X Y,$ (3.14)

$(\nabla_X N)Y=\nabla_X^{\perp}NY-N\nabla_X Y,$ (3.15)

$(\nabla_X t)V=\nabla_X tV-t\nabla_X^{\perp}V$ (3.16)

and

$(\nabla_X n)V=\nabla_X^{\perp}nV-n\nabla_X^{\perp}V.$ (3.17)

For any $X,Y\in\Gamma(TM)$.

Through direct calculations, the following formulas are obtained:

$(\nabla_X T)Y=A_{NY}X+t\sigma(X,Y)$ (3.18)

and

$(\nabla_X N)Y=n\sigma(X,Y)-\sigma(X,TY).$ (3.19)

Similary, for all $V\in\Gamma(T^{\perp}M)$, we have

$(\nabla_X t)V=A_{nV}X-TA_VX$ (3.20)

and

$(\nabla_X n)V=-\sigma(tV,X)-NA_VX.$ (3.21)

Corollary 1. Let M be a submanifolds of a Silver Riemann manifold $(\widetilde{M},g,\varphi)$. If M are $\varphi-$ anti invariant and invariant submanifold, the following properties are satisfied: ,

If M is $\varphi -$ invariant Submanifold	If M is $\varphi -$anti$-$ invariant submanifold
$N = 0$	$T = 0,$
$(\nabla_X T)Y = t\sigma(X,Y),$	$(\nabla_X N)Y = n\sigma(X,Y),$
$(\nabla_X n)V = -\sigma(tV,X)$	$(\nabla_X t)V = A_{nV}X,$
$n\sigma(X,Y) = \sigma(X,TY)$	$A_{NY}X = -t\sigma(X,Y)$
$A_{nV}Y = A_V TY$	$A_{NY}Z = -A_{NZ}Y$

for all $X, Y, Z \in \Gamma(TM)$, for any $V \in \Gamma(T^{\perp}M)$.

4. PSEUDO-SLANT SUBMANIFOLDS Of A SILVER RIEMANN MANIFOLD

Some characterizations of pseudo-slant submanifoldss in a Silver Riemann manifold have been provided.

Definition 2. Let (M, g) be a submanifolds of a Silver Riemann manifold $(\widetilde{M}, g, \varphi)$. For each $X \neq 0$ tangential to M at x, the angle $\theta(x) \in \left[0, \frac{\pi}{2}\right]$, between φX and $T_x M$ is called the slant angle of M. If this slant is constant, the submanifolds is known as a slant submanifolds. When $\theta = 0$ the submanifolds is called an invariant submanifolds, and when $\theta = \frac{\pi}{2}$, it is called an anti-invariant submanifolds. If the slant angel $\theta(x) \in (0, \frac{\pi}{2})$ then the submanifolds is classified as a proper-slantsubmanifolds (Cabrerizo et al, 2000).

Theorem 3. Let (M, g) be a submanifolds of a Silver Riemann manifold $(\widetilde{M}, g, \varphi)$. M is considered a slant submanifold $\Leftrightarrow$there exists a constant $\varrho \in [0,1]$ such that:

$$T^2 = \varrho(2\varphi + I), \qquad (4.1)$$

and

$$\varphi^2 = \frac{1}{\varrho} T^2 \qquad (4.2)$$

furthermore, if θ slant angel of M, then $\varrho = cos^2\theta$ (Cabrerizo et al, 2000).

Lemma 1. Let (M, g) be a submanifolds of a Silver Riemann manifold $(\widetilde{M}, g, \varphi)$. Then, we have

$$g(TX, TY) = cos^2\theta\{g(X, Y) + 2g(X, TY)\} \qquad (4.3)$$

and

$$g(NX, NY) = sin^2\theta\{g(X, Y) + 2g(TX, Y)\}. \qquad (4.4)$$

for all X, Y ∈ Γ(TM).

Proof. From (3.8) and (4.1), we can conclude that

$$g(TX, TY) = g(X, T^2Y) = \varrho g(X, 2\varphi Y + = cos^2\theta\{g(X, Y) + 2g(X, TY)\}$$

The equations in (3.10) and (4.3) result in

$$\begin{aligned} g(NX, NY) &= g(X, Y) + 2g(X, TY) - g(TX, TY) \\ &= g(X, Y) + 2g(X, TY) \\ &\quad -cos^2\theta\{g(X, Y) + 2g(X, TY)\} \\ &= sin^2\theta\{g(X, Y) + 2g(TX, Y)\}. \end{aligned}$$

Definition 3 . Let M be a submanifolds of a Silver Riemann manifold $(\widetilde{M}, g, \varphi)$. M is pseudo-slant submanifold if there exist two orthogonal distributions D_θ and $D^\perp$, exist on M such that

(1) The tangent bundle TM has an orthogonal direct sum decomposition expressed as

$$TM = D^\perp \oplus D_\theta,$$

(2) $D^\perp$ is anti-invariant , which means that $\varphi D^\perp \subset (T^\perp M)$,

(3) D_θ is a slant, $\theta \neq \frac{\pi}{2}$, implying that the angle between D_θ and $\varphi(D_\theta)$ remains constant (Khan, 2007).

Remartk 1. Let us asume that M is a pseudo slant submanifolds of a Silver Riemann manifold $(\widetilde{M}, g, \varphi)$.

Let p =dim($D^\perp$) and q=dim(D_θ). We can distinguish the following six cases:

(1) When q = 0, M is anti-invariant,
(2) If $p = 0$ and $\theta = 0$, then M is invariant.
(3) If p = 0 and $\theta \in (0, \frac{\pi}{2})$, then M is classified as proper slant.
(4) When $\theta = \frac{\pi}{2}$, M is anti-invariant.
(5) If p ≠ 0 and q≠0 with $\theta = 0$, then M is a semi-invariant.
(6). If p ≠ 0 and q≠0 with $\theta \in (0, \frac{\pi}{2})$, then M is considered pseudo-slant.

Let μ, represent the orthogonal complement of φTM in $T^{\perp}M$. In this case, $T^{\perp}M$ can be expressed as the following decomposition:

$$T^{\perp}M = \varphi TM \oplus \mu = ND^{\perp} \oplus ND_{\theta} \oplus \mu,\ ND_{\theta} \perp ND^{\perp}. \tag{4.5}$$

Definition 4. Let (M, g) be a submanifolds of a Silver Riemann manifold $(\widetilde{M}, g, \varphi)$. The submanifolds is called D_{θ}-geodesic (or $D^{\perp}$-geodesic) if $\sigma(X, Y) = 0$ for any $X, Y \in \Gamma(D_{\theta})$ (or $\sigma(Z, W) = 0$ for any $Z, W \in \Gamma(D^{\perp})$, respectively). If for any $X \in \Gamma(D_{\theta})$ and $Z \in \Gamma(D^{\perp})$, $\sigma(X, Z) = 0$, then M is called $a\ D^{\perp} - D_{\theta}$ mixed geodesic submanifolds.

Theorem 4. Let M be a pseudo slant submanifolds of a locally Silver Riemann manifold $(\widetilde{M}, g, \varphi)$. The distribution D_{θ} −integrable, and its leaves are D_{θ} −geodesic in M if the following condition holds:

$$g(\sigma(X, Y), \varphi Z) = 0$$

for any $X, Y \in \Gamma(D_{\theta})$ and $Z \in \Gamma(D^{\perp})$.

Proof. Asume that the distribution D_{θ} is integrable, and each leaf of D_{θ} is D_{θ}-geodesic in M. Additionally, $\nabla_X Y \in \Gamma(D_{\theta})$ for all $X, Y \in \Gamma(D_{\theta})$ and $Z \in \Gamma(D^{\perp})$. Using the result from (3.1), we obtain the following:

$$\begin{aligned} g(\sigma(X, Y), \varphi Z) &= g(\tilde{\nabla}_X Y - \nabla_X Y, \varphi Z) \\ &= g(\tilde{\nabla}_X Y, \varphi Z) = g(\varphi \tilde{\nabla}_X Y, Z) \\ &= g(\tilde{\nabla}_X \varphi Y - (\tilde{\nabla}_X \varphi) Y, Z). \end{aligned}$$

Using the result from Theorem 1, we obtain the following:

$$g(\sigma(X, Y), \varphi Z) = g(\tilde{\nabla}_X \varphi Y, Z)$$

using equation (3.1), we derive the following:

$$g(\sigma(X, Y), \varphi Z) = g(\nabla_X \varphi Y + \sigma(X, \varphi Y), Z) = g(\nabla_X \varphi Y, Z) \qquad = g(\nabla_X Y \varphi, Z) = 0$$

for all $X, Y \in \Gamma(D_{\theta})$ and $Z \in \Gamma(D^{\perp})$.

Theorem 5. Let M be a pseudo slant submanifolds of a locally Silver Riemann manifold $(\widetilde{M}, g, \varphi)$. D_{θ} is integrable if he following condition hold:

$$g(\nabla_X U, 2\varphi Y) - g(\nabla_Y U, 2\varphi X = g(\sigma(X, \varphi Y), \varphi U) - g(\sigma(Y, \varphi X), \varphi U)$$

for any $X, Y \in \Gamma(D_{\theta})$ and $U \in \Gamma(D^{\perp})$.

Proof. From (2.1), (3.1),(3.2) and (3.3), we can conclude the following:

$$\begin{aligned} g(\sigma(X,\varphi Y),\varphi U) &= g\big(A_{\varphi U}X,\varphi Y\big) \\ &= g(\nabla_X^{\perp}\varphi U,\varphi Y) - g(\tilde{\nabla}_X\varphi U,\varphi Y) \\ &= g(\nabla_X^{\perp}\varphi U,\varphi Y) - g\left(\big(\tilde{\nabla}_X\varphi\big)U,\varphi Y\right) \\ &\qquad -g(\varphi\tilde{\nabla}_X U,\varphi Y) \\ &= -g(\tilde{\nabla}_X U,\varphi^2 Y) = -g(\tilde{\nabla}_X U,(2\varphi\ + I)Y) \\ &= -g(\nabla_X U,2\varphi Y) - g(\nabla_X U,Y). \end{aligned}$$

Thus,

$$g(\nabla_X Y,U) = g(\sigma(X,\varphi Y),\varphi U) + g(\nabla_X U,2\varphi Y)$$

in the equation above, if we replace X with Y,we obtain the following:

$$g(\nabla_Y X,U) = g(\sigma(Y,\varphi X),\varphi U) + g(\nabla_Y U,2\varphi X).$$

If we subtract the two equations side by side, we get the following:

$$\begin{aligned} g(\nabla_X Y,U) - g(\nabla_Y X,U) &= g(\sigma(X,\varphi Y),\varphi U) + g(\nabla_X U,2\varphi Y) \\ &\qquad -g(\sigma(Y,\varphi X),\varphi U) - \ g(\nabla_Y U,2\varphi X), \\ g(U,[X,Y]) &= g(\nabla_X U,2\varphi Y) + g(\sigma(X,\varphi Y),\varphi U) \\ &\qquad -g(\nabla_Y U,2\varphi X) - g(\sigma(Y,\varphi X),\varphi U). \end{aligned}$$

Since D_θ is integrable, it follows that:

$$g(\nabla_X U,2\varphi Y) - g(\nabla_Y U,2\varphi X) = g(\sigma(X,\varphi Y),\varphi U) - g(\sigma(Y,\varphi X),\varphi U).$$

Theorem 6. Let M be a pseudo slant submanifolds of a locally Silver Riemann manifold $(\widetilde{M},g,\varphi)$. n is parallel $\Leftrightarrow$ A_V satisfies the condition:

$$A_V tW = -A_W tV$$

for any $V,W \in \Gamma(T^{\perp}M)$.

Proof. If n is parallel, then $\nabla n = 0$. From (3.3) and (3.21) , we obtain the following:

$$0 = g(\sigma(tV,X) + NA_V X,W)$$

$$= g(A_W tV, X) + g(\ A_V X, tW)$$

$$= g(A_W tV + \ A_V tW, X)$$

for any $V,\ W \in \Gamma(T^{\perp}M)$ and for any $X \in \Gamma(TM)$.

Theorem 7. Let M be a pseudo slant submanifolds of a locally Silver Riemann manifold $(\widetilde{M}, g, \varphi)$. If N is parallel, In this case, M is either a mixed geodesic or an anti-invariant submanifolds.

Proof. t is parallel $\Leftrightarrow$ if N is parallel, If t is parallel, then $\nabla t = 0$. which means M is invariant. For all $X \in \Gamma(D_\theta), Y \in \Gamma(D^{\perp})$, $V \in \Gamma(T^{\perp}M)$. We can conclude this from (3.19) and (3.20).

$$A_{nV}X - TA_V X = 0,$$

$$0 = g(A_{nV}X - TA_V X, Y)$$

$$= g(\sigma(X,Y), nV) - g(TA_V X, Y)$$

$$= g(\sigma(X,Y), nV) - g(\sigma(X,TY), V)$$

$$= g(n\sigma(X,Y), V) - g(\sigma(X,TY), V),$$

so

$n\sigma(X,Y) = \sigma(X,TY)$

for $Y \in \Gamma(D^{\perp})$, we have $TY = 0$. Therefore, it follows that:

$n\sigma(X,Y) = 0$

By replacing X with TX in the above equation, we obtain

$n\sigma(TX,Y) = 0.$

By replacing X with TX in the above equation and using (4.1) , we have

$$n\sigma(T^2X,Y) = n\cos^2\theta\sigma((2\varphi + I)X,Y) = 0.$$

Thus, we conclude that either $\sigma = 0$ (indicating that M is mixed geodesic) or $\cos\theta = 0$ which leads to $\theta = \frac{\pi}{2}$ (indicating M is anti-invariant).

Theorem 8 . Let M be a totally umbilical pseudo slant submanifolds of a locally Silver Riemann manifold $(\widetilde{M}, g, \varphi)$. If N is parallel, In this case, M can be classified as either a minimal, an anti-invariant submanifolds.

Proof. N is parallel $\Leftrightarrow$ t is parallel, If t is parallel, then $\nabla t = 0$. which means M is invariant. For all $X \in \Gamma(D_\theta), Y \in D^\perp$, $V \in \Gamma(T^\perp M)$. We can conclude this from (3.19) and (3.20).

$$A_{nV}X - TA_VX = 0,$$

so

$$\begin{aligned} 0 &= g(A_{nV}X - TA_VX, Y), \\ &= g(\sigma(X,Y), nV) - g(TA_VX, Y) \\ &= g(\sigma(X,Y), nV) - g(\sigma(X,TY), V) \\ &= g(n\sigma(X,Y), V) - g(\sigma(X,TY), V) \end{aligned}$$

for $Y \in \Gamma(D^\perp)$, we have $TY = 0$. Therefore, it follows that:

$$n\sigma(X,Y) = 0.$$

By replacing X with TX in the above eq. we obtain

$$n\sigma(TX,Y) = 0.$$

Therefore, since M is totally umbilical submanifolds, we can refer to the findings in (3.5)

$$ng(TX,Y)K = 0.$$

Replacing X by TX in the above eq. and using (4.1) , we have

$$\begin{aligned} ng(T^2X,Y)K &= ncos^2\theta g((2\varphi + I)X,Y)K \\ &= ncos^2\theta\{g(2\varphi X,Y) + g(X,Y)\}K \\ &= ncos^2\theta\{g(X,Y)\}K = 0. \end{aligned}$$

Hence we conclude that either $K = 0$ (indicating that M is minimal), or $cos\theta = 0$ which leads to $\theta = \frac{\pi}{2}$ (indicating that M is anti-invariant).

Theorem 9. Let M be a pseudo-slant submanifolds in a locally Silver Riemann manifold $(\widetilde{M}, g, \varphi)$. $D^\perp$ is integrable $\Leftrightarrow A_{ND^\perp}D^\perp = 0$,

for all $Z, U \in \Gamma(D^\perp)$.

Proof. If M is a pseudo-slant submanifolds in a locally silver Riemann manifold(M, g, φ). Then, for all $Z, U \in \Gamma(D^\perp)$, we have $TZ = TU = 0$, which implies $\nabla_Z TU = \nabla_U TZ = 0$.

By using (3.14), we get $T([Z,U]) = 0$ if and only if $A_{NZ}U = A_{NU}Z$ holds, for all $U \in \Gamma(D^{\perp})$. From (3.14), for all $X \in \Gamma(TM)$ and $Z, U \in \Gamma(D^{\perp})$, we get

$$g\big((\nabla_X T)Z, U\big) = g(A_{NZ}X, U) + g(th(X,Z), U) = -g(\nabla_X Z, TU) = 0,$$

which implies $g(A_{NZ}X, U) = -g(th(X,Z), U)$. From

$$g(A_{NZ}X, U) = g(A_{NZ}U, X) = g(A_{NU}Z, X) = g(h(X,Z), = g(th(X,Z), U),$$

we obtain $g(A_{NZ}U, X) = 0$ for all $X \in \Gamma(TM)$ and $Z, U \in \Gamma(D^{\perp})$. so, $A_{NZ}U = 0$, for all $Z, U \in \Gamma(D^{\perp})$.

Conversely, if $A_{NZ}U = 0$, for all $Z, U \in \Gamma(D^{\perp})$ then from

$$g(th(X,Z), U) = g(h(X,Z), NU) = g(A_{NU}Z, X) = 0$$

and (3.14), we get

$$0 = g\big((\nabla_Z T)U, X\big) = -g(T\nabla_Z U, X) = -g(\nabla_Z U, TX),$$

for any $Z, U \in \Gamma(D^{\perp})$, $X \in \Gamma(D_{\theta})$. From $T(D_{\theta}) = D_{\theta}$, we obtain $\nabla_Z U \in \Gamma(D^{\perp})$ which implies $[Z,U] \in \Gamma(D^{\perp})$.

Theorem 10. Let M be a pseudo slant submanifolds in a locally silver Riemann manifold $(\widetilde{M}, g, \varphi)$. In this case, $D^{\perp}$ is integrable $\Leftrightarrow$

$$(\nabla_Z T)U = (\nabla_U T)Z$$

for all $Z, U \in \Gamma(D^{\perp})$.

Proof. For all $Z, U \in \Gamma(D^{\perp})$. Using (3.18) , we obtain

$$(\nabla_Z T)U = A_{NU}Z + t\sigma(Z,U) \qquad (4.6)$$

Replacing Z by U in the above equation, we have

$$(\nabla_U T)Z = A_{NZ}U + t\sigma(U,Z) \qquad (4,7)$$

Then, (4.6), (4.7) and (from Theorem 9 we arrive at the conclusion.

Finally, let's support the topic with an example.

Example 2 . To construct a pseudo slant submanifolds of a Silver Riemann manifold based on the provided parametrization $\chi(u,v)$, we first need to analyze the given mapping and then define the associated Riemann structure.the mapping is defined as:

$$\chi(u,v) = (3u\sin\alpha, -v\cos\alpha, -4u\sin\alpha, v\cos\alpha)$$

this mapping $\chi: \mathbb{R}^2 \to \mathbb{R}^4$ defines a submanifold M in $\mathbb{R}^4$. To ensure M is a submanifold of $\mathbb{R}^4$,we will consider the tangent vectors and the embedding The parametriziation consist of two parameters (u, v). Next, we calculate the tangent vector of M by differentiating χ with respect to each parameter:

$$\mathrm{E}_1 = \frac{\partial \chi}{\partial \mathrm{u}} = (3\sin\alpha, 0, -4\sin\alpha, 0)$$

$$\mathrm{E}_2 = \frac{\partial \chi}{\partial \mathrm{v}} = (0, -\cos\alpha, 0, \cos\alpha)$$

For the Silver Riemann structure φ of $\mathbb{R}^4$, the coordinat system is given by (x_1, y_1, x_2, y_2).

$$\varphi(\frac{\partial}{x_i}) = \frac{\partial}{y_i}, \varphi(\frac{\partial}{y_j}) = -\frac{\partial}{x_j}, \qquad 1 \leqslant i, j \leqslant 2$$

then we obtain

$$\varphi E_1 = (0, 3sin\alpha, 0, -4sin\alpha)$$

$$\varphi E_2 = (cos\alpha, 0, -cos\alpha, 0).$$

Through direct calculations, we determine that $\mathrm{D}_\theta = \mathrm{Sp}\{\mathrm{E}_1, \mathrm{E}_2\}$ defines a slant distribution with a slant angle of

$$\cos\theta = \frac{\mathrm{g}(\mathrm{E}_{1,}\varphi\mathrm{E}_2)}{\|\mathrm{E}_{1,}\|\|\varphi\mathrm{E}_2\|} = \frac{3\sin\alpha.\cos\alpha + 4\sin\alpha.\cos\alpha}{\sqrt{3^2\sin^2\alpha + (-4)^2\sin^2\alpha}.\sqrt{2\cos^2\alpha}} = \frac{7}{5\sqrt{2}}$$

$\theta = \arccos\left(\frac{7}{5\sqrt{2}}\right)$. Consequently, M is a 2-dinensionel proper pseudo-slant submanifold of $\mathbb{R}^4$ endowed with its standard Silver Riemann structure.

Conclusion . In this study of pseudo-slant submanifoldss within the framework of a Silver Riemann manifold, we have explored their unique geometric properties and the intrinsic connections to the Silver ratio. Pseudo-slant submanifoldss reveal fascinating characteristics, particularly in how their tangent spaces interact with the ambient manifold's structure.

REFERENCES

Atceken, M., & Dirik, S. (2014). On the geometry of pseudo-slant submanifolds of a Kenmotsu manifold. Gulf journal of Mathematics, 2(2).

Bahadır, O., & Uddin, S. (2018). Slant Submanifolds of Golden Riemannian Manifolds , Journal of Mathematical Extension Vol. 13, No. 4, (2019), 23-39 .

Cabrerizo, J. L., Carriazo, A., Fernandez, L. M., & Fernandez, M. (2000). Slant submanifolds in Sasakian manifolds. Glasgow Mathematical Journal, 42(1), 125-138.

Chen, B. Y. (1990). Slant immersions. Bulletin of the Australian Mathematical Society, 41(1), 135-147.

Chen, B. Y. (1990). Geometry of slant submanifolds, Katholieke Univ. Leuven, Louvain, 1, 990.

Crasmareanu, M., & Hreţcanu, C. E. (2008). Golden differential geometry. Chaos, Solitons & Fractals, 38(5), 1229-1238..

Dirik, S., & Atçeken, M. (2016). Pseudo-slant submanifolds in Cosymplectic space forms. Acta Universitatis Sapientiae, Mathematica, 8(1), 53-74.

Goldberg, S. I., & Yano, K. (1970). Polynomial structures on manifolds. In Kodai Mathematical Seminar Reports (Vol. 22, No. 2, pp. 199-218). Department of Mathematics, Tokyo Institute of Technology.

Hretcanu, C. E. (2007). Submanifolds in Riemannian manifold with Golden structure. In Workshop on Finsler geometry and its applications, Hungary..

Hretcanu, C. E., & Crasmareanu, M. (2007). On some invariant submanifolds in a Riemannian manifold with golden structure. An. Stiint. Univ. Al. I. Cuza Iasi. Mat.(NS), 53(1), 199-211.

Hretcanu, C. E., & Crasmareanu, M. (2009). Applications of the golden ratio on Riemannian manifolds. Turkish Journal of Mathematics, 33(2), 179-191.

Hretcanu, C. E., & Blaga, A. M. (2018). Slant and Semi-Slant Submanifolds in Metallic Riemannian Manifolds. Journal of Function Spaces, 2018(1), 2864263.

Khan, V. A., & Khan, M. A. (2007). Pseudo-slant submanifolds of a Sasakian manifold. Indian Journal of pure and applied Mathematics, 38(1), 31.

Livio, M. (2008). The golden ratio: The story of phi, the world's most astonishing number. Crown.

Lotta, A. (1996). Slant submanifolds in contact geometry. Bulletin mathématique de la Société des Sciences Mathématiques de Roumanie, 183-198.

Özkan, M. (2014). Prolongations of golden structures to tangent bundles. Differential Geometry-Dynamical Systems, 16.

Papaghuic N., (2009). Semi-slant submanifolds of a Kaehlarian manifold, An. St. Univ. Al. I. Cuza. Univ. Iasi. 40,55-61

Yano, K. (1982). On a Structure Defined by a Tensor Field f of Type (1, 1) Satisfying f3+ f= 0. In North-Holland Mathematics Studies (Vol. 70, pp. 251-261). North-Holland.

Yano, K., & Kon, M. (1984). Structures on manifolds, Series in Pure Mathematics 3, World Scientific Publ. Co., Singapore..

Özkan, M., & Peltek, B. (2016). A new structure on manifolds: silver structure. International Electronic Journal of Geometry, 9(2), 59-69.

Crasmareanu, M., & Hreţcanu, C. E. (2008). Golden differential geometry. Chaos, Solitons & Fractals, 38(5), 1229-1238.

Chandra, M., & Rani, M. (2009). Categorization of fractal plants. Chaos, Solitons & Fractals, 41(3), 1442-1447.

Gezer, A., Cengiz, N., & Salimov, A. (2013). On integrability of Golden Riemannian structures. Turkish Journal of Mathematics, 37(4), 693-703.

Isah, I., Isah, M. A., Baba, M. U., Hassan, T. L., & Kabir, K. D. (2021). On integrability of silver Riemannian structure. International Journal of Advanced Academic Research, 7(12), 2488-9849.

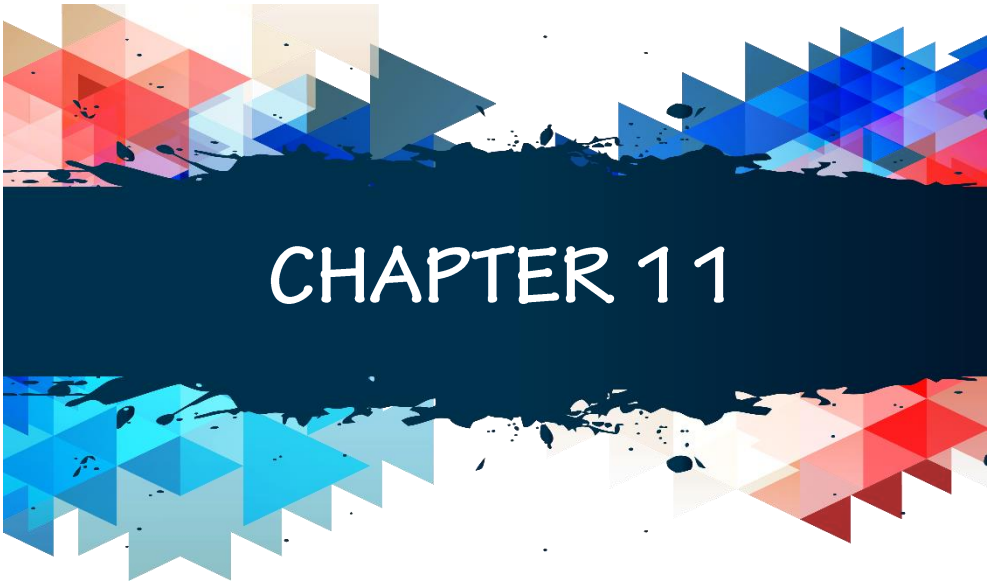

Effect of Chemical Composition on the Biological Activities of Royal Jelly

***Gulsah Aydin*[1]**

1 Asst. Prof. Dr., Ordu University, Ulubey Vocational School, Department of Chemistry and Chemical Processing Technologies, ORCID: 0000-0002-5376-0690

INTRODUCTION

Bees are one of nature's most important creatures, playing a vital role for humanity for centuries(Jarvis, 2023). All products that are the gift of miraculous bees to nature have many biological activities with their rich chemical content. Bee products stand out as health supporters in these aspects. Bee products such as honey, royal jelly, beeswax, propolis and bee venom can play a supportive role in the treatment of many diseases with their important bioactive component contents. The components contained in honey strengthen the immune system. Honey also stands out with its antioxidant, antimicrobial and anti-inflammatory aspects. Propolis, known for its antibacterial, antiviral and antifungal properties, is an important bee product with many remarkable biological activities. Pollen, another bee product, has a high protein content. Bees collect these proteins from various plants. Pollen, which supports digestive health, stands out with its antioxidant, antibacterial, antifungal, antimicrobial, and anti-inflammatory activities. Bee venom secreted from the venom glands of worker bees (*Apis mellifera*) is an important product used in the regulation of the immune system and the treatment of inflammatory diseases. Royal jelly is a product with high nutritional value produced to feed the queen bee. It stands out as a food product rich in vitamins, minerals and amino acids.

Here, studies on the chemical composition, biological activities, side effects and toxic effects of royal jelly are included. Royal jelly is a viscous liquid rich in many minerals, including carbohydrates, lipids, proteins, essential amino acids, fatty acids, phenolic compounds, water-soluble B vitamins and fat-soluble vitamins A, C, D and E, calcium, potassium, magnesium and sodium. Royal jelly stands out as an important functional food with its antihypertensive, anticancer, antidiabetic, immune-boosting, cardiovascular health-improving, memory-boosting, anti-aging and wound-healing biological functions due to the effects of the chemical components it contains with high antimicrobial, anti-inflammatory and antioxidant activities.

ROYAL JELLY

The yellowish white acidic secretion synthesized by nurse honey bees and secreted by the hypopharynx and mandibular glands to feed the larvae is called royal jelly. While the larvae that will become male and worker bees are fed royal jelly for three days, queen bees are fed royal jelly for their entire life. Royal jelly plays an important role in the development and nutrition of the queen bee, who is vital to the survival and growth of the colony as the reproductive center of the hive. The queen bee is fed royal jelly for her entire life, giving her an improved

size, longevity and fertility compared to worker bees. The medical importance of royal jelly has been known since ancient times. In 1922, it was suggested in France that it could be used in human therapy. Following this, studies examining the effects of royal jelly on pathogenic processes in various animal models have increased. Royal jelly, which is a rich source of certain bioactive components, has been used as a functional and nutritious food by people in different parts of the world for the last twenty years. It is also one of the most widely used natural products in the pharmaceutical and cosmetic industries. Royal jelly exhibits numerous physiological and pharmacological properties, including antihypercholesterolemic, anti-inflammatory, vasodilator, hypotensive, immunomodulatory, antidiabetic, antioxidant, neuroprotective, antimicrobial, anti-aging, estrogenic, antiallergic, antiosteoporotic and antitumor effects. The pharmacological effects of royal jelly have been included in many preclinical and clinical studies. Royal jelly can reduce menopausal symptoms and has remarkable biological and therapeutic activities on the reproductive system. These biological activities are due to various bioactive substances such as proteins, essential fatty acids, peptides, minerals and phenolics. Royal jelly, used as a food supplement, in cosmetic products and for therapeutic purposes, is a natural product with high nutritional value with its rich bioactive component content. Its consumption provides numerous health benefits for humans, earning it the reputation of a "superfood"(Bagameri, Botezan, Bobis, Bonta, & Dezmirean, 2023; Fang, Feng, Ma, Rueppell, & Li, 2023; Li et al., 2021; Mutlu, Akbulut, Aydın, & Mutlu, 2023). Interest in royal jelly is increasing due to its potential benefits, and the effectiveness of this superfood should be demonstrated by more preclinical and clinical studies.

CHEMICAL CONTENT AND NUTRITIONAL VALUE OF ROYAL JELLY

Since royal jelly will be offered for use as a traditional natural product, standardization in sensory analysis and chemical component analysis data is important. Sensory analysis, also known as organoleptic analysis, is of great importance in ISO standards. Royal jelly should be liquid at normal temperature(Lercker, 2003). It should have a milky white, pale yellow color, pure, acidic (pH: 3.4-4.5) viscous structure. The sensory quality of royal jelly is determined after statistical analysis of data and application of quality control measures(Marx, Veloso, Casal, Pereira, & Peres, 2021).

Water Content

Water is an important inorganic component of royal jelly since the processability, usability, quality and shelf life of royal jelly depend on its moisture content. The moisture content of fresh royal jelly is in the range of 60-70%. The moisture content of freeze-dried royal jelly is reduced by 3.8%(Piana, 1996). The moisture content of the hive is kept constant. This is thought to be related to the constant supply of new royal jelly by the nurse bees(Kanelis et al., 2015).

Lipid Composition

Most fatty acids contain phospholipids. 10–Hydroxy–2–Decenoic Acid **(**10-HDA), a monounsaturated fatty acid, makes up more than half of the total fatty acids in royal jelly. 10–HDA, also known as queen bee acid, stands out as the primary fatty acid compound of royal jelly(Honda et al., 2015). This compound is largely responsible for the pharmacological activities of royal jelly, accounting for approximately 70% of the total fatty acids. 10-HDA concentration is one of the parameters used to determine the quality of royal jelly. 10-HDA is considered an indicator component and international standard for the freshness and quality of royal jelly (Takikawa et al., 2013). According to the international standard ISO 12824:2106 royal jelly, the minimum 10-HDA concentration in pure royal jelly is estimated to be 1.4% (Sabatini, Marcazzan, Caboni, Bogdanov, & Almeida-Muradian, 2009).

Amino Acid Content

The amino acids with the highest percentage in the free amino acid content of royal jelly are determined as serine, proline, lysine, β-alanine, aspartate, glutamate and phenylalanine. Approximately 12-15% of raw royal jelly consists of proteins. The major royal jelly proteins (MRJPs), which constitute 80% of royal jelly proteins, constitute a protein family consisting of ten different proteins. Apis mellifera is thought to produce ten major royal jelly protein genes (MRJP1-10) through gene duplication of a single-copy protein. These genes are highly expressed in the hypopharyngeal glands of nurse bees and constitute a significant portion of the chemical content of royal jelly, which is a very important nutrient for the development of bee larvae (Dai et al., 2021). MRJP1, MRJP2, MRJP3 and MRJP5 are the most abundant royal jelly proteins. Also known as royal actin, MRJP1 accounts for more than 45% of the water-soluble proteins in royal jelly. MRJP1 is considered a freshness marker to assess the quality and authenticity of royal jelly(L.-r. Shen et al., 2015). MRJP1 is crucial in accelerating larval development and queen differentiation in honeybees by increasing body size,

promoting ovary development, and reducing developmental time(Kamakura, 2011). MRJPs are effective in curing many diseases. It is believed that most of the therapeutic advantages of royal jelly come from MRJPs (Hossen, Nahar, Gan, & Khalil, 2019). Royal jelly proteins are important for larval development. While MRJP1, MRJP4 and MRJP5 proteins are important for meeting basic amino acid needs, MRJP2 and MRJP5 proteins are important as nitrogen reserves.

Sugar Content

The amount of sugar in royal jelly plays an important role in evaluating its quality. The sugar content of royal jelly consists of fructose, glucose and sucrose. The sugar content of fresh royal jelly samples constitutes 7-18%. In lyophilized royal jelly, this value reaches 1.28% by freeze-drying the carbohydrates(Kausar & More, 2019). The amount of sugar in royal jelly samples varies depending on many factors, including geographical origin, harvest season and the availability of food sources such as nectar and pollen compatible with the natural diet of bees.

Vitamins and Minerals

Pantothenic acid and niacin stand out as the most abundant vitamins in royal jelly (Collazo et al., 2021; Sharma, Pant, Brar, Thakur, & Nanda, 2023). Apart from these, there are biotin, folate, inositol, pyridoxine, riboflavin, thiamine and ascorbic acid (Kunugi & Mohammed Ali, 2019; Melliou & Chinou, 2014). It has not been reported that fat-soluble vitamins A, D, E and K are also present in royal jelly (Stocker, Schramel, Kettrup, & Bengsch, 2005). Royal jelly also contains 1.5% salts of iron, aluminum, potassium, calcium, lead, magnesium, sodium, copper, phosphorus, zinc, manganese and cadmium minerals. Royal jelly contains relatively higher levels of potassium and lower levels of cadmium compared to other minerals(J. Guo et al., 2021). Royal jelly also contains trace amounts of the elements nickel, tin, chromium, antimony, tungsten, titanium and bismuth (Bogdanov, 2011).

Phenolic Compounds

Royal jelly contains various phenolic compounds with antioxidant properties(Ibrahim, Nanbu, & Miyata, 2021). Ferulic acid, which constitutes 68% of the total phenolic content, is the main phenolic acid found in royal jelly(López-Gutiérrez, del Mar Aguilera-Luiz, Romero-González, Vidal, & Frenich, 2014). The composition of royal jelly contains abundant flavonoids such as flavone derivatives such as apigenin, acacetin, chrysin and luteolin glycosides, flavanone derivatives such as naringenin, hesperetin and isosakuranetin, flavonol derivatives such as kaempferol glycosides and isorhamnetin, and isoflavonoid

derivatives such as coumestrol, genistein and formononetin (Kocot, Kiełczykowska, Luchowska-Kocot, Kurzepa, & Musik, 2018; Kunugi & Mohammed Ali, 2019). Royal jelly is considered a rich source of phenolics (23.3 g/mg) and flavonoids (1.28 g/mg)(Kunugi & Mohammed Ali, 2019).

Other Compounds

Acetylcholine (ACh) was detected in royal jelly at 1 mg/g dry weight(Bogdanov, 2011; J. Guo et al., 2021). ACh synthesis by royal jelly is affected by glucose metabolism and insulin levels by regulating choline acetyltransferase activity (Kunugi & Mohammed Ali, 2019). ACh, a neurotransmitter, plays a role in memory development and cognitive performance. Nucleotides such as guanosine, adenosine and uridine and phosphates such as adenosine monophosphate, adenosine diphosphate and adenosine triphosphate are also abundant in the composition of royal jelly(Bălan et al., 2020).

FACTORS AFFECTING THE CHEMICAL COMPOSITION OF ROYAL JELLY

The chemical content of royal jelly is affected by factors such as the nutrition of bee larvae, differences in honey bee species, environmental conditions, and harvest time. Differences are also observed in the expected biological activities of natural products depending on the differences in the compounds they contain. Royal jelly is subjected to some sensory and content analyses to determine content standards. Moisture, sugar, 10-HDA and protein contents are the main parameters in the evaluation of royal jelly quality(Wytrychowski et al., 2013). There are studies showing that certain vitamins, amines, amino acids and carbohydrates stand out as quality indicators for royal jelly(Virgiliou et al., 2020).

Environmental Conditions and Nutrition

For the safe use of royal jelly, it is important to standardize the chemical compounds with prominent biological activity and ensure quality production. The quality of royal jelly can be affected by various factors such as environmental conditions, bee nutrition and plant extract source. Since the quality of royal jelly is closely related to its protein content, all factors affecting the protein content, such as consumption of feeds with different protein content and temperature, affect the quality of royal jelly. Changing diets and changing seasons, as well as external environmental effects, play a role in determining the protein content and amino acid composition of bee products. Different proteins are present in the royal jelly of bees fed with different pollen flower origins in different flowering

seasons(Kausar & More, 2019). Nutritional and environmental effects affect not only the protein but also the lipid profiles of royal jelly, leading to differences in the bioactivity and quality of the product (Yan et al., 2022).

Effect of Honeybee Species

Various factors such as genetics, colony conditions, nutrient flow and queen egg laying can affect royal jelly production. Beekeepers use crossbreeding techniques to increase productivity. The Italian bee strain hybrid Apis mellifera ligustica can produce royal jelly at a rate 10 times higher than Italian honeybees(Han et al., 2015). Different honey bee races living in different environments differ from each other in terms of their productivity, the rate of colony expansion, ways of collecting and storing pollen, and the differences in the amounts of bee products produced under different conditions(Khan, Ghramh, Ahmad, El-Niweiri, & Ahamed Mohammed, 2021; Mouro & Toledo, 2004).

Effect of Harvest Time

Harvest time affects the yield and chemical composition of royal jelly(Virgiliou et al., 2020). Royal jelly harvested 72 hours after larval inoculation had the highest yield, maximum crude protein, ash, fructose and glucose concentrations and lowest water content compared to royal jelly harvested 24 and 48 hours after inoculation. It was reported that the highest lipid content was obtained in royal jelly harvested 24 hours after inoculation(S. Al-Kahtani & Taha, 2021). The best antioxidant capacity and total polyphenol amount were also determined 24 hours after collection(Cemek et al., 2010; Kocot et al., 2018).

Effect of Storage Conditions

Post-harvest storage conditions are very important in preventing the loss of chemical components of royal jelly. In a study conducted with royal jelly samples stored at different temperatures for 12 months, it was reported that protein content was affected by temperature. The highest concentrations of minerals, including Mg, Ca, K, Na, Fe, Cu and Mn, were determined to be 48 hours and 72 hours after royal jelly inoculation(S. N. Al-Kahtani & Taha, 2020). The shelf life of royal jelly varies depending on storage conditions. A dark, translucent or opaque ceramic, glass or plastic container is suitable for storing royal jelly. Storing royal jelly frozen helps preserve nutritional quality for longer by preventing the active proteins from deteriorating(Bogdanov, 2011). Fresh royal jelly can be stored for up to two years below -18 ^{o}C, while it has a storage period of six months at +4 ^{o}C.

BIOLOGICAL ACTIVITIES

Foods that contain high amounts of chemical components needed to stay healthy are in the functional food class (Collazo et al., 2021). Royal jelly was first used as a functional food in the food industry in the 1850s(Fratini, Cilia, Mancini, & Felicioli, 2016). After this date, royal jelly began to be commercially produced in capsule, ampoule and powder forms. 60% of royal jelly in the world market is produced in China and distributed to Europe, Japan and the USA(Collazo et al., 2021). Royal jelly contains bioactive components such as amino and gamma globulins, unsaturated fatty acids, hormones, enzymes and other proteins that support the immune system(Maghsoudlou, Mahoonak, Mohebodini, & Toldra, 2019). The biological and pharmacological properties of royal jelly are based on its composition, which includes water, 10-HDA, protein and sugar content. It is known that MRJPs have antioxidant and neuroprotective immune system strengthening properties and may help improve physical and mental performance(W. Wang et al., 2023). The food supplement prepared by adding different levels of royal jelly to skim milk can be used in the treatment of patients with conditions such as hypertension, cancer and type 2 diabetes(Alu'datt et al., 2015).

Immunomodulatory Activity

Bioactive proteins and fatty acids in royal jelly exhibit immunomodulatory properties(Melliou & Chinou, 2014). In immunodeficient mice treated with cyclophosphamide, the number of macrophages increased with the administration of MRJP1, MRJP2 and MRJP3 proteins. As expected, immunity increased in parallel with the increase in macrophages. This resulted in an improvement in the microorganism content of the intestinal flora of the mice (W. Wang et al., 2023). MRJP3 glycoprotein exhibits anti-inflammatory properties by suppressing the production of TNF-α, IL-4, IFN-γ and IL-2 IL-6 and IL-1 by T cells in vitro(Okamoto et al., 2003). The immunomodulatory activity of royal jelly against Graves' disease is mainly due to the decrease in TNF-α and the increase in IFN-γ and Th1/Th2 cytokine level ratios in lymphocytes (Erem, Deger, Ovali, & Barlak, 2006). In serum-deprived environments, MRJP3 glycoproteins derived from royal jelly increase lymphocyte cell proliferation(Maghsoudlou et al., 2019). Both 10-HDA and 10-H2DA compounds found in royal jelly exhibit immunomodulatory effects in terms of reducing the proliferation of peripheral blood mononuclear cells (PBMC) and the levels of interleukin-2 production (IL-2)(Dzopalic et al., 2011; Vucevic et al., 2007). IL-2 secretion from PBMCs changes with age(Meydani et al., 1990). Royal jelly appears to have immunostimulatory effects to promote PBMC proliferation in both elderly and

young individuals. High 10-HDA concentrations have been hypothesized to act as immunoenhancers and promote Th1 immune responses(Mihajlovic, Rajkovic, Chinou, & Colic, 2013). The combined application of royal jelly with alum showed synergistic effects, improving immunological parameters such as total antibody production and IgM, IgG1, IgG2A and IgG2B isotypes (Okamoto et al., 2003). It has been observed that three months of royal jelly treatment showed significant improvement in children with systemic lupus erythematosus (SLE) (Zahran et al., 2016).

Antimicrobial Activity

Royal jelly exhibits strong antimicrobial properties against different pathogens due to the presence of special proteins, peptides and 10-HDA(Fratini et al., 2016; Han et al., 2014; Kim et al., 2019). Jelleins and royalisins act on bacteria by altering the function of the bacterial cell membrane through their hydrophobic residues. Halogenation of gellenins caused them to bind more tightly to the bacterial cell wall, thus increasing their antimicrobial and antibiofilm activity by 1-8 times and their proteolytic stability by 10-100 times (Lima, Brito, Verly, & Lima, 2024; Zhou et al., 2021). Flavonoids, which occupy a large place in the chemical composition of royal jelly, are the main components responsible for antimicrobial activity (Kocot et al., 2018; Nabas, Haddadin, Haddadin, & Nazer, 2014). When royal jelly is used together with antibiotics, it creates a synergistic effect and increases the effectiveness of antibiotics. In other words, antibiotics can be effective at lower doses when used together with royal jelly. Studies on genetically modified animal models highlight the importance of IL-6 in the anti-infective role (Rose-John, Winthrop, & Calabrese, 2017). Royal jelly exhibits antibacterial properties against *Staphylococcus aureus*, *Streptococcus alactolyticus, Staphylococcus xylosus, Salmonella choleraesuis, Staphylococcus intermedius B., Vibro parahaemolyticus* and *Escherichia coli* in animals and humans(Alkhaibari & Alanazi, 2022). The main antibacterial effect of royal jelly is associated with 10-HDA, which exhibits growth inhibitory activity in bacteria (Collazo et al., 2021). 10-HDA has been shown to have significant activity against gram-positive and gram-negative bacteria by disrupting bacterial cell membranes(Uthaibutra, Kaewkod, Prapawilai, Pandith, & Tragoolpua, 2023). One of the most important components of antibacterial action is antimicrobial peptides (AMPs). AMPs are molecules that are successful in killing bacteria that contain chains resistant to ordinary antibiotics. Cationic AMPs are important components that interact with negatively charged phospholipids in bacterial membranes, changing membrane electrochemical potentials and leading to bacterial death (Ahmad, Campos, Fratini, Altaye, & Li,

2020). Royal jelly bioactive compounds that can be categorized as AMPs include gelleins, royalicin, MRJPs, royalactin, apisimine aspimine, and Apolipophorin III (apoLp-III) analog(Collazo et al., 2021). Jelleins are a class of antimicrobial peptides found in royal jelly (Zhou et al., 2021). Natural gelleins can inhibit gram-positive bacteria, *Bacillus subtilis*, *Micrococcus flavus* and *Staphyloccocus aureus* by damaging their cell walls and cell membranes(L. Shen et al., 2012). Some MRJPs, such as MRJP 2 and MRJP4, may exhibit broad-spectrum antibacterial activity against gram-positive and gram-negative bacteria, fungi and yeasts(H. G. Park et al., 2019; M. J. Park et al., 2019). MRJP2, MRJP3, MRJP4, MRJP5 and MRJP7 show antibacterial activity against gram-negative E. Coli(H. G. Park et al., 2019). It has been reported that Royalisin can strongly inhibit many types of gram-positive and gram-negative bacteria (Bílikova, Huang, Lin, Šimuth, & Peng, 2015). Glucose oxidase enzyme found in the bee process shows antimicrobial activity by catalyzing the oxidation of glucose to oxygen peroxide (Crailsheim & Riessberger-Gallé, 2001).

Antiinflammatory Activity

The inflammatory process is stimulated by cytokines, adhesion molecules, pro-inflammatory enzymes and hormone-like compounds, as well as enzymatic breakdown of tissues(Libby, Ridker, & Maseri, 2002). Royal jelly may attenuate the inflammatory response by regulating the levels of these inflammatory mediators (You et al., 2018). Royal jelly may help improve the negative effects of autoimmune diseases by regulating immunity (Kohno et al., 2004). Fatty acid types such as 10-HDA, sebacic acid and 10-HDAA found in the lipid composition of royal jelly may exhibit anti-inflammatory activity by suppressing the secretion of proinflammatory cytokines such as IL-1, IL-12 and TNF-α (Kobayashi et al., 2023). Since these cytokines cause inflammation and cytotoxicity, their suppression also suppresses inflammation. Compared to other components in royal jelly, the fatty acid 10-HDA stands out with its many biological activities and also stands out with its anti-inflammatory effects (Ratajczak et al., 2021). In mice treated with MRJP3 protein, it was observed that inflammation was eliminated by suppressing the production of proinflammatory cytokines (El-Seedi et al., 2022).

Antioxidant Activity

Organic acids in royal jelly form complex compounds with metals, causing the effect of total polyphenolic compounds to increase. This contributes to the increase in antioxidant activity. The main chemical compounds responsible for the antioxidant activity of royal jelly are flavonoids and phenolic compounds,

which have significant ability to scavenge free radicals (Bagameri et al., 2023). Flavonoids found in royal jelly are divided into four main groups as flavanones such as hesperetin, isosakuranetin and naringenin, flavones such as acacetin, apigenin, chrysin and luteolin glycoside, flavonols such as quercetin, galangin, fisetin, isorhamnetin and kaempferol glycosides and isoflavonoids such as coumestrol, formononetin and genistein (Nabas et al., 2014). The 10-H2DA component stands out in many biological activities of royal jelly as well as in its antioxidant activity(Balkanska, Marghitas, & Pavel, 2017). Fatty acids such as benzoic acid, octanoic acid, dodecanoic acid, and 2-hexenedioic acid, which make up the lipid composition of royal jelly, increase its antioxidant capacity. Free amino acids, dipeptide and tripeptide components obtained by hydrolysis of royal jelly proteins exhibit significant hydroxyl radical and hydrogen peroxide scavenging activities(Chiu et al., 2017; Kocot et al., 2018). MRJPs are potent antioxidant proteins with DPPH radical scavenging ability. MRJP-2 acted as a cytoprotector by reducing Caspase-3 activity and oxidative stress-induced cell apoptosis (M. J. Park et al., 2019). Royal jelly can eliminate cadmium-induced genotoxicity and oxidative stress in mice (Çavuşoğlu, Yapar, & Yalçin, 2009). In the diet of Sprague-Dawley rats fed with fumonisin (200 mg/kg), a mycotoxin produced by mold fungi, and royal jelly for three weeks, royal jelly alleviated the harmful effects of fumonisin by improving glutathione peroxidase formation (H. Guo, Kouzuma, & Yonekura, 2009; Martinello & Mutinelli, 2021). In radiation-induced lung and liver injury in Sprague-Dawley rats, royal jelly was effective in reducing oxidative stress and increasing antioxidant properties (Karadeniz et al., 2011).

Effect on Wound Healing

The wound healing process is completed in four phases: hemostasis, inflammation, proliferation, maturation and remodeling. In vivo and in vitro studies show that royal jelly plays an important role in the wound healing process (Majd, Khorasgani, Zaker, Khezri, & Veshareh, 2022; Parhizkari et al., 2023; Pasupuleti, Sammugam, Ramesh, & Gan, 2017; Saadeldin et al., 2023; Tan et al., 2023) Royal jelly dressing is an effective technique for treating diabetic foot ulcers (Vazhacharickal, 2021). It achieves this effect by expanding the blood vessels around the wound, increasing the blood flow rate and preventing the wound from being infected by microorganisms in the environment (Cihan, ÖZTÜRK, & Gokalp, 2013). Royal jelly activity shortened the time required for healing of exfoliated skin lesions in streptozotocin-induced diabetic rats(Y. Lin et al., 2020; Majd et al., 2022). Oral treatment with royal jelly can enhance the wound healing process in diabetic mice(Taniguchi et al., 2003). The positive

effects of royal jelly in the treatment of inflammatory wounds in the mouth caused by the side effects of chemoradiotherapy in patients with head and neck cancer have been demonstrated in in vivo experimental studies (Daugėlaitė, Užkuraitytė, Jagelavičienė, & Filipauskas, 2019; Severo et al., 2022; Suemaru et al., 2008). The demonstration that MRJPs, the basic proteins in royal jelly, can provide cell proliferation in humans clearly demonstrates its wound healing effectiveness (Chen, Xin, Qian, Yu, & Shen, 2016). MRJPs have important biological effects on cell proliferation and wound healing. A protein fraction containing MRJP2, MRJP3 and MRJP7 accelerates wound healing by inducing proliferation and migration of human epidermal keratinocytes(Lin et al., 2019). Additionally, certain peptide regions of MRJP3 contribute to wound healing by directly enhancing cell growth and wound repair(Renard, Gueydan, & Aron, 2022). It has been reported that the defensin-1 peptide found in royal jelly will cause an increase in the expression of matrix metalloproteinase-9 (MMP9) and the migration of keratinocytes, which are the components responsible for keratin production (Bucekova et al., 2017). This results in increased cell renewal and an acceleration of the wound healing process. 10-HDA contributes to the wound healing process by supporting the fibroblast tissue of the collagenous matrix, which is the cell responsible for the production of collagen protein, which is the main substance of connective tissue and has a function in wound healing(Kotronoulas et al., 2021).

Antihypercholesterolemic Activity

Dyslipidemia is a high risk factor for cardiovascular disease, which is worsened by poor eating habits (Tsigos et al., 2008). Administration of royal jelly to patients has been associated with a significant reduction in total blood lipids and cholesterol levels (Chiu et al., 2017). The use of royal jelly as a food supplement has been reported to reduce low-density lipoprotein levels, total serum lipid levels, and total cholesterol (Kamakura, Moriyama, & Sakaki, 2006). Additionally, a study conducted on rats reported that royal jelly reduced plasma triglyceride and insulin levels (Zamami et al., 2008).After consuming 3.15 g of royal jelly per day for 12 weeks, there was a further improvement in the level of dehydroepiandrosterone sulfate hormone and a decrease in serum total cholesterol concentration(Chiu et al., 2017). Royal jelly contains bile acid binding proteins that can induce hypocholesterolemic effect(Chiu et al., 2017). MRJP-1 protein interacts with bile acids and increases the excretion of bile acids and cholesterol in the feces, thus contributing to the lowering of cholesterol (Kashima et al., 2014). MRJP1 may inhibit bile acid reabsorption, which may lead to lower blood cholesterol levels(Viuda-Martos, Pérez-Alvarez, &

Fernández-López, 2017). It was reported that antioxidants in royal jelly may contribute to hypolipidemic effects. (Asgari, Asle-Rousta, & Sofiabadi, 2017).

Aging and Impact on Memory

With aging, there is an increase in neuropsychiatric disorders such as Alzheimer's and depression due to decreased cell proliferation, new lymphocyte and cytokine production (Bouamama, Merzouk, Latrech, Charif, & Bouamama, 2021; Calder, Carr, Gombart, & Eggersdorfer, 2020; Xin et al., 2016). Aging is associated with a decline in cognitive functions. This is the most dangerous factor that causes neurodegenerative diseases (Kumari & Jat, 2021). In humans, it has been reported that royal jelly intake can significantly delay age-related motor dysfunction(Ji, Zhang, Wei, & Hu, 2016; Moraru et al., 2024). Royal jelly increases the lifespan of queen honey bees and several other species(Fratini et al., 2016). Royal jelly has anti-aging and brain health protective activities thanks to its effects such as regulation of neurotransmission, improvement of memory, neuroprotection, regulation of neurotrophins, protection against oxidative stress, reduction of apoptosis, etc (Karimi et al., 2024; Raoufi, Salavati, Komaki, Shahidi, & Zarei, 2023; Zamani, Reisi, Alaei, & Pilehvarian, 2012). 10-HDA, the most abundant fatty acid in royal jelly, is used to increase lifespan in *C. Elegans* (Honda et al., 2011). Royal jelly promotes cellular proliferation in vitro by increasing PBMCs proliferation and cytokine release (Natarajan et al., 2021). Regular consumption of royal jelly has been reported to extend the life of creatures such as bees, crickets, nematodes and mice (X. Wang, Cook, Grasso, Cao, & Dong, 2015). MRJPs contained in royal jelly increased the lifespan of Drosophila by supporting the anti-epidermal growth factor receptor (EGFR)-mediated signaling pathway (Qiu et al., 2020; Xin et al., 2016). In a study in which human embryonic lung fibroblast cell line (HFL-I) was treated with different concentrations of MRJP, positive effects of MRJPs on cell proliferation, senescence and telomere length were reported (Liu et al., 2023). Royalactin (MRJP1), a glycoprotein from royal jelly, extends the lifespan of C. elegans by promoting epidermal growth factor (EGF) and its receptors signaling (Detienne, De Haes, Ernst, Schoofs, & Temmerman, 2014). MRJPs can improve spatial memory ability of aged rats by affecting cysteine, taurine and energy metabolism (Chen, Liu, Wan, Lai, & Shen, 2017). MRJP proteins increase the production of neuroprotective molecules such as cysteic acid in aged rats. Royal jelly (administered at a dose of 100 mg/kg body weight for 56 days) has been shown to prevent fluoride-induced brain damage through antioxidant effects (Aslan et al., 2023). Royal jelly has been reported to reduce skin pigmentation in mice (Peng ChiChung, Sun HuiTzu, Lin IPing, Kuo PingChung, & Li JenChieh, 2017).

Royal jelly may act as a protective agent against skin aging. It is also possible that it can prevent skin aging. 10-H2DA and 10-HDA may have the potential to protect skin against ultraviolet (uvβ)-induced photoaging by improving collagen production (Park et al., 2011; Vazhacharickal, 2021). Control of collagen metabolism is important not only for cosmetic purposes but also for therapeutic applications. During natural aging, a decrease in collagen due to estrogen deficiency results in decreased skin elasticity. The skin level of type I procollagen protein is improved by administering 1% royal jelly to estrogen-free female Sprague-Dawley rats(Bălan et al., 2020). This suggests that taking royal jelly as a supplement after menopause may improve the natural aging process of the skin.

Effect On Reproduction

Royal jelly increases sperm quality in men, while it increases fertility in women by improving the quality of the ovaries (Ahmadnia, Sharifi, Alizadeh, Roohani, & SAFARI, 2015). Royal jelly has been shown to improve levels of male hormones, sperm count, motility, and reduce damage to the reproductive tract (Al-Sanafi, Mohssin, & Abdulla, 2007; Temamogullari, Aral, & Yilmaz, 2018). Royal jelly improved sperm count, live sperm percentage, testosterone levels, glutathione and malondialdehyde levels (El Helew, Hamed, Moustafa, & Sakkara, 2024). Royal jelly has been shown to protect spermatozoa and increase their motility during the freezing process (Shahzad et al., 2016). A study conducted on male rabbits has shown that the use of royal jelly has positive effects on libido, blood testosterone, sperm production and quality, and plasma total proteins (El-Hanoun, Elkomy, Fares, & Shahien, 2014). Long-term royal jelly feeding halted the age-related decline in testicular function in male hamsters and increased testosterone levels and spermatogenesis [108]. It has been reported that 4 weeks of treatment with royal jelly protects the testicular structure from the harmful effects of diabetic oxidative stress (El Helew et al., 2024). Simultaneous administration of royal jelly and cod liver oil may improve sperm characteristics under heat stress conditions (Mahdivand, Najafi, Nejati, Shalizar-Jalali, & Rahmani, 2019). Royal jelly administration improves fertility parameters by promoting follicular growth and ovarian hormones in immature female rats (Ghanbari, Khazaei, Khazaei, & Nejati, 2016). Oral and intramuscular administration of royal jelly with exogenous progesterone improves estrus effect and pregnancy rate in awassi sheep (Husein & Kridli, 2002). Royal jelly has an estrogenic response in in vivo and in vitro models by altering gene expression and cell proliferation through interaction with estrogen receptors (Mishima et al., 2005). Royal jelly improved memory impairment in ovariectomized (OVX) rats. With its estrogen-like activity, royal jelly may help reduce postmenopausal

symptoms by alleviating postmenopausal osteoporosis in women (Aydın, Atar, & Pirgon, 2021; Sharif & Darsareh, 2019) Consuming royal jelly is supportive in alleviating premenstrual syndrome (Taavoni, Barkhordari, Goushegir, & Haghani, 2014).

Anticancer Activity

The anticancer activities of royal jelly have been investigated in in vitro studies on many tumor cells including Ehrlich Solid Carcinoma, Ehrlich Ascites Carcinoma, lymphosarcoma (6C3HED), sarcoma 180, AKR mouse leukemia, Lymphatic L1210 and P388 leukemia cells (Attia, Gabry, & Othman, 2007; Oršolić, Sacases, Sert, & Bašić, 2007). Royal jelly is known to exhibit anticancer potential by inhibiting tumor growth and metastasis (Peng, Sun, Lin, Kuo, & Li, 2017). E2 regulates the proliferation of lymphocytes and inhibits the tumoricidal activity of normal macrophages. Ehrlich asit tümörü olan farelerde arıtılmış tedavi yöntemi, prostaglandin E2'yi azaltarak kemik iliği kan listesi yapımını iyileştirerek yaşam süresini uzatabilir (Bincoletto, Eberlin, Figueiredo, Luengo, & Queiroz, 2005). A mixture containing royal jelly has been observed to have a cytotoxic effect on human glioblastoma multiforme brain tumor (Borawska et al., 2014). Royal jelly plays a role in reducing the cytotoxic effects of the chemotherapeutic drug doxorubicin on prostate cancer cell line (PC3) (Abandansari et al., 2018). Cases of synergistic effects of royal jelly and chemotherapy drugs have been reported. Royal jelly affects N-acetylation and inhibits the metabolism of 2-aminofluorene metabolites in human liver tumor cell line and reduces 2-aminofluorene in human hepatocellular carcinoma (J5) cells in a dose-dependent manner(Premratanachai & Chanchao, 2014). Bisphenol A is an endocrine disruptor with a weak binding affinity to estrogen receptors, which adversely affects human health, especially in women (Kwon, 2022). Raw royal jelly stops the damage caused by bisphenol a, which causes the growth of human breast cancer cells (Nakaya et al., 2007). Royal jelly treatment of the 4T1 breast cancer mouse model reduced tumor weight (Zhang, Shao, Geng, & Su, 2017). Royal jelly inhibited tumor-induced angiogenesis. It stimulated the immune response by increasing the production of T lymphocytes, which play a role in eliminating viruses and tumor cells (Vucevic et al., 2007). Royal jelly may have inhibitory effect on tumor growth and metastasis in the liver and lung (Kimura, 2008). Lipophilic extract of royal jelly can inhibit the proliferation of human neuroblastoma (SH-SY5Y) cells and exhibit antiproliferative effect on human glioblastoma (U373) (Gismondi, Trionfera, Canuti, Di Marco, & Canini, 2017; Ozek, 2024). Lipophilic extracts of royal jelly exhibit antitumor effects by slowing the growth of human neuroblastoma (Gismondi et al., 2017). RJP30

protein fraction showed 50% cytotoxic effect in hela cells (Kimura, 2008). Anticancer activity in Lewis lung carcinoma and colorectal adenocarcinoma cells treated with royal jelly has been attributed to 10-HDA. 10-HDA, an inhibitor of MMPs, has been shown to have antitumor activity in leukemia and various ascites tumors [47,88]. 4-Hydroperoxy-2-decenoic acid ethyl ester, a derivative of 10-HDA, induced apoptosis of A549 human lung cancer cells (X.-M. Lin et al., 2020). 3,10-dihydroxydecanoic acid found in royal jelly enhanced tumor inhibition by stimulating the maturation and Th1-polarizing abilities of monocyte-derived dendritic cells (Salama et al., 2022). Royal jelly MRJP2 protein and its subtype x1 can promote Caspase-dependent apoptosis and inhibit Bcl-2 and p53 expression in Hep G2 cells, which may be a promising strategy against hepatic cancer (Abu-Serie & Habashy, 2019). The effects of royal jelly were also studied in ehrlich solid and ascites tumors (EST and EAT) (Albalawi et al., 2022). Treatment of mice with EST with royal jelly caused a significant decrease in the amount of tumor markers such as alpha-fetoprotein (AFP) serum level and carcinoembryonic antigen tumors (CAE). Treatment of mice carrying EAT with royal jelly increased the number of bone marrow cells and the number of cells in the peripheral circulation. Royal jelly treatment caused a decrease in the in vitro viability of EAT cells (Attia et al., 2007; Oršolić et al., 2007).

Antidiabetic Activity

Long-term royal jelly administration has been shown to inhibit glucose-6-phosphatase, an important enzyme in hepatic gluconeogenesis, thereby improving hyperglycemia (Yoneshiro et al., 2018; Yoshida et al., 2017). In a clinical study, serum glucose levels decreased significantly after royal jelly administration in healthy individuals (Asgari et al., 2017; Münstedt, Bargello, & Hauenschild, 2009). It has been shown that daily consumption of royal jelly (3 g) for six months improves glucose tolerance, cognitive and erythropoiesis in patients (Elena & de Visser, 2003). Royal jelly contains compounds that are functionally and structurally similar to insulin (Pourfard et al., 2023). Royal jelly may reduce insulin resistance through its antioxidant effects, as insulin resistance is associated with increased levels of oxidative stress (Khazaei, Ansarian, & Ghanbari, 2018). It has been reported that including royal jelly in the diet of patients with type 2 diabetes results in an increase in total antioxidant capacity and a decrease in insulin resistance [174]. Antioxidant peptides found in royal jelly are responsible for insulin resistance (Gohari, Khajehlandi, & Mohammadi, 2022; Maleki et al., 2019). On the other hand, 10-HDA can improve hyperglycemia and insulin resistance by activating PGC-1α expression (Watadani et al., 2017).

Organo-Protective Activity

Royal jelly stands out for its protective effects on many tissues and organs damaged by chemotherapy, especially the liver and kidneys (Almeer, Alarifi, et al., 2018; Focak & Suljevic, 2023; Qu et al., 2022). It has been reported that royal jelly treatment improves neural functions and protects the brain from oxidative damage by causing the regeneration of hippocampal granule cells, which play an important role in memory and orientation (Cİhan, Arsav, & Göcen, 2011). In rats treated with 300 mg/kg of royal jelly, there was a decrease in the Bax/Bcl-2 ratio and an increase in the levels of telomerase enzymes, and an improvement in the survival rate of liver, kidney and especially brain cells. Thanks to these anti-apoptotic effects, organ health-protective effects were observed (Khani-Eshratabadi et al., 2022). Royal jelly provides a protective effect against cadmium exposure-induced nephrotoxicity in mice by facilitating cadmium excretion (Almeer et al., 2019). Royal jelly also ameliorated liver cell damage caused by exposure to tetrachloromethane, cadmium, and paracetamol (Almeer, Soliman, et al., 2018; Tohamy et al., 2022). Moreover, it has been revealed that the nephroprotective effect with cisplatin toxicity is provided by the consumption of royal jelly (Karadeniz et al., 2011; Osama et al., 2017). Other components in royal jelly may have cholesterol-lowering and blood pressure effects (Pan et al., 2019). High blood cholesterol is a risk factor for cardiovascular diseases. In this respect, it has an indirect protective effect on heart health (H. Guo et al., 2007). Another study reported that the use of royal jelly for three months may have a protective effect against cardiovascular diseases by reducing total cholesterol and LDL-C levels and improving HDL-C levels (Hadi et al., 2018). Royal jelly may help treat nonalcoholic fatty liver disease (NAFLD) (Kobayashi et al., 2023). Royal jelly could regulate 267 liver genes in mice, of which 148 genes were upregulated and 119 genes were downregulated (Kamakura et al., 2006). Royal jelly can restore antioxidants (SOD, CAT, GSH) and MDA in the liver and alleviate liver damage by reducing AST, ALT levels (Cemek et al., 2010).

TOXIC/SIDE EFFECTS

Royal jelly is a natural product that is considered safe and has a wide pharmacological effect due to its rich bioactive component content, and is important for the cosmetics, food and health industries. Like all natural products, improper use of royal jelly can have harmful effects on health. Excessive use, use with certain drugs and use in certain diseases can lead to toxic effects. In addition, some components found in royal jelly can cause side effects such as allergic reactions in some individuals. MRJP1, MRJP2 and MRJP3, which are among the basic proteins of royal jelly, have been identified as allergens (Hata et al., 2020;

Mizutani et al., 2011). Royal jelly can cause contact dermatitis, gastrointestinal problems, hemorrhagic colitis, allergic rhinitis, acute asthma, intestinal bleeding, respiratory stress, eczema and skin rashes, atopy, anaphylactic shock and even death due to the presence of major allergens MRJP-1 and MRJP-2 (Katayama, Aoki, & Kawana, 2008; Laporte, Ibanez, Vendrell, & Ballarin, 1996; Peacock, Murray, & Turton, 1995; Torrijos et al., 2016). Individuals with a history of allergic disease should be careful when consuming royal jelly products (Hata et al., 2020). It may be unsafe for babies, young children, pregnant and breastfeeding women and people who are allergic to bee stings or other bee products such as honey, propolis, or pollen to use royal jelly (Thien et al., 1996). Application of royal jelly may lead to inflammation of nerves in cultured PC12 neuroendocrine cell line (Hattori, Nomoto, Fukumitsu, Mishima, & Furukawa, 2007).

CONCLUSION

Royal jelly is a natural product secreted from the glands of nurse honey bees and used for the nutrition of queen bees and larvae. Rich in bioactive compounds such as proteins, peptides, essential fatty acids, phenolics and flavonoids, royal jelly has many biological activities, including immunomodulatory, antimicrobial, anticancer, antihypertensive and antidiabetic effects. Royal jelly also plays a supporting role in many biological processes such as wound healing, tissue regeneration, energy metabolism and memory. Royal jelly, which is also effective against multidrug-resistant bacteria, also provides potential benefits in the fight against pathogens such as Sars-Cov-2 virus. With these aspects, royal jelly is widely used in medical, cosmetic and industrial applications. The biological activities of royal jelly come from various bioactive substances such as proteins, essential fatty acids, peptides, minerals and phenolics. The main components responsible for biological activity are 10-HDA and MRJP proteins, known as queen bee acid. It has been stated that royal jelly can cause allergic reactions in some people and its use should be limited in certain diseases or conditions.

The study detailed the biological effects of the bioactive components of royal jelly and explained its benefits on human health. Studies have shown that royal jelly is a versatile natural product that offers a wide range of effects that support health with its bioactive components. In order to fully benefit from the potential health benefits of royal jelly, standardization of the components it contains, quality control, increased research on preclinical and clinical applications, and determination of safe doses are necessary. In addition, toxicity profiles, drug interactions, and side effects should be examined in detail and situations where use or dose should be limited should be clearly determined. Thus, the safe use of this natural product with high therapeutic potential can be ensured.

Referanslar

Abandansari, R. M., Parsian, H., Kazerouni, F., Porbagher, R., Zabihi, E., & Rahimipour, A. (2018). Effect of simultaneous treatment with royal jelly and doxorubicin on the survival of the prostate cancer cell line (pc3): an in vitro study. *International Journal of Cancer Management, 11*(4).

Abu-Serie, M. M., & Habashy, N. H. (2019). Two purified proteins from royal jelly with in vitro dual anti-hepatic damage potency: Major royal jelly protein 2 and its novel isoform X1. *International Journal of Biological Macromolecules, 128*, 782-795.

Ahmad, S., Campos, M. G., Fratini, F., Altaye, S. Z., & Li, J. (2020). New insights into the biological and pharmaceutical properties of royal jelly. *International journal of molecular sciences, 21*(2), 382.

Ahmadnia, H., Sharifi, N., Alizadeh, S., Roohani, Z., & SAFARI, M. S. (2015). @ WONDERFUL EFFECTS OF ROYAL JELLY ON TREATMENT OF MALE-FACTOR RELATED INFERTILITY.

Al-Kahtani, S., & Taha, E.-K. A. (2021). Effect of harvest time on royal jelly yield and chemical composition. *Journal of the Kansas Entomological Society, 93*(2), 132-139.

Al-Kahtani, S. N., & Taha, E.-K. A. (2020). Post grafting time significantly influences royal jelly yield and content of macro and trace elements. *PloS one, 15*(9), e0238751.

Al-Sanafi, A. E., Mohssin, S. A., & Abdulla, S. M. (2007). Effect of royal jelly on male infertility. *Thi-Qar Med. J, 1*(1), 1-12.

Albalawi, A. E., Althobaiti, N. A., Alrdahe, S. S., Alhasani, R. H., Alaryani, F. S., & BinMowyna, M. N. (2022). Antitumor activity of royal jelly and its cellular mechanisms against Ehrlich solid tumor in mice. *BioMed research international, 2022*(1), 7233997.

Alkhaibari, A. M., & Alanazi, A. D. (2022). Insecticidal, antimalarial, and antileishmanial effects of royal jelly and its three main fatty acids, trans-10-hydroxy-2-decenoic acid, 10-hydroxydecanoic acid, and sebacic acid. *Evidence-Based Complementary and Alternative Medicine, 2022*(1), 7425322.

Almeer, R. S., Alarifi, S., Alkahtani, S., Ibrahim, S. R., Ali, D., & Moneim, A. (2018). The potential hepatoprotective effect of royal jelly against cadmium chloride-induced hepatotoxicity in mice is mediated by suppression of oxidative stress and upregulation of Nrf2 expression. *Biomedicine & Pharmacotherapy, 106*, 1490-1498.

Almeer, R. S., AlBasher, G. I., Alarifi, S., Alkahtani, S., Ali, D., & Abdel Moneim, A. E. (2019). Royal jelly attenuates cadmium-induced nephrotoxicity in male mice. *Scientific reports, 9*(1), 5825.

Almeer, R. S., Soliman, D., Kassab, R. B., AlBasher, G. I., Alarifi, S., Alkahtani, S., . . . Abdel Moneim, A. E. (2018). Royal jelly abrogates cadmium-induced oxidative challenge in mouse testes: involvement of the Nrf2 pathway. *International journal of molecular sciences, 19*(12), 3979.

Alu'datt, M. H., Rababah, T., Obaidat, M. M., Ereifej, K., Alhamad, M. N., Mhaidat, N., . . . Ayadi, W. (2015). Probiotics in milk as functional food: characterization and nutraceutical properties of extracted phenolics and peptides from fermented skimmed milk inoculated with royal jelly. *Journal of Food Safety, 35*(4), 509-522.

Asgari, M., Asle-Rousta, M., & Sofiabadi, M. (2017). Effect of royal jelly on blood glucose and lipids in streptozotocin induced type 1 diabetic rats. *Journal of Arak University of Medical Sciences, 20*(5), 48-56.

Aslan, A., Beyaz, S., Gok, O., Parlak, G., Can, M. I., Agca, C. A., . . . Parlak, A. E. (2023). Royal jelly protects brain tissue against fluoride-induced damage by activating Bcl-2/NF-κB/caspase-3/caspase-6/Bax and Erk signaling pathways in rats. *Environmental Science and Pollution Research, 30*(17), 49014-49025.

Attia, W., Gabry, M., & Othman, G. (2007). Immunostimulatory effect of royal jelly and its relation with host resistance against tumor in mice. *Egypt. J. Exp. Biol.(Zool.), 3*, 241-250.

Aydın, B., Atar, M., & Pirgon, Ö. (2021). The effect of royal jelly supplementation for three months on bone markers in postmenopausal osteoporotic women. *Mellifera, 21*(1), 59-68.

Bagameri, L., Botezan, S., Bobis, O., Bonta, V., & Dezmirean, D. S. (2023). Molecular insights into royal jelly anti-inflammatory properties and related diseases. *Life, 13*(7), 1573.

Bălan, A., Moga, M. A., Dima, L., Toma, S., Elena Neculau, A., & Anastasiu, C. V. (2020). Royal jelly—A traditional and natural remedy for postmenopausal symptoms and aging-related pathologies. *Molecules, 25*(14), 3291.

Balkanska, R., Marghitas, L.-A., & Pavel, C. I. (2017). Antioxidant activity and total polyphenol content of royal jelly from Bulgaria. *Int. J. Curr. Microbiol. Appl. Sci, 6*(10), 578-585.

Bílikova, K., Huang, S.-C., Lin, I.-P., Šimuth, J., & Peng, C.-C. (2015). Structure and antimicrobial activity relationship of royalisin, an antimicrobial peptide from royal jelly of Apis mellifera. *Peptides, 68*, 190-196.

Bincoletto, C., Eberlin, S., Figueiredo, C. A., Luengo, M. B., & Queiroz, M. L. (2005). Effects produced by Royal Jelly on haematopoiesis: relation with host resistance against Ehrlich ascites tumour challenge. *International immunopharmacology, 5*(4), 679-688.

Bogdanov, S. (2011). Royal jelly, bee brood: composition, health, medicine: a review. *Lipids, 3*(8), 8-19.

Borawska, M. H., Markiewicz-Żukowska, R., Naliwajko, S. K., Moskwa, J., Bartosiuk, E., Socha, K., . . . Mariak, Z. (2014). The interaction of bee products with temozolomide in human diffuse astrocytoma, glioblastoma multiforme and astroglia cell lines. *Nutrition and cancer, 66*(7), 1247-1256.

Bouamama, S., Merzouk, H., Latrech, H., Charif, N., & Bouamama, A. (2021). Royal jelly alleviates the detrimental effects of aging on immune functions by enhancing the in vitro cellular proliferation, cytokines, and nitric oxide release in aged human PBMCS. *Journal of Food Biochemistry, 45*(2), e13619.

Bucekova, M., Sojka, M., Valachova, I., Martinotti, S., Ranzato, E., Szep, Z., . . . Majtan, J. (2017). Bee-derived antibacterial peptide, defensin-1, promotes wound reepithelialisation in vitro and in vivo. *Wound Healing Southern Africa, 10*(2), 25-35.

Calder, P. C., Carr, A. C., Gombart, A. F., & Eggersdorfer, M. (2020). Optimal nutritional status for a well-functioning immune system is an important factor to protect against viral infections. *Nutrients, 12*(4), 1181.

Cemek, M., Aymelek, F., Büyükokuroğlu, M. E., Karaca, T., Büyükben, A., & Yilmaz, F. (2010). Protective potential of Royal Jelly against carbon tetrachloride induced-toxicity and changes in the serum sialic acid levels. *Food and Chemical Toxicology, 48*(10), 2827-2832.

Chen, D., Liu, F., Wan, J.-B., Lai, C.-Q., & Shen, L.-r. (2017). Effect of major royal jelly proteins on spatial memory in aged rats: Metabolomics analysis in urine. *Journal of Agricultural and Food Chemistry, 65*(15), 3151-3159.

Chen, D., Xin, X.-x., Qian, H.-c., Yu, Z.-y., & Shen, L.-r. (2016). Evaluation of the major royal jelly proteins as an alternative to fetal bovine serum in culturing human cell lines. *Journal of Zhejiang University. Science. B, 17*(6), 476.

Chiu, H.-F., Chen, B.-K., Lu, Y.-Y., Han, Y.-C., Shen, Y.-C., Venkatakrishnan, K., . . . Wang, C.-K. (2017). Hypocholesterolemic efficacy of royal jelly in healthy mild hypercholesterolemic adults. *Pharmaceutical biology, 55*(1), 497-502.

Cihan, Y., ÖZTÜRK, A., & Gokalp, S. (2013). Protective role of royal jelly against radiation-induced oxidative stress in rats. *UHOD-ULUSLARARASI HEMATOLOJI-ONKOLOJI DERGISI, 23*(2).

Cİhan, Y. B., Arsav, V., & Göcen, E. (2011). Radyasyonun İndüklediği Beyin Hasarına Karşı Arı Sütünün Koruyucu Etkisi. *Journal of Neurological Sciences, 28*(4).

Collazo, N., Carpena, M., Nuñez-Estevez, B., Otero, P., Simal-Gandara, J., & Prieto, M. A. (2021). Health promoting properties of bee royal jelly: Food of the queens. *Nutrients, 13*(2), 543.

Crailsheim, K., & Riessberger-Gallé, U. (2001). Honey bee age-dependent resistance against American foulbrood. *Apidologie, 32*(1), 91-103.

Çavuşoğlu, K., Yapar, K., & Yalçin, E. (2009). Royal jelly (honey bee) is a potential antioxidant against cadmium-induced genotoxicity and oxidative stress in albino mice. *Journal of medicinal food, 12*(6), 1286-1292.

Dai, J., Shu, R., Liu, J., Xia, J., Jiang, X., & Zhao, P. (2021). Transcriptome analysis of Apis mellifera under benomyl stress to discriminate the gene expression in response to development and immune systems. *Journal of Environmental Science and Health, Part B, 56*(6), 594-605.

Daugėlaitė, G., Užkuraitytė, K., Jagelavičienė, E., & Filipauskas, A. (2019). Prevention and treatment of chemotherapy and radiotherapy induced oral mucositis. *Medicina, 55*(2), 25.

Detienne, G., De Haes, W., Ernst, U. R., Schoofs, L., & Temmerman, L. (2014). Royalactin extends lifespan of Caenorhabditis elegans through epidermal growth factor signaling. *Experimental gerontology, 60*, 129-135.

Dzopalic, T., Vucevic, D., Tomic, S., Djokic, J., Chinou, I., & Colic, M. (2011). 3, 10-Dihydroxy-decanoic acid, isolated from royal jelly, stimulates Th1 polarising capability of human monocyte-derived dendritic cells. *Food Chemistry, 126*(3), 1211-1217.

El-Hanoun, A., Elkomy, A., Fares, W., & Shahien, E. (2014). Impact of royal jelly to improve reproductive performance of male rabbits under hot summer conditions. *World Rabbit Science, 22*(3), 241-248.

El-Seedi, H. R., Eid, N., Abd El-Wahed, A. A., Rateb, M. E., Afifi, H. S., Algethami, A. F., . . . Tahir, H. E. (2022). Honey bee products: preclinical and clinical studies of their anti-inflammatory and immunomodulatory properties. *Frontiers in Nutrition, 8*, 761267.

El Helew, E. A., Hamed, W. S., Moustafa, A. M., & Sakkara, Z. A. (2024). Structural changes in testes of Streptozotocin induced diabetic rats and possible protective effect of royal jelly: light and electron microscopic study. *Ultrastructural Pathology, 48*(1), 1-15.

Elena, S. F., & de Visser, J. A. G. (2003). Environmental stress and the effects of mutation. *Journal of biology, 2*, 1-4.

Erem, C., Deger, O., Ovali, E., & Barlak, Y. (2006). The effects of royal jelly on autoimmunity in Graves' disease. *Endocrine, 30*, 175-183.

Fang, Y., Feng, M., Ma, C., Rueppell, O., & Li, J. (2023). Major royal jelly proteins influence the neurobiological regulation of the division of labor among honey bee workers. *International Journal of Biological Macromolecules, 225*, 848-860.

Focak, M., & Suljevic, D. (2023). Ameliorative effects of propolis and royal jelly against CCl4-induced hepatotoxicity and nephrotoxicity in Wistar rats. *Chemistry & Biodiversity, 20*(1), e202200948.

Fratini, F., Cilia, G., Mancini, S., & Felicioli, A. (2016). Royal Jelly: An ancient remedy with remarkable antibacterial properties. *Microbiological research, 192*, 130-141.

Ghanbari, E., Khazaei, M., Khazaei, M., & Nejati, V. (2016). Royal jelly promotes ovarian follicles growth and increases steroid hormones in immature rats. 2018; 11 (4): 263-269. doi: 10.22074/ijfs. 2018.5156. *Received, 22*, 263-269.

Gismondi, A., Trionfera, E., Canuti, L., Di Marco, G., & Canini, A. (2017). Royal jelly lipophilic fraction induces antiproliferative effects on SH-SY5Y human neuroblastoma cells. *Oncology Reports, 38*(3), 1833-1844.

Gohari, I., Khajehlandi, A., & Mohammadi, A. (2022). Effect of high-intensity interval training with royal jelly consumption on serum levels of glucose, insulin, and insulin resistance index of overweight and obese middle-aged men: A quasi-experimental study. *Jundishapur Journal of Chronic Disease Care, 11*(4).

Guo, H., Kouzuma, Y., & Yonekura, M. (2009). Structures and properties of antioxidative peptides derived from royal jelly protein. *Food Chemistry, 113*(1), 238-245.

Guo, H., Saiga, A., Sato, M., Miyazawa, I., Shibata, M., Takahata, Y., & Morimatsu, F. (2007). Royal jelly supplementation improves lipoprotein metabolism in humans. *Journal of nutritional science and vitaminology, 53*(4), 345-348.

Guo, J., Wang, Z., Chen, Y., Cao, J., Tian, W., Ma, B., & Dong, Y. (2021). Active components and biological functions of royal jelly. *Journal of Functional Foods, 82*, 104514.

Hadi, A., Najafgholizadeh, A., Aydenlu, E. S., Shafiei, Z., Pirivand, F., Golpour, S., & Pourmasoumi, M. (2018). Royal jelly is an effective and relatively safe alternative approach to blood lipid modulation: A meta-analysis. *Journal of Functional Foods, 41*, 202-209.

Han, B., Fang, Y., Feng, M., Hu, H., Qi, Y., Huo, X., . . . Li, J. (2015). Quantitative neuropeptidome analysis reveals neuropeptides are correlated with social behavior regulation of the honeybee workers. *Journal of proteome research, 14*(10), 4382-4393.

Han, B., Fang, Y., Feng, M., Lu, X., Huo, X., Meng, L., . . . Li, J. (2014). In-depth phosphoproteomic analysis of royal jelly derived from western and eastern honeybee species. *Journal of proteome research, 13*(12), 5928-5943.

Hata, T., Furusawa-Horie, T., Arai, Y., Takahashi, T., Seishima, M., & Ichihara, K. (2020). Studies of royal jelly and associated cross-reactive allergens in atopic dermatitis patients. *PloS one, 15*(6), e0233707.

Hattori, N., Nomoto, H., Fukumitsu, H., Mishima, S., & Furukawa, S. (2007). Royal jelly-induced neurite outgrowth from rat pheochromocytoma PC12 cells requires integrin signal independent of activation of extracellular signalregulated kinases. *Biomedical Research, 28*(3), 139-146.

Honda, Y., Araki, Y., Hata, T., Ichihara, K., Ito, M., Tanaka, M., & Honda, S. (2015). 10-Hydroxy-2-decenoic acid, the major lipid component of royal jelly, extends the lifespan of Caenorhabditis elegans through dietary restriction and target of rapamycin signaling. *Journal of Aging Research, 2015*(1), 425261.

Honda, Y., Fujita, Y., Maruyama, H., Araki, Y., Ichihara, K., Sato, A., . . . Ito, M. (2011). Lifespan-extending effects of royal jelly and its related substances on the nematode Caenorhabditis elegans. *PloS one, 6*(8), e23527.

Hossen, M. S., Nahar, T., Gan, S. H., & Khalil, M. I. (2019). Bioinformatics and therapeutic insights on proteins in royal jelly. *Current Proteomics, 16*(2), 84-101.

Husein, M., & Kridli, R. (2002). Reproductive responses following royal jelly treatment administered orally or intramuscularly into progesterone-treated Awassi ewes. *Animal reproduction science, 74*(1-2), 45-53.

Ibrahim, H. R., Nanbu, F., & Miyata, T. (2021). Potent antioxidant peptides derived from honey major protein enhance tolerance of eukaryotic cells toward oxidative stress. *Food Production, Processing and Nutrition, 3*, 1-10.

Jarvis, C. (2023). The effects of urbanization on disease prevalence in managed honey bee hives in Hamilton County, TN.

Ji, W., Zhang, C., Wei, W., & Hu, F. (2016). The in vivo antiaging effect of enzymatic hydrolysate from royal jelly in d-galactose induced aging mouse. *J. Chin. Inst. Food Sci. Technol, 16*(1), 18-25.

Kamakura, M. (2011). Royalactin induces queen differentiation in honeybees. *Nature, 473*(7348), 478-483.

Kamakura, M., Moriyama, T., & Sakaki, T. (2006). Changes in hepatic gene expression associated with the hypocholesterolaemic activity of royal jelly. *Journal of pharmacy and pharmacology, 58*(12), 1683-1689.

Kanelis, D., Tananaki, C., Liolios, V., Dimou, M., Goras, G., Rodopoulou, M. A., . . . Thrasyvoulou, A. (2015). A suggestion for royal jelly specifications. *Arhiv za higijenu rada i toksikologiju, 66*(4), 275-284.

Karadeniz, A., Simsek, N., Karakus, E., Yildirim, S., Kara, A., Can, I., . . . Turkeli, M. (2011). Royal jelly modulates oxidative stress and apoptosis in liver and kidneys of rats treated with cisplatin. *Oxidative medicine and cellular longevity, 2011*(1), 981793.

Karimi, E., Arab, A., Sepidarkish, M., Khorvash, F., Saadatnia, M., & Amani, R. (2024). Effects of the royal jelly consumption on post-stroke complications in patients with ischemic stroke: results of a randomized controlled trial. *Frontiers in Nutrition, 10*, 1227414.

Kashima, Y., Kanematsu, S., Asai, S., Kusada, M., Watanabe, S., Kawashima, T., . . . Nagaoka, S. (2014). Identification of a novel hypocholesterolemic protein, major royal jelly protein 1, derived from royal jelly. *PloS one, 9*(8), e105073.

Katayama, M., Aoki, M., & Kawana, S. (2008). Case of anaphylaxis caused by ingestion of royal jelly. *The Journal of dermatology*, *35*(4), 222-224.

Kausar, S. H., & More, V. (2019). Royal Jelly. Organoleptic characteristics and physicochemical properties. *Lipids*, *6*(2), 20-24.

Khan, K. A., Ghramh, H. A., Ahmad, Z., El-Niweiri, M. A., & Ahamed Mohammed, M. E. (2021). Queen cells acceptance rate and royal jelly production in worker honey bees of two Apis mellifera races. *PloS one*, *16*(4), e0248593.

Khani-Eshratabadi, M., Talebpuor, A., Bagherzadeh, A., Mehranfar, P., Khanmiri, J. M., Ghorbani, M., & Abtahi-Eivary, S.-H. (2022). Potential Anti-Apoptotic Impacts and Telomerase Activity of Royal Jelly on Different Tissues of Rats. *Archives of Medical Laboratory Sciences*, *8*, 1-8 (e3).

Khazaei, M., Ansarian, A., & Ghanbari, E. (2018). New findings on biological actions and clinical applications of royal jelly: a review. *Journal of dietary supplements*, *15*(5), 757-775.

Kim, B. Y., Lee, K. S., Jung, B., Choi, Y. S., Kim, H. K., Yoon, H. J., . . . Jin, B. R. (2019). Honeybee (Apis cerana) major royal jelly protein 4 exhibits antimicrobial activity. *Journal of Asia-Pacific Entomology*, *22*(1), 175-182.

Kimura, Y. (2008). Antitumor and antimetastatic actions of various natural products. *Studies in Natural Products Chemistry*, *34*, 35-76.

Kobayashi, G., Okamura, T., Majima, S., Senmaru, T., Okada, H., Ushigome, E., . . . Okamoto, H. (2023). Effects of Royal Jelly on Gut Dysbiosis and NAFLD in db/db Mice. *Nutrients*, *15*(11), 2580.

Kocot, J., Kiełczykowska, M., Luchowska-Kocot, D., Kurzepa, J., & Musik, I. (2018). Antioxidant potential of propolis, bee pollen, and royal jelly: Possible medical application. *Oxidative medicine and cellular longevity*, *2018*(1), 7074209.

Kohno, K., Okamoto, I., Sano, O., Arai, N., Iwaki, K., Ikeda, M., & Kurimoto, M. (2004). Royal jelly inhibits the production of proinflammatory cytokines by activated macrophages. *Bioscience, biotechnology, and biochemistry*, *68*(1), 138-145.

Kotronoulas, A., de Lomana, A. L. G., Karvelsson, S. T., Heijink, M., Stone II, R., Giera, M., & Rolfsson, O. (2021). Lipid mediator profiles of burn wound healing: Acellular cod fish skin grafts promote the formation of EPA and DHA derived lipid mediators following seven days of treatment. *Prostaglandins, Leukotrienes and Essential Fatty Acids*, *175*, 102358.

Kumari, R., & Jat, P. (2021). Mechanisms of cellular senescence: cell cycle arrest and senescence associated secretory phenotype. *Frontiers in cell and developmental biology*, *9*, 645593.

Kunugi, H., & Mohammed Ali, A. (2019). Royal jelly and its components promote healthy aging and longevity: from animal models to humans. *International journal of molecular sciences*, *20*(19), 4662.

Kwon, Y. (2022). Potential pro-tumorigenic effect of bisphenol A in breast cancer via altering the tumor microenvironment. *Cancers, 14*(12), 3021.

Laporte, J.-R., Ibanez, L., Vendrell, L., & Ballarin, E. (1996). Bronchospasm induced by royal jelly.

Lercker, G. (2003). La gelatina reale: composizione, autenticità ed adulterazione. *Atti del Convegno "Strategie per la valorizzazione dei prodotti dell'alveare". Università degli Studi del Molise*, 67-81.

Li, S., Tao, L., Yu, X., Zheng, H., Wu, J., & Hu, F. (2021). Royal jelly proteins and their derived peptides: Preparation, properties, and biological activities. *Journal of Agricultural and Food Chemistry, 69*(48), 14415-14427.

Libby, P., Ridker, P. M., & Maseri, A. (2002). Inflammation and atherosclerosis. *Circulation, 105*(9), 1135-1143.

Lima, W. G., Brito, J. C. M., Verly, R. M., & Lima, M. E. d. (2024). Jelleine, a Family of Peptides Isolated from the Royal Jelly of the Honey Bees (Apis mellifera), as a Promising Prototype for New Medicines: A Narrative Review. *Toxins, 16*(1), 24.

Lin, X.-M., Liu, S.-B., Luo, Y.-H., Xu, W.-T., Zhang, Y., Zhang, T., . . . Lu, B.-X. (2020). 10-HDA Induces ROS-Mediated Apoptosis in A549 Human Lung Cancer Cells by Regulating the MAPK, STAT3, NF-κB, and TGF-β1 Signaling Pathways. *BioMed research international, 2020*(1), 3042636.

Lin, Y., Shao, Q., Zhang, M., Lu, C., Fleming, J., & Su, S. (2019). Royal jelly-derived proteins enhance proliferation and migration of human epidermal keratinocytes in an in vitro scratch wound model. *BMC complementary and alternative medicine, 19*, 1-16.

Lin, Y., Zhang, M., Wang, L., Lin, T., Wang, G., Peng, J., & Su, S. (2020). The in vitro and in vivo wound-healing effects of royal jelly derived from Apis mellifera L. during blossom seasons of Castanea mollissima Bl. and Brassica napus L. in South China exhibited distinct patterns. *BMC Complementary Medicine and Therapies, 20*, 1-13.

Liu, Z., Liang, Q., Ren, Y., Guo, C., Ge, X., Wang, L., . . . Han, X. (2023). Immunosenescence: molecular mechanisms and diseases. *Signal transduction and targeted therapy, 8*(1), 200.

López-Gutiérrez, N., del Mar Aguilera-Luiz, M., Romero-González, R., Vidal, J. L. M., & Frenich, A. G. (2014). Fast analysis of polyphenols in royal jelly products using automated TurboFlow™-liquid chromatography–Orbitrap high resolution mass spectrometry. *Journal of Chromatography B, 973*, 17-28.

Maghsoudlou, A., Mahoonak, A. S., Mohebodini, H., & Toldra, F. (2019). Royal jelly: chemistry, storage and bioactivities. *Journal of apicultural Science, 63*(1), 17-40.

Mahdivand, N., Najafi, G., Nejati, V., Shalizar-Jalali, A., & Rahmani, F. (2019). Royal jelly protects male rats from heat stress-induced reproductive failure. *Andrologia, 51*(3), e13213.

Majd, S. A., Khorasgani, M. R., Zaker, S. R., Khezri, M., & Veshareh, A. A. (2022). Comparative Efficacy Study of N-Chromosome Royal Jelly Versus Semelil (ANGIPARS) on Wound Healing of Diabetic Rats. *Iranian journal of diabetes and obesity*.

Maleki, V., Jafari-Vayghan, H., Saleh-Ghadimi, S., Adibian, M., Kheirouri, S., & Alizadeh, M. (2019). Effects of Royal jelly on metabolic variables in diabetes mellitus: A systematic review. *Complementary therapies in medicine, 43*, 20-27.

Martinello, M., & Mutinelli, F. (2021). Antioxidant activity in bee products: A review. *Antioxidants, 10*(1), 71.

Marx, Í. M., Veloso, A. C., Casal, S., Pereira, J. A., & Peres, A. M. (2021). Sensory analysis using electronic tongues. In *Innovative food analysis* (pp. 323-343): Elsevier.

Melliou, E., & Chinou, I. (2014). Chemistry and bioactivities of royal jelly. *Studies in Natural Products Chemistry, 43*, 261-290.

Meydani, S. N., Barklund, M. P., Liu, S., Meydani, M., Miller, R. A., Cannon, J. G., . . . Blumberg, J. B. (1990). Vitamin E supplementation enhances cell-mediated immunity in healthy elderly subjects. *The American journal of clinical nutrition, 52*(3), 557-563.

Mihajlovic, D., Rajkovic, I., Chinou, I., & Colic, M. (2013). Dose-dependent immunomodulatory effects of 10-hydroxy-2-decenoic acid on human monocyte-derived dendritic cells. *Journal of Functional Foods, 5*(2), 838-846.

Mishima, S., Suzuki, K.-M., Isohama, Y., Kuratsu, N., Araki, Y., Inoue, M., & Miyata, T. (2005). Royal jelly has estrogenic effects in vitro and in vivo. *Journal of ethnopharmacology, 101*(1-3), 215-220.

Mizutani, Y., Shibuya, Y., Takahashi, T., Tsunoda, T., Moriyama, T., & Seishima, M. (2011). Major royal jelly protein 3 as a possible allergen in royal jelly-induced anaphylaxis.

Moraru, D., Alexa, E., Cocan, I., Obiștioiu, D., Radulov, I., Simiz, E., . . . Vintilă, T. (2024). Chemical Characterization and Antioxidant Activity of Apilarnil, Royal Jelly, and Propolis Collected in Banat Region, Romania. *Applied Sciences, 14*(3), 1242.

Mouro, G. F., & Toledo, V. d. A. A. d. (2004). Evaluation of Apis mellifera Carniolan and Africanized honey bees in royal jelly production. *Brazilian Archives of Biology and Technology, 47*, 469-476.

Mutlu, G., Akbulut, D., Aydın, N. S., & Mutlu, C. (2023). FONKSİYONEL BİR ARICILIK ÜRÜNÜ OLAN ARI SÜTÜNÜN BAZI ÖZELLİKLERİ ve SAĞLIK ÜZERİNE ETKİLERİ. *Uludağ Arıcılık Dergisi, 23*(1), 138-152.

Münstedt, K., Bargello, M., & Hauenschild, A. (2009). Royal jelly reduces the serum glucose levels in healthy subjects. *Journal of medicinal food, 12*(5), 1170-1172.

Nabas, Z., Haddadin, M. S., Haddadin, J., & Nazer, I. K. (2014). Chemical composition of royal jelly and effects of synbiotic with two different locally isolated probiotic strains on antioxidant activities. *Polish Journal of Food and Nutrition Sciences, 64*(3).

Nakaya, M., Onda, H., Sasaki, K., Yukiyoshi, A., Tachibana, H., & Yamada, K. (2007). Effect of royal jelly on bisphenol A-induced proliferation of human breast cancer cells. *Bioscience, biotechnology, and biochemistry, 71*(1), 253-255.

Natarajan, O., Angeloni, J. T., Bilodeau, M. F., Russi, K. E., Dong, Y., & Cao, M. (2021). The immunomodulatory effects of royal jelly on defending against bacterial infections in the Caenorhabditis elegans model. *Journal of medicinal food, 24*(4), 358-369.

Okamoto, I., Taniguchi, Y., Kunikata, T., Kohno, K., Iwaki, K., Ikeda, M., & Kurimoto, M. (2003). Major royal jelly protein 3 modulates immune responses in vitro and in vivo. *Life sciences, 73*(16), 2029-2045.

Oršolić, N., Sacases, F., Sert, P. d., & Bašić, I. (2007). Antimetastatic ability of honey bee products.

Osama, H., Abdullah, A., Gamal, B., Emad, D., Sayed, D., Hussein, E., . . . Medhat, S. (2017). Effect of honey and royal jelly against cisplatin-induced nephrotoxicity in patients with cancer. *Journal of the American college of nutrition, 36*(5), 342-346.

Ozek, N. S. (2024). Exploring the in vitro potential of royal jelly against glioblastoma and neuroblastoma: impact on cell proliferation, apoptosis, cell cycle, and the biomolecular content. *Analyst, 149*(6), 1872-1884.

Pan, Y., Rong, Y., You, M., Ma, Q., Chen, M., & Hu, F. (2019). Royal jelly causes hypotension and vasodilation induced by increasing nitric oxide production. *Food Science & Nutrition, 7*(4), 1361-1370.

Parhizkari, N., Eidi, M., Mahdavi-Ortakand, M., Ebrahimi-Kia, Y., Zarei, S., & Pazoki, Z. (2023). The effect of oral treatment of royal jelly on the expression of the PDGF-β gene in the skin wound of male mice. *Journal of Tissue Viability, 32*(4), 536-540.

Park, H. G., Kim, B. Y., Park, M. J., Deng, Y., Choi, Y. S., Lee, K. S., & Jin, B. R. (2019). Antibacterial activity of major royal jelly proteins of the honeybee (Apis mellifera) royal jelly. *Journal of Asia-Pacific Entomology, 22*(3), 737-741.

Park, H. M., Hwang, E., Lee, K. G., Han, S.-M., Cho, Y., & Kim, S. Y. (2011). Royal jelly protects against ultraviolet B–induced photoaging in human skin fibroblasts via enhancing collagen production. *Journal of medicinal food, 14*(9), 899-906.

Park, M. J., Kim, B. Y., Park, H. G., Deng, Y., Yoon, H. J., Choi, Y. S., . . . Jin, B. R. (2019). Major royal jelly protein 2 acts as an antimicrobial agent and antioxidant in royal jelly. *Journal of Asia-Pacific Entomology, 22*(3), 684-689.

Pasupuleti, V. R., Sammugam, L., Ramesh, N., & Gan, S. H. (2017). Honey, propolis, and royal jelly: a comprehensive review of their biological actions and health benefits. *Oxidative medicine and cellular longevity, 2017*(1), 1259510.

Peacock, S., Murray, V., & Turton, C. (1995). Respiratory distress and royal jelly. *BMJ: British Medical Journal, 311*(7018), 1472.

Peng, C.-C., Sun, H.-T., Lin, I.-P., Kuo, P.-C., & Li, J.-C. (2017). The functional property of royal jelly 10-hydroxy-2-decenoic acid as a melanogenesis inhibitor. *BMC complementary and alternative medicine, 17*, 1-8.

Peng ChiChung, P. C., Sun HuiTzu, S. H., Lin IPing, L. I., Kuo PingChung, K. P., & Li JenChieh, L. J. (2017). The functional property of royal jelly 10-hydroxy-2-decenoic acid as a melanogenesis inhibitor.

Piana, L. (1996). Value-added products from beekeeping–Royal jelly. *FAO Agric. Serv. Bull, 124*, 195-226.

Pourfard, H., Ahmadi, A., Habibi, Z., Asadi-Samani, M., Shahinfard, N., & Soleimani, A. (2023). The Effect of Tang Forte (Royal Jelly) Capsule on Hypoglycemia and Clinical Course in COVID-19 Patients Under Corticosteroid Therapy. *Journal of Evidence-Based Integrative Medicine, 28*, 2515690X231165333.

Premratanachai, P., & Chanchao, C. (2014). Review of the anticancer activities of bee products. *Asian Pacific journal of tropical biomedicine, 4*(5), 337-344.

Qiu, W., Chen, X., Tian, Y., Wu, D., Du, M., & Wang, S. (2020). Protection against oxidative stress and anti-aging effect in Drosophila of royal jelly-collagen peptide. *Food and Chemical Toxicology, 135*, 110881.

Qu, L., Wang, L., Ji, H., Fang, Y., Lei, P., Zhang, X., . . . Dong, H. (2022). Toxic mechanism and biological detoxification of fumonisins. *Toxins, 14*(3), 182.

Raoufi, S., Salavati, Z., Komaki, A., Shahidi, S., & Zarei, M. (2023). Royal jelly improves learning and memory deficits in an amyloid β-induced model of Alzheimer's disease in male rats: Involvement of oxidative stress. *Metabolic Brain Disease, 38*(4), 1239-1248.

Ratajczak, M., Kaminska, D., Matuszewska, E., Hołderna-Kedzia, E., Rogacki, J., & Matysiak, J. (2021). Promising antimicrobial properties of bioactive compounds from different honeybee products. *Molecules, 26*(13), 4007.

Renard, T., Gueydan, C., & Aron, S. (2022). DNA methylation and expression of the egfr gene are associated with worker size in monomorphic ants. *Scientific reports, 12*(1), 21228.

Rose-John, S., Winthrop, K., & Calabrese, L. (2017). The role of IL-6 in host defence against infections: immunobiology and clinical implications. *Nature Reviews Rheumatology, 13*(7), 399-409.

Saadeldin, I. M., Tanga, B. M., Bang, S., Maigoro, A. Y., Kang, H., Cha, D., . . . Cho, J. (2023). MicroRNA profiling of royal jelly extracellular vesicles and their potential role in cell viability and reversing cell apoptosis. *Functional & Integrative Genomics, 23*(3), 200.

Sabatini, A. G., Marcazzan, G. L., Caboni, M. F., Bogdanov, S., & Almeida-Muradian, L. B. d. (2009). Quality and standardisation of royal jelly. *Journal of ApiProduct and ApiMedical Science, 1*(1), 1-6.

Salama, S., Shou, Q., Abd El-Wahed, A. A., Elias, N., Xiao, J., Swillam, A., . . . Wang, K. (2022). Royal jelly: Beneficial properties and synergistic effects with chemotherapeutic drugs with particular emphasis in anticancer strategies. *Nutrients, 14*(19), 4166.

Severo, M. L. B., Thieme, S., Silveira, F. M., Tavares, R. P. M., Gonzaga, A. K. G., Zucolotto, S. M., . . . da Silveira, É. J. D. (2022). Comparative study of royal jelly, propolis, and photobiomodulation therapies in 5-fluorouracil-related oral mucositis in rats. *Supportive Care in Cancer*, 1-12.

Shahzad, Q., Mehmood, M. U., Khan, H., ul Husna, A., Qadeer, S., Azam, A., . . . Ahmad, M. (2016). Royal jelly supplementation in semen extender enhances post-thaw quality and fertility of Nili-Ravi buffalo bull sperm. *Animal reproduction science, 167*, 83-88.

Sharif, S. N., & Darsareh, F. (2019). Effect of royal jelly on menopausal symptoms: A randomized placebo-controlled clinical trial. *Complementary therapies in clinical practice, 37*, 47-50.

Sharma, A., Pant, K., Brar, D. S., Thakur, A., & Nanda, V. (2023). A review on Apiproducts: Current scenario of potential contaminants and their food safety concerns. *Food Control, 145*, 109499.

Shen, L.-r., Wang, Y.-r., Zhai, L., Zhou, W.-x., Tan, L.-l., Li, M.-l., . . . Xiao, F. (2015). Determination of royal jelly freshness by ELISA with a highly specific antiapalbumin 1, major royal jelly protein 1 antibody. *Journal of Zhejiang University. Science. B, 16*(2), 155.

Shen, L., Liu, D., Li, M., Jin, F., Din, M., Parnell, L. D., & Lai, C.-Q. (2012). Mechanism of action of recombinant acc-royalisin from royal jelly of Asian honeybee against gram-positive bacteria.

Stocker, A., Schramel, P., Kettrup, A., & Bengsch, E. (2005). Trace and mineral elements in royal jelly and homeostatic effects. *Journal of Trace Elements in Medicine and Biology, 19*(2-3), 183-189.

Suemaru, K., Cui, R., Li, B., Watanabe, S., Okihara, K., Hashimoto, K., . . . Araki, H. (2008). Topical application of royal jelly has a healing effect for 5-fluorouracil-

induced experimental oral mucositis in hamsters. *Methods and findings in experimental and clinical pharmacology*, *30*(2), 103-106.

Taavoni, S., Barkhordari, F., Goushegir, A., & Haghani, H. (2014). Effect of Royal Jelly on premenstrual syndrome among Iranian medical sciences students: A randomized, triple-blind, placebo-controlled study. *Complementary therapies in medicine*, *22*(4), 601-606.

Takikawa, M., Kumagai, A., Hirata, H., Soga, M., Yamashita, Y., Ueda, M., . . . Tsuda, T. (2013). 10-Hydroxy-2-decenoic acid, a unique medium-chain fatty acid, activates 5'-AMP-activated protein kinase in L 6 myotubes and mice. *Molecular nutrition & food research*, *57*(10), 1794-1802.

Tan, D., Zhu, W., Liu, L., Pan, Y., Xu, Y., Huang, Q., . . . Rao, L. (2023). In situ formed scaffold with royal jelly-derived extracellular vesicles for wound healing. *Theranostics*, *13*(9), 2811.

Taniguchi, Y., Kohno, K., Inoue, S.-i., Koya-Miyata, S., Okamoto, I., Arai, N., . . . Kurimoto, M. (2003). Oral administration of royal jelly inhibits the development of atopic dermatitis-like skin lesions in NC/Nga mice. *International immunopharmacology*, *3*(9), 1313-1324.

Temamogullari, F., Aral, F., & Yilmaz, R. (2018). Royal jelly protection on flunixin meglumine-induced spermiotoxicity and testicular degeneration in mice. *Polish journal of veterinary sciences*, *21*(3).

Thien, F., Leung, R., Baldo, B., Weinbr, J., Plomley, R., & Czarny, D. (1996). Asthma and anaphylaxis induced by royal jelly. *Clinical & Experimental Allergy*, *26*(2), 216-222.

Tohamy, H. G., El-Neweshy, M. S., Soliman, M. M., Sayed, S., Shukry, M., Ghamry, H. I., & Abd-Ellatieff, H. (2022). Protective potential of royal jelly against hydroxyurea-induced hepatic injury in rats via antioxidant, anti-inflammatory, and anti-apoptosis properties. *PloS one*, *17*(3), e0265261.

Torrijos, E. G., Diaz, Y. M., Segade, J. M. B., Brito, J. F. F., Arias, T. A., Bonilla, P. A. G., . . . Rodríguez, R. G. (2016). Occupational allergic respiratory disease due to royal jelly. *Annals of allergy, asthma & immunology: official publication of the American College of Allergy, Asthma, & Immunology*, *117*(1), 102-103.

Tsigos, C., Hainer, V., Basdevant, A., Finer, N., Fried, M., Mathus-Vliegen, E., . . . Schutz, Y. (2008). Management of obesity in adults: European clinical practice guidelines. *Obesity facts*, *1*(2), 106-116.

Uthaibutra, V., Kaewkod, T., Prapawilai, P., Pandith, H., & Tragoolpua, Y. (2023). Inhibition of skin pathogenic bacteria, antioxidant and anti-inflammatory activity of royal jelly from Northern Thailand. *Molecules*, *28*(3), 996.

Vazhacharickal, P. J. (2021). A review on health benefits and biological action of honey, propolis and royal jelly. *J. Med. Plants Stud*, *9*(5), 1-13.

Virgiliou, C., Kanelis, D., Pina, A., Gika, H., Tananaki, C., Zotou, A., & Theodoridis, G. (2020). A targeted approach for studying the effect of sugar bee feeding on the metabolic profile of Royal Jelly. *Journal of Chromatography A, 1616*, 460783.

Viuda-Martos, M., Pérez-Alvarez, J. A., & Fernández-López, J. (2017). Royal jelly: Health benefits and uses in medicine. *Bee Products-Chemical and Biological Properties*, 199-218.

Vucevic, D., Melliou, E., Vasilijic, S., Gasic, S., Ivanovski, P., Chinou, I., & Colic, M. (2007). Fatty acids isolated from royal jelly modulate dendritic cell-mediated immune response in vitro. *International immunopharmacology, 7*(9), 1211-1220.

Wang, W., Li, X., Li, D., Pan, F., Fang, X., Peng, W., & Tian, W. (2023). Effects of major royal jelly proteins on the immune response and gut microbiota composition in cyclophosphamide-treated mice. *Nutrients, 15*(4), 974.

Wang, X., Cook, L. F., Grasso, L. M., Cao, M., & Dong, Y. (2015). Royal jelly-mediated prolongevity and stress resistance in Caenorhabditis elegans is possibly modulated by the interplays of DAF-16, SIR-2.1, HCF-1, and 14-3-3 proteins. *Journals of Gerontology Series A: Biomedical Sciences and Medical Sciences, 70*(7), 827-838.

Watadani, R., Kotoh, J., Sasaki, D., Someya, A., Matsumoto, K., & Maeda, A. (2017). 10-Hydroxy-2-decenoic acid, a natural product, improves hyperglycemia and insulin resistance in obese/diabetic KK-Ay mice, but does not prevent obesity. *Journal of Veterinary Medical Science, 79*(9), 1596-1602.

Wytrychowski, M., Chenavas, S., Daniele, G., Casabianca, H., Batteau, M., Guibert, S., & Brion, B. (2013). Physicochemical characterisation of French royal jelly: Comparison with commercial royal jellies and royal jellies produced through artificial bee-feeding. *Journal of Food Composition and Analysis, 29*(2), 126-133.

Xin, X.-x., Chen, Y., Chen, D., Xiao, F., Parnell, L. D., Zhao, J., . . . Shen, L.-r. (2016). Supplementation with major royal-jelly proteins increases lifespan, feeding, and fecundity in Drosophila. *Journal of Agricultural and Food Chemistry, 64*(29), 5803-5812.

Yan, S., Wang, X., Sun, M., Wang, W., Wu, L., & Xue, X. (2022). Investigation of the lipidomic profile of royal jelly from different botanical origins using UHPLC-IM-Q-TOF-MS and GC-MS. *LWT, 169*, 113894.

Yoneshiro, T., Kaede, R., Nagaya, K., Aoyama, J., Saito, M., Okamatsu-Ogura, Y., . . . Terao, A. (2018). Royal jelly ameliorates diet-induced obesity and glucose intolerance by promoting brown adipose tissue thermogenesis in mice. *Obesity research & clinical practice, 12*(1), 127-137.

Yoshida, M., Hayashi, K., Watadani, R., Okano, Y., Tanimura, K., Kotoh, J., . . . Maeda, A. (2017). Royal jelly improves hyperglycemia in obese/diabetic KK-Ay mice. *Journal of Veterinary Medical Science, 79*(2), 299-307.

You, M.-M., Chen, Y.-F., Pan, Y.-M., Liu, Y.-C., Tu, J., Wang, K., & Hu, F.-L. (2018). Royal jelly attenuates LPS-induced inflammation in BV-2 microglial cells through modulating NF-κB and p38/JNK signaling pathways. *Mediators of inflammation, 2018*(1), 7834381.

Zahran, A. M., Elsayh, K. I., Saad, K., Eloseily, E. M., Osman, N. S., Alblihed, M. A., . . . Mahmoud, M. H. (2016). Effects of royal jelly supplementation on regulatory T cells in children with SLE. *Food & nutrition research, 60*(1), 32963.

Zamami, Y., Takatori, S., Goda, M., Koyama, T., Iwatani, Y., Jin, X., . . . Kawasaki, H. (2008). Royal jelly ameliorates insulin resistance in fructose-drinking rats. *Biological and pharmaceutical bulletin, 31*(11), 2103-2107.

Zamani, Z., Reisi, P., Alaei, H., & Pilehvarian, A. A. (2012). Effect of Royal Jelly on spatial learning and memory in rat model of streptozotocin-induced sporadic Alzheimer's disease. *Advanced biomedical research, 1*(1), 26.

Zhang, S., Shao, Q., Geng, H., & Su, S. (2017). The effect of royal jelly on the growth of breast cancer in mice. *Oncology letters, 14*(6), 7615-7621.

Zhou, J., Zhang, L., He, Y., Liu, K., Zhang, F., Zhang, H., . . . Fareed, M. S. (2021). An optimized analog of antimicrobial peptide Jelleine-1 shows enhanced antimicrobial activity against multidrug resistant P. aeruginosa and negligible toxicity in vitro and in vivo. *European journal of medicinal chemistry, 219*, 113433.

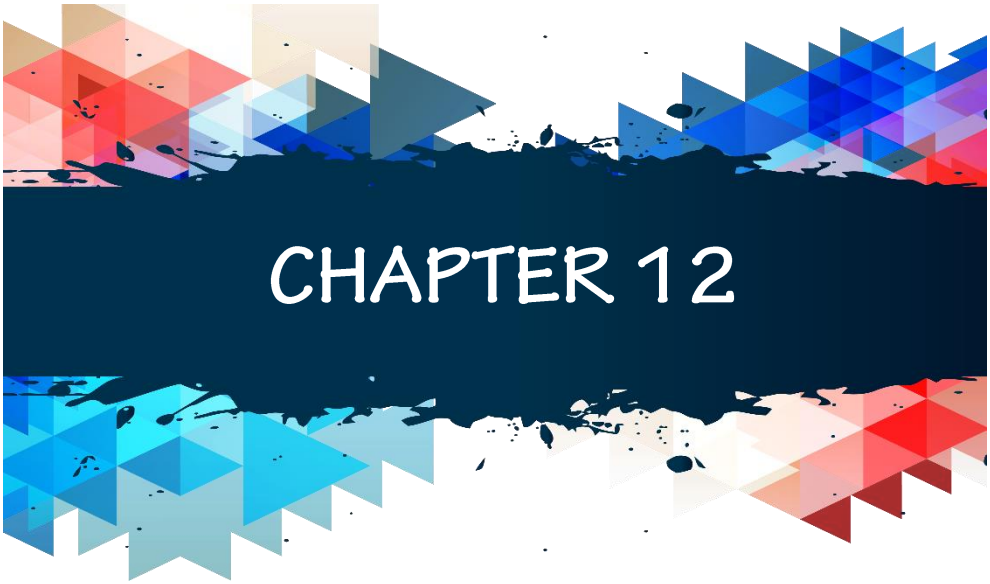

Changes in Hemocyte Count and Behaviors of *Galleria mellonella* L. (Lepidoptera: Pyralidae) at Different Developmental Stages

Aylin Er[1] & Fevzi Uçkan[2]

1 Prof. Department of Biology, Faculty of Science and Letters, Balıkesir University, TÜRKİYE, 0000-0002-8108-8950
[2] Asst. Prof., Department of Biology, Faculty of Science and Letters, Kocaeli University, TÜRKİYE, 0000-0001-9304-4296

INTRODUCTION

In holometabolous insects, numerous significant physiological changes occur during metamorphosis, transitioning from the actively feeding larval stage to the immobile pupal stage and eventually to the sexually reproductive adult stage. (Meylaers et al., 2007). Research studies have identified significant qualitative and quantitative changes in protein and hormone levels during both larval and pupal stages, in addition to morphological differentiation. (Beetz et al., 2008, Kanost et al., 1990; Riddiford, 1991). Furthermore, various studies in the literature have documented changes in both the quantity and morphology of hemocytes, referred to as insect blood cells, during metamorphosis (Beetz et al., 2008, Jalali and Salehi 2008, Gardiner and Strand, 1999).

Insects possess a robust natural immune system against microbes, parasitic organisms, and a wide range of macroorganisms. Pathogens and parasites that breach the insect's physiochemical barriers and enter the body cavity are met with immune responses triggered by the insect's recognition of non-self entities. In insect immunity, two main components are distinguished: humoral immunity and cellular immunity. Humoral immunity encompasses the synthesis of antimicrobial peptides and various effector molecules by fat body or hemocytes, leading to their release into the insect hemolymph, as well as melanization responses resulting from phenoloxidase activity around foreign particles and clotting of hemolymph for wound healing. Cellular immune responses involve defense reactions executed by hemocytes, such as encapsulation, nodulation, and phagocytosis (Lavine and Strand, 2002, Strand and Pech, 1995). In insects, hemocytes can vary in morphology, type, and number from species to species, as well as exhibit differences across the physiological states and developmental stages of the insect. Classification schemes are available in the literature to facilitate their identification, taking into account these variations (Jones and Gupta 1979, Strand, 2008). The most commonly identified hemocyte types in the Lepidoptera order, which includes the greater wax moth G. mellonella, are prohemocytes, plasmatocytes, granulocytes, oenocytoids, and spherulocytes, based on their histological, morphological, and functional characteristics (Senior and Titball 2020, Lu and Zang 2022). Although there are various approaches to the formation and differentiation of insect hemocytes, the general consensus is that prohemocytes differentiate into plasmatocytes in hematopoietic organs. Afterward, other hemocyte types differentiate from plasmatocytes, and the populations of hemocytes in the hemolymph are maintained through ongoing cell divisions (Ribeiro and Brehelin 2006, Ling and Yu 2006).

The most definitive way to elucidate cellular immunity in insects is to determine the total and different types of hemocytes circulating in the hemolymph and to assess the magnitude of the encapsulation response against a specific antigen. Studies demonstrating hemocyte counts and behaviors are often conducted during the larval stage across different insect species, while studies specifically focusing on pupal encapsulation responses are limited in number (Lavine and Strand 2002). Changes in hemocyte counts at different stages of development have been documented in several studies across various insect orders. (Beetz et al., 2004, 2008, Jalali and Salehi, 2008, Gardiner and Strand, 1999,2000, Lanot et al., 2001). The changes in hemocyte counts and behaviors during metamorphosis are crucial for determining the period of lowest immunity in combating harmful insects. Therefore, in this study, focusing on *G. mellonella*, a well-known harmful moth species among beekeepers, total and different hemocyte counts, mitotic index of hemocytes, and encapsulation behaviors of hemocytes were determined and statistically compared during the larval and pupal stages.

2. MATERIALS AND METHODS

2.1. Establishment of Insect Cultures

Laboratory colonies of the greater wax moth *G. mellonella* were established using combs obtained from beehives in the Balıkesir region. Throughout the culture maintenance and all experimental procedures, environmental conditions were maintained at 28 ± 1°C temperature, 60 ± 5% relative humidity, and a 12:12-hour (Light:Dark) photoperiod in the laboratory. Natural darkened combs were used for successive cultures to feed the larvae and allow oviposition by adult females. Two females and two males were introduced into 1-liter jars containing some comb pieces to maintain the culture. Larvae of *G. mellonella* obtained in this manner were transferred to jars containing folded paper to pupate. The final instar larvae and resulting pupae were utilized for both the continuation of insect culture and experimentation. Additionally, when rapid production of *G. mellonella* cultures and obtaining pupae were necessary, incubators set at 30-35°C were utilized.

2.2 Total hemocyte counts in larval and pupal stages of

G. mellonella

For the determination of total hemocyte counts in the pupal stage of *G. mellonella*, pupae were punctured in the abdominal region to obtain hemolymph. 4 µl hemolymph was collected with a microcapillary tube (Sigma), which was

then transferred to Eppendorf tubes containing 20 µl of anticoagulant solution (0.098 M NaOH, 0.186 M NaCl, 0.017 M Na2EDTA, and 0.041 M citric acid, pH = 4.5) and kept on ice. Subsequently, 10 µl of the diluted hemolymph suspension was loaded onto a Neubauer hemocytometer (Improved Neubauer Hemocytometer; Superior, Germany) using a micropipette.

In the larval stage, hemolymph samples were obtained from the first hind leg using a microcapillary tube. Collected 4 µl of hemolymph was diluted in 36 µl of anticoagulant solution, resulting in a 1:10 dilution, and then loaded onto the Neubauer hemocytometer. The hemocytes were counted under an Olympus light microscope, and the hemocyte count was determined per milliliter of hemolymph.

For the determination of total hemocyte counts in both larval and pupal stages, 15 larvae and 15 pupae were used in each replicate, and all experiments were repeated three times.

2.3. Differential Hemocyte Counts and Mitotic Index in *G. mellonella* Larval and Pupal Stages

To determine the different hemocyte counts and mitotic index in *G. mellonella* larvae and pupae, the larvae and pupae were first wiped with 95% ethanol. Hemolymph was collected by puncturing the abdominal part of the pupae and the first rear leg of the larvae with a dissection needle, and 5 µl of hemolymph was obtained using a microcapillary tube. The hemolymph was spread onto slides cleaned with alcohol and left to dry. After drying, the slides were placed in methanol for 5 minutes and then dried again. To identify different hemocytes, these slides were stained with freshly prepared Giemsa stain solution. Preparations were left in the stain solution for 10 minutes for pupal hemolymph and 15 minutes for larval hemolymph. The slides were then washed with distilled water, passed through PBS, and left to dry. The dried preparations were examined under a light microscope at 1000x magnification.

2.4. In Vivo Encapsulation in *G. mellonella* Larval and Pupal Stages

In studies comparing the encapsulation behaviors of *G. mellonella* larval and pupal hemocytes, Sephadex DEAE A-25 (40-120 µm) beads were selected as the encapsulation material. To facilitate the detection of beads within the insect body cavity, they were stained with a 1% Coomassie Blue solution (Brilliant Blue G Sigma) prepared in PBS. After 1 hour, the supernatant was removed from the dye solution, and the beads were washed with PBS. From the stock bead solution containing 15-20 Sephadex A-25 beads, 10 µl was drawn using a Hamilton microinjector (50 µl capacity with a 22 gauge needle) and injected into the host

larvae and pupae. At 4 and 24 hours post-injection, *G. mellonella* larvae and pupae were dissected under a stereo microscope, and the extracted beads were transferred onto slides containing PBS for microscopic examination. The obtained beads were categorized into three different groups as non-encapsulated, weakly encapsulated, and strongly encapsulated, as described in previous studies.

2.5. Statistics

The experimental results were compared using one-way analysis of variance (ANOVA). Differences between means were determined using Tukey's Honestly Significant Difference (Tukey HSD) tests. SPSS statistical software was used for data analysis. Percentage values were normalized by taking the arcsine square roots, but results were presented as percentages. The results were found to be significant at $P < 0.05$.

3. RESULTS AND DISCUSSION

The total hemocyte counts detected in the larval and pupal stages of *G. mellonella* are presented in Table 1. In *G. mellonella* larvae, the total hemocyte count was found to be an average of 16.92 x 10^6 cells/ml, while in the pupal stage, this count decreased to 10.91 x 10^6 cells/ml. This difference in total hemocyte counts between the larval and pupal stages was found to be statistically significant.

Table 1. Total hemocyte counts in the circulation of *G. mellonella* larva and pupa (x10^6 cell/ml)

Phase	Total hemocyte counts (x10^6 cell /ml)		
	N	**Min. – Max.**	**(Mean ± SE) #**
Larva	45	8.40 – 37.40	16.92 ± 0.9 **a**
Pupa	45	2.70 – 24.50	10.91 ± 0.7 **b**

#Each represents the mean total hemocyte count for 45 larvae and pupae. *Values within the same column bearing different letters (a-b) indicate a statistically significant difference ($P < 0.05$).

Reductions in total hemocyte counts during the transition from the larval to the pupal stage have been observed in various studies (Jalali and Salehi 2008). The decrease in hemocyte counts during the pupal stage may be due to the adhesion of hemocytes to different organs. In *G. mellonella*, hemocytes are classified as granulocytes, plasmatocytes, spherulocytes, prohemocytes, and oenocytoids. However, when determining different hemocyte counts in the larval

and pupal stages, hemocytes were categorized as granulocytes, plasmatocytes, and others. No difference was observed in the different hemocyte counts between the larval and pupal stages (Table 2). The evaluation of preparations made from the larval hemolymph of *G. mellonella* revealed that the proportion of hemocytes in mitosis was 2.16%. In the pupal stage, this proportion was calculated as 1.44%. The decrease in the mitotic index observed in the pupal stage compared to the larval stage was significant (Table 3). In Lepidoptera, circulating hemocytes are released from the hematopoietic organ, and the mitotic division of existing circulating hemocytes also contributes to this process (Liu and Wang 2017, Wang and Zhang 2020). Our results are consistent with findings in *B. mori* and *E. Declarata*, where approximately 1-8% of circulating hemocytes are normally in the mitotic phase (Nakahara et al., 2009)

Following the injection of Sephadex A-25 beads in *G. mellonella*, 46.2% of the beads dissected from the larvae 4 hours after the injection were strongly encapsulated, while this rate was calculated to be 10.2% in the pupal stage (Table 4). In the 24-hour period following the injection, this rate increased to 84.8% in the larvae, whereas it was found to be 48.5% in the pupal stage. The strong encapsulation response observed in the larval stage during the 4 and 8-hour periods was statistically significant. The encapsulation response observed at 24 hours after the injection was stronger compared to the response at 4 hours in both the larval and pupal stages ($P<0.05$).

In our study, the total hemocyte count and mitotic index were found to be higher in the larval stage compared to the pupal stage, and the encapsulation behavior of hemocytes occurred faster and more robustly in the larval stage compared to the pupal stage. This suggests that cellular defense responses are weaker in the pupal stage, which lacks feeding and movement activity.

Table 2. Differential hemocyte counts (DHC) in the larval and pupal stages of *G. mellonella* (cells / 1000)

Hemocyte Type	Phase	DHC (cells / 1000)		
		N	Min. – Max.	(Mean ± SE) #
Granulocyte	Larvae	12	545 – 689	589.0 ± 11.1**a**
	Pupa	12	478 – 633	574.3 ± 10.9**a**
Plasmatocyte	Larvae	12	297 – 444	400.3 ± 11.5**a**
	Pupa	12	358 – 506	415 ± 10.3**a**
Others	Larvae	12	6 – 17	10.7 ± 1.1**a**
	Pupa	12	6 – 19	10.8 ± 1.2**a**

Each column represents the mean granulocyte, plasmatocyte, and other hemocyte counts for 12 larvae and pupae.*Values sharing the same letter within the same column are not statistically different (P > 0.05).

Table 3. Circulating mitotic hemocyte counts (cells / 100) in the larval and pupal stages of *G. mellonella.*

Phase	Mitotic Index (cells /100)		
	N	Min. – Max.	(Mean ± SE) #
Larva	9	7 – 15	2.16 ± 0.9 **a**
Pupa	9	4 – 11	1.44 ± 0.8 **b**

Each shows the mean mitotic hemocyte counts of 9 larvae and pupae. *Values sharing the same letter within the same column are not statistically different (P > 0.05).

The study of insect metamorphosis, particularly in species undergoing complete metamorphosis, reveals significant transformations across the larval, pupal, and adult stages. This process is not only morphological but also involves profound changes in immune function, which are crucial for pest management strategies. Insects like *G. mellonella* exhibit distinct morphological changes throughout their life cycle. Our observations indicate that during the transition from larva to pupa, there is a notable reduction in total hemocyte counts, which

are critical for immune responses. While the total number of hemocytes decreases during this transition, the diversity of hemocyte types remains relatively stable. This suggests that although the immune capacity may be compromised during the pupal stage, the types of cells involved in immunity do not drastically change.

The immune system of insects undergoing complete metamorphosis is highly dynamic. For instance, studies on other species such as *Brithys crini* and *Apis cerana* have shown that their intestinal structures and gut microbiota adapt significantly during metamorphosis to enhance resistance against pathogens. In *G. mellonella*, we found that encapsulation rates, an indicator of cellular immunity were lower in the pupal stage compared to the larval stage. This decline in encapsulation efficiency may reflect a temporary vulnerability during metamorphosis when tissues undergo extensive remodeling.

Understanding the molecular mechanisms underlying the immune transformations in insects can facilitate the development of effective biopesticides. By identifying critical genes or proteins involved in immunity during the larval-to-adult transition in *G. mellonella*, researchers can better target pest management strategies. For instance, leveraging knowledge about how immune responses change can inform the timing and application of biological control agents such as entomopathogens or natural enemies which rely on these immune systems for efficacy.

The findings regarding hemocyte dynamics and immune system changes during metamorphosis highlight crucial aspects of insect biology that can be exploited for pest management. As we deepen our understanding of these processes, particularly in economically significant pests, we pave the way for innovative strategies that could mitigate their impact on agriculture. This discussion underscores the importance of integrating developmental biology with immunology to enhance pest control measures effectively. Further research into these interconnected systems will be essential for advancing agricultural practices and ensuring sustainable pest management solutions.

Table 4. Proportions of non-encapsulated, weakly encapsulated, and strongly encapsulated hemocytes in the larval and pupal stages of *G. mellonella* (%)

Phase	**Number of Beads Recovered**		**Non-Encapsulated**			**Weakly Encapsulated**			**Strongly Encapsulated**		
	4s	**24s**	**4s**		**24s**	**4s**		**24s**	**4s**		**24s**
Larva	12	11	1 (%8,3)	0	(%0,0)	5	(%41,7)	0 (%0,0)	6 (%50,0)	11	(%100,0)
	10	14	0 (%0,0)	0	(%0,0)	5	(%50,0)	2 (%14,3)	5 (%50,0)	12	(%85,7)
	9	8	1 (%11,1)	0	(%0,0)	3	(%33,3)	2 (%25,0)	5 (%55,6)	6	(%75,0)
	12	11	0 (%0,0)	0	(%0,0)	6	(%50,0)	2 (%18,2)	6 (%50,0)	9	(%81,8)
	13	12	0 (%0,0)	0	(%0,0)	3	(%23,1)	0 (%0,0)	10 (%76,9)	12	(%100,0)
	12	12	2 (%16,7)	0	(%0,0)	4	(%33,3)	2 (%16,7)	6 (%50,0)	10	(%83,3)
	11	8	0 (%0,0)	0	(%0,0)	10	(%90,9)	0 (%0,0)	1 (%9,1)	8	(%100,0)
	12	12	1 (%8,3)	0	(%0,0)	7	(%58,3)	1 (%8,3)	4 (%33,3)	11	(%91,7)
	8	12	0 (%0,0)	1	(%8,3)	3	(%37,5)	2 (%16,7)	5 (%62,5)	9	(%75,0)
	9	9	1 (%11,1)	1	(%11,1)	3	(%33,3)	2 (%22,2)	5 (%55,6)	6	(%66,7)
	11	12	0 (%0,0)	0	(%0,0)	8	(%72,7)	0 (%0,0)	3 (%27,3)	12	(%100,0)
	10	10	2 (%20,0)	2	(%20,0)	4	(%40,0)	3 (%30,0)	4 (%40,0)	5	(%50,0)
	13	13	3 (%23,1)	1	(%7,7)	6	(%46,2)	2 (%15,4)	4 (%30,8)	10	(%76,9)
	10	9	2 (%20,0)	0	(%0,0)	4	(%40,0)	0 (%0,0)	4 (%40,0)	9	(%100,0)
	8	14	0 (%0,0)	2	(%14,3)	3	(%37,5)	0 (%0,0)	5 (%62,5)	12	(%85,7)
(Ort±SH)[#]			%7,8 ± 2,2**a**		%4,1±1,7**a**	%45,9± 4,4**a**		%10,9±2,7**a**	%46,2±4,3**a**		%84,8 ± 3,7**a**
Pupa	10	8	0 (%0,0)	0	(%0,0)	6	(%60,0)	4 (%50,0)	4 (%40,0)	4	(%50,0)
	9	11	0 (%0,0)	2	(%18,2)	9	(%100)	5 (%45,5)	0 (%0,0)	4	(%36,4)
	8	14	1 (%12,5)	1	(%7,1)	7	(%87,5)	8 (%57,1)	0 (%0,0)	5	(%35,7)
	12	12	2 (%16,7)	1	(%8,3)	10	(%83,3)	9 (%75,0)	0 (%0,0)	2	(%16,7)
	10	15	1 (%10,0)	1	(%6,7)	9	(%90,0)	5 (%33,3)	0 (%0,0)	9	(%60,0)
	8	8	1 (%12,5)	0	(%0,0)	7	(%87,5)	0 (%0,0)	0 (%0,0)	8	(%100)
	13	14	1 (%7,7)	1	(%7,1)	12	(%92,3)	5 (%35,7)	0 (%0,0)	8	(%57,1)
	11	12	1 (%9,1)	0	(%0,0)	9	(%81,8)	5 (%41,7)	1 (%9,1)	7	(%58,3)

8	9	0	(%0,0)	0	(%0,0)	6	(%75,0)	6	(%66,7)	2	(%25,0)	3	(%33,3)
7	11	1	(%14,3)	1	(%9,1)	5	(%71,4)	3	(%27,3)	1	(%14,3)	7	(%63,6)
7	10	0	(%0,0)	2	(%20,0)	4	(%57,1)	4	(%40,0)	3	(%42,9)	4	(%40,0)
8	10	0	(%0,0)	0	(%0,0)	7	(%87,5)	5	(%50,0)	1	(%12,5)	5	(%50,0)
10	11	0	(%0,0)	0	(%0,0)	10	(%100)	4	(%36,4)	0	(%0,0)	7	(%63,6)
10	11	1	(%10,0)	0	(%0,0)	8	(%80,0)	9	(%81,8)	1	(%10,0)	2	(%18,2)
9	11	0	(%0,0)	1	(%9,1)	9	(%100)	5	(%45,5)	0	(%0,0)	5	(%45,5)
(Ort±SH)#		%6,2 ± 2**b**		%5,7±1,7**b**		%83,5 ± 3,4**b**		%45,7±5**b**		%10,2±3,8**b**		%48,5±5,3**b**	

*Values sharing the same letter within the same column are not statistically different (P > 0.05).

4. REFERENCES

Beetz, S., Kaftan, F., & Kroeger, A. (2008). Hemocyte differentiation during larval and pupal metamorphosis in holometabolous insects. Developmental Biology, 323(2), 273-283.

Beetz, S., Holthusen, T. K., Koolman, J., & Trenczek, T. (2004). Proteomic profiling of hemocyte immunity in Manduca sexta. Insect Biochemistry and Molecular Biology, 34(10).

Gardiner, E. M. M., & Strand, M. R. (1999). Hemocyte dynamics in insects during metamorphosis. Developmental & Comparative Immunology, 23(2), 215-224.

Gardiner, E. M., & Strand, M. R. (2000). Hematopoietic organ dynamics in lepidopteran larvae. Archives of Insect Biochemistry and Physiology, 43(3), 147-164.

Jalali, M. A., & Salehi, A. (2008). Changes in hemocyte number and morphology in metamorphosis of Lepidopteran insects. Zoological Studies, 47(3), 329-335.

Jalali, J., & Salehi, R. (2008). Differential roles of hemocyte types in insect immunity. Archives of Insect Biochemistry and Physiology, 67(4), 174-186.

Jones, J. C., & Gupta, A. P. (1979). Pathways and pitfalls in the classification and study of insect hemocytes. In Insect Hemocytes: Development, Forms, Functions and Techniques (pp. 279–300). Cambridge University Press.

Kanost, M. R., Jiang, H., & Yu, X. Q. (1990). Roles of insect hemolymph proteins in immunity. Advances in Insect Physiology, 27, 1-62.

Lanot, R., Zachary, D., Holder, F., & Meister, M. (2001). Hematopoiesis in Drosophila melanogaster. Development, 128(22), 4891-4899.

Lavine, M. D., & Strand, M. R. (2002). Insect hemocytes and their role in cellular immune responses. Insect Biochemistry and Molecular Biology, 32(10), 1295–1309.

Liu, L., & Wang, L. (2017). Hematopoiesis and hemocyte dynamics in Lepidoptera: Insights from the silkworm Bombyx mori. Insect Biochemistry and Molecular Biology, 81, 1-10.

Ling, E., & Yu, X. Q. (2006). Prophenoloxidase binds to plasmatocyte surfaces in Manduca sexta hemolymph. Insect Biochemistry and Molecular Biology, 36(8), 751–759.

Lu, Z., & Zhang, X. (2022). Immune responses of *Galleria mellonella* hemocytes in antimicrobial defense. Frontiers in Immunology, 13, 1-12.

Meylaers, K., Huybrechts, R., & De Loof, A. (2007). Metamorphosis in insects: A major change in the hormonal regulation of hemocytes. Invertebrate Survival Journal, 4(1), 85-91.

Nakahara, K., Sato, R., & Hoshino, S. (2009). Two hemocyte lineages exist in silkworm larval hematopoietic organ. PLOS ONE, 4(9), e7182.

Ribeiro, C., & Brehelin, M. (2006). Insect hemocytes: What type of cell is that? Journal of Insect Physiology, 52(5), 417–429.

Riddiford, L. M. (1991). Hormonal regulation of hemocyte changes during insect metamorphosis. Annual Review of Entomology, 36, 511-532.

Strand, M. R., & Pech, L. L. (1995). Immunological defense mechanisms in insects. Annual Review of Entomology, 40(1), 353–375.Strand, M. R. (2008). The insect cellular immune response. Insect Science, 15(1), 1–14.

Senior, N. J., & Titball, R. W. (2020). Isolation and primary culture of Galleria mellonella hemocytes for infection studies. F1000Research, 9(1392), 1-10.

Wang, Y., & Zhang, Y. (2020). Dynamics of hemocyte proliferation and differentiation in lepidopteran insects. Journal of Insect Physiology, 121, 103-110.

CHAPTER 13

On Planes and Angles of Double Rotations By Quaternions

Melek Erdoğdu[1]

1 Assoc. Prof., Department of Mathematics and Computer Sciences, Necmettin Erbakan University, Orcid: 0000-0001-9610-6229

In the realm of physical sciences and mechanics, one of the most crucial types of transformations are those that preserve distances transformations that leave the structure of space unchanged. These are known as rigid motions, and they serve as the foundation for describing the motion of rigid bodies. The identity transformation, which leaves everything unchanged, is a prime example of a rigid motion. Even more fascinating, the composition of rigid motions results in another rigid motion.

In the case of Euclidean space, this group of rigid motions is called the Euclidean group. Every rigid motion within this group is essentially a combination of two key components: a linear transformation and a translation. The focus of our discussion lies in the linear transformation part, which is of particular interest. This component is an orthogonal transformation, and it plays a critical role in understanding the behavior of rigid bodies in motion.

Consider an $n \times n$ matrix R with real entries that satisfies the condition:

$$R^T R = R R^T = I$$

where I is the identity matrix of order n. This condition tells us that R is an orthogonal matrix in E^n, meaning that the transpose of R is also its inverse. As a result, orthogonal matrices preserve lengths, which is a key property for rigid motions, as they do not distort the space they act upon.

What makes orthogonal matrices particularly fascinating is that they form a group under matrix multiplication and taking inverses. This group is called the orthogonal group, denoted $O(n)$. The elements of this group represent all possible rigid motions that preserve the geometry of space.

But the story doesn't end there. The orthogonal group $O(n)$ is not just an abstract group it's a smooth manifold of dimension $\frac{n(n-1)}{2}$ within the space of all $n \times n$ real matrices, denoted $GL(n, \mathbb{R})$. Even more intriguing, The orthogonal group $O(n)$ is not just a group, but a compact Lie group a structure rich in geometric and algebraic properties, with deep connections to the study of symmetries and rigid motions in Euclidean space [6,20].

The orthogonal group $O(n)$ is split into two distinct components, driven by the determinant of the matrices it contains. Since the determinant of any orthogonal matrix is either $+1$ or -1, we can categorize these matrices into two groups. The first component, consisting of orthogonal matrices with determinant $+1$ (and including the identity matrix), forms a subgroup of $O(n)$. This subgroup is known as the special orthogonal group, denoted $SO(n)$. Matrices in $SO(n)$

represent rotations, and they capture the essence of rigid motions that preserve orientation in space. The second component, which consists of orthogonal matrices with determinant -1, corresponds to the set of reflections, representing transformations that reverse orientation.

The primary focus of this paper is on the first type of orthogonal transformations rotations. To explore this intriguing aspect, we will utilize the powerful mathematical tool of quaternions, which offer a compact and elegant way to describe and manipulate rotations in space.

There are various techniques for constructing rotations, each with its own unique strengths and applications. Some of the most notable methods include Clifford algebras, the Rodrigues' rotation formula, Cayley formula, Householder transformations, and quaternions. Each of these approaches is particularly suited to different types of spaces. For instance, while some methods are applicable to spaces of any dimension, others are specialized for specific cases, such as three- and four-dimensional spaces. However, two of the most fascinating and elegant ways to explore rotations are through Clifford algebras and quaternions. These mathematical tools not only provide deep insights into rotational symmetries but also offer compact, efficient representations that are particularly powerful in higher-dimensional spaces [2, 7, 9, 12, 24].

Isoclinic rotation is a particular case of a double rotation in which there are infinitely many invariant orthogonal planes with same rotation angle $\theta_1 = \pm\theta_2$. If the rotation angle of both planes are the same i.e. $\theta_1 = \theta_2$, then the rotation is called left isoclinic, if the rotation angle of both plane have opposite sign i.e. $\theta_1 = -\theta_2$,then the rotation is called right isoclinic. The $4D$ rotations can be decomposed into one left and one right isoclinic rotations which is called Cayley's factorizations of $4D$ rotations. The $4D$ rotations are represented by $Cl_{4,0,0}$ with the use of Cayley's factorizations in [8].

In [15], rotations around non-null axes in Minkowski 3-space are explored using unit timelike split quaternions. It is further shown that the type of a Lorentzian rotation whether Euclidean or hyperbolic can be determined by examining the scalar part of the split quaternion, as discussed in [16].

For rotations involving null rotation axes, the study employs Rodrigues' formula and Cayley's formula, utilizing a pseudo-orthonormal frame. Additionally, it is demonstrated in [14] that any unit timelike split quaternion with a null vector part corresponds to a rotation around a null axis. Finally, in [21], rotations within a given null-cone are derived using a combination of Rodrigues'

formula, Cayley's formula, and hyperbolic quaternions, offering a rich framework for understanding these unique transformations.

Rotations for a given hyperboloid are thoroughly examined in [22], providing insights into their unique geometric properties. In [18], elliptical rotations are explored through various methods, including Rodrigues' rotation formula, Cayley's formula, the union of an even number of Householder transformations, and the use of elliptic quaternions. Meanwhile, rotations in Minkowski spacetime are extensively discussed in [14] and [17], with both Cayley and Rodrigues formulas playing a central role in the analysis. Further developments based on these results are presented in [10] and expanded upon in [11], offering additional perspectives on the topic.

On a different note, Lorentzian rotations are also studied using Lorentzian matrix multiplications in [19] and [13], providing another approach to understanding these transformations. Additionally, the homothetic Cayley formula and its corresponding transformation are introduced, with Rodrigues and Euler parameters for homothetic motion derived in [23], offering a new framework for understanding motions in this context.

Quaternions and Rotations in Euclidean 3 Space

In 1843, the Irish mathematician Sir William Rowan Hamilton introduced the concept of quaternions, extending the idea of complex numbers into higher dimensions. A quaternion can be expressed as:

$$H = \{q = q_0 + q_1 i + q_2 j + q_3 k : q_0, q_1, q_2, q_3 \in \mathbb{R}\}.$$

where i, j, and k are the fundamental quaternionic units. These units satisfy the following relations:

$$i^2 = j^2 = k^2 = -1, ij = -ji = k, jk = -kj = i, ki = -ik = j.$$

One of the most remarkable properties of quaternions is that their multiplication is noncommutative that is, the order of multiplication matters, a feature that distinguishes quaternions from familiar real and complex numbers. This noncommutativity gives quaternions a rich algebraic structure, making them incredibly useful in fields such as 3D rotations, computer graphics, and theoretical physics [25, 26].

For any $q = q_0 + q_1 i + q_2 j + q_3 k \in H$, $S_q = q_0$ is the scalar part of q and $V_q = (q_1, q_2, q_3)$ is vector part of q. And norm of the quaternion q is defined by

$$N_q = \sqrt{q_0^2 + q_1^2 + q_2^2 + q_3^2}.$$

Every quaternion can be written in the form:

$$q = N_q(\cos\theta + u\sin\theta),$$

where

$$\cos\theta = \frac{q_0}{N_q}, \sin\theta = \frac{\sqrt{q_1^2 + q_2^2 + q_3^2}}{N_q},$$
$$u = u_1 i + u_2 j + u_3 k = \frac{q_1 i + q_2 j + q_3 k}{\sqrt{q_1^2 + q_2^2 + q_3^2}} \text{ and } \langle u, u \rangle = 1.$$

The set of unit quaternions is denoted by

$$H_1 = \{q = q_0 + q_1 i + q_2 j + q_3 k : q_0^2 + q_1^2 + q_2^2 + q_3^2 = 1\}. \quad (1)$$

A quaternion can encode a rotation using just four numbers, with the only requirement being that the quaternion must have a unit norm meaning its magnitude must equal 1. This simplicity and elegance make quaternions an incredibly powerful tool for describing rotations, as they provide a compact and efficient way to manipulate and calculate rotations in three-dimensional space. Every unit quaternion

$$q = \cos\theta + u\sin\theta = \cos\theta + (u_1 i + u_2 j + u_3 k)\sin\theta \quad (2)$$

represents a rotation about the rotation axis u by angle 2θ by the linear transformation

$$R_q : E^3 \to E^3$$

which is defined as

$$R_q(x) = qxq^{-1} = qx\bar{q}. \quad (3)$$

Here $x = x_1 i + x_2 j + x_3 k \in E^3$ is a pure quaternion. By a unit quaternion q, the following rotation matrix $R = [R_{ij}]$ is obtained:

$$\begin{bmatrix} q_0^2 + q_1^2 - q_2^2 - q_3^2 & -2q_0q_3 + 2q_1q_2 & 2q_0q_2 + 2q_1q_3 \\ 2q_1q_2 + 2q_0q_3 & q_0^2 - q_1^2 + q_2^2 - q_3^2 & 2q_2q_3 - 2q_1q_0 \\ -2q_0q_2 + 2q_1q_3 & 2q_2q_3 + 2q_1q_0 & q_0^2 - q_1^2 - q_2^2 + q_3^2 \end{bmatrix} \quad (4)$$

[1,3]. Conversely, the unit quaternion q corresponding to a given rotation matrix in E^3 can be given by the following formulas:

$$q_0^2 = \frac{1}{4}(1 + R_{11} + R_{22} + R_{33}) \quad (5)$$

$$q_1 = \frac{1}{4q_0}(R_{32} - R_{23}) \quad (6)$$

$$q_2 = \frac{1}{4q_0}(R_{13} - R_{31}) \quad (7)$$

$$q_3 = \frac{1}{4q_0}(R_{21} - R_{12}) \quad (8)$$

when $q_0 \neq 0$. If $q_0 = 0$, then the unit quaternion q can be given by the equations:

$$q_2 = \frac{1}{2q_1}R_{12}, q_3 = \frac{1}{2q_1}R_{13} \text{ and } q_1^2 = 1 - q_2^2 - q_3^2. \quad (9)$$

The function $f: S_3 \cong H_1 \to SO(3)$, which sends q to matrix R, is a homomorphism of groups [15,24].

Eigenvalue and Eigenvectors of Rotations in E^4 by Quaternions

In four-dimensional space E^4, instead of a simple axis of rotation, we encounter the concept of a plane of rotation—an abstract yet powerful tool used to describe rotations. A plane of rotation for a given transformation is the plane that remains invariant under the rotation; that is, the rotation maps all vectors within this plane to other vectors in the same plane. While the plane itself is not fixed in position, every vector within it is transformed in a way that preserves the plane's structure.

These rotations in E^4 are closely tied to the eigenvalues and eigenvectors of the rotation matrix, providing a deeper insight into the transformation. Since rotations in four-dimensional space can have at most two planes of rotation, we

can classify these rotations based on the specific planes involved. This classification allows for a more refined understanding of the complex rotational symmetries in higher-dimensional spaces.

Double Rotations

A rotation involving two planes of rotation is known as a double rotation. In this type of rotation, the transformation occurs simultaneously within both planes, which are orthogonal to each other. Each plane has its own distinct angle of rotation—denoted θ for the first plane and φ for the second. These two angles fully specify the rotation, provided that neither angle is zero (in which case, the rotation reduces to a simpler form).

Points in the first plane rotate by the angle θ, while points in the second plane rotate by the angle φ. Points that lie outside of these planes experience a rotation that is a blend of θ and φ, depending on their position relative to the two planes.

For any general double rotation, the two planes and their respective rotation angles are unique, offering a distinct and fascinating way to characterize rotations in higher-dimensional spaces.

Every unit quaternions

$$q = q_0 + q_1 i + q_2 j + q_3 k = e^{\theta u} = \cos\theta + \sin\theta u$$

and

$$p = p_0 + p_1 i + p_2 j + p_3 k = e^{\varphi v} = \cos\varphi + \sin\varphi v$$

represent a double rotation by the linear transformation

$$R_{p,q}^{double}(x) = pxq. \tag{10}$$

The matrix representation of this linear transformation can be found as follows:

$$R_{p,q}^{double} = [r_{ij}] \tag{11}$$

where

$$r_{11} = p_0 q_0 - p_1 q_1 - p_2 q_2 - p_3 q_3,$$

$$r_{21} = p_0 q_1 + p_1 q_0 + p_2 q_3 - p_3 q_2,$$

$$r_{31} = p_0 q_2 - p_1 q_3 + p_2 q_0 + p_3 q_1,$$

$$r_{41} = p_0q_3 + p_1q_2 - p_2q_1 + p_3q_0,$$

$$r_{12} = -p_0q_1 - p_1q_0 + p_2q_3 - p_3q_2,$$

$$r_{22} = p_0q_0 - p_1q_1 + p_2q_2 - p_3q_3,$$

$$r_{32} = -p_0q_3 - p_1q_2 - p_2q_1 + p_3q_0,$$

$$r_{42} = p_0q_2 - p_1q_3 - p_2q_0 - p_3q_1,$$

$$r_{13} = -p_0q_2 - p_1q_3 - p_2q_0 + p_3q_1,$$

$$r_{23} = p_0q_3 - p_1q_2 - p_2q_1 - p_3q_0,$$

$$r_{33} = p_0q_0 + p_1q_1 - p_2q_2 + p_3q_3,$$

$$r_{43} = -p_0q_1 + p_1q_0 - p_2q_3 - p_3q_2,$$

$$r_{14} = -p_0q_3 + p_1q_2 - p_2q_1 - p_3q_0,$$

$$r_{24} = -p_0q_2 - p_1q_3 + p_2q_0 - p_3q_1,$$

$$r_{34} = p_0q_1 - p_1q_0 - p_2q_3 - p_3q_2,$$

$$r_{44} = p_0q_0 + p_1q_1 + p_2q_2 - p_3q_3.$$

Theorem 1. Let $p = (p_0, p_1, p_2, p_4)$ and $q = (q_0, q_1, q_2, q_3)$ be two unit quaternions, then eigenvalues of the double rotation matrix $R_{p,q}^{doub}$ which is generated by p and q are

$$\lambda_1 = p_0q_0 + \sqrt{(1-p_0^2)(1-q_0^2)} + \left(q_0\sqrt{1-p_0^2} - p_0\sqrt{1-q_0^2}\right)i,$$

$$\lambda_2 = p_0q_0 + \sqrt{(1-p_0^2)(1-q_0^2)} - \left(q_0\sqrt{1-p_0^2} - p_0\sqrt{1-q_0^2}\right)i,$$

$$\lambda_3 = p_0q_0 + \sqrt{(1-p_0^2)(1-q_0^2)} + \left(q_0\sqrt{1-p_0^2} + p_0\sqrt{1-q_0^2}\right)i,$$

$$\lambda_4 = p_0q_0 + \sqrt{(1-p_0^2)(1-q_0^2)} - \left(q_0\sqrt{1-p_0^2} + p_0\sqrt{1-q_0^2}\right)i.$$

That is, eigenvalues depend only the first components of the unit quaternions p and q.

Proof. Let $R_{p,q}^{doub}$ be the double rotation matrix generated by unit quaternions $p = (p_0, p_1, p_2, p_4)$ and $q = (q_0, q_1, q_2, q_3)$. By considering the matrix $R_{p,q}^{doub}$ given in Equation 11, we find the eigenvalues of $R_{p,q}^{doub}$ as follows:

$$\lambda_1 = p_0q_0 + \sqrt{(p_1^2 + p_2^2 + p_3^2)(q_1^2 + q_2^2 + q_3^2)} + \sqrt{\begin{matrix}2p_0q_0\sqrt{(p_1^2 + p_2^2 + p_3^2)(q_1^2 + q_2^2 + q_3^2)} \\ -p_1^2q_0^2 - p_0^2q_2^2 - p_2^2q_0^2 - p_3^2q_0^2 - p_0^2q_1^2\end{matrix}},$$

$$\lambda_2 = p_0q_0 + \sqrt{(p_1^2 + p_2^2 + p_3^2)(q_1^2 + q_2^2 + q_3^2)} - \sqrt{\begin{matrix}2p_0q_0\sqrt{(p_1^2 + p_2^2 + p_3^2)(q_1^2 + q_2^2 + q_3^2)} \\ -p_1^2q_0^2 - p_0^2q_2^2 - p_2^2q_0^2 - p_3^2q_0^2 - p_0^2q_1^2\end{matrix}},$$

$$\lambda_3 = p_0q_0 - \sqrt{(p_1^2 + p_2^2 + p_3^2)(q_1^2 + q_2^2 + q_3^2)} + \sqrt{\begin{matrix}-2p_0q_0\sqrt{(p_1^2 + p_2^2 + p_3^2)(q_1^2 + q_2^2 + q_3^2)} \\ -p_1^2q_0^2 - p_0^2q_2^2 - p_2^2q_0^2 - p_3^2q_0^2 - p_0^2q_1^2\end{matrix}},$$

$$\lambda_4 = p_0q_0 - \sqrt{(p_1^2 + p_2^2 + p_3^2)(q_1^2 + q_2^2 + q_3^2)} - \sqrt{\begin{matrix}-2p_0q_0\sqrt{(p_1^2 + p_2^2 + p_3^2)(q_1^2 + q_2^2 + q_3^2)} \\ -p_1^2q_0^2 - p_0^2q_2^2 - p_2^2q_0^2 - p_3^2q_0^2 - p_0^2q_1^2\end{matrix}}.$$

Since p and q are unit quaternions, we have $p_0^2 + p_1^2 + p_2^2 + p_3^2 = 1$ and $q_0^2 + q_1^2 + q_2^2 + q_3^2 = 1$. Using these equalities, we obtain the eigenvalues as:

$$\lambda_1 = p_0q_0 + \sqrt{(1 - p_0^2)(1 - q_0^2)} + \left(q_0\sqrt{1 - p_0^2} - p_0\sqrt{1 - q_0^2}\right)i,$$

$$\lambda_2 = p_0q_0 + \sqrt{(1 - p_0^2)(1 - q_0^2)} - \left(q_0\sqrt{1 - p_0^2} - p_0\sqrt{1 - q_0^2}\right)i,$$

$$\lambda_3 = p_0q_0 + \sqrt{(1 - p_0^2)(1 - q_0^2)} + \left(q_0\sqrt{1 - p_0^2} + p_0\sqrt{1 - q_0^2}\right)i,$$

$$\lambda_4 = p_0 q_0 + \sqrt{(1-p_0^2)(1-q_0^2)} - \left(q_0\sqrt{1-p_0^2} + p_0\sqrt{1-q_0^2}\right) i.$$

Theorem 2. Every unit quaternions

$$q = \cos\theta + \sin\theta u \text{ and } p = \cos\varphi + \sin\varphi v$$

represent a double rotation $R_{p,q}^{doub}$ with the angle $\varphi - \theta$ and $\varphi + \theta$.

Proof. Let

$$q = q_0 + q_1 i + q_2 j + q_3 k$$

and

$$p = p_0 + p_1 i + p_2 j + p_3 k$$

be unit quaternions. The eigenvalues of a double rotation $R_{p,q}^{doub}$ are obtained by previous theorem. Since $q_0 = \cos\theta$ and $p_0 = \cos\varphi$, we can rewrite the eigenvalues as follows:

$$\lambda_1 = \cos\varphi\cos\theta + \sin\varphi\sin\theta + (\cos\theta\sin\varphi - \cos\varphi\sin\theta)i,$$

$$\lambda_2 = \cos\varphi\cos\theta + \sin\varphi\sin\theta - (\cos\theta\sin\varphi - \cos\varphi\sin\theta)i,$$

$$\lambda_3 = \cos\varphi\cos\theta - \sin\varphi\sin\theta + (\cos\theta\sin\varphi + \cos\varphi\sin\theta)i,$$

$$\lambda_4 = \cos\varphi\cos\theta - \sin\varphi\sin\theta - (\cos\theta\sin\varphi + \cos\varphi\sin\theta)i.$$

By using trigonometric identities, we obtain

$$\lambda_1 = \cos(\varphi - \theta) + \sin(\varphi - \theta)\, i,$$

$$\lambda_2 = \cos(\varphi - \theta) - \sin(\varphi - \theta)\, i,$$

$$\lambda_3 = \cos(\varphi + \theta) + \sin(\varphi + \theta)\, i,$$

$$\lambda_4 = \cos(\varphi + \theta) - \sin(\varphi + \theta)\, i.$$

Thus, the rotation angles of $R_{p,q}^{doub}$ are $\varphi - \theta$ and $\varphi + \theta$.

Theorem 3. Let $R_{p,q}^{doub}$ be the double rotation which is obtained by unit quaternions $q = \cos\theta + \sin\theta u$ and $p = \cos\varphi + \sin\varphi v$.

i) If $v = u$, then $R_{p,q}^{doub}$ represents a double rotation on the plane $span\{e_1, e_2\}$ with the angle $\varphi + \theta$ and on the plane $(span\{e_1, e_2\})^{\perp}$ with angle $\varphi - \theta$.

ii) If $v = -u$, then $R_{p,q}^{doub}$ represents a double rotation on the plane $span\{e_1, e_2\}$ with the angle $\varphi - \theta$ and on the plane $(span\{e_1, e_2\})^{\perp}$ with angle $\varphi + \theta$.

iii) If $v \neq \pm u$, then $R_{p,q}^{doub}$ represents a double rotation with rotation plane $span\{e_3, e_4\}$ by angle $\varphi - \theta$ and on the plane $span\{e_5, e_6\}$ by angle $\varphi + \theta$.

Here

$$e_1 = (1,0,0,0)$$

$$e_2 = (0, u_1, u_2, u_3)$$

$$e_3 = (0, v_1 - u_1, v_2 - u_2, v_3 - u_3)$$

$$e_4 = (u_1v_1 + u_2v_2 + u_3v_3 - 1, u_2v_3 - u_3v_2, u_1v_3 - u_3v_1, u_1v_2 - u_2v_1)$$

$$e_5 = (0, v_1 + u_1, v_2 + u_2, v_3 + u_3)$$

$$e_6 = (u_1v_1 + u_2v_2 + u_3v_3 + 1, u_2v_3 - u_3v_2, u_1v_3 - u_3v_1, u_1v_2 - u_2v_1).$$

Proof. Let $R_{p,q}^{doub}$ be the double rotation which is obtained by unit quaternions

$$q = q_0 + q_1 i + q_2 j + q_3 k = \cos\theta + \sin\theta u$$

and

$$p = p_0 + p_1 i + p_2 j + p_3 k = \cos\varphi + \sin\varphi v.$$

i) Suppose that $u = v$. Then we have

$$q_1 = u_1 \sin\theta\,, q_2 = u_2 \sin\theta\,, q_3 = u_3 \sin\theta,$$

$$p_1 = u_1 sin\varphi, p_2 = u_2 sin\varphi, q_3 = u_3 sin\varphi.$$

By using trigonometric identities and the relation

$$u_1^2 + u_2^2 + u_3^2 = 1,$$

we obtain

$$R_{p,q}^{doub}(e_1) = (\cos\alpha)e_1 + (\sin\alpha)e_2,$$

$$R_{p,q}^{doub}(e_2) = (-\sin\alpha)e_1 + (\cos\alpha)e_2$$

where $\varphi + \theta = \alpha$. This means $R_{p,q}^{doub}$ represents a double rotation on the plane $span\{e_1, e_2\}$ with angle $\varphi + \theta = \alpha$. So that, the other rotation occurs on the plane $(span\{e_1, e_2\})^{\perp}$ with angle $\varphi - \theta = \beta$.

ii) Suppose that $v = -u$. Then we have

$$q_1 = u_1 \sin\theta\,, q_2 = u_2 \sin\theta\,, q_3 = u_3 \sin\theta,$$

$$p_1 = -u_1 sin\varphi, p_2 = -u_2 sin\varphi, q_3 = -u_3 sin\varphi.$$

By using trigonometric identities and the relation

$$u_1^2 + u_2^2 + u_3^2 = 1,$$

we obtain

$$R_{p,q}^{doub}(e_1) = (\cos\beta)e_1 - (\sin\beta)e_2,$$

$$R_{p,q}^{doub}(e_2) = (\sin\beta)e_1 + (\cos\beta)e_2$$

Where $\varphi - \theta = \beta$. Thus, $R_{p,q}^{doub}$ represents a double rotation on the plane $span\{e_1, e_2\}$ with angle $\varphi - \theta = \beta$. So that, the other rotation occurs on the plane $(span\{e_1, e_2\})^{\perp}$ with angle $\varphi + \theta = \alpha$.

iii) Suppose that $v \neq \pm u$. Then we have

$$q_1 = u_1 \sin\theta\,, q_2 = u_2 \sin\theta\,, q_3 = u_3 \sin\theta,$$

$$p_1 = v_1 sin\varphi, p_2 = v_2 sin\varphi, q_3 = v_3 sin\varphi.$$

By using trigonometric identities and the relations

$$u_1^2 + u_2^2 + u_3^2 = 1$$

and

$$v_1^2 + v_2^2 + v_3^2 = 1,$$

we obtain

$$R_{p,q}^{doub}(e_3) = cos(\varphi - \theta)e_3 + sin(\varphi - \theta)\, e_4,$$

$$R_{p,q}^{doub}(e_4) = -sin(\varphi - \theta)e_3 + \cos(\varphi - \theta)\, e_4.$$

This means $R_{p,q}^{doub}$ represents a double rotation on the plane $span\{e_3, e_4\}$ with angle $\varphi - \theta$. Similarly, we can see that

$$R_{p,q}^{doub}(e_5) = cos(\varphi + \theta)e_5 - sin(\varphi + \theta)\, e_6,$$

$$R_{p,q}^{doub}(e_6) = sin(\varphi + \theta)e_5 + \cos(\varphi + \theta)\, e_6.$$

So that, the other rotation occurs on the plane $span\{e_5, e_6\}$ with angle $\varphi + \theta$.

Corollary 4. Let $R_{p,q}^{doub}$ be the double rotation which is obtained by unit quaternions

$$q = cos\theta + sin\theta u \text{ and } p = cos\varphi + sin\varphi v.$$

If $\langle u, v\rangle = 0$, then $R_{p,q}^{doub}$ represents a double rotation on the plane $span\{e_3, e_4^*\}$ with the angle $\varphi - \theta$ and on the plane $span\{e_5, e_6^*\}$ with angle $\varphi + \theta$. Here

$$e_3 = (0, v_1 - u_1, v_2 - u_2, v_3 - u_3),$$

$$e_4{}^* = (-1, u_2v_3 - u_3v_2, u_1v_3 - u_3v_1, u_1v_2 - u_2v_1),$$

$$e_5 = (0, v_1 + u_1, v_2 + u_2, v_3 + u_3),$$

$$e_6{}^* = (1, u_2v_3 - u_3v_2, u_1v_3 - u_3v_1, u_1v_2 - u_2v_1).$$

Proof. Let $R_{p,q}^{doub}$ be the double rotation which is obtained by unit quaternions $q = q_0 + q_1i + q_2j + q_3k = \cos\theta + \sin\theta u$ and $p = p_0 + p_1i + p_2j + p_3k = \cos\varphi + \sin\varphi v$. Suppose that $\langle u, v\rangle = 0$. Thus, we have $u_1v_1 + u_2v_2 + u_3v_3 = 0$. By iii) of previous theorem, we get the result.

Conclusion

The main purpose of this paper to analyze how quaternions can be used to rotate objects with use of geometric meaning of eigenvalue problem for rotation matrices. For this purpose, the real matrix representations of the linear transformations $R_{p,q}^{doub}\ is$ introduced, which corresponds to double rotation in E^4. Then, the eigenvalues of these rotation matrices are obtained in terms of the scalar (real) part of the unit quaternions q and p for each cases. Furthermore, the eigenvectors of of these rotation matrices are also expressed according to the components of the unit quaternions q and p for all types of the rotation matrices. With the help of the obtained data, one can easily find the plane(s) of rotation for any given rotation matrix in E^4. Therewithal, we can also classify the rotation matrices in E^4: as simple, double and isoclinic by using their eigenvalues and eigenvectors.

References

[1] Altmann, S.L., Rotations, Quaternions and Double Groups. Republication of Oxford Edition, (1986).

[2] Aragon, G., Aragon, J.L., Rodriguez, M.A., Clifford Algebras and Geometric Algebra. Advances in Applied Clifford Algebras. **7,** 91-102 (1997).

[3] Dam, E.B., Koch, M., Lillholm, M., Quaternion, Interpolation and Animation. Technical Report DIKU-TR-98/5, Department of Computer Science University of Copenhagen, Denmark (1998).

[4] Erdoğdu, M., Özdemir, M., Cayley Formula in Minkowski Space-time. International Journal of Geometric Methods in Modern Physics. **12,** (2015).

[5] Erdoğdu, M., Özdemir, M., Simple, Double and Isoclinic Rotations with a Viable Algorithm. Mathematical Sciences and Applications E-Notes. **8(1)**, 11-24, (2020)

[6] Friedberg, A.J., Insel, L.E., Spence, L.E., Linear Algebra. Prentice Hall Pearson Education International, New Jersey (2003).

[7] Gonzalez, G.A., Aragon, J.L., Rodriguez-Andrade, M.A., Verde Star, L., Reflections, Rotations and Pythagorean Numbers. Advances in Applied Clifford Algebras. **19**, 1-14 (2009).

[8] Gracia, A.P., Thomas, F., On Cayley's Factorization of 4D Rotations and Applications. Advances in Applied Clifford Algebras. 27, 523-538 (2017).

[9] Gürlebeck, K., Sprössig, W., Quaternionic and Clifford Calculus for Physicists and Engineers, Series: Mathematical Methods in Practice 1. Wiley (1997).

[10] Jadczyk, A., Szulga, J., A Comment on "On the Rotation Matrix in Minkowski Space-time" by Özdemir and Erdoğdu. Reports on Mathematical Physics. **74**, 39-44 (2014).

[11] Jadczyk, A., Szulga, J., Lorentzian Transformations from Elementary Point of View. The Electronic Journal of Linear Algebra. **31**, 794-813 (2016).

[12] Kantor, I.L., Solodovnikov, A.S., Hypercomplex Numbers, An Elementary Introduction to Algebras. Springer-Verlag, New York (1989).

[13] Keçelioğlu, O., Özkaldı, S., Gündoğan, H., Rotations and Screw Motion with Timelike Vector in 3-Dimensional Lorentzian Space. Advances in Applied Clifford Algebras. **22**, 1081-1091 (2012).

[14] Nesovic, E., On Rotation About Lightlike Axis in Three Dimensional Minkowski Space. Advances in Applied Clifford Algebras. **26,** 237-251 (2016).

[15] Özdemir, M., Ergin, A.A., Rotations with unit timelike quaternions in Minkowski 3-space. Journal of Geometry and Physics. **56,** 322-336 (2006).

[16] Özdemir, M., Erdoğdu, M., Şimşek, H., On the Eigenvalues and Eigenvectors of a Lorentzian Rotation Matrix by Using Split Quaternions. Advances in Applied Clifford Algebras. **24,** 179-192 (2014).

[17] Özdemir, M., Erdoğdu, M., On the Rotation Matrix in Minkowski Space-time. Reports on Mathematical Physics. **74**, 27-38 (2014).

[18] Özdemir, M., An Alternative Approach to Elliptical Motion. Advances in Applied Clifford Algebras. **26,** 279-304 (2016).

[19] Özkaldı, S., Gündoğan, H., Cayley Formula, Euler Parameters and Rotations in 3-Dimensional Lorentzian Space. Advances in Applied Clifford Algebras. **20**, 367-377 (2010).

[20] Roman, S., Advanced Linear Algebra, Graduate text in mathematics. Springer, USA (2008).

[21] Şimşek, H., Özdemir, M., Rotations on Lightcone in Minkowski 3-Space. Advances in Applied Clifford Algebras. **27**, 2841-2853 (2017).

[22] Şimşek, H., Özdemir, M., Generating Hyperbolical Rotation Matrix for a Given Hyperboloid. Linear Algebra and Its Applications. **496**, 221-245 (2016).

[23] Ünal, D., Güngör, M.A., Tosun, M., Homethetic Cayley Formula and Its Applications. Advances in Applied Clifford Algebras. **26**, 809-824 (2016).

[24] Weiner, J.L., Wilkens, G.R., Quaternions and Rotations in E^4. The Mathematical Association of America Monthly, **112** (2005).

[25] Wilkins, D.R., On Quaternions or On A New System of Imaginaries in Algebra by William Rowan Hamilton (Philosophical Magazine, 1844-1850).

[26] Zhang, F., Quaternions and Matrices of Quaternions. Linear Algebra and Its Applications. **251**, 21-57 (1997).

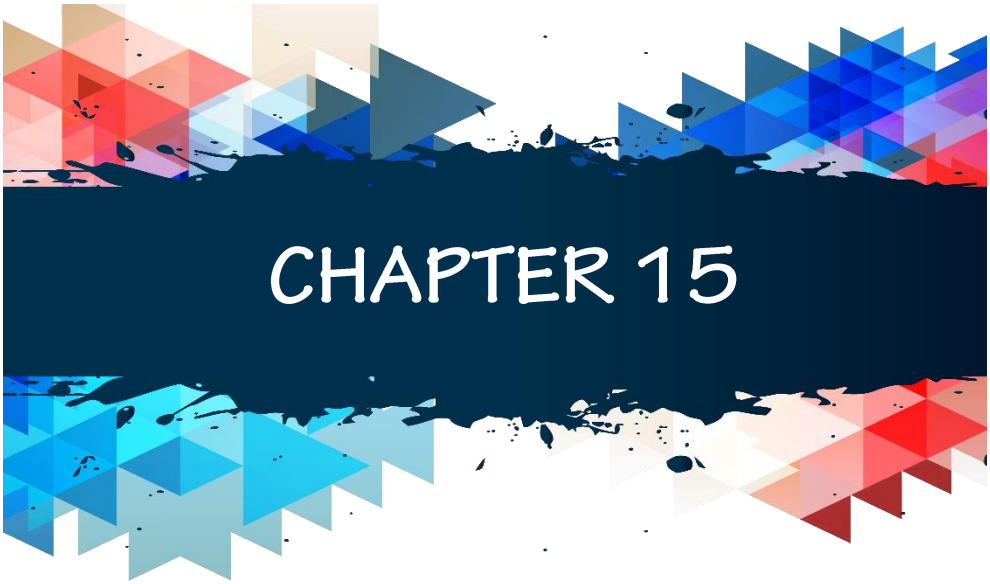

Parametric and Non-Parametric Survival Regression Modelling: An Analysis of Lung Cancer Data Set

***Özlem Gürünlü Alma*[1]**

1 Prof.Dr., Muğla Sıtkı Koçman University, Department of Statistics, Muğla, ORCID: 0000-0001-6978-9810

1. INTRODUCTION

The goal of survival analysis is to describe and predict survival, usually defined over the time domain (Klein and Moeschberger (2003), Cox and Oakes (1984), Kalbfleisch and Prentice (2002), and Hosmer and Lemeshow (1999)). There are three approaches to survival analysis, parametric, nonparametric, and semiparametric. Parametric methods require knowledge of the distribution of survival times. Survival analysis focuses on the distribution of survival times. Although there are well-known methods for estimating unconditional survival distributions, the most interesting survival modeling examines the relationship between survival and one or more predictors, often referred to as covariates in the survival analysis literature. While studies on adding covariate variables to the model were not very common until the 1970s, important steps were taken in survival analysis with the Cox regression model developed by Cox (1972). The Cox proportional hazards (CPH) model is well known for analyzing survival data due to its simplicity as it does not make any assumptions regarding the survival distribution. CPH helps in finding the hazard ratio based on the coefficients. These coefficients are easy to interpret and are clinically meaningful. In parametric survival models, the survival time is assumed to follow known distributions such as Weibull, exponential, log-normal, loglogistic, and generalized gamma distributions. Parametric models can be acceleration failure time (AFT) and CPH models. AFT models are useful for comparing survival times, while CPH can be applied for comparing hazards. Parametric models are better than CPH in terms of sample size and relative efficiencies (Kumar et all., 2020). In most medical studies designed to determine survival of cancer patients, Cox regression has been used because it is more flexible and does not require estimation of the underlying hazard function. Although the observed survival time distribution in Cox regression is not clear, the CPH assumption should be investigated. If the proportional hazards assumptions are not met, meaning that the linear component of the model changes with time, this is called disproportionate hazards. There are three options to overcome these shortcomings, namely, removing independent variables that do not meet the model's assumptions, using the stratified Cox model, or applying the extended Cox model **(**Wulandari, I., Kurnia, A., Sadik, K., 2021). Since violation of this assumption impairs the validity of the results of Cox regression, it would be better to use parametric models such as Exponential, Weibull, Log-Logistic, Log-Normal and Gamma instead of the Cox model. Compared to the Cox model, parametric models have both greater validity and higher accuracy in parameter

estimates and also do not require checking the proportional hazards assumption (Hosseini Teshnizi, and Taghi Ayatollahi, 2017).

Cancer is a class of diseases when a cell or group of cells display uncontrolled growth, invasion and sometimes spread to other locations in the body via lymph or blood (metastasis). American Cancer Society reports 9.7 million global 2024 cancer deaths. Lung cancer (both small cell and non-small cell) is the second most common cancer in both men and women in the United States. About 125,070 patients died from lung cancer (65,790 in men and 59,280 in women) in the USA. Lung cancer mainly occurs in older people. Most people diagnosed with lung cancer are 65 or older; a very small number of people diagnosed are younger than 45. The average age of people when diagnosed is about 70. Lung cancer is by far the leading cause of cancer death in the US, accounting for about 1 in 5 of all cancer deaths. Each year, more people die of lung cancer than of colon, breast, and prostate cancers combined (American Cancer Society, November 2024).

In general, the aim of this study was to compare the parametric methods and Cox's regression model to determine the independent factors in the survival of lung cancer patients' data.

2. METHODS

Survival analysis includes nonparametric (KM method), semiparametric (CPH model), and parametric methods. In this section, we will briefly explain these methods.

2.1. Nonparametric Model

In medical and health applications, nonparametric methods have significant advantages in terms of their flexibility to account for variations in the survival process of living organisms. The most widely used of nonparametric model is the product limit estimator, also known as the Kaplan-Meier estimator. This estimator, first proposed by Kaplan and Meier (1958), is the product over the failure times of the conditional probabilities of surviving to the next failure time. KM is the most frequent survival analysis method used in randomized (phase III and some phase II) medical clinical trials in which the following criteria are met:

- Patients are randomly assigned to different treatment arms,
- All patients do not enter the study at the same time,
- Patients drop out of or are lost from the study at different time intervals after entering the study; and
- The outcome variable of interest may or may not occur during the study observation period (Rich et al., 2010).

The minimal set of information to construct a KM survival curve includes the time to the event of interest for example, days, months, and years, and the binary variable indicating patients' status: presence/absence of the condition at that point in time. The time between the enrolment and the terminal event or end of observation is represented by a random variable T (T > 0) defined as survival time. By considering n patients and t_1, t_2,…, tj (j≤ n) the observed times to event, the survival time, at time i, is $T_i = t_j - t_i$. Basically, the KM method estimates the conditional probability of survival calculated at specific time points dictated by the occurrence of the event. The conditional probability or cumulative probability or cumulative survival is the probability $\widehat{S(t)}$ that a patient survives x days after entering a study conditional to the fact that the same patient survives the days before (D'Arrigo et all., 2021). For example, in a hypothetical setting in which a patient admitted to an intensive care unit survives for three days, the cumulative survival (calculated by the product rule of conditional probabilities) is the product of survival probabilities at day 1 (p_1), at day 2 (p_2), and at day 3 (p_3), that is:

$$\widehat{S(t)} = p_1 * p_2 * p_3. \quad (1)$$

Formally, it is given by, d_j, the number of subjects present the event of interest (for example, death) at time t_j and with n_j, the number of individuals at risk at time t_j. The individual probability $\widehat{q(t)}$ to die at t_j conditional to be alive at t_{j-1} is:

$$\widehat{q_j} = \frac{d_j}{n_j}. \quad (2)$$

Therefore, the probability of surviving at time t_j is as follows:

$$\widehat{p_j} = 1 - \frac{d_j}{n_j} = \frac{n_{j-d_j}}{n_j}. \quad (3)$$

By multiplying the estimates of the conditional probabilities of surviving, we obtain the estimate of the cumulative probability of living beyond the instant t_j is given as below (D'Arrigo et all., 2021)

$$\widehat{S(t)} = \prod_{j \le t} \widehat{p_j}. \quad (4)$$

2.2. Semiparametric Model

The KM model is used to analyze survival times. In addition to survival time data, information such as gender, age, heart rate, tumor size, tumor type, hemoglobin, smoking, physical activity, diet, etc. may also be analyzed. These factors that may play a role in a patient's survival time are specified as explanatory variables. It is also possible to model the network survival time in a patient using these explanatory variables. A multiple regression model is used to determine how much of the dependent variable is explained by the explanatory variables. Cox's proportional hazards model is similar to the multiple regression model, allowing the factors affecting the survival of certain patient groups to be determined and the differences between these factors to be tested. In this model, the response/dependent variable is hazard. Hazard is the probability of patients dying or experiencing the event in question if they had survived to a certain point in time, or the risk of death at that time. The proportional hazards (PH) model, originally proposed by Cox (1972) for the analysis of data from clinical trials.

In Cox's model no assumption is made about the probability distribution of the hazard. However, it is assumed that if the risk for dying at a particular point in time in one group is, say, twice that in the other group, then at any other time it will still be twice that in the other group. In other words, the hazard ratio does not depend on time (Bewick, Cheek, and Ball ,2004). The Cox regression model, defined as,

$$h(t|x) = h_0(t)\exp\left(\beta_1 x_1 + \beta_2 x_2 + \cdots + \beta_p x_p\right) = h_0(t)\exp(\boldsymbol{X'\beta}) \quad (5)$$

where $h_0(t)$ is baseline hazard function, i.e the hazard function for an individual in which all the variables in the model is zero, $X'=(x_1,...,x_p)$ is 1xp vector of explanatory variables and β is px1 vector of regression coefficients (Cox dan Oakes, 1984, Azimmatul I., 2015). What's interesting about this approach is the lack of clarity of the Cox baseline hazard form does not cause problems in the estimation, so keep a good estimate can be obtained from the regression coefficient β, and the hazard ratio (HR). Cox regression model is also called the Cox proportional hazard regression models (PH) due to the form of proportional HR (independent of time). Hazard Ratio of two individuals with different covariate values are as follows (Azimmatul I., 2015):

$$HR = \frac{h_0(t)\exp\left(x^{'}\beta\right)}{h_0(t)\exp\left(x^{*'}\beta\right)} = \exp\left(x^{'} - x^{*'}\right)\beta \tag{6}$$

2.3. Parametric Model

While semi-parametric model focuses on the influence of covariates on hazard, fully parametric model can also calculate the distribution form of survival time. The parametric model assumes that the distribution underlying survival time follows a certain distribution. Advantages of parametric model in survival analysis include: (I) the distribution of survival time can be estimated; (II) full maximum likelihood can be used to estimate parameters; (III) residuals can represent the difference between observed and estimated values of time; (IV) estimated parameters provide clinically meaningful estimates of effect (Zhang Z.,2016). The probability density function of time (t) is assumed to follow a distribution that can be expressed in terms of unknown parameters. When the probability density function for survival times is specified, the survival function (t) and the hazard function corresponding to the probability density function can be found. Parametric survival models tend to produce estimates that are consistent with the theoretical survival distribution (Kleinbaum and Klein, 2010). To choose the parametric model in survival analysis, several tests are needed. Particularly, two approaches can be done to measure the proximity of empirical and theoretical distribution, namely the graph approach and analysis approach. The popular first approach used is the probability plot (PP and QQ plot), and stabilized probability. The next approach that is most commonly used is Kolmogorov-Smirnov, Cramer-von Mises, and Anderson Darling. Whereas to choose the best model, Akaike's Information Criterion (AIC) and Bayesian Information Criterion (BIC) can be used **(**Wulandari, I., Kurnia, A., Sadik, K., 2021)**.** The commonly used parametric regression models are exponential, Weibull, log-normal, log-logistic, and generalized gamma regression models. If the survival times of individuals have an exponential distribution, it would be appropriate to use the exponential regression model, if they have a Weibull distribution, it would be appropriate to use the Weibull regression model, if they have a log-normal distribution, it would be appropriate to use the log-normal regression model, and if they are suitable for the log-logistic distribution, it would be appropriate to use the log-logistic regression model. In this study we will examine these distributions: exponential, Weibull, log-logistic, log-normal and generalized gamma distribution.

2.3.1. Exponential Model: The exponential regression model is the most basic and simplest parametric regression model used in the field of survival analysis **(Kleinbaum and Klein 2010).** The only parameter of the exponential distribution is the scale parameter λ. This parameter is defined as the constant hazard ratio. High λ values give high risk and short survival time, while low λ values give low risk and long survival time (Hosmer et al., 1999). In the exponential regression model, $t=(t_1,t_2,...,t_n)'$ survival times are assumed to be independent, homogeneous and each has an exponential distribution with the parameter λ. Its survival function is

$$S(t) = \exp(-\lambda t), \lambda > 0, t > 0.$$

The density function is

$$f(t) = \lambda \exp(-\lambda t)$$

and it is characterized by a constant hazard function

$$h(t) = \lambda.$$

One important characteristic of the exponential distribution is the lack of memory property

$$Pr(T \geq t + z \mid T \geq t) = Pr(T \geq z).$$

It follows that the mean residual life, that is the conditional expected life at time t, is constant

$$E(T - t \mid T > t) = E(T) = \frac{1}{\lambda}.$$

Since the exponential distribution has a constant hazard rate, it leads to a rather restrictive assumption in many applications. The exponential distribution is limited in its applicability because it has only one parameter, the scale parameter λ. In survival analysis, exponential regression is commonly used to model the time until an event occurs, such as failure or death. The exponential regression model assumes that the time-to-event follows an exponential distribution, which is often used when the event's occurrence rate (or hazard) is constant over time. This model is frequently applied when the assumption of constant hazard rate is reasonable. The exponential regression model can be described by the following equation:

$$h(t|X) = \lambda \exp(X^T \beta).$$

Where:

- h(t|X) is the hazard rate at time t, conditional on the covariates X. The hazard function h(t|X) describes the rate at which the event is expected to occur, given that the individual has survived up to time t. In the case of the exponential model, the hazard function is assumed to be constant, meaning that the rate of occurrence of the event does not change over time.
- λ is the baseline hazard, a constant that represents the hazard when all covariates are zero.
- X^T represents the vector of covariates, independent variables or predictors for a given individual or unit. The covariates X are explanatory variables that are hypothesized to affect the hazard rate. These might include factors like age, sex, treatment, and other demographic or clinical variables. The covariates are combined with their corresponding regression coefficients β, which describe the direction and strength of their effect on the hazard.
- β is the vector of regression coefficients for the covariates, which quantify the relationship between the covariates and the hazard rate. If $\beta_j > 0$, it means that as the covariate X_j increases, the hazard rate increases, implying a shorter survival time, higher likelihood of event occurring earlier. If $\beta_j < 0$, it means that as the covariate X_j increases, the hazard rate decreases, implying a longer survival time, lower likelihood of event occurring earlier.

The survival function S(t|X) gives the probability that the event has not occurred by time *t*, given the covariates *X*. It is related to the hazard function via the following relationship:

$$S(t|X) = \exp\left(-\int_0^t h(u|X)du\right).$$

For the exponential model, where the hazard is constant:

$$S(t|X) = \exp(-\lambda e^{X^T \beta} t).$$

This survival function describes how the probability of survival decreases over time as a function of the covariates.

Adding a shape parameter makes the distribution more flexible and can fit more types of data. A generalization of the exponential distribution to include the shape parameter is the Weibull distribution.

2.3.2. Weibull Model: The exponential distribution is limited in its applicability due to its memoryless property. The assumption that a lifetime has a constant failure rate is often too restrictive or inappropriate. For example, mechanical items often deteriorate over time, and therefore their lifetimes are more likely to follow a probability distribution with a strictly increasing hazard function. The Weibull distribution, named after Swedish mathematician Waloddi Weibull, is a generalization of the exponential distribution that is suitable for modeling lifetimes with constant, strictly increasing, or strictly decreasing hazard functions (Leemis, L., 2023). The **Weibull distribution** is widely used in survival analysis because it can model a variety of hazard functions. The **Weibull distribution** is a flexible model that can accommodate increasing, constant, or decreasing hazard rates, depending on the value of its shape parameter, γ also called the shape or slope parameter. The probability density function (PDF) for the Weibull distribution is:

$$f(t|\gamma,\lambda)=\frac{\gamma}{\lambda}\left(\frac{t}{\lambda}\right)^{\gamma-1}\exp\left(-\left(\frac{t}{\lambda}\right)^{\gamma}\right).$$

Where:

- t is the survival time variable.
- γ is shape parameter which controls the hazard function's shape:
    - If $\gamma=1$, the hazard is constant the model reduces to the exponential distribution.
    - If $\gamma>1$, the hazard increases over time, used to model situations where the failure rate increases as time progresses.
    - If $\gamma<1$, the hazard decreases over time, it used to model situations where the failure rate decreases over time.
- λ is scale parameter. It is a constant that scales the distribution, it determines the scale of the distribution and is related to the mean survival time.

The cumulative distribution function (CDF), which gives the probability that the event has occurred by time t, and the **survival function** $S(t|\gamma,\lambda)$, which is the probability that the event has not yet occurred by time t, it is the complement of the CDF. These are given as below:

$$F(t|\gamma,\lambda)=1-\exp\left(-\left(\frac{t}{\lambda}\right)^{\gamma}\right) \text{ and } S(t|\gamma,\lambda)=1-F(t|\gamma,\lambda)=\exp\left(-\left(\frac{t}{\lambda}\right)^{\gamma}\right).$$

The **hazard function** $h(t|\gamma,\lambda)$ of the Weibull distribution, which gives the instantaneous event rate at time t, is the ratio of the probability density function (PDF) to the survival function:

$$h(t|\gamma,\lambda)=\frac{f(t|\gamma,\lambda)}{S(t|\gamma,\lambda)}=\frac{\gamma}{\lambda}\left(\frac{t}{\lambda}\right)^{\gamma-1}.$$

This hazard function is **time-dependent**, and the shape of the hazard function depends on the value of γ. If $\gamma>1$, the hazard increases over time, while if $\gamma<1$, the hazard decreases over time. If $\gamma=1$, the hazard is constant (exponential distribution).

The Weibull regression model extends the Weibull distribution to include covariates or predictors that can affect the survival time. In survival analysis, the goal is to model the survival function $S(t|X)$ or the hazard function $h(t|X)$ while accounting for the effects of covariates X (e.g., age, treatment, gender) on the event rate. In a Weibull regression model, the survival time's t is modeled as a function of covariates X. The model assumes that the survival time t follows a Weibull distribution with parameters that depend on X, the vector of covariates. The hazard function of the Weibull regression model can be written as:

$$h(t|X)=\lambda e^{X^{T}\beta}\left(\frac{t}{\lambda}\right)^{\gamma-1}.$$

Where:

- λ is the scale parameter of the Weibull distribution, which is typically modeled as a baseline hazard.

- γ is the shape parameter, controlling the hazard's behavior over time.
- X is the vector of covariates.
- β is the vector of regression coefficients associated with the covariates.

This model assumes that both the scale parameter λ and the shape parameter γ are influenced by covariates. Scale parameter λ is typically modeled as an exponential function of covariates:

$$\lambda = \exp(X^T \beta_\lambda)$$

Where β_λ are the coefficients associated with the covariates that affect the scale parameter.

Shape parameter γ can be modeled as a constant, or it can depend on covariates as well:

$$\gamma = 1 + \exp(X^T \beta_\gamma).$$

Here β_γ are the coefficients for the covariates affecting the shape parameter.

The **survival function** $S(t|X)$ in the Weibull regression model is given by:

$$S(t|X) = \exp\left(-\left(\frac{t}{\lambda}\right)^\gamma\right) \exp(X^T \beta).$$

This equation represents the probability that the event has not occurred by time t, given the covariates X.

To estimate the parameters of the Weibull regression model, we typically use the **maximum likelihood estimation (MLE)** approach. The log-likelihood function for the Weibull regression model is based on the probability density function (PDF) and is expressed as:

$$\log L(\gamma, \beta, \lambda) = \sum_{i=1}^{n} \left[\delta_i \log h(t_i|X_i) - h(t_i|X_i)\right].$$

Where:

- δ_i is the censoring indicator (1 if the event occurred, 0 if censored).
- t_i is the observed survival time for the i-th individual.
- X_i is the vector of covariates for the i-th individual.
- $h(t_i | X_i)$ is the hazard function at time t_i for the i-th individual, given the covariates X_i.

The regression coefficients β are associated with the covariates in the model. A positive coefficient indicates that as the covariate increases, the hazard increases and shorter survival time. A negative coefficient indicates that as the covariate increases, the hazard decreases and longer survival time. The coefficients for the covariates are typically interpreted in terms of hazard ratios exp(βj), which represents the relative change in the hazard for a one-unit increase in the covariate X_j. In this model, the shape parameter γ:

- If γ>1, the hazard increases over time, implying that the event becomes more likely as time progresses.
- If γ=1, the hazard is constant over time, and the model reduces to an exponential distribution.
- If γ<1, the hazard decreases over time, indicating that the event becomes less likely as time passes.

2.3.3. Log-Logistic Model: The most commonly used distribution for modeling survival and failure time data is the Weibull. However, its use is limited by the fact that the hazard function must be monotonic, regardless of the parameter values, although it may increase or decrease. This may not be appropriate in cases where the course of the disease is such that mortality peaks after a certain period of time and then slowly declines (Bennett S., 1983). The log-logistic distribution is used in survival analysis to model the survival times of individuals. The probability density function of the log-logistic distribution is:

$$f(t)=\frac{\beta t^{\beta-1}}{\theta^{\beta}\left(1+\left(\frac{t}{\theta}\right)^{\beta}\right)^{2}},$$

here, t is the survival time, β is the shape parameter of the distribution, and θ is the scale parameter. The **cumulative distribution function (CDF)** and **hazard function** of the log-logistic distribution are:

$$F(t) = \frac{1}{1 + \left(\frac{t}{\theta}\right)^{-\beta}} \quad \textbf{and} \quad h(t) = \frac{f(t)}{1 - F(t)} = \frac{\beta \left(\frac{t}{\theta}\right)^{\beta - 1}}{\theta \left(1 + \left(\frac{t}{\theta}\right)^{\beta}\right)}.$$

When incorporating covariates into the log-logistic model, we typically use a **log-linear model** for the scale parameter θ. The covariates are used to model the relationship between the predictor variables (e.g., age, gender, treatment) and the survival time. The log-logistic regression model can be specified as:

$$\log(\theta) = \beta_0 + \beta_1 x_1 + \beta_2 x_2 + \ldots + \beta_k x_k$$

Where:

- θ is the scale parameter of the log-logistic distribution, which depends on the covariates,
- $\beta_0, \beta_1, \ldots, \beta_k$ are the regression coefficients, and
- $x_1, x_2, \ldots, x_k$ are the covariates.

$\theta(x_1, x_2, \ldots, x_k)$ is the scale parameter, which depends on the covariates $(x_1, x_2, \ldots, x_k)$. The **scale parameter** θ becomes:

$$\theta = \exp(\beta_0 + \beta_1 x_1 + \ldots + \beta_k x_k).$$

Substituting this expression for θ into the hazard function, we get the **log-logistic hazard function with covariates.**

$$h(t)=\frac{\beta\left(\frac{t}{\theta(x_1,x_2,..,x_k)}\right)^{\beta-1}}{\theta(x_1,x_2,..,x_k)\left[1+\left(\frac{t}{\theta(x_1,x_2,..,x_k)}\right)^{\beta}\right]}$$

$$=\frac{\beta\left(\frac{t}{\exp(\beta_0+\beta_1x_1+...+\beta_kx_k)}\right)^{\beta-1}}{\exp(\beta_0+\beta_1x_1+...+\beta_kx_k)\left[1+\left(\frac{t}{\exp(\beta_0+\beta_1x_1+...+\beta_kx_k)}\right)^{\beta}\right]}$$

For survival analysis, we use the **log-logistic regression** to model the **log of survival times** (logarithmic transformation of t) to estimate the effect of covariates on the survival distribution. The model is typically fitted using maximum likelihood estimation. In this model, the beta coefficients represent the influence of each covariate on the log of the survival time. A positive coefficient implies that the covariate increases the survival time (or decreases the hazard), while a negative coefficient implies that the covariate decreases the survival time (or increases the hazard). The scale parameter (θ) controls the spread of the survival distribution. Larger values theta generally correspond to longer survival times, while smaller values indicate shorter survival times.

The log-logistic model is especially useful when the hazard function is non-monotonic, meaning it initially increases and later decreases, which is more realistic for certain types of survival data, like recovery rates after treatment or aging processes in biological organisms. Unlike the Cox proportional hazards model, the log-logistic model does not assume proportional hazards (i.e., the effect of covariates on the hazard function is not constant over time). This makes the log-logistic model more flexible in situations where this assumption is violated.

The log-logistic model can be compared to other models, such as the exponential, Weibull, or log-normal models, to see which best fits the observed data. It may offer better performance when the hazard function is U-shaped or inverted-U-shaped.

To estimate the parameters $\beta_0,\beta_1,...,\beta_k$, we need to use maximum likelihood estimation. The likelihood function for the log-logistic model, assuming a sample of n independent observations, is:

$$L(\beta_0,\beta_1,\ldots,\beta_k)=\prod_{i=1}^{n}\left[\frac{\beta\left(\frac{t_i}{\exp(\beta_0+\beta_1 x_{i1}+\ldots+\beta_k x_{ik})}\right)^{\beta-1}}{\exp(\beta_0+\beta_1 x_{i1}+\ldots+\beta_k x_{ik})\left[1+\left(\frac{t_i}{\exp(\beta_0+\beta_1 x_{i1}+\ldots+\beta_k x_{ik})}\right)^{\beta}\right]}\right]$$

The log-likelihood is typically computed as the natural logarithm of this likelihood function, and the coefficients $\beta_0,\beta_1,\ldots,\beta_k$ are estimated by maximizing this log-likelihood.

2.3.4. Log-Normal Model: The lognormal distribution is a widely used distribution in reliability and survival analysis. This distribution is an appropriate distribution for life patterns with first increasing and then decreasing danger. There are many studies in the literature on this distribution. For example, Krishnamoorthy and Mathew (2003) derived exact inferential procedures for the means of lognormal distributions, Gupta and Li (2006) discussed a test for equality of means of two independent lognormal populations, Longford (2009) proposed several estimators for the expectation, median and mode of the lognormal distribution, and Balakrishnan and Mitra (2011) developed probability inference for lognormal data with left truncation and right censoring based on the EM algorithm. Balakrishnan and Pal (2013) used Conway–Maxwell Poisson-based cure rate model by assuming the lognormal distribution for the time-to-event variable, and also, they developed the EM algorithm for the estimation of the parameters of different cure rate survival models.

The log-normal distribution models a random variable whose logarithm is normally distributed. Let T represent a survival time $T \sim LogNormal(\mu,\sigma^2)$.The probability density function and the cumulative distribution function of T are given by:

$$f(t;\mu,\sigma)=\frac{1}{t\sigma\sqrt{2\pi}}\exp\left(-\frac{(\ln t-\mu)^2}{2\sigma^2}\right),t>0,$$

$$F(t;\mu,\sigma)=P(T\le t)=\Phi\left(\frac{\ln t-\mu}{\sigma}\right),t>0\text{ and }\Phi(.)\text{is the standard normal CDF.}$$

The survival function S(t), and the hazard function h(t) are given by;

$$S(t;\mu,\sigma)=P(T>t)=1-F(t;\mu,\sigma)=1-\Phi\left(\frac{\ln t-\mu}{\sigma}\right),$$

$$h(t;\mu,\sigma)=\frac{f(t;\mu,\sigma)}{S(t;\mu,\sigma)}=\frac{\frac{1}{t\sigma\sqrt{2\pi}}\exp\left(-\frac{(\ln t-\mu)^2}{2\sigma^2}\right)}{1-\Phi\left(\frac{\ln t-\mu}{\sigma}\right)}.$$

When modeling Log-Normal regression for survival data, the covariates $\mathbf{X}=(X_1, X_2,\ldots,X_p)$ into the log-normal framework. The relationship between the covariates and the survival time is expressed through the parameter μ, which becomes a linear function of the covariates:

$$\mu=X\beta=\beta_0+\beta_1X1+\beta_2X_2+\ldots+\beta_pX_p.$$

f(t;X,β,σ), S(t;X,β,σ), and h(t;X,β,σ) in regression model are given as below;

$$f(t;X,\beta,\sigma)=\frac{1}{t\sigma\sqrt{2\pi}}\exp\left(-\frac{(\ln t-X\beta)^2}{2\sigma^2}\right),$$

$$S(t;X,\beta,\sigma)=1-\Phi\left(\frac{(\ln t-X\beta)^2}{\sigma}\right),$$

$$h(t;X,\beta,\sigma)=\frac{f(t;X,\beta,\sigma)}{S(t;X,\beta,\sigma)}.$$

Where, β_i measures the effect of the i-th covariate X_i on the log-transformed survival time. A positive β_i increases μ, shifting the survival time distribution to the right (i.e., longer survival times). The log-normal regression model is analogous to ordinary linear regression on the log-transformed survival times:

$$\ln T = X\beta + \varepsilon, \varepsilon \sim N(0, \sigma^2)$$

The parameters **β** and σ are estimated by maximizing the log-likelihood function, which is derived from the PDF f(t) for censored and uncensored data. The model naturally accommodates right-censored survival data by modifying the likelihood to account for incomplete observations.

2.3.4. Generalized Gamma Model: The goal of survival analysis is to estimate the probability of survival, recurrence, death, and other events over a given time period. The generalized gamma distribution provides a flexible family of distributions with different shapes and hazard functions that are well suited to model survival data, making the generalized gamma distribution useful in survival analysis.

The three-parameter generalized gamma distribution was first proposed by Stacy (1962). Johnson, Kotz, and Balakrishnan (1994) extended Stacy's three-parameter generalized gamma distribution to a four-parameter generalized gamma distribution by setting the location parameter to zero. Agarwal and Al-Saleh (2001) studied the hazard rate function of the generalized gamma type distribution, while Balakrishnan and Peng (2006) used the generalized gamma distribution to study the frailty model. Another generalization of Stacy's generalized gamma distribution was derived by Cordeiro et all.,(2011). For this purpose, the authors used the exponential method and applied it to study survival data. Balakrishnan and Pal (2015) and Pal and Balakrishnan (2017) used the generalized gamma distribution in the context of the recovery rate model and the catastrophic recovery rate model, respectively. Pal et al (2020) demonstrated the flexibility of the broader class of the generalized gamma distribution to model right-censored survival data. This distribution includes the commonly used gamma, Weibull, and lognormal distributions as particular cases, and this flexibility allows us to discriminate between models to select a lifespan distribution that provides the best fit to a given data set within its class.

The **generalized gamma distribution** with parameters σ (shape), q (shape), and λ (scale) can be expressed as follows. The PDF is given by:

$$f(t;\lambda,\sigma,q) = \frac{|q|}{\lambda\Gamma(1/\sigma)}\left(\frac{t}{\lambda}\right)^{q/\sigma-1}\exp\left(-\left(\frac{t}{\lambda}\right)^{q}\right), t>0.$$

Here, $\lambda>0$, ($\sigma>0$) determines the tail behavior and ($q\neq 0$) adjusts skewness. The CDF is:

$$F(t;\lambda,\sigma,q)=\frac{\gamma\left(1/\sigma,\left(\frac{t}{\lambda}\right)^{q}\right)}{\Gamma(1/\sigma)},\ t>0,$$

where $\gamma(s,x)$ is the lower incomplete gamma function, $\gamma(s,x)=\int_0^x u^{s-1}e^{-u}du$

The survival function S(t), which gives the probability of survival beyond time t, and hazard function are given by:

$$S(t;\lambda,\sigma,q)=1-F(t;\lambda,\sigma,q)=1-\frac{\gamma\left(1/\sigma,\left(\frac{t}{\lambda}\right)^{q}\right)}{\Gamma(1/\sigma)},\ \text{and}$$

$$h(t;\lambda,\sigma,q)=\frac{f(t;\lambda,\sigma,q)}{S(t;\lambda,\sigma,q)}.$$

When modeling generalized gamma regression for survival data, we incorporate covariates $\mathbf{X}$= (X_1, X_2,…,Xp) through the scale parameter λ, while keeping σ and q as constants. The scale parameter λ is related to the covariates via a log-linear model:

$$\ln\lambda=\mathbf{X}\beta=\beta_0+\beta_1X_1+\beta_2X_2+\ldots+\beta_pX_p,$$

Substituting $\lambda=e^{\mathbf{X}\beta}$ into the PDF, we get:

$$f(t;\mathbf{X},\beta,\sigma,q)=\frac{|q|}{e^{\mathbf{X}\beta}\Gamma(1/\sigma)}\left(\frac{t}{e^{\mathbf{X}\beta}}\right)^{q/\sigma-1}\exp\left(-\left(\frac{t}{e^{\mathbf{X}\beta}}\right)^{q}\right),\ t>0.$$

The survival function and hazard function become:

$$S(t;\mathbf{X},\beta,\sigma,q)=1-\frac{\gamma\left(1/\sigma,\left(\frac{t}{e^{\mathbf{X}\beta}}\right)^{q}\right)}{\Gamma(1/\sigma)},\ h(t;\mathbf{X},\beta,\sigma,q)=\frac{f(t;\mathbf{X},\beta,\sigma,q)}{S(t;\mathbf{X},\beta,\sigma,q)}.$$

The generalized gamma model is highly flexible and includes several common distributions as special cases:

- Exponential Distribution: $\sigma = 1$, $q = 1$.
- Weibull Distribution: $\sigma = 1$, $q > 0$.
- Gamma Distribution: $q = 1$, $\sigma > 0$.

For survival data with right censoring, the likelihood function combines contributions from uncensored and censored observations. If t_i is the observed time for individual i, and δ_i is the censoring indicator ($\delta_i = 1$, if uncensored, $\delta_i = 0$ if censored), the likelihood and log-likelihood are:

$$L(\beta, \sigma, q) = \prod_{i=1}^{n} [f(t_i; X_i, \beta, \sigma, q)]^{\delta_i} [S(t_i; X_i, \beta, \sigma, q)]^{1-\delta_i},$$

$$\ell(\beta, \sigma, q) = \sum_{i=1}^{n} \delta_i \ln f(t_i; X_i, \beta, \sigma, q) + (1 - \delta_i) \ln S(t_i; X_i, \beta, \sigma, q).$$

The **generalized gamma distribution (GGD)** as implemented in R, particularly through the flexsurv package, uses a parameterization introduced by Prentice (1974) in this study. This distribution has three key parameters: a location parameter (μ), a scale parameter (σ), and a shape parameter (Q).

The PDF for the generalized gamma distribution is given as:

$$f(x | \mu, \sigma, Q) = \frac{|Q|}{\sigma x \Gamma(Q^{-2})} (Q^2)^{Q^2} \exp[Q^2(Qw - \exp(Qw))],$$

where $w = \frac{\ln(x) - \mu}{\sigma}$. This is numerically stable even for Q values near 0, enabling it to handle transitions to related distributions like log-normal and Weibull.

3. APPLICATION and RESULTS

This study will use the Veterans' Administrative Lung Cancer dataset presented by Prentice (1973), which is maintained by the US Veterans Administration and includes 137 patients with advanced inoperable lung cancer. Of the 137 male patients, 69 received the Standard test and 68 received the

Chemotherapy test, and 64 patients died in each treatment group, with only 9 patients being alive censored at the end of the study. This dataset will be analyzed using life tables to determine whether there is a statistically significant difference between the survival distributions of lung cancer cell types and between the standard test and chemotherapy test treatment groups using the Kaplan Meier method. Various covariates were analyzed using Cox regression to find out whether they have any effect on the mortality of male patients with advanced inoperable lung cancer. Furthermore, exponential, Weibull, log-logistic, log-normal and generalized gamma distribution parametric regression methods were also applied to this dataset. All these applications were analyzed using RStudio software.

The explanation of the variables is presented in Table 1 and Table 2. In these tables, we will give frequencies of categorical variables, and give mean, standard deviation, minimum, maximum, median and range for numeric variables are shown.

Table 1. Frequencies of Categorical Variables

	Treatment		**Cell Type**				**Status**		**Prior Treatment**	
	1	**2**	**Squamous**	**Small Cell**	**Adeno**	**Large**	**0**	**1**	**0**	**10**
Frequency	69	68	35	48	27	27	9	128	97	40

Table 2. Descriptive Statistics of Numeric Variables

Variable	**Mean**	**SD**	**Min**	**Max**	**Median**	**Range**
Time	121.6277372	157.8167220	1	999	80	998
Karno	58.5693431	20.0395916	10	99	60	89
Diagtime	8.7737226	10.6121411	1	87	5	86
Age	58.3065693	10.5416276	34	81	62	47

The dataset consists of two treatment groups (1 and 2) in Table 1. The frequency of patients in each treatment group is almost balanced, with 69 patients in treatment group 1 and 68 patients in treatment group 2. There are four distinct cell types: Squamous, Small Cell, Adeno, and Large. The most common cell type is Small Cell, with 48 patients, followed by Squamous with 35 patients. Both Adeno and Large have 27 patients each, which makes them the least frequent cell

types. This distribution might indicate a higher prevalence of Small Cell cancer in the dataset, but the dataset appears to have a variety of cell types. Status variable seems to represent the survival status of patients, with 0 likely indicating alive and 1 indicating dead. The frequency distribution is highly skewed, with 128 patients recorded as alive (status = 0) and 97 patients recorded as dead (status = 1). The prior treatment status variable has three categories: 0, 1, and 10. The largest group is prior = 0 (no prior treatment) with 40 patients, followed by prior = 1 (previous treatment) with 60 patients. The prior = 10 category, which might represent a different or special treatment condition, has 37 patients.

In Table 2, the mean of time variable is 121.63 days. On average, patients in the study survived for approximately **121.63 days** and the s**tandard deviation (SD)** is 157.82 days. There is a high variability in survival time, as reflected by the large standard deviation. Some patients survived for a much longer or shorter period than the average. The shortest survival time recorded is **1 day**, which could indicate either very rapid decline after diagnosis or data recording. The longest survival time observed is **999 days**, which indicates that some patients survived for nearly three years after the start of the study. The median survival time is **80 days**, meaning that half of the patients survived less than 80 days and half survived more. The median is lower than the mean, which suggests that the distribution of survival times is right-skewed (with a long tail toward higher values).

The mean of **karno (Karnofsky Performance Score) is** 58.57, indicating moderate functional impairment on average and the SD is 20.04. There is significant variation in the karnofsky scores, reflecting differences in the patients' functional status. The lowest recorded karnofsky score is **10**, which could represent patients who are very ill and bedridden. The highest karnofsky score is **99**, indicating patients who are mostly functional with minimal impairments. The median score is **60**, suggesting that half of the patients have scores higher than this, and half have scores lower, indicating a moderate level of functional impairment on average.

The mean of **diagtime (Time Since Diagnosis) variable is** 8.77 months. On average, patients were diagnosed **8.77 months** before the study began, and the SD is 10.61 months. The standard deviation is relatively large, suggesting that the time from diagnosis varies widely among the patients. The shortest time since diagnosis is **1 month**, indicating that some patients were diagnosed very recently. The longest time since diagnosis is **87 months**, which suggests some patients were diagnosed several years before the study. The median time since diagnosis is **5 months**, meaning that half of the patients were diagnosed less than 5 months

before the study, and half were diagnosed more than 5 months ago. The median is lower than the mean, suggesting a skewed distribution with a longer tail for those diagnosed earlier.

The mean of age variable is 58.31 years which is typical for lung cancer patients, as they are usually diagnosed in later adulthood. The SD is 10.54 years, indicating variability in the age of patients within the study. The youngest patient is **34 years old**, which is relatively young for a lung cancer diagnosis but is not unheard of, particularly for certain types of lung cancer or genetic factors. The oldest patient is **81 years old**, reflecting the inclusion of elderly individuals in the study. The median age is **62 years**, meaning that half of the patients are younger than 62, and half are older. This suggests that most patients are middle-aged to older adults.

The log-rank test is commonly used to determine if there is a statistically significant difference between the survival curves of two or more groups. We applied the log-rank test to compare the survival distributions between two treatment groups **(trt = 1** and **trt = 2)** in the **veteran** dataset and get the results are shown in Table 3.

Table 3. The log-rank test results between two treatment groups

	N	Observed	Expected	(O-E)^2/E	(O-E)^2/V
trt=1	69	64	64.5	0.00388	0.00823
trt=2	68	64	63.5	0.00394	0.00823

Chisq= 0 on 1 degrees of freedom, p= 0.9

The **p-value of 0.9** suggests that the observed differences in the number of events (deaths) between the groups are likely due to chance, and there is no strong evidence to suggest that the treatment type has a major impact on survival. The Kaplan Meier curve has been seen in Figure 1. There is no difference in survival functions between the standard treatment and chemotherapy methods applied. It is seen in the Figure 1, the number at risk that is the number of patients who are still being followed at each time point. This helps understand how the sample size decreases over time.

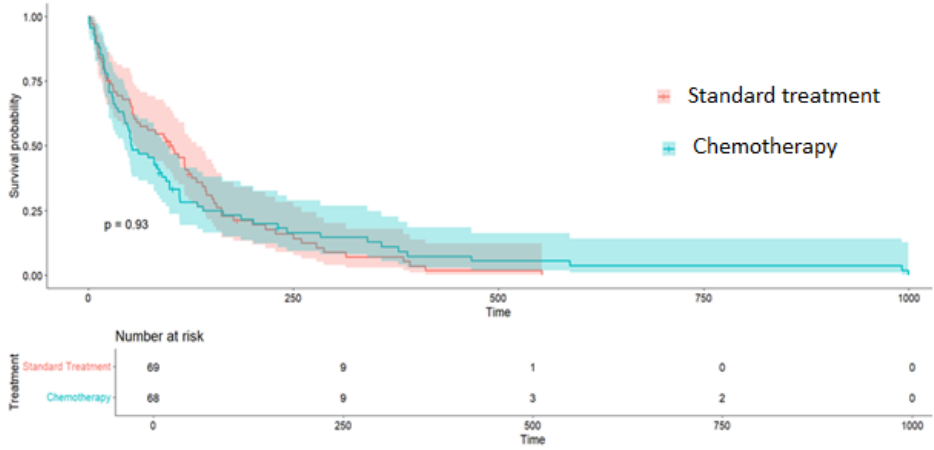

Figure 1. Kaplan Meier Curve for Treatment Variable

At the same time, the Log rank test was also applied to compare whether the cell types have an effect on survival times and the Log rank test results are given in Table 4.

Table 4. The Kaplan-Meier Survival Analysis Results, Stratified by Cell Type

Cell Type	N (Number of Patients)	Observed Deaths	Expected Deaths	(O-E)^2/E	(O-E)^2/V	Median Survival (days)	95% CI for Median Survival (days)
Squamous	35	31	47.7	5.82	10.53	118	[82, 314]
Small Cell	48	45	30.1	7.37	10.20	51	[25, 63]
Adenocarcinoma	27	26	15.7	6.77	8.19	51	[35, 92]
Large Cell	27	26	34.5	2.12	3.02	156	[105, 231]

The results from the Kaplan-Meier survival analysis in Table 4, stratified by **cell type**, provide valuable insights into the survival experiences of patients with different types of lung cancer. The analysis includes four categories: **squamous, small cell, adenocarcinoma**, and **large cell**. In the results, the Chi-Squared test statistic is 25.4 with 3 degree of freedom and the corresponding p-value is 1e-05. Since this p-value is less than 0.05, we reject the null hypothesis. In other words, we have sufficient evidence to say that there is a statistically significant difference in survival between the cell types. The results given in Table 4 can be interpreted as follows.

- The median survival of squamous cell carcinoma is 118 days, with a 95% CI of [82, 314]. The observed survival time is much longer than expected, indicating that these patients survive longer than what the model predicts.
- The median survival of small cell carcinoma is 51 days, with a 95% CI of [25, 63]. This is the shortest survival time among all the cell types. Small cell carcinoma is known for its aggressive nature, and this is reflected in the high observed deaths compared to the expected deaths.
- The median survival of adenocarcinoma is 51 days, with a 95% CI of [35, 92]. Adenocarcinoma has a median survival that is similar to small cell carcinoma, but the survival range is slightly broader.
- The median survival of large cell carcinoma is 156 days, with a 95% CI of [105, 231]. This is the longest survival time among all the cell types, suggesting that patients with large cell carcinoma have the best prognosis.

Overall, small cell carcinoma appears to be the most aggressive, with significantly lower survival, while large cell carcinoma has the best survival, with squamous and adenocarcinoma showing intermediate outcomes. These findings are consistent with the general understanding of lung cancer biology and could help guide clinical decisions and treatment strategies based on the cancer type.

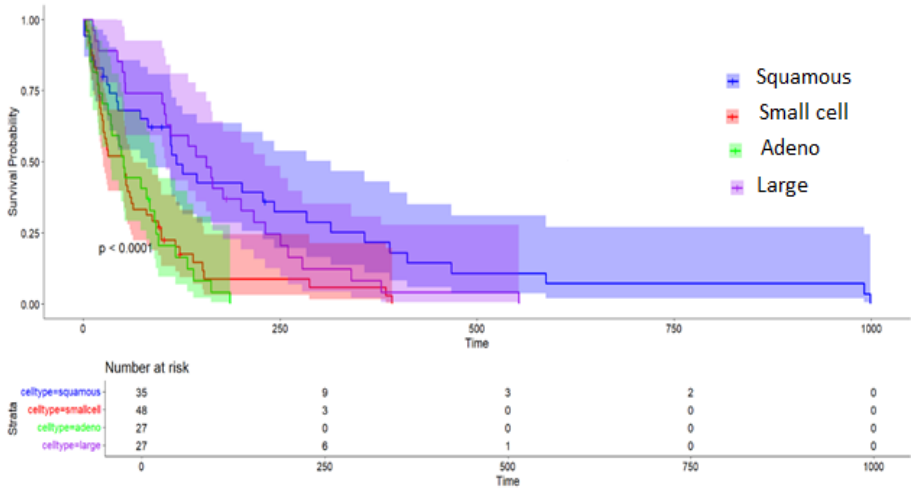

Figure 2. The Kaplan Meier Curve by Cell Types

The Kaplan Meier curve has been seen in Figure 2. It is seen in the Figure 2, the number at risk that is the number of patients who are still being followed at each time point. This helps understand how the sample size decreases over time.

The Cox regression model, which is a semi-parametric method, was also applied to the veteran data set and the results obtained with the R software are given in the output below.

```
                        coef  exp(coef)   se(coef)      z Pr(>|z|)
trt                 2.946e-01  1.343e+00  2.075e-01  1.419  0.15577
celltypesmallcell   8.616e-01  2.367e+00  2.753e-01  3.130  0.00175 **
celltypeadeno       1.196e+00  3.307e+00  3.009e-01  3.975 7.05e-05 ***
celltypelarge       4.013e-01  1.494e+00  2.827e-01  1.420  0.15574
karno              -3.282e-02  9.677e-01  5.508e-03 -5.958 2.55e-09 ***
diagtime            8.132e-05  1.000e+00  9.136e-03  0.009  0.99290
age                -8.706e-03  9.913e-01  9.300e-03 -0.936  0.34920
prior               7.159e-03  1.007e+00  2.323e-02  0.308  0.75794
---
Signif. codes:  0 ‘***’ 0.001 ‘**’ 0.01 ‘*’ 0.05 ‘.’ 0.1 ‘ ’ 1

                   exp(coef) exp(-coef) lower .95 upper .95
trt                   1.3426     0.7448    0.8939    2.0166
celltypesmallcell     2.3669     0.4225    1.3799    4.0597
celltypeadeno         3.3071     0.3024    1.8336    5.9647
celltypelarge         1.4938     0.6695    0.8583    2.5996
karno                 0.9677     1.0334    0.9573    0.9782
diagtime              1.0001     0.9999    0.9823    1.0182
age                   0.9913     1.0087    0.9734    1.0096
prior                 1.0072     0.9929    0.9624    1.0541

Concordance= 0.736  (se = 0.021 )
Likelihood ratio test= 62.1  on 8 df,   p=2e-10
Wald test            = 62.37  on 8 df,   p=2e-10
Score (logrank) test = 66.74  on 8 df,   p=2e-11

 n= 137, number of events= 128
```

The components in the model output related to Cox regression: Coef (Coefficients) determining the effect of each independent variable on survival time, if positive coefficients, the risk of the event (e.g. death) increases with the increase of the relevant variable, and negative coefficients indicate that the risk decreases. exp(coef) or hazard ratio value is shown as the ratio of each variable on the risk. This value expresses how much the risk of the event changes with each unit increase of the relevant variable. If; exp(coef) > 1: Risk increases. exp(coef) < 1: Risk decreases. se(coef) is the Standard Error of the Coefficient, a statistic that measures the accuracy of the coefficients. A small standard error indicates a more reliable coefficient estimate. Z-value tests how much the coefficients differ from zero. Large z-values mean that the coefficients are statistically significant. P-value tests whether the relevant variable is significant in the model. Generally, if $p < 0.05$, we accept that this variable is significant.

The results of the Cox regression output obtained are as follows for each covariate.

1. Coefficients (coef): The coefficients represent the change in the log hazard ratio for a one-unit increase in each covariate.

- **trt (treatment)**: The coefficient is 0.2946, but the p-value (0.15577) is greater than the commonly used threshold (0.05), indicating that the treatment is not significantly associated with survival in this model.
- **celltypesmallcell**: The coefficient is 0.8616 (p-value = 0.00175), which is significant at the 0.01 level. This suggests that the "smallcell" cancer type is associated with a higher risk of the event (death) compared to the reference category (which might be the "large" type or a baseline category not shown here).
- **celltypeadeno**: The coefficient is 1.196 (p-value = 7.05e-05), which is highly significant. "Adeno" type is associated with an even higher risk of the event compared to the reference category, making it one of the most significant predictors of survival.
- **celltypelarge**: The coefficient is 0.4013, and the p-value (0.15574) is greater than 0.05, indicating that the "large" cell type is not significantly associated with survival.
- **karno (Karnofsky performance score)**: The coefficient is -0.03282 (p-value = 2.55e-09), which is highly significant. The negative coefficient suggests that higher Karnofsky scores (better performance) are associated with a reduced risk of the event (better survival).
- **diagtime (time of diagnosis)**: The coefficient is 0.00008132 (p-value = 0.99290), indicating that diagnosis time is not a significant predictor of survival in this model.
- **age**: The coefficient is -0.008706 (p-value = 0.34920), suggesting that age is not a significant predictor of survival.
- **prior (prior treatment)**: The coefficient is 0.007159 (p-value = 0.75794), indicating that prior treatment history is not significantly associated with survival in this model.

2. Exponential of Coefficients (exp(coef)): The exponentiated coefficients (hazard ratios) provide an interpretation of how the risk of the event changes with a one-unit increase in each covariate.

- **trt**: The hazard ratio is 1.3426, meaning that treatment increases the hazard of the event by about 34% (though this is not significant).
- **celltypesmallcell**: Hazard ratio of 2.367, meaning that the smallcell cancer type increases the risk of death by about 137% compared to the reference category. The formula to calculate the percentage increase in risk is:

$$\text{Percentage increase} = (\text{HR} - 1) \times 100.$$

In this case, HR= 2.367. Percentage increase= $(2.367-1)\times 100 = 1.367 \times 100 = 136.7\%$.

- **celltypeadeno**: Hazard ratio of 3.307, meaning the adeno type increases the risk of death by about 231%.
- **celltypelarge**: Hazard ratio of 1.494, indicating a 49% higher risk of death for the large cell type but not statistically significant.
- **karno**: Hazard ratio of 0.9677, indicating that for each unit increase in karnofsky score, the risk of the event decreases by about 3%.
- **diagtime**: Hazard ratio of 1.0001, which essentially means that time of diagnosis has no significant impact on survival.
- **age**: Hazard ratio of 0.9913, indicating a slight decrease in the hazard of the event with increasing age, but this is not statistically significant.
- **prior**: Hazard ratio of 1.0072, meaning prior treatment has a very slight increase in the risk, but not statistically significant.

3.Confidence Intervals: The 95% confidence intervals for the hazard ratios (lower .95 to upper .95) provide the range within which we are 95% confident the true hazard ratio lies.

- For celltypesmallcell and celltypeadeno, the confidence intervals do not cross 1, indicating strong evidence of a relationship between these variables and survival.

- For karno, the interval (0.9573, 0.9782) indicates that karnofsky performance score is a significant predictor, as the interval is entirely below 1 (indicating reduced risk with better performance).
- For trt, celltypelarge, diagtime, age, and prior, the confidence intervals include 1, suggesting no significant effect on survival.

4. Model Evaluation:

- **Concordance**: The concordance index (C-index) is 0.736, which suggests that the model has good discriminatory power, with higher values closer to 1 indicating better performance.
- **Likelihood Ratio Test**: The likelihood ratio test statistic is 62.1 with a p-value of 2e-10, which indicates that the model as a whole is highly significant.
- **Wald Test**: The Wald test statistic is 62.37 (p-value = 2e-10), which further confirms the overall significance of the model.
- **Score (Logrank) Test**: The score test statistic is 66.74 (p-value = 2e-11), again confirming the model's statistical significance.

Fort his cox regression model, significant predictors of survival include celltype (smallcell, adeno), karno (Karnofsky performance score), and the overall model is highly significant. Non-significant predictors include trt (treatment), age, prior treatment, and diagtime. The model shows good discriminatory power with a C-index of 0.736, suggesting it can reasonably separate subjects with different survival times. Finally, the results highlight the importance of cell type and karnofsky score as key factors affecting survival, while treatment, age, and prior treatments do not have significant effects in this dataset.

In order to compare parametric and nonparametric methods in the veteran data set and first decide which distribution is more suitable for the data, the graph of the risk functions of the distributions was drawn as seen in Figure 3. As can be understood from the figure, the most suitable distribution for the data set is seen as the generalized gamma distribution.

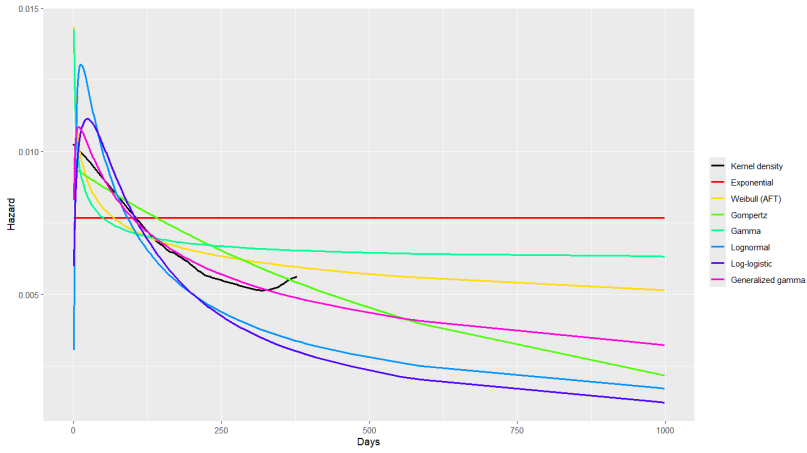

Figure 3. Hazard ratio of data and distributions.

We used AIC, BIC and Log-Lik values to compare Cox regression and exponential, Weibull, log-logistic, log-normal, and generalized gamma regression models.

The Akaike Information Criterion (AIC) is a statistical measure used to assess the fit of a model while penalizing for model complexity. AIC is used for model comparison. It is defined by the following equation:

$$AIC=2k-2\ln(L)$$

Where, k is the number of free parameters in the model. This represents the number of parameters that are estimated by the model. This term penalizes for model complexity. If a model has more parameters, this term increases, causing the AIC value to increase, which discourages overly complex models. L is the likelihood function, which represents the likelihood of the data given the model. This term reflects the model's goodness of fit. The likelihood function measures how well the model explains the observed data. A higher likelihood (better fit) leads to a lower value of $-2\ln(L)$, which decreases the AIC. When comparing multiple models, the model with the lowest AIC is generally considered the best, as it balances between fit and model complexity. A lower AIC indicates a model that provides a good fit to the data while avoiding unnecessary complexity (i.e., overfitting).

The Bayesian Information Criterion (BIC), also known as the Schwarz Information Criterion (SIC), is another statistical measure used to assess the

goodness of fit of a model, similar to AIC. However, BIC incorporates a stronger penalty for the number of parameters in the model, which tends to favor simpler models compared to AIC, especially when the sample size is large. The formula for BIC is:

$$BIC=\ln(n)k-2\ln(L)$$

Where, n is the number of observations. K is the number of free parameters in the. L is the likelihood function, representing the likelihood of the data given the model. Ln(n)k penalizes the model for the number of parameters. The penalty increases with both the number of parameters k and the sample size n. For large sample sizes, this term grows significantly, leading to a stronger penalty for models with more parameters. The second term is $-2\ln(L)$: Like AIC, this term measures the fit of the model. A higher likelihood (better fit) results in a lower value of $-2\ln(L)$, which lowers the BIC. The BIC is more conservative than AIC in terms of penalizing complexity, and as a result, it often favors simpler models, especially when the sample size is large.

The AIC, BIC and Log-Likelihood comparison results are given in Table 5.

Table 5. The AIC, BIC and Log-Likelihood Results of Cox Regression and Distributions

Model	AIC	BIC	Log-Likelihood
Cox Regression	964.7942	987.6105	-474.3971
Exponential	1504.4424	1507.3624	-751.2212
Weibull	1500.1824	1506.0224	-748.0912
Log-logistic	1504.5316	1510.3715	-750.2658
Log-normal	1502.9480	1508.7879	-749.4740
Generalized Gamma	1498.9416	1507.7015	-746.4708

In Table 5, the Cox Regression is clearly the best model for veteran dataset, as it achieves the lowest AIC, BIC, and the highest log-likelihood. This suggests that, despite being a semi-parametric model, it provides the best fit to the survival data when compared to the various fully parametric models.

REFERENCES

Agarwal SK, Al-Saleh JA (2001) Generalized gamma type distribution and its hazard rate function. Commun Stat Theory Methods 30:309–318

American Cancer Society November, (2024).https://www.cancer.org/cancer/types/lung-cancer/about/key-statistics.html

Azimmatul I., (2015). The Use of Cox Regression Model to Analyze the Factors that Influence Consumer Purchase Decision on a Product,Agriculture and Agricultural Science Procedia,3,78-83.

Balakrishnan N, Peng Y (2006) Generalized gamma frailty model. Stat Med 25:2797–2816

Balakrishnan, N., Mitra, D., (2011). Likelihood inference for lognormal data with left truncation and right censoring with an illustration. Journal of Statistical Planning and Inference 141, 3536–3553.

Balakrishnan N., Pal S.,(2013). Lognormal lifetimes and likelihood-based inference for flexible cure rate models based on COM-Poisson family, Computational Statistics & Data Analysis, 67, 41-67.

Balakrishnan N, Pal S (2015) An EM algorithm for the estimation of parameters of a flexible cure rate model with generalized gamma lifetime and model discrimination using likelihood- and informationbased methods. Comput Stat 30:151–189

Bennett S., (1983). Log-Logistic Regression Models for Survival Data, Journal of the Royal Statistical Society Series C: Applied Statistics, 32(2),165–171.

Bewick V, Cheek L, Ball J.,(2004). Statistics review 12: survival analysis. Critical Care. 8(5):389-94.

Cordeiro GM, Ortega EMM, Silva GO (2011) The exponentiated generalized gamma distribution with application to lifetime data. J Stat Comput Simul 81:827–842

Cox DR., (1972). Regression models and life-tables. Journal of theRoyal Statistical Society B, 34(2):187–220.

Cox D. R. and Oakes D (1984). Analysis of Survival Data. Chapman and Hall.

D'Arrigo, G., Leonardis, D., Abd ElHafeez, S., Fusaro, M., Tripepi, G., Roumeliotis, S., (2021). Methods to Analyse Time-to-Event Data: The Kaplan-Meier Survival Curve. Oxid. Med. Cell. Longev. 2290120.

Gupta, R.C., Li, X., (2006). Statistical inference for the common mean of two log-normal distributions and some applications in reliability. Computational Statistics and Data Analysis 50, 3141–3164.

Hosmer, D.W.Jr. and Lemeshow, S. (1999) Applied Survival Analysis, Regression Modeling of Time to Event Data. John Wiley and Sons, Inc., New York.

Hosseini Teshnizi S, Taghi Ayatollahi SM, (2017). Comparison of Cox Regression and Parametric Models: Application for Assessment of Survival of Pediatric Cases of Acute Leukemia in Southern Iran. Asian Pac J Cancer Prev. 1;18(4):981-985

Johnson NL., Kotz S., Balakrishnan N., (1994) Continuous univariate distributions, vol 1, 2nd edn.Wiley, New York

Leemis, L., (2023). Statistical Modeling: Regression, Survival Analysis, and Time Series Analysis *Open Education Resources (OER).*ISBN: 978-0-9829174-3-5.

Longford, N.T., (2009). Inference with the lognormal distribution. Journal of Statistical Planning and Inference 139, 2329–2340.

Kalbfleisch J. and Prentice R. L., (1980). The Statistical Analysis of Failure Time Data. Wiley.

Kaplan, E. L., & Meier, P. (1958). Nonparametric estimation from incomplete observations. Journal of the American Statistical Association, 53, 457–481.

Klein J. P. and Moeschberger M. L., (2003). Survival Analysis. Techniques for Censored and Truncated Data. Springer.

Kleinbaum, D. K., & Klein, M. (2010). Survival analysis, third edition. Springer.

Krishnamoorthy, K., Mathew, T., (2003). Inferences on the means of lognormal distributions using generalized p-values and generalized confidence intervals. Journal of Statistical Planning and Inference 115, 103–121.

Kumar, M.; Sonker, P.K.; Saroj, A. Jain, A.; Bhattacharjee, A.; Saroj, R.K., (2020). Parametric survival analysis using R: Illustration with lung cancer data. Cancer Reports. Vol. 3, e1210.

Pal S, Balakrishnan N (2017) An EM type estimation procedure for the destructive exponentially weighted Poisson regression cure rate model under generalized gamma lifetime. J Stat Comput Simul., 87:1107–1129.

Pal, S., Yu, H., Loucks, Z.D. et al. (2020). Illustration of the Flexibility of Generalized Gamma Distribution in Modeling Right Censored Survival Data: Analysis of Two Cancer Datasets. Ann. Data. Sci. 7, 77–90.

Prentice, R. L. (1973) Exponential survivals with censoring and explanatory variables. Biometrika, 60, 279-288.

Prentice, R. L. (1974). A Log Gamma Model and Its Maximum Likelihood Estimation. Biometrika, 61(3), 539–544.

Rich, J. T., Neely, J. G., Paniello, R. C., Voelker, C. C. J., Nussenbaum, B., & Wang, E. W. (2010). A practical guide to understanding Kaplan-Meier. Otolaryngology Head and Neck Surgery, 143(3), 331–336.

Stacy EW., (1962). A generalization of the gamma distribution. Ann Math Stat 33:1187–1192.

Wulandari, I., Kurnia, A., Sadik, K. (2021). Weibull Regression and Stratified Cox Regression in Modelling Exclusive Breastfeeding Duration. Journal of Physics: Conference Series, 1940(1), 012001.

Zhang Z. Parametric regression model for survival data: Weibull regression model as an example. Annals of Translational Medicine. 4(24):484.

CHAPTER 16

The Effects of Nanoparticles on Some Vertebrates

Özlem Önen Çelebi[1]

1 Dr., Kafkas University, Faculty of Arts and Sciences, Biology Department, Kars, ORCID: 0000-0002-9103-1720

Introduction

In recent years, nanoparticles have emerged as a significant class of nanomaterials employed during the advancement of novel nanotechnologies. Nanoparticles are utilized Across various trade fields today, ranging from medical devices and cosmetics to electronics and environmental remediation. Due to their unique properties, they hold the potential to revolutionize production and technology. However, as you mentioned, we still lack comprehensive knowledge about their prolonged impact on health and the environment. The potential risks associated with nanoparticles include toxic effects on livings' health, environmental bioaccumulation, and harm to ecosystems. Of particular concern are how nanoparticles penetrate the organism (through breathing, swallowing, or skin absorption), how they interact with cells, and how they accumulate within biological systems—areas that require further research.

With the progress of technology, the environmental release of nanoparticles has emerged as a fact that negatively impacts all living organisms over time, posing a significant threat to life in the long term through biological accumulation.

Research on the toxic effects of nanoparticles on vertebrates has been submitted, evaluated, and summarized to serve as a reference for future studies.

This review examines the toxic impacts of various nanoparticles on selected vertebrates using different methodologies. It has been reported that exposure to nanoparticles induces abnormalities in certain biological parameters of affected organisms and, in some populations, results in numerical declines. The reviewed reports indicate that nanoparticles induce sensitivity in certain vertebrates, with biological changes increasing in correlation with dose escalation. However, no evidence of chemical-specific sensitivity was observed. The findings recorded in the evaluated studies were generally consistent, and it was observed that exposure to nanoparticles is pernicious to the vertebrates in question.

Organisms are constantly exposed to hundreds of chemical and biological materials. Without exception, a wide range of substances that influence living organisms in various ways is present everywhere.

Paracelsus, regarded as the founder of modern toxicology, asserted that all substances are toxic, that no substance is entirely free from toxicity, and that the difference between a poison and a remedy is determined by the dose. As establishing the safety thresholds of substances is a fundamental area of research for toxicologists, dose constitutes the core principle of toxicology.

On the other hand, while some substances do not induce toxic effects when consumed in large quantities, others can threaten an organism's life even at very low concentrations. In this regard, toxic substances have consistently attracted attention throughout history.

The term "nano" refers to one billionth of a physical quantity. One nanometer (nm) represents a unit of length equal to one billionth of a meter (m) (Ateş et al., 2013; Alberts et al., 2015).

The majority of the sources of nanocomponents are of natural origin and they can be constantly found in the environment (Wigginton et al., 2007).

Comparative Assessments

Colloids suspended in water, fine-grained desert sand, oil smoke, smoke from volcanic activities or forest fires, and some atmospheric dust represent nanoparticles produced in nature.

In addition, many biological processes in living things occur in the nanoscale range and can be nanoscale and can be regarded as manifestations of nanotechnology in nature (Fig. 1; Bundschuh, et al., 2016). In addition, ribosomes work like a nanoscale factory that makes proteins by arranging amino acids in a specific order (Alberts, 2004; Ashby et al., 2009; Ateş et al., 2013, and hemoglobin, a protein that transfers oxygen in some cells (Figure 2).

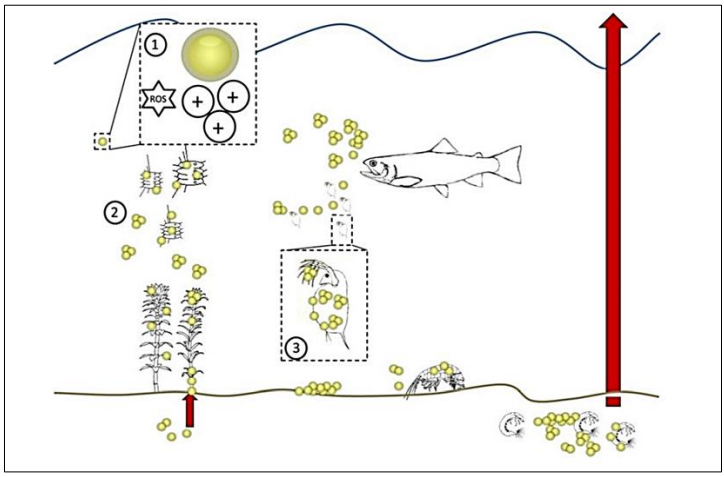

Fig. 1. Exposure and possible paths (indicated in red) for poisonousness of nanoparticles in the water habitats, (1) poisonous features, (2) bioexpansion capacity triggered by surface assimilation resulting in integration, (3) soaking up onto underwater structures. (Bundschuh, et al., 2016).

Other examples of nanomaterials include car exhaust, industrial emissions, and solder fumes used in welding. These are unintentionally released into the environment from anthropogenic sources as a byproduct of human activities (Nowack & Bucheli, 2007).

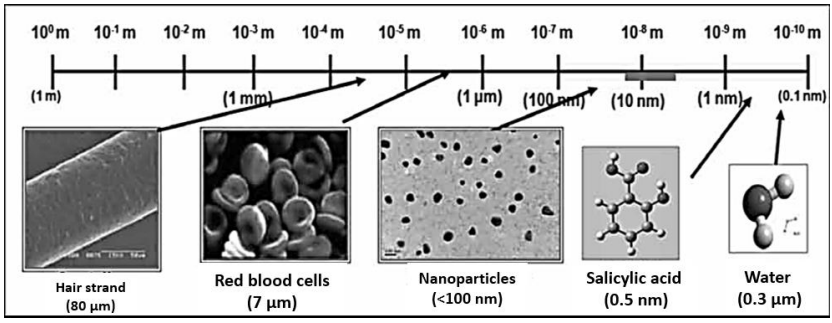

Fig. 2. Nanometer-scale size and visibly models of this gradation (Ateş et al., 2013).

Man-made engineered nanomaterials are specifically produced to take advantage of their unique properties that emerge at the nanoscale. Man-made or naturally occurring nanoparticles can be found in all aquatic environments such as surface water, groundwater, oceans, glaciers and atmospheric waters (Wigginton et al., 2007).

Nanoparticles constitute a very active field in the defense industry, textile, automotive industry, construction, electronics, new treatment methods and the pharmaceutical industry.

The toxicity of nanoparticles can occur either by directly causing poisoning or by triggering a side effect. Currently, relatively little is known about what nanoparticles do once they enter living cells (Kulkarni, 2010).

As the production of nanocomponents increases, so does the likelihood of human exposure and the spontaneous discharge of these materials into the habitats.

The release or unintentional leakage of these nanoparticles into the habitat also causes poisonous impacts on aquatic organisms (Turan et al., 2019; Habumugisha et al., 2024).

Even though the pathway of toxicity has not been fully explained, current ecotoxicological results on the impacts of nanocomponents on water-dwelling advanced organisms (vertebrates etc.) indicate that this toxicity is in the form of free radical damage, mutagenity and influence on the immune function (Handy and Shaw, 2007).

The hazardous mechanism of nanocomponents stated that the toxicity that occurs due to their physicochemical properties is related to ROS (reactive oxygen species) accumulation (Fig. 3; Xuan et al., 2023).

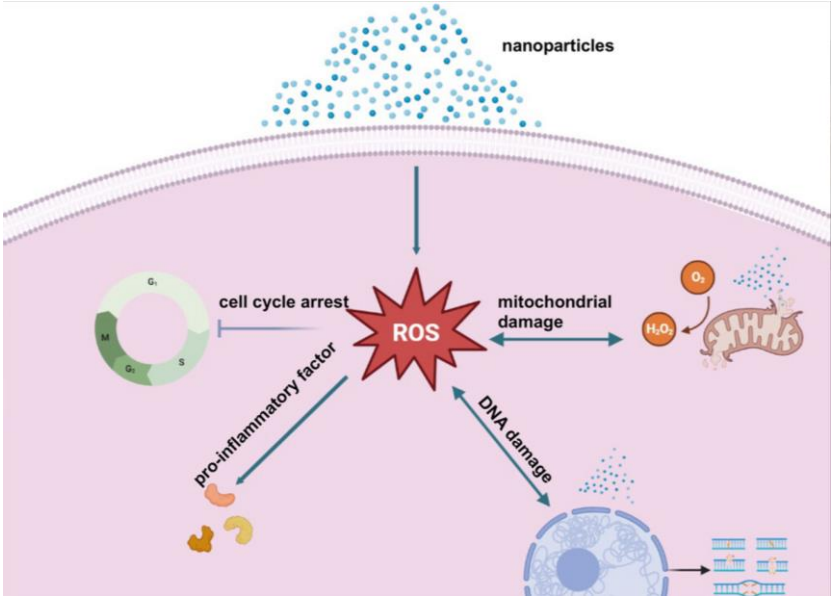

Fig. 3. The association of the harmfulness process induced by ROS piling up with nanoparticles (Xuan et al., 2023).

Despite the obvious benefits of nanomaterials, there are many questions about whether these innovative characteristics seen at the nanosize exposure a danger to the surroundings and, if so, to what extent (Buzea et al., 2007).

The toxicity of nanoparticles can occur either by direct toxic effects or by triggering a side effect. Currently, relatively little is known about what nanoparticles do once they enter living cells (Kulkarni, 2010).

With the increasing production of nanomaterials, the probability of human exposure and inadvertent discharge into the surroundings also increases. The release or unintentional leakage of these nanoparticles into the environment also causes harmful impacts on aquatic organisms (Turan et al., 2019).

Although the mechanism of poisonousness has not been fully clarified, available hazard science throughput regarding the impacts of nanocomponents on backboned animals that live in water indicate that this toxicity occurs in the form of oxidative damage, mutagenic potential and influences on the natural defenses function (Handy and Shaw, 2007).

Ecotoxicity test data on fish indicate that nanoparticles pose a low hazard potential, nevertheless, researches on their non-destructive impacts have shown free radical damage in the brains of sea perch subjected to buckyball (Fig. 4; Oberdörster, 2004; Lovern and Klaper, 2006; Lovern et al., 2007, Oberdörster et al., 2006; Smith et al., 2007, Ateş et al., 2013; Haghighat et al., 2021).

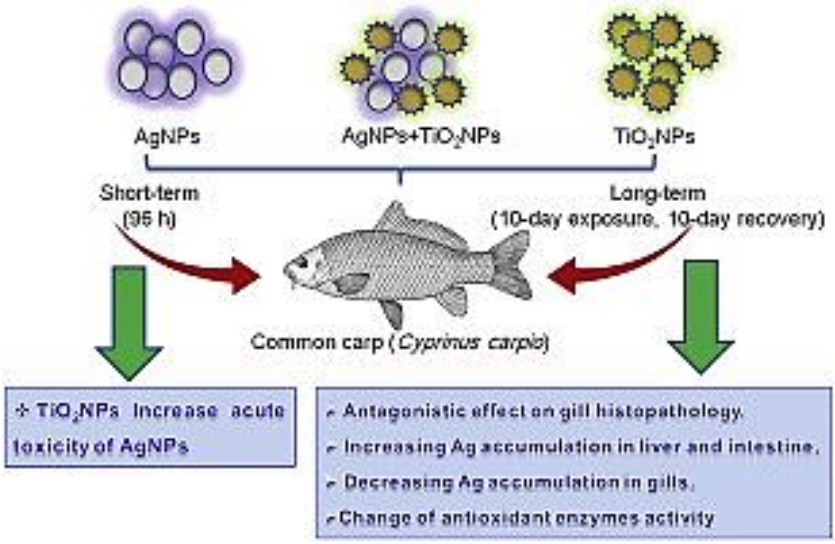

Fig. 4. Nanoparticle toxicity, individually and together, causes bioaccumulation in some organs of living beings and changes in antioxidant enzyme activity (Haghighat et al., 2021).

Oxidative damage to lipids has been reported in the gills, brain and liver of young carp and rainbow trout exposed to TiO_2 and Ag nanoparticles, demonstrating that the mentioned structures are under free radical imbalance (Federici et al., 2007, Linhua et al., 2009).

Nanoparticles have been indicated to be taken up by fish eggs and accumulate in the branchial and gut tissues of adult teleost, and nanoparticles have also been detected in the brain, testes, liver and blood (Nowack and Bucheli, 2007).

In a study investigating the non-lethal effects on a freshwater teleost *Prochilodus lineatus*, known to be sensitive to copper, it was noted that the gills of fish exposed to copper nanoparticles experienced negative effects, including elevated copper accumulation, inhibition of H^+-ATPase and Ca^{2+}-ATPase activities, and certain histological damages such as the proliferation of mitochondria-rich cells and/or mucosal cells.

Furthermore, lipid peroxidation amounts were rised in the hepatic tissue of fish subjected to copper nanoparticles and oxidative stress occurred. Copper nanoparticle exposure was stated to lower Ht (hematocrit), and Hb (hemoglobin) concentrations, suggesting anemia, and to elevate branchial Na+-K+-ATPase and H+-ATPase activities, potentially representing a compensatory mechanism for metabolic acidosis. (Fig. 5; Tesser et al., 2020).

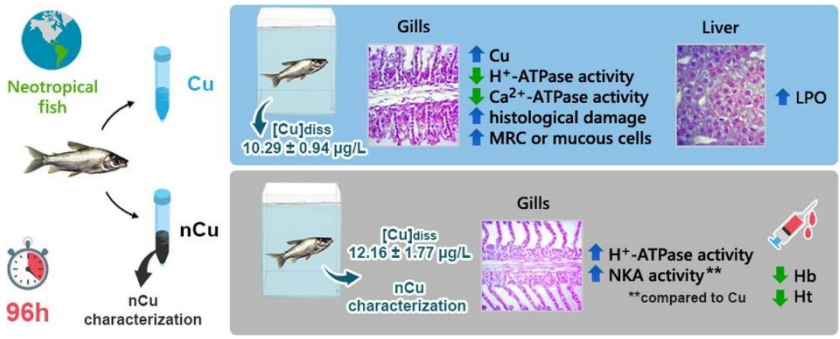

Fig. 5. Adverse effects on some tissues of fish (*Prochilodus sp.*) exposed to Cu nanoparticles; LPO: lipid peroxidation, MRC: mitochondria-rich cells, Cu: copper chloride, nCu: copper nanoparticles, Hb: hemoglobin, Ht: hematocrit, NaKATP: Na^+-K^+-ATPase (Tesser et al., 2020).

In a study analyzing the lethal and mutatory impacts of zincite nanocomponents and their solubilized equivalents on amphibians, *Lithobates sp.*, it was reported that significant DNA damage, micronucleated and anucleated erythrocyte counts were found in the exposed tadpoles in comparison the reference group, demonstrating the possible clastogenic and mutagenic impacts of zincite nanoparticles for Amphibious species (Fig. 6; Motta et al., 2020).

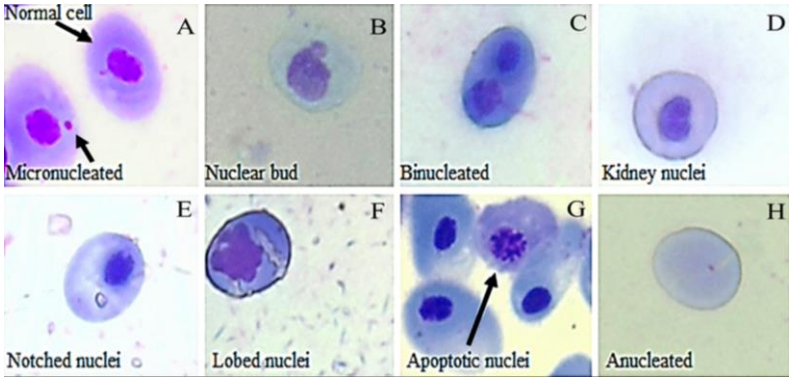

Fig. 6. Micrograph showing micronuclei and else aberrations in nucleus of *Lithobates sp.* porwigles subjected to Cu nanoparticles. Micronucleus-bearing nucleus (A), budded nucleus (B), binuclear cell (C), reniform nucleus (D), indented nucleus (E), segmented nucleus (F), programmed cell death nucleus (G), nucleusless cell (H) [Motta et al., 2020].

In a research examining the effects of zinc oxide nanoparticles on hatchlings of *Podocnemis expansa* (Amazon turtle), it was reported that these nanoparticles caused aberrations in nucleus like micronucleus-bearing nucleus and binuclear cell, are linked to cancer-causing mechanisms and defects in the Mitosis-related mechanism.

The reduced "zone in nucleus:zone of erythrocyte" proportion and an expanded cytoplasmic zone examined in exposed organisms were reported to indicate the presence of erythrocyte exchange induction, which is probably associated with energy deficit equilibrium/metabolic function interferences and/or oxygen transport performance by red blood cells (da Costa Araújo et al., 2019).

In a study exploring the impacts of silver nanoparticles on broiler chickens, it was reported that degeneration, necrosis, mononuclear permeation and localized clustering of immune cells increased in liver, kidney, spleen and duodenum tissues in parallel with increasing doses (Fig. 7; Al-Sultan et al., 2022).

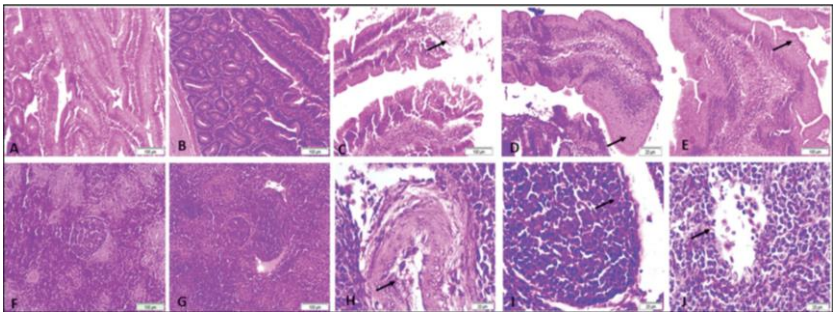

Fig. 7. Microphotographs of duodenum and spleen of broilers exposed to AgNP, H&E stain. (A) Duodenum from reference group. (B) Duodenum from low dose group, normal intestinal villi structure. (C) Duodenum from medium dose group, cell death and epithelial desquamation (arrow). (D-E) Duodenum from high dose group, metaplastic epithelium-related differentiation (arrow). (F) Spleen from control group. (G) Spleen from low dose group indicating normal red and white pulp with normal lymph-related follicles. (H) Vascular dilation, desquamation of the endothelial layer (arrow) and permeation around blood vessels in the spleen from the medium dose group. (I-J) Cell death of lymph-related follicles in the spleen from the high dose group (arrow) [Al-Sultan et al., 2022].

According to a study using cattle fallopian tube membranous cells and early-stage organisms as experimental models to study if subject to styrofoam nanocomponents affects proliferative activity and embryonic growth in mammals; karyotype analysis of cells exposed to nanoparticles showed no chromosomal abnormalities as per the reference, but tetraploid metaphase plates were more prevalent in the former.

IVF trials aimed at determining if subject to nanocomponents affects preimplantation development showed that incubation with nanoparticles reduced the ratio of 8-cell embryos and blastocysts in a dose-dependent manner.

Even if the eligibility of the blastocysts regarding the average percentage of cells of the DNA-fragmented blastomeres was found to be the just as in the subjected blastocysts in comparison with the references, the data obtained indicated that subject to nanoparticles may disrupt growth, which may influence the mitosis degree in early stage organisms and result in A reduced ability to progress to the blastocyst stage.

In accordance with the aforementioned study results, it was reported that the release into the environment and subsequent accumulation in life forms must be closely observed to avoid cytotoxic effects that could impact the reproductive success of styrofoam nanocomponents (Barbato et al., 2020).

Conclusion

Based on the information examined, it was determined that toxins may pose hazard at various levels relying on the living group exposed and the form of exposure. It was also concluded that toxicity rises in proportion to the quantity of the toxin exposed and the duration of subjection. It is also thought that the effects may differ relying on the kind of toxin. Consequently, the analyzed investigation data were determined to be consistent in relation to one another.

References

Alberts, B., Bray, D., Hopkin, K., Johnson, A. D., Lewis, J., Raff, M., Roberts, K., & Walter, P. (2015). *Essential Cell Biology*. Garland Science. ISBN 978-0-8153-4454-4

Al-Sultan, S. I., Hereba, A. R. T., Hassanein, K. M., Abd-Allah, S. M., Mahmoud, U. T., & Abdel-Raheem, S. M. (2022). The impact of dietary inclusion of silver nanoparticles on growth performance, intestinal morphology, caecal microflora, carcass traits and blood parameters of broiler chickens. *Italian Journal of Animal Science*, *21*(1), 967-978. https://doi.org/10.1080/1828051X.2022.2083528

Ates, M., Daniels, J., Arslan, Z., Farah, I. O., & Rivera, H. F. (2013). Comparative evaluation of impact of Zn and ZnO nanoparticles on brine shrimp (*Artemia salina*) larvae: effects of particle size and solubility on toxicity. *Environmental Science: Processes & Impacts*, *15*(1), 225-233. https://doi.org/10.1039/C2EM30540B

Barbato, V., Talevi, R., Gualtieri, R., Pallotta, M. M., Di Nardo, M., Costanzo, V., Catapano G., & Capriglione, T. (2020). Polystyrene nanoparticles may affect cell mitosis and compromise early embryo development in mammals. *Theriogenology*, *145*, 18-23. https://doi.org/10.1016/j.theriogenology.2020.01.007

Buzea, C., Pacheco, I. I., & Robbie, K. (2007). Nanomaterials and nanoparticles: sources and toxicity. *Biointerphases*, *2*(4), MR17-MR71. https://doi.org/10.1116/1.2815690

da Costa Araújo, A. P., Lima, V. S., de Andrade Vieira, J. E., Mesak, C., & Malafaia, G. (2019). First report on the mutagenicity and cytotoxicity of ZnO nanoparticles in reptiles. *Chemosphere*, *235*, 556-564. https://doi.org/10.1016/j.chemosphere.2019.06.164

Federici, G., Shaw, B. J., & Handy, R. D. (2007). Toxicity of titanium dioxide nanoparticles to rainbow trout (*Oncorhynchus mykiss*): gill injury, oxidative stress, and other physiological effects. *Aquatic Toxicology*, *84*(4), 415-430. https://doi.org/10.1016/j.aquatox.2007.07.009

Habumugisha, T., Zhang, Z., Uwizewe, C., Yan, C., Ndayishimiye, J. C., Rehman, A., & Zhang, X. (2024). Toxicological review of micro-and nano-plastics in aquatic environments: Risks to ecosystems, food web dynamics and human health. *Ecotoxicology and Environmental Safety*, *278*, 116426. https://doi.org/10.1016/j.ecoenv.2024.116426

Haghighat, F., Kim, Y., Sourinejad, I., Yu, I. J., & Johari, S. A. (2021). Titanium dioxide nanoparticles affect the toxicity of silver nanoparticles in common carp (*Cyprinus carpio*). *Chemosphere*, *262*, 127805. https://doi.org/10.1016/j.chemosphere.2020.127805

Handy, R. D., & Shaw, B. J. (2007). Toxic effects of nanoparticles and nanomaterials: implications for public health, risk assessment and the public perception of nanotechnology. *Health, Risk & Society*, *9*(2), 125-144. https://doi.org/10.1080/13698570701306807

Linhua, H. A. O., Zhenyu, W. A. N. G., & Baoshan, X. I. N. G. (2009). Effect of subacute exposure to TiO_2 nanoparticles on oxidative stress and histopathological changes in Juvenile Carp (*Cyprinus carpio*). *Journal of Environmental Sciences*, *21*(10), 1459-1466. https://doi.org/10.1016/S1001-0742(08)62440-7

Lovern, S. B., & Klaper, R. (2006). *Daphnia magna* mortality when exposed to titanium dioxide and fullerene (C_{60}) nanoparticles. *Environmental Toxicology and Chemistry: An International Journal*, *25*(4), 1132-1137. https://doi.org/10.1897/05-278R.1

Lovern, S. B., Strickler, J. R., & Klaper, R. (2007). Behavioral and physiological changes in *Daphnia magna* when exposed to nanoparticle suspensions (titanium dioxide, nano-C_{60}, and $C_{60}HxC_{70}Hx$). *Environmental Science & Technology*, *41*(12), 4465-4470. https://doi.org/10.1021/es062146p

Motta, A. G. C., do Amaral, D. F., Benvindo-Souza, M., Rocha, T. L., & e Silva, D. D. M. (2020). Genotoxic and mutagenic effects of zinc oxide nanoparticles and zinc chloride on tadpoles of *Lithobates catesbeianus* (Anura: Ranidae). *Environmental Nanotechnology, Monitoring & Management*, *14*, 100356. https://doi.org/10.1016/j.enmm.2020.100356

Nowack, B., & Bucheli, T. D. (2007). Occurrence, behavior and effects of nanoparticles in the environment. *Environmental Pollution*, *150*(1), 5-22. https://doi.org/10.1016/j.envpol.2007.06.006

Oberdörster, E. (2004). Manufactured nanomaterials (fullerenes, C_{60}) induce oxidative stress in the brain of juvenile largemouth bass. *Environmental health perspectives*, *112*(10), 1058-1062. https://doi.org/10.1289/ehp.7021

Oberdörster, E., Zhu, S., Blickley, T. M., McClellan-Green, P., & Haasch, M. L. (2006). Ecotoxicology of carbon-based engineered nanoparticles: effects of fullerene (C_{60}) on aquatic organisms. *Carbon*, *44*(6), 1112-1120. https://doi.org/10.1016/j.carbon.2005.11.008

Kulkarni, V. S. (2010). William Andrew is an imprint of Elsevier The Boulevard, Langford Lane, Kidlington, Oxford, OX5 1GB, UK 30 Corporate Drive, Suite 400, Burlington, MA 01803, USA First edition 2010 Copyright© 2010, Vitthal S. Kulkarni. Published by Elsevier Inc. All rights reserved. ISBN: 978-0-8155-2025-2

Smith, C. J., Shaw, B. J., & Handy, R. D. (2007). Toxicity of single walled carbon nanotubes to rainbow trout, (*Oncorhynchus mykiss*): respiratory toxicity, organ pathologies, and other physiological effects. *Aquatic Toxicology*, *82*(2), 94-109. https://doi.org/10.1016/j.aquatox.2007.02.003

Tesser, M. E., de Paula, A. A., Risso, W. E., Monteiro, R. A., Santo Pereira, A. D. E., Fraceto, L. F., & dos Reis Martinez, C. B. (2020). Sublethal effects of waterborne copper and copper nanoparticles on the freshwater Neotropical teleost *Prochilodus lineatus*: A comparative approach. *Science of the Total Environment*, *704*, 135332. https://doi.org/10.1016/j.scitotenv.2019.135332

Turan, N. B., Erkan, H. S., Engin, G. O., & Bilgili, M. S. (2019). Nanoparticles in the aquatic environment: Usage, properties, transformation and toxicity—A review. *Process safety and environmental protection*, *130*, 238-249. https://doi.org/10.1016/j.psep.2019.08.014

Wigginton, N. S., Haus, K. L., & Hochella Jr, M. F. (2007). Aquatic environmental nanoparticles. *Journal of Environmental Monitoring*, *9*(12), 1306-1316. https://doi.org/10.1039/B712709J

Xuan, L., Ju, Z., Skonieczna, M., Zhou, P. K., & Huang, R. (2023). Nanoparticles-induced potential toxicity on human health: applications, toxicity mechanisms, and evaluation models. *MedComm*, *4*(4), e327. https://doi.org/10.1002/mco2.327

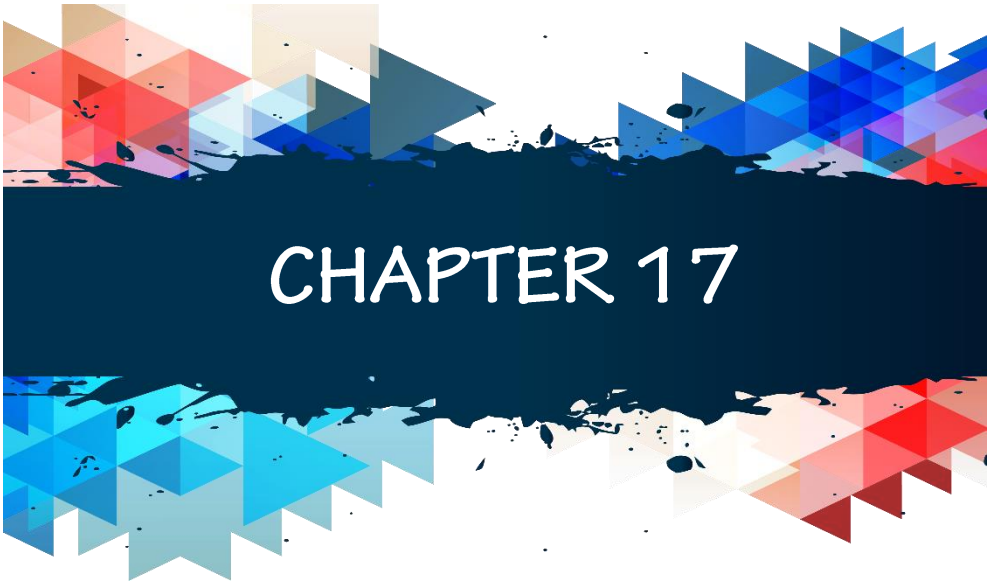

Free Radicals and Their Effects on the Human Body

***Nurhan Gümrükçüoğlu*[1]**

1 Prof. Dr. Nurhan GÜMRÜKÇÜOĞLU, Karadeniz Technical University, Vocational School of Health Sciences, Department of Medical Services and Techniques, 61080, Trabzon, TURKEY,
ORCID No: 0000-0002-9669-6318

1. Free Radicals (Oxidants)

An atom has electrons revolving around a nucleus consisting of protons and neutrons. Electrons are found at certain energy levels and each orbital can hold a maximum of two electrons, which have opposite spins. Atoms become stable by completing the number of electrons in their orbits or try to complete this number to maintain their stability. Free radicals can be defined as atoms, ions or molecules that contain one or more unpaired electrons in their outermost orbit [1]. The unpaired electron of a free radical is indicated by a dot (.) on or next to the atom or group (such as OH^-) [2]. The reactivity of radicals is very high because the presence of unshared electrons in their outer orbitals increases the reactivity of these chemical species tremendously [3]. Free radicals generally have short lifespans and are electrically positively charged, negatively charged or uncharged [4]. The chemical structures of free radicals are unstable and in order to pass into a stable structure, they react with another molecule in a series by sharing their unpaired electrons. Since they react with free radicals, one electron of the molecules is lost and they become reactive and carry out the reaction in a chain reaction. The most important free radicals in biological systems are those originating from oxygen. The importance of oxygen is generally associated with free oxygen radicals. These radicals can be formed by the division of any part of a covalently bonded molecule by taking one of its shared electrons, by adding electrons or by electron transfer. In biological systems, free oxygen radicals are mostly formed as a result of electron transfer [5].

Free radicals are formed as a result of reactions that occur in every living cell that uses oxygen (Aerobic). Free radicals, which are sourced from oxygen or nitrogen, have a dual effect in biological systems; in other words, we can say that they are both beneficial and harmful. When formed in high concentrations, free radicals can lead to the destruction of membrane lipids, proteins and nucleic acids, which can be harmful. However, in addition to antioxidant enzymes, non-enzymatic antioxidant systems can also balance these effects [6]. It has been determined that oxygen increases radiation damage in cell cultures of animals and bacteria exposed to radiation [7]. Although the oxidation ability of molecular oxygens is generally low; the activity of reactive oxygen species (ROS)

such as superoxide and hydrogen peroxide is much higher. At high radical concentrations, antioxidant systems that will remove the mentioned reactive species may be insufficient and especially unsaturated fatty acids may undergo oxidation. For this reason, nerve and membrane tissues with high lipid content can easily suffer oxidative damage when oxygen concentration is high [8]. The disruption of the balance by the dominance of free radicals is called oxidative stress.

2. Free Radical Sources

Oxygen molecules are not reactive by nature because their electron configuration is stable. However, when energy or electrons are provided to the oxygen molecule, this restriction is lifted and the formation of reactive species occurs spontaneously. This process occurs through electron donors such as heavy metal ions. The formation of reactive oxygen species can occur by both enzymatic and non-enzymatic means. Reactive oxygen species (ROS) can form as by-products in the chloroplast, mitochondrial structure and plasma membrane electron transport chain [9].

Living in an environment where oxygen is present provides a significant advantage in the production of adenosine triphosphate (ATP) through oxidative phosphorylation, but it also brings some risks. Free radicals can occur from biological, intracellular fluids or toxic substances. These sources can be divided into two main categories: endogenous and exogenous. Free radicals can be produced by metabolic reactions, cells converting food into ATP, intense exercise, environmental pollution and external factors such as ionizing radiation. They can also be formed in different ways such as adding an electron to a stable molecule [1]. Studies have shown that environmentally persistent free radicals contain a single electron, such as oxygen-containing or oxygen-centered free radicals, and have recently been studied as long-term and dangerous substances. The main source of free radicals in the body is physiological metabolism, but in addition to reactive oxygen species and oral bacteria, external factors such as ionizing and ultraviolet radiation, food and air pollution, alcohol and cigarettes can also contribute to the formation of free radicals. Oral tissues are frequently exposed to reactive oxygen species after consumption of beverages and food, which can cause adverse health

effects in the oral cavity [6]. Life with the presence of oxygen provides a significant advantage through the production of adenosine triphosphate (ATP) through oxidative phosphorylation. However, this situation can also bring some risks. These risks can be biological, intracellular fluids or toxic substances. These sources are generally divided into two general categories: endogenous or exogenous.

2.1. Endogenous Sources

2.1.1. Mitochondrial Electron Transport Chain

Mitochondria, where cellular respiration takes place, reduce a large portion of oxygen to water in energy metabolism, while a small portion (1-5%) is used in the production of superoxide. The reason for this situation is the electron leakage from electron carriers such as NADH dehydrogenase and coenzyme Q to oxygen [10].

2.1.2. Microsomal Electron Transport Chain

Many P450 and flavin monooxygenase (FMO) enzyme systems are located in the endoplasmic reticulum and nuclear membranes. Enzyme systems oxidize unsaturated fatty acids and foreign substances in the organism to form free radicals [11].

2.1.3. Proteins

Reactive oxygen species interact with proteins and form protein carbonyl derivatives after oxidative damage from many amino acid residues such as proline, histidine, arginine, glycine or in the peptide backbone. At the same time, free radicals cause oxidative protein damage by causing oxidation of thiols (-SH) in proteins [12].

2.1.4. Activation of the Arachidonic Acid Cycle

The arachidonic acid cycle is an important mechanism where reactive oxygen species are synthesized. With the stimulation of phagocytic cells, activation of phospholipase and protein kinase enzymes and release of arachidonic acid from the plasma membrane occur. Free radical products are formed as a result of the enzymatic oxidation of arachidonic acids [13].

2.1.5. Oxidative Stress-Causing Situations (Trauma, Ischemia, Reperfusion)

Free radical production always occurs during the metabolic process. However, the free radicals formed are neutralized by endogenous and exogenous

antioxidant systems and a balance is achieved. If this balance is disrupted against the free radicals, this is called oxidative stress. Trauma usually causes structural damage by transferring kinetic, thermal or chemical energy to tissues. This can lead to loss of normal homeostatic mechanisms and an increase and disruption of physiological needs.

2.1.6. Phagocytic Cells

Phagocytic cells, which initiate the cellular response in the body against infections, include various cell types such as neutrophils, monocytes and macrophages, eosinophils, lymphocytes and endothelial cells. These cells can produce compounds such as hydrogen peroxide or hypochlorous acid to destroy bacteria during phagocytosis.

2.1.7. Peroxisomes

High levels of oxidases become the main source of cellular hydrogen peroxide production. These structures include oxidase enzymes of D-amino acid, urate, L-alpha-hydroxy acid and acyl CoA (coenzyme A) compounds, and they are present in quite high amounts. [14].

2.1.8. Plasma Membrane

Intracellularly formed free radicals must either pass through the plasma membrane or cause toxic reactions in the membrane in order to interact with other parts of the cell. Membrane components such as unsaturated fatty acids, phospholipids, glycolipids, glycerol and sterols, and membrane proteins containing oxidizable amino acids are sensitive to free radical damage. Lipid peroxidation caused by free radicals or oxidation of structural proteins can disrupt the ion permeability of the membrane, cause damage to secretion functions and inhibit cellular metabolic events.

Lipoxygenase, prostaglandin synthetase in the plasma membrane structure, and NADPH oxidase in phagocytes are free radical sources that trigger lipid peroxidation. During phagocytosis, it increases superoxide and therefore hydrogen peroxide production with increased oxygen consumption. In this way, the plasma membrane of phagocytic cells becomes an important source of free radical formation via NADPH oxidase. Free radicals are formed during the conversion of arachidonic acid into biologically active products (prostaglandin, leukotriene, thromboxane) by enzymes with microsomal structure, such as lipoxygenase and cyclooxygenase, which are also in the plasma membrane [13].

2.1.9. Transition Metals

Heavy metals such as copper and iron play a role in reduction-oxidation reactions. They accelerate oxidative damage by carrying electrons for DNA (Deoxyribonucleic acid), proteins and lipids, and iron and copper become elemental with the destruction of ceruloplasmin proteins containing iron and copper, which accumulate in the form of ferritin and hemosiderin in the cell as a result of cell lysis. In this case, Fe and Cu released to the surrounding tissues act as catalysts and increase oxidative damage [11]. Metal ions also catalyze the breakdown of lipid peroxides (LOOH) and the chain reaction of lipid peroxidation. Thus, radical damage increases.

2.2. Exogenous Sources

2.2.1. Drugs, Metal Ions and Pollutants

Herbicides, pesticides and paracetamol, aminotriazoles, acetaminophen, bleomycin, doxorubicin, clonazine, closapine, MDMA, nitrofurantoins, ciprofloxacins, cyclosporines, tricyclic antidepressants and troglitazones are drugs that cause free radical formation [15].

Free radical formation is caused especially by ions of transition metals such as iron, copper, cadmium, nickel, chromium and mercury [15].

Fibers found in asbestos structure, mineral particles, ozone, carbon monoxide radical, nitric oxide, nitrogen dioxide, silica and some solvents, toxins, hypochlorite ion, sulfur dioxide and pollutants such as plumbagin and juglone, which are ketone group compounds, constitute the source of free radicals [15].

2.2.2. Radiation

Ultraviolet light, X-rays and gamma rays can trigger radical formation.

3. Formation of Free Radicals

Free radicals are constantly formed in cellular conditions and in the environment, this formation is caused by physical factors and chemical events. Free radicals emerge through three different mechanisms [16].

• By homolytic breaking: Radicals can form as a result of homolytic separation of covalent bonds. In this case, during the breaking of the bond, the electrons belonging to the bond are distributed equally between both atoms. This causes each atom to become a radical.

X ⁚ Y X • + Y •

• By single electron transfer: Radical formation can occur as a result of a molecule that does not have radical properties losing or gaining an electron that is normally paired. This occurs when a molecule loses an electron and leaves an unpaired electron in its outer orbital, or when a molecule gains an electron and takes an additional electron to its outer orbital.

• By losing electrons: The presence of an unpaired electron in the outer orbital of a molecule that is not a radical can trigger radical formation.

In biological systems, the most common formation mechanism of free radicals occurs as a result of electron transport. The charge of the free radical can be positive, negative, or free radicals can be neutral. The most important radicals found in a biological system are usually free oxygen radicals, but they are also found in radicals derived from atoms such as C, N, S and inorganic molecules. Transition metals such as Cu2+, Fe3+, Mn2+, Mo5+ are generally not considered free radicals even though they have unpaired electrons. In addition, the contribution of these ions to the formation of free radicals by catalyzing reactions is very important [17].

4. Types of Free Radicals

Some of the free radicals and non-radical reactive species are shown in Table 1.

Table 1. Types of Free Radicals

Free Radicals	**Non-Radical Reactive Types**
Reactive Oxygen Species	Reactive Oxygen Species
Singlet Oxygen ($O_2^{\downarrow}$) Superoxide Radical ($O_2^{\bullet -}$) Hydroxy Radical ($HO^{\bullet}$) Alkoxyl Radical ($RO^{\bullet}$) Peroxyl Radical ($ROO^{\bullet}$) Hydroperoxyl Radical ($HO_2^{\bullet}$) Carbonate Radical ($CO_3^{\bullet -}$)	Ozone (O_3) Hydrogen Peroxide (H_2O_2) Organic Peroxides (ROOH) Peroxynitrite Radical ($ONOO^-$) Peroxonitrate (O_2NOO^-) Peroxynitric acid (ONOOH) Peroxomonocarbonate ($HOOCO_2^-$) Hipobromik asid (HOBr)
Reactive Chloride Species	Reactive Chloride Species
Chlorine Radical (Cl•)	Hypochlorous Acid (HOCl) Nitrile Chloride (NO_2Cl) Chlorine Gas (Cl_2) Bromine Chloride (BrCl)
Reactive Bromine Species	Reactive Bromine Species
Brom Radically ($Br^{\bullet}$)	Hypobromic Acid (HOBr) Bromine gas (Br_2) Bromine chloride (BrCl)
Reactive Nitrogen Species	Reactive Nitrogen Species

Nitrogen Dioxide ($NO_2^{\bullet}$)	Nitric acid (HNO_3)
Nitrate Radicals ($NO_3^{\bullet}$)	Nitrosyl cation (NO^+)
Nitric Oxide ($NO^{\bullet}$)	Nitrosyl anion (NO^-)
Nitrous Trioxide ($N_2O_3^{\bullet}$)	Nitronium cation (NO_2^+)
	Dinitrogen tetraoxide (N_2O_4)
	Alkyl peroxynitrites (ROONO)
	Alkyl peroxynitrates (RO_2NO_2)
	Peroxyacetyl nitrate ($CH_3C(O)O_2NO_2$)
	Peroxynitric acid (ONOOH)
	Peroxynitrate ($OONOO^-$)
	Nitrile chloride ($ClNO_2$)
	Peroxynitrite ($OONO^-$)

4.1. Reactive Species of Oxygen

Reactive species of oxygen are formed when a free electron is added to the O2 molecule during the cellular respiration process in the mitochondria. Different biochemical reactions produce various molecules such as oxygen ions, free radicals, superoxide anions, nitric oxide and hydrogen peroxides [18]. They are highly reactive small molecules with unpaired electrons derived from cellular metabolism and other external sources. Reactive oxygen species (ROS) cause harmful damage to organisms by disrupting the balance of fixed molecules; therefore, the presence of low levels of antioxidants and high levels of ROS can lead to the emergence of oxidative stress [19].

In some cases, free radicals with high reactivity and unbalanced energy are formed. These reactive oxygen species or free radical structures can be formed as a result of factors such as lipid peroxidation, radiation, pro-oxidative enzyme systems, smoking, glycation and air pollution [20].

The molecular activity of oxygen can be achieved by different physical, chemical and biological events [21]. Of course, these methods may have disadvantages such as high energy consumption and low efficiency [22]. In recent years, light-catalyzed molecular oxygen activation has attracted the attention of

researchers as a practical method. This process, which is carried out using solar energy, produces highly beneficial reactive oxygen species with the effect of carrier or electron-hole pair, while also disrupting spin-forbidden reactions [23]. Although it is continuously activated by light-excitation and does not take part in the oxygen activation process, it plays an important role in light-catalyzed, light-catalytic molecular oxygen activation [24].

With the help of heavy metals (such as Cu^{+2}, Fe^{+3}) located in the active centers of many oxidases and oxygenases in the organism, the spin restriction of oxygen can be overcome by transferring a single electron to the oxygen molecule. Another way to overcome the spin restriction is to make oxygen enter an excited state by energy absorption [25]. As a result of this event, singlet oxygen is formed.

Oxygen radicals are obtained as a result of physical and chemical effects and metabolic reactions that occur involuntarily in the environment where oxygen is present. Oxygen radicals are very important free radicals found in biological structures. Of these radicals, superoxide and hydroxyl radicals and the hydrogen peroxide compound that does not exhibit radical properties are known as reactive oxygen species (ROS). The reduction of oxygen to water and the formation of other oxygen species are shown in Figure 1.

4.2. Reactive Oxygen Sources of the Cell

4.2.1. Biological Sources

4.2.1.1. *Oxidative Burst*

Respiratory burst is an important phenomenon that occurs when phagocyte cells (such as neutrophils, macrophages, and dendritic cells), which are components of the immune system, interact with microbes. This process occurs when microbes are taken in by phagocytosis or interact with phagocyte cells.

During the respiratory burst, phagocyte cells rapidly release molecules called reactive oxygen species (ROS) to destroy microbes.

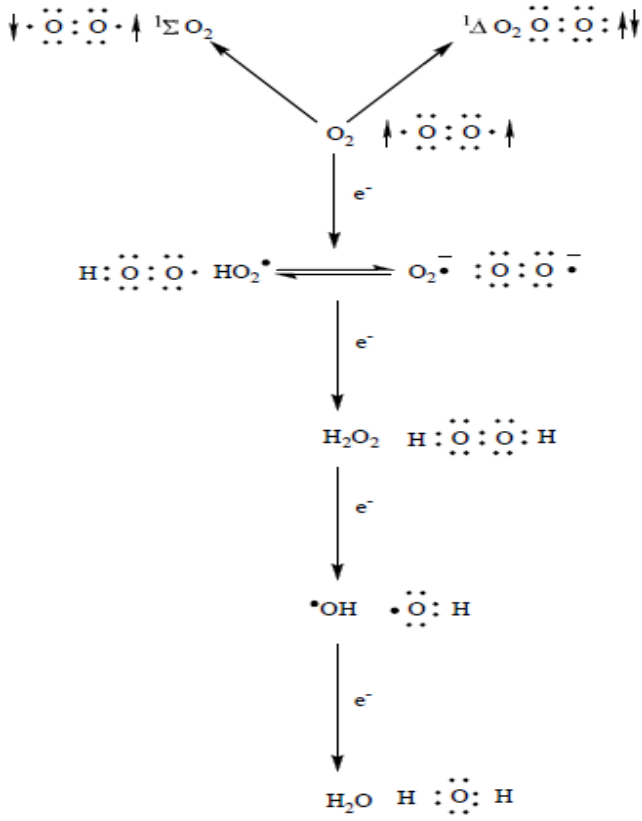

Figure 1. Reduction of Oxygen to Water and Formation of Other Oxygen Species

Superoxide radicals (O2-•), hydrogen peroxides (H_2O_2), and hydroxyl radicals (•OH) are reactive oxygen species. These reactive oxygen species are produced in the phagosome where microbes are taken in or interact with, and play a critical role in the destruction of microbes. Reactive oxygen species cause damage to microbes and oxidative stress within the cell. This process acts as a rapid defense mechanism of the immune system and helps control the infection.

However, excessive production of reactive oxygen species can cause damage to cells. Therefore, it is important that the respiratory burst process is tightly regulated and controlled. In addition, the respiratory burst process is vital for the normal function of the immune system, but if excessive or uncontrolled, it can lead to pathological conditions. This process is shown in Figure 2.

4.2.1.2. Environmental Factors and Radiation

Factors such as harmful drugs, polluted air, smoke, arenes, solvents, drugs can trigger oxidant formation.

4.2.1.3. Antineoplastic Factors

These types of drugs constitute a subgroup of chemical treatment drugs used in cancer treatment. Antineoplastic drugs can kill cancer cells or control their growth by inhibiting the DNA replication of cancer cells or by stopping cell division. These types of drugs can contain many different chemicals commonly used in cancer treatment [26].

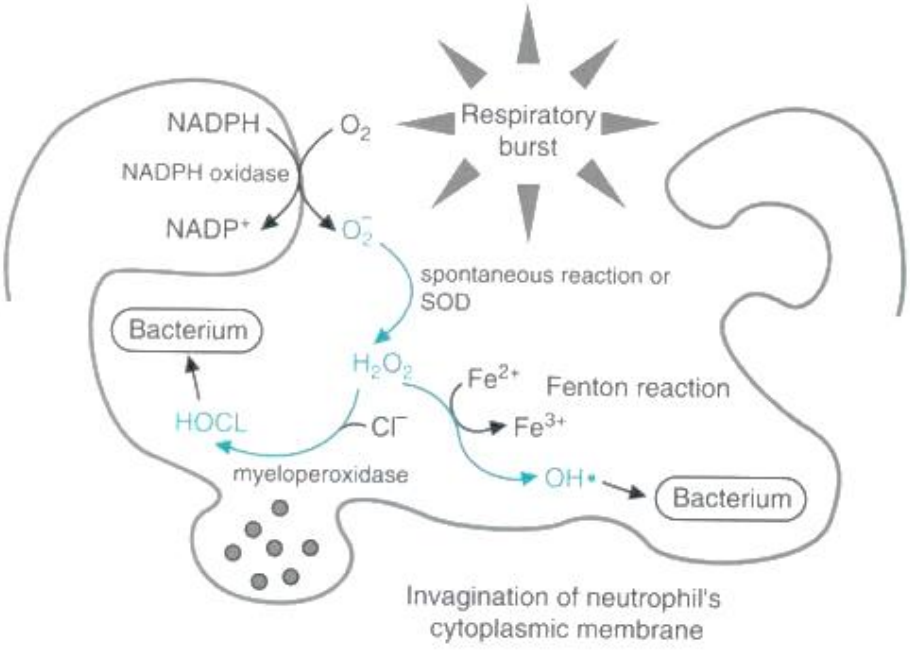

Figure 2. Neutrophil Membrane

4.2.1.4. Stress

Catecholamines are chemical compounds synthesized in the adrenal glands and nerve endings that regulate the stress response. These include adrenaline (epinephrine), noradrenaline (norepinephrine), and dopamine. In cases of nervous stimulation or stress, the body produces and secretes these hormones. These hormones help various systems in the body cope with and adapt to stress. Stress causes an increase in catecholamines, which in turn causes the formation of free

radicals. This is important in terms of providing a relationship between the progression of the disease in this case and the formation of free radicals [17].

4.3. Intracellular Sources

Free radicals can be formed as a result of various processes within the cell. Some of the intracellular sources and their classification are given below.

Mitochondrial Sources: Redox reactions occurring in mitochondria during electron transport chain (ETC) reactions can lead to the formation of free radicals. Particularly, radius free radicals occurring in complex I and complex III of the ETC are the main source of mitochondrial-derived free radicals.

Peroxisomes: Peroxisomes play a role in the production of hydrogen peroxide (H_2O_2) within the cell. Although hydrogen peroxide is not a free radical molecule, it can cause the formation of free radicals in peroxisomes under metal catalysts.

Cytoplasmic Sources: Redox reactions located in the cytoplasm, especially processes such as oxidation of proteins or lipid peroxidation, can lead to the formation of free radicals.

Endoplasmic Reticulum (ER): The endoplasmic reticulum performs important functions such as protein synthesis and lipid metabolism within the cell. Byproducts formed during these processes can contribute to the formation of free radicals.

NADPH Oxidase: The NADPH oxidase enzyme complex is found in the cell membrane and produces superoxide radical (O2•-) by reducing oxygen in the cytoplasm. This enzyme is found especially in immune cells (such as neutrophils and macrophages) and plays an important role in the production of free radicals during interaction with pathogens.

These sources contribute to the formation of free radicals as a result of various processes occurring within the cell. Understanding these mechanisms is important in terms of controlling free radical sources and preventing oxidative stress.

4.4. Effects of Free Radicals on the Human Body

The intense reactive properties of free radicals can quickly interact with all cell structures. If these radicals are not cleaned by the cell's defense mechanisms, they can interact with biological molecules and initiate a chain reaction, causing the production of new free radicals. The effect of free radicals on the cell is shown in Figure 3.

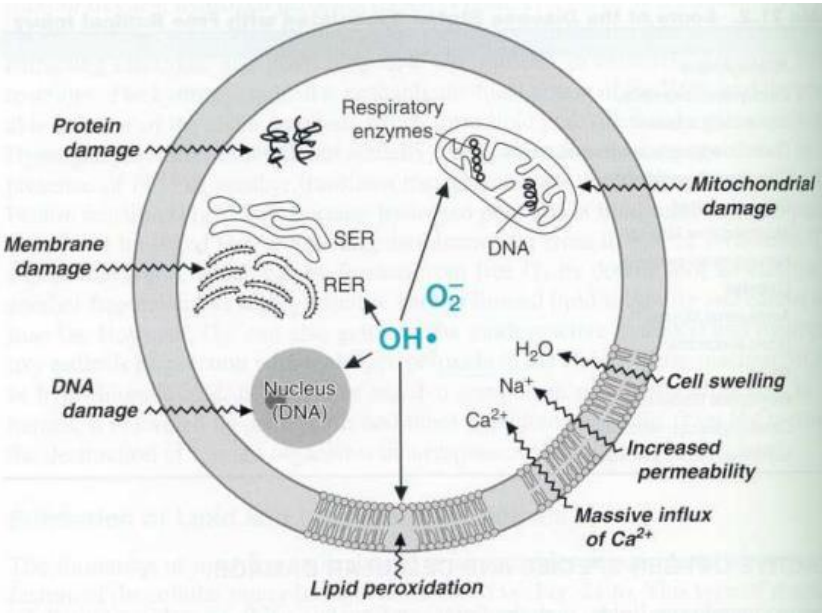

Figure 3. Effect of Free Radicals on the Cell

4.4.1. Oxidative Stress

Reactive oxygen and nitrogen species (ROS and RAT) are constantly produced in the body and the antioxidant system tries to balance their undesirable effects. However, when this balance is disrupted in favor of oxidants, oxidative stress occurs. In the event of oxidative stress, there is an increase in the amount of ROS and RAT and therefore an increase in the reaction rates of these species. This can have negative effects on many systems in metabolism, especially lipids, proteins and nucleic acids. The affected systems also negatively affect other peripheral systems. This situation continues as a chain reaction until the radical chain reaction is stopped by the antioxidant system. Otherwise, these reagents can cause the cell to die directly or indirectly [27].

The presence of high concentrations of reactive oxygen species can be an indicator of significant damage to cell structures, nucleic acids, lipids and proteins. It is known that the hydroxyl radical interacts with all elements of the DNA molecule and as a result of this interaction, it can damage purine and pyrimidine bases as well as the deoxyribose skeleton [28]. New research highlights the importance of base damage as a marker of oxidative DNA damage. Cu^{2+} ions located in G-C rich regions affect the guanine base, which is most susceptible to oxidative damage in DNA. Therefore, the most commonly

measured base damage is 8-hydroxy-2'-deoxyguanose (8-OHdG), which is considered to be an indicator of oxidative DNA base damage [29]. Oxidative damage is the first step in a process that can lead to permanent damage to genetic material, mutations, cancer formation, and the onset of aging.

Metal-induced reactive oxygen species can damage not only DNA but also other cellular components that are highly susceptible to oxidation, such as various unsaturated fatty acids and phospholipid residues [30]. In lipid peroxidation, the main aldehyde product is 4-hydroxy-2-nonenal (HNE), rather than malondialdehyde. Monoaldehyde is a substance that exhibits carcinogenic properties in bacteria and mammalian cells, as well as in rats. Although HNE exhibits weak mutagenic properties, it is a major toxic product in lipid peroxidation. Reactive oxygen and nitrogen species are shown in Figure 4.

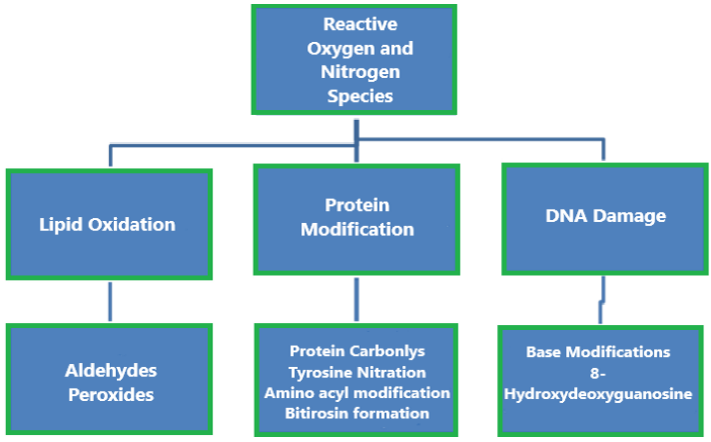

Figure 4. Reactive Oxygen and Nitrogen SpecieS

4.4.2. Free Radical Effect on Lipids

Lipids are the biomolecules most sensitive to the effects of free radicals. Cholesterol and fatty acids in cell membranes and foods react rapidly with free radicals to form peroxidation products. The oxidative destruction of polyunsaturated fatty acids by the effect of free radicals is called non-enzymatic lipid peroxidation and progresses as a chain reaction.

Lipid peroxidation in the organism begins with the loss of an H atom from the conjugated double bonds found in polyunsaturated fatty acids (PUFA) in the membrane structure, especially by the OH radical. This is the initial stage of the radical reaction. In this process, the fatty acid chain becomes a lipid radical (L˙)

and more stable conjugated dienes are formed. In aerobic conditions, lipid peroxyl radicals (LOO˙) are formed as a result of the combination of the conjugated diene with the oxygen molecule. The formation of LOO˙ becomes very important. Because it also affects other polyunsaturated fatty acids in the membrane structure and forms new lipid radicals (L˙). In addition, it itself takes a hydrogen atom and turns into lipid peroxides (LOOH) and can attack membrane proteins. In this way, the reaction proceeds autocatalytically. This represents the advanced stage of lipid peroxidation [25]. Lipid peroxidation ends with the breakdown of lipid peroxides into aldehydes and other carbonyl compounds. In this final stage, biologically effective aldehyde compounds are usually formed. These compounds are metabolized in the cell or spread from the region where they were first formed to the cell and damage other regions. As a result of peroxidation of fatty acids containing three or more double bonds, MDA, which is accepted as an indicator of lipid peroxidation level, is formed. Lipid peroxidation is an irreversible process that directly damages the cell membrane and indirectly damages other cell components through the reactive aldehydes it forms [31]. Under the influence of free radicals, especially in the presence of heavy metals that act as catalysts of reduction-oxidation events, lipid peroxidation in the cell membrane and intracellular membranes increases. This situation is shown in Figure 5.

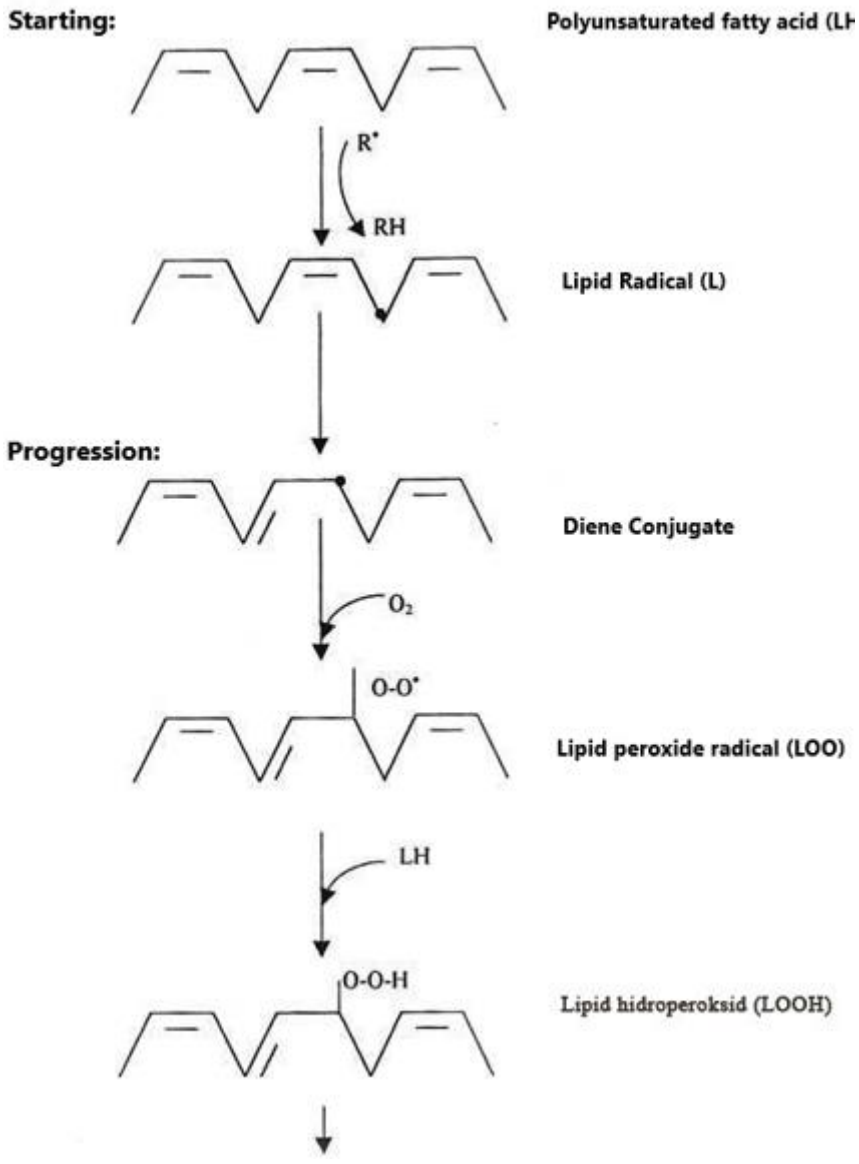

Decomposition products (aldehydes and other carbonyl compounds, ethane, pentane etc.) Figure 5. Lipid Peroxidation Degradation Products

4.4.3. Free Radical Effects on Proteins

Proteins may be less sensitive than polyunsaturated fatty acids, but the degree to which they are affected by radical damage varies depending on the amino acid content of the protein. Especially amino acids containing double bonds such as tryptophan, tyrosine, phenylalanine, histidine and sulfur in their structure such as methionine and cysteine increase the sensitivity of proteins to free radicals [32]. As a result of these reactions, organic radicals and sulfur radical structures with a carbon center are formed. These reactions disrupt the tertiary structure of proteins containing many disulfide bonds such as albumin and immunoglobulin G (IgG). In addition, the ferrous iron (Fe+2) of hemoglobin is oxidized by reacting with superoxide and some other oxidizing agents and loses its ability to carry oxygen, forming methemoglobin [33]. Protein bond and peptide bond breakage are shown in Figure 1.9.

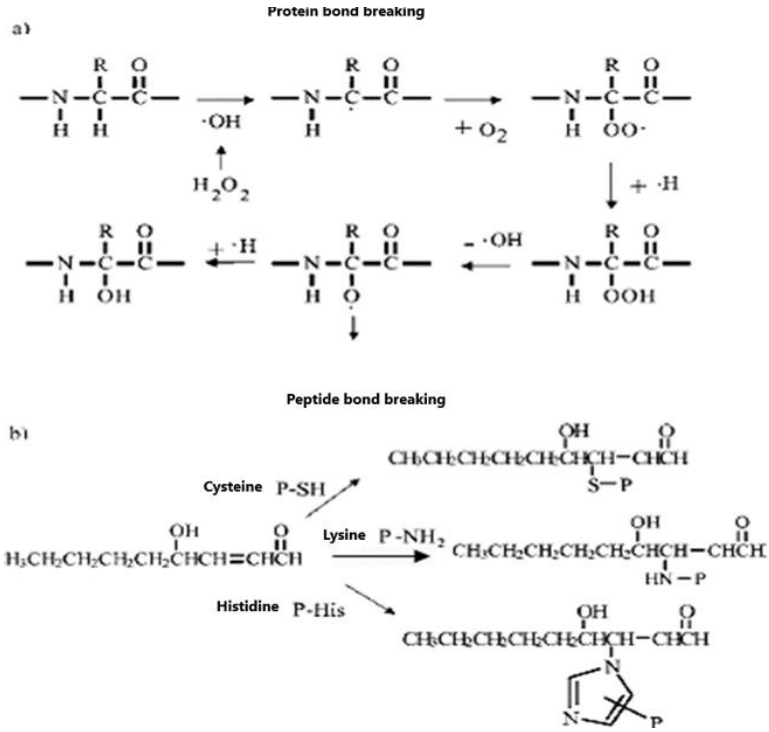

Figure 6. Protein Bond and Peptide Bond Breakage

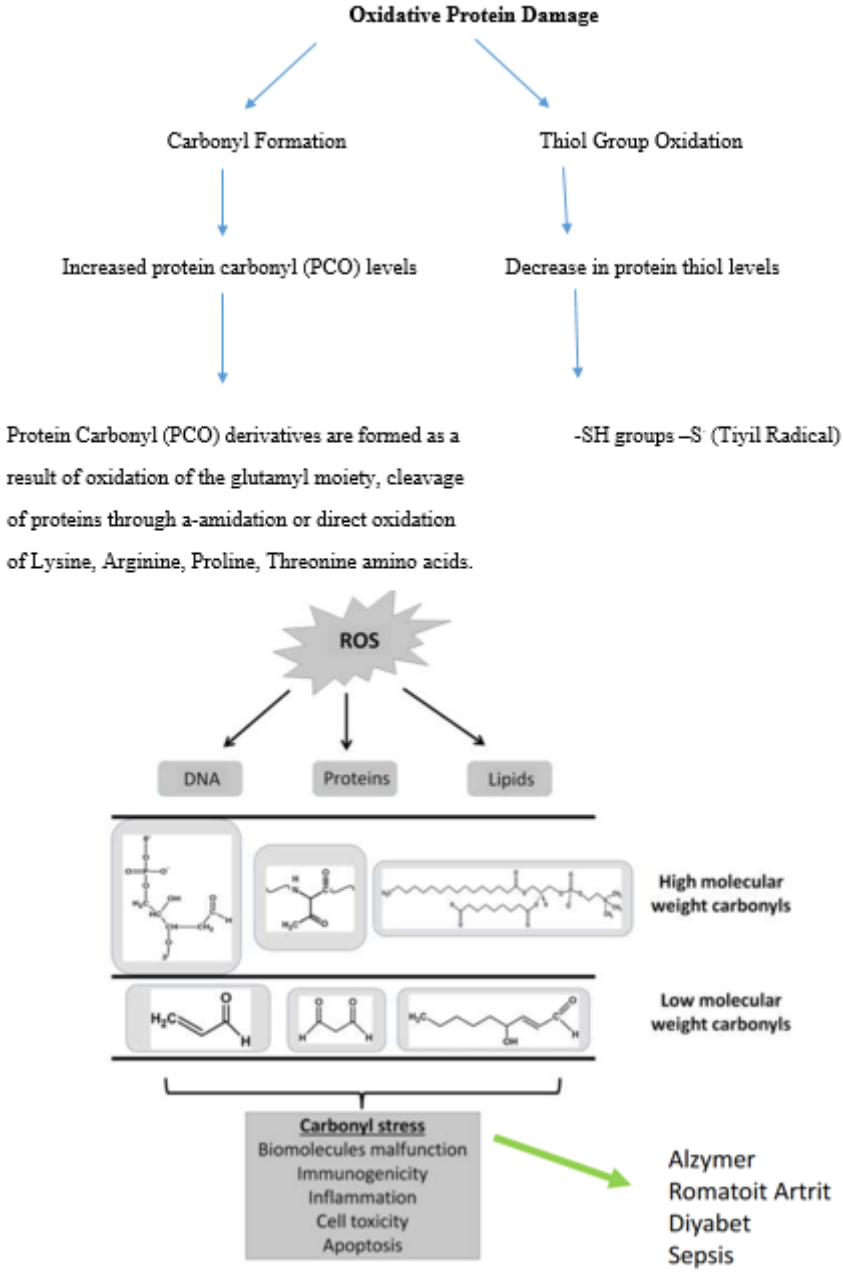

4.4.4. Free Radical Effects on Nucleic Acids and DNA

DNA, a target that is immediately affected by free radicals, can be affected by radicals caused by ionizing radiation, which can cause cell changes and loss.

H2O2 released from activated neutrophils can pass through cell membranes and reach the cell nucleus, where the hydroxyl radical formed reacts rapidly with DNA bases and causes base conversion [34]. If DNA damage is not prevented, it can lead to cell disorder and even cell death. The effects of free radicals on nucleic acids and DNA are shown in Figure 7.

Ionizing Radiation
Toxic Molecules
UV radiation
ROS, RNS, RSS produced as a result of normal metabolism

Sugar Lesions
Base Lesions
Protein DNA cross-links
Single-strand breaks
Single-strand breaks

Cytotoxic
Mutagenic

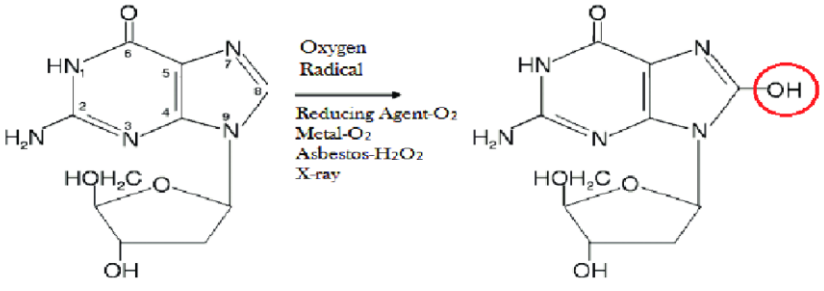

2-deoxy Guanosine

8-hydroxy-2-deoxy Guanosine

8-OhdG can be detected in tissue, serum, urine and other biological materials. Among purines and pyridines, guanine is the most sensitive base to oxidation. This is because it has the lowest ionization potential among other bases. The most important radical that causes damage to biomolecules is the hydroxyl radical. This radical can be produced by various mechanisms including the Fenton reaction of hydrogen peroxide and other endogenous and exogenous ROS metals. The interaction of the hydroxyl radical with a nucleobase such as guanine results in the formation of C8-hydroxyguanine or its nucleoside 8-OhdG. 8-OHdG is formed as a result of the attachment of the hydroxyl radical to the 8th carbon atom of guanine in DNA.

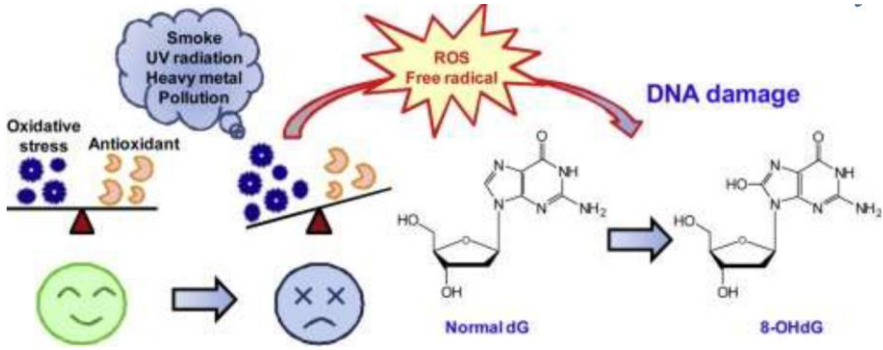

Figure 7. Effects of Free Radicals on Nucleic Acids and DNA

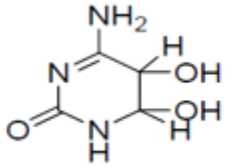

cytosine glycol

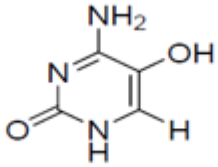

5-hydroxy cytosine

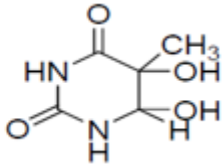

thymine glycol

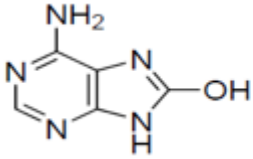

8-hydroxy adenine

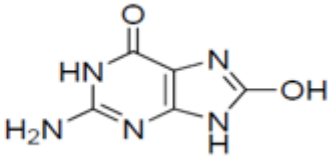

8-hydroxy guanine

Figure 8. Nucleic acid base modifications caused by free radicals and ROS

4.4.5. Free Radical Effect on Carbohydrates

Free radicals also have important effects on carbohydrates. Glucose, mannose and deoxy sugars undergo autooxidation under physiological conditions, producing superoxide and hydrogen peroxide. It is suggested that autooxidation of monosaccharides causes protein cross-linking, causing them to aggregate, as well as thickening of the basement membrane and ultimately the development of cataracts and microangiopathy.

The effects of free radical structures on carbohydrates include polysaccharide depolymerization and especially auto-oxidation of single sugars. Superoxides and oxaldehydes formed as a result of auto-oxidation of single sugars play a role in diseases associated with diabetes and smoking. Oxaldehydes also have an inhibitory effect on cell division due to their binding properties to DNA, RNA and proteins. Therefore, they may also be effective in cancer and aging processes.

Hyaluronic acid, a significant mucopolysaccharide of connective tissue, is abundantly present in intracellular fluid. Oxidation of hyaluronic acid by free radicals has been definitively established in inflammatory joint diseases such as rheumatoid arthritis [35].

Free radicals occur in living organisms during normal metabolic behavior and in pathological stages. Since such free radicals are cleared by cellular protection

mechanisms, ROS production is controlled by antioxidant protection systems. However, sometimes much more reactive oxygen species may occur in cells due to reasons such as metabolism of toxins, excessive oxygen exposure, imbalance of phagocytic activation, and inadequate intake of antioxidant compounds. When more ROS are produced during the process of cellular defense mechanisms cleaning ROS, the phenomenon of "oxidative stress" occurs. Oxidative stress is a condition that disrupts the balance between oxidants and antioxidants, causing cell damage. In addition to cell damage caused by ROS, oxidative stress is thought to contribute to many diseases. Studies have highlighted the importance of free oxygen radicals in clinical cases such as intestinal inflammation [36], ischemia/reperfusion injury [37], atherosclerosis, aging [38], diabetes, Alzheimer's dementia; Parkinson's syndrome [39], problems caused by smoking and air pollution, and lung diseases such as Chronic Obstructive Pulmonary Disease [38]; various cancers; stroke; hypertension; autoimmune disorders such as rheumatoid arthritis and multiple sclerosis; allergies; asthma; septic shock; inflammation; acute pancreatitis; diseases caused by aging, and cataracts [40]. However, while investigating the importance and effects of free radicals on these vital diseases, the importance of distinguishing whether free radical formation is the source or the result of diseases is emphasized.

CONCLUSION

Rapidly developing and constantly advancing technology, radiation, environmental pollution, heavy metals, drugs used in agriculture, and many other factors such as oxygen metabolism in living cells cause the formation of free radicals. It is extremely normal for oxidation to occur in living metabolism. Under normal conditions, oxidants and antioxidants are in balance in the living body. This situation shifts in favor of oxidants as a result of excess formation of oxidants or decrease in antioxidants.

Free radicals are reactive forms of oxygen and damage body cells. For this reason, they pave the way for the emergence of many diseases such as cardiovascular diseases, gastrointestinal diseases, respiratory and excretory disorders, cancer, diabetes, aging, sperm dysfunction and infertility. In order to find a solution to these diseases, it is possible to eliminate the damage caused by free radicals and thus prevent the emergence of diseases. Therefore, it should be ensured that oxidant substances are in balance with antioxidants.

REFERENCES

[1] Ardoin, S. P., Sundy, S. J. 2006. Update on Non-Steroidal Anti-Inflammatory Drugs. Current Opinion in Rheumatology. 18: 221-226.

[2] Halliwell, B. 1991. Reactive Oxygen Species in Living Systems. The American Journal of Medicine. 91: 14-21.

[3] Türe, T. 1998. Akut Miyokard İnfarktüsünde SOD ve GSHPX Enzimleri ile E ve C Vitaminlerinin Düzeyleri. T. C Sağlık Bakanlığı İzmir Atatürk Eğitim Hastanesi Biyokimya Anabilim Dalı, Uzmanlık Tezi, İzmir.

[4] Çevrim, E. 2000. Sigara İçenlerde Antioksidan Enzimler, Ferritin ve Hemoglobin Düzeylerinin Değerlendirilmesi. Dumlupınar Üniversitesi, Fen Bilimleri Enstitüsü, Biyokimya Anabilim Dalı, Yüksek Lisans Tezi, Kütahya pp. 38-40.

[5] Goodyear-Brunch, C., Pierce, J. D. 2002. Oxidative Stress in Critically III Patient. American Journal of Critical Care. 11: 543-551.

[6] Kise, Y., Yoshimura, S., Akieda, K., Umezawa, K., Okada, K., Yoshitake, N., Shiramizu, H., Yamamoto, I., Inokuchi, S. 2004. Acute Oral Selenium Intoxication with Ten Times the Lethal Dose Resulting in Deep Gastric Ulcer. The Journal of Emergency Medicine. 26: 183-187.

[7] Gutterige, J. M.C. 1989. Iron and Oxygen: A Biologically Damaging Mixture. Acta Pediatrica Scandinavica Supplement. 361: 78-85.

[8] Sohal, R. S. 2002. Role of Oxidative Stress and Protein Oxidation in the Aging Process. Free Radical Biology and Medicine. 33: 37-44.

[9] Blokhina, O., Virolainen, E., Fagerstedt, K. V. 2003. Antioxidants, Oxidative Damage and Oxygen Deprivation Stress: A Review, Annals of Botany. 91: 179-194.

[10] Kılınç K., Kılınç, A. 2002. Oksijen Toksisitesinin Araç Molekülleri Olarak Oksijen Radikalleri. Hacettepe Tıp Dergisi. 33: 110-118.

[11] Hasani, A. 1999. Sıçanlarda Kafa Travması Sonrası Artan Serbest Oksijen Radikalleri Üzerine Sevofluranın Etkisi. Marmara Üniversitesi Tıp Fakültesi Anesteziyoloji ve Reanimasyon Anabilim Dalı, İstanbul pp.23-24.

[12] Çakatay, U., Telci A. 2000. Oksidatif Protein Hasarı ve Saptanmasında Kullanılan Markerlar. İstanbul Üniversitesi Tıp Fakültesi Mecmuası. 63: 314-317.

[13] Çelik, S. 2001. APS ile Opere Edilen Tavşanların Kan ve Karaciğer Dokularındaki Serbest Oksijen Radikallerin Antioksidan Enzim Düzeylerinin Tayini. Dumlupınar Üniversitesi, Fen Bilimleri Enstitüsü, Moleküler Biyoloji Anabilim Dalı, Yüksek Lisans Tezi, Kütahya pp. 34-35.

[14] Kavas, G. 1989. Serbest Radikaller ve Organizma Üzerine Etkileri. Türkiye Klinikleri. 9: 1-8.

[15] Abdollahi, M., Ranjbar, A., Shadnia, S., Nikfar, S., Rezaie, A. 2004. Pesticides and Oxidative Stress: A Review, Medical Science and Monitoring. 10: 141-147.

[16] Halliwell, B. 1997. Antioxidants and Human Disease: A General Introduction. Nutrition Reviews. 55: 544-549.

[17] Akkuş, I. 1995. Serbest Radikaller ve Fizyopatolojik Etkileri. Mimoza Yayınları, 5. Sağlık Dizisi 38: 4.

[18] Pham-Huy, L. A., He, H., & Pham-Huy, C. (2008). Free radicals, antioxidants in disease and health. International journal of biomedical science : IJBS, 4(2), 89-96. Retrieved from https://pubmed.ncbi.nlm.nih.gov/23675073

[19] Popiołek, Ł., Rzymowska, J., Kosikowska, U., Hordyjewska, A., Wujec, M., and Malm, A. (2014). Synthesis, antiproliferative and antimicrobial activity of new Mannich bases bearing 1, 2, 4-triazole moiety, Journal of Enzyme Inhibition and Medicinal Chemistry, 29 (6), pp: 786-795

[20] Stief, T. W. 2003. The Physiology and Pharmacology of Singlet Oxygen. Medical Hypothesis. 60: 567-572.

[21] Anglada, J. M., Martins-Costa, M., Francisco, J. S., & Ruiz-Lopez, M. F. (2015). Interconnection of reactive oxygen species chemistry across the interfaces of atmospheric, environmental, and biological processes. Accounts of chemical research, 48(3), 575-583.

[22] Di Mascio, P., Martinez, G. R., Miyamoto, S., Ronsein, G. E., Medeiros, M. H., & Cadet, J. (2019). Singlet molecular oxygen reactions with nucleic acids, lipids, and proteins. Chemical reviews, 119(3), 2043-2086.

[23] Li, B., Liu, S., Lai, C., Zeng, G., Zhang, M., Zhou, M., . . . Li, Z. (2020). Unravelling the interfacial charge migration pathway at atomic level in 2D/2D interfacial Schottky heterojunction for visible-light-driven molecular oxygen activation. Applied Catalysis B: Environmental, 266, 118650.

[24] Wisser, F. M., Duguet, M., Perrinet, Q., Ghosh, A. C., Alves-Favaro, M., Mohr, Y., Farrusseng, D. (2020). Molecular Porous Photosystems Tailored for Long-Term Photocatalytic CO2 Reduction. Angewandte Chemie, 132(13), 5154-5160.

[25] Halliwell, B., Gutteridge, J. M. C. 1990. Role of Free Radicals and Catalytic Metal Ions in Human Disease: An Overview. In: Methods in Enzymology. 186: 1-85.

[26] Weijl, N. I., Cleton F. J., Osanto, S. 1997. Free Radicals and Antioxidants in Chemothraphy-Induced Toxicity. Cancer Treatment Reviews. 23: 209-240.

[27] Moldovan, L., Moldovan, N. I. 2004. Oxygen Free Radicals and Redox Biology of Organalles. Histochemical and Cell Biology. 122: 395-412.

[28] Hallilwell, B., Gutteridge, J. M. C. 1999. Free Radicals in Biology and Medicine. 3rd ed. Oxford University Press. 2: 1059-1094.

[29] Aruoma, O. I. 1998. Free Radicals Oxdative Stress and Antioxidants in Human Health an Disease. Journal of the American Oil Chemist's Society.75: 199-212.

[30] Siems, W. G., Grune, T., Esterbauer, H. 1995. 4-Hydroxynonenal Formation During Ischemia and Reperfusion of Rat Small-Instestine. Life Sciences. 57: 758-789.

[31] Onat, T., Emerk, K., Sözmen, E. Y. 2002. İnsan Biyokimyası. Palme Yayıncılık. Ankara pp. 665-674.

[32] Van Der Vlient, A., O'neill, C. A., Halliwell, B., Cross, C., Kaur, H. 1994. Aromatic Hydroxylation and Phenylalanine and Tyrosine by Peroxynitrite. FEBS Letters. 339: 89-92.

[33] Murray, R. K., Granner, D. K., Mayes, P.A., Rodwell, V. W. 1996. Harper'ın Biyokimyası. pp. 978-975-953-311-3. Barış Kitabevi. İstanbul.

[34] Halliwell, B. 1994. Free Radicals and Antioxidants: A Personal View. Nutrition Reviews. 52: 253-265.

[35] Hawkins, C. L., Davies M. J. 1998. Degradation of Hyaluronic acid, Poly-and Mono-saccharides and model compounds by Hypochlorite: Evidence for Radical Intermediates and Fragmentation. Free Radical Biology and Medicine. 24: 1396-1410.

[36] Cruthirds, D. L., Novak, L., Akhi, K. M., Sanders, P. W., Thompsan, J. A.2003. Mitochondrial Targets of Oxidative Stress During Renal Ischemia/Reperfusion. Archives Biochemistry and Biophysics. 412: 27-33.

[37] Mosley, R. L., Benner, E. J., Kadiu, I., Thomas, M., Boska, M. D. 2006. Neuroinflammation Oxidative Stress and the Pathogenesisi of Parkinson's Disease. Clinical Neuroscience Research. 6: 261-281.

[38] Hipkiss, A.R. 2007. Biological Aspects of Ageing. Psychiatry. 6: 476-479.

[39] Bowler, R. P., Barnes, P. J., Crapo, J. D. 2004. The Role of Oxidative Stres in Chronic Obstructive Pulmonary Disease. Journal of Chronic Obstructive Pulmonary Disease. 1: 255-277.

[40] Anderson, R. A., 2007. Prescribing Antioxidants. Chapter 103, pp.1083-2094. In Rakel: Integrative Medicine, 2nd ed., Saunders.

CHAPTER 18

Cytotoxic potential of *Ferula* (Apiaceae)

***Ela Nur Şimşek Sezer*[1]**

1 Assoc. Prof. Dr., Selçuk University, 0000-0003-2805-7204

Cancer is the second leading cause of death after cardiovascular diseases today. Despite the use of various methods (chemotherapy, radiotherapy, etc.) in cancer treatment, mortality rates are increasing day by day. This situation has led scientists to seek new treatments. More than 60% of the current cytotoxic agents have been obtained directly from natural sources, including plants, marine organisms and microorganisms, or through chemical synthesis based on natural precursor compounds (Newman et al., 2003; Cragg et al., 2005). Plants that have been used in many areas from ancient times to the present and have provided various benefits to humanity are the first solutions that come to mind here. Extracts and/or metabolites obtained from plants are used to treat many types of cancer today. In addition to treatment, plants are evaluated as alternative and complementary treatments. From this point of view, it is essential first to determine the cytotoxic potential of the extracts or metabolites obtained from plants. Cytotoxicity tests are performed on cell cultures to determine whether there is a cytotoxic potential or not. The data obtained from these tests provide preliminary information about the cytotoxic potential of the extract in vitro. Cell-based cytotoxicity studies have become quite preferred due to their ease of application and ability to provide information for in vivo tests.

To investigate the cytotoxic effect, first of all, the plant to be studied must be selected and the extraction must be done. When we look at the past and present, it is seen that there are numerous studies investigating the potential of various plant extracts. Medicinal plants are rich sources of secondary metabolites and have an effective role in cancer treatment or cancer protection. The increasing interest in plant metabolites, especially secondary metabolites, has revealed the therapeutic importance of their biological activities and diversity. Therefore, the demand for effective and safe natural products is increasing. Considering the anticancer roles of secondary metabolites, it is of particular importance to examine the biological activities of plants, reveal their various properties and confirm their therapeutic effects on human health. *Ferula* genus is a genus that has been extensively studied for its cytotoxic potential.

Ferula L. is the largest genus of the Apiaceae family with more than 185 species distributed worldwide (Pimenov, 1993; Akalın et al., 2020). Following a phytochemical examination of over 70 species, the genus *Ferula* has been identified as an excellent source of bioactive chemicals, particularly terpenoid derivatives (Tamemoto et al., 2001; Motai et al., 2004; Iranshahi et al., 2007,2009). Several species of the genus *Ferula* have been reported to be valuable for various biologically active phytochemicals including galactose, arabinose, rhamnose, daucan esters, glucuronic acid, sulphur-containing

derivatives, coumarins, coumarin esters, sesquiterpenes, sesquiterpene lactones and sesquiterpene coumarins (Nazari and Iranshahi, 2011; Asghari et al., 2016; Maggi et al., 2016; Razavi et al., 2016). The genus *Ferula* L. is a rich source of biologically active secondary metabolites. For this reason, numerous biological activity tests have been conducted on extracts and compounds isolated from *Ferula* species in the last two decades. Plants of this genus have been used in traditional medicine since ancient times, mostly as contraceptives, antispasmodics, antipyretics, anthelmintics, antidiarrhoeals, anticarcinogenics, antidiabetics, wound healing agents, and aphrodisiacs. In addition, *Ferula* species have been reported to be used in traditional medicine for skin infections and hysteria (Sadraei et al., 2001; Sayyah et al., 2002; Iranshahi et al., 2008; Gamal-Eldeen and Hegazy, 2010; Iranshahy and Iranshahi, 2011; Nazari and Iranshahi, 2011; Yaqoob et al., 2016). According to a number of studies, extracts from *Ferula* species exhibit a broad spectrum of biological activities, such as antimicrobial, antioxidant, antibacterial, anti-inflammatory, and anticancer effects (Motai et al. 2004; Poli et al., 2005; Geroushi et al., 2011; Ibraheim et al., 2012; Huang et al., 2013; Sahpaz et al., 2013; Znati et al., 2014; Iranshahi et al., 2014; Zang et al., 2016; Bagheri et al., 2017; Bouratoua et al., 2018; Wang et al., 2018; Mohammadhosseini et al., 2019). In this chapter, the examinations conducted with the *Ferula* species in recent years are compiled and presented.

CYTOTOXICITY STUDIES ABOUT GENUS

Throughout history, researchers have looked at the cytotoxic effects of many plant species. Among these species is the *Ferula* species. The cytotoxic activity of extracts, essential oils, and different metabolites extracted from different *Ferula* species using various techniques and solvents has been studied in recent years, based on our literature review. From this vantage point, we can state that there is still much to be done and that interest in the cytotoxic effects of *Ferula* species is growing. Table 1 summarises the *Ferula* species, preparation, and cell lines that have been investigated for their cytotoxic effects during the last years.

Table 1. *Ferula* species and cell lines used in cytotoxic activity studies between 2012 and 2024.

Species and extract/phytochemical	Part	Cell Line	Cytotoxicity test	Reference
F.assafoetida	Resin	HepG2 and L929	MTT	Sadooghi et al., 2013
F.assafoetida	Resin	HOS-CRL	MTT	Shafri et al., 2015
*F.assafoetida (*sesquiterpene coumarin-gummosin*)*	Gum	MCF-7 and PC-3	Ala-marB-lue	Iranshahy et al., 2019
F.assafoetida ethanol extract	Upper part	PC12 and MCF7	MTT	Abroudi et al., 2020
F.assafoetida ethanol extract	Herb	SKOV-3 and MIAPaca-2	MTT	Aali et al., 2021
F.assafoetida hydroalcoholic extracts	Resin	K562	MTT	Talebpour et al., 2022
F.assafoetida essential oil	Gum	MCF-7 and MDA-MB-468	MTT	Moulazadeh et al., 2022
F.assafoetida extracts	Gum	CT-26, HT-29, SW-742 and WiDr	MTT	Ali et al., 2023
F.assafoetida ethanolic extract	Resin	KB and L929	MTT	Gavanji et al., 2023
F.assafoetida essential oil	Resin	SW620 and CT26	MTT	Verma et al., 2023
F. assafoetida oleo-gum	Resin	HT-29	MTT	Elarabany et al., 2023
F. caspica (Sesquiterpene Coumarins, Chromones, and Acetophenone Derivatives)	Root	COLO 205, K-562, and MCF-7	MTS	Kuran et al., 2024
F. communis extracts	Aerial parts (flower, fruit, and stem)	HL-60	Trypan blue exclusion	Rahali et al., 2019
F.communis acetone and water extracts	Root	MCF-7,HeLa and Saos-2	MTT	Maiuolo et al., 2022

F.communis ethanol and methanol extracts	Leaf	MCF-7 and MDA-MB-231	Trypan blue exclusion	Kavaz and Faraj 2023
F.communis acetone and water extracts	Root	HeLa	Alamar Blue	Ulusu, 2023
F. flabelliloba (Conferone-coumarin)	Root	ATL	Alamar blue	Rafatpanah et al., 2023
F. gummosa ethanolic extract	Seed and Gum	BHY, SKMEL-3 and MCF-7	MTT	Gudarzi et al.,2015
F. gummosa gum	Root	ACHN	MTT	Hosseini et al., 2017
F. gummosa extract	Root	PC12 and N2a	MTT	Sadeghnia et al., 2017
F. gummosa gum	Resin	NB4 and HL-60	AlamarBlue	Moradzadeh et al., 2017
F.gummosa	Resin	HeLa	MTT	Forouzmand et al., 2018
F.gummosa	Gum	U87	MTT	Afshari et al.,2022
F. gummosa	Gum	PC-3	MTT	Eizadifard et al., 2023
F.gummosa	Gum	HepG2	MTT	Bashiri-Nahnjeh et al.,2023
F. gummosa	Gum	SW-480	MTT	Bahavar and Tafrihi 2023
F. gummosa gum	Root	A375 and HEK293T	MTT	Eizadifard and Tafrihi 2024
F.gummosa	Root	MCF-7 and L929	MTT	Rashidi et al., 2024
F.heuffelii chloroform and methanol extracs and metabolites	Underground parts	HeLa, K562 and MCF-7	MTT	Pavlovic et al., 2015
F. hermonis hexane extract	Root	MDA-MB-231 and LoVo	MTT	Abutaha et al.,2019
F. hezarlalehzarica methanol extracts and fractions	Aerial parts	HeLa, HepG2, K562, Raji and EL4	MTT	Asemani et al., 2018
F. hezarlalehzarica dichloromethane extract	Root	PANC-1	WST-8	Alilou et al.,2020

F. huber-morathii (sesquiterpene coumarin ethers *)*	Root	COLO 205, MCF-7, K-562, and HUVEC	MTS	Eruçar et al., 2023
F. lapidosa (iridoid glicosite-ferlapioside)	Root	HL-60, A549, SMMC-7721, MDA-MB-231 and SW480	MTS	Li et al., 2024
F.lutea extracts and compounds	Flower	K562	MTT	Znati et al., 2014
F. lutea essential oil	Root	HT-29 and HCT-116	MTT	Ben Salem et al., 2016
F. macrecolea essential oil	Aerial part	J774-A1	MTT	Mahmoudvand et al., 2022
F.mervynii sesquiterpene esters	Root	Colo 205, K562,MCF-7 and HUVEC	MTT	Yazıcı Bektaş et al., 2023
F. persica essential oil	Gum	CT26 and Vero	MTT	Hosseinzadeh et al., 2020
F.persica var. *persica* and *F.hezarlalehzarica* methanol extract and fractions	Aerial part	HepG2, A549,HT29,MCF-7 and MDBK	MTT	Hajimehdipoor et al., 2012
F.pseudalliacea methanolic extract	Root	HCT-116	MTT	Bamehr et al., 2018
F. tabasensis ethyl acetate extract, methanol extract, and fractions	Aerial roots	J774-A1	MTT	Saraei et al., 2023
F.tenuissima (sesquiterpene esters) hexane, chloroform (CHCl3), and methanol (MeOH) extracts	Root	PC-3	WST	Aydoğan et al., 2019
F. tingitana essential oil	Flower, leaves	MCF7, HeLa and HepG2	sulforhodamine B	Elghwaji et al., 2017
F. communis subsp. *communis* *F. drudeana* *F. duranii*	Root	PC-3	WST	Baykan et al., 2019

F. elaeochytris *F. halophila* *F. huber-morat-hii* *F. lycia* *F. orientalis* *F. rigidula* *F. szowitsiana* *F. tenuissima* *F. tingitana* *n-hexane, chlo-roform, methanol extracts*				
F. latisecta *F. ovina* *F. flabelliloba*	Root	HCT116,HeLa, A549 and A2780	Alamar Blue	Soltani et al., 2019

When the table is evaluated in detail, it is seen that extracts/essential oils obtained from different species have been studied in cell lines of various origins. When the cell lines studied according to the literature review are evaluated in terms of cancer types; cytotoxic effects of *Ferula* species on various cancer types have been studied. These are; liver, breast, prostate, ovary, uterine cancer, colorectal cancer, leukaemia, lymphoma, osteosarcoma, oral squamous cancer, neuroblastoma and renal carcinoma. The most frequently used cell lines in current studies are MCF-7, HeLa, HepG2 and K562. On the other hand, when we look at the cancer types in which the cytotoxic effects of *Ferula* species are studied the most, it is seen that the order is colon, breast, leukaemia, cervix and liver cancers (Figure1).

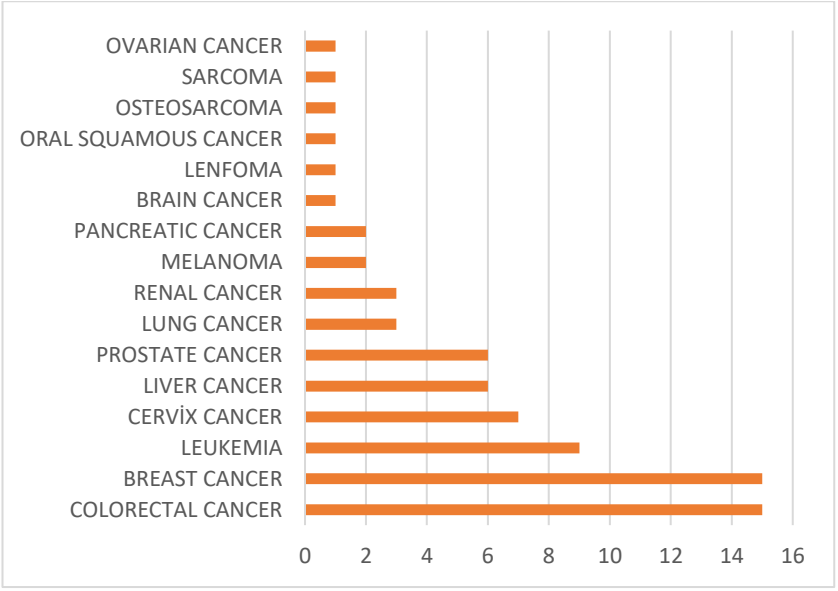

Figure 1. The sources and dispersion of cell lines used to study *Ferula* species from 2012 to 2024 are depicted in this pie chart.

When the studies about the *Ferula* species are examined, it is seen that although different plant parts have been used to reveal their cytotoxic potential, mostly the root and resin are used in extraction. On the other hand, although different cytotoxicity tests have been preferred to reveal the cytotoxic potential of the species (Tryphan blue, Alamar blue, MTS, WST, sulforhodamine B), the most commonly used cytotoxicity test is the MTT test. As given in the table, it is seen the cytotoxic effects of *Ferula* extracts and their fractions as well as their metabolites have been investigated. Especially the cytotoxic effects of sesquiterpene coumarins, chromones, acetophenone derivatives and iridoid glycosides have been investigated and reported (Iranshahy et al., 2019; Aydoğan et al., 2019; Yazıcı Bektaş et al., 2023; Eruçar et al., 2023; Rafatpanah et al., 2023; Kuran et al., 2024; Li et al., 2024).

This review therefore makes it abundantly evident that *Ferula* species possess a considerable capacity for cytotoxic effects. Research involving species from the genus has garnered a lot of interest in recent years. However, the impact of the plant on anticancer pathways will become more clear as more research of this kind is conducted.

REFERENCES

1. Aali, E., Aamadi, S., Bajelan, A., & Ghaebi, M. (2021). Cytotoxic effects of methanolic extract of *Ferula assa-foetida* on Skov-3 and Mia Paca-2 cells. Annals of Cancer Research and Therapy, 29(1), 110-113.
2. Abroudi, M., Fard, A. G., Dadashizadeh, G., Gholami, O., & Mahdian, D. (2020). Antiproliferative effects of *Ferula assa-foetida*'s extract on PC12 and MCF7 cancer cells. Int J Biomed Engg Clin Sci, 6(3), 60-67.
3. Abutaha, N., Nasr, F. A., Al-Zharani, M., Alqahtani, A. S., Noman, O. M., Mubarak, M., ... & Wadaan, M. A. (2019). Effects of hexane root extract of *Ferula hermonis* boiss. On human breast and colon cancer cells: an in vitro and in vivo study. BioMed Research International, 2019(1), 3079895.
4. Afshari, A. R., Mousavi, S. H., Mousavi, G., Moghadam, S. D., Maghrouni, A., Javid, H., ... & Hosseini, A. (2022). *Ferula gummosa* gum exerts cytotoxic effects against human malignant glioblastoma multiforme in vitro. Research in Pharmaceutical Sciences, 17(5), 585-593.
5. Akalın, E., Tuncay, H. O., Olcay, B., & Miski, M. (2020). A New *Ferula* (Apiaceae) Species from Southwest Anatolia: Ferula pisidica Akalın & Miski. Plants, 9(6), 740.
6. Ali, A. N. M., Raghad, J. F., Nuaman, R. S., Mahmod, Z. S., & Alamery, N. D. (2023). Anticancer Potentiality of *Ferula assa-foetida* Gum Extract against CT-26, HT-29, SW742 and WiDr Colorectal Cancer Cell Lines. South Asian Res J Bio Appl Biosci, 5(1), 1-6.
7. Alilou, M., Dibwe, D. F., Schwaiger, S., Khodami, M., Troppmair, J., Awale, S., & Stuppner, H. (2020). Antiausterity activity of secondary metabolites from the roots of *Ferula hezarlalehzarica* against the PANC-1 human pancreatic cancer cell line. Journal of natural products, 83(4), 1099-1106.
8. Asemani, Y., Azadmehr, A., Hajiaghaee, R., & Amirghofran, Z. (2018). Anticancer potential of *Ferula hezarlalehzarica* Y. Ajani fraction in Raji lymphoma cell line: induction of apoptosis, cell cycle arrest, and changes in mitochondrial membrane potential. Daru Journal of Pharmaceutical Sciences, 26, 143-154.
9. Asghari J, Atabaki V, Baher E, Mazaheritehrani M. (2016). Identification of sesquiterpene coumarins of oleo-gum resin of *Ferula assa-foetida* L. from the Yasuj region. Nat Prod Res, 30:350-353.
10. Aydoğan, F., Baykan, Ş., & Bütüner, B. D. (2019). Cytotoxic activity of sesquiterpenoids isolated from endemic *Ferula tenuissima* hub.-mor & peşmen. Turkish Journal of Pharmaceutical Sciences, 16(4), 476.
11. Bagheri, S. M., Abdian-Asl, A., Moghadam, M. T., Yadegari, M., Mirjalili, A., Zare-Mohazabieh, F., & Momeni, H. (2017). Antitumor effect of *Ferula assa foetida* oleo gum resin against breast cancer induced by 4T1 cells in BALB/c mice. Journal of Ayurveda and integrative medicine, 8(3), 152-158.

12. Bahavar, P., & Tafrihi, M. (2024). Exploring the anticancer properties of the gum of *Ferula gummosa*: impact on cytotoxicity, caspase 3/7 activity and apoptosis, and gene expression in SW-480 cells. International Journal of Environmental Health Research, 34(3), 1810-1823.

13. Bamehr, H., Saidijam, M., Dastan, D., Amini, R., Pourjafar, M., & Najafi, R. (2019). *Ferula pseudalliacea* induces apoptosis in human colorectal cancer HCT-116 cells via mitochondria-dependent pathway. Archives of physiology and biochemistry, 125(3), 284-291.

14. Bashiri-Nahnjeh, M., Sarihi, A., Ebadi, A., Dastan, D., & Mohammadi, M. (2023). In silico molecular modeling, neuro-behavioral profile, and toxicity assessment of the essential oil of *Ferula gummosa* Boiss. As an anti-seizure agent. Journal of Ethnopharmacology, 309, 116347.

15. Baykan, S., Aydogan, F., Ozturk, M. B., Debelec-Butuner, B., Yengin, Ç., & Ozturk, B. (2020). Ferutinin content and cytotoxic effects of various *Ferula* L. species on prostate cancer (PC-3) cell line. J. Res. Pharm, 24, 142-149.

16. Ben Salem, S., Znati, M., Jabrane, A., Casanova, J., & Ben Jannet, H. (2016). Chemical composition, antimicrobial, anti-acetylcholinesterase and cytotoxic activities of the root essential oil from the Tunisian *Ferula lutea* (Poir.) Maire (Apiaceae). Journal of Essential Oil Bearing Plants, 19(4), 897-906.

17. Bouratoua, A., Khalfallah, A., Bensouici, C., Kabouche, Z., Alabdul Magid, A., Harakat, D., ... & Kabouche, A. (2018). Chemical composition and antioxidant activity of aerial parts of *Ferula longipes* Coss. ex Bonnier and Maury. Natural product research, 32(16), 1873-1880.

18. Cragg, G. M., Kingston, D. G., & Newman, D. J. (2005). Anticancer agents from natural products. CRC press.

19. Eizadifard, F., & Tafrihi, M. (2024). Unveiling the Cytotoxic and Inhibitory Effects of *Ferula gummosa* Gum on A-375 Skin Cancer Cells: An in Vitro Study. Jentashapir Journal of Cellular and Molecular Biology, 15(4).

20. Eizadifard, F., Tafrihi, M., & Mohadjerani, M. (2023). Antioxidant, cytotoxic, and genotoxic potentials of the gum of *Ferula gummosa* Boiss on PC-3 cells. Avicenna Journal of Phytomedicine, 13(3), 316.

21. Elarabany, N., Hamad, A., & Alzamel, N. M. (2023). Antitumor and Phytochemical Properties of *Ferula assa-foetida* L. Oleo-Gum–Resin against HT-29 Colorectal Cancer Cells In Vitro and in a Xenograft Mouse Model. Molecules, 28(24), 8012.

22. Elghwaji, W., El-Sayed, A. M., El-Deeb, K. S., & ElSayed, A. M. (2017). Chemical composition, antimicrobial and antitumor potentiality of essential oil of *Ferula tingitana* L. Apiaceae grow in Libya. Pharmacognosy magazine, 13(Suppl 3), S446.

23. Eruçar, F. M., Kuran, F. K., Altıparmak Ülbegi, G., Özbey, S., Karavuş, Ş. N., Arcan, G. G., ... & Miski, M. (2023). Sesquiterpene coumarin ethers with selective cytotoxic activities from the roots of *Ferula huber-morathii* Peşmen (Apiaceae) and unequivocal determination of the absolute stereochemistry of samarcandin. Pharmaceuticals, 16(6), 792.

24. Forouzmand, S. H., Mousavi, S. H., Vazifedan, V., Nourbakhsh, M., Chamani, J., Hoseini, A., & Fanipakdel, A. (2018). Synergistic effects of *Ferula gummosa* and radiotherapy on induction of cytotoxicity in HeLa cell line. Avicenna Journal of Phytomedicine, 8(5), 439.

25. Gamal-Eldeen AM, Hegazy MEF. (2010). A crystal lapiferin derived from *Ferula vesceritensis* induces apoptosis pathway in MCF-7 breast cancer cells. Natl Prod Res, 24:246-257.

26. Gavanji S., Bakhtari A., Baghshahi H., Hamami Chamgordani Z., (2023). Evaluation of the Cytotoxicity effects of ethanolic extract of *Ferula assafoetida* resin on oral Squamous Cells Carcinoma (KB) compared with L929 cells; The New Armenian Medical Journal. 17(2): 14-20.

27. Geroushi, A., Auzi, A. A., Elhwuegi, A. S., Elzawam, F., Elsherif, A., Nahar, L., & Sarker, S. D. (2011). Antiinflammatory sesquiterpenes from the root oil of *Ferula hermonis*. Phytotherapy Research, 25(5), 774-777.

28. Gudarzi, H., Salimi, M., Irian, S., Amanzadeh, A., Mostafapour Kandelous, H., Azadmanesh, K., & Salimi, M. (2015). Ethanolic extract of *Ferula gummosa* is cytotoxic against cancer cells by inducing apoptosis and cell cycle arrest. Natural product research, 29(6), 546-550.

29. Hajimehdipoor, H., Esmaeili, S., Ramezani, R., Jafari Anaraki, M., & Mosaddegh, M. (2012). The cytotoxic effects of *Ferula* persica var. persica and *Ferula hezarlalehzarica* against HepG2, A549, HT29, MCF7 and MDBK cell lines. Iranian Journal of Pharmaceutical Sciences, 8(2), 113-117.

30. Hosseini, A., Bakhtiari, E., Rad, A. K., Shahraki, S., Mousavi, S. H., Havakhah, S., & Amiri, M. S. (2017). The evaluation and comparing of cytotoxic effects of *Ferula gummosa* gum, *Scutellaria lindbergii*, *Kelussia odoratissima* and *Artemisia kopetdaghensis* extracts on ACHN cell line. Iranian Journal of Pharmaceutical Research: IJPR, 16(3), 1104.

31. Hosseinzadeh, N., Shomali, T., Hosseinzadeh, S., Raouf Fard, F., Pourmontaseri, M., & Fazeli, M. (2020). Green synthesis of gold nanoparticles by using *Ferula persica* Willd. gum essential oil: production, characterization and in vitro anti-cancer effects. Journal of Pharmacy and Pharmacology, 72(8), 1013-1025.

32. Huang, J., Han, H. Y., Li, G. Y., Wang, H. Y., Zhang, C., Zhang, K., ... & Wang, J. H. (2013). Two new terpenoid benzoates with antitumor activity from the roots of *Ferula dissecta*. Journal of Asian natural products research, 15(10), 1100-1106.

33. Ibraheim, Z. Z., Abdel-Mageed, W. M., Dai, H., Guo, H., Zhang, L., & Jaspars, M. (2012). Antimicrobial antioxidant daucane sesquiterpenes from *Ferula hermonis* Boiss. Phytotherapy Research, 26(4), 579-586.

34. Iranshahi, M., Arfa, P., Ramezani, M., Jaafari, M. R., Sadeghian, H., Bassarello, C., ... & Pizza, C. (2007). Sesquiterpene coumarins from *Ferula szowitsiana* and in vitro antileishmanial activity of 7-prenyloxycoumarins against promastigotes. Phytochemistry, 68(4), 554-561.

35. Iranshahi, M., Mojarab, M., Sadeghian, H., Hanafi-Bojd, M. Y., & Schneider, B. (2008). Polar secondary metabolites of *Ferula persica* roots. Phytochemistry, 69(2), 473-478.

36. Iranshahi, M., Rezaee, R., Sahebkar, A., Bassarello, C., Piacente, S., & Pizza, C. (2009). Sesquiterpene coumarins from the fruits of *Ferula badrakema*. Pharmaceutical biology, 47(4), 344-347.

37. Iranshahy, M., & Iranshahi, M. (2011). Traditional uses, phytochemistry and pharmacology of asafoetida (*Ferula* assa-foetida oleo-gum-resin)—A review. Journal of ethnopharmacology, 134(1), 1-10.

38. Iranshahi, M., Barthomeuf, C., Bayet-Robert, M., Chollet, P., Davoodi, D., Piacente, S., ... & Sahebkar, A. (2014). Drimane-type sesquiterpene coumarins from *Ferula gummosa* fruits enhance doxorubicin uptake in doxorubicin-resistant human breast cancer cell line. Journal of Traditional and Complementary Medicine, 4(2), 118-125.

39. Iranshahy, M., Farhadi, F., Paknejad, B., Zareian, P., Iranshahi, M., Karami, M., & Abtahi, S. R. (2019). Gummosin, a sesquiterpene coumarin from *Ferula assa-foetida* is preferentially cytotoxic to human breast and prostate cancer cell lines. Avicenna Journal of Phytomedicine, 9(5), 446.

40. Kavaz, D., & Faraj, R. (2023). Investigation of composition, antioxidant, antimicrobial and cytotoxic characteristics from Juniperus sabina and *Ferula communis* extracts. Scientific reports, 13(1), 7193.

41. Kuran, F. K., Altıparmak Ülbegi, G., Arcan, G. G., Eruçar, F. M., Karavuş, Ş. N., Aksoy Sağırlı, P., ... & Miski, M. (2024). Sesquiterpene Coumarins, Chromones, and Acetophenone Derivatives with Selective Cytotoxicities from the Roots of *Ferula caspica* M. Bieb.(Apiaceae). Pharmaceuticals, 17(10), 1254.

42. Li, X. X., Khasanova, K. I., Shang, J. H., Babekov, A. U., Li, W. J., Li, J. J., ... & Zhang, Y. J. (2024). Ferlapioside: a new bromine substituted iridoid glycoside from the roots of *Ferula lapidosa* Korovin. Natural Product Research, 1-8.

43. Maggi F, Papa F, Dall'Acqua S, Nicoletti M. (2016). Chemical analysis of essential oils from different parts of *Ferula communis* L. growing in central Italy. Nat Prod Res, 30:806-813.

44. Mahmoudvand, H., Yadegari, J. G., Khalaf, A. K., Hashemi, M. J., Dastyarhaghighi, S., & Salimikia, I. (2022). Chemical composition, antileishmanial,

and cytotoxic effects *Ferula macrecolea* essential oil against *Leishmania tropica*. Parasite Epidemiology and Control, 19, e00270.

45. Maiuolo, J., Musolino, V., Guarnieri, L., Macrì, R., Coppoletta, A. R., Cardamone, A., ... & Mollace, V. (2022). *Ferula communis* L.(Apiaceae) Root Acetone-Water Extract: Phytochemical Analysis, Cytotoxicity and In Vitro Evaluation of Estrogenic Properties. Plants, 11(15), 1905.

46. Mohammadhosseini, M., Venditti, A., Sarker, S. D., Nahar, L., & Akbarzadeh, A. (2019). The genus *Ferula*: Ethnobotany, phytochemistry and bioactivities–A review. Industrial crops and products, 129, 350-394.

47. Moradzadeh, M., Sadeghnia, H. R., Mousavi, S. H., Mahmoodi, M., & Hosseini, A. (2017). *Ferula gummosa* gum induces apoptosis via ROS mechanism in human leukemic cells. Cellular and Molecular Biology, 63(11), 17-22.

48. Motai, T., Daikonya, A., & Kitanaka, S. (2004). Sesquiterpene coumarins from Ferula fukanensis and nitric oxide production inhibitory effects. Journal of natural products, 67(3), 432-436.

49. Moulazadeh, A., Ranjbar, R., Dakhili Ardestani, A., Ranjbar, K., Farjadfar, A., Kouhpayeh, S. A., ... & Najafipour, S. (2022). Cytotoxic effects of Trachyspermum ammi and *Ferula assafoetida* on MCF-7 and MDA-MB-468 breast cancer cell lines. Beni-Suef University Journal of Basic and Applied Sciences, 11(1), 147.

50. Nazari ZE, Iranshahi M. (2011). Biologically active sesquiterpene coumarins from *Ferula* species. Phytother Res, 25:315-323.

51. Newman, D. J., Cragg, G. M., & Snader, K. M. (2003). Natural products as sources of new drugs over the period 1981− 2002. Journal of natural products, 66(7), 1022-1037.

52. Pavlović, I., Radenković, M., Branković, S., Milenković, M. T., Niketić, M., Ušjak, L., & Petrović, S. (2022). Spasmolytic, gastroprotective and antioxidant activities of dry methanol extract of *Ferula heuffelii* underground parts. Chemistry & Biodiversity, 19(5), e202200047.

53. Pimenov, M. G. (1993). The Genera of the Umbelliferae: A Nomenclator. Royal Botanic Gardens, Kew and London Botanical Garden of Moscow University, 156.

54. Poli, F., Appendino, G., Sacchetti, G., Ballero, M., Maggiano, N., & Ranelletti, F. O. (2005). Antiproliferative effects of daucane esters from *Ferula communis* and *F. arrigonii* on human colon cancer cell lines. Phytotherapy Research: An International Journal Devoted to Pharmacological and Toxicological Evaluation of Natural Product Derivatives, 19(2), 152-157.

55. Rafatpanah, H., Golizadeh, M., Mahdifar, M., Mahdavi, S., Iranshahi, M., & Rassouli, F. B. (2023). Conferone, a coumarin from *Ferula flabelliloba*, induced

toxic effects on adult T-cell leukemia/lymphoma cells. International Journal of Immunopathology and Pharmacology, 37, 03946320231197592.

56. Rahali, F. Z., Kefi, S., Bettaieb Rebey, I., Hamdaoui, G., Tabart, J., Kevers, C., ... & Hamrouni Sellami, I. (2019). Phytochemical composition and antioxidant activities of different aerial parts extracts of *Ferula communis* L. Plant Biosystems-An International Journal Dealing with all Aspects of Plant Biology, 153(2), 213-221.

57. Rashidi, R., Roohbakhsh, A., Mohtashami, L., Mobasheri, L., Kheradmand, H., Amiri, M. S., ... & Mousavi, S. H. (2024). Cytotoxic and apoptotic effects of *Ferula gummosa* Boiss: extract on human breast adenocarcinoma cell line. Molecular Biology Reports, 51(1), 592.

58. Razavi SM, Nahar L, Talischi H, Sarker SD. (2016). Ferulone A and ferulone B: two new coumarin esters from *Ferula orientalis* L. roots. Nat Prod Res, 30:2183-2189.

59. Sadeghnia, H. R., Rajabian, A., Ghorbani, A., Moradzadeh, M., & Hosseini, A. (2017). Effects of standardized extract of *Ferula gummosa* root on glutamate-induced neurotoxicity. Folia neuropathologica, 55(4), 340-346.

60. Sadooghi, S. D., Nezhad Shahrokh Abadi, K., & Zafar Balanzhad, S. (2013). Investigating the cytotoxic effects of ethanolic extract of *Ferula assa-foetida* resin on HepG2 cell line. Feyz Medical Sciences Journal, 17(4), 323-330.

61. Sadraei, H., Asghari, G. R., Hajhashemi, V., Kolagar, A., & Ebrahimi, M. (2001). Spasmolytic activity of essential oil and various extracts of *Ferula gummosa* Boiss. on ileum contractions. Phytomedicine, 8(5), 370-376.

62. Sahpaz, S., Neut, C., Abedini, A., & Miski, M. (2013). Antimicrobial activity of the sesquiterpene esters of *Ferula halophila* Peşmen. Planta Medica, 79(10), PN19.

63. Saraei, S., Soozangar, N., Miran, M., Ghaffarifar, F., Mohammadi-Ghalehbin, B., Molaei, S., & Asfaram, S. (2023). In vitro Evaluation of the Potent Antileishmanial Activity of *Ferula tabasensis* Alone or in Combination with Shark Cartilage Extract Against the Standard Iranian Strain of Leishmania major (MRHO/IR/75/ER). Iranian Journal of Pharmaceutical Research: IJPR, 22(1).

64. Sayyah, M., Mandgary, A., & Kamalinejad, M. (2002). Evaluation of the anticonvulsant activity of the seed acetone extract of *Ferula gummosa* Boiss. against seizures induced by pentylenetetrazole and electroconvulsive shock in mice. Journal of ethnopharmacology, 82(2-3), 105-109.

65. Shafri, M. A. M., Yusof, F. A., & Zain, A. Z. M. (2015). In vitro cytotoxic activity of *Ferula assafoetida* on osteosarcoma cell line (HOS CRL). Jurnal Teknologi, 77(3).

66. Soltani, S., Amin, G., Salehi-Sourmaghi, M. H., & Iranshahi, M. (2019). Histone deacetylase inhibitory and cytotoxic activities of the constituents from the roots of three species of *Ferula*. Iranian Journal of Basic Medical Sciences, 22(1), 93.

67. Talebpour, A., Alipour, R., Sajjadi, S. M., Osmani, F., & Sarab, G. A. (2022). In Vitro cytotoxicity of *Ferula asafoetida* Gum extract on human chronic myelogenous leukemia K562 cells. Pharmaceutical Chemistry Journal, 56(2), 245-253.

68. Tamemoto K, Takais Y, Chen B, Kawazoe K, Shibata H, Higuti T, Honda G, Ito M, Takeda Y, Kodzhimatov OK, Ashurmetov O. (2001). Sesquiterpenoids from the fruits of *Ferula kuhistanica* and antibacterial activity of the constituents of *F. kuhistanica*. Phytochemistry 2001, 58:763–767.

69. Ulusu, F. (2023). In vitro evaluation of antioxidant and cytotoxic activities on human cervical cancer cells in three different plant extracts from Turkey. Journal of Scientific Reports-A, (054), 338-352.

70. Verma, S., Joshi, S., Kothari, V., & Seshadri, S. (2023). Anti-proliferative and apoptotic potential of *Ferula asafoetida*'s essential oil on Colon Cancer via inhibiting NF-kB and TNF-alpha receptors pathway. Iranian Journal of Colorectal Research, 11(1), 15-21.

71. Yaqoob U, Nawchoo IA, Ahmad M. (2016). Phytochemical screening of the root tuber extracts of *Ferula jaeschkeana* vatke. J Essent Oil Bear Pl, 19:208-211.

72. Yazici Bektas, N., Altiparmak Ulbegi, G., Aksoy Sagirli, P., & Miski, M. (2023). Novel Cytotoxic Sesquiterpene Ester Derivatives from the Roots of *Ferula mervynii*. Chemistry & Biodiversity, 20(3), e202201058.

73. Wang, J., Gao, Y., Wang, H., Chen, L., Cao, L., Xu, J., ... & Si, J. (2018). Apoptosis induction and cell cycle arrest induced by Sinkiangenone B, a novel phenylpropanoid derivative from the resin of *Ferula sinkiangensis* KM Shen. RSC advances, 8(8), 4093-4103.

74. Zhang, X., Lin, D., Jiang, R., Li, H., Wan, J., & Li, H. (2016). Ferulic acid exerts antitumor activity and inhibits metastasis in breast cancer cells by regulating epithelial to mesenchymal transition. Oncology Reports, 36(1), 271-278.

75. Znati, M., Ben Jannet, H., Cazaux, S., & Bouajila, J. (2014). Chemical composition, biological and cytotoxic activities of plant extracts and compounds isolated from *Ferula lutea*. Molecules, 19(3), 2733-2747.

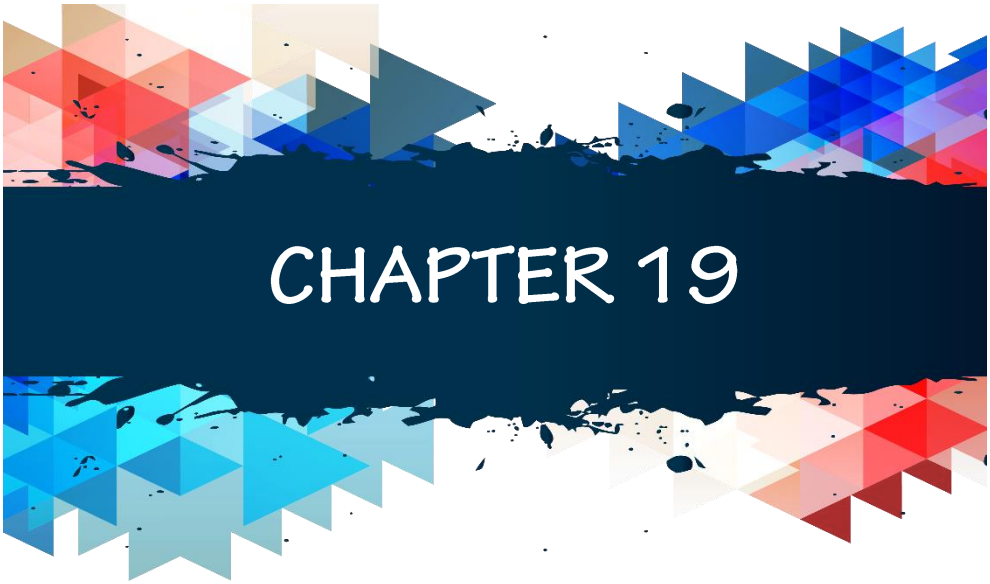

Ecology of Algae and Microorganisms Biological Basis and Physical Factors

Elif Tezel Ersanlı[1] & Cem Cüneyt Ersanlı[2]

1 Prof. Dr., Sinop University, Faculty of Arts and Sciences, Department of Biology, Sinop/Turkey, ORCID: 0000-0003-0608-9344

[2] Prof. Dr., Sinop University, Faculty of Arts and Sciences, Department of Physics, Sinop/Turkey ORCID: 0000-0002-8113-5091

Introduction

Aquatic ecosystems are one of the richest areas of biodiversity and harbor a wide range of life, from microorganisms to macroorganisms. Aquatic environments such as lakes, rivers, oceans and marshes are in a constant state of balance thanks to the interactions of living things with each other and with their environment. The functioning of these ecosystems is fundamentally determined by energy flow and nutrient cycles (Wetzel, 2001). One of the main steps of energy flow in aquatic ecosystems is algae, which are photosynthetic organisms. Algae are known as the main primary producers of aquatic ecosystems and fulfill this role by converting light energy into chemical energy through photosynthesis. This energy they produce forms the basis of the aquatic food web and is important for the sustainability of life in aquatic ecosystems (Reynolds, 2006).

Besides algae, microorganisms also play a vital role in aquatic ecosystems. Microorganisms are involved in many ecological processes, from the breakdown of organic matter to key stages in nutrient cycling. The function of microorganisms is to process energy and nutrients produced by other organisms and to recycle substances in the aquatic environment (Falkowski and Raven, 2007). The biological and ecological relationships between these organisms directly affect the health and functionality of aquatic environments (Azam, 1998).

Besides algae, microorganisms also play a vital role in aquatic ecosystems. Microorganisms are involved in many ecological processes, from the breakdown of organic matter to key stages in nutrient cycling. The function of microorganisms is to process energy and nutrients produced by other organisms and to recycle substances in the aquatic environment (Falkowski and Raven, 2007). The biological and ecological relationships between these organisms directly affect the health and functionality of aquatic environments (Azam, 1998).

Aquatic algae and microorganisms not only interact biologically with each other, but also with their physical environment. Physical factors in the aquatic environment influence the distribution, growth rate and metabolic processes of these organisms. Factors such as light, temperature, nutrients and water movement shape the photosynthetic capacity of algae and the metabolic activity of microorganisms. For example, the amount and quality of light varies with parameters such as water depth and turbidity, and this affects the photosynthetic mechanisms of algae depending on depth (Kirk, 1994). Similarly, temperature changes are one of the main factors affecting the activities and living conditions of microorganisms. Water currents and movements also directly interfere with ecosystem dynamics by affecting the distribution, nutrient uptake and oxygen

levels of algae and microorganisms (Häder et al., 2007). In this context, the interaction between the biological characteristics of algae and microorganisms and physical environmental factors is a key determinant of the ecological balance of aquatic ecosystems.

The roles played by algae and microorganisms in ecosystems are not limited to energy production and nutrient cycling; they also play a critical role in maintaining ecosystem health. The presence of algae and microorganisms in aquatic ecosystems is also used as water quality indicators. Changes in the populations of these organisms can be an indicator of changes in the chemical and physical structure of water. For example, algal overgrowth can indicate water pollution and eutrophication, which can destabilize aquatic ecosystems, causing mortality and even loss of biodiversity (Smith and Schindler, 2009).

Algae in aquatic ecosystems have a great biodiversity. Ranging from single-celled microalgae to multicellular macroalgae, these organisms live in a variety of environments at the surface and at depth. Microalgae are part of plankton communities, commonly known as phytoplankton, and are commonly found in different bodies of water, from oceans to lakes. Thanks to their photosynthetic pigments, they convert sunlight into chemical energy, providing food for themselves and other members of the ecosystem. Phytoplankton are considered the starting point of the aquatic food chain and form the basis of energy flow in aquatic ecosystems (Lalli and Parsons, 1997). They also play an important role in the global carbon cycle, absorbing much of the carbon dioxide in the atmosphere (Falkowski, 1994).

In marine ecosystems, macroalgae are usually dense in rocky coastal areas and form important structures that provide habitat for the ecosystem. Macroalgae are large, multicellular algae, particularly seaweeds. These algae provide shelter and protection as well as a source of food for many marine species. In marine ecosystems, algae also play an important role in the formation of habitats such as reefs. Algae also play an important role in oxygen production and the cycling of matter.

Like algae, microorganisms play an indispensable role in the functioning of aquatic ecosystems. Bacteria, protozoa and archaea contribute to nutrient cycling by breaking down organic matter in aquatic ecosystems. Bacteria are involved in the breakdown of dead organisms and organic wastes, while the nutrients produced as a result of this process meet the nutritional needs of algae and other aquatic organisms. Microorganisms are also known to play a role in symbiotic relationships. Some microorganisms form symbiotic relationships with algae.

Such symbiotic relationships are particularly common in coral reefs and are among the important factors that increase the biodiversity of aquatic ecosystems (Knowlton and Rohwer, 2003).

This biodiversity, which sustains the health and functioning of aquatic ecosystems, is also used as an indicator of water quality. Sudden increases or decreases in populations of algae and microorganisms can be the result of water pollution, nutrient overload or changes in oxygen levels. In particular, in a process called eutrophication, algal blooms occur as a result of nutrient overload, which reduces the oxygen level of the water and disrupts the ecosystem balance. As a result of algal blooms, living conditions for aquatic life forms become difficult, causing serious damage to the ecosystem. Therefore, algae and microorganisms play a critical role in assessing not only the biological dynamics of aquatic ecosystems, but also water quality and ecosystem health (Schindler, 2006). In this chapter, we will take a closer look at the biological characteristics of aquatic algae and microorganisms, their role in ecosystems and their interactions with the physical environment. The photosynthetic processes of algae, the functions of microorganisms in nutrient cycling and the effects of physical factors on these organisms will provide important insights into the complex structure of aquatic ecosystems. We will also discuss how algae and microorganisms play a critical role in the conservation and sustainable management of these ecosystems.

1. Biological Basis of Algae

1.1. General Characteristics and Diversity of Algae

Found in both fresh and saltwater ecosystems, algae have a wide ecological diversity. They can live in different aquatic environments such as oceans, lakes, rivers and marshes and range in size from single-celled microalgae to multicellular macroalgae. This wide diversity makes it easy for algae to adapt to the physical and chemical characteristics of their environment (Wetzel, 2001; Falkowski and Raven, 2007).

Algae are an important part of the carbon cycle through their photosynthetic activities in aquatic ecosystems. They take carbon dioxide from the atmosphere and use sunlight to convert it into chemical energy. This process allows algae to play important roles both in initiating the flow of energy within the ecosystem and in producing much of the oxygen in the biosphere. For this reason, algae are described as the main producers of aquatic ecosystems and form the basis of the entire food chain (Odum, 1971).

The diversity of algae varies greatly depending on the conditions of their environment. In freshwater ecosystems, the most common algae are the microscopic ones. These can be cyanobacteria, green algae or diatoms. These algae are found especially in stagnant or slowly flowing waters such as lakes, rivers and marshes, where they make a major contribution to aquatic environments through their photosynthetic activity. Algae photosynthesize by absorbing sunlight thanks to the pigments they contain and contribute to the ecological cycle with the organic matter and oxygen they produce (Round, 1981; Wetzel, 2001).

In the seas and oceans, microscopic algae are found as well as macroscopic ones, such as red algae and brown algae. Their diversity is shaped by ecological conditions. Red algae are particularly common in the deep sea. Thanks to their red pigments, these algae are capable of photosynthesis even in deep water with little light. The presence of these algae is important for the continuity of life in the deep sea (Lee, 2008). Brown algae are especially common along coastlines and tidal zones. Brown algae provide shelter and food for many marine species (Schiel and Foster, 2006). Algae are at the bottom of the aquatic food chain, providing a food source for zooplankton and other small organisms. These small organisms are consumed by larger predators in aquatic ecosystems, such as fish and mammals.

The role of algae in ecosystems is not limited to energy production and forming the basis of the food chain. They also directly affect the physical and chemical properties of water. Macroalgae, in particular, can form large structures on the seafloor and provide shelter for many organisms, while at the same time regulating the flow rate of water and sediment accumulation. These structural functions of algae are important for maintaining ecosystem dynamics. For example, the presence of macroalgae in coastal areas helps prevent erosion and regulates water mobility, maintaining biodiversity in the marine environment (Lobban and Harrison, 1997).

The contribution of algae to water quality is a decisive factor in maintaining ecosystem health. Especially by balancing the concentration of nutrients in aquatic environments, algae prevent excessive nutrient accumulation. For example, in environments rich in phosphorus and nitrogen, algae proliferate rapidly and consume these nutrients, thereby maintaining the chemical balance of the water (Smith and Schindler, 2009).

1.2. Role of Microalgae and Phytoplankton

Phytoplankton are the most important photosynthetic organisms in aquatic ecosystems. Despite their microscopic size, these organisms form large populations in the upper layers of oceans, lakes and rivers (Falkowski and Raven, 2007; Mann and Lazier, 2006). Phytoplankton produce organic matter through photosynthesis and absorb large amounts of carbon dioxide. Thanks to these properties, phytoplankton play a critical role in the global carbon cycle. The oceans are one of the largest natural carbon pools, absorbing carbon dioxide from the atmosphere, and phytoplankton play an important role in this process. The conversion of carbon dioxide into organic matter through photosynthesis both reduces greenhouse gas levels in the atmosphere and initiates energy flow in marine ecosystems (Falkowski et al., 1998; Field et al., 1998).

Another important function of phytoplankton is to form the base of the food chain. Phytoplankton provide the organic matter they produce through photosynthesis as a food source for zooplankton and small aquatic organisms. These small organisms are consumed by larger aquatic animals and energy is thus transported upwards along the food chain. At the bottom of this chain, phytoplankton are the organisms that initiate the energy flow of all aquatic ecosystems. Phytoplankton indirectly provide food for top predators such as large marine mammals and fish, and thus play a critical role in the sustainability of aquatic ecosystems (Odum, 1971; Round, 1981).

The organic matter produced by phytoplankton is consumed by other members of aquatic ecosystems. This food production is an important food source for zooplankton and other microscopic organisms. Zooplankton is consumed by fish, crustaceans and other aquatic organisms. The productivity of phytoplankton directly affects the biodiversity and ecological health of oceans, lakes and rivers. Particularly large phytoplankton blooms can create an abundance of nutrients in ecosystems, but uncontrolled increases can also sometimes have detrimental effects. For example, excessive phytoplankton growth can lead to eutrophication, causing oxygen deficiency and the formation of dead zones (Carpenter, 2005; Smith and Schindler, 2009).

The oceans cover more than 70% of the Earth's surface and phytoplankton make up the bulk of the biomass in this huge body of water. The importance of phytoplankton in ecosystems is not limited to the carbon cycle. These organisms also provide a large part of the world's oxygen production. By releasing oxygen into the atmosphere through the process of photosynthesis, phytoplankton produce about 50% of the world's oxygen. This indicates that phytoplankton play

a critical role in the ecological importance of phytoplankton for the ecosystem. Phytoplankton are vital for the maintenance of both aquatic and terrestrial life, producing a large proportion of the oxygen required for respiration worldwide (Field et al., 1998; Falkowski et al., 1998).

Microalgae are also used as important biological indicators to monitor the health of ecosystems because of their ability to respond rapidly to environmental changes. In particular, the increase or decrease of phytoplankton populations in the sea can be an indicator of changes in the chemical composition of water. For example, increased nutrients (such as nitrogen and phosphorus) in the seas can rapidly increase phytoplankton populations, leading to algal blooms. Such algal blooms can lead to lower oxygen levels in aquatic ecosystems and the extinction of many species. Thus, monitoring phytoplankton has an important role in maintaining ecosystem health in water bodies (Smayda, 1990; Cloern, 2001).

Compared to terrestrial ecosystems, the productivity of phytoplankton in aquatic environments is highly dependent on environmental factors. Factors such as the amount of light, temperature, nutrient content and water mobility affect the growth rate of phytoplankton. For example, phytoplankton reproduce rapidly where sunlight is abundant on the ocean surface. However, in deep water where light is limited or at extremely low temperatures, the growth of these organisms slows down. Similarly, changes in the chemical composition of water also affect the biological activity of phytoplankton. For example, an abundance of nutrients such as nitrogen and phosphorus can lead phytoplankton to multiply rapidly. However, excessive phytoplankton growth can lead to oxygen depletion in the water body, which in turn can reduce biodiversity in ecosystems (Round, 1981; Wetzel, 2001).

2. Ecology and Role of Microorganisms

2.1. Types of Microorganisms and Ecosystem Functions

Microorganisms are one of the smallest but most influential components of aquatic ecosystems. Different microorganisms such as bacteria, archaea, protozoa and microscopic fungi are important elements that increase biodiversity and influence ecosystem dynamics. These microscopic organisms perform many ecological functions in aquatic environments, such as the breakdown of organic matter, nutrient recycling and biological degradation processes. Although invisibly small, these organisms play critical roles in aquatic ecosystems and maintain biochemical cycles in aquatic environments (Atlas and Bartha, 1998; Madigan et al., 2017).

One of the main tasks of microorganisms in aquatic ecosystems is the decomposition of organic matter. Organic matter consists of biological waste that has accumulated in the ecosystem, such as the remains of dead organisms. These organic substances are broken down by microorganisms and recycled to organisms higher up in the food chain. Bacteria in particular are the most effective group in this decomposition process. Bacteria break down organic matter into its simpler components, allowing nutrients to circulate in aquatic ecosystems. This process is essential for the maintenance of energy flow and nutrient cycling in ecosystems (Fenchel, 1988; Kirchman, 2012).

Nitrogen cycling is another critical role of microorganisms in aquatic ecosystems. Nitrogen is one of the essential nutrients required for the survival of plants and animals, but nitrogen must undergo various transformation processes to become bioavailable. Microorganisms play a vital role in these conversion processes. In particular, denitrifying bacteria complete the biological cycle of nitrogen in aquatic ecosystems. These bacteria convert nitrates into nitrogen gas, allowing nitrogen to cycle regularly in the aquatic environment. This process is critical for the healthy functioning of ecosystems and the maintenance of the chemical balance of water (Galloway and Cowling, 2002; Capone and Knapp, 2007).

Bacteria and archaea not only decompose organic matter, but also form part of the food chain in aquatic ecosystems. At the same time, bacteria themselves provide food for zooplankton and other microorganisms. They thus ensure the continuity of energy and nutrient cycling in aquatic ecosystems. These microorganisms also help regulate the chemical composition of water, keeping the pH and other chemical parameters in balance (Azam et al., 1983; Ducklow, 2000).

Microorganisms also play an important role in biodegradation and waste management in aquatic ecosystems. Chemicals and organic wastes that enter water as a result of industrial pollution and human activities are biodegraded by microorganisms. This process protects water quality by allowing pollutants to decompose naturally. Microorganisms have a great contribution especially in the removal of organic pollutants such as oil and hydrocarbons from aquatic ecosystems. In this process, microorganisms break down pollutants into simpler and harmless components and thus protect the health of aquatic ecosystems (Leahy and Colwell, 1990; Head et al., 2006).

Microorganisms not only act as decomposers in aquatic ecosystems, but also establish symbiotic relationships, further strengthening ecosystem dynamics.

Algae and cyanobacteria develop mutually beneficial symbiotic relationships with other aquatic organisms. These symbiotic relationships increase the productivity and biodiversity of aquatic ecosystems. One example is the symbiotic relationship between corals and algae. Coral reefs are one of the most biodiverse aquatic ecosystems and their health depends on the relationship between algae and corals. Algae photosynthesize in coral tissues to produce organic matter, which is used by corals as an energy source. At the same time, algae support the production of calcium carbonate, which is essential for coral reef growth. This symbiotic relationship ensures the healthy growth and development of coral reefs. Since coral reefs provide shelter to many aquatic organisms in ecosystems, this relationship is critical for maintaining ecosystem dynamics (Muscatine and Porter, 1977; Hoegh-Guldberg, 1999).

Microorganisms also support other important symbiotic relationships in aquatic ecosystems that increase biodiversity and maintain ecosystem balance. For example, microscopic fungi form mycorrhizal relationships with aquatic plants, enhancing their nutrient uptake. These relationships allow plants to take up nutrients and water more efficiently, thus increasing plant productivity and biodiversity in ecosystems. Similarly, some bacteria develop symbiotic relationships with aquatic invertebrates and support the digestive processes of these organisms. Such relationships are of great importance for the sustainability of aquatic ecosystems and the maintenance of biodiversity (Smith and Read, 2008).

Microorganisms can also be called ecosystem engineers. Apart from decomposing organic matter, maintaining nutrient cycling and establishing symbiotic relationships, microorganisms also play a role in biofilm formation, oxygen production and regulation of physical properties of water in aquatic ecosystems. Biofilms are structures formed by microbial communities in aquatic ecosystems, which can affect the movement and chemical composition of water. In some cases, these biofilms can slow the flow rate of water or provide protection for organisms living on submerged surfaces. In addition, microorganisms maintain the chemical balance of the water, protecting its overall health (Costerton et al., 1995; Stal, 2012).

3. Effects of Physical Factors on Algae and Microorganisms

3.1. Light and Photosynthetic Activity

Light is a critical source of energy production for algae and photosynthetic microorganisms living in aquatic ecosystems. Through the process of photosynthesis, algae use carbon dioxide in the atmosphere to produce oxygen and synthesize organic compounds. This process is essential for the growth of algae and the production of nutrients for other organisms in the ecosystem. However, the amount and quality of light required for photosynthesis varies depending on environmental factors such as water depth, turbidity and water surface (Falkowski and Raven, 2007).

In the water column, light intensity decreases with depth. Near the surface of the water body, the intensity of sunlight is higher and algae perform a more active photosynthesis process. However, as you move deeper into the water, the light intensity decreases rapidly and photosynthesis becomes impossible after a certain depth. This depth is a result of factors that limit light penetration, and these factors include water turbidity, suspended particles and the chemical composition of the water (Kirk, 1994; Wetzel, 2001).

Photosynthetically active radiation (PAR) refers to the spectrum of light that algae need to photosynthesize. PAR includes wavelengths between 400 and 700 nanometers of the visible light spectrum, and these wavelengths provide the energy that algae use in their photosynthetic processes. The concentration of PAR in the water column directly affects the energy production capacity of the ecosystem and the growth rate of algae (Sverdrup et al., 1942). Algae produce energy through photosynthesis when exposed to sufficient amounts of PAR, but this process comes to a standstill when light intensity drops below a certain level. Red algae, especially those living in the deep sea, have evolved to adapt to low light conditions and use even small amounts of light (Dring, 1982).

While reduced light intensity limits the photosynthetic activity of algae, excessive light intensity can also negatively affect photosynthesis. Excess light reduces the capacity of algae to photosynthesize, a process called photoinhibition. Photoinhibition occurs as a result of damage to the photosystems of algae when light is excessive. This is seen in algae exposed to intense sunlight, especially near the water surface (Powles, 1984). As a result of photoinhibition, algae significantly reduce their energy production, which affects the energy cycle of the ecosystem. Thus, when light intensity is both low and high, the photosynthetic processes of algae can be negatively affected, limiting energy production in aquatic ecosystems.

3.2. Temperature and Thermal Conditions

Temperature is one of the most important physical factors that directly affect the metabolic activities of organisms such as algae and microorganisms in aquatic ecosystems. There is a specific temperature range in which algae and microorganisms can perform their biological functions most efficiently. This temperature range differs for each organism and is related to the ability of organisms to adapt to environmental conditions. Temperature affects many fundamental biological processes, from photosynthetic activity to reproductive rate, so sudden changes in water temperature can severely affect populations of these organisms (Graham and Wilcox, 2000).

In general, the metabolic rates of algae and microorganisms increase as temperature increases. Temperature can increase the growth rate of these organisms by accelerating biochemical reactions. However, temperatures above a certain threshold can disrupt these processes. Extremely high temperatures can lead to denaturation of protein structures, disrupting photosynthesis and other metabolic processes. As a result, algae and microorganisms are damaged and their growth rate is reduced. Temperature increases, especially at the water surface, can lead to higher densities of these organisms in the upper layers, but extreme temperatures can also cause population collapses.

Algae are organisms that are particularly sensitive to temperature changes. The fact that different algal species are adapted to specific temperature ranges further complicates the effects of temperature on ecosystem dynamics. For example, some algal species adapted to cold waters may experience a decrease in their growth rate with an increase in temperature. Conversely, tropical algae species adapted to warmer waters can increase their growth rates when temperatures rise. However, temperature increases beyond a certain level can cause metabolic stress even in tropical algae, which can inhibit growth (Staehr and Birkeland, 2006).

Microorganisms show a similar sensitivity to temperature changes. Bacteria, in particular, can respond rapidly to temperature changes and temperature increases often accelerate their metabolic activity. However, high temperatures can degrade the enzymes of microorganisms, causing them to lose their function. Microorganisms reach their highest efficiency within a certain temperature range, especially when performing their decomposing functions. If the temperature rises outside this range, it can lead to disruptions in basic ecosystem functions such as the decomposition of organic matter (Allison and Treseder, 2011).

Climate change is significantly affecting temperature dynamics in aquatic ecosystems. Global warming causes various effects on algae and microorganisms by directly or indirectly affecting water temperatures in seas, lakes and rivers. In particular, increasing sea surface temperatures can lead to more frequent and severe algal blooms (e.g. harmful algal blooms or "red tide" events). These events can disrupt the balance of aquatic ecosystems, negatively affecting both biodiversity and water quality (Paerl and Huisman, 2008).

Algal blooms usually occur as a result of overloading the water with excessive amounts of nutrients (especially nitrogen compounds such as phosphorus and nitrate) and accompanying temperature increases. The rise in temperature increases the photosynthetic activity of the algae and thus causes them to multiply rapidly. However, these blooms are often harmful to the ecosystem, as excessive algal growth depletes the oxygen content of the water, making living conditions difficult for other aquatic life. Furthermore, some algal species produce toxins that can have lethal effects on fish and other aquatic organisms (Sellner et al., 2003).

Climate change is not limited to temperature increases; it also creates changes in the thermal structure of water. For example, thermal stratification (the separation of the water column into different temperature layers) in lakes and seas affects the distribution of algae and microorganisms in the ecosystem. An increase in temperature at the surface can affect stratification, limiting the access of organisms in the lower layers to vital resources such as nutrients and light. This can make living conditions difficult, especially for organisms living in deep waters (Wetzel, 2001).

Temperature increase has similar consequences for microorganisms. Especially microorganisms such as denitrifying bacteria, which play important roles in aquatic ecosystems, regulate their activities in response to changes in water temperature. Temperature increase can accelerate the processes in the nitrogen cycle by increasing the metabolic rate of these bacteria, but excessive acceleration of these processes can lead to disruptions in ecosystem balances. However, in extreme cases of temperature increase, bacterial populations can collapse and essential ecosystem functions, such as the nitrogen cycle, can be disrupted.

Temperature changes not only affect biological processes, but also reshape relationships between ecosystems. Symbiotic relationships in particular are greatly affected by temperature changes. For example, the relationship between corals and symbiotic algae is extremely sensitive to increases in water

temperature. Algae living on coral reefs provide corals with oxygen and nutrients, but a rise in water temperature disrupts this symbiotic relationship and leads to a phenomenon called coral bleaching. Coral bleaching occurs when the algae detach from the coral, reducing the corals' chances of survival. The disruption of such symbiotic relationships poses serious threats not only to corals, but also to many other organisms living on coral reefs (Hoegh-Guldberg, 1999).

3.3. Nutrients and Eutrophication

Nutrients are critical for the growth of algae and microorganisms in aquatic ecosystems. Essential elements such as nitrogen and phosphorus are used in the metabolic processes of these organisms and support vital functions such as energy production through photosynthesis. However, too much nutrient input into water has serious consequences that can upset ecosystem balance. This process is known as eutrophication and has particularly dramatic effects on algae. Eutrophication is usually caused by human activities and is accelerated by the introduction of agricultural fertilizers into rivers, lakes and seas (Carpenter et al., 1998).

The process of eutrophication leads to rapid growth of algae and intense algal blooms. These blooms cover large areas of the water surface, preventing sunlight from reaching the lower water layers. The lack of light means a struggle for survival for plants and photosynthetic organisms living in the lower layers of the water column. The cessation of photosynthesis limits energy production in these areas and causes oxygen levels to drop. With the collapse of underwater vegetation, the health of the ecosystem deteriorates rapidly. In the later stages of this process, hypoxia (low oxygen levels) or anoxia (lack of oxygen) occurs, with fatal consequences for aquatic life (Dodds, 2006).

Overloading of nutrients into water is often associated with anthropogenic activities. Fertilizers used in agriculture, rich in phosphorus and nitrogen, cause a heavy accumulation of nutrients in aquatic ecosystems when they flow into rivers, lakes and seas. Similarly, industrial and domestic wastewater also increases the nutrient load. When these substances enter the water, they create an ideal growth environment for algae and other aquatic plants. However, this overgrowth disrupts the ecosystem balance and has negative effects on other organisms in the food chain. In particular, fast-growing algal species can overshadow slower-growing plants that are critical to the ecosystem and cause their extinction (Carpenter, 2005).

Algal blooms, one of the most obvious consequences of eutrophication, severely affect oxygen levels in aquatic ecosystems. Dense masses of algae cover

the water surface, preventing sunlight from reaching the lower layers. Lack of light stops photosynthesis, which limits oxygen production in the lower water layers. As a result of the rapid growth and reproduction of algae, large quantities of organic matter enter the water when these organisms die. During the decomposition process of this organic matter, bacteria consume the available oxygen. Thus, the oxygen level of the water drops rapidly and oxygen deficiency becomes a serious threat to aquatic life (Conley et al., 2009).

Reduced oxygen levels put great pressure on aquatic life, especially fish and other aquatic organisms with high oxygen requirements. In conditions of hypoxia or anoxia, these organisms struggle to survive and often suffer mass mortality. This has negative impacts on fisheries and aquatic ecosystem services. For example, fish kills in lakes and seas can severely damage local fishing industries and have economic consequences. Biodiversity is also threatened; algal blooms and oxygen deficiency can lead to the extinction of many species in aquatic ecosystems (Diaz and Rosenberg, 2008).

The negative effects of algal blooms on ecosystems are not limited to reduced oxygen levels. Some algal species produce toxins, which can pose serious health risks to aquatic organisms, humans and other animals. Such algal blooms are often referred to as “harmful algal blooms”. This can have fatal effects, especially on shellfish, fish and mammals. When toxins get into the water, they can contaminate water supplies, which can lead to serious problems in the drinking water supply. In addition, people can face serious health problems when they eat seafood that has consumed these toxins. Toxin-producing algal blooms can also negatively affect activities such as tourism and recreational water sports (Anderson et al., 2002).

Various strategies have been developed to prevent eutrophication and reduce its impacts. The most important of these strategies is the regulation of agricultural and industrial activities. Controlling the use of fertilizers can help reduce nutrients entering the water. In particular, sustainable agricultural practices can prevent water pollution by preventing the addition of excess nutrients to the soil. Similarly, efficient operation of industrial wastewater treatment plants and treatment of domestic wastewater can contribute to reducing the nutrient load.

Biological control methods can also be used in aquatic ecosystems to mitigate the effects of eutrophication. These include reintroducing organisms that can balance the nutrient surplus into the ecosystem. For example, some aquatic plants and plankton can help reduce this excess by absorbing excess nutrients. Also, protecting predatory species high up the food chain can help keep algal blooms

in check. Such strategies can contribute to maintaining ecosystem balances and minimizing the negative effects of eutrophication (Scheffer et al., 1993).

The impacts of eutrophication are not limited to local aquatic ecosystems; the process also affects global water resources and biodiversity. Large river deltas and coastal areas are particularly threatened by eutrophication in areas with intensive agricultural activities. For example, in many parts of the world, large rivers carry large amounts of nutrients into the sea, which can cause algal blooms in coastal ecosystems. It is therefore clear that eutrophication is a global problem and needs to be addressed with international cooperation as well as local governments (Vitousek et al., 1997).

3.4. Currents and Water Movements

Currents and water movements in aquatic environments have significant impacts on algae and microorganisms and play a critical role in the dynamics of aquatic ecosystems. Currents refer to the horizontal and vertical movements of water, which determine the distribution and transport of algae and microorganisms and their role in ecosystems. The strength, direction and character of water movements are important factors affecting the living conditions of these organisms and ecosystem functioning (Hofmann and Kremer, 1981; Mann and Lazier, 2006).

Effects of Currents on Algae and Microorganisms

Currents determine the position and distribution of algae and microorganisms in water. The direction and speed of water currents affect where these organisms are concentrated and how they move. For example, strong ocean currents can spread surface phytoplankton over large areas, which can cause these organisms to spread over large marine regions. At the same time, currents regulate the flow of nutrients and energy in aquatic ecosystems by transporting nutrients and other solvents to different parts of the water. This transport process is critical for the efficiency of nutrient cycling and algal access to food resources (Butman et al., 1994).

Water movements affect the settlement of algae and microorganisms as well as their growth and reproduction periods. Currents can cause algae and microorganisms to move away from their established sites or move to new areas. These movements shape the adaptation of organisms to environmental conditions and population dynamics. Currents, especially in lakes and rivers, can affect the dispersal and community structure of freshwater algae and microorganisms (Reynolds and Descy, 1996).

Oxygen Distribution and Water Mixing

Currents also significantly affect the distribution of oxygen in the water column. Water movements allow oxygen to diffuse from the surface to the depths and vice versa. This distribution determines the living conditions of aquatic organisms and ecosystem health. For example, strong currents can increase oxygen levels in deep water layers by facilitating the transport of oxygen from the surface to the depths. This is vital for organisms living in deep water layers.

In areas of high water mixing, oxygen distribution is more homogeneous, providing favorable living conditions for microorganisms. The even distribution of oxygen allows organisms in the aquatic environment to utilize nutrients and other resources more efficiently. Furthermore, currents contribute to the healthy functioning of biological processes in aquatic ecosystems by regulating water oxygen levels (Diaz and Rosenberg, 2008).

Nutrient Transport and Nutrient Cycle

Currents also affect the transport of nutrients in water. Nutrients are transported by currents to different parts of the water and this process shapes the nutrient cycling of ecosystems. For example, river currents can transport nutrients from agricultural land into lakes and seas. This transport can stimulate the growth of algae and microorganisms, affecting nutrient loading, especially in freshwater ecosystems (Galloway et al., 2004).

Currents regulate the functioning of the food chain in aquatic ecosystems by affecting the distribution and concentrations of nutrients. Depending on the speed and direction of currents, nutrients can diffuse to different parts of the water, affecting the access of algae and microorganisms. Furthermore, currents regulate the flow of energy and matter in aquatic ecosystems, contributing to the efficient functioning of nutrient cycling (Schlesinger, 1997).

Maintaining Ecosystem Balance

Currents and water movements play an important role in maintaining the balance of aquatic ecosystems. Water currents regulate the flow of nutrients and energy within ecosystems, shaping interactions and relationships between organisms. Furthermore, currents contribute to the maintenance of water quality by influencing the distribution of pollutants and waste materials in the aquatic environment. In particular, they protect the health of aquatic organisms and ecosystems by limiting the spread of pollutants and toxins in the aquatic environment (Nixon, 1995).

The protective effects of water movements on ecosystem balance are particularly evident in coastal areas and lagoons. In these areas, water movements allow the dispersion of nutrients and organic matter and provide cleanup. In addition, coastal currents create habitats for seaweeds and other aquatic plants, supporting their role in the ecosystem (Mann and Lazier, 2006).

4. Algal-Microorganism Interactions and Ecosystem Health

4.1. Algae-Microorganism Relationships

Interactions between algae and microorganisms play a critical role in the health and functioning of aquatic ecosystems. These relationships directly affect the energy flow, nutrient cycling and biodiversity of ecosystems. The interactions between algae and microorganisms maintain the overall health of aquatic environments by increasing the balance and productivity in ecosystems (Azam et al., 1983; Falkowski et al., 1998).

Role of Microorganisms in Nutrient Cycling

The relationships between algae and microorganisms also play an important role in nutrient cycling. Microorganisms break down dead cells and organisms and other organic matter, returning nutrients to the aquatic environment in a reusable form. This process ensures that the nutrient cycle functions efficiently and contributes to the continuous supply of nutrients necessary for algae growth. For example, bacteria and fungi decompose dead algal cells and other organic material, recycling nutrients from the aquatic environment. This decomposition process completes the cycling of nutrients in aquatic ecosystems and provides the nutrients that algae need for growth. In this way, microorganisms support the efficient growth of algae while maintaining the health of ecosystems (Pomeroy, 1974; Azam et al., 1983).

Impacts of Interactions on Ecosystem Health

Interactions between algae and microorganisms have a wide range of impacts on ecosystem health. These interactions affect energy flow, nutrient cycling and biodiversity in aquatic ecosystems, ensuring the functioning and balance of ecosystems. The interactions of algae and microorganisms increase productivity in ecosystems, while also contributing to biodiversity conservation and increasing the resilience of ecosystems. For example, the interactions of algae and microorganisms support the healthy functioning of the food chain in aquatic ecosystems. The growth of algae, the contribution of microorganisms to nutrient cycling and symbiotic relationships regulate energy flow and nutrient cycling in ecosystems. This regulation supports biodiversity in aquatic ecosystems and

maintains the overall health of ecosystems (Fenchel, 1987; Cotner and Biddanda, 2002).

Interactions with Temperature and Nutrients

Interactions between algae and microorganisms are also directly related to environmental factors. Water temperature and nutrients determine the efficiency and impact of these interactions. Temperature changes can affect the growth rate of algae and microorganisms, which in turn can alter the efficiency of symbiotic relationships. Furthermore, the amount and type of nutrients influence the interactions of microorganisms and algae, regulating nutrient cycles and energy flow in ecosystems (Shiah and Ducklow, 1994; Rivkin and Legendre, 2001).

Maintaining Ecosystem Balance

Interactions between algae and microorganisms play a critical role in maintaining ecosystem balance. These interactions regulate the flow of energy and nutrients in aquatic ecosystems, enable nutrient cycling and support biodiversity. Furthermore, these interactions increase the resilience of ecosystems to environmental stressors in aquatic environments and ensure the healthy functioning of ecosystems (Azam et al., 1983; Falkowski et al., 1998).

4.2. Ecosystem Management and Conservation Strategies

Algae and microorganisms are considered important indicators for monitoring the health and functioning of aquatic ecosystems. These organisms are determinants of water quality and ecosystem balance and are sensitive to changes in aquatic environments. Thus, changes in algae and microorganisms can reflect the overall health of aquatic ecosystems. Sustainable management and conservation of water resources requires a critical strategy to achieve the goals of protecting the biodiversity of these organisms and ecosystem functions (Reynolds, 2006; Schindler, 2006).

Monitoring Water Quality and Ecosystem Balance

Water quality degradation directly affects populations of algae and microorganisms and can destabilize the ecosystem. To monitor water quality, algae and microorganisms can be used as indicators of the health of ecosystems. Changes in the populations of these organisms indicate changes in the physical, chemical and biological properties of water. For example, overgrowth of algae or abnormalities in microscopic organisms can often indicate water pollution or nutrient excesses. Therefore, algal and microorganism monitoring is an effective tool to assess water quality and protect ecosystem health (Heisler et al., 2008; Smith and Schindler, 2009).

Eutrophication and Pollution Problems

Eutrophication is a process that occurs when excessive amounts of nutrients enter aquatic environments. This leads to algal blooms. Eutrophication can lead to reduced oxygen levels in aquatic ecosystems, degraded water quality and reduced biodiversity. Increased pollution and nutrient loading can disrupt the balance of algal and microorganism populations, negatively affecting ecosystem function. Control of pollution sources and nutrient management are important for preventing eutrophication (Carpenter et al., 1998; Paerl and Huisman, 2008).

Climate Change and Ecosystem Impacts

Climate change is leading to significant changes in aquatic ecosystems. Increases in water temperatures, changes in flow patterns and fluctuations in water levels can have major impacts on algae and microorganisms. In particular, temperature increases can alter the composition and distribution of algal and microorganism populations, trigger harmful algal blooms and disrupt the balance in aquatic ecosystems. Developing adaptation strategies to cope with climate change and protect water resources is important to mitigate these negative impacts (IPCC, 2014; Woodward et al., 2010).

Sustainable Management Strategies

Sustainable management of water requires developing comprehensive strategies to protect the health of algae and microorganisms and ecosystem functions. These strategies may include:

Control of Pollution Sources: Controlling industrial, agricultural and domestic pollution sources can reduce the introduction of harmful substances into aquatic environments. This can help improve water quality and prevent eutrophication (Carpenter et al., 1998).

Nutrient Management: The management of nutrients such as nitrogen and phosphorus can control nutrient loading in aquatic ecosystems. Efficient use of these substances in agricultural practices and regulations on nutrient load reduction in water treatment plants are important steps to be taken in this regard (Smith and Schindler, 2009).

Tackling Climate Change: Developing climate change adaptation strategies can help aquatic ecosystems adapt to changing conditions. Monitoring water temperatures and flow patterns can be part of these strategies (IPCC, 2014).

Protected Areas and Management: Establishing and managing protected areas is an effective way to protect aquatic ecosystems and promote biodiversity.

Regulations in these areas can maintain ecosystem health and organism populations (Allan et al., 1997).

Education and Public Awareness: Raising public awareness and providing environmental education raises public awareness about the conservation and sustainable management of water resources. This plays an important role in protecting aquatic ecosystems (Orr, 2004).

Conclusion

Algae and microorganisms are the biological basis of aquatic ecosystems and play a critical role in the dynamics of ecosystems. These organisms exhibit various biological characteristics depending on the physical conditions of the environment in which they live. Physical factors such as light, temperature, nutrients and water movement are important factors that determine the populations of algae and microorganisms and their effects on the ecosystem.

Light is a major source for the photosynthetic activity of algae and varies depending on factors such as light intensity in the water column, water depth and turbidity. Photosynthetically active radiation includes the wavelengths of light at which algae can photosynthesize. Changes in light intensity affect the photosynthetic capacity of algae and can therefore limit the energy production of ecosystems. Furthermore, excessive light intensity can lead to a process called photoinhibition in some algal species and stop photosynthesis.

Temperature directly affects the metabolic rate of algae and microorganisms in aquatic environments. Within the optimal temperature range, these organisms perform their biological functions most efficiently. However, sudden changes in water temperature can cause algal blooms or the collapse of microorganism populations. Factors such as climate change can disrupt ecosystem balances by altering water temperatures and trigger harmful algal blooms.

Nutrients, especially nitrogen and phosphorus, are critical for the growth of algae. However, excessive nutrient inputs into the aquatic environment can initiate the process of eutrophication. Algae overgrow and can upset the balance of the aquatic ecosystem. Algal blooms can cover the water surface, blocking sunlight from reaching the lower layers and causing oxygen levels to drop. This can be fatal for aquatic life and threaten biodiversity.

Water movements and currents affect the distribution and transport of algae and microorganisms. The strength and direction of currents allow plankton and nutrients to be transported from one place to another. Furthermore, currents and water movements affect the distribution of oxygen in the water column,

determining the living conditions for microorganisms. In areas of high water mixing, populations of algae and microorganisms can be more homogeneously distributed and nutrient cycling can function more efficiently.

The relationships between algae and microorganisms play an important role in maintaining ecosystem health. Some microorganisms support algae by forming symbiotic relationships with them. These symbiotic relationships allow nutrient cycles in aquatic ecosystems to function more efficiently and maintain ecosystem balances. Deterioration in water quality can affect populations of these organisms and disrupt ecosystem balance.

In this context, sustainable management and conservation of water resources should include the goals of protecting the biodiversity of algae and microorganisms and ecosystem functions. Strategies such as monitoring water quality, controlling pollution sources, nutrient management, combating climate change, creating protected areas and raising public awareness are effective methods to maintain the health and balance of aquatic ecosystems. Sustainable management strategies ensure the efficient and sustainable functioning of aquatic ecosystems and promote ecosystem health.

In conclusion, algae and microorganisms are determinants of the health and functioning of aquatic ecosystems. The biological basis of these organisms and their interactions with the physical environment shape the dynamics and balance of ecosystems. The effects of physical factors determine the populations of algae and microorganisms and their impact on the ecosystem. Sustainable management and conservation of water resources is critical to achieve the goals of maintaining the health of these organisms. Maintaining ecosystem health and managing water resources sustainably will be vital for future aquatic ecosystems.

References

Allan, J. D., Erickson, D. L., and Fay, J. (1997). The influence of catchment land use on stream integrity across multiple spatial scales**,** *Freshwater Biology*, 37(1), 149-161. https://doi.org/10.1046/j.1365-2427.1997.d01-546.x.

Allison, S. D. and Treseder, K. K. (2011). Climate change feedbacks to microbial decomposition in boreal soils. *Fungal Ecology*, 4(6), 362-374. https://doi.org/ 10.1016/j.funeco.2011.01.003.

Anderson, D. M., Gilbert, P. M., and Burkholder, J. M. (2002). Harmful Algal Blooms and Eutrophication: Nutrient Sources, Composition and Consequences. *Estuaries*, 25(4), 704-726. https://doi.org/10.1007/ BF02804901.

Atlas, R. M. and Bartha, R. (1998). Microbial ecology: fundamentals and applications. 4th edn. Addison Wesley Longman, New York, pp 556-588.

Azam, F. (1998). Microbial control of oceanic carbon flux: The plot thickens. *Science*, 280(5364), 694-696. ISSN: 0036-8075, 1095-9203.

Azam, F., Fenchel, T., Field, J. G., Gray, J. S., Meyer-Reil, L. A., and Thingstad, F. (1983). The Ecological Role of Water-Column Microbes in the Sea. *Marine Ecology-Progress Series*, 10, 257-263. http://dx.doi.org/ 10.3354/meps010257.

Butman, C. A., Fréchette, M., Geyer, W. R., and Starczak, V. R. (1994).Watercourse experiments on nutrient supply to the blue mussel *Mytilus edulis* L. as a function of boundary layer flow. *Limnology and Oceanography*, 32(2), 453-463. https://doi.org/10.4319/lo.1994.39.7.1755.

Capone, D. G. and Knapp, A. N. (2007). A marine nitrogen cycle fix?. *Nature*, 445, 159-160.

Carpenter, S. R. (2005). Eutrophication of aquatic ecosystems: bistability and soil phosphorus. Proc Natl Acad Sci, 102(29), 10002-10005. https://doi.org/10.1073/pnas. 0503959102.

Carpenter, S. R., Caraco, N. F., Correll, D. L., Howarth, R. W., Sharpley, A. N., and Smith, V. H. (1998). Nonpoint Pollution of Surface Waters with Phosphorus and Nitrogen. *Ecological Applications*, 8(3), 559-568. https://doi.org/10.2307/2641247.

Cloern, J. E. (2001). Our Evolving Conceptual Model of the Coastal Eutrophication Problem. *Marine Ecology Progress Series*, 210, 223-253. http://dx.doi.org/10.3354/ meps210223.

Conley, D. J., Paerl, H. W., Howarth, R. W., Boesch, D. F., Seitzinger, S. P., Havens, K. E., Lancelot, C., and Likens, G. E. (2009). Controlling Eutrophication: Nitrogen and Phosphorus. *Science*, 323, 5917, 1014-1015. http://dx.doi.org/10.1126/science.1167755.

Costerton, J. W., Lewandowski, Z., Caldwell, D. E., Korber, D. R., and Lappin-Scott, H. M. (1995). Microbial Biofilms. *Annual Review of Microbiology*, 49, 711-745. http://dx.doi.org/10.1146/annurev.mi.49.100195.003431.

Cotner, J. B. and Biddanda, B. A. (2002). Small Players, Large Role: Microbial Influence on Biogeochemical Processes in Pelagic Aquatic Ecosystems. *Ecosystems*, 5(2), 105-121. http://dx.doi.org/10.1007/s10021-001-0059-3.

Diaz, R. J. and Rosenberg, R. (2008). Spreading Dead Zones and Consequences for Marine Ecosystems. *Science*, 321(5891), 926-929. http://dx.doi.org/10.1126/science. 1156401.

Dodds, W. K. (2006). Eutrophication and Trophic State in Rivers and Streams. *Limnology and Oceanography*, *51*, *671-680*. http://dx.doi.org/10.4319/lo.2006.51.1_part_2. 0671.

Dring, M. J. (1982). The *biology of marine plants.* Published by *London:* E. *Arnold, 1982*., 1986. ISBN 10: 0713128607 / ISBN 13: 9780713128604.

Ducklow, H. W. (2000). Bacterial production and biomass in the oceans. p. 85-120. In: *Microbial ecology of the oceans*. Kirchman, D.L. (Eds). Wiley-Liss, New York.

Falkowski, P. G., Barber, R. T., and Smetacek, V. (1998). Biogeochemical controls and feedbacks on ocean primary production. *Science*, 281, 200-206. http://dx.doi.org/10.1126/science.281.5374.200.

Falkowski, P. G. and Raven, J. A. (2007), Aquatic Photosynthesis. 2nd Edition, *Princeton University Press*, Princeton. https://doi.org/10.1515/9781400849727.

Fenchel, R. T. (1987). Ecology of Protozoa-the Biology of Free-living Phagotrophic Protists. X+197S., 47 Abb. Berlin-Heidelberg-New York-London-Paris-Tokyo. Springer-Verlag. DM 94,00. ISBN: 3-540-16960-1**.**

Fenchel, T. (1988). Marine plankton food chains. Annual Review of Ecology and Systematics, 19(1), 19-38. https://doi.org/10.1146/annurev.es.19.110188.000315.

Field, C. B., Behrenfeld, M. J., Randerson, J. T., and Falkowski, P. (1998). Primary production of the biosphere: integrating terrestrial and oceanic components. *Science*, 281(5374), 237-240.

Galloway, J. N. and Cowling, E. B. (2002). *Reactive Nitrogen and the World: 200 Years of Change*. *Ambio*, 31, 64-71. https://doi.org/10.1579/0044-7447-31.2.64.

Galloway, J. N., Dentener, F. J., Capone, D. G., Boyer, E. W., Howarth, R. W., Seitzinger, S. P., Asner, G. P., Cleveland, C. C., Green, P. A., Holland, E. A., Karl, D. M., Michaels, A. F., Porter, J. H., Townsend, A. R., and Vörösmarty, C. J. (2004). Nitrogen cycles: Past, present, and future. *Biogeochemistry*, *70*(2), 153-226. https://doi.org/10.1007/s10533-004-0370-0.

Graham, L. E. and Wilcox, L.W. (2000) Algae. Prentice Hall, Upper Saddle River, 640 p.

Häder, D.-P., Kumar, H. D., Smith, R. C., and Worrest, R. C. (2007). Effects of solar UV radiation on aquatic ecosystems and interactions with climate change, *Photochem. Photobiol. Sci*., 6, 267-285.

Head, I. M., Jones, D. M., and Röling, W. F. M. (2006). Marine microorganisms make a meal of oil. *Nat. Rev. Microbiol.*, 4, 173-182. https://doi.org/10.1038/nrmicro 1348.

Heisler, J., Glibert, P. M., Burkholder, J. M., Anderson, D. M., Cochlan, W., Dennison, W. C., Dortch, Q., Gobler, C. J., Heil, C. A., Humphries, E., Lewitus, A., Magnien, R., Marshall, H. G., Sellner, K., Stockwell, D. A., Stoecker, D. K., and Suddleson, M. (2008). Eutrophication and harmful algal blooms: A scientific consensus. *Harmful Algae*, 8(1), 3-13. https://doi.org/10.1016/j.hal.2008. 08.006.

Hoegh-Guldberg, O. (1999) Climate Change, Coral Bleaching and the Future of the World's Coral Reefs. *Marine and Freshwater Research*, 50, 839-866. http://dx.doi.org/10.1071/MF99078.

Intergovernmental Panel on Climate Change (IPCC). (2014). Climate Change 2014: Impacts, Adaptation and Vulnerability. Cambridge University Press.

Kirchman, D. L. (2012). Processes in Microbial Ecology. Oxford University Press, Oxford.

Kirk, J. T. O. (1994). Light and Photosynthesis in Aquatic Ecosystems. Cambridge University Press, Cambridge, p. 509. https://doi.org/10.1017/CBO9780511623370.

Knowlton, N. and Rohwer, F. (2003). *Multispecies microbial* mutualisms on *coral reefs:* The *host* as a *habitat*. *American Naturalist*, 162(4), S51-S62. https://doi.org/ 10.1086/378684.

Lalli,C. M. and Parsons, T. R., (1997). Biological Oceanography: An introduction. *Butterworth-Heinemann* publ., Oxford.

Leahy, J. G. and Colwell, R. R. (1990). Microbial Degradation of Hydrocarbons in the Environment. *Microbiological Reviews*, 54, 305-315.

Lee, R. E. (2008). Phycology, 4th Edition, Cambridge University Press, New York, 645 p.

Lobban, C. S. and Harrison, P. J. (1994). Seaweed Ecology and Physiology. Cambridge University Press, Cambridge, 384 p. http://dx.doi.org/10.1017/CBO97805116 26210.

Madigan, M. T., Martinko, J. M., and Parker, J. (1997). Brock Biology of Microorganisms. 8th Edition, Prentice Hall International, Inc., New York.

Mann, K. H. and Lazier, J. R. N. (2006). Dynamics of Marine Ecosystems: Biological-Physical Interactions in the Oceans. 3rd edn. (Blackwell Science: Malden, MA, USA).

Muscatine, L. and Porter, J. W. (1977). Reef Corals: Mutualistic Symbioses Adapted to Nutrient-Poor Environments. *BioScience*, *27*(7), 454-460. https://doi.org/10.2307/1297526.

Nixon, S. W. (1995) Coastal Marine eutrophication: A definition, social causes, and future concerns. *Ophelia*, 41, 199-219. https://doi.org/10.1080/00785236.1995.104220 44.

Orr, D. W. (2004). Earth in Mind: On Education, Environment, and the Human Prospect. Washington DC: Island Press.

Paerl, H. W. and Huisman, J. (2008). Climate-Blooms Like It Hot. *Science*, 320(5872), 57-58. http://dx.doi.org/ 10.1126/science.1155398.

Pomeroy, L. R. (1974). The ocean's food web, a changing paradigm. BioScience, 24(9), 499-504.

Powles, S. B. (1984). Photoinhibition of Photosynthesis Induced by Visible Light. *Annual Review of Plant Physiology and Plant Molecular Biology*, 35, 15-44. https://doi.org/10.1146/annurev.pp.35.060184.000311.

Reynolds, C. S. (*2006*). The *Ecology* of *Phytoplankton. Cambridge University Press*, Cambridge. https://doi.org/10.1017/CBO9780511542145.

Reynolds, C. S. and Descy, J. P. (1996). The production, biomass and structure of phytoplankton in large rivers. *Archiv fur Hydrobiologie*, 10, 161-187.

Rivkin, R. B. and Legendre, L. (2001). Biogenic carbon cycling in the upper ocean: Effects of microbial respiration. *Science*, 291(5512), 2398-2400.

Round, F. E. (1981). The Ecology of Algae. Cambridge University Press, Cambridge, 653 p.

Scheffer, M., Hosper, S. H., Meijer, M-L., Moss, B., Jeppesen, E. (1993). Alternative equilibria in shallow lakes. *Trends in Ecology & Evolution* 8(8), 275-279. https://doi.org/10.1016/0169-5347(93)90254-M.

Sellner, K. G., Doucette, G. J., and Kirkpatrick, G. J. (2003). Harmful Algal Blooms: Causes, Impacts and Detection. *Journal of Industrial Microbiology and Biotechnology*, 30, 383-406. https://doi.org/10.1007/s10295-003-0074-9.

Schiel, D. R. and Foster, M. S. (2006). The *biology* and *ecology* of *Giant Kelp forests*. University of California Press. Berkeley, *California*, USA. 416 p.

Schinkler, D. W. (2006). Recent Advances in the Understanding and Management of Eutrophication. *Limnology and Oceanography*, 51, 356-363. https://doi.org/10.4319 /lo.2006.51.1_part_2.0356.

Schlesinger, W. H. (1997). Biogeochemistry. An Analysis of Global Change. 2nd Edition, Academic Press, San Diego, London, Boston, New York, Sydney, Tokyo, Toronto, 588 p.

Shiah, F. K. and Ducklow, H. W. (1994). Temperature and substrate regulation of bacterial abundance, production and specific growth-rate in Chesapeake Bay, U.S.A. *Mar. Ecol. Prog. Series* 103, 297-308. https://doi.org/10.3354/meps103297.

Smayda, T. J. (1990). Novel and nuisance phytoplankton blooms in the sea: Evidence for a global epidemic. In: E. Graneli, B. Sundstrom, L. Edler and D.M. Anderson (cds). *Toxic marine phytoplankton.* Elsevier, New York, pp. 29-40.

Smith, S. E. and Read, D. J. (2008). Mycorrhizal Symbiosis. 3rd Edition, Academic Press, London.

Smith, V. H. and Schindler, D. W. (2009). eutrophication science: where do we go from here?. *Trends in Ecology and Evolution*, 24, 201-207. https://doi.org/10.1016/j.tree.2008.11.009.

Smith, V. H., Tilman, G. D., and Nekola, J. C. (1999). Eutrophication: impacts of excess nutrient inputs on freshwater. Marine, and Terrestrial Ecosystems. *Environmental Pollution*, 100, 179-196.

Stal, L. J. (2012). Cyanobacterial mats and stromatolites. In: Whitton BA, ed. Ecology of Cyanobacteria II. Netherlands: Springer, 65-125.

Sverdrup, H. U., Johnson, M. W., and Fleming, R. H. (1942). The Oceans, Their Physics, Chemistry, and General Biology. Prentice-Hall, New York. http://ark.cdlib.org/ark:/13030/kt167nb66r/.

Vitousek, P. M., Aber, J. D., Howarth, R. W., Likens, G. E., Matson, P. A., Schindler, D. W., Schindler, W. H., and Tilman, D. G. (1997). Human Alteration of the Global Nitrogen Cycle: Sources and Consequences. *Ecological Applications*, 7, 737-750.

Wetzel, R. G. (2001). Limnology: Lake and River Ecosystems. Third Edition, Academic Press, San Diego, 1006 p.

Woodward, G., Perkins, D. M., and Brown, L. E. (2010). Climate Change and Freshwater Ecosystems: Impacts across Multiple Levels of Organization. *Philosophical Transactions of the Royal Society B*, 365, 2093-2106. https://doi.org/10.1098/rstb.2010.0055.

CHAPTER 20

Recent Advances in Purification Methods for Glycomics

Hacı Mehmet Kayılı[1]

1 Doç. Dr., Karabük Üniversitesi, Mühendislik Fakültesi, Biyomedikal Mühendisliği, Karabük., https://orcid.org/0000-0002-6740-0645

Introduction

Over the past ten years, glycomics, the study of glycans and their roles in health or disease has been of paramount focus. Unfortunately, due to this complexity, many means of sample preparation are needed to ensure accurate analytical results. Fortunately, several sample preparation methods have been improved to meet the requirements of more efficient and reliable glycomic analyses aiming at high-throughput and clinical diagnostic contexts.

High throughput methodologies (e.g., 96-well plate format) – which allows for concurrent processing of several samples – are high throughput methodologies adapted for glycomics sample preparation. This strategy cut down the time needed to prepare the samples and increased reproducibility. Furthermore, the streamlining of glycomics workflows has been flagged as an important factor in improving the practicality and user-friendliness of these procedures in clinical practice (Zhang, Ma, Chin, & Li, 2020). Given the degree of complexity associated with glycomic analyses, a significant requirement for integrating glycan biomarkers into clinical practice is the automation of processes involved in sample preparation.

Mass spectrometry (MS) has been used frequently in glycomics, and improvements in ionization and separation methods over the past decade have resulted in better structural elucidation and quantitation of glycans. Dong et al. emphasized that there is now excellent workflow streamlining for glycan release, purification, and derivatization through advancements in MS-based techniques, which are key to successful and accurate glycomic analysis(Dong et al., 2018). Furthermore, the importance of efficient sample preparation methods was spotlighted by the emergence of quantitative glycomics, which enables the comparison of glycan profiles of different biological conditions(Peng et al., 2021). The new techniques improve sensitivity and specificity in glycan detection and assist in detecting changes in glycosylation patterns associated with diseases.

Advancements in microseparation have thus opened up new possibilities in glycomics. Liu et.al. presented a detailed analysis of the challenges and resolutions concerning ionization efficiency in microscale environments, making a solid case for innovative approaches to enhancing glycan recovery rates(Liu, 2024). This holds in field situations where an analysis relies on a limited sample, such as cerebrospinal fluid analyses(Cho, Reyes, & Mechref, 2021). Well-deserved recognition of biological effects and the feasibility of biomarkers depends upon the practical analysis of low-abundant glycan forms.

The recent advances in sample preparation methods for glycomics have significantly enhanced the field's analytical capabilities. Improving throughput, automation, and sensitivity pave the way for more comprehensive glycomic analyses that can contribute to our understanding of glycans in terms of health and disease. As the field evolves, ongoing research and development will be essential to address remaining challenges and further refine these methodologies.

This book chapter aims to provide insights into purification methods for glycomics analysis. Recent advancements in these preparation techniques are reviewed, highlighting their role in facilitating glycomics research. Additionally, detailed comparisons of the advantages and challenges of these methods are presented to offer researchers a comprehensive understanding of their application in glycomics studies.

Challenges in Glycan Analysis

The challenge of identifying, analyzing, and quantifying glycans is mainly due to these macromolecules' intricate structures and innate diversity. An unusually diverse array of isomers exists, all structural and stereoisomers, implying no simple identification and measurement. Analytical advances thus far to counter the challenge still pose quite a hurdle. Discrimination in isomeric structures is one major challenge in glycan analysis and was thus developed as a SERS sensor form(Hu et al., 2023). Such innovative approaches suggest better methods by which glycan isomers could be differentiated, a requisite aspect during proper glycomic profiling.

Furthermore, glycans derived from extracellular vesicles (EVs) pose another tough problem in glycan analysis. Wang et al. mentioned that the glycome of EVs has an important role in several biological processes, but the measurement technologies currently limit the analysis of EV glycans(Wang et al., 2020). In addition, the growing number of biological sample sources often contains so many glycan structures that make the analysis difficult. More refined analytical tools are needed to adapt to the unique characteristics of EV glycans. Mass spectrometry (MS) has turned out to be the backbone technique within glycan analysis, although it fails to distinguish between isomeric forms.

Glycans often have a complicated structure and are subject to low abundance in biological samples, especially clinical diagnostic ones. For example, Lageveen-Kammeijer et al. highlighted the dynamic range of glycan abundances and serious difficulty characterizing minor glycoforms in expensive clinical samples(Lageveen-Kammeijer et al., 2019). This requires extremely sensitive and highly efficient sample processing methods to capture and enrich glycans

before analysis. In addition, advanced methods such as capillary electrophoresis coupled with electrospray ionization mass spectrometry (CE-ESI-MS) have been utilized for enhancing detection sensitivity, though still facing problems in acquiring complete glycomic profiles. In addition, O-glycan analyses pose a unique problem compared to N-glycans as there are no consensus sequences for the glycosylation sites, and microheterogeneity is the rule for *O*-glycosylation(Xu, Goonatilleke, Wongkham, & Lebrilla, 2020). This certainly requires a very targeted approach to tackle these complexities associated with O-glycan analysis. As mentioned by Helms et al., these challenges would probably be magnified by advanced informatics tools for application in microheterogeneity contexts(Helms, Escobar, Vainauskas, Taron, & Brodbelt, 2023).

Table 1 summarizes key challenges in glycan analysis, including structural complexity, isomeric diversity, and low abundance in samples, which complicate detection and characterization. It highlights issues with current technologies like mass spectrometry and computational tools and the need for sensitive methods to process and enrich glycans, especially in complex biological and clinical samples.

Table 1. Summary of the challenges in Glycan Analysis.

Challenge	Description	Notes
Structural and Isomeric Diversity	Glycans have convoluted structures with a wide variety of isomers, including structural and stereoisomers, making identification and measurement complex.	- Discrimination between isomeric forms is a significant challenge.
Isomeric Analysis	Mass spectrometry (MS) struggles with resolving isomeric forms.	- Tandem MS and approaches like the reciprocal best-hit method offer some improvement.
Low Abundance in Biological Samples	Glycans often occur in low abundance, particularly in clinical diagnostic samples, necessitating sensitive and efficient sample processing methods.	- Advanced techniques like CE-ESI-MS enhance detection sensitivity but still lack comprehensive profiling.
Dynamic Range of Glycan Abundances	A wide dynamic range of glycan abundances complicates the detection and characterization of minor glycoforms.	- Minor glycoforms are particularly difficult to identify in expensive clinical samples.
Need for Advanced Informatics Tools	Computational tools are required to handle complex glycan structures and microheterogeneity, particularly in O-glycan contexts.	- Informatics solutions are underdeveloped for these complexities.

Purification Approaches for N-Glycan Analysis

Purification of glycans is an important step in glycomics research and directly influences the accuracy and reliability of subsequent analysis. The inherent complexity of the structure of glycans and their low abundance in biological samples have raised an urgent need for the development of effective purification techniques. Various strategies have been tried to enhance glycan purification, all with unique pros and cons. For example, solid-phase extraction (SPE) improves

glycan recovery and concentration from diverse biological matrices and is one of the most widely used glycan purification methods. Recently, Guan et al. have compared different N-glycan preparation techniques and identified solid-phase permethylation followed by nanoLC-MS/MS as having superior purification efficiency over conventional methods(Guan, Zhang, Wang, & Schlüter, 2021).

Another hopeful purification technique is one that also employs carbon nanoparticles (CNPs) and graphene nanosheets as matrix materials in matrix-assisted laser desorption/ionization (MALDI) mass spectrometry. Banazadeh et al. showed these benefits for glycan profiling with increased sensitivity and specificity by employing analysis via MALDI(Banazadeh, Peng, Veillon, & Mechref, 2018). Zhong et al. used a CNP-based solid-phase purification method and sensitive MALDI-MS analysis of permethylated N-glycans while achieving minimal losses in the sample and avoiding using toxic solvents for analysis(Zhong, Banazadeh, Peng, & Mechref, 2018). Thus, the advances underscore nanomaterials' possibilities in improving glycan purification processes. Other innovative techniques have been developed in addition to solid-phase extraction to facilitate glycan purification. The glycoblotting method described by Montalban and Hinou has proven effective for N-glycan extraction from human serum with an efficiency of recovery of 72.5%(Montalban & Hinou, 2023). Such integrated systems could lessen the time and complexity associated with the older purification methods.

Automated purification techniques have been found to gain some ground in glycomics research as well. Vreeker et al. presented a method of using high-throughput plates for automated glycan purification; however, they observed variability with batch to batch(Vreeker et al., 2018). Automation of the glycan purification process is significant in clinical settings where the speed of handling samples is critical. In addition to this, magnetic nanoparticles were reported as very efficient tools in glycans purification. According to Kayili et al., poly(amidoamine) dendrimer-coated magnetic nanoparticles were used to rapidly purify and selectively enrich glycopeptides and glycans(Kayili, Ertürk, Elmacı, & Salih, 2019). This supplements glycan recovery, making it easier and more amenable to high-throughput applications.

HILIC covers a wide interface for polar compound separation and is effectively used for glycan purification. This methodology further exploits that glycans are hydrophilic, which retains and elutes glycans from the stationary phase. On the other hand, lectin affinity chromatography (LAC) is another powerful glycan purification method, leveraging lectins' specific binding properties to isolate glycan structures. Lectins are carbohydrate-binding proteins

that exhibit high specificity for specific glycan motifs, making them invaluable tools in glycomics. Kanao et al. emphasized the utility of lectins in profiling glycan structures on extracellular vesicles, showcasing their ability to provide detailed information on glycosylation patterns(Kanao et al., 2022). This approach allows for profiling native glycoproteins and is particularly advantageous for screening biological samples. Furthermore, lectin-based methods can be integrated with mass spectrometry for enhanced glycan characterization. Despite these advances, challenges persist regarding the optimal purification of glycans. The need to make further purification steps might induce losses and degradation of glycans. Thus, Hu insists that the development of a methodology that allows for direct analysis of unprocessed biological samples is necessary(Hu, 2024).

Purification Approaches for O-Glycan Analysis

The conventional method of reductive β-elimination for O-glycan release has been utilized extensively because of its efficiency in cleaving O-glycans from glycoproteins. Fu et al. showed that this method released O-glycans in their alditol form, which could then be profiled on porous graphitized carbon columns and analyzed online LC-MS(Fu et al., 2019). However, specific glycans are lost in this procedure, and others may not work effectively, especially those considered sensitive to the harsh conditions used in this method of reductive β-elimination. Song et al. introduced an oxidative release method based on DMSO/NaOH/iodomethane for inducing O-glycan release and providing permethylation(Song et al., 2016). This strategy resulted in diverse O-glycans from mouse stomach samples for functional glycomics. The oxidative method appears to be an attractive alternative to classical methods, mainly when these studies are performed on complex biological samples and involve high diversity in O-glycans.

One more novel technique was using ammonium carbamate to release O-glycans, as explained(Miura et al., 2010). Thus, O-glycans are released from glycoproteins, which can then be analyzed. They emphasized that such an approach is advantageous for glycoproteins available in scant amounts in biological fluids, as this could increase the yield of target O-glycans through immunoprecipitation procedures. Other than these, the advancements in solid-phase extraction methods have shown promising results in better O-glycan purification. Yang et al. proposed a solid-phase capture technique that directly analyzes glycoproteins without further purification(Yang, Li, Shah, & Zhang, 2013). This method decreases the loss of the sample and increases the sensitivity of detection, thus making it possible to obtain low amounts of O-glycans. This

method is much more versatile as glycan modifications can be done directly on the solid phase.

Furthermore, advanced chromatographic approaches, such as C18 nanoliquid chromatography, have been employed for the in-depth analysis of O-glycan isomers. Haan et al. have shown from the reports that the method works pretty well for analyzing O-glycan isomers from human cells and inferring subsequent structures of added or missing glycosylation(Haan et al., 2022). It is perfect for rupturing isomers as the fine details of their anatomy significantly impact their interactions and functions, so this is a good step toward understanding biological functions concerning O-glycans.

Conclusion and Future Perspectives

Glycomics has made exciting strides in sample preparation and analytical techniques, making important steps toward tackling the challenges in complexity, diversity, and low abundance associated with glycan analyses in biological samples. High-throughput methods have converted such workflows into higher reproducibility and efficiency formats, such as 96-well plate formats. Automation and microscale techniques have opened new possibilities for the clinical sphere by allowing analyses of tiny sample volumes with much higher sensitivity. Purification techniques have come a long way, with current innovative solid-phase extraction, HILIC, lectin affinity chromatography, and nanomaterial-assisted techniques, which have led to new, reliable and efficient workflows. Mainly, it will improve glycan recovery and the detection of minor glycoforms and isomers, which are crucial for understanding events related to glycan biology and disease mechanisms.

Improved methods, such as oxidative release and advanced chromatographic approaches, gave a significant nudge towards comprehensive glycomic profiling for both N-glycan and O-glycan analyses. However, challenges still lie ahead in the search for more sensitive, specific, and scalable purification techniques that can be smoothly incorporated into high-throughput systems. Emerging research and innovative practices are thus eliminating obstacles to more accurate, practical analyses in glycomics. Such innovations will better understand the complex glycan functions in health and disease, resulting in disruptive progress in biomedical research and personalized medicine.

References

Banazadeh, A., Peng, W., Veillon, L., & Mechref, Y. (2018). Carbon Nanoparticles and Graphene Nanosheets as MALDI Matrices in Glycomics: A New Approach to Improve Glycan Profiling in Biological Samples. *Journal of the American Society for Mass Spectrometry, 29*(9), 1892-1900. doi:10.1007/s13361-018-1985-z

Cho, B. G., Reyes, C. D. G., & Mechref, Y. (2021). N-Glycomics of Cerebrospinal Fluid: Method Comparison. *Molecules, 26*(6), 1712. doi:10.3390/molecules26061712

Dong, X., Huang, Y., Cho, B. G., Zhong, J., Gautam, S., Peng, W., Mechref, Y. (2018). Advances in Mass Spectrometry-based Glycomics. *Electrophoresis, 39*(24), 3063-3081. doi:10.1002/elps.201800273

Fu, Q., Li, G., Wang, C., Ya, W., Li, Q., Hao, J., & Yu, G. (2019). Profiling and Structural Characterization of High Neu5Gc or Sulfate-Containing O-Glycans From Hyla Rabbit Intestinal Mucin. *Molecules, 24*(7), 1365. doi:10.3390/molecules24071365

Guan, Y., Zhang, M., Wang, J., & Schlüter, H. (2021). Comparative Analysis of Different N-Glycan Preparation Approaches and Development of Optimized Solid-Phase Permethylation Using Mass Spectrometry. *Journal of Proteome Research, 20*(5), 2914-2922. doi:10.1021/acs.jproteome.1c00135

Haan, N. d., Narimatsu, Y., Aasted, M. K. M., Larsen, I. S. B., Marinova, I. N., Dabelsteen, S., . . . Wandall, H. H. (2022). In-Depth Profiling of O-Glycan Isomers in Human Cells Using C18 Nanoliquid Chromatography–Mass Spectrometry and Glycogenomics. *Analytical Chemistry, 94*(10), 4343-4351. doi:10.1021/acs.analchem.1c05068

Helms, A., Escobar, E. E., Vainauskas, S., Taron, C. H., & Brodbelt, J. S. (2023). Ultraviolet Photodissociation Permits Comprehensive Characterization of O-Glycopeptides Cleaved With O-Glycoprotease IMPa. *Analytical Chemistry, 95*(24), 9280-9287. doi:10.1021/acs.analchem.3c01111

Hu, Q. (2024). Direct Glycan Analysis of Biological Samples and Intact Glycoproteins by Integrating Machine Learning-Driven Surface-Enhanced Raman Scattering and Boronic Acid Arrays. *Acs Measurement Science Au, 4*(3), 307-314. doi:10.1021/acsmeasuresciau.4c00014

Hu, Q., Kuai, D., Park, H., Clark, H., Balbuena, P. B., Kwon, J., & Wu, H. J. (2023). Advancing Glycan Analysis: A New Platform Integrating SERS, Boronic Acids, and Machine Learning Algorithms. doi:10.1101/2023.02.03.527030

Kanao, E., Wada, S., Nishida, H., Kubo, T., Tanigawa, T., Imami, K., . . . Ishihama, Y. (2022). Classification of Extracellular Vesicles Based on Surface Glycan Structures by Spongy-Like Separation Media. *Analytical Chemistry, 94*(51), 18025-18033. doi:10.1021/acs.analchem.2c04391

Kayili, H. M., Ertürk, A., Elmacı, G., & Salih, B. (2019). Poly(amidoamine) Dendrimer-coated Magnetic Nanoparticles for the Fast Purification and Selective Enrichment of Glycopeptides and Glycans. *Journal of Separation Science, 42*(20), 3209-3216. doi:10.1002/jssc.201900492

Lageveen-Kammeijer, G. S. M., Haan, N. d., Mohaupt, P., Wagt, S., Filius, M., Nouta, J., Wuhrer, M. (2019). Highly Sensitive CE-ESI-MS Analysis of N-Glycans From Complex Biological Samples. *Nature Communications, 10*(1). doi:10.1038/s41467-019-09910-7

Liu, C. (2024). Recent Advances in Microscale Separation Techniques for Glycome Analysis. *Journal of Separation Science, 47*(11). doi:10.1002/jssc.202400170

Miura, Y., Kato, K., Takegawa, Y., Kurogochi, M., Furukawa, Y., Shinohara, Y., Nishimura, S. I. (2010). Glycoblotting-Assisted O-Glycomics: Ammonium Carbamate Allows for Highly Efficient O-Glycan Release From Glycoproteins. *Analytical Chemistry, 82*(24), 10021-10029. doi:10.1021/ac101599p

Montalban, B. M., & Hinou, H. (2023). Glycoblotting Enables Seamless and Straightforward Workflow for MALDI-TOF/MS-based Sulphoglycomics of N and O-glycans. *Proteomics, 23*(19). doi:10.1002/pmic.202300012

Peng, W., Reyes, C. D. G., Gautam, S., Yu, A., Cho, B. G., Goli, M.,Mechref, Y. (2021). MS-based Glycomics and Glycoproteomics Methods Enabling Isomeric Characterization. *Mass Spectrometry Reviews, 42*(2), 577-616. doi:10.1002/mas.21713

Song, X., Ju, H., Lasanajak, Y., Kudelka, M. R., Smith, D. F., & Cummings, R. D. (2016). Oxidative Release of Natural Glycans for Functional Glycomics. *Nature Chemical Biology, 13*(6), 528-534. doi:10.1038/nmeth.3861

Vreeker, G. C. M., Nicolardi, S., Bladergroen, M. R., Corné, J. v. d. P., Mesker, W. E., Tollenaar, R. A., Wuhrer, M. (2018). Automated Plasma Glycomics With Linkage-Specific Sialic Acid Esterification and Ultrahigh Resolution MS. *Analytical Chemistry, 90*(20), 11955-11961. doi:10.1021/acs.analchem.8b02391

Wang, Z., Sun, X., Natalia, A., Tang, C., Ang, C. B. T., Ong, C.-A. J., . . . So, J. B. Y. (2020). Dual-Selective Magnetic Analysis of Extracellular Vesicle Glycans. *Matter, 2*(1), 150-166. doi:10.1016/j.matt.2019.10.018

Xu, G., Goonatilleke, E., Wongkham, S., & Lebrilla, C. B. (2020). Deep Structural Analysis and Quantitation of O-Linked Glycans on Cell Membrane Reveal High Abundances and Distinct Glycomic Profiles Associated With Cell Type and Stages of Differentiation. *Analytical Chemistry, 92*(5), 3758-3768. doi:10.1021/acs.analchem.9b05103

Yang, S., Li, Y., Shah, P., & Zhang, H. (2013). Glycomic Analysis Using Glycoprotein Immobilization for Glycan Extraction. *Analytical Chemistry, 85*(11), 5555-5561. doi:10.1021/ac400761e

Zhang, Q., Ma, C., Chin, L. S., & Li, L. (2020). Integrative Glycoproteomics Reveals Protein N-Glycosylation Aberrations and Glycoproteomic Network Alterations in Alzheimer's Disease. *Science Advances, 6*(40). doi:10.1126/sciadv.abc5802

Zhong, J., Banazadeh, A., Peng, W., & Mechref, Y. (2018). A Carbon Nanoparticles-based Solid-phase Purification Method Facilitating Sensitive MALDI–MS Analysis of Permethylated N-glycans. *Electrophoresis, 39*(24), 3087-3095. doi:10.1002/elps.201800254

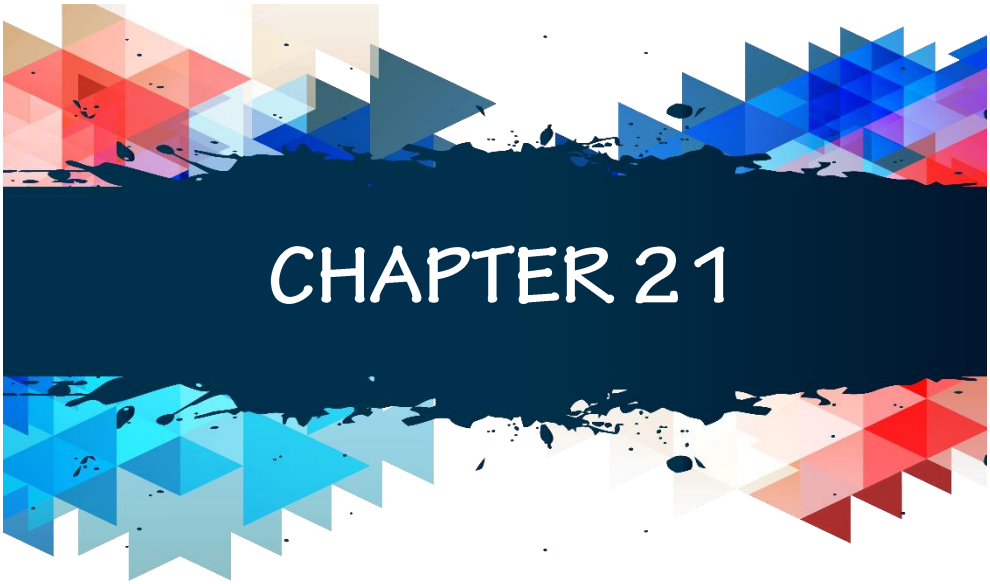

Mass Spectrometry-Based Approaches for the Analysis of Glycans

Hacı Mehmet Kayılı[1]

1 Doç. Dr., Karabük Üniversitesi, Mühendislik Fakültesi, Biyomedikal Mühendisliği, Karabük., https://orcid.org/0000-0002-6740-0645

Introduction

Mass spectrometry (MS) has become a powerful tool in glycomics, enabling glycans' structural characterization and quantitative analysis (Dong et al., 2018; Wuhrer, 2012). Glycans, complex carbohydrates linked to proteins and lipids, have important roles in various biological processes and are frequently altered in disease states(Sethi & Fanayan, 2015; Yoshida et al., 2016). Advances in separation methods and bioinformatics, along with the advancement of MS-based techniques, have led to significant advances in the field of glycomics (Dong et al., 2018; Rojas-Macias et al., 2019). Liquid chromatography-tandem mass spectrometry (LC-MS/MS) has emerged as the tool of choice for comprehensive glycan analysis, allowing the identification, structural elucidation, and quantification of glycans from complex biological samples(Kim et al., 2015; Kronewitter et al., 2012; Nwosu et al., 2012).

Glycomics studies have provided valuable insights into the role of glycans in disease mechanisms and are being used to identify potential glycan-based biomarkers for various diseases(Haci Mehmet Kayili & Salih, 2021). MS-based glycomics are important because they allow the detection of low amounts of glycans and precisely characterize their structure, making them a valuable tool in biomarker discovery (Liu et al., 2023). Besides, developing standard bioinformatics workflows and public repositories allows the integration of MS-based glycomics data by other omics fields. This enables more comprehensive and reproducible analyses(Rojas-Macias et al., 2019). Moreover, advances in quantitative glycomics approaches have increased the reliability and efficiency of glycan quantification(Zhou et al., 2016).

Glycomics studies have led to the discovery of potential glycan-based biomarkers for various diseases. This could significantly improve the early detection of diseases, disease monitoring, and the development of targeted therapies. The ability of MS-based glycomics to detect low amounts of glycans and precisely characterize their structure has been helpful in this respect. However, the transition of glycan-based biomarkers from detection to the clinical phase poses several challenges, including the widespread heterogeneity of distinguished glycoforms and the sensitivity of the glycosylation machinery to the biological situation. Standardizing analytical methods, bioinformatics workflows, and developing high-throughput and reliable glycan analysis tools are needed for the broader adoption of clinical glycomics. Moreover, integrating glycomics data with other “omics” approaches, such as genomics and proteomics, can provide a more comprehensive understanding of disease mechanisms and facilitate the development of personalized diagnostic and therapeutic strategies.

The rise of systems glycobiology and personalized glycomics demonstrates the importance of glycan analysis in clinical settings.

Mass spectrometry (MS) is the most widely used analytical technique for characterizing glycans and glycoconjugates(Grabarics et al., 2021; Puranik et al., 2022). Due to the structural diversity of glycans, their comprehensive analysis is quite challenging. In addition, the analysis of structural isomers of glycans requires sensitive analytical techniques capable of distinguishing these changes. Mass spectrometric systems combined with complementary methods such as liquid chromatography (LC) or capillary electrophoresis (CE) provide the sensitivity and resolution required for these purposes. The development of new sample preparation and derivatization techniques, such as fluorescent labeling and stable isotope labeling, has significantly improved the sensitivity, quantification, and separation of different glycan types in MS-based analyses(Pallister et al., 2020; Zheng et al., 2016). This has enabled a more comprehensive and accurate characterization of glycans and glycoconjugates.

In glycan analysis, different mass spectrometers are used to examine glycans' complex structures and variations in detail. Matrix-assisted laser Desorption/Ionization (MALDI-MS) is the method of choice for fast and sensitive glycan profile analysis and improves ionization efficiency, especially for ethyl-esterified and permethylated glycans. Electrospray Ionization (ESI-MS) integrated liquid chromatographic (LC) methods having tandem mass spectrometry (MS/MS) capabilities to analyze branching and binding information of glycan structures. Ion Mobility Spectrometry (IMS-MS) can distinguish structural isomers and provide an additional dimension to the m/z ratio by examining the three-dimensional properties of glycans. The cross-sectional areas of glycans can be calculated using this method. On the other hand, ultra-high mass resolution instruments, including Orbitrap and Fourier-Transform Ion Cyclotron Resonance (FT-ICR-MS) mass analyzers, enable sensitive and accurate mass measurements and structural analysis of glycans. These various methods play a critical role in understanding the biological functions of glycans and their relationship to disease. In addition, mass spectrometry is often supplemented by pre-treatments used to characterize glycans better. Derivatization techniques such as permethylation and reductive amination improve the ionization of glycans and increase spectral resolution(Shajahan, Supekar, Heiss, & Azadi, 2019). These technologies play a critical role in understanding the biological functions of glycans, investigating their association with diseases, and discovering potential biomarkers. Thus, mass spectrometry has become an vital technique for the structural examination of glycans.

This book chapter aims to provide information about glycomics analysis performed by mass spectrometric methods. Recent developments in these analyses are reviewed in this book chapter. In addition, detailed comparisons of the advantages and difficulties of the analyses are presented to provide researchers with a better understanding of these methods.

Functions of Glycans

Glycans play critical characters in different biological processes including cell-cell communication and cell-microorganism interactions. For example, cell surface glycans help immune system recognize infected/damaged cells(Nishihara, 2018; Schnaar, 2015). Glycan-binding proteins such as selectins and galectins regulate the immune response and inflammation, making the functions of glycans in the immune system more prominent(Eckardt, Weber, & Hundelshausen, 2019). Furthermore, glycans have an important role in cell signalling; for example, signalling pathways regulated by glycans play key roles in processes such as cell growth, differentiation, and apoptosis(Briard, Jiang, Moremen, Macauley, & Wu, 2018). In addition, glycans have been reported to act as a protective barrier in biological systems(Viswanathan et al., 2010). Surrounding the cell surface, glycans form a physical barrier against pathogens and protect the cell from mechanical damage. On the other hand, glycosylated proteins are less susceptible to proteolytic enzymes. Studies show that they also play an active role in regulating the immune response(Schnaar, 2015). Furthermore, glycans are involved in various pathogen-binding mechanisms; viruses, bacteria, and parasites target glycan structures to attach to the cell and initiate infection. Thus, glycans can act both as an entry point for pathogens and as a marker for the immune system to recognize these pathogens. On the other hand, the misregulation of glycans plays an important role in many pathological conditions(Kitov et al., 2019). These functions define glycans as essential regulatory molecules in biological systems.

Glycans are classified into several types according to their structural properties and biological functions (Figure 1). Generally, glycans are divided into categories according to the linked monosaccharide units, chain length, and branching properties. N-linked glycans are glycans linked to the side chain of the amino acid asparagine (Asn) and are one of the most common types of protein glycosylation. These glycans usually start with an N-acetylglucosamine (GlcNAc) molecule and can form complex structures. N-linked glycans are divided into three main subtypes: high mannose, complex and hybrid. These play important roles in protein folding, stabilization, and cell-cell interactions. O-linked glycans are attached to the hydroxyl groups of serine (Ser) or threonine

(Thr) amino acids. These glycans usually start with N-acetylgalactosamine (GalNAc) and can form short, linear structures or complex branched chains. Glycans in mucus proteins are usually O-linked and provide a protective barrier on mucosal surfaces.

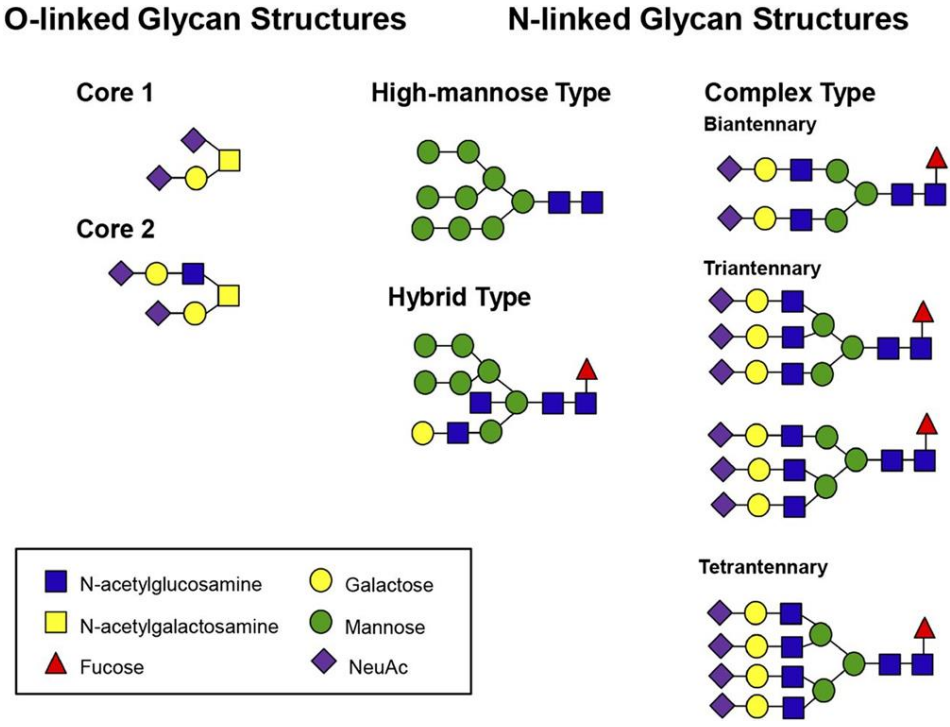

Figure 1. *N*- and *O*-linked glycans.

Figure 1 shows the main structural features and types of the two main types of glycans, *O*-linked and *N*-linked glycans. O-linked glycans have a core structure (Core 1 or Core 2) attached to the amino acid serine or threonine and are usually short-chain and branched structures. N-linked glycans bind to the amino acid of asparagine and are divided into three main subtypes. These are high-mannose, hybrid, and complex types. High-mannose structures contain only mannose with GlcNAc. Complex types include diverse monosaccharides such as galactose, sialic acid, and fucose. N-linked complex glycans are classified as biantennary, triantennary, or tetraantennary according to their degree of branching. The coloured symbols in the figure represent the basic building blocks of these glycans.

Sample Preparation Strategies for Mass Spectrometry-based Glycomics

Sample preparation steps are important to achieve a successful result in glycomic analyses based on mass spectrometry (MS). Proper sample preparation is the most critical point in analyzing glycans reliably and reproducibly. The first step in glycan analysis is the release of glycans from the biological sample to be analyzed. This process usually involves the enzymatic or chemical liberation of glycan modifications of proteins. N-glycans are usually liberated by the enzyme peptide-N-glycosidase F (PNGase F), while O-glycans are removed by chemical β-elimination methods(H. Mehmet Kayili, Atakay, Hayatu, & Salih, 2022). Recently, a much faster process has been achieved in *O*-glycan analysis. In this process, only O-glycans are released and analyzed by HPLC-HILIC-FLD-MS/MS or MALDI-MS(Kameyama, Thet Tin, Toyoda, & Sakaguchi, 2019). The protocols applied must be carefully optimized to maintain the specificity and structural integrity of the glycans. The released glycans should be cleaned and concentrated prior to mass spectrometry analysis. A cleanup step is often necessary to eliminate impurities, which suppresses the signal during analysis. Solid-phase extraction (SPE) methods are widely used to purify glycans from impurities(Haci Mehmet Kayili & Salih, 2021). Glycans can be analyzed in their natural form or after derivatization. For high-sensitivity analysis, glycans can be chemically treated such as permethylation or ethyl-esterification, especially for MALDI-MS analysis(Hu, Desantos-Garcia, & Mechref, 2013). This process increases the ionization efficiency of glycans and provides stronger signals in the analysis. On the other hand, glycans can also be labeled and analyzed by reductive amination(Reider, Szigeti, & Guttman, 2018).

Derivatization is an important step for the structural characterization of glycans. For example, fluorescent labeling facilitates the separation of glycans by high-performance liquid chromatography (HPLC) and detection by MS. Similarly, modifications such as permethylation or ethyl-esterification increase the sensitivity of analysis by reducing the polarity of glycans. Especially in MALDI-MS analysis, sialic acids are made more stable, allowing MALDI-MS analysis to be performed efficiently(Masri et al., 2024).

Figure 2 presents a step-by-step process flow describing analyzing glycans from glycoproteins. The analysis starts with the release of the glycans of the glycoproteins, which is performed by two different methods. The PNGase F enzyme releases N-glycans, while O-glycans are released by β-elimination. These two methods are designed to target different types of glycans, and the choice of the method used at the initial stage of analysis depends on the characteristics of

the glycoprotein to be analyzed. Both methods provide a suitable basis for preparing glycans for subsequent derivatization or labeling steps.

Following the release, the glycans are prepared for analysis by one of two different processing routes. The first route involves derivatization of the glycans by permethylation or ethyl esterification, which increases the stability of the glycans and makes them suitable for mass spectrometry analysis(Haci Mehmet Kayili et al., 2023). The second route involves labelling glycans by fluorescent labelling, which is helpful for visualization and detection. At the end of both processing routes, the glycans are purified by solid phase extraction (SPE) and then analyzed by mass spectrometry (MS). This combination of methods offers an efficient process for glycans' structural and quantitative characterization. The figure summarizes the key steps of this process and how the different pathways can be combined.

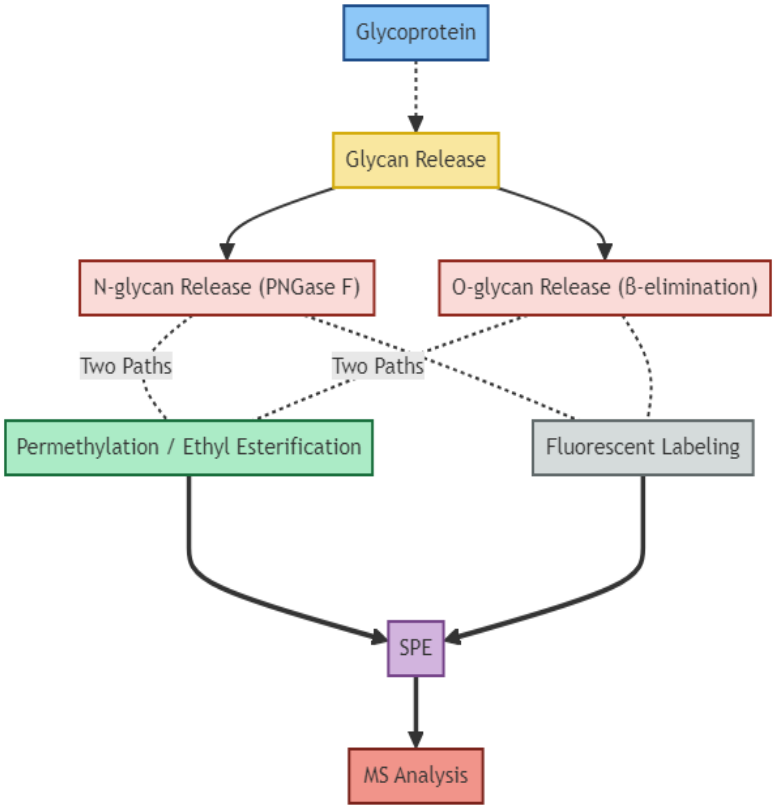

Figure 2. *N- and O*-glycan Analysis Workflow for MS-based glycomics.

MALDI-MS Analysis of Glycans

Matrix-assisted laser Desorption/Ionization Mass Spectrometry (MALDI-MS) is a fast and sensitive technique that is widely used in glycan analysis. This method is helpful for structural identification, profiling and determination of isomeric variations of glycans(Atakay, Kayılı, & Salih, 2024). MALDI-MS allows the acquisition of spectra of glycans with high resolution. Since glycans are generally polar and highly soluble in water, MALDI-MS conveniently enables the analysis of such molecules by matrix-assisted laser ionization(Demirhan, Yılmaz, Erol, Kayili, & Salih, 2023). In a MALDI-MS analysis, the glycans are mixed with a matrix, which protects the glycans before exposure to the laser beam and promotes ionization. One of the matrices commonly used in glycan analysis is 2,5-dihydroxybenzoic acid (DHB). MALDI-MS is often supported by pre-treatments such as permethylation, which increases the ionization efficiency of glycans, resulting in more consistent and powerful spectra. On the other hand, binding-specific ethyl-esterification is also useful. Permethylated or ethyl-esterified glycans increase signal intensity in MALDI-MS analysis and provide structural information more reliable.

MALDI-MS is highly effective in determining the structures of glycans, but even more so when combined with tandem mass spectrometry (MS/MS). MS/MS modes can resolve glycans' branching points and isomers in detail. This combination can distinguish glycan isomers, and glycan profiles can be accurately determined. In addition, MALDI-MS is an ideal tool for analyzing the high number of batches of samples due to its high throughput. It has been particularly critical in identifying glycoform changes associated with conditions such as cancer, diabetes and neurological diseases. For example, changes in sialylation and fucosylation levels can be employed to identify disease conditions and monitor their advancement. On the other hand, with the integration of artificial intelligence applications such as machine learning into data analysis, the MALDI-MS may make significant contributions to the development of glycan science by offering fast diagnosis.

ESI-MS Analysis of Glycans

ESI-MS is a powerful technique for analyzing biomolecules. It works by ionizing molecules in a solution and transferring them into the gas phase. ESI-MS is particularly valuable in protecting structural details. It is also useful for delicate glycan modifications like sialic acids. The resulting mass spectra provide critical information such as glycans' composition, molecular weight, and charge state. They are essential for structural characterization. A significant strength of

ESI-MS in glycan analysis is its compatibility with tandem mass spectrometry (MS/MS) techniques. Through MS/MS, glycan precursor ions are fragmented in the gas phase, producing fragmentation spectra that provide critical insights into structural characteristics like linkage positions and branching sites(H. M. Kayili, 2020). Commonly used fragmentation methods, such as collision-induced dissociation (CID) and high-energy collision dissociation (HCD), are especially valuable for in-depth structural investigations. This capability enables the determination of the structural conformation of glycans(H. M. Kayili & Salih, 2022).

One of the significant advantages of ESI-MS in glycan analysis is its ability to handle complex mixtures commonly found in biological samples. ESI-MS provides detailed structural information about glycans, including monosaccharide composition, linkage positions, and branching patterns, which are crucial for understanding their biological roles and investigating their potential as biomarkers. Many studies have demonstrated the application of ESI-MS in the analysis of N-linked and O-linked glycans, glycosphingolipids, and glycosaminoglycans. The integration of ESI-MS with liquid chromatography (LC-ESI-MS) or capillary electrophoresis (CE-ESI-MS) has further increased its separation and detection capabilities, enabling the analysis of complex glycan mixtures with brilliant sensitivity and resolution(Tahhan, Aksoy, Kayili, & Salih, 2023). Furthermore, advances in ionization techniques, such as using dopant-enriched nitrogen gas (DEN-gas) at the ESI interface, have significantly improved the sensitivity and reproducibility of glycan analysis(Madunić, Wagt, Zhang, Wuhrer, & Lageveen-Kammeijer, 2021). This innovation has been beneficial for detecting low-abundance and labile glycans that are difficult to analyze using traditional ESI-MS methods. Beyond structural characterization, ESI-MS is also used for quantitative analysis of glycans, facilitating the study of glycan heterogeneity and the identification of disease-associated glycan signatures. Combining ESI-MS with affinity-based methods such as capture and release ESI-MS has further expanded its capabilities by enabling the discovery of glycan-binding proteins and their interactions.

Ion Mobility-Mass Spectrometry (IM-MS) Analysis of Glycans

Ion mobility-mass spectrometry (IM-MS) has emerged as a powerful analytical technique for structurally characterizing complex carbohydrates, including glycans(Atakay, Kayılı, Güler, & Salih, 2024). IM-MS combines the benefits of mass spectrometry, such as high sensitivity and mass accuracy, with the ability to separate ions based on their size, shape, and charge, allowing for the discrimination of isomeric glycans(Pagel & Harvey, 2013).

The IM-MS approach provides several advantages for glycan analysis. Firstly, mass spectrometry alone can resolve indistinguishable isomeric glycans (Manz & Pagel, 2018). This is particularly important given glycans' structural complexity and heterogeneity, which often contain numerous regio- and stereoisomers. The collision cross-section (CCS) values obtained from IM-MS can be used as an additional search parameter for database analyses of glycans(Re et al., 2018). Furthermore, IM-MS has been successfully applied to the analysis of *N*-linked glycans, glycopeptides, and other glycoconjugates(Pallister et al., 2020).

The technique can separate glycans from peptides in the same digest without purification, enabling the comprehensive characterization of glycoproteins. IM-MS has also been used to study the retention of anomericity in glycosidic bonds upon collision-induced dissociation (CID). Several studies have demonstrated the utility of IM-MS for the structural elucidation of glycans. They have used IM-MS to determine the CCS values of sodiated N-linked glycans, highlighting the potential to implement IM-derived CCS information in glycan database analyses(Pagel & Harvey, 2013). They also showed that IM-MS can discriminate between epimeric glycans and glycopeptides, suggesting its potential for carbohydrate sequencing.

MALDI-Imaging Analysis (MALDI-IMS) of Glycans

MALDI-IMS has emerged as a powerful technique for spatial profiling and characterization of N-linked glycans in tissue sections(Drake et al., 2020; Mittal et al., 2020; Powers, Holst, Wuhrer, Mehta, & Drake, 2015).This approach enables visualization of glycan distribution and changes associated with various diseases, especially cancer. MALDI-IMS analysis is typically performed on formalin-fixed paraffin-embedded (FFPE) tissue sections. N-linked glycans are enzymatically released from glycoproteins using PNGase F digestion. Glycan purification and desalting steps are crucial to improve MALDI-IMS detection(Banazadeh, Williamson, Zabet, Hussien, & Mechref, 2018).

Glycan ion images are generated using software such as flexImaging, and glycan structures are identified by matching them with databases(Scott et al., 2019). MALDI-IMS can detect changes in glycan expression and branching patterns associated with diseases such as cancer(West et al., 2018). Sialic acid derivatization strategies stabilize labile glycans for enhanced MALDI-IMS detection(Holst et al., 2016). Novel MALDI matrices, such as carbon nanoparticles and graphene nanosheets, can improve glycan ionization and detection(Banazadeh, Peng, Veillon, & Mechref, 2018).

MALDI-IMS has been used to profile N-linked glycans in various tissues, including kidney, liver, prostate, and ovarian cancer(Mittal et al., 2020). Cancer tissues have been observed to have increased branching, fucosylation, and high-mannose-type glycans compared to healthy controls (Powers et al., 2014). MALDI-IMS can provide spatial information on glycan changes during disease progression, such as liver fibrosis and hepatocellular carcinoma(Ochoa-Rios, 2024).

References

Atakay, M., Kayılı, H. M., Güler, Ü., & Salih, B. (2024). Ion Mobility-Mass Spectrometry for Macro-molecule Analysis. *Applications of Modern Mass Spectrometry: Volume 2*, 1.

Atakay, M., Kayılı, H. M., & Salih, B. (2024). Sample preparation for glycoproteins.

Banazadeh, A., Peng, W., Veillon, L., & Mechref, Y. (2018). Carbon Nanoparticles and Graphene Nanosheets as MALDI Matrices in Glycomics: A New Approach to Improve Glycan Profiling in Biological Samples. *Journal of the American Society for Mass Spectrometry, 29*(9), 1892-1900. doi:10.1007/s13361-018-1985-z

Banazadeh, A., Williamson, S. D., Zabet, M., Hussien, A. M., & Mechref, Y. (2018). Magnetic Carbon Nanocomposites as a MALDI Co-Matrix Enhancing MS-based Glycomics. *Analytical and Bioanalytical Chemistry, 410*(28), 7395-7404. doi:10.1007/s00216-018-1345-7

Briard, J. G., Jiang, H., Moremen, K. W., Macauley, M., & Wu, P. (2018). Cell-Based Glycan Arrays for Probing Glycan–glycan Binding Protein Interactions. *Nature Communications, 9*(1). doi:10.1038/s41467-018-03245-5

Demirhan, D. B., Yılmaz, H., Erol, H., Kayili, H. M., & Salih, B. (2023). Prediction of gastric cancer by machine learning integrated with mass spectrometry-based N-glycomics. *Analyst, 148*(9), 2073-2080. doi:10.1039/D2AN02057B

Dong, X., Huang, Y., Cho, B. G., Zhong, J., Gautam, S., Peng, W., . . . Mechref, Y. (2018). Advances in Mass Spectrometry-based Glycomics. *Electrophoresis, 39*(24), 3063-3081. doi:10.1002/elps.201800273

Drake, R., McDowell, C., West, C. A., David, F., Powers, T. W., Nowling, T. K., . . . Copland, J. A. (2020). Defining the Human Kidney N-glycome in Normal and Cancer Tissues Using MALDI Imaging Mass Spectrometry. *Biological Mass Spectrometry, 55*(4). doi:10.1002/jms.4490

Eckardt, V., Weber, C., & Hundelshausen, P. v. (2019). Glycans and Glycan-Binding Proteins in Atherosclerosis. *Thrombosis and Haemostasis, 119*(08), 1265-1273. doi:10.1055/s-0039-1692720

Grabarics, M., Lettow, M., Kirschbaum, C., Greis, K., Manz, C., & Pagel, K. (2021). Mass Spectrometry-Based Techniques to Elucidate the Sugar Code. *Chemical Reviews, 122*(8), 7840-7908. doi:10.1021/acs.chemrev.1c00380

Holst, S., Heijs, B., Haan, N. d., René, J. M. v. Z., Bruijn, I. H. B., Pelt, G. W. v., Wuhrer, M. (2016). Linkage-Specific in Situ Sialic Acid Derivatization for N-Glycan Mass Spectrometry Imaging of Formalin-Fixed Paraffin-Embedded Tissues. *Analytical Chemistry, 88*(11), 5904-5913. doi:10.1021/acs.analchem.6b00819

Hu, Y., Desantos-Garcia, J. L., & Mechref, Y. (2013). Comparative Glycomic Profiling of Isotopically Permethylated N-glycans by Liquid Chromatography/Electrospray Ionization Mass Spectrometry. *Rapid Communications in Mass Spectrometry, 27*(8), 865-877. doi:10.1002/rcm.6512

Kameyama, A., Thet Tin, W. W., Toyoda, M., & Sakaguchi, M. (2019). A practical method of liberating O-linked glycans from glycoproteins using hydroxylamine and an organic superbase. *Biochemical and Biophysical Research Communications, 513*(1), 186-192. doi:https://doi.org/10.1016/j.bbrc.2019.03.144

Kayili, H. M. (2020). Identification of bisecting N-glycans in tandem mass spectra using a procainamide labeling approach for in-depth N-glycan profiling of biological samples. *International Journal of Mass Spectrometry, 457*. doi:10.1016/j.ijms.2020.116412

Kayili, H. M., Atakay, M., Hayatu, A., & Salih, B. (2022). Sample preparation methods for N-glycomics. *Advances in Sample Preparation, 4*, 100042. doi:https://doi.org/10.1016/j.sampre.2022.100042

Kayili, H. M., Barlas, N., Demirhan, D. B., Yaman, M. E., Atakay, M., Güler, Ü., Salih, B. (2023). Utilizing linkage-specific ethyl-esterification approach to perform in-depth analysis of sialylated N-glycans present on milk whey glycoproteins. *Food Chemistry, 421*, 136166. doi:https://doi.org/10.1016/j.foodchem.2023.136166

Kayili, H. M., & Salih, B. (2021). N-glycan Profiling of Glycoproteins by Hydrophilic Interaction Liquid Chromatography with Fluorescence and Mass Spectrometric Detection. *Journal of visualized experiments : JoVE,* (175). doi:10.3791/62751. (Accession No. 34633372)

Kayili, H. M., & Salih, B. (2022). Site-specific N-glycosylation analysis of human thyroid thyroglobulin by mass spectrometry-based Glyco-analytical strategies. *Journal of Proteomics, 267*. doi:10.1016/j.jprot.2022.104700

Kim, K. J., Kim, Y. W., Kim, Y. G., Park, H. M., Jin, J. M., Kim, Y. H., Saghatelian, A. (2015). Stable Isotopic Labeling-based Quantitative Targeted Glycomics. *Biotechnology Progress, 31*(3), 840-848. doi:10.1002/btpr.2078

Kitov, P. I., Kitova, E. N., Han, L., Li, Z., Jung, J., Rodrigues, E.,Klassen, J. S. (2019). A Quantitative, High-Throughput Method Identifies Protein–glycan Interactions via Mass Spectrometry. *Communications Biology, 2*(1). doi:10.1038/s42003-019-0507-2

Kronewitter, S. R., Maria Lorna, A. D. L., Strum, J. S., An, H. J., Dimapasoc, L. M., Guerrero, A., Leiserowitz, G. S. (2012). The Glycolyzer: Automated Glycan Annotation Software for High Performance Mass Spectrometry and Its Application to Ovarian Cancer Glycan Biomarker Discovery. *Proteomics, 12*(15-16), 2523-2538. doi:10.1002/pmic.201100273

Liu, M., Treves, G., Amicucci, M. J., Guerrero, A., Xu, G., Gong, T.,Lebrilla, C. B. (2023). GlycoNote With Iterative Decoy Searching and Open-Search Component Analysis for High-Throughput and Reliable Glycan Spectral Interpretation. *Analytical Chemistry, 95*(21), 8223-8231. doi:10.1021/acs.analchem.3c00083

Madunić, K., Wagt, S., Zhang, T., Wuhrer, M., & Lageveen-Kammeijer, G. S. M. (2021). Dopant-Enriched Nitrogen Gas for Enhanced Electrospray Ionization of Released Glycans in Negative Ion Mode. *Analytical Chemistry, 93*(18), 6919-6923. doi:10.1021/acs.analchem.1c00023

Manz, C., & Pagel, K. (2018). Glycan Analysis by Ion Mobility-Mass Spectrometry and Gas-Phase Spectroscopy. *Current Opinion in Chemical Biology, 42*, 16-24. doi:10.1016/j.cbpa.2017.10.021

Masri, S., Aksoy, S., Duman, H., Karav, S., Kayili, H. M., & Salih, B. (2024). Distinguishing Turkish pine honey from multi-floral honey through MALDI-MS-based N-glycomics and machine learning. *Journal of Food Measurement and Characterization, 18*(7), 5673-5682. doi:10.1007/s11694-024-02597-5

Mittal, P., Briggs, M. T., Klingler-Hoffmann, M., Kaur, G., Packer, N. H., Oehler, M. K., & Hoffmann, P. (2020). Altered N-Linked Glycosylation in Endometrial Cancer. *Analytical and Bioanalytical Chemistry, 413*(10), 2721-2733. doi:10.1007/s00216-020-03039-z

Nishihara, S. (2018). Glycans in Stem Cell Regulation: From <i>Drosophila</I> Tissue Stem Cells to Mammalian Pluripotent Stem Cells. *Febs Letters, 592*(23), 3773-3790. doi:10.1002/1873-3468.13167

Nwosu, C., Aldredge, D., Lee, H., Lerno, L., Zivkovic, A. M., German, J. B., & Lebrilla, C. B. (2012). Comparison of the Human and Bovine Milk N-Glycome via High-Performance Microfluidic Chip Liquid Chromatography and Tandem Mass Spectrometry. *Journal of Proteome Research, 11*(5), 2912-2924. doi:10.1021/pr300008u

Ochoa-Rios, S. (2024). Spatial Omics Reveals That Cancer-Associated Glycan Changes Occur Early in Liver Disease Development in a Western Diet Mouse Model of MASLD. *Journal of Proteome Research*. doi:10.1021/acs.jproteome.3c00672

Pagel, K., & Harvey, D. J. (2013). Ion Mobility–Mass Spectrometry of Complex Carbohydrates: Collision Cross Sections of Sodiated N-Linked Glycans. *Analytical Chemistry, 85*(10), 5138-5145. doi:10.1021/ac400403d

Pallister, E., Choo, M. S. F., Walsh, I., jn, t., S, T., Yang, Y. S., . . . Nguyen-Khuong, T. (2020). Ion-Mobility Mass Spectrometry of Glycans and Glycopeptides Using Both Intact and Glycan Sequencing Approaches in Positive Ion Mode Facilitates Glycan Isomer and Glycan Motif Identification. doi:10.26434/chemrxiv.12117243.v1

Powers, T. W., Holst, S., Wuhrer, M., Mehta, A., & Drake, R. (2015). Two-Dimensional N-Glycan Distribution Mapping of Hepatocellular Carcinoma Tissues by

MALDI-Imaging Mass Spectrometry. *Biomolecules, 5*(4), 2554-2572. doi:10.3390/biom5042554

Powers, T. W., Neely, B. A., Shao, Y., Tang, H., Troyer, D. A., Mehta, A., Drake, R. (2014). MALDI Imaging Mass Spectrometry Profiling of N-Glycans in Formalin-Fixed Paraffin Embedded Clinical Tissue Blocks and Tissue Microarrays. *Plos One, 9*(9), e106255. doi:10.1371/journal.pone.0106255

Puranik, A., Goswami, R., Sutar, P., Tupe, D., Rasam, P., Dandekar, P., & Jain, R. (2022). Mass Spectrometry-based Glycoprofiling of Biopharmaceuticals by Using an Automated Data Processing Tool: SimGlycan. *Journal of Separation Science, 46*(3). doi:10.1002/jssc.202200521

Re, S., Watabe, S., Nishima, W., Muneyuki, E., Yamaguchi, Y., MacKerell, A. D., & Sugita, Y. (2018). Characterization of Conformational Ensembles of Protonated N-Glycans in the Gas-Phase. *Scientific Reports, 8*(1). doi:10.1038/s41598-018-20012-0

Reider, B., Szigeti, M., & Guttman, A. (2018). Evaporative Fluorophore Labeling of Carbohydrates via Reductive Amination. *Talanta, 185*, 365-369. doi:10.1016/j.talanta.2018.03.101

Rojas-Macias, M. A., Mariethoz, J., Andersson, P., Jin, C., Venkatakrishnan, V., Aoki, N. P., . . . Karlsson, N. G. (2019). Towards a Standardized Bioinformatics Infrastructure for N- And O-Glycomics. *Nature Communications, 10*(1). doi:10.1038/s41467-019-11131-x

Schnaar, R. L. (2015). Glycans and Glycan-Binding Proteins in Immune Regulation: A concise Introduction to Glycobiology for the Allergist. *Journal of Allergy and Clinical Immunology, 135*(3), 609-615. doi:10.1016/j.jaci.2014.10.057

Scott, D. A., Casadonte, R., Cardinali, B., Spruill, L., Mehta, A., Carli, F., . . . Drake, R. (2019). Increases in Tumor N-Glycan Polylactosamines Associated With Advanced HER2-Positive and Triple-Negative Breast Cancer Tissues. *Proteomics - Clinical Applications, 13*(1). doi:10.1002/prca.201800014

Sethi, M. K., & Fanayan, S. (2015). Mass Spectrometry-Based N-Glycomics of Colorectal Cancer. *International Journal of Molecular Sciences, 16*(12), 29278-29304. doi:10.3390/ijms161226165

Shajahan, A., Supekar, N., Heiss, C., & Azadi, P. (2019). High-Throughput Automated Micro-permethylation for Glycan Structure Analysis. *Anal Chem, 91*(2), 1237-1240. doi:10.1021/acs.analchem.8b05146

Tahhan, N., Aksoy, S., Kayili, H. M., & Salih, B. (2023). Integration of high-pH fractionation and cotton-HILIC enrichment approaches for analyzing N-glycopeptides. *Advances in Sample Preparation, 8*. doi:10.1016/j.sampre.2023.100098

Viswanathan, K., Chandrasekaran, A., Srinivasan, A., Raman, R., Sasisekharan, V., & Sasisekharan, R. (2010). Glycans as Receptors for Influenza Pathogenesis. *Glycoconjugate Journal, 27*(6), 561-570. doi:10.1007/s10719-010-9303-4

West, C. A., Wang, M., Herrera, H., Liang, H., Black, A., Angel, P., Mehta, A. (2018). N-Linked Glycan Branching and Fucosylation Are Increased Directly in HCC Tissue as Determined Through in Situ Glycan Imaging. *Journal of Proteome Research, 17*(10), 3454-3462. doi:10.1021/acs.jproteome.8b00323

Wuhrer, M. (2012). Glycomics Using Mass Spectrometry. *Glycoconjugate Journal, 30*(1), 11-22. doi:10.1007/s10719-012-9376-3

Yoshida, Y., Furukawa, Y., Naito, S., Higashino, K., Numata, Y., & Shinohara, Y. (2016). Quantitative Analysis of Total Serum Glycome in Human and Mouse. *Proteomics, 16*(21), 2747-2758. doi:10.1002/pmic.201500550

Zheng, X., Zhang, X., Schocker, N. S., Renslow, R., Orton, D. J., Khamsi, J., . . . Baker, E. (2016). Enhancing Glycan Isomer Separations With Metal Ions and Positive and Negative Polarity Ion Mobility Spectrometry-Mass Spectrometry Analyses. *Analytical and Bioanalytical Chemistry, 409*(2), 467-476. doi:10.1007/s00216-016-9866-4

Zhou, S., Hu, Y., Veillon, L., Snovida, S. I., Rogers, J. C., Saba, J., & Mechref, Y. (2016). Quantitative LC–MS/MS Glycomic Analysis of Biological Samples Using AminoxyTMT. *Analytical Chemistry, 88*(15), 7515-7522. doi:10.1021/acs.analchem.6b00465

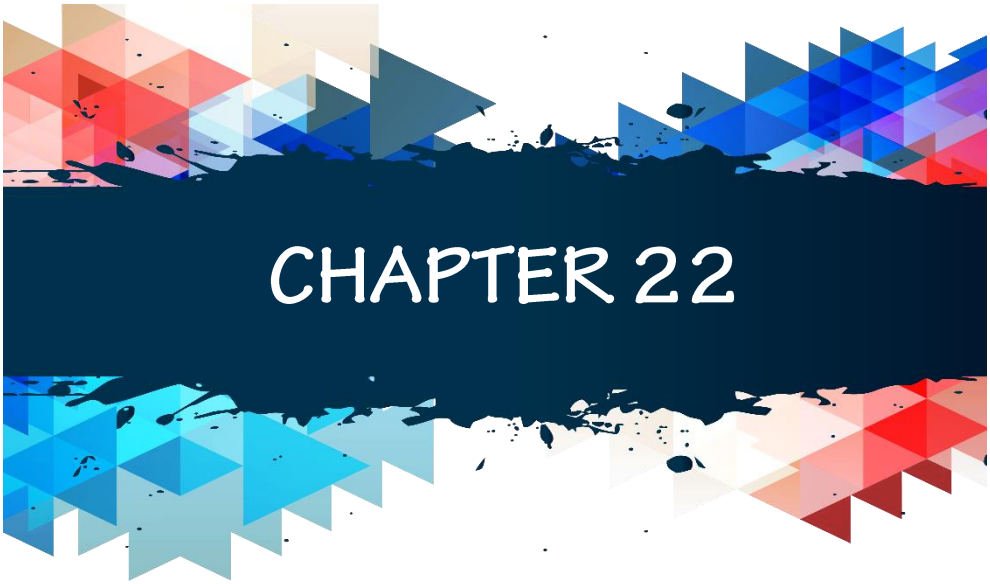

Bernstein Type Operators Based on Multiple Representation Parameters

Gurel Bozma[1] & Nazmiye Gonul Bılgın[2]

1 PhD Student, Zonguldak Bulent Ecevit University, Faculty of Sciences, Department of Mathematics, Zonguldak, Turkey,ORCID: 0000-0002-0916-5894
[2] Assoc. Prof. Dr., Zonguldak Bulent Ecevit University, Faculty of Sciences, Department of Mathematics, Zonguldak, Turkey, ORCID:0000-0001-6300-6889

1. INTRODUCTION

In 1854, Chebyshev's claim that continuous functions can be approximated by elements from the family of polynomials of degree at most n was clarified by Weierstrass in 1885 with the theorem he stated and proved. According to this theorem, continuous functions can be uniformly approximated by polynomials over a finite interval with any predetermined error. In the following periods, this theorem of Weierstrass was given in different ways by many mathematicians, especially Bernstein, Volterra and Picard. However, the simplest and most well-known version of this theorem on the interval [0,1] was proved by Bernstein. Bernstein showed the approximation of a sequence of operators to a function continuous on the interval. After this theorem, which brought a different perspective to the literature, different operators were defined and their approximation properties were studied. Later studies made it possible to calculate the approximation speed.

After the polynomials defined by Bernstein, with the statement and proof of Korovkin's theorem, many linear and positive operators that satisfy this theorem have been defined. Examples of these operators are Bernstein Schurer, Baskokov and Balazs operators. In the following periods, both different generalizations of existing operators and completely new operators were established.

Inspired by the operator introduced in the literature by Arab et al. in 2018, which is constructed with the help of equations provided by nth order polynomials and two sequences where approximation is achieved by state evaluation, this section will present a new approach defined to obtain a better approximation degree for Bernstein type operators.

After this study, similar operator structures were examined by different authors from different perspectives. Some of these studies are as follows:

Acu and Agrawal obtained a more useful version of the Bernstein-Durrmeyer type operator in their work in 2018. The convergence speed was calculated with two types of the continuity modulus. The findings were supported with asymptotic formulas and numerical examples.

In (Baytunç et al. 2024), a new class of blending type Bernstein-Kantorovich operators was introduced. They defined the operator depending on three parameters. They also calculated the approach speed with the help of the first and second order continuity modulus of the operator they defined.

(Kaur and Goyal 2024) also obtained a new modification on the Baskakov-Durrmeyer operators with changes that will improve the approximation. The

asymptotic approximation properties with Voronovskaja type formulas were also investigated. The usefulness of the changes made to the operator was seen by comparing with the classical operator.

(Jabbar and Hassan 2024) defined two new operators for the Baskakov type operator. They obtained results on the convergence rate of this operator and presented visual results.

First, the operator existing in the literature will be given, which will be modified by the method in (Arab et al, 2018).

Definition 1.1.

Let p and s, be a function of x,

$$(p+s)^{\mathfrak{z}} = \sum_{r=0}^{\mathfrak{z}} \binom{\mathfrak{z}}{r} \big(p(x)\big)^r,$$

let

$$b_{\mathfrak{z},r}(x) = \binom{\mathfrak{z}}{r} \big(p(x)\big)^r \big(s(x)\big)^{\mathfrak{z}-r} \qquad (1.1)$$

then Bernstein type operator is given as

$$Z_{\mathfrak{z}}(f,x) = \left(\frac{\mathfrak{z}+1}{2(\mathfrak{z}+2)}\right)^{\mathfrak{z}} \sum_{r=0}^{\mathfrak{z}} b_{\mathfrak{z},r}(x) f\left(\left(\frac{2r}{\mathfrak{z}}-1\right)\frac{2+\mathfrak{z}}{1+\mathfrak{z}}\right) \qquad (1.2)$$

(Bilgen, 2023)

In the following section, a modification using operator (1.2) will be constructed and the equalities and important approximation properties of this operator will be given.

2. Structure of the Operator

First, the following equations between the polynomials $b_{\mathfrak{z},r}(x), b_{\mathfrak{z},\mathfrak{z}-r}(x)$, $b_{\mathfrak{z}-1,r-1}(x)$ and $b_{\mathfrak{z}-1,r}(x)$ will be given in the structure of the operator.

Lemma 2.1

Let for $p(x) = \frac{2+\mathfrak{z}}{1+\mathfrak{z}} + x, s(x) = \frac{2+\mathfrak{z}}{1+\mathfrak{z}} - x$,

$$b_{\mathfrak{z},r}(x) = \big(p(x)\big)^r \big(s(x)\big)^{\mathfrak{z}-r} \binom{\mathfrak{z}}{r},$$

for $\tilde{p}(x)=\frac{\mathfrak{z}+2}{\mathfrak{z}+1}-x,\ \ \tilde{s}(x)=x+\frac{\mathfrak{z}+2}{\mathfrak{z}+1}$,

$b_{\mathfrak{z},\mathfrak{z}-r}(x)=\binom{\mathfrak{z}}{\mathfrak{z}-r}\left(\tilde{p}(x)\right)^{r}\left(\tilde{s}(x)\right)^{\mathfrak{z}-r}$.

In this case, the equations

i) $b_{\mathfrak{z},r}(x)=b_{\mathfrak{z},\mathfrak{z}-r}(x)$,

ii) $b_{\mathfrak{z},r}(x)=\left(\frac{2+\mathfrak{z}}{1+\mathfrak{z}}-x\right)b_{\mathfrak{z}-1,r}(x)+\left(\frac{2+\mathfrak{z}}{1+\mathfrak{z}}+x\right)b_{\mathfrak{z}-1,r-1}(x)$

are valid.

Proof.

i) For all $x\in\left[-\frac{2+\mathfrak{z}}{\mathfrak{z}+1},\frac{2+\mathfrak{z}}{1+\mathfrak{z}}\right]$ clearly

$b_{\mathfrak{z},r}(x)=\binom{\mathfrak{z}}{r}\left(p(x)\right)^{r}\left(s(x)\right)^{\mathfrak{z}-r}$

$=\binom{\mathfrak{z}}{r}\left(\frac{2+\mathfrak{z}}{1+\mathfrak{z}}+x\right)^{r}\left(\frac{2+\mathfrak{z}}{1+\mathfrak{z}}-x\right)^{\mathfrak{z}-r}$.

On the other hand,

$b_{\mathfrak{z},\mathfrak{z}-r}(x)=\binom{\mathfrak{z}}{\mathfrak{z}-r}\left(\tilde{s}(x)\right)^{\mathfrak{z}-(\mathfrak{z}-r)}\left(\tilde{p}(x)\right)^{\mathfrak{z}-r}$

$=\binom{\mathfrak{z}}{\mathfrak{z}-r}\left(\frac{2+\mathfrak{z}}{\mathfrak{z}+1}-x\right)^{\mathfrak{z}-r}\left(x+\frac{2+\mathfrak{z}}{\mathfrak{z}+1}\right)^{\mathfrak{z}-(\mathfrak{z}-r)}$.

is obtained. So,

$b_{\mathfrak{z},r}(x)=b_{\mathfrak{z},\mathfrak{z}-r}(x)$

is written.

ii) For $p(x)=\frac{2+\mathfrak{z}}{1+\mathfrak{z}}+x, s(x)=\frac{\mathfrak{z}+2}{1+\mathfrak{z}}-x$, using

$b_{\mathfrak{z},r}(x)=\binom{\mathfrak{z}}{r}\left(p(x)\right)^{r}\left(s(x)\right)^{\mathfrak{z}-r}$,

$\boldsymbol{b_{\mathfrak{z}-1,r}(x)=\binom{\mathfrak{z}-1}{r}\left(p(x)\right)^{r}\left(s(x)\right)^{\mathfrak{z}-r}}$

$$\boldsymbol{b_{\mathfrak{Z}-1,r}(x)=\left(\frac{2+\mathfrak{Z}}{1+\mathfrak{Z}}-x\right)^{\mathfrak{Z}-1-r}\left(x+\frac{2+\mathfrak{Z}}{1+\mathfrak{Z}}\right)^{r}\ \binom{\mathfrak{Z}-1}{r}} \qquad (\mathbf{2.1})$$

$$\boldsymbol{b_{\mathfrak{Z}-1,r-1}(x)=\binom{\mathfrak{Z}-1}{r-1}\left(\frac{2+\mathfrak{Z}}{\mathfrak{Z}+1}-x\right)^{\mathfrak{Z}-r}\left(x+\frac{\mathfrak{Z}+2}{\mathfrak{Z}+1}\right)^{r-1}} \qquad (\mathbf{2.2})$$

is getting. Here, $\boldsymbol{b_{\mathfrak{Z}-1,-1}(x)=0}$, $\boldsymbol{b_{\mathfrak{Z}-1,\mathfrak{Z}}(x)=0}$. Then, for $\boldsymbol{r=0}$, using $\boldsymbol{b_{\mathfrak{Z}-1,-1}(x)=0}$

$$\boldsymbol{b_{\mathfrak{Z},0}(x)=\left(\frac{2+\mathfrak{Z}}{\mathfrak{Z}+1}-x\right)b_{\mathfrak{Z}-1,0}(x)+\left(\frac{2+\mathfrak{Z}}{1+\mathfrak{Z}}+x\right)b_{\mathfrak{Z}-1,-1}(x)} \qquad (2.3)$$

is obtained. Similarly, for $\boldsymbol{r=\mathfrak{Z}}$ using $\boldsymbol{b_{\mathfrak{Z}-1,\mathfrak{Z}}(x)=0}$

$$\boldsymbol{b_{\mathfrak{Z},\mathfrak{Z}}(x)=\left(x+\frac{2+\mathfrak{Z}}{1+\mathfrak{Z}}\right)^{\mathfrak{Z}}}$$

$$\boldsymbol{=\left(\frac{2+\mathfrak{Z}}{\mathfrak{Z}+1}-x\right)b_{\mathfrak{Z}-1,\mathfrak{Z}}(x)+\left(x+\frac{2+\mathfrak{Z}}{1+\mathfrak{Z}}\right)b_{\mathfrak{Z}-1,\mathfrak{Z}-1}(x)} \qquad (\mathbf{2.4})$$

is written. Thus, for $\boldsymbol{1\le r\le \mathfrak{Z}}$, if the equations (2.1) and (2.2) are multiplied by $\left(\frac{2+\mathfrak{Z}}{1+\mathfrak{Z}}-x\right)$ and $\left(x+\frac{2+\mathfrak{Z}}{1+\mathfrak{Z}}\right)$, respectively,

$$\boldsymbol{\left(\frac{2+\mathfrak{Z}}{\mathfrak{Z}+1}-x\right).b_{\mathfrak{Z}-1,r}(x)+\left(x+\frac{\mathfrak{Z}+2}{\mathfrak{Z}+1}\right).b_{\mathfrak{Z}-1,r-1}(x)}$$

$$\boldsymbol{=\left(\frac{2+\mathfrak{Z}}{\mathfrak{Z}+1}-x\right)^{\mathfrak{Z}-r}\left(\frac{2+\mathfrak{Z}}{\mathfrak{Z}+1}+x\right)^{r}\binom{\mathfrak{Z}-1}{r}}$$

$$\boldsymbol{+\left(\frac{2+\mathfrak{Z}}{\mathfrak{Z}+1}-x\right)^{\mathfrak{Z}-r}\left(x+\frac{\mathfrak{Z}+2}{\mathfrak{Z}+1}\right)^{r}\binom{\mathfrak{Z}-1}{r-1}}$$

$$= \left(\frac{\mathbf{2}+\mathbf{\mathfrak{z}}}{\mathbf{\mathfrak{z}}+\mathbf{1}} - \boldsymbol{x}\right)^{\mathfrak{z}-\boldsymbol{r}} \left(\boldsymbol{x} + \frac{\mathbf{2}+\mathbf{\mathfrak{z}}}{\mathbf{1}+\mathbf{\mathfrak{z}}}\right)^{\boldsymbol{r}} \cdot \left[\binom{\mathfrak{z}-\mathbf{1}}{\boldsymbol{r}} + \binom{\mathfrak{z}-\mathbf{1}}{\boldsymbol{r}-\mathbf{1}}\right]$$

$$= \left(\frac{\mathbf{2}+\mathbf{\mathfrak{z}}}{\mathbf{\mathfrak{z}}+\mathbf{1}} - \boldsymbol{x}\right)^{\mathfrak{z}-\boldsymbol{r}} \left(\frac{\mathbf{2}+\mathbf{\mathfrak{z}}}{\mathbf{1}+\mathbf{\mathfrak{z}}} + \boldsymbol{x}\right)^{\boldsymbol{r}} \cdot \left[\frac{\boldsymbol{r}+(\mathfrak{z}-\boldsymbol{r})}{\mathfrak{z}}\right] \cdot \frac{\mathfrak{z}!}{(\mathfrak{z}-\mathbf{1})!\,\boldsymbol{r}!}$$

$$= \boldsymbol{b}_{\mathfrak{z},\boldsymbol{r}}(\boldsymbol{x}).$$

Remark 2.1

Using Lemma 2.1, for the operator given in Definition 1.1

$$Z_{\mathfrak{z}}(f;x) = \sum_{r=0}^{\mathfrak{z}} \left(\left(\frac{2+\mathfrak{z}}{\mathfrak{z}+1} - x\right) b_{\mathfrak{z}-1,r}(x) + \left(x + \frac{2+\mathfrak{z}}{1+\mathfrak{z}}\right) b_{\mathfrak{z}-1,r-1}(x) \right)$$

$$\times f\left(\frac{2+\mathfrak{z}}{1+\mathfrak{z}}\left(\frac{2r}{\mathfrak{z}} - 1\right)\right) \qquad (2.5)$$

is getting.

Definition 2.1

For $x \in \left[-\frac{2+\mathfrak{z}}{1+\mathfrak{z}}, \frac{2+\mathfrak{z}}{1+\mathfrak{z}}\right]$and $\mathfrak{z} = 0,1,2, \ldots, i = 0,1$, Let $\alpha_i(\mathfrak{z})$, be two sequences whose properties are given in Lemma 2.2. The sequence $\alpha\left(\frac{\mathfrak{z}+2}{\mathfrak{z}+1} \mp x, \mathfrak{z}\right)$ is given by

$$\alpha\left(\frac{\mathfrak{z}+2}{\mathfrak{z}+1} \mp x, \mathfrak{z}\right) = \alpha_1(\mathfrak{z})\left(\frac{\mathfrak{z}+2}{\mathfrak{z}+1} \mp x\right) + \alpha_0(\mathfrak{z})$$

Also, here

$$\alpha_1(\mathfrak{z}) + \alpha_0(\mathfrak{z})\left(\frac{2+\mathfrak{z}}{\mathfrak{z}+1}\right) = 1.$$

Then, for $p(x) = \frac{\mathfrak{z}+2}{\mathfrak{z}+1} + x, s(x) = \frac{2+\mathfrak{z}}{1+\mathfrak{z}} - x,$

$$b^*_{\mathfrak{z},r}(x) = \alpha\left(\frac{2+\mathfrak{z}}{1+\mathfrak{z}} + x, \mathfrak{z}\right) b_{\mathfrak{z}-1,r}(x) + \alpha\left(\frac{2+\mathfrak{z}}{\mathfrak{z}+1} - x, \mathfrak{z}\right) b_{\mathfrak{z}-1,r-1}(x) \qquad (2.6)$$

and modification of Bernstein type operators is given as

$$Z_{\mathfrak{Z}}^{*}(f;x)=\left(\frac{\mathfrak{Z}+1}{2(\mathfrak{Z}+2)}\right)^{\mathfrak{Z}}\sum_{r=0}^{\mathfrak{Z}}b_{\mathfrak{Z},r}^{*}f\left(\frac{\mathfrak{Z}+2}{\mathfrak{Z}+1}\left(\frac{2r}{\mathfrak{Z}}-1\right)\right) \qquad (2.7)$$

Here, if $r<0$ or $r>\mathfrak{Z}$, then $b_{\mathfrak{Z},r}(x)=0$.

Lemma 2.2

When the equality $\alpha_1(\mathfrak{Z})+\alpha_0(\mathfrak{Z})\left(\frac{\mathfrak{Z}+1}{\mathfrak{Z}+2}\right)=1$ valid for the sequences $\alpha_0(\mathfrak{Z})$ and $\alpha_1(\mathfrak{Z})$ is examined, the following is true for $p(x)=\frac{2+\mathfrak{Z}}{1+\mathfrak{Z}}+x, s(x)=\frac{2+\mathfrak{Z}}{\mathfrak{Z}+1}-x$.

Case 1. If $\alpha_1(\mathfrak{Z})=0$, $\alpha_0(\mathfrak{Z})=\frac{\mathfrak{Z}+2}{\mathfrak{Z}+1}$.

Case 2. If $0<\alpha_1(\mathfrak{Z})<\frac{\mathfrak{Z}+2}{\mathfrak{Z}+1}$, then $\alpha_0(\mathfrak{Z})>0$.

Case 3. If $\alpha_1(\mathfrak{Z})=1$, then $\alpha_0(\mathfrak{Z})=0$.

Case 4. If $\alpha_1(\mathfrak{Z})>1$, then $\alpha_0(\mathfrak{Z})<0$.

Case 5. If $\alpha_1(\mathfrak{Z})<0$, then $\alpha_0(\mathfrak{Z})>0$ and $\alpha_1(\mathfrak{Z})+\alpha_0(\mathfrak{Z})>0$.

Case 6. If $\alpha_1(\mathfrak{Z})=-1$, then $\alpha_0(\mathfrak{Z})=\frac{2(\mathfrak{Z}+2)}{\mathfrak{Z}+1}$.

Remark 2.2

It can be easily seen that if Case 6 is satisfied, i.e., for $\alpha_1(\mathfrak{Z})=-1$, $\alpha_0(\mathfrak{Z})=\frac{2(\mathfrak{Z}+2)}{\mathfrak{Z}+1}$, the operator (2.7) reduces to the Bernstein-type operator in (1.1).

Lemma 2.3

For $\boldsymbol{p(x)=x+\frac{\mathfrak{Z}+2}{\mathfrak{Z}+1}, s(x)=\frac{\mathfrak{Z}+2}{\mathfrak{Z}+1}-x}$, let $\boldsymbol{b_{\mathfrak{Z},r}(x)=\binom{\mathfrak{Z}}{r}\left(p(x)\right)^{r}\left(s(x)\right)^{\mathfrak{Z}-r}}$. In this case the following equalities hold.

i) $\boldsymbol{\sum_{r=0}^{\mathfrak{Z}}b_{\mathfrak{Z},r}(x)=\left(\frac{2+\mathfrak{Z}}{\mathfrak{Z}+1}\right)^{\mathfrak{Z}}2^{\mathfrak{Z}}}$,

ii) $$\sum_{r=0}^{\mathfrak{z}} b_{\mathfrak{z}-1,r}(x) = \sum_{r=0}^{\mathfrak{z}} b_{\mathfrak{z}-1,r-1}(x) = 2^{\mathfrak{z}-1}\left(\frac{2+\mathfrak{z}}{1+\mathfrak{z}}\right)^{\mathfrak{z}-1}. \qquad (2.8)$$

Proof

i) For $x \in \left[-\frac{2+\mathfrak{z}}{\mathfrak{z}+1}, \frac{2+\mathfrak{z}}{\mathfrak{z}+1}\right]$

$$\sum_{r=0}^{\mathfrak{z}} b_{\mathfrak{z},r}(x) = \sum_{r=0}^{\mathfrak{z}} \binom{\mathfrak{z}}{r}\left(x+\frac{\mathfrak{z}+2}{\mathfrak{z}+1}\right)^{r}\left(\frac{2+\mathfrak{z}}{1+\mathfrak{z}}-x\right)^{\mathfrak{z}-r}$$

$$= \left(\frac{2+\mathfrak{z}}{\mathfrak{z}+1}\right)^{\mathfrak{z}} 2^{\mathfrak{z}}$$

ii) $$\sum_{r=0}^{\mathfrak{z}} b_{\mathfrak{z}-1,r}(x) = \sum_{r=0}^{\mathfrak{z}} \binom{\mathfrak{z}-1}{r}\left(x+\frac{2+\mathfrak{z}}{\mathfrak{z}+1}\right)^{r}\left(\frac{2+\mathfrak{z}}{\mathfrak{z}+1}-x\right)^{\mathfrak{z}-r-1}$$

$$= \sum_{r=0}^{\mathfrak{z}-1} \frac{(\mathfrak{z}-1)!}{r!\,(\mathfrak{z}-r-1)!}\left(x+\frac{\mathfrak{z}+2}{\mathfrak{z}+1}\right)^{r}\left(\frac{2+\mathfrak{z}}{1+\mathfrak{z}}-x\right)^{\mathfrak{z}-r-1}$$

$$= 2^{\mathfrak{z}-1}\left(\frac{2+\mathfrak{z}}{1+\mathfrak{z}}\right)^{\mathfrak{z}-1}.$$

So,

$$\sum_{r=0}^{\mathfrak{z}} b_{\mathfrak{z}-1,r-1}(x) = \sum_{r=0}^{\mathfrak{z}} \binom{\mathfrak{z}-1}{r-1}\left(x+\frac{\mathfrak{z}+2}{\mathfrak{z}+1}\right)^{r-1}\left(\frac{\mathfrak{z}+2}{\mathfrak{z}+1}-x\right)^{\mathfrak{z}-r}$$

$$= \sum_{r=1}^{\mathfrak{z}} \frac{(\mathfrak{z}-1)!}{(r-1)!\,(\mathfrak{z}-r)!}\left(x+\frac{2+\mathfrak{z}}{1+\mathfrak{z}}\right)^{r-1}\left(\frac{2+\mathfrak{z}}{1+\mathfrak{z}}-x\right)^{\mathfrak{z}-r}$$

$$= \left(\frac{2+\mathfrak{z}}{\mathfrak{z}+1}\right)^{\mathfrak{z}-1} 2^{\mathfrak{z}-1}$$

is obtained.

Lemma 2.4

Let $\alpha_1(\mathfrak{z}), \alpha_0(\mathfrak{z}) \geq 0$. Then, $Z_{\mathfrak{z}}^{*}(f;x)$ is a linear positive operator.

Proof

The linearity of the operator is clear.

Positivity:

Let $\mathfrak{Z}, r \in \mathbb{N}$ and for all $x \in \left[-\frac{\mathfrak{Z}+2}{\mathfrak{Z}+1}, \frac{\mathfrak{Z}+2}{\mathfrak{Z}+1}\right]$, $f(x) \geq 0$. So, for the

$$Z_{\mathfrak{Z}}^{*}(f;x) = \left(\frac{1+\mathfrak{Z}}{2(2+\mathfrak{Z})}\right)^{\mathfrak{Z}} \sum_{r=0}^{\mathfrak{Z}} b_{\mathfrak{Z},r}^{*} f\left(\frac{2+\mathfrak{Z}}{1+\mathfrak{Z}}\left(\frac{2r}{\mathfrak{Z}}-1\right)\right),$$

to satisfy the inequality $b_{\mathfrak{Z},r}^{*}(x) \geq 0$, the condition $A + B \geq 0$ must be satisfied where

$$A = \alpha\left(x + \frac{\mathfrak{Z}+2}{\mathfrak{Z}+1}, \mathfrak{Z}\right) b_{\mathfrak{Z}-1,r}(x) \text{ and } B = \alpha\left(\frac{\mathfrak{Z}+2}{\mathfrak{Z}+1} - x, \mathfrak{Z}\right) b_{\mathfrak{Z}-1,r-1}(x)$$

Here, using

$$A = \left(\alpha_1(\mathfrak{Z})\left(\frac{2+\mathfrak{Z}}{1+\mathfrak{Z}} + x\right) + \alpha_0(\mathfrak{Z})\right)$$

$$\times \left(x + \frac{2+\mathfrak{Z}}{1+\mathfrak{Z}}\right)^{r} \left(\frac{2+\mathfrak{Z}}{1+\mathfrak{Z}} - x\right)^{\mathfrak{Z}-r-1} \binom{\mathfrak{Z}-1}{r},$$

$$B = \left(\alpha_1(\mathfrak{Z})\left(\frac{2+\mathfrak{Z}}{1+\mathfrak{Z}} - x\right) + \alpha_0(\mathfrak{Z})\right)$$

$$\times \binom{\mathfrak{Z}-1}{r-1}\left(x + \frac{2+\mathfrak{Z}}{1+\mathfrak{Z}}\right)^{r-1} \left(\frac{2+\mathfrak{Z}}{1+\mathfrak{Z}} - x\right)^{\mathfrak{Z}-r},$$

we get

$$A + B = \alpha_1(\mathfrak{Z}) \binom{\mathfrak{Z}-1}{r}\left(x + \frac{2+\mathfrak{Z}}{1+\mathfrak{Z}}\right)^{r+1} \left(\frac{2+\mathfrak{Z}}{1+\mathfrak{Z}} - x\right)^{\mathfrak{Z}-r-1}$$

$$+\alpha_0(\mathfrak{Z}) \binom{\mathfrak{Z}-1}{r}\left(x + \frac{\mathfrak{Z}+2}{\mathfrak{Z}+1}\right)^{r} \left(\frac{\mathfrak{Z}+2}{\mathfrak{Z}+1} - x\right)^{\mathfrak{Z}-r-1}$$

$$+\alpha_1(\mathfrak{Z}) \binom{\mathfrak{Z}-1}{r-1}\left(x + \frac{\mathfrak{Z}+2}{\mathfrak{Z}+1}\right)^{r-1} \left(\frac{\mathfrak{Z}+2}{\mathfrak{Z}+1} - x\right)^{\mathfrak{Z}-r+1}$$

$$+\alpha_0(\mathfrak{Z}) \binom{\mathfrak{Z}-1}{r-1}\left(x + \frac{\mathfrak{Z}+2}{\mathfrak{Z}+1}\right)^{r-1} \left(\frac{\mathfrak{Z}+2}{\mathfrak{Z}+1} - x\right)^{\mathfrak{Z}-r}$$

$$= \left(x + \frac{\frac{z}{3}+2}{\frac{z}{3}+1}\right)^{2} \left(\frac{\frac{z}{3}+2}{\frac{z}{3}+1} - x\right)^{-1} \left(\frac{\frac{z}{3}}{r} - 1\right) \alpha_1\left(\frac{z}{3}\right) \frac{\left(\frac{z}{3}-1\right)!}{(r-1)!\left(\frac{z}{3}-r\right)!}$$

$$\times \left(x + \frac{\frac{z}{3}+2}{\frac{z}{3}+1}\right)^{r-1} \left(\frac{\frac{z}{3}+2}{\frac{z}{3}+1} - x\right)^{\frac{z}{3}-r} + \left(x + \frac{\frac{z}{3}+2}{\frac{z}{3}+1}\right) \left(\frac{\frac{z}{3}+2}{\frac{z}{3}+1} - x\right)^{-1}$$

$$\times \left(\frac{\frac{z}{3}}{r} - 1\right) \alpha_0\left(\frac{z}{3}\right) \frac{\left(\frac{z}{3}-1\right)!}{(r-1)!\left(\frac{z}{3}-r\right)!} \left(x + \frac{\frac{z}{3}+2}{\frac{z}{3}+1}\right)^{r-1} \left(\frac{\frac{z}{3}+2}{\frac{z}{3}+1} - x\right)^{\frac{z}{3}-r}$$

$$+ \left(\frac{\frac{z}{3}+2}{\frac{z}{3}+1} - x\right) \alpha_1\left(\frac{z}{3}\right) \frac{\left(\frac{z}{3}-1\right)!}{(r-1)!\left(\frac{z}{3}-r\right)!}$$

$$\times \left(x + \frac{\frac{z}{3}+2}{\frac{z}{3}+1}\right)^{r-1} \left(\frac{\frac{z}{3}+2}{\frac{z}{3}+1} - x\right)^{\frac{z}{3}-r} + \alpha_0\left(\frac{z}{3}\right) \frac{\left(\frac{z}{3}-1\right)!}{(r-1)!\left(\frac{z}{3}-r\right)!}$$

$$\times \left(x + \frac{\frac{z}{3}+2}{\frac{z}{3}+1}\right)^{r-1} \left(\frac{\frac{z}{3}+2}{\frac{z}{3}+1} - x\right)^{\frac{z}{3}-r}$$

$$= \frac{\left(\frac{z}{3}-1\right)!}{(r-1)!\left(\frac{z}{3}-r\right)!} \left(x + \frac{\frac{z}{3}+2}{\frac{z}{3}+1}\right)^{r-1} \left(\frac{\frac{z}{3}+2}{\frac{z}{3}+1} - x\right)^{\frac{z}{3}-r}$$

$$\times \left(\left(x + \frac{\frac{z}{3}+2}{\frac{z}{3}+1}\right)^{2} \left(\frac{\frac{z}{3}+2}{\frac{z}{3}+1} - x\right)^{-1} \left(\frac{\frac{z}{3}}{r} - 1\right) \alpha_1\left(\frac{z}{3}\right) + \left(\frac{\frac{z}{3}+2}{\frac{z}{3}+1} - x\right) \alpha_1\left(\frac{z}{3}\right) \right.$$

$$\left. + \left(x + \frac{\frac{z}{3}+2}{\frac{z}{3}+1}\right) \left(\frac{\frac{z}{3}+2}{\frac{z}{3}+1} - x\right)^{-1} \left(\frac{\frac{z}{3}}{r} - 1\right) \alpha_0\left(\frac{z}{3}\right) + \alpha_0\left(\frac{z}{3}\right) \right)$$

$$= \frac{\left(\frac{z}{3}-1\right)!}{(r-1)!\left(\frac{z}{3}-r\right)!} \left(x + \frac{\frac{z}{3}+2}{\frac{z}{3}+1}\right)^{r-1} \left(\frac{\frac{z}{3}+2}{\frac{z}{3}+1} - x\right)^{\frac{z}{3}-r}$$

$$\times \left(\frac{\left(x + \frac{\frac{z}{3}+2}{\frac{z}{3}+1}\right)^{2}}{\left(\frac{\frac{z}{3}+2}{\frac{z}{3}+1} - x\right)} \left(\frac{\frac{z}{3}}{r} - 1\right) \alpha_1\left(\frac{z}{3}\right) + \left(\frac{\frac{z}{3}+2}{\frac{z}{3}+1} - x\right) \alpha_1\left(\frac{z}{3}\right) \right.$$

$$\left. + \frac{\left(x + \frac{\frac{z}{3}+2}{\frac{z}{3}+1}\right)}{\left(\frac{\frac{z}{3}+2}{\frac{z}{3}+1} - x\right)} \left(\frac{\frac{z}{3}}{r} - 1\right) \alpha_0\left(\frac{z}{3}\right) + \alpha_0\left(\frac{z}{3}\right) \right)$$

$$= \frac{\left(\frac{z}{3}-1\right)!}{(r-1)!\left(\frac{z}{3}-r\right)!} \left(x + \frac{\frac{z}{3}+2}{\frac{z}{3}+1}\right)^{r-1} \left(\frac{\frac{z}{3}+2}{\frac{z}{3}+1} - x\right)^{\frac{z}{3}-r}$$

$$\times\left(\frac{\left(x+\frac{\mathfrak{Z}+2}{\mathfrak{Z}+1}\right)\left(\frac{\mathfrak{Z}}{r}-1\right)}{\left(\frac{\mathfrak{Z}+2}{\mathfrak{Z}+1}-x\right)}\left(\left(x+\frac{\mathfrak{Z}+2}{\mathfrak{Z}+1}\right)\alpha_1(\mathfrak{Z})+\alpha_0(\mathfrak{Z})\right)\right.$$

$$\left.+\left(\left(\frac{\mathfrak{Z}+2}{\mathfrak{Z}+1}-x\right)\alpha_1(\mathfrak{Z})+\alpha_0(\mathfrak{Z})\right)\right).$$

$$=b_{\mathfrak{Z}-1,r-1}(x)\left(\frac{\left(x+\frac{\mathfrak{Z}+2}{\mathfrak{Z}+1}\right)\left(\frac{\mathfrak{Z}}{r}\right)}{\left(\frac{\mathfrak{Z}+2}{\mathfrak{Z}+1}-x\right)}\left(\alpha_1(\mathfrak{Z})\left(x+\frac{\mathfrak{Z}+2}{\mathfrak{Z}+1}\right)+\alpha_0(\mathfrak{Z})\right)\right.$$

$$\left.+\frac{2x}{\left(x-\frac{\mathfrak{Z}+2}{\mathfrak{Z}+1}\right)}\left(\alpha_1(\mathfrak{Z})+\alpha_0(\mathfrak{Z})\right)\right) \qquad (2.9)$$

In other words, for the positivity of the operator, this equality that emerged at the stage of showing the positivity of $b^*_{\mathfrak{Z},r}(x)$ should be evaluated by taking into account the interval to which x belongs, and the states $\alpha_1(\mathfrak{Z})$ and $\alpha_0(\mathfrak{Z})$.

For $\left(\left(x+\frac{\mathfrak{Z}+2}{\mathfrak{Z}+1}\right)\alpha_1(\mathfrak{Z})+\alpha_0(\mathfrak{Z})\right)\geq 0$

if $x=-\frac{\mathfrak{Z}+2}{\mathfrak{Z}+1}$ then $\alpha_0(\mathfrak{Z})\geq 0$.

If $x=\frac{\mathfrak{Z}+2}{\mathfrak{Z}+1}$ then $2\frac{\mathfrak{Z}+2}{\mathfrak{Z}+1}\alpha_1(\mathfrak{Z})+\ \alpha_0(\mathfrak{Z})\geq 0$.

If $-\frac{\mathfrak{Z}+2}{\mathfrak{Z}+1}<x<\frac{\mathfrak{Z}+2}{\mathfrak{Z}+1}$ then $\ -\frac{\mathfrak{Z}+2}{\mathfrak{Z}+1}+\frac{\mathfrak{Z}+2}{\mathfrak{Z}+1}<x+\frac{\mathfrak{Z}+2}{\mathfrak{Z}+1}<\frac{\mathfrak{Z}+2}{\mathfrak{Z}+1}+\frac{\mathfrak{Z}+2}{\mathfrak{Z}+1}$

$0<x+\frac{\mathfrak{Z}+2}{\mathfrak{Z}+1}<2\frac{\mathfrak{Z}+2}{\mathfrak{Z}+1}$.

If the condition that $\alpha_1(\mathfrak{Z}),\alpha_0(\mathfrak{Z})\geq 0$ is removed, the positivity of the operator may be broken according to the following cases of $\alpha_1(\mathfrak{Z})$ and $\alpha_0(\mathfrak{Z})$ in equation (2.9).

Case 1. If $0\leq\alpha_1(\mathfrak{Z})\leq 1$, then $\alpha_0(\mathfrak{Z})\geq 0$ and $\alpha_1(\mathfrak{Z})+\alpha_0(\mathfrak{Z})\geq 0$.

Case 2. If $\alpha_1(\mathfrak{Z})<0$, then $\alpha_0(\mathfrak{Z})>0$ and $\alpha_1(\mathfrak{Z})+\alpha_0(\mathfrak{Z})>0$.

Case 3. If $\alpha_1(\mathfrak{Z})>1$, then $\alpha_0(\mathfrak{Z})<0$.

Lemma 2.5 For $b_{\mathfrak{z}-1,r}$ and $b_{\mathfrak{z}-1,r-1}$, given in Lemma 2.3

i) $\sum_{r=0}^{\mathfrak{z}} b_{\mathfrak{z}-1,r}(x)\left(\frac{\mathfrak{z}+2}{\mathfrak{z}+1}\left(\frac{2r}{\mathfrak{z}}-1\right)\right)$

$= 2^{\mathfrak{z}-1}\left(\frac{\mathfrak{z}+2}{\mathfrak{z}+1}\right)^{\mathfrak{z}-1}\left(\left(1-\frac{1}{\mathfrak{z}}\right)x-\frac{1}{\mathfrak{z}}\left(\frac{\mathfrak{z}+2}{\mathfrak{z}+1}\right)\right)$,

ii) $\sum_{r=0}^{\mathfrak{z}} b_{\mathfrak{z}-1,r-1}(x)\left(\frac{\mathfrak{z}+2}{\mathfrak{z}+1}\left(\frac{2r}{\mathfrak{z}}-1\right)\right)$

$= 2^{\mathfrak{z}-1}\left(\frac{\mathfrak{z}+2}{\mathfrak{z}+1}\right)^{\mathfrak{z}-1}\left(\left(1-\frac{1}{\mathfrak{z}}\right)x+\frac{1}{\mathfrak{z}}\left(\frac{\mathfrak{z}+2}{\mathfrak{z}+1}\right)\right)$ (2.10)

is obtained.

Proof.

i) $\sum_{r=0}^{\mathfrak{z}} b_{\mathfrak{z}-1,r}(x)\left(\frac{\mathfrak{z}+2}{\mathfrak{z}+1}\left(\frac{2r}{\mathfrak{z}}-1\right)\right)$

$= \frac{t+2}{t+1}\sum_{r=0}^{t}\binom{t-1}{r}\left(x+\frac{t+2}{t+1}\right)^{r}\left(\frac{t+2}{t+1}-x\right)^{t-r-1}\left(\frac{2r}{t}-1\right)$

$= \frac{2}{\mathfrak{z}}\frac{\mathfrak{z}+2}{\mathfrak{z}+1}\sum_{r=1}^{\mathfrak{z}}\frac{(\mathfrak{z}-1)!}{(r-1)!\,(\mathfrak{z}-r-1)!}$

$\times\left(x+\frac{\mathfrak{z}+2}{\mathfrak{z}+1}\right)^{r}\left(\frac{\mathfrak{z}+2}{\mathfrak{z}+1}-x\right)^{\mathfrak{z}-r-1}$

$-\frac{\mathfrak{z}+2}{\mathfrak{z}+1}\sum_{r=0}^{\mathfrak{z}-1}\frac{(\mathfrak{z}-1)!}{r!\,(\mathfrak{z}-r-1)!}\left(x+\frac{\mathfrak{z}+2}{\mathfrak{z}+1}\right)^{r}\left(\frac{\mathfrak{z}+2}{\mathfrak{z}+1}-x\right)^{\mathfrak{z}-r-1}$

$= \frac{2}{\mathfrak{z}}\frac{\mathfrak{z}+2}{\mathfrak{z}+1}\sum_{r=0}^{\mathfrak{z}-1}\frac{(\mathfrak{z}-1)!}{r!\,(\mathfrak{z}-r-2)!}\left(x+\frac{\mathfrak{z}+2}{\mathfrak{z}+1}\right)^{r+1}\left(\frac{\mathfrak{z}+2}{\mathfrak{z}+1}-x\right)^{\mathfrak{z}-r-2}$

$-\frac{\mathfrak{z}+2}{\mathfrak{z}+1}2^{\mathfrak{z}-1}\left(\frac{\mathfrak{z}+2}{\mathfrak{z}+1}\right)^{\mathfrak{z}-1}$

$$= \frac{2(\mathfrak{Z}-1)}{\mathfrak{Z}}\frac{\mathfrak{Z}+2}{\mathfrak{Z}+1}\left(x+\frac{\mathfrak{Z}+2}{\mathfrak{Z}+1}\right)$$

$$\times \sum_{r=0}^{\mathfrak{Z}-2}\frac{(\mathfrak{Z}-2)!}{r!\,(\mathfrak{Z}-r-2)!}\left(x+\frac{\mathfrak{Z}+2}{\mathfrak{Z}+1}\right)^{r}\left(\frac{\mathfrak{Z}+2}{\mathfrak{Z}+1}-x\right)^{\mathfrak{Z}-r-2}$$

$$-2^{\mathfrak{Z}-1}\left(\frac{\mathfrak{Z}+2}{\mathfrak{Z}+1}\right)^{\mathfrak{Z}}$$

$$= 2^{\mathfrak{Z}-1}\left(\frac{\mathfrak{Z}+2}{\mathfrak{Z}+1}\right)^{\mathfrak{Z}-1}\left(\left(1-\frac{1}{\mathfrak{Z}}\right)x-\frac{1}{\mathfrak{Z}}\left(\frac{\mathfrak{Z}+2}{\mathfrak{Z}+1}\right)\right).$$

ii) $$\sum_{r=0}^{\mathfrak{Z}} b_{\mathfrak{Z}-1,r-1}(x)\left(\frac{\mathfrak{Z}+2}{\mathfrak{Z}+1}\left(\frac{2r}{\mathfrak{Z}}-1\right)\right)$$

$$= \frac{\mathfrak{Z}+2}{\mathfrak{Z}+1}\sum_{r=0}^{\mathfrak{Z}}\binom{\mathfrak{Z}-1}{r-1}\left(x+\frac{\mathfrak{Z}+2}{\mathfrak{Z}+1}\right)^{r-1}\left(\frac{\mathfrak{Z}+2}{\mathfrak{Z}+1}-x\right)^{\mathfrak{Z}-r}\left(\frac{2r}{\mathfrak{Z}}-1\right)$$

$$= \frac{2}{\mathfrak{Z}}\frac{\mathfrak{Z}+2}{\mathfrak{Z}+1}\sum_{r=1}^{\mathfrak{Z}}\frac{(\mathfrak{Z}-1)!}{(r-1)!\,(\mathfrak{Z}-r)!}\left(x+\frac{\mathfrak{Z}+2}{\mathfrak{Z}+1}\right)^{r-1}\left(\frac{\mathfrak{Z}+2}{\mathfrak{Z}+1}-x\right)^{\mathfrak{Z}-r} r$$

$$-\frac{\mathfrak{Z}+2}{\mathfrak{Z}+1}\sum_{r=1}^{\mathfrak{Z}}\frac{(\mathfrak{Z}-1)!}{(r-1)!\,(\mathfrak{Z}-r)!}\left(x+\frac{\mathfrak{Z}+2}{\mathfrak{Z}+1}\right)^{r-1}\left(\frac{\mathfrak{Z}+2}{\mathfrak{Z}+1}-x\right)^{\mathfrak{Z}-r}$$

$$= \frac{2}{\mathfrak{Z}}\frac{\mathfrak{Z}+2}{\mathfrak{Z}+1}\sum_{r=0}^{\mathfrak{Z}-1}\frac{(\mathfrak{Z}-1)!}{r!\,(\mathfrak{Z}-r-1)!}$$

$$\times\left(x+\frac{\mathfrak{Z}+2}{\mathfrak{Z}+1}\right)^{r}\left(\frac{\mathfrak{Z}+2}{\mathfrak{Z}+1}-x\right)^{\mathfrak{Z}-r-1}(r+1)$$

$$-\frac{\mathfrak{Z}+2}{\mathfrak{Z}+1}\sum_{r=0}^{\mathfrak{Z}-1}\frac{(\mathfrak{Z}-1)!}{r!\,(\mathfrak{Z}-r-1)!}\left(x+\frac{\mathfrak{Z}+2}{\mathfrak{Z}+1}\right)^{r}\left(\frac{\mathfrak{Z}+2}{\mathfrak{Z}+1}-x\right)^{\mathfrak{Z}-r-1}$$

$$= \frac{2(\mathfrak{Z}-1)}{\mathfrak{Z}}\frac{\mathfrak{Z}+2}{\mathfrak{Z}+1}\left(x+\frac{\mathfrak{Z}+2}{\mathfrak{Z}+1}\right)$$

$$\times \sum_{r=0}^{\mathfrak{Z}-2} \frac{(\mathfrak{Z}-2)!}{r!\,(\mathfrak{Z}-r-2)!}\left(x+\frac{\mathfrak{Z}+2}{\mathfrak{Z}+1}\right)^{r}\left(\frac{\mathfrak{Z}+2}{\mathfrak{Z}+1}-x\right)^{\mathfrak{Z}-r-2}$$

$$+\frac{1}{\mathfrak{Z}}2^{\mathfrak{Z}}\left(\frac{\mathfrak{Z}+2}{\mathfrak{Z}+1}\right)^{\mathfrak{Z}}-2^{\mathfrak{Z}-1}\left(\frac{\mathfrak{Z}+2}{\mathfrak{Z}+1}\right)^{\mathfrak{Z}}$$

$$=\frac{2(\mathfrak{Z}-1)}{\mathfrak{Z}}\frac{\mathfrak{Z}+2}{\mathfrak{Z}+1}\left(x+\frac{\mathfrak{Z}+2}{\mathfrak{Z}+1}\right)2^{\mathfrak{Z}-2}\left(\frac{\mathfrak{Z}+2}{\mathfrak{Z}+1}\right)^{\mathfrak{Z}-2}$$

$$+\frac{1}{\mathfrak{Z}}2^{\mathfrak{Z}}\left(\frac{\mathfrak{Z}+2}{\mathfrak{Z}+1}\right)^{\mathfrak{Z}}-2^{\mathfrak{Z}-1}\left(\frac{\mathfrak{Z}+2}{\mathfrak{Z}+1}\right)^{\mathfrak{Z}}$$

$$=2^{\mathfrak{Z}-1}\left(\frac{\mathfrak{Z}+2}{\mathfrak{Z}+1}\right)^{\mathfrak{Z}-1}\left(\left(1-\frac{1}{\mathfrak{Z}}\right)\left(x+\frac{\mathfrak{Z}+2}{\mathfrak{Z}+1}\right)+\frac{2}{\mathfrak{Z}}\left(\frac{\mathfrak{Z}+2}{\mathfrak{Z}+1}\right)\right.$$

$$\left.-\left(\frac{\mathfrak{Z}+2}{\mathfrak{Z}+1}\right)\right)$$

$$=2^{\mathfrak{Z}-1}\left(\frac{\mathfrak{Z}+2}{\mathfrak{Z}+1}\right)^{\mathfrak{Z}-1}\left(\left(1-\frac{1}{\mathfrak{Z}}\right)x+\frac{1}{\mathfrak{Z}}\left(\frac{\mathfrak{Z}+2}{\mathfrak{Z}+1}\right)\right)$$

Lemma 2.6

The following equations are valid.

i) $$\sum_{r=0}^{\mathfrak{Z}} b_{\mathfrak{Z}-1,r}(x)\left(\frac{\mathfrak{Z}+2}{\mathfrak{Z}+1}\left(\frac{2r}{\mathfrak{Z}}-1\right)\right)^{2}$$

$$=2^{\mathfrak{Z}-1}\left(\frac{\mathfrak{Z}+2}{\mathfrak{Z}+1}\right)^{\mathfrak{Z}-1}\left(\frac{\mathfrak{Z}^2-3\mathfrak{Z}+2}{\mathfrak{Z}^2}x^2+\frac{2-2\mathfrak{Z}}{\mathfrak{Z}^2}\left(\frac{\mathfrak{Z}+2}{\mathfrak{Z}+1}\right)x\right.$$

$$\left.+\frac{1}{\mathfrak{Z}}\left(\frac{\mathfrak{Z}+2}{\mathfrak{Z}+1}\right)^{2}\right),$$

ii) $$\sum_{r=0}^{\mathfrak{Z}} b_{\mathfrak{Z}-1,r-1}(x)\left(\frac{\mathfrak{Z}+2}{\mathfrak{Z}+1}\left(\frac{2r}{\mathfrak{Z}}-1\right)\right)^{2}$$

$$=2^{\mathfrak{Z}-1}\left(\frac{\mathfrak{Z}+2}{\mathfrak{Z}+1}\right)^{\mathfrak{Z}-1}\left(\frac{\mathfrak{Z}^2-3\mathfrak{Z}+2}{\mathfrak{Z}^2}x^2+\frac{2\mathfrak{Z}-2}{\mathfrak{Z}^2}\left(\frac{\mathfrak{Z}+2}{\mathfrak{Z}+1}\right)x\right.$$

$$+\frac{1}{\mathfrak{z}}\left(\frac{\mathfrak{z}+2}{\mathfrak{z}+1}\right)^2\Bigg). \qquad (2.11)$$

Proof

Using Lemma 2.3

$$\textbf{i)}\sum_{r=0}^{\mathfrak{z}} b_{\mathfrak{z}-1,r}(x)\left(\frac{\mathfrak{z}+2}{\mathfrak{z}+1}\left(\frac{2r}{\mathfrak{z}}-1\right)\right)^2$$

$$=\left(\frac{\mathfrak{z}+2}{\mathfrak{z}+1}\right)^2\sum_{r=0}^{\mathfrak{z}}\binom{\mathfrak{z}-1}{r}\left(x+\frac{\mathfrak{z}+2}{\mathfrak{z}+1}\right)^r\left(\frac{\mathfrak{z}+2}{\mathfrak{z}+1}-x\right)^{\mathfrak{z}-r-1}$$

$$\times\left(\frac{2r}{\mathfrak{z}}-1\right)^2$$

$$=\left(\frac{\mathfrak{z}+2}{\mathfrak{z}+1}\right)^2\sum_{r=0}^{\mathfrak{z}}\binom{\mathfrak{z}-1}{r}\left(x+\frac{\mathfrak{z}+2}{\mathfrak{z}+1}\right)^r\left(\frac{\mathfrak{z}+2}{\mathfrak{z}+1}-x\right)^{\mathfrak{z}-r-1}$$

$$\times\left(\frac{4r^2}{\mathfrak{z}^2}-\frac{4r}{\mathfrak{z}}+1\right)$$

$$=\left(\frac{\mathfrak{z}+2}{\mathfrak{z}+1}\right)^2\frac{4}{\mathfrak{z}^2}\sum_{r=0}^{\mathfrak{z}-2}\frac{(\mathfrak{z}-1)!}{r!\,(\mathfrak{z}-r-3)!}$$

$$\times\left(x+\frac{\mathfrak{z}+2}{\mathfrak{z}+1}\right)^{r+2}\left(\frac{\mathfrak{z}+2}{\mathfrak{z}+1}-x\right)^{\mathfrak{z}-r-3}$$

$$+\left(\frac{\mathfrak{z}+2}{\mathfrak{z}+1}\right)^2\left(\frac{4}{\mathfrak{z}^2}-\frac{4}{\mathfrak{z}}\right)\sum_{r=0}^{\mathfrak{z}-1}\frac{(\mathfrak{z}-1)!}{r!\,(\mathfrak{z}-r-2)!}$$

$$\times\left(x+\frac{\mathfrak{z}+2}{\mathfrak{z}+1}\right)^{r+1}\left(\frac{\mathfrak{z}+2}{\mathfrak{z}+1}-x\right)^{\mathfrak{z}-r-2}+2^{\mathfrak{z}-1}\left(\frac{\mathfrak{z}+2}{\mathfrak{z}+1}\right)^{\mathfrak{z}+1}$$

$$=\left(\frac{\mathfrak{z}+2}{\mathfrak{z}+1}\right)^2\frac{4(\mathfrak{z}-1)(\mathfrak{z}-2)}{\mathfrak{z}^2}\sum_{r=0}^{\mathfrak{z}-3}\frac{(\mathfrak{z}-3)!}{r!\,(\mathfrak{z}-r-3)!}$$

$$\times\left(x+\frac{\mathfrak{z}+2}{\mathfrak{z}+1}\right)^{r+2}\left(\frac{\mathfrak{z}+2}{\mathfrak{z}+1}-x\right)^{\mathfrak{z}-r-3}$$

$$+\left(\frac{\mathfrak{z}+2}{\mathfrak{z}+1}\right)^2\left(\frac{4}{\mathfrak{z}^2}-\frac{4}{\mathfrak{z}}\right)(\mathfrak{z}-1)$$

$$\times\sum_{r=0}^{\mathfrak{z}-2}\frac{(\mathfrak{z}-2)!}{r!\,(\mathfrak{z}-r-2)!}\left(x+\frac{\mathfrak{z}+2}{\mathfrak{z}+1}\right)^{r+1}\left(\frac{\mathfrak{z}+2}{\mathfrak{z}+1}-x\right)^{\mathfrak{z}-r-2}$$

$$+2^{\mathfrak{z}-1}\left(\frac{\mathfrak{z}+2}{\mathfrak{z}+1}\right)^{\mathfrak{z}+1}$$

$$=\left(\frac{\mathfrak{z}+2}{\mathfrak{z}+1}\right)^2\frac{4(\mathfrak{z}-1)(\mathfrak{z}-2)}{\mathfrak{z}^2}\left(x+\frac{\mathfrak{z}+2}{\mathfrak{z}+1}\right)^2 2^{\mathfrak{z}-3}\left(\frac{\mathfrak{z}+2}{\mathfrak{z}+1}\right)^{\mathfrak{z}-3}$$

$$+\left(\frac{1}{\mathfrak{z}^2}-\frac{1}{\mathfrak{z}}\right)(\mathfrak{z}-1)\left(x+\frac{\mathfrak{z}+2}{\mathfrak{z}+1}\right)2^{\mathfrak{z}}\left(\frac{\mathfrak{z}+2}{\mathfrak{z}+1}\right)^{\mathfrak{z}}+2^{\mathfrak{z}-1}\left(\frac{\mathfrak{z}+2}{\mathfrak{z}+1}\right)^{\mathfrak{z}+1}$$

$$=2^{\mathfrak{z}-1}\left(\frac{\mathfrak{z}+2}{\mathfrak{z}+1}\right)^{\mathfrak{z}-1}\left(\frac{(\mathfrak{z}-1)(\mathfrak{z}-2)}{\mathfrak{z}^2}\left(x+\frac{\mathfrak{z}+2}{\mathfrak{z}+1}\right)^2\right.$$

$$\left.+2\left(\frac{1}{\mathfrak{z}^2}-\frac{1}{\mathfrak{z}}\right)(\mathfrak{z}-1)\left(x+\frac{\mathfrak{z}+2}{\mathfrak{z}+1}\right)\left(\frac{\mathfrak{z}+2}{\mathfrak{z}+1}\right)+\left(\frac{\mathfrak{z}+2}{\mathfrak{z}+1}\right)^2\right),$$

$$=2^{\mathfrak{z}-1}\left(\frac{\mathfrak{z}+2}{\mathfrak{z}+1}\right)^{\mathfrak{z}-1}\left(\frac{\mathfrak{z}^2-3\mathfrak{z}+2}{\mathfrak{z}^2}x^2+\frac{2-2\mathfrak{z}}{\mathfrak{z}^2}\left(\frac{\mathfrak{z}+2}{\mathfrak{z}+1}\right)x\right.$$

$$\left.+\frac{1}{\mathfrak{z}}\left(\frac{\mathfrak{z}+2}{\mathfrak{z}+1}\right)^2\right)$$

is obtained.

ii) $$\sum_{r=0}^{\mathfrak{z}}b_{\mathfrak{z}-1,r-1}(x)\left(\frac{\mathfrak{z}+2}{\mathfrak{z}+1}\left(\frac{2r}{\mathfrak{z}}-1\right)\right)^2$$

$$=\left(\frac{\mathfrak{z}+2}{\mathfrak{z}+1}\right)^2\sum_{r=0}^{\mathfrak{z}}\binom{\mathfrak{z}-1}{r-1}\left(x+\frac{\mathfrak{z}+2}{\mathfrak{z}+1}\right)^{r-1}\left(\frac{\mathfrak{z}+2}{\mathfrak{z}+1}-x\right)^{\mathfrak{z}-r}$$

$$\times\left(\frac{2r}{\mathfrak{z}}-1\right)^2$$

$$=\left(\frac{\mathfrak{z}+2}{\mathfrak{z}+1}\right)^2\frac{4}{\mathfrak{z}^2}\sum_{r=1}^{\mathfrak{z}}\frac{(\mathfrak{z}-1)!}{(r-1)!\,(\mathfrak{z}-r)!}$$

$$\times\left(x+\frac{\beth+2}{\beth+1}\right)^{r-1}\left(\frac{\beth+2}{\beth+1}-x\right)^{\beth-r}r^2$$

$$-\frac{4}{\beth}\left(\frac{\beth+2}{\beth+1}\right)^2\sum_{r=1}^{\beth}\frac{(\beth-1)!}{(r-1)!\,(\beth-r)!}$$

$$\times\left(x+\frac{\beth+2}{\beth+1}\right)^{r-1}\left(\frac{\beth+2}{\beth+1}-x\right)^{\beth-r}r$$

$$+\left(\frac{\beth+2}{\beth+1}\right)^2\sum_{r=1}^{\beth}\frac{(\beth-1)!}{(r-1)!\,(\beth-r)!}\left(x+\frac{\beth+2}{\beth+1}\right)^{r-1}\left(\frac{\beth+2}{\beth+1}-x\right)^{\beth-r}$$

$$=\left(\frac{\beth+2}{\beth+1}\right)^2\frac{4(\beth-1)(\beth-2)}{\beth^2}$$

$$\times\sum_{r=0}^{\beth-3}\frac{(\beth-3)!}{r!\,(\beth-r-3)!}\left(x+\frac{\beth+2}{\beth+1}\right)^{r+2}\left(\frac{\beth+2}{\beth+1}-x\right)^{\beth-r-3}$$

$$+\left(\frac{\beth+2}{\beth+1}\right)^2\left(\frac{12}{\beth^2}-\frac{4}{\beth}\right)(\beth-1)$$

$$\times\sum_{r=0}^{\beth-2}\frac{(\beth-2)!}{r!\,(\beth-r-2)!}\left(x+\frac{\beth+2}{\beth+1}\right)^{r+1}\left(\frac{\beth+2}{\beth+1}-x\right)^{\beth-r-2}$$

$$+\left(\frac{\beth+2}{\beth+1}\right)^2\left(\frac{4}{\beth^2}-\frac{4}{\beth}+1\right)2^{\beth-1}\left(\frac{\beth+2}{\beth+1}\right)^{\beth-1}$$

$$=\left(\frac{\beth+2}{\beth+1}\right)^2\frac{4(\beth-1)(\beth-2)}{\beth^2}\left(x+\frac{\beth+2}{\beth+1}\right)^2 2^{\beth-3}\left(\frac{\beth+2}{\beth+1}\right)^{\beth-3}$$

$$+\left(\frac{\beth+2}{\beth+1}\right)^2\left(\frac{12}{\beth^2}-\frac{4}{\beth}\right)(\beth-1)\left(x+\frac{\beth+2}{\beth+1}\right)2^{\beth-2}\left(\frac{\beth+2}{\beth+1}\right)^{\beth-2}$$

$$+\left(\frac{\beth+2}{\beth+1}\right)^2\left(\frac{4}{\beth^2}-\frac{4}{\beth}+1\right)2^{\beth-1}\left(\frac{\beth+2}{\beth+1}\right)^{\beth-1}$$

$$=2^{\beth-1}\left(\frac{\beth+2}{\beth+1}\right)^{\beth-1}\left(\frac{\beth^2-3\beth+2}{\beth^2}x^2+\frac{2\beth-2}{\beth^2}\left(\frac{\beth+2}{\beth+1}\right)x\right.$$

$$+\frac{1}{\mathfrak{Z}}\left(\frac{\mathfrak{Z}+2}{\mathfrak{Z}+1}\right)^2\Bigg).$$

Lemma 2.7

For $Z_{\mathfrak{Z}}^*(f;x)$,

i) $Z_{\mathfrak{Z}}^*(e_0;x)=1$,

ii) $Z_{\mathfrak{Z}}^*(e_1;x)=x\left(\alpha_1(\mathfrak{Z})+\alpha_0(\mathfrak{Z})\left(\frac{\mathfrak{Z}+1}{\mathfrak{Z}+2}\right)\right)-x\left(\frac{2\alpha_1(\mathfrak{Z})+\alpha_0(\mathfrak{Z})\left(\frac{\mathfrak{Z}+1}{\mathfrak{Z}+2}\right)}{\mathfrak{Z}}\right)$,

iii) $Z_{\mathfrak{Z}}^*(e_2;x)=x^2\left(\alpha_1(\mathfrak{Z})+\alpha_0(\mathfrak{Z})\left(\frac{\mathfrak{Z}+1}{\mathfrak{Z}+2}\right)\right)$

$$+\frac{2x^2\left(2\alpha_1(\mathfrak{Z})+\alpha_0(\mathfrak{Z})\left(\frac{\mathfrak{Z}+1}{\mathfrak{Z}+2}\right)\right)}{\mathfrak{Z}^2}$$

$$+\frac{\left(\left(\frac{\mathfrak{Z}+2}{\mathfrak{Z}+1}\right)^2-5x^2\right)\alpha_1(\mathfrak{Z})+\left(\left(\frac{\mathfrak{Z}+2}{\mathfrak{Z}+1}\right)-3\left(\frac{\mathfrak{Z}+1}{\mathfrak{Z}+2}\right)x^2\right)\alpha_0(\mathfrak{Z})}{\mathfrak{Z}}$$

equalities are valid.

Proof.

i) $Z_{\mathfrak{Z}}^*(e_0;x)=\left(\frac{\mathfrak{Z}+1}{2(\mathfrak{Z}+2)}\right)^{\mathfrak{Z}}\sum_{r=0}^{\mathfrak{Z}}b_{\mathfrak{Z},r}^*$

$$=\left(\frac{\mathfrak{Z}+1}{2(\mathfrak{Z}+2)}\right)^{\mathfrak{Z}}\sum_{r=0}^{\mathfrak{Z}}\Bigg(\left(\alpha_1(\mathfrak{Z})\left(x+\frac{\mathfrak{Z}+2}{\mathfrak{Z}+1}\right)+\alpha_0(\mathfrak{Z})\right)$$

$$\times b_{\mathfrak{Z}-1,r}(x)+\left(\alpha_1(\mathfrak{Z})\left(\frac{\mathfrak{Z}+2}{\mathfrak{Z}+1}-x\right)+\alpha_0(\mathfrak{Z})\right)b_{\mathfrak{Z}-1,r-1}(x)\Bigg)$$

$$=\left(\frac{\mathfrak{Z}+1}{2(\mathfrak{Z}+2)}\right)^{\mathfrak{Z}}\Bigg(\sum_{r=0}^{\mathfrak{Z}}\Bigg(\left(\alpha_1(\mathfrak{Z})\left(x+\frac{\mathfrak{Z}+2}{\mathfrak{Z}+1}\right)+\alpha_0(\mathfrak{Z})\right)b_{\mathfrak{Z}-1,r}(x)\Big)$$

$$+\sum_{r=0}^{\mathfrak{Z}}\left(\left(\alpha_1(\mathfrak{Z})\left(\frac{\mathfrak{Z}+2}{\mathfrak{Z}+1}-x\right)+\alpha_0(\mathfrak{Z})\right)b_{\mathfrak{Z}-1,r-1}(x)\right)\Bigg)$$

$$=\left(\frac{\mathfrak{Z}+1}{2(\mathfrak{Z}+2)}\right)^{\mathfrak{Z}}\left(\left(\alpha_1(\mathfrak{Z})\left(x+\frac{\mathfrak{Z}+2}{\mathfrak{Z}+1}\right)+\alpha_0(\mathfrak{Z})\right)2^{\mathfrak{Z}-1}\left(\frac{\mathfrak{Z}+2}{\mathfrak{Z}+1}\right)^{\mathfrak{Z}-1}\right.$$

$$\left.+\left(\alpha_1(\mathfrak{Z})\left(\frac{\mathfrak{Z}+2}{\mathfrak{Z}+1}-x\right)+\alpha_0(\mathfrak{Z})\right)2^{\mathfrak{Z}-1}\left(\frac{\mathfrak{Z}+2}{\mathfrak{Z}+1}\right)^{\mathfrak{Z}-1}\right)$$

$$=\frac{1}{2}\left(\frac{\mathfrak{Z}+1}{\mathfrak{Z}+2}\right)\left(\left(\alpha_1(\mathfrak{Z})\left(x+\frac{\mathfrak{Z}+2}{\mathfrak{Z}+1}\right)+\alpha_0(\mathfrak{Z})\right)\right.$$

$$\left.+\left(\alpha_1(\mathfrak{Z})\left(\frac{\mathfrak{Z}+2}{\mathfrak{Z}+1}-x\right)+\alpha_0(\mathfrak{Z})\right)\right)$$

$$=\frac{\mathfrak{Z}+1}{\mathfrak{Z}+2}\left(\left(\alpha_1(\mathfrak{Z})\left(\frac{\mathfrak{Z}+2}{\mathfrak{Z}+1}\right)+\alpha_0(\mathfrak{Z})\right)\right)$$

$$=1.$$

ii) Here, using Definition 2.1.,

$$Z_{\mathfrak{Z}}^{*}(e_1;x)=\frac{1}{2^{\mathfrak{Z}}}\left(\frac{\mathfrak{Z}+1}{\mathfrak{Z}+2}\right)^{\mathfrak{Z}}\sum_{r=0}^{\mathfrak{Z}}b_{\mathfrak{Z},r}^{*}\left(\frac{\mathfrak{Z}+2}{\mathfrak{Z}+1}\left(\frac{2r}{\mathfrak{Z}}-1\right)\right)$$

$$=\frac{1}{2^{\mathfrak{Z}}}\left(\frac{\mathfrak{Z}+1}{\mathfrak{Z}+2}\right)^{\mathfrak{Z}}\sum_{r=0}^{\mathfrak{Z}}\left(\alpha\left(x+\frac{\mathfrak{Z}+2}{\mathfrak{Z}+1},\mathfrak{Z}\right)b_{\mathfrak{Z}-1,r}(x)\right.$$

$$\left.+\alpha\left(\frac{\mathfrak{Z}+2}{\mathfrak{Z}+1}-x,\mathfrak{Z}\right)b_{\mathfrak{Z}-1,r-1}(x)\right)\left(\frac{\mathfrak{Z}+2}{\mathfrak{Z}+1}\left(\frac{2r}{\mathfrak{Z}}-1\right)\right)$$

$$=\frac{1}{2^{\mathfrak{Z}}}\left(\frac{\mathfrak{Z}+1}{\mathfrak{Z}+2}\right)^{\mathfrak{Z}}\left(\left(\alpha_1(\mathfrak{Z})\left(x+\frac{\mathfrak{Z}+2}{\mathfrak{Z}+1}\right)+\alpha_0(\mathfrak{Z})\right)\right.$$

$$\times 2^{\mathfrak{z}-1}\left(\frac{\mathfrak{z}+2}{\mathfrak{z}+1}\right)^{\mathfrak{z}-1}\left(\left(1-\frac{1}{\mathfrak{z}}\right)x-\frac{1}{\mathfrak{z}}\left(\frac{\mathfrak{z}+2}{\mathfrak{z}+1}\right)\right)$$

$$+\left(\alpha_1(\mathfrak{z})\left(\frac{\mathfrak{z}+2}{\mathfrak{z}+1}-x\right)+\alpha_0(\mathfrak{z})\right)$$

$$\times 2^{\mathfrak{z}-1}\left(\frac{\mathfrak{z}+2}{\mathfrak{z}+1}\right)^{\mathfrak{z}-1}\left(\left(1-\frac{1}{\mathfrak{z}}\right)x+\frac{1}{\mathfrak{z}}\left(\frac{\mathfrak{z}+2}{\mathfrak{z}+1}\right)\right)\Bigg)$$

$$=\left(x\left(1-\frac{1}{\mathfrak{z}}\right)\left(\alpha_1(\mathfrak{z})+\alpha_0(\mathfrak{z})\left(\frac{\mathfrak{z}+1}{\mathfrak{z}+2}\right)\right)-\frac{\alpha_1(\mathfrak{z})}{\mathfrak{z}}x\right)$$

$$=x\left(\alpha_1(\mathfrak{z})+\alpha_0(\mathfrak{z})\left(\frac{\mathfrak{z}+1}{\mathfrak{z}+2}\right)\right)-x\left(\frac{2\alpha_1(\mathfrak{z})+\alpha_0(\mathfrak{z})\left(\frac{\mathfrak{z}+1}{\mathfrak{z}+2}\right)}{\mathfrak{z}}\right) \qquad (2.12)$$

is hold.

iii) Similarly, by making some calculations,

$$Z_{\mathfrak{z}}^{*}(e_2;x)=\frac{1}{2^{\mathfrak{z}}}\left(\frac{\mathfrak{z}+1}{\mathfrak{z}+2}\right)^{\mathfrak{z}}\sum_{r=0}^{\mathfrak{z}}b_{\mathfrak{z},r}^{*}\left(\frac{\mathfrak{z}+2}{\mathfrak{z}+1}\left(\frac{2r}{\mathfrak{z}}-1\right)\right)^2$$

$$=\frac{1}{2^{\mathfrak{z}}}\left(\frac{\mathfrak{z}+1}{\mathfrak{z}+2}\right)^{\mathfrak{z}}\sum_{r=0}^{\mathfrak{z}}\left(\alpha\left(x+\frac{\mathfrak{z}+2}{\mathfrak{z}+1},\mathfrak{z}\right)b_{\mathfrak{z}-1,r}(x)\right.$$

$$\left.+\alpha\left(\frac{\mathfrak{z}+2}{\mathfrak{z}+1}-x,\mathfrak{z}\right)b_{\mathfrak{z}-1,r-1}(x)\right)\left(\frac{\mathfrak{z}+2}{\mathfrak{z}+1}\left(\frac{2r}{\mathfrak{z}}-1\right)\right)^2$$

$$=\frac{1}{2^{\mathfrak{z}}}\left(\frac{\mathfrak{z}+1}{\mathfrak{z}+2}\right)^{\mathfrak{z}}\Bigg(\left(\alpha_1(\mathfrak{z})\left(x+\frac{\mathfrak{z}+2}{\mathfrak{z}+1}\right)+\alpha_0(\mathfrak{z})\right)$$

$$\times 2^{\mathfrak{z}-1}\left(\frac{\mathfrak{z}+2}{\mathfrak{z}+1}\right)^{\mathfrak{z}-1}\left(\frac{\mathfrak{z}^2-3\mathfrak{z}+2}{\mathfrak{z}^2}x^2+\frac{2-2\mathfrak{z}}{\mathfrak{z}^2}\left(\frac{\mathfrak{z}+2}{\mathfrak{z}+1}\right)x\right.$$

$$\left.+\frac{1}{\mathfrak{z}}\left(\frac{\mathfrak{z}+2}{\mathfrak{z}+1}\right)^2\right)+\left(\alpha_1(\mathfrak{z})\left(\frac{\mathfrak{z}+2}{\mathfrak{z}+1}-x\right)+\alpha_0(\mathfrak{z})\right)$$

$$\times 2^{\frac{z}{3}-1}\left(\frac{\frac{z}{3}+2}{\frac{z}{3}+1}\right)^{\frac{z}{3}-1} 2^{\frac{z}{3}-1}\left(\frac{\frac{z}{3}+2}{\frac{z}{3}+1}\right)^{\frac{z}{3}-1}\left(\frac{\frac{z^2}{3^2}-3\frac{z}{3}+2}{\frac{z^2}{3^2}}x^2\right.$$

$$\left.+\frac{2\frac{z}{3}-2}{\frac{z^2}{3^2}}\left(\frac{\frac{z}{3}+2}{\frac{z}{3}+1}\right)x+\frac{1}{\frac{z}{3}}\left(\frac{\frac{z}{3}+2}{\frac{z}{3}+1}\right)^2\right)$$

$$=x^2\left(\alpha_1\left(\frac{z}{3}\right)+\alpha_0\left(\frac{z}{3}\right)\left(\frac{\frac{z}{3}+1}{\frac{z}{3}+2}\right)\right)$$

$$+\frac{2x^2\left(2\alpha_1\left(\frac{z}{3}\right)+\alpha_0\left(\frac{z}{3}\right)\left(\frac{\frac{z}{3}+1}{\frac{z}{3}+2}\right)\right)}{\frac{z^2}{3^2}}$$

$$+\frac{\left(\left(\frac{\frac{z}{3}+2}{\frac{z}{3}+1}\right)^2-5x^2\right)\alpha_1\left(\frac{z}{3}\right)+\left(\left(\frac{\frac{z}{3}+2}{\frac{z}{3}+1}\right)-3\left(\frac{\frac{z}{3}+1}{\frac{z}{3}+2}\right)x^2\right)\alpha_0\left(\frac{z}{3}\right)}{\frac{z}{3}} \qquad (2.13)$$

is written.

Theorem 2.1

Let $\alpha_1\left(\frac{z}{3}\right)$ and $\alpha_0\left(\frac{z}{3}\right)$, be two sequences that make the operator (2.5) positive. In this case, for every $f \in C\left[-\frac{\frac{z}{3}+2}{\frac{z}{3}+1}, \frac{\frac{z}{3}+2}{\frac{z}{3}+1}\right]$,

$$\lim_{\frac{z}{3}\to\infty}\left\|Z_{\frac{z}{3}}^*(f;x)-f(x)\right\|_{C\left[-\frac{\frac{z}{3}+2}{\frac{z}{3}+1},\frac{\frac{z}{3}+2}{\frac{z}{3}+1}\right]}=0$$

is valid.

Proof. For $i=0,1\ \frac{z}{3}=0,1,2,\ldots$ let $\alpha_i\left(\frac{z}{3}\right)$ satisfy the positivity conditions. Using (2.12) and (2.13),

$$\lim_{\frac{z}{3}\to\infty} Z_{\frac{z}{3}}^*(e_0;x)=1,$$

$$\lim_{\frac{z}{3}\to\infty} Z_{\frac{z}{3}}^*(e_1;x)=\lim_{\frac{z}{3}\to\infty}\left(x\left(\alpha_1\left(\frac{z}{3}\right)+\alpha_0\left(\frac{z}{3}\right)\left(\frac{\frac{z}{3}+1}{\frac{z}{3}+2}\right)\right)\right.$$

$$\left.-x\left(\frac{2\alpha_1\left(\frac{z}{3}\right)+\alpha_0\left(\frac{z}{3}\right)\left(\frac{\frac{z}{3}+1}{\frac{z}{3}+2}\right)}{\frac{z}{3}}\right)\right)$$

$$= \lim_{ʒ\to\infty} x - \lim_{ʒ\to\infty} x\left(\frac{2\alpha_1(ʒ)+\alpha_0(ʒ)\left(\frac{ʒ+1}{ʒ+2}\right)}{ʒ}\right)$$

$$= x,$$

$$\lim_{ʒ\to\infty} Z_ʒ^*(e_2;x) = \lim_{ʒ\to\infty}\left(x^2\left(\alpha_1(ʒ)+\alpha_0(ʒ)\left(\frac{ʒ+1}{ʒ+2}\right)\right)\right.$$

$$+\frac{2x^2\left(2\alpha_1(ʒ)+\alpha_0(ʒ)\left(\frac{ʒ+1}{ʒ+2}\right)\right)}{ʒ^2}$$

$$\left.+\frac{\left(\left(\frac{ʒ+2}{ʒ+1}\right)^2-5x^2\right)\alpha_1(ʒ)+\left(\left(\frac{ʒ+2}{ʒ+1}\right)-3\left(\frac{ʒ+1}{ʒ+2}\right)x^2\right)\alpha_0(ʒ)}{ʒ}\right)$$

$$= \lim_{ʒ\to\infty} x^2 + \lim_{ʒ\to\infty}\frac{2x^2\left(2\alpha_1(ʒ)+\alpha_0(ʒ)\left(\frac{ʒ+1}{ʒ+2}\right)\right)}{ʒ^2}$$

$$+\lim_{ʒ\to\infty}\frac{\left(\left(\frac{ʒ+2}{ʒ+1}\right)^2-5x^2\right)\alpha_1(ʒ)+\left(\left(\frac{ʒ+2}{ʒ+1}\right)-3\left(\frac{ʒ+1}{ʒ+2}\right)x^2\right)\alpha_0(ʒ)}{ʒ}$$

$$= x^2.$$

So, for $j = 0,1,2,$

$$\lim_{ʒ\to\infty}\left\|Z_ʒ^*(e_j;x)-e_j(x)\right\|_{C\left[-\frac{ʒ+2}{ʒ+1},\frac{ʒ+2}{ʒ+1}\right]} = 0$$

is written. Then from Korovkin's theorem, for all $f \in C\left[-\frac{ʒ+2}{ʒ+1},\frac{ʒ+2}{ʒ+1}\right]$,

$$\lim_{ʒ\to\infty}\left\|Z_ʒ^*(f;x)-f(x)\right\|_{C\left[-\frac{ʒ+2}{ʒ+1},\frac{ʒ+2}{ʒ+1}\right]} = 0.$$

Theorem 2.2 (Voronovskaja Theorems)

Let f, be bounded on $\left[-\frac{ʒ+2}{ʒ+1},\frac{ʒ+2}{ʒ+1}\right]$ and the operator (2.5) be positive.

i) If $2\alpha_1(ʒ)+\alpha_0(ʒ)\left(\frac{ʒ+1}{ʒ+2}\right) = 0$ and second derivative $f''(x)$ exists at a given point $x \in \left[-\frac{ʒ+2}{ʒ+1},\frac{ʒ+2}{ʒ+1}\right]$,

$$\lim_{\mathfrak{Z}\to\infty} 2\mathfrak{Z}\left(Z_{\mathfrak{Z}}^{*}(f;x)-f(x)\right)$$

$$=\lim_{\mathfrak{Z}\to\infty}\left(\left(\left(\frac{\mathfrak{Z}+2}{\mathfrak{Z}+1}\right)^{2}-5x^{2}\right)\alpha_{1}(\mathfrak{Z})\right.$$

$$\left.+\left(\left(\frac{\mathfrak{Z}+2}{\mathfrak{Z}+1}\right)-3\left(\frac{\mathfrak{Z}+1}{\mathfrak{Z}+2}\right)x^{2}\right)\alpha_{0}(\mathfrak{Z})f''(x)\right. . \qquad (2.14)$$

Also, if $f''\in C\left[-\frac{\mathfrak{Z}+2}{\mathfrak{Z}+1},\frac{\mathfrak{Z}+2}{\mathfrak{Z}+1}\right]$, then the equality is uniformly on $\left[-\frac{\mathfrak{Z}+2}{\mathfrak{Z}+1},\frac{\mathfrak{Z}+2}{\mathfrak{Z}+1}\right]$.

ii) If $2\alpha_{1}(\mathfrak{Z})+\alpha_{0}(\mathfrak{Z})\left(\frac{\mathfrak{Z}+1}{\mathfrak{Z}+2}\right)\neq 0$ and first derivative $f'(x)$ exists at a given point $x\in\left[-\frac{\mathfrak{Z}+2}{\mathfrak{Z}+1},\frac{\mathfrak{Z}+2}{\mathfrak{Z}+1}\right]$,

$$\lim_{\mathfrak{Z}\to\infty}\mathfrak{Z}\left(Z_{\mathfrak{Z}}^{*}(f;x)-f(x)\right)$$

$$=\lim_{\mathfrak{Z}\to\infty}(-x)\left(2\alpha_{1}(\mathfrak{Z})+\alpha_{0}(\mathfrak{Z})\left(\frac{\mathfrak{Z}+1}{\mathfrak{Z}+2}\right)\right)f'^{(x)}.$$

Also if $f'\in C\left[-\frac{\mathfrak{Z}+2}{\mathfrak{Z}+1},\frac{\mathfrak{Z}+2}{\mathfrak{Z}+1}\right]$, then the equality is uniformly on $\left[-\frac{\mathfrak{Z}+2}{\mathfrak{Z}+1},\frac{\mathfrak{Z}+2}{\mathfrak{Z}+1}\right]$.

Proof

Only i) will be proven. ii) can be proven in a similar way. Let

$2\alpha_{1}(\mathfrak{Z})+\alpha_{0}(\mathfrak{Z})\left(\frac{\mathfrak{Z}+1}{\mathfrak{Z}+2}\right)=0$. Using Theorem 1.6.6 in (Davis, 1975),

$$f(y)=f(x)+f'(x)(y-x)+\frac{f''(x)(y-x)^{2}}{2}+h(y)(y-x)^{2}$$

is written. Here, $\lim_{y\to x}h(y)=0$. Then, if $y=\frac{\mathfrak{Z}+2}{\mathfrak{Z}+1}\left(\frac{2r}{\mathfrak{Z}}-1\right)$ is taken

$$f\left(\frac{\mathfrak{Z}+2}{\mathfrak{Z}+1}\left(\frac{2r}{\mathfrak{Z}}-1\right)\right)=f(x)+f'(x)\left(\frac{\mathfrak{Z}+2}{\mathfrak{Z}+1}\left(\frac{2r}{\mathfrak{Z}}-1\right)-x\right)$$

$$+\frac{1}{2}f''(x)\left(\frac{\mathfrak{Z}+2}{\mathfrak{Z}+1}\left(\frac{2r}{\mathfrak{Z}}-1\right)-x\right)^{2}$$

$$+h\left(\frac{\mathfrak{Z}+2}{\mathfrak{Z}+1}\left(\frac{2r}{\mathfrak{Z}}-1\right)\right)\left(\frac{\mathfrak{Z}+2}{\mathfrak{Z}+1}\left(\frac{2r}{\mathfrak{Z}}-1\right)-x\right)^{2} \qquad (2.15)$$

is getting. If we multiply both sides of (2.15) by $b_{ʒ,r}^{*}\left(\frac{ʒ+1}{2(ʒ+2)}\right)^{ʒ}$ and take the sum from $r=0$ to $r=ʒ$, using (2.11), (2.12) ve (2.13) and $\alpha_1(ʒ)+\alpha_0(ʒ)\left(\frac{ʒ+1}{ʒ+2}\right)=1$,

$$\left(\frac{ʒ+1}{2(ʒ+2)}\right)^{ʒ}\sum_{r=0}^{ʒ}b_{ʒ,r}^{*}\,f\left(\frac{ʒ+2}{ʒ+1}\left(\frac{2r}{ʒ}-1\right)\right)$$

$$=\left(\frac{ʒ+1}{2(ʒ+2)}\right)^{ʒ}\sum_{r=0}^{ʒ}b_{ʒ,r}^{*}\,f(x)$$

$$+\left(\frac{ʒ+1}{2(ʒ+2)}\right)^{ʒ}\sum_{r=0}^{ʒ}b_{ʒ,r}^{*}\,f'(x)\left(\frac{ʒ+2}{ʒ+1}\left(\frac{2r}{ʒ}-1\right)-x\right)$$

$$+\left(\frac{ʒ+1}{2(ʒ+2)}\right)^{ʒ}\sum_{r=0}^{ʒ}b_{ʒ,r}^{*}\,\frac{1}{2}f''(x)\left(\frac{ʒ+2}{ʒ+1}\left(\frac{2r}{ʒ}-1\right)-x\right)^{2}$$

$$+\left(\frac{ʒ+1}{2(ʒ+2)}\right)^{ʒ}\sum_{r=0}^{ʒ}b_{ʒ,r}^{*}\,h\left(\frac{ʒ+2}{ʒ+1}\left(\frac{2r}{ʒ}-1\right)\right)$$

$$\times\left(\frac{ʒ+2}{ʒ+1}\left(\frac{2r}{ʒ}-1\right)-x\right)^{2}.$$

$$Z_{ʒ}^{*}(f;x)=Z_{ʒ}^{*}(e_0;x)f(x)+f'(x)\left(Z_{ʒ}^{*}(e_1;x)-x\right)$$

$$+\frac{1}{2}f''(x)\left(Z_{ʒ}^{*}(e_2;x)-2xZ_{ʒ}^{*}(e_1;x)+x^2Z_{ʒ}^{*}(e_0;x)\right)$$

$$+Z_{ʒ}^{*}(h(e_1)(e_1-x)^2;x)$$

$$=f(x)+f'(x)(x-x)$$

$$+\frac{1}{2}f''(x)\left(Z_{ʒ}^{*}(e_2;x)-2xZ_{ʒ}^{*}(e_1;x)+x^2Z_{ʒ}^{*}(e_0;x)\right)$$

$$+Z_{ʒ}^{*}(h(e_1)(e_1-x)^2;x)$$

$$=f(x)+\frac{1}{2}f''(x)(x^2$$

$$+\frac{\left(\left(\frac{\text{ʒ}+2}{\text{ʒ}+1}\right)^2-5x^2\right)\alpha_1(\text{ʒ})+\left(\left(\frac{\text{ʒ}+2}{\text{ʒ}+1}\right)-3\left(\frac{\text{ʒ}+1}{\text{ʒ}+2}\right)x^2\right)\alpha_0(\text{ʒ})}{\text{ʒ}}$$

$$-2x^2+x^2)+Z_{\text{ʒ}}^*(h(e_1)(e_1-x)^2;x)$$

$$=f(x)$$

$$+\frac{1}{2}\text{f}''(\text{x})\left(\frac{\left(\left(\frac{\text{m}+2}{\text{m}+1}\right)^2-5\text{x}^2\right)\alpha_1(\text{m})}{\text{m}}+\frac{\left(\left(\frac{\text{m}+2}{\text{m}+1}\right)-3\left(\frac{\text{m}+1}{\text{m}+2}\right)\text{x}^2\right)\alpha_0(\text{m})}{\text{m}}\right)$$

$$+Z_{\text{ʒ}}^*(h(e_1)(e_1-x)^2;x).$$

is getting. Let $\varepsilon>0$ be given. There exists a $\delta>0$ such that $|y-x|<\delta$ then $|h(y)|<\varepsilon$.

Let

$$\mathcal{A}=\left\{r:\left|\frac{\text{ʒ}+2}{\text{ʒ}+1}\left(\frac{2r}{\text{ʒ}}-1\right)-x\right|<\delta,r=0,1,2,\ldots\text{ʒ}\right\},$$

$$\mathcal{B}=\left\{r:\left|\frac{\text{ʒ}+2}{\text{ʒ}+1}\left(\frac{2r}{\text{ʒ}}-1\right)-x\right|\geq\delta,r=0,1,2,\ldots\text{ʒ}\right\}.$$

Then

$$Z_{\text{ʒ}}^*(h(e_1)(e_1-x)^2;x)$$

$$=\left(\frac{\text{ʒ}+1}{2(\text{ʒ}+2)}\right)^{\text{ʒ}}\sum_{r=0}^{\text{ʒ}}b_{\text{ʒ},r}^*(x)$$

$$\times h\left(\frac{\text{ʒ}+2}{\text{ʒ}+1}\left(\frac{2r}{\text{ʒ}}-1\right)\right)\left(\frac{\text{ʒ}+2}{\text{ʒ}+1}\left(\frac{2r}{\text{ʒ}}-1\right)-x\right)^2.$$

Here, $b_{\text{ʒ},r}^*(x)$, is defined in (2.6). Using (2.11), (2.12) and (2.13), for $\alpha_1(\text{ʒ})+\alpha_0(\text{ʒ})\left(\frac{\text{ʒ}+1}{\text{ʒ}+2}\right)=1$ and $i=0,1$, using $|a_i(\text{ʒ})|\leq M$

$$M=\sup_{-\frac{\text{ʒ}+2}{\text{ʒ}+1}\leq y\leq\frac{\text{ʒ}+2}{\text{ʒ}+1}}h(y)\,(y-x)^2.$$

In this case,

$$\left|Z_{\text{ʒ}}^*(h(e_1)(e_1-x)^2;x)\right|$$

$$= \left(\frac{\mathfrak{Z}+1}{2(\mathfrak{Z}+2)}\right)^{\mathfrak{Z}} \left| \sum_{r\in\mathcal{A}} b^*_{\mathfrak{Z},r}(x)\, h\left(\frac{\mathfrak{Z}+2}{\mathfrak{Z}+1}\left(\frac{2r}{\mathfrak{Z}}-1\right)\right) \right.$$

$$\times \left(\frac{\mathfrak{Z}+2}{\mathfrak{Z}+1}\left(\frac{2r}{\mathfrak{Z}}-1\right)-x\right)^2 + \sum_{r\in\mathcal{B}} b^*_{\mathfrak{Z},r}(x)\, h\left(\frac{\mathfrak{Z}+2}{\mathfrak{Z}+1}\left(\frac{2r}{\mathfrak{Z}}-1\right)\right)$$

$$\left.\left(\frac{\mathfrak{Z}+2}{\mathfrak{Z}+1}\left(\frac{2r}{\mathfrak{Z}}-1\right)-x\right)^2 \right|$$

$$\leq \varepsilon \left(\frac{\mathfrak{Z}+1}{2(\mathfrak{Z}+2)}\right)^{\mathfrak{Z}} \sum_{r=0}^{\mathfrak{Z}} \left| b^*_{\mathfrak{Z},r}(x) \right|$$

$$+ \frac{M}{\delta^2}\left(\frac{\mathfrak{Z}+1}{2(\mathfrak{Z}+2)}\right)^{\mathfrak{Z}} \sum_{r=0}^{\mathfrak{Z}} b^*_{\mathfrak{Z},r}(x) \left(\frac{\mathfrak{Z}+2}{\mathfrak{Z}+1}\left(\frac{2r}{\mathfrak{Z}}-1\right)-x\right)^2$$

$$= \varepsilon + \frac{M}{\delta^2}\left(Z^*_{\mathfrak{Z}}(e_2;x) - 2xZ^*_{\mathfrak{Z}}(e_1;x) + x^2 Z^*_{\mathfrak{Z}}(e_0;x)\right)$$

$$= \varepsilon + \frac{M}{\delta^2}\left(x^2 + \frac{\left(\left(\frac{\mathfrak{Z}+2}{\mathfrak{Z}+1}\right)^2 - 5x^2\right)\alpha_1(\mathfrak{Z})}{\mathfrak{Z}}\right.$$

$$\left. + \frac{\left(\left(\frac{\mathfrak{Z}+2}{\mathfrak{Z}+1}\right) - 3\left(\frac{\mathfrak{Z}+1}{\mathfrak{Z}+2}\right)x^2\right)\alpha_0(\mathfrak{Z})}{\mathfrak{Z}} - 2x^2 + x^2 \right)$$

$$= \varepsilon + \frac{M}{\delta^2}\left(\frac{\left(\left(\frac{\mathfrak{Z}+2}{\mathfrak{Z}+1}\right)^2 - 5x^2\right)\alpha_1(\mathfrak{Z})}{\mathfrak{Z}} \right.$$

$$\left. + \frac{\left(\left(\frac{\mathfrak{Z}+2}{\mathfrak{Z}+1}\right) - 3\left(\frac{\mathfrak{Z}+1}{\mathfrak{Z}+2}\right)x^2\right)\alpha_0(\mathfrak{Z})}{\mathfrak{Z}} \right) \leq \varepsilon', \qquad (2.16)$$

is getting. Since ε is arbitrary, the desired result is shown in (2.14). Let $f'' \in C\left[-\frac{\mathfrak{Z}+2}{\mathfrak{Z}+1}, \frac{\mathfrak{Z}+2}{\mathfrak{Z}+1}\right]$. Here, f'' is uniformly continuous. Since the equality (2.16) is independent of $x \in \left[-\frac{\mathfrak{Z}+2}{\mathfrak{Z}+1}, \frac{\mathfrak{Z}+2}{\mathfrak{Z}+1}\right]$ (2.14), uniformly on $\left[-\frac{\mathfrak{Z}+2}{\mathfrak{Z}+1}, \frac{\mathfrak{Z}+2}{\mathfrak{Z}+1}\right]$.

Theorem 2.3

Let the function f be bounded at $x \in \left[-\frac{\mathfrak{Z}+2}{\mathfrak{Z}+1}, \frac{\mathfrak{Z}+2}{\mathfrak{Z}+1}\right]$ and the operator (2.5) be positive. Then,

$$\left\|Z_{\mathfrak{Z}}^{*}(f,x) - f(x)\right\|_{C\left[-\frac{\mathfrak{Z}+2}{\mathfrak{Z}+1}, \frac{\mathfrak{Z}+2}{\mathfrak{Z}+1}\right]} \leq 6\left(\frac{\mathfrak{Z}+2}{\mathfrak{Z}+1}\right)\omega\left(\frac{1}{\sqrt{\mathfrak{Z}}}\right). \qquad (2.17)$$

Proof

$$\left|Z_{\mathfrak{Z}}^{*}(f;x) - f(x)\right| \leq \left|\alpha_1(\mathfrak{Z})\left(x + \frac{\mathfrak{Z}+2}{\mathfrak{Z}+1}\right) + \alpha_0(\mathfrak{Z})\right|$$

$$\times\left(\left(\frac{\mathfrak{Z}+1}{2(\mathfrak{Z}+2)}\right)^{\mathfrak{Z}}\sum_{r=0}^{\mathfrak{Z}} b_{\mathfrak{Z},r}(x)\left|f\left(\frac{\mathfrak{Z}+2}{\mathfrak{Z}+1}\left(\frac{2r}{\mathfrak{Z}}-1\right)\right) - f(x)\right|\right)$$

$$+\left|\alpha_1(\mathfrak{Z})\left(\frac{\mathfrak{Z}+2}{\mathfrak{Z}+1} - x\right) + \alpha_0(\mathfrak{Z})\right|\left(\left(\frac{\mathfrak{Z}+1}{2(\mathfrak{Z}+2)}\right)^{\mathfrak{Z}}\right.$$

$$\left.\times\sum_{r=0}^{\mathfrak{Z}} b_{\mathfrak{Z}-1,r-1}(x)\left|f\left(\frac{\mathfrak{Z}+2}{\mathfrak{Z}+1}\left(\frac{2r}{\mathfrak{Z}}-1\right)\right) - f(x)\right|\right)$$

$$\leq \left|\alpha_1(\mathfrak{Z})\left(x + \frac{\mathfrak{Z}+2}{\mathfrak{Z}+1}\right) + \alpha_0(\mathfrak{Z})\right|$$

$$\times\left(\left(\frac{\mathfrak{Z}+1}{2(\mathfrak{Z}+2)}\right)^{\mathfrak{Z}}\sum_{r=0}^{\mathfrak{Z}} b_{\mathfrak{Z}-1,r}(x)\,\omega\left(\left|\frac{\mathfrak{Z}+2}{\mathfrak{Z}+1}\left(\frac{2r}{\mathfrak{Z}}-1\right) - x\right|\right)\right)$$

$$+\left|\alpha_1(\mathfrak{Z})\left(\frac{\mathfrak{Z}+2}{\mathfrak{Z}+1} - x\right) + \alpha_0(\mathfrak{Z})\right|$$

$$\times\left(\left(\frac{\mathfrak{Z}+1}{2(\mathfrak{Z}+2)}\right)^{\mathfrak{Z}}\sum_{r=0}^{\mathfrak{Z}} b_{\mathfrak{Z}-1,r-1}(x)\,\omega\left(\left|\frac{\mathfrak{Z}+2}{\mathfrak{Z}+1}\left(\frac{2r}{\mathfrak{Z}}-1\right) - x\right|\right)\right).$$

Using

$$\omega\left(\left|\frac{\mathfrak{z}+2}{\mathfrak{z}+1}\left(\frac{2r}{\mathfrak{z}}-1\right)-x\right|\right)$$

$$=\omega\left(\sqrt{\mathfrak{z}}\left|\frac{\mathfrak{z}+2}{\mathfrak{z}+1}\left(\frac{2r}{\mathfrak{z}}-1\right)-x\right|\frac{1}{\sqrt{\mathfrak{z}}}\right)$$

$$\leq\left(1+\sqrt{\mathfrak{z}}\left|\frac{\mathfrak{z}+2}{\mathfrak{z}+1}\left(\frac{2r}{\mathfrak{z}}-1\right)-x\right|\right)\omega\left(\frac{1}{\sqrt{\mathfrak{z}}}\right)$$

property of the modulus of continuity,

$$\left|Z_{\mathfrak{z}}^{*}(f;x)-f(x)\right|\leq\left|\alpha_1(\mathfrak{z})\left(x+\frac{\mathfrak{z}+2}{\mathfrak{z}+1}\right)+\alpha_0(\mathfrak{z})\right|\omega\left(\frac{1}{\sqrt{\mathfrak{z}}}\right)$$

$$\times\left(1+\sqrt{\mathfrak{z}}\left(\frac{\mathfrak{z}+1}{2(\mathfrak{z}+2)}\right)^{\mathfrak{z}}\sum_{r=0}^{\mathfrak{z}}b_{\mathfrak{z}-1,r}(x)\left|\frac{\mathfrak{z}+2}{\mathfrak{z}+1}\left(\frac{2r}{\mathfrak{z}}-1\right)-x\right|\right)$$

$$+\left|\alpha_1(\mathfrak{z})\left(\frac{\mathfrak{z}+2}{\mathfrak{z}+1}-x\right)+\alpha_0(\mathfrak{z})\right|\omega\left(\frac{1}{\sqrt{\mathfrak{z}}}\right)(1$$

$$+\sqrt{\mathfrak{z}}\left(\frac{\mathfrak{z}+1}{2(\mathfrak{z}+2)}\right)^{\mathfrak{z}}\sum_{r=0}^{\mathfrak{z}}b_{\mathfrak{z}-1,r-1}(x)\left|\frac{\mathfrak{z}+2}{\mathfrak{z}+1}\left(\frac{2r}{\mathfrak{z}}-1\right)-x\right|\Bigg)$$

is written. With the help of Schwarz inequality and equations (2.8), (2.9) and (2.10)

$$\left(\frac{\mathfrak{z}+1}{2(\mathfrak{z}+2)}\right)^{\mathfrak{z}}\sum_{r=0}^{\mathfrak{z}}b_{\mathfrak{z}-1,r}(x)\left|\frac{\mathfrak{z}+2}{\mathfrak{z}+1}\left(\frac{2r}{\mathfrak{z}}-1\right)-x\right|$$

$$\leq\left(\left(\frac{\mathfrak{z}+1}{2(\mathfrak{z}+2)}\right)^{\mathfrak{z}}\sum_{r=0}^{\mathfrak{z}}b_{\mathfrak{z}-1,r}(x)\left(\frac{\mathfrak{z}+2}{\mathfrak{z}+1}\left(\frac{2r}{\mathfrak{z}}-1\right)-x\right)^{2}\right)^{\frac{1}{2}}$$

$$\times\left(\left(\frac{\mathfrak{z}+1}{2(\mathfrak{z}+2)}\right)^{\mathfrak{z}}\sum_{r=0}^{\mathfrak{z}}b_{\mathfrak{z}-1,r}(x)\right)^{\frac{1}{2}}$$

$$= \left(x^2 \frac{1}{2}\left(\frac{\overline{3}+1}{\overline{3}+2}\right) - 2x\frac{1}{2}\left(\frac{\overline{3}+1}{\overline{3}+2}\right)\left(\left(1-\frac{1}{\overline{3}}\right)x - \frac{1}{\overline{3}}\left(\frac{\overline{3}+2}{\overline{3}+1}\right)\right)\right.$$

$$\left. + \frac{1}{2}\left(\frac{\overline{3}+1}{\overline{3}+2}\right)\left(\frac{\overline{3}^2-3\overline{3}+2}{\overline{3}^2}x^2 + \frac{2-2\overline{3}}{\overline{3}^2}\left(\frac{\overline{3}+2}{\overline{3}+1}\right)x\right.\right.$$

$$\left.\left. + \frac{1}{\overline{3}}\left(\frac{\overline{3}+2}{\overline{3}+1}\right)^2\right)\right)^{\frac{1}{2}} \left(\frac{1}{2}\left(\frac{\overline{3}+1}{\overline{3}+2}\right)\right)^{\frac{1}{2}}$$

$$= \left(\frac{1}{2}\left(\frac{\overline{3}+1}{\overline{3}+2}\right)\right)^{\frac{1}{2}} \left(x^2 - 2x\left(\left(1-\frac{1}{\overline{3}}\right)x - \frac{1}{\overline{3}}\left(\frac{\overline{3}+2}{\overline{3}+1}\right)\right)\right.$$

$$\left. + \left(\frac{\overline{3}^2-3\overline{3}+2}{\overline{3}^2}x^2 + \frac{2-2\overline{3}}{\overline{3}^2}\left(\frac{\overline{3}+2}{\overline{3}+1}\right)x + \frac{1}{\overline{3}}\left(\frac{\overline{3}+2}{\overline{3}+1}\right)^2\right)\right)^{\frac{1}{2}}$$

$$\times \left(\frac{1}{2}\left(\frac{\overline{3}+1}{\overline{3}+2}\right)\right)^{\frac{1}{2}}$$

$$= \left(\frac{2-\overline{3}}{\overline{3}^2}x^2 + \frac{2}{\overline{3}^2}\left(\frac{\overline{3}+2}{\overline{3}+1}\right)x + \frac{1}{\overline{3}}\left(\frac{\overline{3}+2}{\overline{3}+1}\right)^2\right)^{\frac{1}{2}} \left(\frac{1}{2}\left(\frac{\overline{3}+1}{\overline{3}+2}\right)\right) \qquad (2.18)$$

and

$$\left(\frac{\overline{3}+1}{2(\overline{3}+2)}\right)^{\overline{3}} \sum_{r=0}^{\overline{3}} b_{\overline{3}-1,r-1}(x) \left|\frac{\overline{3}+2}{\overline{3}+1}\left(\frac{2r}{\overline{3}}-1\right) - x\right|$$

$$= \left(x^2 \frac{1}{2}\left(\frac{\overline{3}+1}{\overline{3}+2}\right) - 2x\frac{1}{2}\left(\frac{\overline{3}+1}{\overline{3}+2}\right)\left(\left(1-\frac{1}{\overline{3}}\right)x + \frac{1}{\overline{3}}\left(\frac{\overline{3}+2}{\overline{3}+1}\right)\right)\right.$$

$$\left. + \frac{1}{2}\left(\frac{\overline{3}+1}{\overline{3}+2}\right)\left(\frac{\overline{3}^2-3\overline{3}+2}{\overline{3}^2}x^2 + \frac{2\overline{3}-2}{\overline{3}^2}\left(\frac{\overline{3}+2}{\overline{3}+1}\right)x\right.\right.$$

$$\left.\left. + \frac{1}{\overline{3}}\left(\frac{\overline{3}+2}{\overline{3}+1}\right)^2\right)\right)^{\frac{1}{2}} \left(\frac{1}{2}\left(\frac{\overline{3}+1}{\overline{3}+2}\right)\right)^{\frac{1}{2}}$$

$$= \left(\frac{4-3\zeta}{\zeta^2}x^2 - \frac{2}{\zeta^2}\left(\frac{\zeta+2}{\zeta+1}\right)x + \frac{1}{\zeta}\left(\frac{\zeta+2}{\zeta+1}\right)^2\right)^{\frac{1}{2}}\left(\frac{1}{2}\left(\frac{\zeta+1}{\zeta+2}\right)\right) \qquad (2.19)$$

is getting. From (2.18) and (2.19)

$$\max_{x\in\left[-\frac{\zeta+2}{\zeta+1},\frac{\zeta+2}{\zeta+1}\right],\zeta>2}\left(\frac{2-\zeta}{\zeta^2}x^2 + \frac{2}{\zeta^2}\left(\frac{\zeta+2}{\zeta+1}\right)x + \frac{1}{\zeta}\left(\frac{\zeta+2}{\zeta+1}\right)^2\right)^{\frac{1}{2}}$$

$$\times\left(\frac{1}{2}\left(\frac{\zeta+1}{\zeta+2}\right)\right) = \frac{\sqrt{(\zeta-3)(\zeta+1)}}{2\zeta\sqrt{(\zeta-2)}}$$

$$\max_{x\in\left[-\frac{\zeta+2}{\zeta+1},\frac{\zeta+2}{\zeta+1}\right],1\le\zeta\le3}\left(\frac{4-3\zeta}{\zeta^2}x^2 - \frac{2}{\zeta^2}\left(\frac{\zeta+2}{\zeta+1}\right)x\right.$$

$$\left.+\frac{1}{\zeta}\left(\frac{\zeta+2}{\zeta+1}\right)^2\right)^{\frac{1}{2}}\left(\frac{1}{2}\left(\frac{\zeta+1}{\zeta+2}\right)\right) = \frac{\sqrt{6-2\zeta}}{2\zeta}.$$

The following expressions are valid for maximum, limited and critical points.

i) For $x = -\frac{\zeta+2}{\zeta+1}$,

$$\left(\frac{2-\zeta}{\zeta^2}\left(\frac{\zeta+2}{\zeta+1}\right)^2 - \frac{2}{\zeta^2}\left(\frac{\zeta+2}{\zeta+1}\right)^2 + \frac{1}{\zeta}\left(\frac{\zeta+2}{\zeta+1}\right)^2\right)^{\frac{1}{2}}\left(\frac{1}{2}\left(\frac{\zeta+1}{\zeta+2}\right)\right)$$

$= 0.$

For $x = \frac{\zeta+2}{\zeta+1}$,

$$\left(\frac{2-\zeta}{\zeta^2}\left(\frac{\zeta+2}{\zeta+1}\right)^2 + \frac{2}{\zeta^2}\left(\frac{\zeta+2}{\zeta+1}\right)^2 + \frac{1}{\zeta}\left(\frac{\zeta+2}{\zeta+1}\right)^2\right)^{\frac{1}{2}}\left(\frac{1}{2}\left(\frac{\zeta+1}{\zeta+2}\right)\right)$$

$$= \frac{1}{\zeta}\left(\frac{\zeta+2}{\zeta+1}\right)\frac{1}{2}\left(\frac{\zeta+1}{\zeta+2}\right) = \frac{1}{2\zeta},$$

is written. Then for $x = \frac{\zeta+2}{(\zeta-2)(\zeta+1)}$,

$$\left(\frac{2-\zeta}{\zeta^2}\left(\frac{\zeta+2}{(\zeta-2)(\zeta+1)}\right)^2 - \frac{2}{\zeta^2}\left(\frac{\zeta+2}{\zeta+1}\right)\frac{\zeta+2}{(\zeta-2)(\zeta+1)}\right.$$

$$+\frac{1}{\mathfrak{Z}}\left(\frac{\mathfrak{Z}+2}{\mathfrak{Z}+1}\right)^2\Bigg)^{\frac{1}{2}}\left(\frac{1}{2}\left(\frac{\mathfrak{Z}+1}{\mathfrak{Z}+2}\right)\right)$$

$$=\left(\frac{\mathfrak{Z}(\mathfrak{Z}-2)-3}{\mathfrak{Z}^2(\mathfrak{Z}-2)}\left(\frac{\mathfrak{Z}+2}{\mathfrak{Z}+1}\right)^2\right)^{\frac{1}{2}}\left(\frac{1}{2}\left(\frac{\mathfrak{Z}+1}{\mathfrak{Z}+2}\right)\right)$$

$$=\frac{\sqrt{(\mathfrak{Z}-3)(\mathfrak{Z}+1)}}{2\mathfrak{Z}\sqrt{(\mathfrak{Z}-2)}}.$$

ii) For $x=-\frac{\mathfrak{Z}+2}{\mathfrak{Z}+1}$,

$$\left(\frac{4-3\mathfrak{Z}}{\mathfrak{Z}^2}\left(\frac{\mathfrak{Z}+2}{\mathfrak{Z}+1}\right)^2+\frac{2}{\mathfrak{Z}^2}\left(\frac{\mathfrak{Z}+2}{\mathfrak{Z}+1}\right)^2+\frac{1}{\mathfrak{Z}}\left(\frac{\mathfrak{Z}+2}{\mathfrak{Z}+1}\right)^2\right)^{\frac{1}{2}}\left(\frac{1}{2}\left(\frac{\mathfrak{Z}+1}{\mathfrak{Z}+2}\right)\right)$$

$$=\frac{\sqrt{6-2\mathfrak{Z}}}{\mathfrak{Z}}\left(\frac{\mathfrak{Z}+2}{\mathfrak{Z}+1}\right)\frac{1}{2}\left(\frac{\mathfrak{Z}+1}{\mathfrak{Z}+2}\right)=\frac{\sqrt{6-2\mathfrak{Z}}}{2\mathfrak{Z}}.$$

For $x=\frac{\mathfrak{Z}+2}{\mathfrak{Z}+1}$,

$$\left(\frac{4-3\mathfrak{Z}}{\mathfrak{Z}^2}\left(\frac{\mathfrak{Z}+2}{\mathfrak{Z}+1}\right)^2-\frac{2}{\mathfrak{Z}^2}\left(\frac{\mathfrak{Z}+2}{\mathfrak{Z}+1}\right)^2+\frac{1}{\mathfrak{Z}}\left(\frac{\mathfrak{Z}+2}{\mathfrak{Z}+1}\right)^2\right)^{\frac{1}{2}}\left(\frac{1}{2}\left(\frac{\mathfrak{Z}+1}{\mathfrak{Z}+2}\right)\right)$$

$$=\frac{\sqrt{2-2\mathfrak{Z}}}{\mathfrak{Z}}\left(\frac{\mathfrak{Z}+2}{\mathfrak{Z}+1}\right)\frac{1}{2}\left(\frac{\mathfrak{Z}+1}{\mathfrak{Z}+2}\right)=\frac{\sqrt{2-2\mathfrak{Z}}}{2\mathfrak{Z}}.$$

For $x=\frac{\mathfrak{Z}+2}{(4-3\mathfrak{Z})(\mathfrak{Z}+1)}$,

$$\left(\frac{4-3\mathfrak{Z}}{\mathfrak{Z}^2}\left(\frac{\mathfrak{Z}+2}{(4-3\mathfrak{Z})(\mathfrak{Z}+1)}\right)^2\right.$$

$$\left.-\frac{2}{\mathfrak{Z}^2}\left(\frac{\mathfrak{Z}+2}{\mathfrak{Z}+1}\right)\frac{\mathfrak{Z}+2}{(4-3\mathfrak{Z})(\mathfrak{Z}+1)}+\frac{1}{\mathfrak{Z}}\left(\frac{\mathfrak{Z}+2}{\mathfrak{Z}+1}\right)^2\right)^{\frac{1}{2}}\left(\frac{1}{2}\left(\frac{\mathfrak{Z}+1}{\mathfrak{Z}+2}\right)\right)$$

$$=\left(\frac{\mathfrak{Z}(4-3\mathfrak{Z})-1}{\mathfrak{Z}^2(4-3\mathfrak{Z})}\left(\frac{\mathfrak{Z}+2}{\mathfrak{Z}+1}\right)^2\right)^{\frac{1}{2}}\left(\frac{1}{2}\left(\frac{\mathfrak{Z}+1}{\mathfrak{Z}+2}\right)\right)$$

$$= \frac{\sqrt{(1-3\mathfrak{Z})(\mathfrak{Z}-1)}}{2\mathfrak{Z}\sqrt{(4-3\mathfrak{Z})}}$$

is obtained. Then,

$$\left(\frac{\mathfrak{Z}+1}{2(\mathfrak{Z}+2)}\right)^{\mathfrak{Z}} \sum_{r=0}^{\mathfrak{Z}} b_{\mathfrak{Z}-1,r}(x) \left|\frac{\mathfrak{Z}+2}{\mathfrak{Z}+1}\left(\frac{2r}{\mathfrak{Z}}-1\right)-x\right|$$

$$\leq \frac{1}{2\sqrt{\mathfrak{Z}}} \frac{\sqrt{(\mathfrak{Z}-3)(\mathfrak{Z}+1)}}{\sqrt{\mathfrak{Z}(\mathfrak{Z}-2)}}$$

$$\left(\frac{\mathfrak{Z}+1}{2(\mathfrak{Z}+2)}\right)^{\mathfrak{Z}} \sum_{r=0}^{\mathfrak{Z}} b_{\mathfrak{Z}-1,r-1}(x) \left|\frac{\mathfrak{Z}+2}{\mathfrak{Z}+1}\left(\frac{2r}{\mathfrak{Z}}-1\right)-x\right|$$

$$\leq \frac{1}{2\sqrt{\mathfrak{Z}}} \frac{\sqrt{2(3-\mathfrak{Z})}}{\sqrt{\mathfrak{Z}}}$$

is getting. On the other hand, using

$$\frac{1}{2\sqrt{\mathfrak{Z}}} \frac{\sqrt{(\mathfrak{Z}-3)(\mathfrak{Z}+1)}}{\sqrt{\mathfrak{Z}(\mathfrak{Z}-2)}} \leq \frac{1}{2\sqrt{\mathfrak{Z}}} \frac{\sqrt{2(3-\mathfrak{Z})}}{\sqrt{\mathfrak{Z}}}$$

and $\alpha_1(\mathfrak{Z}) + \alpha_0(\mathfrak{Z})\left(\frac{\mathfrak{Z}+1}{\mathfrak{Z}+2}\right) = 1$ For *m* sufficiently large

$$\left|Z_{\mathfrak{Z}}^{*}(f;x) - f(x)\right|$$

$$\leq 3\left(\left|\alpha_1(\mathfrak{Z})\left(x+\frac{\mathfrak{Z}+2}{\mathfrak{Z}+1}\right)+\left(1-\alpha_1(\mathfrak{Z})\right)\left(\frac{\mathfrak{Z}+2}{\mathfrak{Z}+1}\right)\right|\right.$$

$$\left.+\left|\alpha_1(\mathfrak{Z})\left(\frac{\mathfrak{Z}+2}{\mathfrak{Z}+1}-x\right)+\left(1-\alpha_1(\mathfrak{Z})\right)\left(\frac{\mathfrak{Z}+2}{\mathfrak{Z}+1}\right)\right|\right)\omega\left(\frac{1}{\sqrt{\mathfrak{Z}}}\right)$$

$$\leq 6\left(\frac{\mathfrak{Z}+2}{\mathfrak{Z}+1}\right)\omega\left(\frac{1}{\sqrt{\mathfrak{Z}}}\right)$$

is obtained. Thus the proof is completed.

Conclusion

It is thought that by using this type of generalizations, in which the basic functions of operators, which are among the popular topics of recent years, are expressed as additive, new studies can be revealed with the help of q-analysis, (p,q)-analysis in the field of approximation theory, and moreover, it can be carried to different paths with the help of parametric generalization and function preservation properties that exist in the literature. It is a useful study since it contains detailed solutions for researchers who will work in this field. It is foreseen that it is possible to establish a two-dimensional generalization considering that interdisciplinary studies can be done.

REFERENCES

Acu, A. M., Cetin, N., & Tachev, G. (2024). Approxımatıon By Perturbed Baskakov–Type Operators. Journal Of Mathematical Inequalities, 18(2).

Acu, A. M., & Agrawal, P. N. (2018). Better Approximation Of Functions By Genuine Bernstein-Durrmeyer Type Operators. Arxiv Preprint Arxiv:1810.06822.

Baytunç, E., Gezer, H., & Aktuğlu, H. (2024). Kantorovich Variant of the Blending Type Bernstein Operators. Bulletin of the Iranian Mathematical Society, 50(6), 82.

Bernstein Operators: Theory And Applications. Numerical Algorithms, 77, 111-150.

Bilgen, Z. (2023). Simetrik Aralık Üzerinde Bernstein Polinomlarının Bir Modifikasyonu (Doctoral Dissertation,Harran Üniversitesi, Şanlıurfa).

Davis, P. J. (1975). Interpolation and approximation. Courier Corporation.

Gupta, V., Tachev, G., & Acu, A. M. (2019). Modified Kantorovich Operators With Better Approximation Properties. Numerical Algorithms, 81, 125-149.

Jabbar, A. F., & Hassan, A. K. (2024). Better Approximation Properties By New Modified Baskakov Operators. Journal Of Applied Mathematics, 2024(1), 8693699.

Kaur, J., & Goyal, M. (2024). Improved Convergence And Approximation Properties Of Baskakov-Durrmeyer Operators. Arxiv Preprint Arxiv:2411.06250.

Khosravian-Arab, H., Dehghan, M., & Eslahchi, M. R. (2018). A New Approach to Improve the Order of Approximation of the

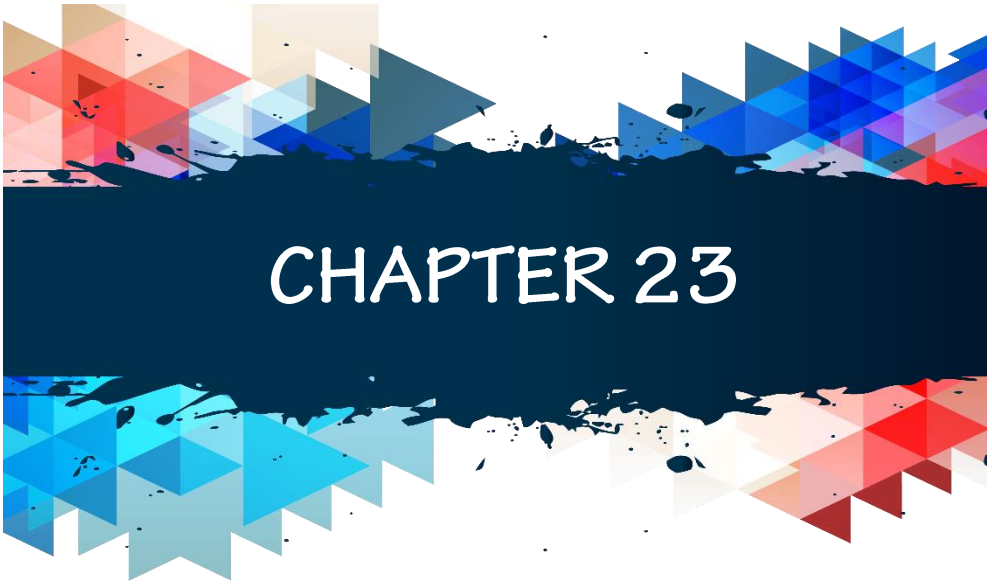

Regular Lucas Matrix and Fractional Difference Sequence Spaces

Ayşe Metin Karakaş [1] ***& Murat Karakaş*** [2]

1 Assoc. Prof. Dr., Bitlis Eren Üniversitesi, ORCID: 0000-0003-3552-0105
[2] Prof. Dr., Bitlis Eren Üniversitesi, ORCID: 0000-0002-5174-0282

1. INTRODUCTION

The gamma function which is denoted by $\Gamma(s)$ for all real numbers $s \notin \{0, -1, -2, \ldots\}$ can be stated the following integral

$$\Gamma(s) = \int_0^\infty e^{-x} x^{s-1} dx \qquad (1)$$

Throughout the paper, we make use of some well-known properties of Gamma function by using the above equality as follows:

i. $\Gamma(s+1) = s!$ for $s \in \mathbb{N}$,

ii. $\Gamma(s+1) = s\Gamma(s)$ for any real number $s \notin \{0, -1, -2, \ldots\}$,

iii. $\Gamma(1) = \Gamma(2) = 1, \Gamma(3) = 2!, \Gamma(4) = 3!, \ldots$

The linear space of all real sequences is denoted by ω. Any vector subspace of ω is named sequence space. We use the notations ℓ_∞, c, c_0 for the spaces of all bounded, null and convergent sequences, respectively. Also, the norm on the spaces ℓ_∞, c, c_0 is defined by $\|x\|_\infty = \sup_i |x_i|$. For the space of absolutely p—summable series, we use the notation $\ell_p, 1 \leq p < \infty$. By $e^{(i)}$, we mean the sequences whose only non-zero term is 1 in the i^{th} place for $i \in \mathbb{N}$ and write $e = \{1,1,1,\ldots\}$.

A sequence space μ with a linear topology is named a K—space provided each of the maps $\tau_i : \mu \to \mathbb{C}, \tau_i(x) = x_i$ is continuous for all $i \in \mathbb{N}$. If a K—space μ is a complete linear metric space, then we say that μ is an FK—space. An FK—space whose topology is normable is named a BK—space. According to this definition, the sequence space ℓ_p is a BK—space with the following norm:

$$\|x\| = \left(\sum_i |x_i|^p \right)^{1/p}.$$

In some instances, we use an infinite matrix to state the most general linear operator between two sequence spaces. Assume that $B=(b_{nk})$ is an infinite matrix of real or complex numbers b_{nk}, where $n,k\in\mathbb{N}$ and $x=(x_k)\in\omega$. Then, we transform the sequence x into the sequence $Bx=\{(Bx)_n\}$ with

$$(Bx)_n=\sum_k b_{nk}x_k \qquad (2)$$

if the above series converge for each $n\in\mathbb{N}$. Suppose that λ and μ be two sequence spaces. Then, it is said that B defines a matrix mapping from λ into μ if for every $x\in\lambda$, $Bx\in\mu$. We symbolize it by $B:\lambda\to\mu$. $(\lambda:\mu)$ represents the class of all matrices B such that $B:\lambda\to\mu$. Also, the domain of an infinite matrix B is a sequence space which is defined by

$$\lambda_B=\{x\in\omega:Bx\in\lambda\}. \qquad (3)$$

The following famous theorem which is named Silverman-Toeplitz characterises the class (c,c,P) and gives the necessary and sufficient conditions for the regularity of an infinite matrix. The matrices in the class (c,c,P) are called Toeplitz matrices or regular matrices.

Theorem 1.1 $B\in(c,c,P)$ if and only if the following conditions hold:

i. $\sup_n \sum_k |b_{nk}| < \infty$,

ii. $\lim_{n\to\infty} b_{nk}=0$,

iii. $\lim_{n\to\infty}\sum_k a_{nk}=1$, Choudary and Nanda (1989).

Kızmaz (1981) defined the difference sequence spaces $\ell_\infty(\Delta), c(\Delta), c_0(\Delta)$ where $\Delta x=(x_k-x_{k+1})$. Then, Et (1993) defined the sequence spaces $\ell_\infty(\Delta^2), c(\Delta^2), c_0(\Delta^2)$. Later, Et and Çolak (1995) generalized these spaces and introduced the difference sequence spaces $\ell_\infty(\Delta^m), c(\Delta^m), c_0(\Delta^m)$ for $m\in\mathbb{N}$. After then many authors studied a variety of sequence spaces of integer order using the difference operator Δ such as Tripathy and Esi (2006), Bektaş et al. (2004), Mursaleen and Noman (2010), Başarır and Kara (2011), Et and Işık (2012).

In some number sequences, there is a recurrence relation. One of the most studied and researched number sequence with recurrence relation is Lucas sequence. There is a very close relationship between the Lucas numbers and the golden ratio. So, new theorems and properties about the Lucas numbers help us to obtain various results.

In 1876, the French mathematician Francois Edouard Anatole Lucas discovered the Lucas number sequences. In this sequence, first term is 2 and the second term is 1. Each subsequent term equals to the sum of the previous two terms, that is, $L_0=2, L_1=1$ and $L_j=L_{j-1}+L_{j-2}, j\geq 2$. Hence, the first few terms of Lucas sequence are 2,1,3,4,7,11,18,29,47,76,123,… The ratio between two consecutive terms of the Lucas number sequence also tends to the golden ratio. Some of the main properties of Lucas numbers are as follows:

i. $\lim_{j\to\infty}\frac{L_{j+1}}{L_j}\simeq 1,618=\phi(\text{golden ratio}),$

ii. $\sum_{i=1}^{j}L_i=L_{j+2}-3, j\geq 1,$

iii. $\sum_{i=1}^{j}L_i^2=L_jL_{j+1}-2, j\geq 1.$

There are a lot of identities about the Lucas numbers and it can be found in Koshy (2001) and Vajda (1989). In recent years, so many authors have used the approach for creating a sequence space by using matrix domain of a particular limitation method, e.g. Candan (2015), Debnath et al. (2015), Ercan and Bektaş (2017), Kara (2013), Karakaş et al. (2019), Karakaş and Karakaş (2017,2018), Mohiuddine et al. (2021), Demiriz and Ellidokuzoglu (2018).

The concept of difference operator was generalized by Baliarsingh (2013) and introduced the fractional difference operator Δ^{α} such that $\left(\Delta^{\alpha}x\right)_i=\sum_{j=0}^{\infty}(-1)^j\frac{\Gamma(\alpha+1)}{j!\Gamma(\alpha-j+1)}x_{i+j}, i\in\mathbb{N}$. After then, Baliarsingh and Dutta (2015) identified the following difference operators for real α and $x\in\omega$:

$$\left(\Delta^{(\alpha)}x\right)_i=\sum_{j=0}^{\infty}(-1)^j\frac{\Gamma(\alpha+1)}{j!\Gamma(\alpha-j+1)}x_{i-j}, \tag{4}$$

$$\left(\Delta^{(-\alpha)}x\right)_i=\sum_{j=0}^{\infty}(-1)^j\frac{\Gamma(1-\alpha)}{j!\Gamma(1-\alpha-j)}x_{i-j}. \tag{5}$$

It is supposed that the summation given in (4) and (5) is convergent and also the above difference operators can be represented by triangular matrices. However, in the special case $\alpha=1$ for the operator $\Delta^{(\alpha)}$, it is obtained that the operator $\left(\Delta^{(1)}x\right)_j=x_j-x_{j-1}$ given by Malkowsky and Parashar (1997). The operator $\Delta^{(\alpha)}$ is represented the following matrix:

$$\left(\Delta^{(\alpha)}x\right)_{ij}=\begin{cases}(-1)^{i-j}\dfrac{\Gamma(\alpha+1)}{(i-j)!\Gamma(\alpha-i+j+1)}, & 0\le j\le i\\ 0, & j>i\end{cases} \tag{6}$$

It can be equivalently written for the above matrix

$$\begin{bmatrix} 1 & 0 & 0 & 0 & \dots \\ -\alpha & 1 & 0 & 0 & \dots \\ \frac{\alpha(\alpha-1)}{2!} & -\alpha & 1 & 0 & \dots \\ -\frac{\alpha(\alpha-1)(\alpha-2)}{3!} & \frac{\alpha(\alpha-1)}{2!} & -\alpha & 1 & \dots \\ \vdots & \vdots & \vdots & \vdots & \ddots \end{bmatrix}$$

Some studies related to fractional difference operator can be found in Kadak (2017), Baliarsingh and Nayak (2018), Kadak and Baliarsingh (2015), Yaying et al. (2021) and Nayak et al. (2019).

Now, let us call to mind that the well-recognized concept of Schauder basis. Let λ be a normed sequence space. If λ involves a sequence (a_j) which has the property that there is a unique sequence of scalars (γ_j) for every $x \in \lambda$ such that $\lim_{j\to\infty} \| x - (\gamma_0 a_0 + \gamma_1 a_1 + ... + \gamma_j a_j) \| = 0$, then (a_j) is named Schauder basis (or shortly basis).

Our main purpose in this study is to combine the difference operator $\Delta^{(\alpha)}$ and the Lucas matrix. Then, we establish the new Lucas difference sequence space by using fractional Lucas difference operator. Besides, we investigate the topological and geometrical structure of our sequence space.

2. SOME TOPOLOGICAL PROPERTIES

In this part of the study, we first introduce the Lucas sequence space $\ell_p\left(H^{(\alpha)}\right), 1 \le p \le \infty$. To do this, we consider the following Lucas matrix defined by Karakas and Dönmez (2020) :

$$\hat{H}=\left(L_{ij}\right)=\begin{cases}\dfrac{L_j}{L_{i+2}-3}, & 1\le j\le i\\ 0, & j>i\end{cases}. \tag{7}$$

Now, we compound the Lucas matrix in (7) with the operator $\Delta^{(\alpha)}$ in (6) and establish the following fractional Lucas difference operator:

$$H^{(\alpha)}=\begin{cases}\displaystyle\sum_{n=j}^{i}(-1)^{n-j}\frac{\Gamma(\alpha+1)}{(n-j)!\Gamma(\alpha-n+j+1)}\frac{L_n}{L_{i+2}-3}, & 1\le j\le i\\ 0, & j>i\end{cases} \tag{8}$$

The inverses of the difference matrix $\Delta^{(\alpha)}$, Lucas matrix $\hat{H}$ and the fractional Lucas matrix $H^{(\alpha)}$ are as follows, respectively:

$$\left(\Delta^{(-\alpha)}x\right)_{ij}=\begin{cases}(-1)^{i-j}\dfrac{\Gamma(1-\alpha)}{(i-j)!\Gamma(1-\alpha-i+j)}, & 0\le j\le i\\ 0, & j>i\end{cases},$$

$$\hat{H}^{-1}=\begin{cases}\dfrac{L_{i+2}-3}{L_j}, & j=i\\ -\dfrac{L_{i+1}-3}{L_{j+1}}, & j=i-1\\ 0, & \text{other}\end{cases},$$

$$H^{(-\alpha)}=\begin{cases}\displaystyle\sum_{n=j}^{i+1}(-1)^{i-j}\frac{\Gamma(1-\alpha)}{(i-n)!\Gamma(1-\alpha-i+n)}\frac{L_{j+2}-3}{L_n}, & 1\le j<i\\ \dfrac{L_{j+2}-3}{L_j}, & j=i\\ 0, & j>i\end{cases}. \tag{9}$$

Now, we introduce the following fractional Lucas Banach sets

$$\ell_p\left(H^{(\alpha)}\right)=\left\{x\in\omega: H^{(\alpha)}x\in\ell_p\right\}, 1\le p<\infty,$$

and

$$\ell_\infty\left(H^{(\alpha)}\right)=\left\{x\in\omega: H^{(\alpha)}x\in\ell_\infty\right\}.$$

However, let us demonstrate the $H^{(\alpha)}$ –transform of the sequence $x=(x_i)$ with

$$y_i=\sum_{j=0}^{i}\sum_{n=j}^{i}(-1)^{n-j}\frac{\Gamma(\alpha+1)}{(n-j)!\Gamma(\alpha-n+j+1)}\frac{L_n}{L_{i+2}-3}x_j. \qquad (10)$$

In the below theorems, we present some topological properties of the sequence spaces $\ell_p\left(H^{(\alpha)}\right)$ and $\ell_\infty\left(H^{(\alpha)}\right)$.

Theorem 2.1 The Lucas sequence spaces $\ell_p\left(H^{(\alpha)}\right)$ and $\ell_\infty\left(H^{(\alpha)}\right)$ are BK-spaces normed by

$$\|x\|_{\ell_p\left(H^{(\alpha)}\right)}=\left\|H^{(\alpha)}x\right\|_{\ell_p}=\left(\sum_j\left|H_j^{(\alpha)}x\right|^p\right)^{1/p}, \qquad (11)$$

and

$$\|x\|_{\ell_\infty\left(H^{(\alpha)}\right)}=\left\|H^{(\alpha)}x\right\|_{\ell_\infty}=\sup_j\left|H_j^{(\alpha)}x\right|. \qquad (12)$$

Proof Using the matrix domain of $H^{(\alpha)}$, our spaces can be reidentified as follows:

$$\ell_p\left(H^{(\alpha)}\right)=\left(\ell_p\right)_{H^{(\alpha)}} \text{ and } \ell_\infty\left(H^{(\alpha)}\right)=\left(\ell_\infty\right)_{H^{(\alpha)}}. \qquad (13)$$

The matrix $H^{(\alpha)}$ is triangle and also the sequence spaces ℓ_p and ℓ_∞ are BK-spaces by means of their usual norms. So, we obtain the requested result from Theorem 4.3.12 of Wilansky (1984).

Theorem 2.2 $\ell_p\left(H^{(\alpha)}\right)\cong\ell_p$ and $\ell_\infty\left(H^{(\alpha)}\right)\cong\ell_\infty$ where $1\leq p\leq\infty$.

Proof As a beginning, let us define the mapping $Z:\ell_p\left(H^{(\alpha)}\right)\to\ell_p, y=Zx=H^{(\alpha)}x$ by use of the sequence in (10). The mapping Z is linear and $Zx=0\Rightarrow x=0$. So, Z is obviously injective. Now, consider the sequences $y=\left(y_j\right)\in\ell_p$ for $1\leq p\leq\infty$ and

$$x_j=\sum_{k=0}^{j-1}\sum_{n=k}^{j-1}(-1)^{j-k}\frac{\Gamma(1-\alpha)}{(j-n)!\Gamma(1-\alpha-j+n)}\frac{L_{k+2}-3}{L_n}y_k+\frac{L_{j+2}-3}{L_j} \tag{14}$$

Hence, we obtain for $p=\infty$,

$$\|x\|_{\ell_\infty\left(H^{(\alpha)}\right)}=\sup_j\left|H_j^{(\alpha)}(x)\right|=\sup_j|y_j|=\|y\|_{\ell_\infty}<\infty,$$

and for $1\leq p<\infty$,

$$\|x\|_{\ell_p\left(H^{(\alpha)}\right)}=\left(\sum_j\left|H_j^{(\alpha)}(x)\right|^p\right)^{1/p}$$

$$=\left(\sum_j\left|\sum_{k=0}^{j}\sum_{n=k}^{j}(-1)^{n-k}\frac{\Gamma(\alpha+1)}{(n-k)!\Gamma(\alpha-n+k+1)}\frac{L_n}{L_{j+2}-3}x_k\right|^p\right)^{1/p}$$

$$=\left(\sum_j\left|\delta_{jk}y_k\right|^p\right)^{1/p}=\left(\sum_j|y_j|^p\right)^{1/p}=\|y\|_{\ell_p}<\infty.$$

The last two equalities indicate that $x \in \ell_p\left(H^{(\alpha)}\right), 1 \leq p \leq \infty$. Therefore, the mapping Z is norm preserving and surjective. As a consequence, the sequence space $\ell_p\left(H^{(\alpha)}\right)$ is linearly isomorphic to the space ℓ_p for $1 \leq p \leq \infty$.

From Theorem 2.2, we say that the inverse image of the basis for the space ℓ_p provides a basis for the sequence space $\ell_p\left(H^{(\alpha)}\right)$. To see this, we'll give the following theorem:

Theorem 2.3 The following sequence $\left\{h^{(j)}\right\}_{j \in \mathbb{N}}$ is a Schauder basis for the Lucas sequence space $\ell_p\left(H^{(\alpha)}\right)$ and any $x = (x_j) \in \ell_p\left(H^{(\alpha)}\right)$ has a unique representation of the form $x = \sum_j \gamma_j h^{(j)}$.

$$h_i^{(j)} = \begin{cases} \sum_{n=j}^{i+1} (-1)^{i-j} \dfrac{\Gamma(1-\alpha)}{(i-n)!\,\Gamma(1-\alpha-i+n)} \dfrac{L_{j+2}-3}{L_n}, & 1 < j < i \\ \dfrac{L_{j+2}-3}{L_j}, & j = i \\ 0, & 1 \leq k < n-1 \text{ or } k > n \end{cases} \quad (15)$$

Theorem 2.1 and Theorem 2.3 give us the following result:

Corollary 2.4 The fractional Lucas sequence space $\ell_p\left(H^{(\alpha)}\right)$ is a seperable space for $1 \leq p < \infty$.

3. KOTHE-TOEPLITZ DUALS

In this section of the paper, we determine the $\alpha-, \beta-, \gamma-$duals of the space $\ell_p\left(H^{(\alpha)}\right)$. We'll only consider the case $1 < p \leq \infty$since for $p = 1$ the proof can

be obtained by similar way. Let us first give the following well-known lemmas which are essential for our consideration by Stieglitz and Tietz (1977). Throughout this section, we will use the symbol $\mathcal{K}$ for the collection of all finite subsets of $\mathbb{N}$.

Lemma 3.1 $H\in(\ell_p:\ell_1)$ if and only if

$$\sup_{G\in\mathcal{K}}\sum_j\left|\sum_{i\in G}h_{ij}\right|^q<\infty. \tag{16}$$

Lemma 3.2 $H\in(\ell_p:c)$ if and only if

$$\lim_i h_{ij} \text{ exists for every } j\in\mathbb{N}, \tag{17}$$

$$\sup_i\sum_j|h_{ij}|^q<\infty. \tag{18}$$

Lemma 3.3 $H\in(\ell_\infty:c)$ if and only if (17) holds and

$$\lim_i\sum_j|h_{ij}|=\sum_j\left|\lim_i h_{ij}\right|. \tag{19}$$

Lemma 3.4 $H\in(\ell_p:\ell_\infty)$ if and only if (18) holds for $1<p\le\infty$.

Theorem3.5 The $\alpha-$dual of the space $\ell_p\left(H^{(\alpha)}\right)$ is $\delta_1^q=\left\{h=(h_j)\in\omega:\sup_{G\in\mathcal{K}}\sum_j\left|\sum_{i\in G}t_{ij}\right|^q<\infty\right\}$ for $1<p\le\infty$.

Proof Let $1<p\le\infty$ and define the matrix $T=(t_{ij})$ for all $i,j\in\mathbb{N}$ and $h=(h_j)\in\omega$ by

$$t_{ij}=\begin{cases}\sum_{n=j}^{i+1}(-1)^{i-j}\dfrac{\Gamma(1-\alpha)}{(i-n)!\Gamma(1-\alpha-i+n)}\dfrac{L_{j+2}-3}{L_n}h_j, & 1\le j<i\\ \dfrac{L_{i+2}-3}{L_i}h_i, & j=i\\ 0, & j>i\end{cases}.$$

Then, we have from (10) and (14)

$$h_ix_i=\sum_{n=0}^{i+1}\sum_{k=n}^{i+1}(-1)^{i-n}\frac{\Gamma(1-\alpha)}{(i-k)!\Gamma(1-\alpha-i+k)}\frac{L_{n+2}-3}{L_k}h_iy_n+\frac{L_{i+2}-3}{L_i}h_iy_i$$

$$=T_i(y) \qquad (20)$$

for each $i\in\mathbb{N}$. Thus, we have by (20) that $hx=(h_ix_i)\in\ell_1$ whenever $x\in\ell_p(H^{(\alpha)})$ if and only if $Ty\in\ell_1$ whenever $y\in\ell_p$. Finally, we derive from Lemma 3.1 that $\sup_{G\in\mathcal{K}}\sum_j\left|\sum_{i\in G}t_{ij}\right|^q<\infty$ which means that $\left\{\ell_p(H^{(\alpha)})\right\}^{\alpha}=\delta_1^q$.

Theorem 3.6 Define the following sets:

$$\delta_2^q=\left\{h=(h_j)\in\omega:\sum_j\left|\Delta^{(\alpha)}\left(\frac{h_j}{L_j}\right)(L_{j+2}-3)\right|^q<\infty\right\};$$

$$\delta_3=\left\{h=(h_j)\in\omega:\sup_j\left|\frac{L_{j+2}-3}{L_j}h_j\right|<\infty\right\};$$

$$\delta_4=\left\{h=(h_j)\in\omega:\lim_j\frac{L_{j+2}-3}{L_j}h_j=0\right\}$$

where

$$\Delta^{(\alpha)}\left(\frac{h_j}{L_j}\right)=\frac{h_j}{L_j}+\sum_{k=j+1}^{i}(-1)^{k-j}h_k\sum_{n=j}^{k-1}\frac{\Gamma(1-\alpha)}{(k-n)!\Gamma(1-\alpha-k+n)L_n}.$$

Then $\left\{\ell_p\left(H^{(\alpha)}\right)\right\}^{\beta}=\delta_2^1\cap\delta_3$ and $\left\{\ell_\infty\left(H^{(\alpha)}\right)\right\}^{\beta}=\delta_2^1\cap\delta_4$.

Proof Let $h=(h_j)\in\omega$ and take into account the following equality,

$$\begin{aligned}\sum_{j=0}^{i}h_jx_j&=\sum_{j=0}^{i}h_j\left[\sum_{n=0}^{j-1}\sum_{k=n}^{j-1}(-1)^{j-n}\frac{\Gamma(1-\alpha)}{(j-k)!\Gamma(1-\alpha-j+k)}\frac{L_{n+2}-3}{L_k}y_n+\frac{L_{j+2}-3}{L_j}y_j\right]\\&=\sum_{j=0}^{i-1}\left[\frac{h_j}{L_j}+\sum_{k=j+1}^{i}(-1)^{k-j}h_k\sum_{n=j}^{k-1}\frac{\Gamma(1-\alpha)}{(k-n)!\Gamma(1-\alpha-k+n)L_n}\right](L_{j+2}-3)y_j\\&\quad+\frac{L_{i+2}-3}{L_i}h_iy_i\\&=\sum_{j=0}^{i-1}\Delta^{(\alpha)}\left(\frac{h_j}{L_j}\right)(L_{j+2}-3)y_j+\frac{L_{i+2}-3}{L_i}h_iy_i \qquad (21)\\&=S_i(y), \text{ for each } i\in\mathbb{N} \qquad (22)\end{aligned}$$

where $S=(s_{ij})$ is defined by

$$s_{ij}=\begin{cases}\Delta^{(\alpha)}\left(\frac{h_j}{L_j}\right)(L_{j+2}-3), & j<i\\ \frac{L_{i+2}-3}{L_i}h_i, & j=i.\\ 0, & j>i\end{cases}$$

Hence, by using Lemma 3.2 with (22) that $hx=(h_jx_j)\in cs$ whenever $(x_j)\in\ell_p\left(H^{(\alpha)}\right)$ if and only if $Sy\in c$ whenever $y=(y_j)\in\ell_p$. So, this gives

that $h=(h_j)\in\left\{\ell_p\left(H^{(\alpha)}\right)\right\}^{\beta}$ if and only if $S\in(\ell_p,c),1\le p<\infty$. Hence, from (21), we see that

$$\sum_j\left|\Delta^{(\alpha)}\left(\frac{h_j}{L_j}\right)(L_{j+2}-3)\right|^q<\infty \text{ and } \sup_j\left|\frac{L_{j+2}-3}{L_j}h_j\right|<\infty.$$

Consequently, $\left\{\ell_p\left(H^{(\alpha)}\right)\right\}^{\beta}=\delta_2^q\cap\delta_3$ for $1<p<\infty$. In the case $p=\infty$, it can be similarly proved using Lemma 3.3.

Theorem 3.7 $\left\{\ell_p\left(H^{(\alpha)}\right)\right\}^{\gamma}=\delta_2^q\cap\delta_3$ for $1<p\le\infty$.

Proof If Lemma 3.4 is used in place of Lemma 3.2, the proof is similar to the previous theorem.

4. SOME MATRIX MAPPINGS

In this part of the paper, we characterize the classes $\left(\ell_p\left(H^{(\alpha)}\right),X\right)$ for $1\le p\le\infty$ and $X\in\{c_0,c,\ell_\infty,\ell_1\}$. For simplicity in notation, we write for all $i,j\in\mathbb{N}$

$$\Delta^{(\alpha)}\left(\frac{h_{ij}}{L_j}\right)=\left(\frac{h_{ij}}{L_j}+\sum_{k=j+1}^{i}(-1)^{k-j}h_{ik}\sum_{n=j}^{i+1}\frac{\Gamma(1-\alpha)}{(k-n)!\Gamma(1-\alpha-k+n)L_n}\right) \tag{23}$$

and

$$\Delta_\infty^{(\alpha)}\left(\frac{h_{ij}}{L_j}\right)=\left(\frac{h_{ij}}{L_j}+\sum_{k=j+1}^{\infty}(-1)^{k-j}h_{ik}\sum_{n=j}^{i+1}\frac{\Gamma(1-\alpha)}{(k-n)!\Gamma(1-\alpha-k+n)L_n}\right). \tag{24}$$

Besides, using equality (21), we have

$$\sum_{j=0}^{\infty} h_{ij} x_j = \sum_{j=0}^{u-1} \Delta^{(\alpha)}\left(\frac{h_{ij}}{L_j}\right)\left(L_{j+2}-3\right) y_j + \frac{L_{u+2}-3}{L_u} h_{iu} y_u. \qquad (25)$$

Now, we consider the conditions below:

$$\left(\frac{L_{j+2}-3}{L_j} h_{ij}\right)_{j=0}^{\infty} \in \ell_\infty \text{ for every } i \in \mathbb{N}, \qquad (26)$$

$$\lim_j \frac{L_{j+2}-3}{L_j} h_{ij} = 0 \text{ for all } i \in \mathbb{N}, \qquad (27)$$

$$\sup_i \sum_j \left|\Delta_\infty^{(\alpha)}\left(\frac{h_{ij}}{L_j}\right)\left(L_{j+2}-3\right)\right|^q < \infty, \qquad (28)$$

$$\sup_{i,j} \left|\Delta_\infty^{(\alpha)}\left(\frac{h_{ij}}{L_j}\right)\left(L_{j+2}-3\right)\right| < \infty, \qquad (29)$$

$$\sup_i \sum_j \left|\Delta_\infty^{(\alpha)}\left(\frac{h_{ij}}{L_j}\right)\left(L_{j+2}-3\right)\right| < \infty, \qquad (30)$$

$$\exists \mu_j \in \mathbb{R} \text{ such that } \lim_i \sum_j \left|\Delta_\infty^{(\alpha)}\left(\frac{h_{ij}}{L_j}\right)\left(L_{j+2}-3\right) - \mu_j\right| = 0 \ \forall j \in \mathbb{N}, \qquad (31)$$

$$\exists \mu_j \in \mathbb{R} \text{ such that } \lim_i \left|\Delta_\infty^{(\alpha)}\left(\frac{h_{ij}}{L_j}\right)\left(L_{j+2}-3\right) - \mu_j\right| = 0 \ \forall j \in \mathbb{N}, \qquad (32)$$

$$\lim_i \sum_j \left|\Delta_\infty^{(\alpha)}\left(\frac{h_{ij}}{L_j}\right)\left(L_{j+2}-3\right)\right| = 0, \qquad (33)$$

$$\lim_i \left|\Delta_\infty^{(\alpha)}\left(\frac{h_{ij}}{L_j}\right)\left(L_{j+2}-3\right)\right| = 0 \text{ for all } j \in \mathbb{N}. \qquad (34)$$

Hence, we instantly derive the following results from Stieglitz and Tietz (1977) and Theorem 3.6 with (25):

Theorem 4.1

(i) $\left(h_{ij}\right) \in \left(\ell_1\left(H^{(\alpha)}\right), c_0\right)$ if and only if (26), (29) and (34) hold.

(ii) $\left(h_{ij}\right) \in \left(\ell_1\left(H^{(\alpha)}\right), c\right)$ if and only if (26), (29) and (32) hold.

(iii) $\left(h_{ij}\right) \in \left(\ell_1\left(H^{(\alpha)}\right), \ell_\infty\right)$ if and only if (26) and (29) hold.

Theorem 4.2

(i) $\left(h_{ij}\right) \in \left(\ell_p\left(H^{(\alpha)}\right), c_0\right)$ if and only if (26), (28) and (34) hold.

(ii) $\left(h_{ij}\right) \in \left(\ell_p\left(H^{(\alpha)}\right), c\right)$ if and only if (26), (28) and (32) hold.

(iii) $\left(h_{ij}\right) \in \left(\ell_p\left(H^{(\alpha)}\right), \ell_\infty\right)$ if and only if (26) and (28) hold.

Theorem 4.3

(i) $\left(h_{ij}\right) \in \left(\ell_\infty\left(H^{(\alpha)}\right), c_0\right)$ if and only if (27), (33) hold.

(ii) $\left(h_{ij}\right) \in \left(\ell_\infty\left(H^{(\alpha)}\right), c\right)$ if and only if (27), (30), (31) and (32) hold.

(iii) $\left(h_{ij}\right) \in \left(\ell_\infty\left(H^{(\alpha)}\right), \ell_\infty\right)$ if and only if (27) and (30) hold.

5. SOME GEOMETRIC PROPERTIES

ℓ_p-type spaces have a lot of helpful applications by reason of the characteristics of the space ℓ_p. As the space ℓ_p is convex and reflexive, it can be naturally take into consideration the geometrical form of these spaces. Now, let us begin with some geometric properties of sequence spaces.

Let $B(Y)$ and $S(Y)$ be the unit ball and the unit sphere of the normed linear space Y. For $0\leq\varepsilon\leq 2$, Clarkson's modulus of convexity is introduced by Clarkson (1936) as follows:

$$\delta_Y(\varepsilon)=\inf\left\{1-\frac{\|u+v\|}{2}: u,v\in S(Y), \|u-v\|=\varepsilon\right\}.$$

Uniformly convex spaces are qualified in the case $\delta_Y(\varepsilon)>0$ for all $\varepsilon\in(0,2]$. After Clarkson, the Gurarii's modulus of convexity is established by Gurarii (1967) for $0\leq\varepsilon\leq 2$ as

$$\beta_Y(\varepsilon)=\inf\left\{1-\inf_{\gamma\in[0,1]}\|\gamma u+(1-\gamma)v\|: u,v\in S(Y), \|u-v\|=\varepsilon\right\}. \quad (35)$$

It can be easily seen that $\delta_Y(\varepsilon)\leq\beta_Y(\varepsilon)\leq 2\delta_Y(\varepsilon)$ for any $\varepsilon\in[0,2]$. However, it is said that Y is uniformly convex if $0<\beta_Y(\varepsilon)<1$ and also Y is strictly convex if $\beta_Y(\varepsilon)\leq 1$. After than Sanchez and Ullan (1998) showed that the inequality $\beta_{\ell_p}(\varepsilon)\leq 1-\left(1-\left(\frac{\varepsilon}{2}\right)^p\right)^{1/p}$ is hold.

Let Y be a Banach space. Then, we say that Y has the Banach-Saks property if every bounded sequence $(y_i)\in Y$ possess a subsequence (u_i) such that the sequence $\{t_j(u)\}$ is convergent in norm Diestel (2012), in case

$$t_j(u)=\frac{1}{j+1}(u_0+u_1+\ldots+u_j), j\in\mathbb{N}. \quad (36)$$

A Banach space Y is said to have the weak Banach-Saks property if for any weakly null sequence $(y_i)\subset Y$, there is a subsequence (u_i) in case the sequence $\{t_j(u)\}$ is strongly convergent to zero.

Let $1<p<\infty$. A Banach space holds the Banach-Saks property of type p whenever every weakly null sequence (y_i) possess a subsequence (y_{i_j}) in case

$$\left\| \sum_{j=0}^{k} y_{i_j} \right\| < C(k+1)^{1/p} \tag{37}$$

for some $C>0$ and all $k \in \mathbb{N}$, Knaust (1992).

Before giving our results in this part of the study, let us mention the following coefficient introduced by Garcia-Falset (1997):

$$R(Y)=\sup\left\{\liminf_{j\to\infty}\|y_j-y\| : (y_j)\subset B(Y), y_j \xrightarrow{w} 0, y\in B(Y)\right\}.$$

Remark 5.1 A Banach space Y which holds the inequality $R(Y)<2$ possess the weak fixed point property Garcia-Falset (1997).

Now, we can investigate the geometric properties of the space $\ell_p\left(H^{(\alpha)}\right)$ for $1<p<\infty$.

Theorem 5.2 The Lucas sequence space $\ell_p\left(H^{(\alpha)}\right)$ possess the property $(BS)_p$ for $1<p<\infty$.

Proof Let (y_j) be a weakly null sequence in $B\left(\ell_p\left(H^{(\alpha)}\right)\right)$ and (ζ_j) be a sequence of positive numbers so much so that $\sum \zeta_j \leq \frac{1}{2}$. Take $u_0=y_0=0$ and $u_1=y_{j_1}=y_1$. Therefore, there is $n_1 \in \mathbb{N}$ such that

$$\left\| \sum_{i=n_1+1}^{\infty} u_1(i)e^{(i)} \right\|_{\ell_p\left(H^{(\alpha)}\right)} < \zeta_1.$$

Since $y_j \xrightarrow{w} 0$ indicates $y_j \to 0$ coordinatewise, there is $j_2 \in \mathbb{N}$ such that for $j \geq j_2$,

$$\left\| \sum_{i=1}^{n_1} y_j(i) e^{(i)} \right\|_{\ell_p(H^{(\alpha)})} < \zeta_1.$$

Now, take $u_2 = y_{j_2}$. Then, there is $n_2 > n_1$ such that

$$\left\| \sum_{i=n_2+1}^{\infty} u_2(i) e^{(i)} \right\|_{\ell p\left(H^{(\alpha)}\right)} < \zeta_2.$$

Again taking account of the fact that $y_j \to 0$ coordinatewise, there is $j_3 \geq j_2$ such that for $j \geq j_3$,

$$\left\| \sum_{i=1}^{n_2} y_j(i) e^{(i)} \right\|_{\ell p\left(H^{(\alpha)}\right)} < \zeta_2.$$

If we continue this method, we obtain two increasing subsequences (n_k) and (j_k) such that for $j \geq j_{k+1}$,

$$\left\| \sum_{i=1}^{n_k} y_j(i) e^{(i)} \right\|_{\ell p\left(H^{(\alpha)}\right)} < \zeta_k,$$

and

$$\left\| \sum_{i=n_k+1}^{\infty} u_k(i) e^{(i)} \right\|_{\ell_p(H^{(\alpha)})} < \zeta_k,$$

where $u_k = y_{j_k}$. Herefrom,

$$\left\| \sum_{k=1}^{j} u_k \right\|_{\ell_p(H^{(\alpha)})}$$

$$= \left\| \sum_{k=1}^{j} \left(\sum_{i=1}^{n_{k-1}} u_k(i) e^{(i)} + \sum_{i=n_{k-1}+1}^{n_k} u_k(i) e^{(i)} + \sum_{i=n_k+1}^{\infty} u_k(i) e^{(i)} \right) \right\|_{\ell_p(H^{(\alpha)})}$$

$$\leq \left\| \sum_{k=1}^{j} \left(\sum_{i=n_{k-1}+1}^{n_k} u_k(i) e^{(i)} \right) \right\|_{\ell_p(H^{(\alpha)})} + 2 \sum_{k=1}^{j} \zeta_k .$$

In addition to this, it is clear that $\|y\|_{\ell_p(H^{(\alpha)})} < 1$. Accordingly, we get

$$\left\| \sum_{k=1}^{j} \left(\sum_{i=n_{k-1}+1}^{n_k} u_k(i) e^{(i)} \right) \right\|_{\ell_p(H^{(\alpha)})}^{p}$$

$$= \sum_{k=1}^{j} \sum_{i=n_{k-1}+1}^{n_k} \left| H_i^{(\alpha)}(u_k) \right|^p \leq \sum_{k=1}^{j} \sum_{i=1}^{\infty} \left| H_i^{(\alpha)}(u_k) \right|^p \leq j$$

Hence, we find

$$\left\| \sum_{k=1}^{j} u_k \right\|_{\ell_p(H^{(\alpha)})} \leq j^{1/p} + 1 \leq 2 j^{1/p},$$

since $\sum_{k=1}^{\infty}\zeta_k \leq \frac{1}{2}$. Consequently, $\ell_p\left(H^{(\alpha)}\right)$ has the Banach-Saks property of type p.

Remark 5.3 Since $\ell_p\left(H^{(\alpha)}\right)$ is linearly isomorphic to the ℓ_p, we have

$$R\left(\ell_p\left(H^{(\alpha)}\right)\right)=R\left(\ell_p\right)=2^{1/p}.$$

Then, it follows from the Remark 5.1 that the Lucas sequence space $\ell_p\left(H^{(\alpha)}\right)$ holds the weak fixed point property.

Theorem 5.4 Gurarii's modulus of convexity for the Lucas sequence space $\ell_p\left(H^{(\alpha)}\right)$ is

$$\beta_{\ell_p\left(H^{(\alpha)}\right)}(\varepsilon)\leq 1-\left(1-\left(\frac{\varepsilon}{2}\right)^p\right)^{1/p}, 0\leq\varepsilon\leq 2.$$

Proof Let $x\in\ell_p\left(H^{(\alpha)}\right)$. Then,

$$\|x\|_{\ell_p\left(H^{(\alpha)}\right)}=\left\|H^{(\alpha)}x\right\|_{\ell_p}=\left(\sum_j\left|H_j^{(\alpha)}x\right|^p\right)^{1/p}.$$

Let $0\leq\varepsilon\leq 2$ and take in consideration the following sequences:

$$r=(r_j)=\left(\left(H^{(-\alpha)}\left(1-\left(\frac{\varepsilon}{2}\right)^p\right)\right)^{1/p}, H^{(-\alpha)}\left(\frac{\varepsilon}{2}\right), 0,0,\ldots\right),$$

$$s=(s_j)=\left(\left(H^{(-\alpha)}\left(1-\left(\frac{\varepsilon}{2}\right)^p\right)\right)^{1/p}, H^{(-\alpha)}\left(-\frac{\varepsilon}{2}\right), 0,0,\ldots\right).$$

Afterwards, we have $\|r\|_{\ell p\left(H^{(\alpha)}\right)}=\left\|H^{(\alpha)}r\right\|_{\ell p}=1$, $\|s\|_{\ell_p(H^{(\alpha)})} = \|H^{(\alpha)}s\|_{\ell_p} = 1$, in a word, $r,s\in S\left(\ell p\left(H^{(\alpha)}\right)\right)$ and $\left\|H^{(\alpha)}r-H^{(\alpha)}s\right\|_{\ell p}=\|r-s\|_{\ell p\left(H^{(\alpha)}\right)}=\varepsilon$. Hence for $\gamma\in[0,1]$,

$$\|\gamma r+(1-\gamma)s\|^{p}_{\ell p\left(H^{(\alpha)}\right)}=\left\|\gamma H^{(\alpha)}r+(1-\gamma)H^{(\alpha)}s\right\|^{p}_{\ell p}=1-\left(\frac{\varepsilon}{2}\right)^{p}+|2\gamma-1|\left(\frac{\varepsilon}{2}\right)^{p}$$

.

and then, $\inf_{0\le\gamma\le1}\|\gamma r+(1-\gamma)s\|^{p}_{\ell p\left(H^{(\alpha)}\right)}=1-\left(\frac{\varepsilon}{2}\right)^{p}$. As a result, we obtain that

$$\beta_{\ell p\left(H^{(\alpha)}\right)}(\varepsilon)\le1-\left(1-\left(\frac{\varepsilon}{2}\right)^{p}\right)^{1/p}.$$

Corollary 5.5 $\ell p\left(H^{(\alpha)}\right)$ is strictly convex for $\varepsilon=2$.

Corollary 5.6 $\ell p\left(H^{(\alpha)}\right)$ is uniformly convex for $0<\varepsilon<2$.

Corollary 5.7 For $\gamma=\frac{1}{2}$, $\delta_{\ell p\left(H^{(\alpha)}\right)}(\varepsilon)=\beta_{\ell p\left(H^{(\alpha)}\right)}(\varepsilon)$.

6. CONCLUSION

There are so many studies related to the notions of fractional difference operator and Lucas numbers. But, the concept of fractional Lucas difference operator are not included in summability theory. In this work, we consider a fractional difference operator with the Lucas numbers and so introduce the new sequence spaces. Also, we investigate the topological and geometrical structure of these spaces. However, we give Köthe Toeplitz duals and some matrix mappings for the defined spaces. Finally, we examine the geometic structure of the space $\ell_p(H^{(\alpha)})$ for $1<p<\infty$.

REFERENCES

1. Baliarsingh, P. (2013), Some new difference sequence spaces of fractional order and their dual spaces, *Applied Mathematics and Computation*, 219(18), 9737-9742.
2. Baliarsingh, P., Dutta, S. (2015), A unifying approach to the difference operators and their applications, *Boletim da Sociedade Paranaense de Matematica*, 33(1), 49-57.
3. Baliarsingh, P., Nayak, L. (2018), A note on fractional difference operators, *Alexandria Engineering Journal*, 57(2), 1051-1054.
4. Başarır, M., Kara, EE. (2011), On some difference sequence spaces of weighted means and compact operators, *Annals of Functional Analysis*, 2(2), 114-129.
5. Bektaş, CA., Et, M., Colak, R. (2004), Generalized difference sequence spaces and their dual spaces, *Journal of Mathematical Analysis and Applications*, 292(2), 423-432.
6. Candan, M. (2015), A new approach on the spaces of generalized Fibonacci difference null and convergent sequences, *Mathematica Aeterna*. 5(1), 191-210.
7. Choudhary, B., Nanda, S. (1989), *Functional Analysis with Applications*, New Delhi: Wiley.
8. Clarkson, JA. (1936), Uniformly convex spaces, *Transactions of the American Mathematical Society*, 40(3), 396-414.
9. Debnath, S., Datta, AJ., Saha, S. (2015), Regular matrix of interval numbers based on Fibonacci numbers, *Afrika Matematika*, 26(7-8), 1379-1385.
10. Demiriz, S., Ellidokuzoğlu, HB. (2018), On some new paranormed Lucas sequence spaces and Lucas core, *Conference Proceedings of Science and Technology*. 1(1), 7-10.
11. Diestel, J. (2012), *Sequences and series in Banach spaces*, New York: Springer-Verlag.
12. Ercan, S., Bektaş, CA. (2017), Some topological and geometric properties of a new BK-space derived by using regular matrix of Fibonacci numbers, *Linear and Multilinear Algebra*, 65(5), 909-921.
13. Et, M. (1993), On some difference sequence spaces, *Turkish Journal of Mathematics*, 17, 18-24.
14. Et, M., Çolak, R. (1995), On some generalized difference sequence spaces, *Soochow Journal of Mathematics*, 21(4), 377-386.
15. Et, M., Işık, M. (2012), On pα-dual spaces of generalized difference sequence spaces, *Applied Mathematics Letters*, 25 (10), 1486-1489.

16. Garcia-Falset, J. (1997), The fixed point property in Banach spaces with the NUS-property, *Journal of Mathematical Analysis and Applications*, 215(2), 532-542.

17. Gurarii, VI. (1967), Differential properties of the convexity moduli of Banach spaces, *Matematicheskie Issledovaniya*, 2 (1), 141-148.

18. Kadak, U. (2017), Generalized weighted invariant mean based on fractional difference operator with applications to approximation theorems for functions of two variables, *Results in Mathematics*, 72(3), 1181-1202.

19. Kadak, U., Baliarsingh, P. (2015), On certain Euler difference sequence spaces of fractional order and related dual properties, *Journal of Nonlinear Science and Applications*, 8(6), 997-1004.

20. Kara, EE. (2013), Some topological and geometrical properties of new Banach sequence spaces, *Journal of Inequalities and Applications*, 38, 1-15.

21. Karakaş, M., Akbaş, T., Karakaş, A. (2019), On the Lucas difference sequence spaces defined by modulus function, *Applications and Applied Mathematics*, 14(1), 235-244.

22. Karakaş, M., Dönmez, H. (2020), Lucas type statistical convergence of order α, *BEU Journal of Science*, 9(4), 1537-1544.

23. Karakaş, M., Karakaş, A. (2017), New Banach sequence spaces that is defined by the aid of Lucas numbers, *Iğdır University Journal of the Institute of Science and Technology*, 7(4), 103-111.

24. Karakaş, M., Karakaş, A. (2018), A study on Lucas difference sequence spaces $\ell_p\left(\hat{E}(r,s)\right)$ and $\ell_\infty\left(\hat{E}(r,s)\right)$, *Maejo International Journal of Science and Technology*, 12(1), 70-78.

25. Kızmaz, H. (1981), On certain sequence spaces, *Canadian Mathematical Bulletin*, 24(2), 169-176.

26. Knaust, H. (1992), Orlicz sequence spaces of Banach-Saks type, *Archiv der Mathematik*, 59(6), 562-565.

27. Koshy, T. (2001), *Fibonacci and Lucas numbers with Applications*, Canada: John Wiley & Sons.

28. Malkowsky, E., Parashar, SD. (1997), Matrix transformations in spaces of bounded and convergent difference sequences of order m, *Analysis*, 17(1), 87-98.

29. Mohiuddine, S.A., Raj, K., Choudhary, A. (2022), Difference sequence spaces based on Lucas band matrix and modulus function, *São Paulo Journal of Mathematical Sciences*, 16, 1249-1260.

30. Mursaleen, M., Noman, AK. (2010), On some new difference sequence spaces of non-absolute type, *Mathematical and Computer Modelling*, 52(3-4), 603-617.

31. Nayak, L., Et, M., Baliarsingh, P. (2019), On certain generalized weighted mean fractional difference sequence spaces, *Proceedings of the National Academy of Sciences, India Section A: Physical Sciences*, 89(1), 163-170.

32. Sánchez, L., Ullán, A. (1998), Some properties of Gurarii's modulus of convexity, *Archiv der Mathematik*, 71(5), 399-406.

33. Stieglitz, M., Tietz, H. (1977), Matrixtransformationen von Folgenraumen eine Ergebnisübersicht, *Mathematische Zeitschrift*, 154, 1-16.

34. Tripathy, BC., Esi, A. (2006), A new type of difference sequence spaces, *International Journal of Science and Technology*, 1 (1), 11-14.

35. Vajda, S. (1989), *Fibonacci and Lucas numbers, and the Golden Section: Theory and Applications*, Mineola: Dover publications.

36. Yaying, T., Hazarika, B., Mohiuddine, SA. (2021), On difference sequence spaces of fractional-order involving Padovan numbers, *Asian-European Journal of Mathematics*, 14 (6), 2150095.

37. Wilansky, A. (1984), *Summability through functional analysis*, Amsterdam: Elsevier.

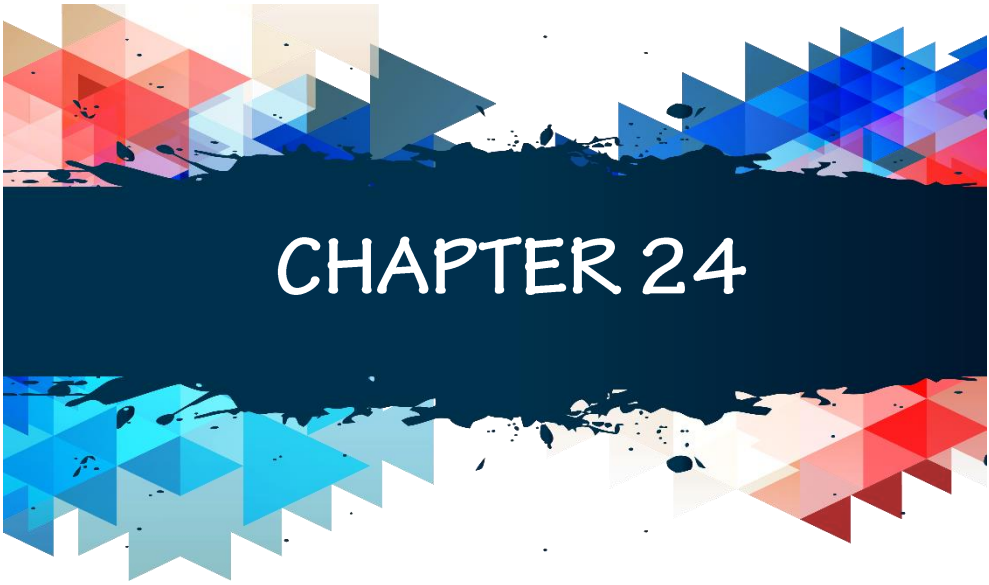

Integrating Microemulsions and Plant Extracts for Innovative Drug Delivery: Enhancing Therapeutic Solutions

Seval Cing Yıldırım [1] ***& Aslıhan Şeyma Dinçer Deniz*** [2]

1 Assoc. Prof. Dr.; Inonu University, Faculty of Arts and Sciences, Department of Biology, Department of Biotechnology, ORCID No: 0000-0001-7163-9512

[2] Graduate Student; Inonu University, Faculty of Arts and Sciences, Department of Biology, Department of Biotechnology, ORCID No: 0000-0002-6082-0567

INTRODUCTION

Due to the limitations of synthetic drugs against emerging diseases and their associated side effects, interest in natural products has grown (Çiftçi and Odabaş, 2020;85). Advances in science and technology have enabled the isolation of therapeutic active substances from plants in their purest form. Natural resources rich in phytochemicals, traditionally used for treating chronic and infectious diseases, are considered safe and effective alternatives to synthetic agents due to fewer side effects, thus allowing the use of plants for therapeutic purposes (Şanda, 2019;1). Plants and their bioactive compounds offer a potential source of medicine, meeting the need for safe and effective treatments. Traditional knowledge, accumulated over years of observation and environmental interaction, has played a key role in modern medicine's evolution (Abraham et al., 2020;43). The growing resistance of microorganisms to antibiotics and the absence or rarity of side effects in natural-origin drugs have prompted researchers to explore natural-origin medicines and led the public to turn to medicinal plants (Koçer and Sugeçti, 2015;28). Medicinal plants, utilized internally or externally for disease treatment, encompass phytotherapy, pharmacy, food, spices, and cosmetics (Göktaş and Gıdık, 2019;145). These plants, known as medicinal and aromatic plants, contain bioactive secondary metabolites like terpenoids, steroids, alkaloids, terpenes, lipids, saponins, and phenolic compounds (Phillipson, 2007;2960). These secondary metabolites exhibit strong antimicrobial, antioxidant, antifungal, antiallergic, antidiabetic, antithyroid, and anti-inflammatory effects, as well as modulation of detoxification enzymes, immune system stimulation, reduction of platelet aggregation, and hormone metabolism modulation (Varlı et al., 2020;24). Plants have long been used to treat and prevent certain human ailments. Their medicinal properties are attributed to the presence of secondary metabolites in their structure and metabolic pathways. Although these metabolites are not essential for plant growth and development, they play vital roles in plant signaling and defense (Ökmen et al., 2017;16). Medicinal and aromatic plants offer an ample source of biologically active compounds, many of which can be utilised for developing new pharmaceuticals (Acıbuca and Budak, 2018;37).

Plants with components such as organic acids, phenolic compounds, and essential oils demonstrate antimicrobial properties that may vary with structural changes (Apaydın and Yolcu, 2017;152). Phenolic compounds are distributed throughout various plant parts, and essential oil extracts derived from them can show antimicrobial effects against numerous microorganisms (Gyawali and Ibrahim, 2014;412 and Aydın, 2020;1). The hydroxyl groups in phenolics play a

role in inhibiting bacteria by disrupting bacterial cell membranes, causing leakage of cellular contents (Xue et al., 2013;12720). These hydroxyl groups function as proton exchangers, diminishing the orientation of bacterial cells on the cytoplasmic membrane and leading to bacterial death by damaging the membrane (Manandhar et al., 2019;1). The biological and antimicrobial efficacy of essential oils depends on their bioactive constituents (Oliveira et al., 2020;717). Generally, the lipophilic ends of lipoteichoic acids in Gram-positive bacteria's cell membrane can enhance the penetration of hydrophobic essential oil compounds. Conversely, the resistance of Gram-negative bacteria to essential oils may be due to the protective functions of outer membrane proteins or bacterial lipopolysaccharides that hinder the diffusion rate of hydrophobic compounds through the lipopolysaccharide layer (Alsamri et al., 2021;73).

The use of natural antimicrobial agents as alternative health solutions has a long history, particularly in the case of agents derived from vegetable oils. The antimicrobial properties of essential oils and spices, which were first discovered by the Egyptians and are still frequently used in Asian countries today, have attracted considerable attention (Tajkarimi et al., 2010;1199). Plants contain a variety of components, including saponins, coumarins, terpenoids, alkaloids, flavonoids, thiosulfinates, phenolics, and organic acids. The antimicrobial effects of these components vary depending on several factors, including the type of microorganism, the extraction method, the culture medium, the inoculum size, the determination method, and the chemical structure and concentration of the components (Şengün and Öztürk, 2018;256).

Turkey's geographical location, climate, soil structure, and geomorphological diversity contribute to its remarkable status as a region of unique plant biodiversity. The number of plant species identified in Turkey has increased from 2,480 in the 1950s to 11,707 today, indicating a significant increase in plant diversity (Kocalar, 2017;68). Turkey's diverse array of habitats fosters a rich variety of plant species, including numerous endemic varieties. The country serves as the native habitat of many plant species and a center for their cultivation, with a total of 3,649 endemic plant species identified within its borders (Ulcay and Şenel, 2020;62). The utilization of plants for therapeutic purposes dates back to antiquity, with humans leveraging the properties of various plants for medicinal, culinary, construction, fuel, animal feed, ornamental, and religious purposes (Deniz et al., 2018;1). These applications have been transmitted across generations, evolving alongside changes and developments over time (Alsataf, 2020;1).

Although essential oils are frequently incorporated into food as flavorings, they can also exert a range of potent effects on the human body. The methods of obtaining these oils can affect their antimicrobial properties, as well as properties such as taste, odour, colour and appearance (Sayın, 2019;1). One of the essential oil components obtained from the GC-MS analysis exhibits hydrophobic properties. This property can result in structural disruptions and increased permeability by breaking down the bacterial cell membrane and mitochondrial lipids (Alsamri et al., 2021;73). These structural alterations to the bacterial cell membrane result in the leakage of intracellular ionic compounds and other cellular contents out of the cell. Bacterial cells can tolerate minor leakage, but the loss of significant quantities of cell contents (such as critical ions and molecules) can result in the death of the bacterial cell (Ghazanfari et al., 2020;1). Antimicrobial agents can inhibit microbial growth even at low concentrations (Güdücü, 2014;1).

Antimicrobial compounds in plants are typically located within the essential oil section. These compounds are responsible for the flavour and flavonoids of plants and are typically obtained through water vapour distillation. In traditional medicine, certain diseases have been treated with herbal drugs, and a significant proportion of the global population has employed plant-based products for basic healthcare (Salık, 2019;1). Plants are capable of transforming water, minerals and other substances obtained from the soil into compounds that can be utilised by the human body. Some primary and secondary metabolites, including carbohydrates, proteins, fats, and vitamins, are the active substances resulting from the metabolism of plants and can be used for medicinal purposes (Tongnuanchan and Benjakul, 2014;1231). The extraction of these active substances is a prerequisite for utilising plants for medicinal purposes (Demirkapı, 2018;1). The extraction and purification of bioactive components from plants can facilitate the development of drugs in the field of pharmacology and medicine. The use of plants in the production of pharmaceuticals is predicated on their rich content of bioactive components. Furthermore, pure herbal components of these plants can be employed for therapeutic or prophylactic purposes. Since antiquity, plants have been prepared for use and employed as medicinal agents. Recent studies corroborate the claims regarding the intended use of plants employed in traditional medicine (Baldemir et al., 2018;45). A study conducted in 2000 demonstrated that the pharmacological properties of plant essential oils and components can be employed in the fields of medicine, cosmetics and industry (Faydaoğlu and Sürücüoğlu, 2013;233). The utilisation of medicinal plants in the management of illnesses is a long-standing

practice that has been observed since the advent of human settlements. These plants are capable of synthesising a range of chemical compounds, including flavonoids, alkaloids, terpenoids, tannins, berberine, quinine and emetine, which are employed in the treatment of numerous microbiological diseases (Ullah and Amin, 2020;1). In light of the often arbitrary nature of the development of synthetic pharmaceuticals, a growing number of pharmaceutical companies are turning their attention to plant-derived drugs (Vital et al., 2010;58). Similarly, in the cosmetics industry, plant raw materials are preferred, particularly in cream formulations. This preference is largely attributed to the fact that plants contain biologically active components of medicinal value and have a wide effect profile due to their rich active ingredient content (Üstündağ et al., 2020;292).

The pursuit of beauty has been a constant throughout human history. The use of herbal extracts for the treatment of skin diseases, scalp problems and general appearance has spanned millennia. A growing body of research indicates that the herbal cosmetics industry is expanding, with an accompanying increase in demand for herbs. This has led to a surge in interest in herbal commerce (Kole et al., 2005;315). In recent years, the herbal industry has witnessed a surge in growth driven by consumers' preference for herbal care products and a decline in trust in modern healthcare. The aforementioned factors, in addition to the historical use of herbal products in diverse cultures and the perception that herbal medicines are natural and superior to synthetic cosmetics, have contributed to the rising popularity of herbal cosmetics (Joshi and Pawar, 2015;1 and Doğan, 2018;49). The range of plant-derived substances used in cosmetic products is expanding rapidly. It is anticipated that new plants will be introduced to the cosmetics industry in the future (Çoklar and Akbulut, 2016;235)

Herbal cosmetics are defined as products that affect the structure and functions of the skin. They contain nutrients for healthy skin and hair and are obtained from different herbal sources. Additionally, they contain phytochemicals (Fathima et al., 2011;140). Cosmetic products, which include items such as cream, facial cleansing gel, cleanser, hair oil, hair colourant, shampoo, hair conditioner, eyeliner, mascara, foundation, perfume, and scented soap, are also considered to be a form of cosmetic. The use of cosmetics containing plant extracts is becoming increasingly prevalent across numerous sectors of the personal care industry. This shift can be attributed to the growing awareness of the detrimental effects of prolonged reliance on synthetic products and chemicals, which have contributed to a rise in health concerns and environmental degradation over the past half-century (Kırbağ, 2006;77 and Joshi and Pawar, 2015;1).

The potential of natural products derived from plant extracts is an area of significant interest for future research; however, further studies are required to gain a deeper understanding of the impact of plant-solvent ratios, active substance contents, and extraction methods (Dedebaş et al., 2021;313).By elucidating the factors that influence the stability of active substances, such as color, odor, clarity, or time-dependent stability, new scientific studies can address limitations associated with plant extracts. It is imperative to acknowledge the distinction between plant extracts and purified therapeutic agents. The primary distinction lies in the lower concentration of plant extracts relative to pure chemicals. Additionally, plants contain supplementary active substances that are intricately linked with the compound responsible for the primary effect, both chemically and therapeutically (Kurban, 2018;1 and Egesel, 2019;87). A range of formulations has been developed for herbal cosmetics, with plant extracts being among the most prevalent. These products can be formulated in various forms, including cream, ointment, lotion, emulsion, powder, and solution (Joshi and Pawar, 2015;1). The efficacy of herbal adjuvants in enhancing the appearance of the skin has been demonstrated, with studies highlighting their potential applications as whitening, moisturizing, emollient, or tanning agents (Kole et al., 2005;315 and Ökmen et al., 2017;16).

The skin is an intricate organ system comprising three distinct layers: the epidermis, dermis, and subcutaneous layers. The dermis, located beneath the epidermis, contains blood vessels, specialized nerve endings, elastin, and collagen fibers.The epidermis is comprised of two main parts: the stratum germinativum and the stratum corneum. The stratum corneum, being the outermost layer of the epidermis, is in direct contact with the external environment due to its high keratin content. This layer is not merely an accumulation of dead cells; it is also a component of the homeostatic system of a complex organism (Zagorska et al., 2020;229).Events occurring in the stratum corneum, including the use of cosmetic products, have an impact on the epidermis and deeper cell layers (Kurban, 2018;1). Adverse effects on the epidermis and dermis layers can result from rapid alterations in the external environment and shifts in the universal homeostatic equilibrium associated with the aging process (Gediya et al., 2011;24).Formulations of cosmetic products containing active ingredients derived from plants are designed to protect the skin against damaging external factors and to restore the disrupted lipid balance within the dermis that occurs during the aging process (Joshi and Pawar, 2015;1 and Berk et al., 2015;185). The topical application of essential oils is a viable approach for the management of dermatological conditions, given their capacity to penetrate the

skin and interact with cellular membranes, thereby exerting prolonged effects on the skin (Gediya et al., 2011;24).

The process of wound healing is a complex biological phenomenon that occurs through four distinct phases: hemostasis, inflammation, cell proliferation, and maturation. These phases result in the death of old tissue and the repair of new tissue (Zagórska et al., 2020;229). However, any disruption or irregularity in this process can result in microbial infections and impaired wound healing (Agra et al., 2013;945). In the context of infected wounds, the process of wound healing can be impeded by the simultaneous death of regenerating cells, which can lead to the formation of toxins and a protracted healing process (Hasmann et al., 2013;245).Therefore, the prevention of microbial infection and the stimulation of tissue repair processes are imperative for expeditious healing (Schiffer et al., 2016;2553). In this regard, herbal medicines derived from natural sources have been shown to play a significant role in health promotion, with approximately 80% of these plants having been demonstrated to have ethnomedicinal use on a global scale.

The herbal medicines in this category include plants such as *Rhus coriaria* L. (sumac) and *Coriandrum sativum* L. (coriander). Sumac is a member of the Anacardiaceae family and contains phytochemicals with antioxidant and antimicrobial properties. Sumac has a long history of medicinal use, with a reputation as a traditional folk remedy for diabetes and mouth sores (Ünver, 2006;1). Coriander, belonging to the Apiaceae family, contains components with various health functions, including antioxidant, anti-hyperglycaemic and anti-anthelmintic properties (Burdock and Carabin, 2009;22). Coriander has been demonstrated to exhibit antibacterial activity, with particular efficacy against E. coli, B. megaterium, S. choleraesuis, and S. aureus (Duman, 2008;1).

Algae are photosynthetic eukaryotes that play an integral role in maintaining the structural and functional integrity of ecosystems. The bioactive components present in the structure of algae demonstrate comparable effects to those of organic and inorganic filters, which are effective in mitigating the detrimental effects of UV radiation in cosmetics (Ak and Cirik, 2017;227). The health-promoting effects of algae are attributed to the presence of sulphated polysaccharides, which possess antioxidant, antitumour, anti-inflammatory and antiviral properties (Soylu and Çebi, 2017;146). Algae-based products in skin care have been demonstrated to offer a range of beneficial outcomes, including enhanced moisture retention, accelerated blood circulation, enhanced cell renewal and augmented skin resilience (Charlier and Chaineux, 2009;838).

Algae are widely employed in medical and dermatological applications, as well as in a variety of cosmetic products. However, there is currently a lack of commercially available products or scientific data in the literature or within the cosmetic industry on microemulsions of sumac and coriander that are capable of penetrating algal cells. This highlights the necessity for further research into microemulsions to gain a deeper understanding of the interaction between these herbal extracts and algae, as well as to assess their potential cosmetic applications.

1. The Role of Microemulsion and Herbal Ingredients in Skin Care

A microemulsion is defined as a transparent or translucent heterogeneous colloidal system containing oil, water, and typically a co-surfactant. It is thermodynamically stable and characterized by low interfacial tension between the oil and water phases (Tartaro, 2020;1657).These systems offer advantages for the delivery of drugs to the skin. These systems are colloidal in nature, comprising oil and water phases, and are stabilized by a mixture of surfactants and co-surfactants (Üstündağ, 2008;292 and Nastiti et al., 2017;37).It has been demonstrated that microemulsions enhance bioavailability while minimizing skin irritation. This enhancement is attributed to the presence of chemical penetration enhancers, which facilitate the penetration of the stratum corneum lipid bilayers. The skin's role as a natural barrier hinders the permeation of drugs and potentially harmful compounds. Consequently, the utilization of microemulsions as a topical and transdermal drug delivery system is advocated, as they enhance penetration through the skin (Lopes, 2014;52).

The small droplet diameters of microemulsions facilitate the direct penetration of oil-soluble active substances into the stratum corneum layer of the skin. This indicates that it may enhance the penetration of the active substance into the skin (Yücel et al., 2019;1). The methods employed to optimise droplet size are of key importance, as the preparation of microemulsions and the method selected have a significant impact on their physicochemical properties. Despite kinetic energy barriers or limitations that delay spontaneous formation, microemulsions are typically formed by applying external energy through stirring or heating processes (Ashkar et al., 2022;1). These advantages of microemulsions are particularly relevant for the delivery of drugs across the stratum corneum layer of the skin.

2. The significance and general characteristics of microemulsions in diverse systems

Microemulsions are colloidal systems comprising oil, water, surfactant and co-surfactant, with droplet sizes typically ranging between 10 and 100 nm (Callender et al., 2017;425). This particular type of colloid is thermodynamically stable and possesses a transparent structure that enables the homogeneous integration of the water and oil phases. The formation of microemulsions is contingent upon a number of factors. The presence of suitable surfactants that facilitate solubility between the water and oil phases is of critical importance in this process. Additionally, the diffusion of surfactants, the change in entropy, alterations in the surface area of droplets, and the maintenance of a constant temperature are significant factors influencing the formation of microemulsions (Prus-Walendziak and Kozlowska, 2021;950). The transparent structure of microemulsions is a consequence of their small droplet sizes, which are below the resolution of the human eye. This characteristic precludes direct observation using an optical microscope. Surface-active ingredients distribute these microscopic droplets in a circular shape, thereby forming the dual-phase structure of microemulsions. This structure functions as a liquid membrane carrier, facilitating the transport of lipophilic compounds in water environments and hydrophilic compounds in lipid environments (Anton and Vandamme, 2010;978). The advantages of microemulsions include efficient transport of herbal drugs and enhanced transdermal drug delivery (Muzaffar et al., 2013;39). Despite their thermodynamic stability, such systems are prone to phase separation due to activation energy (McClements, 2012;1719).

The advantages of microemulsions can be enumerated as follows:

- The formation of a stable structure is achieved without the necessity for external energy input.

- The capacity to maintain stability over an extended period of time, which serves to extend the shelf life of the products.

- They possess a high solubilisation capacity, which enables the efficient transportation of a variety of components.

Furthermore, they facilitate the targeted delivery of active ingredients to specific areas of the body.

They play a significant role in the development of cosmetic and pharmaceutical formulations.

- It ensures that the active ingredients are minimally affected by physiological conditions, which is especially advantageous in the use of sensitive substances.

The versatility of this system allows for its use in a multitude of applications, including transdermal, dermal, topical, oral, and parenteral, thus providing a flexible platform for a diverse range of treatment modalities (Muzaffar et al., 2013;39 and Prus-Walendziak 2021;950).

However, some disadvantages of microemulsions are as follows:

- The formation of stable particles requires the inclusion of high amounts of surface-active ingredients, which may increase the likelihood of the formulation being toxic or irritating.

- The thermodynamic stability of microemulsions is sensitive to environmental factors, especially temperature and pH changes (Özyılmaz et al., 2020:65).

3. Optimal Component Selection and Functions in Microemulsion Formulations

The successful production of microemulsion formulations depends on the selection of components and the determination of the correct proportions of these components (Güngör et al., 2013;116). A wide range of emulsion components and combinations are available. Fatty acids (e.g. oleic acid) and esters of alcohols (isopropyl myristate, isopropyl palmitate, ethyl oleate), medium chain triglycerides, triacetin and terpenes are used as oil phase components in microemulsion formulations and have penetration enhancing properties (Prus-Walendziak and Kozlowska, 2021;950). These components can be used to form the oil phase alone or in combination. The aqueous phase components may include sodium chloride, buffer salts, preservatives and penetration enhancers (Üstündağ, 2008;292). When determining the formulation components, the intended use of the microemulsion is also taken into consideration. When preparing microemulsion for dermal applications, fatty acids are preferred because they increase penetration (Nastiti et al., 2017;37).

A plethora of materials constitute the surfactants and co-surfactants that are employed in microemulsion formulations. Non-ionic surfactants are the preferred option as they are effective at reducing interfacial tension and producing stable emulsions, while causing minimal skin irritation. The most commonly used surfactants include Tween 20 and 80, Span 20, Azone, Labrasol, Plurol isostearate, Plurol oleate, Aerosil and Transcutol (Güngör et al., 2013;116).

4. Formation and Preparation Methods of Microemulsions: Phase Titration and Phase Inversion

Microemulsions are thermodynamically stable colloidal systems that can form spontaneously and are typically prepared through low-energy applications (Dey et al., 2016;327). The formation and preparation of these systems are based on a number of different theoretical frameworks. Two common approaches are known as the phase titration method and the phase inversion method.

The phase titration method is a process whereby microemulsions are prepared through a self-emulsifying method. This method determines the area of microemulsion formation stability using triangular phase diagrams. In this area, microemulsions are formed with various coalescence structures, dependent on the chemical composition and concentration (Muzaffar et al., 2013;39). The oil and water phases are mixed and titrated with the co-surfactant until the microemulsions become transparent. The phase inversion method is a process whereby microemulsions are formed as a result of factors such as temperature effect or addition of an excess of the dispersed phase. The use of non-ionic surfactants allows the system to be transformed into y/s or s/y type microemulsions in accordance with temperature changes (Kruglyakov, 2000;100). In this method, non-ionic surfactants are particularly preferred due to their reduced irritancy and capacity to facilitate the application of microemulsions. The formulation, component selection and preparation methods of microemulsions play a critical role in obtaining stable and effective colloidal systems. Consequently, the formation theories and preparation methods of microemulsions have constituted an important area of research in drug delivery systems and cosmetic applications.

4. The Structural and Physical Characterisation of Microemulsions

The structures of microemulsions are characterised by various physical properties that play a pivotal role in this determination. Ternary phase diagrams are a common tool for illustrating the chemical composition of water, oil, surfactant, and co-surfactant components (Prus-Walendziak and Kozlowska, 2021;950). Mixtures of oil, surfactant and co-surfactant in specified weight ratios are diluted with an aqueous solution under moderate agitation at an ambient temperature of 25 °C. Once equilibrium is reached, clear emulsions are mapped on a phase diagram to demonstrate component combinations, either by visual inspection or polarised light microscopy. Viscosity and electrical conductivity are employed to gain insight into the structure of ME systems and to ascertain phase inversion phenomena. The presence of high conductivity values suggests that the percolation effect, which is characterised by attractive interactions between water droplets, is a defining feature of the continuous structure. Furthermore, these

measurements can be employed to predict the release of drugs from ME (Güngör et al., 2013;116).

The structural and physical characterisation of microemulsions plays an important role in understanding the properties of these special colloidal systems. The information obtained on microemulsions can provide a fundamental guide in the development and characterisation of microcomposite materials. The characterisation of microemulsions for the evaluation of the structural properties of microcomposite materials constitutes a critical research area, guiding researchers in the field of materials science and nanotechnology.

4. Advanced Technology with Plant Derived Materials: Microcomposites

Microcomposites are defined as multi-phase materials obtained by combining two or more materials with different chemical structures through various methods (Turkchem, 2021). The advancement of technology and growing environmental concerns have prompted a decline in petroleum-based products and an increase in demand for sustainable alternatives. This has led to a surge in scientific studies on bio-based products and plant-derived materials, which have in turn facilitated the development of microcomposites (Uzun, 2016;1). The increasing prevalence of costly and side-effect-prone synthetic drugs has underscored the importance of controlled drug release studies with microcomposites (Erdöl, 2018;1). Microcomposites are versatile materials with a range of properties that can be utilised in diverse industrial sectors.

As living standards rise, there is a corresponding increase in the use of medicinal and aromatic plants. These plants have a wide range of applications, including in the fields of medicine, cosmetics, toothpaste, soap, perfume, tea and spices. Furthermore, medicinal plants have attracted the attention of scientists due to their demonstrated activities, including antioxidant, anticarcinogenic, antiallergenic, antimicrobial, and antifungal properties (Şanda, 2019;1). A substantial body of literature exists examining the antimicrobial and antioxidant activities of essential oil extracts derived from medicinal plants. In these studies, the most commonly employed methods for evaluating antimicrobial activity were disc-diffusion and MIC (minimum inhibition concentration). Methods such as DPPH, ABTS, FRAP and ORAC are employed to ascertain antioxidant activity (Sayın, 2019;1). When bacterial cells encounter an antimicrobial agent, a series of degradation processes commence, commencing with the cell wall. As illustrated in Figure 1, this is followed by damage to the cytoplasmic membrane, damage to membrane proteins, leakage of cell contents, coagulation of the

cytoplasm, disruption of electron flow/active transport and depletion of protein repulsive force. This ultimately prevents the proliferation of bacterial cells (Balkan et al., 2016;18).

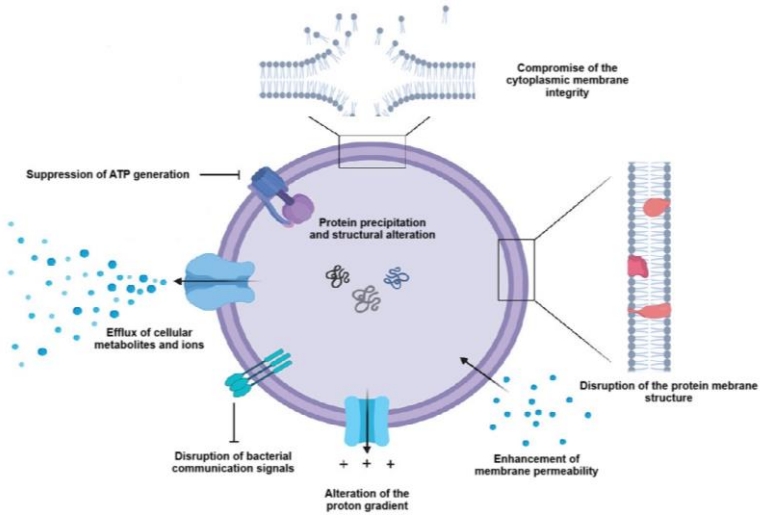

Figure 1. Broad-spectrum antibacterial mechanisms of essential oils (Nazzaro et al., 2020;1).

The broad antimicrobial properties of plant essential oils stem from the diverse chemical interactions of aldehydes, phenolic compounds, and terpenes, which are products of secondary metabolism across various plant tissues. The efficacy of essential oils depends on the capacity of their constituents to engage with the cell membrane, leading to the disruption of microbial integrity and ultimately causing cell death. Nevertheless, the bioactive compounds in essential oils target multiple cellular processes, primarily contributing to cytoplasmic coagulation, inhibition of enzymes responsible for ATP synthesis, disruption of ion transport, cell wall degradation, and bacterial membrane disintegration (Nazzaro et al., 2020;1).

The most crucial of the key parameters in the effective determination of antioxidant content is the presence of phenolic compounds (Guiné et al., 2020;470). While the specific phenolic compound varieties may influence the antioxidant capacity of a spice, it has been reported that there is typically a correlation between phenolic content and antioxidant activity (Torun, 2019;1). The antimicrobial and antioxidant effects can be attributed to the polyphenols and other secondary metabolites present in plant extracts. Nevertheless, further detailed research is required in order to gain a full understanding of the underlying mechanism. Plant-derived preparations have been demonstrated to possess therapeutic properties in the management of certain pathological conditions.

Furthermore, previous studies have indicated that the topical application of antioxidant-containing substances may facilitate wound healing and protect tissues from oxidative damage (Akgül et al., 2016;146).

Microemulsions (MEs) are thermodynamically stable formulations that significantly enhance drug absorption compared to traditional solutions. Their combination with bioadhesive gels holds promise for topical therapeutic applications (Özyılmaz et al., 2020;65). Due to their unique formulation characteristics, including excellent thermodynamic stability and biocompatibility, as well as their ability to enhance the skin penetration of both hydrophilic and lipophilic active substances, MEs serve as effective systems for topical and transdermal drug delivery (Yücel et al., 2019;1). In our study, MEs were utilized in the preparation of microcomposites for these purposes.

As living standards rise, there is an increase in the consumption of medicinal and aromatic plants, which find application in pharmaceuticals, cosmetics, toothpaste, soap, perfumes, teas, and spices (Sanda, 2019;1).Medicinal plants have garnered significant attention from scientists due to their bioactive properties, which include antioxidant, anticancer, antiallergenic, antimicrobial, and antifungal activities (Sayin, 2019;1). Research has been extensively focused on analyzing the antimicrobial and antioxidant properties of essential oils from these plants, utilizing methods like disk diffusion, minimum inhibitory concentration (MIC) for antimicrobial activity, and DPPH, ABTS, FRAP, and ORAC for antioxidant assays (Berber et al., 2013;10).

Antimicrobial agents target bacterial cells, initiating damage at the cell wall, followed by cytoplasmic membrane disruption, protein damage, leakage of cellular contents, and energy depletion, ultimately inhibiting bacterial growth (Balkan et al., 2016;18). For example, studies on extracts from 15 plants in Sinop, Turkey, demonstrated strong antimicrobial activity against various Gram-positive and Gram-negative bacteria (Faydaoglu and Surucuoglu, 2013;233). Similarly, The traditional South African plant extracts were more effective against Gram-positive bacteria, while only methanol extracts inhibited *E. coli* (Kose et al., 2021;141).

Extensive studies on sumac (Rhus coriaria) revealed its strong antimicrobial effects, particularly against Gram-positive bacteria (Erturk, 2010;53 and Demirkol, 2010;1). Additionally, GC-MS analysis of sumac identified over 120 volatile compounds contributing to its antimicrobial properties, with terpenoids and aliphatic compounds being the most active (Yildirim Aybakır, 2015;1). Other studies, such as those by Nasar and Halkman (2004;63), further demonstrated

sumac's effectiveness against foodborne pathogens (Faydaoglu & Surucuoglu, 2013;233). Regarding coriander, its essential oils, rich in linalool, have exhibited broad-spectrum antimicrobial effects, primarily through membrane disruption of both Gram-positive and Gram-negative bacteria (Asgarpanah and Kazemivash, 2012;2340). Studies have shown that coriander extracts are effective against bacteria such as *S. aureus* and *Pseudomonas* spp. (Deniz et al., 2018;1).

CONCLUSION

Microemulsions represent a versatile and innovative approach to drug delivery and cosmetic formulations, offering significant advantages in enhancing bioavailability and minimizing skin irritation. Their thermodynamic stability and ability to create stable, homogeneous systems make them ideal for delivering active ingredients effectively through the skin. The incorporation of plant extracts such as sumac and coriander into microemulsions further enhances their therapeutic potential by providing bioactive compounds with antimicrobial and antioxidant properties. These plant-derived materials offer safe and effective alternatives to synthetic agents, ensuring minimal adverse effects and increased skin resistance. Additionally, the careful selection of components, including oils, aqueous phases, and surfactants, is critical in achieving functional and stable microemulsion formulations. Despite their sensitivity to environmental factors such as temperature and pH, microemulsions continue to show promise in both cosmetic and pharmaceutical applications. Through continued research and development, microemulsions with plant-based microcomposites can unlock new potentials for targeted and controlled drug release, meeting the growing demand for sustainable, plant-derived solutions in the healthcare and personal care industries.

REFERENCES

Abraham, A. M., Alnemari, R. M., Jacob, C., and Keck, C. M. (2020). PlantCrystals—Nanosized Plant Material for Improved Bioefficacy of Medical Plants. Materials, 13(19), 43-68.

Acıbuca, V. and Budak, D. B. (2018). The place and importance of medicinal and aromatic plants in the world and Turkey. Çukurova Tarım ve Gıda Bilimleri Dergisi, 33(1), 37-44.

Agra, I. K., Pires, L. L., Carvalho, P. S., Silva-Filho, E. A., Smaniotto, S. and Barreto, E. (2013). Evaluation of wound healing and antimicrobial properties of aqueous extract from Bowdichia virgilioides stem barks in mice. Anais Da Academia Brasileira de Ciências, 85(3), 945–954.

Ak, L. and Cirik, S. (2017). Blue-green algae (Cyanobacteria) and thermalism. Ege Journal of Fisheries and Aquatic Sciences, 34(2), 227–233.

Akgül, M. B., Şındak, N., Karakoç, Z. and Gülaydın, A. (2016). Effects of topically applied Pistachio oil and glycerin solution on wound healing in Japanese quails (Coturnix coturnix japonica). Harran University Journal of Veterinary Faculty, 5(2), 146-151.

Alsamri, H., Athamneh, K., Pintus, G., Eid, A. H. and Iratni, R. (2021). Pharmacological and antioxidant activities of Rhus coriaria L. (Sumac). Antioxidants, 10(1), 73.

Alsataf, S. (2020). Antimicrobial and biological activities of pomegranate tissue extracts (Master's thesis). Harran University, Institute of Science, Şanlıurfa.

Anton, N. and Vandamme, T. F. (2010). Nano-emulsions and Micro-emulsions: Clarifications of the Critical Differences. Pharmaceutical Research, 28(5), 978–985.

Apaydın, E. and Yolcu, M. (2017). Determination of total phenolic content, total flavonoid content and ion chromatographic anion-cation content of Sakarca (Ornithogalum Umbellatum L.) plant native to Giresun region. Karadeniz Fen Bilimleri Dergisi, 7(2), 152-160.

Ashkar, A., Sosnik, A. and Davidovich-Pinhas, M. (2022). Structured edible lipid-based particle systems for oral drug-delivery. Biotechnology Advances, 54, 107789.

Asgarpanah, J. and Kazemivash, N. (2012). Phytochemistry, pharmacology and medicinal properties of Coriandrum sativum L. African Journal of Pharmacy and Pharmacology, 6(31), 2340-2345.

Aydın, F. G. (2020). Examination of biological activities and analysis of active phenolic compounds of some medicinal plants (Master's thesis). Health Sciences University, Hamidiye Health Sciences Institute, Istanbul.

Baldemir, A., Ekinci, K., İlgün, S., Dalda, A. and Yetişir, H. (2018). Evaluation of total phenolic content and antioxidant capacities of Momordica charantia L. (Bitter melon) fruits. Derim, 35(1), 45-50.

Balkan, C. E., Karamese, M., Celebi, D., Aydogdu, S., Dicle, Y., & Calik, Z. (2016). The Determination of the Antibacterial Activities of Rose, Thyme, Centaury and Ozone Oils Against Some Pathogenic Microorganisms. Kafkas Journal of Medical Sciences, 6(1), 18-22.

Berber, İ., Avşar, C., Çine, N., Bozkurt, N. and Elmas, E. (2013). Determination of antibacterial and antifungal activities of methanolic extracts of some plants grown in Sinop. Karaelmas Science and Engineering Journal, 3(1), 10-16.

Berk, A., Dokumacı, A. H. and Kaymaz, M. B. (2015). Wound healing and medicinal plants used in the treatment of diabetic wounds. Health Science Journal, 24, 185-92.

Burdock, G. A. and Carabin, I. G. (2009). Safety assessment of coriander (Coriandrum sativum L.) essential oil as a food ingredient. Food and Chemical Toxicology, 47(1), 22–34.

Callender, S. P., Mathews, J. A., Kobernyk, K. and Wettig, S. D. (2017). Microemulsion utility in pharmaceuticals: Implications for multi-drug delivery. International Journal of Pharmaceutics, 526(1–2), 425-442.

Charlier, R. H. and Chaineux, M. C. P. (2009). The Healing Sea: A Sustainable Coastal Ocean Resource: Thalassotherapy. Journal of Coastal Research, 254, 838–856.

Çoklar, H. and Akbulut, M. (2016). Effect of different solvents on antioxidant activity and phenolic compounds extraction of Hawthorn (Crataegus orientalis) fruits. Derim, 235–246.

Çiftçi Yegin, S. and Odabaş Alver, D. (2020). The Investigation of Antimicrobial Activities and Hypoglycemic Effect of Sumac (Rhus coriaria L.) Syrups in Different Region. Bitlis Eren Üniversitesi Fen Bilimleri Dergisi, 9(1), 85–90.

Dedebaş, T., Dursun Çapar, T., Ekici, L. and Yalçın, H. (2021). Ultrasonic-assisted extraction method in oily seeds and its advantages. European Journal of Science and Technology, (21), 313-322.

Demirkapı Kalın, D. (2018). Investigation of the effects of extraction methods on the antimicrobial activity of plants (Master's thesis). Kastamonu University, Graduate School of Natural and Applied Sciences, Kastamonu.

Demirkol, G. (2010). Investigation of antibacterial, antifungal, and antioxidant activities of fifty commonly used spice types in Turkey (Master's thesis). Ordu University, Institute of Science, Ordu.

Deniz, E. U., Yeğenoğlu, S., Şahne, B. S. and Özkan, A. M. G. (2018). A review on coriander (Coriandrum sativum L.). Marmara Pharmaceutical Journal, 22(1).

Dey, S., Datta, S., Dasgupta, S., Mazumder, B. and Pathak, Y. V. (2016). Lipid nanoparticles for topical application of drugs for skin diseases. In A. M. Grumezescu (Ed.), Nanobiomaterials in Galenic Formulations and Cosmetics (pp. 327–361). William Andrew Publishing.

Doğan, Ö. and Avcı, A. (2018). Herbal medicine and drug interactions. Turkey Clinics Journal of Public Health-Special Topic, 4(1), 49-54.

Duman Aydın, B. (2008). Investigation of Antibacterial Effects of Some Medicinal Plants and Spices on Food Pathogens. Kafkas Universitesi Veteriner Fakultesi Dergisi. Published.

Egesel, C. and Ordu, O. (2019). Comparison of different extraction methods for carotenoid analysis in corn flour. Çanakkale Onsekiz Mart University Journal of Graduate School of Natural and Applied Sciences, 5(1), 87–98.

Erel-Akbaba, G., Öztürk, İ., & Ay-şenyiğit, Z. (2020). Improvement of the Antimicrobial Activity of Moxifloxacin Using W/O Microemulsion System for Skin Infections. FABAD Journal of Pharmaceutical Sciences, 45(3), 219-227.

Erdöl Aydın, N. (2018). Investigation of drug loading performance of hydroxyapatite-gelatin and hydroxyapatite-chitosan biocomposites produced in artificial body fluid medium. Erzincan University Journal of the Institute of Science and Technology.

Ertürk, Ö. (2010). Antibacterial and antifungal effects of alcoholic extracts of 41 medicinal plants growing in Turkey. Czech Journal of Food Sciences, 28(1), 53–60.

Fathima, A., Varma, S., Jagannath, P. and Akash, M. (2011). General review on herbal cosmetics. International Journal of Drug Formulation and Research, 2(5), 140-165.

Faydaoğlu, E. and Sürücüoğlu, M. (2013). Antimicrobial and antioxidant activities of medicinal and aromatic plants. Erzincan University Journal of Science and Technology, 6(2), 233-265.

Gediya, S. K., Mistry, R. B., Patel, U. K., Blessy, M. and Jain, H. N. (2011). Herbal plants: used as cosmetics. Journal of Natural Products and Plant Resources, 1(1), 24-32.

Gediya, S. K., Mistry, R. B., Patel, U. K., Blessy, M. and Jain, H. N. (2011). Herbal plants: used as a cosmetics. J Nat Prod Plant Resour, 1(1), 24-32.

Ghazanfari, N., Mortazavi, S. A., Yazdi, F. T. and Mohammadi, M. (2020). Microwave-assisted hydrodistillation extraction of essential oil from coriander seeds and evaluation of their composition, antioxidant and antimicrobial activity. Heliyon, 6(9), e04893.

Göktaş, Ö. and Gıdık, B. (2019). Usage areas of medicinal and aromatic plants. Bayburt University Journal of Science, 2(1), 145–151.

Guiné, R. P. F., Gonçalves, F. J. A., Oliveira, S. F. and Correia, P. M. R. (2020). Evaluation of phenolic compounds, antioxidant activity and bioaccessibility in Physalis peruviana L. International Journal of Fruit Science, 20(2), 470–490.

Güdücü, F. (2014). Determination of phenolic contents, DPPH radical scavenging activities, and in vitro antimicrobial effects of Pyrus elaegifolia extracts (Master's thesis). Trakya University, Institute of Science, Edirne.

Güngör, Ö., Zungur, A., Mehmet, K. O. Ç., & Kaymak-Ertekin, F. (2013). Properties of emulsions and the effects of emulsification conditions on the microencapsulation of aromas and oils. Academic Food Journal, 11(2), 116–124.

Gyawali, R. and Ibrahim, S. A. (2014). Natural products as antimicrobial agents. Food Control, 46, 412-429.

Hasmann, A., Wehrschuetz-Sigl, E., Marold, A., Wiesbauer, H., Schoeftner, R., Gewessler, U., Kandelbauer, A., Schiffer, D., Schneider, K. P., Binder, B., Schintler, M. and Guebitz, G. M. (2013). Analysis of myeloperoxidase activity in wound fluids as a marker of infection. Annals of Clinical Biochemistry: International Journal of Laboratory Medicine, 50(3), 245–254.

Joshi, L. S. and Pawar, H. A. (2015). Herbal cosmetics and cosmeceuticals: An overview. El Mednifico Journal, 3(1).

Kırbağ, S. and Zengin, F. (2006). Antimicrobial activities of some medicinal plants from the Elazığ region. Yüzüncü Yıl University Faculty of Agriculture Journal of Agricultural Sciences, 16(2), 77-80.

Kocalar, A. O. (2017). The use of ecological region concept in geography teaching. Marmara Coğrafya Dergisi, 35, 68-73.

Koçer, F. and Sugeçti, S. (2015). Antimicrobial activity of commercial natural extracts against clinical pathogen microorganisms. Anadolu Doğa Bilimleri Dergisi, 6, 28-34.

Kose, L. S., Moteetee, A. and van Vuuren, S. (2021). Ethnobotany, toxicity and antibacterial activity of medicinal plants used in the Maseru District of Lesotho for the treatment of selected infectious diseases. South African Journal of Botany, 143, 141–154.

Kole, P. L., Jadhav, H. R., Thakurdesai, P. and Nagappa, A. N. (2005). Cosmetic potential of herbal extracts. Natural Product Radiance, 4, 315-321.

Kruglyakov, P. M. (2000). Chapter 2 - Stabilising ability of surfactants in emulsification and foam formation. In P. M. Kruglyakov (Ed.), Studies in Interface Science 9, 100–145.

Kurban, B. (2018). Examination of plants used in cosmetic products from a phytotherapy perspective (Master's Thesis). Istanbul University, Institute of Health Sciences, Istanbul.

Lopes, L. (2014). Overcoming the Cutaneous Barrier with Microemulsions. Pharmaceutics, 6(1), 52–77.

Manandhar, S., Luitel, S. and Dahal, R. K. (2019). In vitro antimicrobial activity of some medicinal plants against human pathogenic bacteria. Journal of Tropical Medicine, 2019, 1-5.

McClements, D. J. (2012). Nanoemulsions versus microemulsions: terminology, differences, and similarities. Soft Matter, 8(6), 1719–1729

Muzaffar, F. A. I. Z. I., Singh, U. K. and Chauhan, L. (2013). Review on microemulsion as futuristic drug delivery. Int J Pharm Pharm Sci, 5(3), 39-53.

Nasar-Abbas, S. and Halkman, A. (2004). Antimicrobial effect of water extract of sumac (Rhus coriaria L.) on the growth of some foodborne bacteria including pathogens. International Journal of Food Microbiology, 97(1), 63-69.

Nastiti, C., Ponto, T., Abd, E., Grice, J., Benson, H .and Roberts, M. (2017). Topical Nano and Microemulsions for Skin Delivery. Pharmaceutics, 9(4), 37.

Nazarzadeh, A., Heshmati, A. and Ghojazadeh, M. (2018). Plant-based antimicrobial agents against oral microorganisms: A comprehensive review. Current Pharmaceutical Biotechnology, 19(6), 434–448.

Nazzaro, F., Fratianni, F., Coppola, R. and De Feo, V. (2020). Essential oils as an innovative approach against biofilm of multidrug-resistant Staphylococcus. In K. C. S. de Souza (Ed.), Staphylococcus and biofilm—Molecular mechanisms, role in chronic diseases and preventive strategies (pp. 1–26). IntechOpen.

Ökmen, G., Arslan, A., Vurkun, M., Mammadkhanli, M. and Ceylan, O. (2017). Antimicrobial and antioxidant activities of different spices. Electronic Journal of Microbiology TR, 15(1), 16–28.

Oliveira Ribeiro, S., Fontaine, V., Mathieu, V., Zhiri, A., Baudoux, D., Stévigny, C. and Souard, F. (2020). Antibacterial and cytotoxic activities of ten commercially available essential oils. Antibiotics, 9(10), 717.

Özyılmaz, E. D., Sayıner, Z. and Çomoğlu, T. (2020). Evaluation of Micro and Nanoemulsions in Pharmaceutical Aspect. Journal of Literature Pharmacy Sciences, 9(1), 65–76.

Phillipson, J. D. (2007). Phytochemistry and pharmacognosy. Phytochemistry, 68(22–24), 2960–2972.

Prus-Walendziak, W. and Kozlowska, J. (2021). Lyophilized Emulsions in the Form of 3D Porous Matrices as a Novel Material for Topical Application. Materials, 14(4), 950.

Salık, Y. (2019). Anti-oxidant and antimicrobial activity of Alyssum floribundum Boiss. and Balansa (Brassicaceae) plant extracts (Master's thesis). Mersin University, Institute of Science, Mersin.

Sanda, C. (2019). Determination of volatile compounds in Cirsium creticum (Lam.) D'Urv. (Asteraceae) and investigation of its antifungal/antimicrobial activity (Master's thesis). Institute of Science, Namık Kemal University, Tekirdağ.

Sayın, A. Ü. (2019). Examination of antibacterial effects of some plant essential oils (Master's thesis). Nevşehir Hacı Bektaş Veli University, Institute of Science, Nevşehir.

Schiffer, D., Tegl, G., Vielnascher, R., Weber, H., Herrero-Rollett, A., Sigl, E., Heinzle, A.and Guebitz, G. M. (2016). Myeloperoxidase-responsive materials for infection detection based on immobilized aminomethoxyphenol. Biotechnology and Bioengineering, 113(12), 2553–2560.

Soylu, E. N. and Çebi, A. (2017). DPPH (1,1-diphenyl-2-picrylhydrazyl) Radical Scavenging Activity of Scenedesmus sp. Karadeniz Science Journal, 7(2), 146–151.

Şengün, İ. Y. and Öztürk, B. (2018). Natural antimicrobials from plant sources. Anadolu University Journal of Science and Technology C-Life Sciences and Biotechnology, 7(2), 256-276.

Tajkarimi, M., Ibrahim, S. and Cliver, D. (2010). Antimicrobial herb and spice compounds in food. Food Control, 21(9), 1199–1218.

Tartaro G, Mateos H, Schirone D, Angelico R and Palazzo G. (2020). Microemulsion Microstructure(s): A Tutorial Review. Nanomaterials. 10(9):1657.

Tongnuanchan, P. and Benjakul, S. (2014). Essential oils: extraction, bioactivities, and their uses for food preservation. Journal of Food Science, 79(7),1231-1249.

Torun, L. (2019). Phenolic content and antioxidant activity properties of sumac plant (Master's thesis). Istanbul Aydın University, Institute of Science and Technology, Istanbul.

Turkchem. (2021). Homepage. Retrieved from https://www.turkchem.net/.

Ullah, T., & Amin, N. U. (2020). In Vitro Antibacterial Activity of Medicinal Plant Extracts. Pakistan Journal of Agricultural Research, 33(4).

Ulcay, S. and Şenel, G. (2020). A study on ethnobotanical characteristics of some medicinal and edible plants spreading in the Tokat region. Academic Platform Journal of Engineering and Science, 62–69.

Uzun, G. (2016). Determination of some properties of bio-composites with bio-particle added PHB (Master's thesis). Bartın University, Graduate School of Natural and Applied Sciences, Bartın.

Ünver, A. (2006). Sumak (Rhus coriaria L.) Meyvelerinden Oleorezin Üretimi Üzerine Araştırma (Doktora Tezi). Selçuk Üniversitesi, Fen Bilimleri Enstitüsü, Konya.

Üstündağ Okur, N., Karadağ, A. E., İpekçi, E.and Özcan Bülbül, E. (2020). Cosmetic preparations and plants used in cosmetic preparations. Journal of Literature Pharmacy Sciences, 9(3), 292–303.

Varlı, M., Hancı, H. and Kalafat, G. (2020). Production potential and bioavailability of medicinal and aromatic plants. Research Journal of Biomedical and Biotechnology, 1(1), 24-32.

Vital, P. G., Velasco Jr, R. N., Demigillo, J. M., & Rivera, W. L. (2010). Antimicrobial activity, cytotoxicity and phytochemical screening of Ficus septica Burm and Sterculia foetida L. leaf extracts. Journal of Medicinal Plants Research, 4(1), 058-063.

Xue, J., Davidson, P. M. and Zhong, Q. (2013). Thymol nanoemulsified by whey protein-maltodextrin conjugates: Enhanced emulsifying capacity and antilisterial properties in milk by propylene glycol. Journal of Agricultural and Food Chemistry, 61(51), 12720–12726.

Yıldırım Aybakır, M. (2015). Investigation of the antimicrobial effect of spices within the scope of hurdle technology (Master's thesis). Ankara University, Institute of Science and Technology, Ankara.

Yücel, I., Eren Böncü, T., Şeker Karatoprak, G. and Akpolat, R. N. (2019). Development, characterization, and evaluation of microemulsion and microemulsion gel formulations containing rutin with antioxidant effects. Düzce University Journal of Health Sciences Institute.

Zagórska-Dziok, M., Ziemlewska, A., Nizioł-Łukaszewska, Z. and Bujak, T. (2020). Antioxidant Activity and Cytotoxicity of Medicago sativa L. Seeds and Herb Extract on Skin Cells. BioResearch Open Access, 9(1), 229–242.

Zerrifi, S., el Khalloufi, F., Oudra, B. and Vasconcelos, V. (2018). Seaweed Bioactive Compounds against Pathogens and Microalgae: Potential Uses on Pharmacology and Harmful Algae Bloom Control. Marine Drugs, 16(2), 55.

CHAPTER 25

Leaf Anatomical and Micromorphological Characteristics of the Evergreen *Laurocerasus officinalis* Species depending on Seasons

Öznur Ergen Akçin [1] ***& İsmail Zoroğlu***[2]

1 Prof. Dr., Ordu University, Faculty of Arts and Sciences, Department of Molecular Biology and Genetics, Ordu, Türkiye. ORCID: 0000-0002-6875-6045
[2] Ünye Arif Nihat Asya Vocational and Technical Anatolian High School, Ordu, Türkiye
ORCID: 0009-0003-9469-206X

Introduction

The genus *Laurocerasus* Duhamel. belongs to the family Rosaeceae and subfamily Prunoideae. While the genus has 17 species growing naturally in the world, it is represented by *Laurocerasus officinalis* M. Roem. which is the only species in Turkey (Yıldız and Aktoklu, 2010 Öztürk and Ölçücü, 2016).

The genus *Laurocerasus* are evergreen shrubs or trees up to 6-7 m tall. Leaves are simple, broadly elliptic, leathery and short-petioled. Margins very sparsely toothed, flowers erect, in racemes, fruits olive-sized black drupes. Petals are white in colour. It is widespread in Turkey, especially in the Eastern Black Sea region and is usually found under beech forests together with the genus *Rhododendron* L. The leaves of the plant are poisonous as they carry glycosides (Baytop, 1984; Tanker, 2007).

Although *L. officinalis* species is generally known as ‘taflan and karayemiş, it is also known by local names such as "gürcü kirazı”, "laz kirazı", "laz üzümü", "laz yemişi" (Alpınar and Yazıcıoğlu, 1991; Islam, 2005; Genç, 2009).The fruit of the plant is consumed fresh. It is also used as jam, molasses, salting, pickles and dried (Çalışır and Aydın, 2004). The leaves of Taflan plant are used as a medicinal plant as cough suppressant, antitussive, antispasmodic, anti-nausea and nerve sedative (Alpınar and Yazıcıoğlu, 1991).

In gymnosperm plants, the leaves of evergreen trees are needle or scale-shaped. In angiosperm plants, they are usually thicker and leatherier than those of deciduous trees. In an evergreen tree, the leaf can stay on for two years or more and can fall off in any season. Since the plant is evergreen, the large leaves are on the plant summer and winter. In temperate regions, evergreen species are exposed to large seasonal variations in air temperature and radiation. In response to such environmental changes, leaves change their photosynthetic and anatomical properties (Terashima et al., 2001; 2005).

In this study, it was attempted to determine the anatomical and micromorphological characteristics of the evergreen *L. officinalis* species grown in Ordu and its surroundings in relation to the seasons.

Material and Method

The specimens of *Laurocerasus officınalıs* species selected as the subject of the research were collected from Ordu province, Ünye district at sea level (41º07′35″N, 37º17′21″ E, 10 m, Zoroğlu 1, 15.08.2015, 15.02.2016) in August and February 2015-2016.

Leaves of *L. officinalis* plants were preserved in 70% alcohol for anatomical analyses. Cross and surface sections were taken from the alcohol materials with the help of a razor blade. The sections were made into permanent preparations (Vardar, 1987). For anatomical analyses, leaf transverse thickness, thickness of cuticle layer, thickness of mesophyll layer, palisade parenchyma cells, spongy parenchyma cells, stomata and epidermis cells were measured. The measurements were made using NIS (Nikon Imaging System-Elements Imaging Software 3.00 SP5) programme. Anatomical photographs of the species were taken with Nikon Eclipse E400 microscope. For micromorphological measurements, dry leaf samples were fixed on double-sided carbon tape. The fixed samples were coated with 12.5-15 nm gold. The examinations and photographs were taken with a voltage of 10-15 kilovolts (Kv) in a JSM-7001F scanning electron microscope (SEM) at the Black Sea Advanced Technology Research and Application Centre (KITAM) located at Ondokuz Mayıs University.

Results

The evergreen *L. officinalis* plants collected in August and February were analysed anatomically. When the general anatomical structure of the plant leaf is examined, single-row epidermis cells are observed on the upper and lower surfaces of the leaf cross sections. The upper and lower epidermis cells consist of rectangular and oval shaped cells. The leaf is bifacial type. The vascular bundles are arranged regularly. Palisade parenchyma cells contain dense chloroplasts. Palisade parenchyma cells are in two rows. There are rounded spongy parenchyma cells under the palisade parenchyma cells. Spongy parenchyma cells are in two to three rows. The average leaf thickness of the leaf cross sections was 356.89 ± 7.43 µm in the samples taken in August and 367.83 ± 38.21 µm in the samples taken in February. The average mesophyll thickness of the leaves was 301.43 ± 5.36 µm in summer and 292.95 ± 10.23 µm in winter. In the plants collected in August, the upper epidermis cells were 23.77±4.09 X 30.55±8.12 µm and the lower epidermis cells were 19.49±2.92 X 26.45±6.30 µm. The average thickness of the upper cuticle of the leaves was 3.65±0.58 µm. In the leaves collected in February, the upper cuticle thickness was 6.68±1.05 µm and the upper epidermis cell size was 19.22±3.41 X 42.28±13.67 µm. The average size of the lower epidermis cells was 16.85±3.20 X 35.21±5.81 µm. There was no change in the number of layers of palisade and spongy parenchyma cells in the mesophyll layer of the leaves in February and August. However, changes in the size of the cells were determined. In August, palisade parenchyma cells were 13.76±3.08 µm X 44.84±6.32 µm and spongy parenchyma cells were 22.30±3.69

µm in diameter. In plants collected in February, palisade parenchyma cells were 16.24±2.80 X 37.75±4.46 µm and spongy parenchyma cells were 24.84±6.98 µm in diameter. Stomatal cells were found only on the lower surface of the leaves. Stomata were 29.899 X 37.118 µm in August and 28.543 X 34.048 µm in February (Table1, Figure 1).

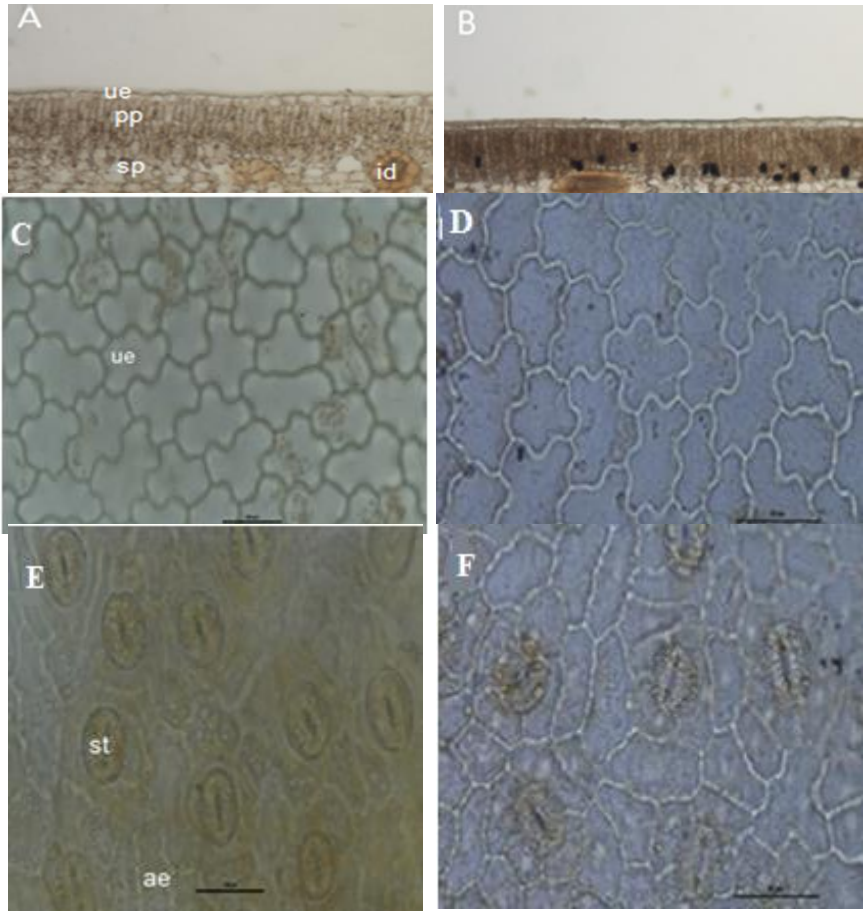

Figure 1. Cross and surface sections of *Laurocerasus officinalis* leaves collected in different seasons. A. Cross leaf section of August. B. Cross leaf section of February. C-D. Upper surface sections of leaves from August- February. E-F. Lower superficial sections of leaves from August -February. (ue: upper epidermis, ae: lower epidermis, pp: palisade parenchyma, sp: spongy parenchyma, id: vascular bundle, st: stomata)

Table 1. *Laurocerasus officinalis* collected in August and February

	August (µm)	**February (µm)**
Cuticle thickness	3.65±0.58	6.60±0.83
Upper epidermis width	23.77±4.09	19.22±3.41
Upper epidermis length	30.55±8.12	42.28±13.67
Lower epidermis width	19.49±2.92	16.85±3.20
Lower epidermis length	26.45±6.30	35.21±5.81
Palisade parenchyma width	13.76±3.08	16.24±2.80
Palisade paren. length	44.84±6.32	37.75±4.46
Spongy paren. diameter	22.30±3.69	24.84±6.98
Leaf thickness	356.89 ± 7.43	367.83±38.21
Palisade parenchyma area	88.81±6.46	90.09±17.14
Spongy parenchyma area	162.27±11.33	184.93±13.32

Micromorphological examinations revealed that the surface of the leaves was covered with a thick wax layer. It was determined that the samples collected in February had a denser wax layer. The epidermis cells on the upper surface of the leaves are oblong in shape. Periclinal and anticlinal walls of the epidermis cells are thick. Epidermal cells on the lower leaf surface are oblong, pentagonal or roundish. Periclinal and anticlinal walls are straight or curved. The walls of these cells are not very distinct. There are no stomata on the upper surface of the leaf, while there are stomata on the lower surface. There are linear cuticular folds around the stomata on the lower surface of the leaf. Stomatal cells are at the same level or slightly higher than the epidermis cells. Stomatal aperture is short and wide (Figure 2).

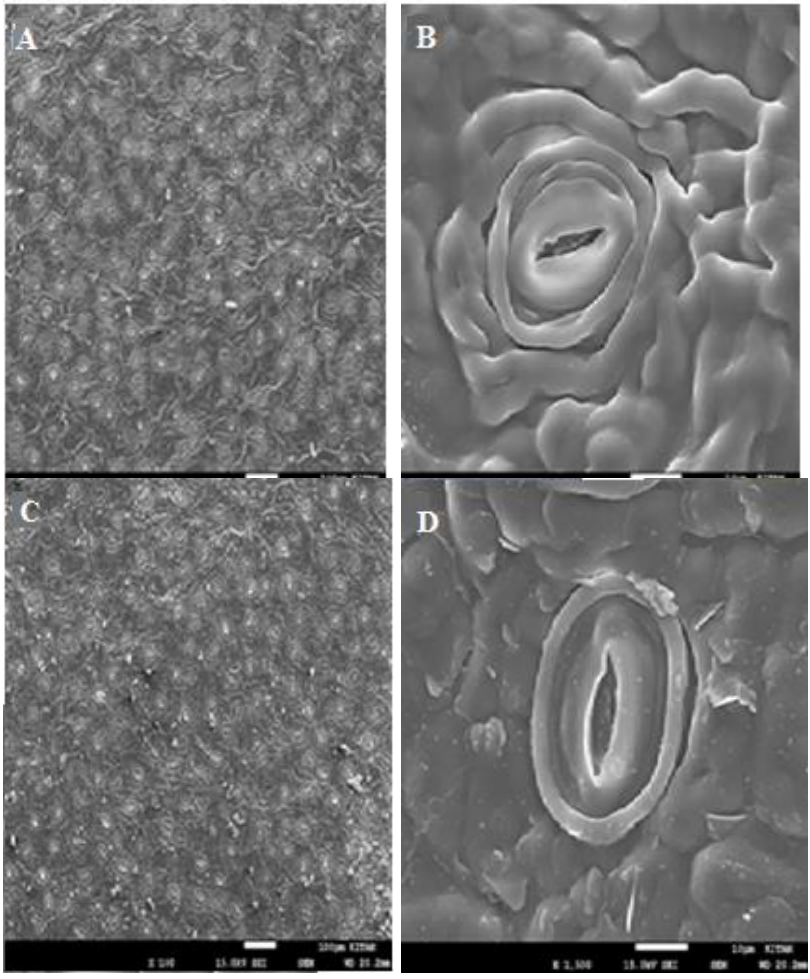

Figure 2. Lower surface SEM images of leaves in August (A-B) and February (C-D). A,C. general leaf surface image. B,D. Stomatal cells.

Discussion

The anatomical and micromorphological characteristics of the leaves of *Laurocerasus officinalis*, an evergreen plant, were examined seasonally. Micromorphological and anatomical studies on plants revealed important characters that can be used in the systematics of taxa (Akçin and Binzet, 2010). Especially the characters obtained by micromorphological and anatomical determination of the leaf and epidermis structures of plants are very important for detailed identification of plants (Akçin et al., 2013). In recent years, anatomical studies on leaf characteristics of woody and shrub forms have increased (Vasic and Dubak, 2012; Bercu and Popoviciu, 2013, Akçin 2023). The environments in which plants live cause changes in morphological and some anatomical characteristics of plants. Environmental conditions affect especially the thickness of leaves, density of stomata, structure of parenchymatic cells and photosynthesis activities. It has been reported that the anatomical and morphological characteristics of leaves change depending on the environmental conditions of plants (Schoettle ve Rochelle, 2000). Changes in environmental conditions cause stress in plants. As a result of this stress, plants show environmental adaptation. These adaptations can be seen in the morphological, physiological and anatomical structure of plants. In evergreen plants, leaves try to adapt to the extract to adapt to winter conditions (Mareri et al., 2022). When leaves are exposed to cold, structural changes in cellular compartments occur as a response to cold and activate a number of protective mechanisms (Wu et al., 2022). These mechanisms include changes in stomatal density, increases in mesophyll cell size, decreases in epidermal cell density and enhanced lignification (Equiza et al., 2001; Lorenzo et al., 2019). Some seasonal anatomical and micromorphological differences were determined in the leaves of *L. officinalis* species. Cuticle thickness, upper and lower epidermis cell lengths, leaf thickness, palisade and spongy parenchyma areas were found to increase in February measurements compared to August. Kofidis et al. (2003) reported that leaf thickness remained more or less constant seasonally in the plants they examined. In many studies, it has been reported that the leaves of evergreen plants are harder and thicker in winter. It has also been reported that nutrient levels are lower in leaves in winter, whereas secondary metabolites are more abundant, which helps to discourage leaf consumption by herbivores (Reich et al., 1992; Givnish, 2002). In evergreen plants, the leaves have a thicker cuticle and epidermis layer than in deciduous plants. This reduces the rate of photosynthesis in the plant. It makes them more drought resistant by reducing the amount of water lost during transpiration (Anonymous, 2023). Our results are consistent with the literature. The cuticle

layer of the leaves collected in winter is quite thick. Thus, the plant adapts to the harsh winter conditions. In addition, the surface of these leaves is covered with a dense wax layer. As a result, it was determined that the evergreen *L. officinalis* species adapts to the harsh winter conditions by showing structural changes such as thickening of the cuticle layer, increase in mesophyll cell size and leaf thickness, and covering the leaf surface with a wax layer.

Acknowledgments

This study was supported by the project numbered TF-1648 of Ordu University Scientific Research Projects Coordination Office. This study is a part of the master thesis prepared by İsmail Zoroğlu. A part of the study was presented as a poster paper at the "IConPB 2022 3rd International Congress on Plant Biology" and the abstract was published in the proceedings book.

References

Akçin, Y. (2023). The Leaf Properties, Stomatal Index and Chlorophyll Content of Turkish Hazelnut (Corylus avellana L.) Cultivars. *Journal of Agricultural Sciences 29*(3), 744-755. https://doi.org/10.15832/ankutbd.1085373

Alpınar, K. & Yazıcıoğlu, E. (1991). 9. Bitkisel ilaç hammadeleri toplantısı bildirisi

Anonymous (2023). The magıc of evergreens by Sarah Ottino, https://salishmagazine.org/magic-of-evergreens.

Baytop, T. (1984). *Therapy with Medicinal Plants in Turkey (Past and Present)* No: 3255. *Istanbul: Publications of the Istanbul University, 359*.

Bercu, R. & Popoviciu, D. R. (2013). Anatomcal Comparative Study Of Larix Decidua Mill. And Picea Abies (L.) Karsten (Pinaceae) Leaf. *Annals of the Romanian Society for Cell Biology*, *18*(2), 172.

Çalışır, S. & Aydın, C. (2004). Some physico-mechanic properties of cherry laurel (*Prunus lauracerasus* L.) fruits. *Journal of Food Engineering*, *65*(1), 145-150.

Equiza, M. A., Mirave, J. P. & Tognetti, J. A. (2001). Morphological, anatomical and physiological responses related to differential shoot vs. root growth inhibition at low temperature in spring and winter wheat. *Ann. Bot*. 2001, *87*, 67–76.

Ergen Akçin, Ö. & Binzet, R. (2010). The micromorphological and anatomical properties of Onosma angustissimum Hausskn Bornm and O cassium Boiss Boraginaceae. *Bangladesh journal of Plant Taxonomy 17*(2),1–8

Ergen Akçin, Ö., Şenel, G. & Akçin, Y. (2013) "Leaf epidermis morphology of some Onosma (Boraginaceae) species from Turkey," *Turkish Journal of Botany 37*(1), 55-64. https://doi.org/10.3906/bot-1202-33

Genç, S. (2009). Taflan çekirdeğinde *(Laurocerasus officinalis* Roem*.)* fonksiyonel bileşik analizi ve antioksidan kapasitesinin araştırılması. Yüksek lisans tezi, Gazi Osman Paşa Üniversitesi, Fen Bilimleri Enstitüsü, Kimya Anabilim Dalı, Tokat

Givnish, T. J. (2002). Adaptive signifi cance of evergreen vs. deciduous leaves: solving the triple paradox. *Silva Fennica 36*(3): 703–743.

İslam, A. (2005). Karayemiş yetiştiriciliği ve önemi. *Ege Karadeniz Dergisi 28*(4):25-32.

Kofidis, G., Bosabalidis, A. M. & Moustakas, M. (2003). Contemporary seasonal and altitudinal variations of leaf structural features in oregano (*Origanum vulgare* L.). *Annals of Botany*, *92*(5), 635-645.

Lorenzo, M., Pinedo, M. L., Equiza, M. A., Fernandez, P. V., Ciancia, M., Ganem, D. & Tognetti, J. A. (2019). Changes in apoplastic peroxidase activity and cell wall composition are associated with cold-induced morpho-anatomical plasticity of wheat leaves. *Plant Biol. 21*, 84–94.

Mareri, L., Parrotta, L. & Cai G.(2022). Environmental Stress and Plants. *Int J Mol Sci*. *23*(10):5416. doi: 10.3390 /ijms23105416.

Öztürk, F. & Ölçücü, C. (2016). The Chorology of Genus Laurocerasus Duhamel (Rosaceae) in East Black Sea Region-*Turkey J. Int. Environmental Application & Science 11*(3), 263 - 266,

Reich, P. B., Walters, M. B. & Ellsworth, D. S. (1992). Leaf lifespan in relation to leaf, plant, and stand characteristics among diverse ecosystems. *Ecological Monographs 62*, 365–392.

Schoettle, A. W. & Rochelle, S. G. (2000). Morphological variation of *Pinus flexilis* (*Pinaceae*), a bird-dispersed pine, across a range of elevations. *American Journal of Botany*, *87*(12), 1797-1806.

Tanker, N. K. (2007). *Farmasötik botanik*. Ankara: Ankara Üniversitesi Eczacılık Fakültesi , 93:288.

Terashima, I., Araya, T., Miyazawa, S., Sone, K. & Yano S. (2005). Construction and Maintenance of the Optimal Photosynthetic Systems of the Leaf, Herbaceous Plant and Tree: an Eco-developmental Treatise, *Annals of Botany* 95(3), 507–519, https://doi.org/10.1093/aob/mci049

Terashima, I., Miyazawa, S. I. & Hanba, Y. T. (2001) Why are sun leaves thicker than shade leaves? Consideration based on analyses of CO_2 diffusion in the leaf. *J Plant Res 114*: 93–105.

Vardar, Y. (1987). *Botanikte preparasyon tekniği*. İzmir: Ege Üniversitesi.

Vasic, P. S. & Dubak, D. V. (2012). Anatomical analysis of red Juniper leaf (*Juniperus oxycedrus*) taken from Kopaonik Mountain, Serbia. *Turkish Journal of Botany*, *36*(5), 473-479.

Wu, J., Nadeem, M., Galagedara, L., Thomas, R. & Cheema, M. (2022). Recent insights into cell responses to cold stress in plants: Signaling, defence, and potential functions of phosphatidic acid. *Environ. Exp. Bot*. *203*, 105068.

Yıldız, B., & Aktoklu, E. (2010). *Bitki sistematiği.* Ankara: Palme Yayınevi.

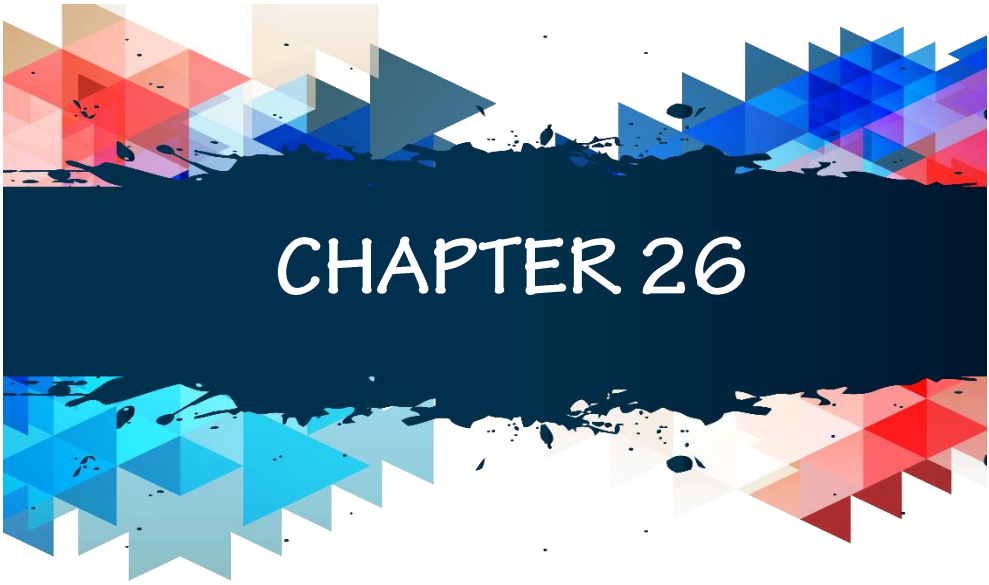

Epigenetic Studies in Insects: Current Advances and Emerging Trends

***Ebru Ceren Fidan*[1]**

1 Dr. Eskişehir Osmangazi Üniversitesi, Fen Fakültesi, Biyoloji Bölümü
ORCID: 0000-0002-6121-4585

Epigenetic investigates how external or environmental variables can affect gene expression without altering the genetic coding. This method examines the inheritable modifications in gene expression that occur without changes to the DNA sequence. This discipline relies on mechanisms like DNA methylation, histone modification, remodeling of chromatin, non-coding RNAs, heredity and genomic imprinting (Gibney & Nolan, 2010).

This is a discipline that has achieved considerable advancements in recent years, with applications across multiple academic fields. The primary focus of this area is; impact of environmental factors on diseases prevalent in clinical and mental health. The concept of epigenetics is studied across several organisms, including its implications for human morphology and behavior. In In the examination of insect epigenetics, distinct topics arise prominently:

A. Epigenetic Regulation of Insect Metamorphosis

Epigenetic pathways are essential in regulating insect metamorphosis, characterized by significant alterations in body structure and function. Specifically, DNA methylation and histone acetylation/deacetylation are essential for governing the intricate process of insect metamorphosis. These systems facilitate significant alterations in bodily form and function and may be inherited, hence influencing the evolution of insect species (Amiri, 2019; Glastad et al., 2019).

- DNA Methylation and Histone Modifications

Insect metamorphosis is regulated by epigenetic variations, including DNA methylation and histone acetylation-deacetylation. The notable changes documented during this phase are made possible by these epigenetic mechanisms (Glastad et al., 2019).

In dragonflies, the transcription factors Kr-h1 and E93 are essential for regulating metamorphosis, akin to their functions in other insects. The transcription factor Broad, a major gene controlling pupation in holometabolous insects, modulates both nymph-specific and adult-specific genes in dragonflies, offering insights into the evolutionary development of this essential transcription factor (Okude et al., 2022).

- Epigenetic Modulation of Gene Expression

During insect metamorphosis, gene expression levels can be controlled by epigenetic mechanisms, such as DNA methylation. Higher levels of methylation are associated with genes and isoforms that show more variable expression across developmental stages or phenotypic castes (Glastad et al., 2019).

- Epigenetic Inheritance and Metamorphosis

Through epigenetic inheritance, epigenetic changes made during metamorphosis may be transmitted to subsequent generations. This could speed up evolutionary adaptations in insect populations and promote the emergence of phenotypic variation (Amiri, 2019; Mukherjee & Dobrindt, 2024).

B. Epigenetic Foundations of Insect Caste Determination

Epigenetic mechanisms have been identified as influencing the differentiation of many castes in social insects like ants and bees (including queens and workers, from a singular genome). The process of caste determination is essential for the creation of phenotypic diversity in insect societies. Histone modifications and DNA methylation are crucial in regulating gene expression patterns particular to caste (Amiri, 2019; Oldroyd & Yagound, 2021; Vaiserman, 2015). Caste-specific gene expression and phenotypic variations, such as workers and long-lived queens, are caused by epigenetic modifications, specifically DNA methylation, which are induced by differential feeding of larvae (Vaiserman, 2015).

In the stingless bee *Melipona scutellaris*, epigenetic modifications, such as DNA methylation/demethylation and variations in histone methylation and phosphorylation between queens and workers, indicate a correlation among genotype, larval diet, and adult social behavior (Cardoso-Júnior et al., 2017). Nonetheless, the functional significance of DNA methylation in defining social insect caste remains ambiguous, as several studies have not identified significant correlations between methylation and caste in honeybees and other species (Oldroyd & Yagound, 2021).

A genomic imprinting model in termites suggests that queen and king-specific epigenetic imprints oppositely influence child sexual development, elucidating all existing empirical data on caste differentiation (Matsuura et al., 2018).

C. Epigenetic Memory and Adaptation in Insect Pests

Researchers have found that epigenetic alterations can be inherited by succeeding generations of insect pests, potentially facilitating the emergence of pesticide resistance and other adaptive characteristics. Recent findings underscore the significant importance of epigenetic memory in enabling swift adaptability and stress resilience in insect pests and populations. The heritability of stress-induced epigenetic alterations may facilitate the emergence of adaptive traits, posing issues for pest management while underscoring the evolutionary significance of epigenetics in insects.

Epigenetic modifications may be inherited by future generations of insect pests, potentially facilitating the emergence of adaptive characteristics like pesticide resistance. Epigenetic inheritance enables fast adaptability to fluctuating environmental conditions, presenting a considerable barrier for pest management (Gupta & Nair, 2022). Research on the brown planthopper, a significant pest of rice, has shown the heritability of stress-induced epigenetic alterations, namely DNA methylation patterns. Nonetheless, these inheritable epigenetic modifications may ultimately be forfeited in the absence of stressors, presenting possible fitness detriments linked to the preservation of the stressed epigenotype (Gupta & Nair, 2022).

The alteration of the methylome in the brown planthopper through 5-azacytidine treatment has been demonstrated to influence the expression levels of stress-responsive genes, underscoring the significance of DNA methylation/demethylation in the stress tolerance of this insect pest (Gupta & Nair, 2022). The innate immune system of insects can respond more swiftly and efficiently to diseases due to prior exposure to antigens. Recent data indicates that epigenetic changes, including DNA/RNA methylation and histone acetylation, can influence the activation of insect immune responses and be inherited by progeny, resulting in the evolution of resistance (Mukherjee & Dobrindt, 2024).

D. Epigenetic Reactions of Insects to Environmental Stressors

Insects have dynamic epigenetic alterations in reaction to several environmental stressors, including temperature fluctuations, pesticide exposure, and nutritional deficits. Epigenetic responses can influence insect physiology and behavior, facilitating swift adaptability to fluctuating environmental conditions. Epigenetic modifications generated by stress, particularly alterations in DNA methylation patterns, can be inherited by successive generations of insects and facilitate the emergence of adaptive features, including pesticide resistance (Chatterjee et al., 2018; Lindeman et al., 2019).

Nilaparvata lugens (Stål) (Hemiptera: Delphacidae) as the brown planthopper, a significant pest of rice, exhibited altered expression levels of stress-responsive genes following 5-azacytidine treatment, indicating the influence of DNA methylation/demethylation on stress tolerance (Lindeman et al., 2019). Environmental stressor-induced epigenetic changes may be inherited and facilitate quick adaptability in insect populations (Chatterjee et al., 2018; Lindeman et al., 2019). However, in the absence of the stressor, these inheritable epigenetic changes can eventually be lost, posing potential fitness costs associated with maintaining the stressed epigenotype (Lindeman et al., 2019).

These results highlight the critical role epigenetic mechanisms play in insects' quick adaptation to changing environmental conditions. Developing effective strategies to manage insect pests and protect beneficial insects requires an understanding of these stress-induced epigenetic responses.

E. Evolutionary Significance of Insect Epigenetics

Insect epigenetics is important for evolution because it plays a crucial role in controlling behavior, development, and adaptation. The function of epigenetic mechanisms in the formation of phenotypic variation in insects has been clarified by recent results (Glastad et al., 2019).

Important components of their evolutionary success include the epigenetic regulation of insect metamorphosis, which includes notable changes in morphology and physiology, the ability of epigenetics to define insect caste and promote phenotypic diversity within a species, the role of epigenetic memory in the emergence of adaptive traits in insects, and the epigenetic modifications they exhibit in response to environmental stressors (Glastad et al., 2019; Oldroyd & Yagound, 2021). Insect physiology and behavior can be influenced by epigenetic reactions, which enable quick adaptation to changing environmental conditions.

According to Amiri (2019) and Mukherjee & Dobrindt (2024), the evolutionary significance of insect epigenetics lies in its ability to control development, provide phenotypic variability, facilitate rapid adaptation to environmental changes, and impact complex behaviors. These results highlight the growing importance of epigenetics in understanding insect biology and ecology, which may have implications for conservation, pest management, and the development of innovative insect-based biotechnologies.

REFERENCES

Amiri, A. (2019). Epigenetic in insects. *Journal of Epigenetics, 1*(1). https://doi.org/10.22111/jep.2019.27953.1007

Cardoso-Júnior, C. A. M., Fujimura, P. T., Santos-Júnior, C. D., Borges, N. A., Ueira-Vieira, C., Hartfelder, K., Goulart, L. R., & Bonetti, A. M. (2017). Epigenetic modifications and their relation to caste and sex determination and adult division of labor in the stingless bee *Melipona scutellaris*. *Genetics and Molecular Biology, 40*(1), 61–68. https://doi.org/10.1590/1678-4685-gmb-2016-0242

Chatterjee, N., Gim, J., & Choi, J. (2018). Epigenetic profiling to environmental stressors in model and non-model organisms: Ecotoxicology perspective. *Environmental Health and Toxicology, 33*(3), e2018015. https://doi.org/10.5620/eht.e2018015

Gibney, E., & Nolan, C. (2010). Epigenetics and gene expression. *Heredity, 105*, 4–13. https://doi.org/10.1038/hdy.2010.54

Glastad, K. M., Hunt, B. G., & Goodisman, M. A. D. (2019). Epigenetics in insects: Genome regulation and the generation of phenotypic diversity. *Annual Review of Entomology, 64*(1), 185–203. https://doi.org/10.1146/annurev-ento-011118-111914

Gupta, A., & Nair, S. (2022). Heritable epigenomic modifications influence stress resilience and rapid adaptations in the brown planthopper (*Nilaparvata lugens*). *International Journal of Molecular Sciences, 23*(15), 8728. https://doi.org/10.3390/ijms23158728

Lindeman, L. C., Thaulow, J., Song, Y., Kamstra, J. H., Xie, L., Asselman, J., Aleström, P., & Tollefsen, K. E. (2019). Epigenetic, transcriptional, and phenotypic responses in two generations of *Daphnia magna* exposed to the DNA methylation inhibitor 5-azacytidine. *Environmental Epigenetics, 5*(3), dvz016. https://doi.org/10.1093/eep/dvz016

Matsuura, K., Mizumoto, N., Kobayashi, K., Nozaki, T., Fujita, T., Yashiro, T., Fuchikawa, T., Mitaka, Y., & Vargo, E. L. (2018). A genomic imprinting model of termite caste determination: Not genetic but epigenetic inheritance influences offspring caste fate. *The American Naturalist, 191*(6), 677–690. https://doi.org/10.1086/697238

Mukherjee, K., & Dobrindt, U. (2024). Epigenetic remodeling in insect immune memory. *Frontiers in Immunology, 15*, 1397521. https://doi.org/10.3389/fimmu.2024.1397521

Okude, G., Moriyama, M., Kawahara-Miki, R., Yajima, S., Fukatsu, T., & Futahashi, R. (2022). Molecular mechanisms underlying metamorphosis in the most-ancestral winged insect. *Proceedings of the National Academy of Sciences, 119*(9), e2114773119. https://doi.org/10.1073/pnas.2114773119

Oldroyd, B. P., & Yagound, B. (2021). The role of epigenetics, particularly DNA methylation, in the evolution of caste in insect societies. *Philosophical Transactions of the Royal Society B: Biological Sciences, 376*(1826), 20200115. https://doi.org/10.1098/rstb.2020.0115

Vaiserman, A. (2015). Developmental epigenetic programming of caste-specific differences in social insects: An impact on longevity. *Current Aging Science, 7*(3), 176–186. https://doi.org/10.2174/1874609807666141129173749

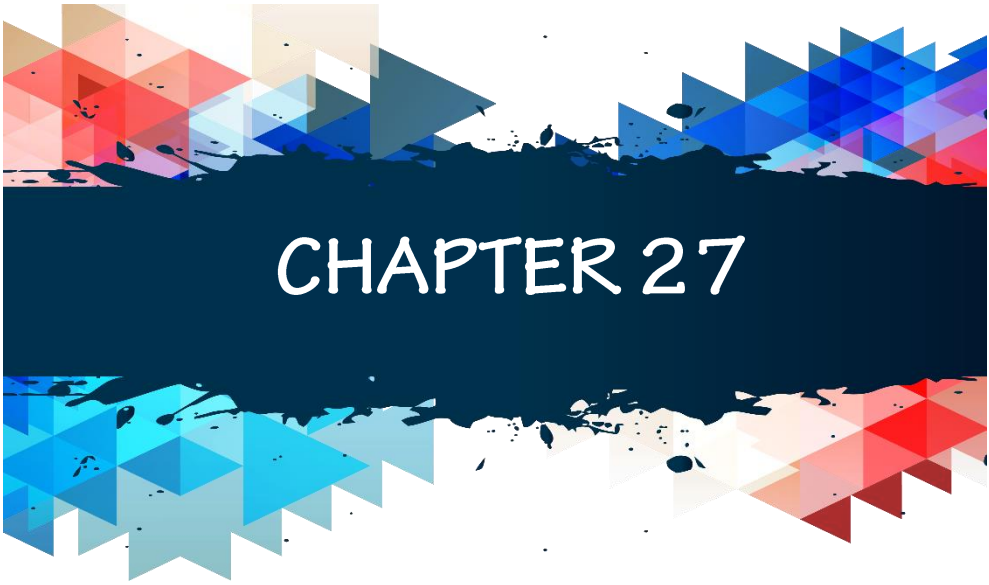

Determination of Antioxidant and Antimicrobial Properties of Bioactive Compounds of Some Macroalgae By Supercritical Carbon Dioxide Method.

MinaaAqeel Adil & Cengiz Akköz[1]

[1] Selcuk University, Faculty of Science, Department of Biology, Konya, Turkey.
*Corresponding author ORCID Code: https://orcid.org/0000-0003-3268-0189

INRODUCTION

Algae, known as primary producers in the aquatic ecosystem, are known to produce a wide variety of secondary metabolites with unique biological activities. (König vd., 1994), Algae are very simple chlorophyll containing organisms (Bold and Wynne, 1985). composed of one cell or grouped together in colonies or as organisms with many cells, sometimes collaborating together as simple tissues. They vary greatly in size unicellular of 3–10 lm (microns) to giant kelps up to 70 m long and growing at up to 50 cm per day (Hillison, 1977).

Algae are found everywhere on earth: in the sea, rivers and lakes, on soil and walls, in animal and plants (as symbionts-partners collaborating together); infact just about everywhere there is a light to carry out photosynthesis. Algae are heterogeneous group of plants with a long fossil history. Two major types of algae can be identified: the macroalgae (seaweeds) occupy the littoral zone, which included green algae, brown algae and red algae, and the micro algae are found in both bentheic and littoral habitats and also throughout the ocean waters as phytoplankton (Garson, 1989)(El Gamal, 2010).

In addition to being used as a food source, they are also used in wastewater treatment and agriculture. On the other hand, living mass can also be used in the production of some chemical substances such as methane gas, antibiotics, carrageenan, and agar (Goldman, 1979)(Demir, 2015).

Recent studies on algae have revealed that bioactive molecules obtained from algae have antibiotic, anticancer, antifungal, antibacterial, anti-inflammatory, hypocholesterolemic, enzyme inhibition, as well as pharmacological effects. These natural products serve not only as raw materials for drugs but also as structural models in the production of synthetic molecules (Quinn et al., 1993). Reports on antimicrobial and antioxidant activity of algae extracts are quite limited compared to plants and are mostly on marine algae rather than freshwater algae. It has also been reported that the composition of phenolic compounds, as with other chemical compounds, can vary both qualitatively and quantitatively depending on species, environmental conditions and algae locations (Orhan et al., 2003; Ibañez et al., 2011).

Macroalgae have a wide application potential in the food, cosmetic and pharmaceutical industries due to the diversity of their composition and the availability of these organisms. In particular, the interest in new natural antimicrobial compounds has been further strengthened by two important trends: the increasing demand for the use of natural ingredients to prevent microbial

contamination and the prevalence of antimicrobial-resistant pathogens (Sharma ve ark., 2020) (Dominguez, 2013) (Li ve ark., 2011).

The identification of antimicrobial compounds from algae and their recovery in environmentally friendly and economical ways, especially through the use of sustainable green extraction technologies, are of great importance in this field.(Sharma ve ark., 2020).

Materials and methods

Collection and preparation of algae

Samples were collected from some macroalgae species belonging to the Chlorophyta *(U. flabellum)*, Rhodophyta (*A. rigida)* and Phaeophyta (*G. barbata)* divisions spread along the coasts of Antalya and Çanakkale.

After the macroalgae collected from the field were washed with pure water, they were placed in an oven set at 40ºc to speed up the drying process and to prevent damage to the phytochemical compounds contained in the samples after this process, and an additional drying process was carried out by keeping them there for 24 hours.

The algae, which were dried appropriately and ground with the help of a homogenizer (ISOLAB), were stored in vacuum bags at room temperature in an airtight manner until the extraction stage. Figure (1), Types of algae.

Gongolaria barbata (Stackhouse) Kuntze *Udotea flabellum*

Amphiroa rigida J.V.Lamour.

Preparation of Macroalgae by Supercritical CO2 Extraction Method

The supercritical extraction of algal species was conducted at Necmettin Erbakan University Medicinal and Cosmetic Plants Practice and Research Center (TİBAM). In accordance with our study purpose in the supercritical CO2 extraction process, 3 different macroalgae types were subjected to extraction process with "P-25 35L Super Critical CO2 Exractor System" (Nantong Borisbang Industrial Technology Co. Ltd) device at 300 bar pressure and 55℃ temperature for 150 minutes in order to obtain the highest phenolic substance yield in the macroalgae content (Keskinkaya et al., 2023).

The solvent used in the supercritical CO2 method is ethanol (ethyl alcohol), a simple chemical compound with the chemical formula C2H6O and a boiling point of 78.4 ° C. Ethanol is a volatile, flammable, colorless liquid with a slightly characteristic odor.

Antioxidant Tests:

Total phenolic determination (TPC) (Folin Ciocalteu Method)

Total phenolic amounts of the extracts were determined using FCR (Folin ciocalteu phenol reagent) as equivalent to gallic acid (Slinkard and singleton, 1977). Solutions containing 1 mg of sample were completed to 1ml (et-oh) and 500µL of FCR and 3 min. Then 300µL of 7.5% Na2Co3 solution were added to this mixture. After the mixture was kept at room temperature for 2 hours with shaking, the absorbances of the samples were read at 765 nm.

Total flavonoid quantification (TFC)

The total flavonoid amounts of the extracts were determined as quercetin equivalents by the aluminum nitrate method. (Moreno et al., 2000). For this purpose, solutions containing 1 mg of sample were completed to 4.8 ml with ethanol and 75µl of 1 M potassium acetate and 5µl of 10% aluminum nitrate solution were added to this mixture. After the samples were kept at room temperature for 40 min, their absorbances were read at 415 nm.

Table 1. TPC and TFC values

Types of Algae	*Determination of Total Phenolic µg GAEs/mg*	***Total Flavinoid Determination µg Qes/mg***
U. flabellum	65.18±0.15	21.69±0.42
A. rigida	19.19±0.004	4.48±0.014
G. barbata	34.85±0.019	12.97±0.074

In our study, antioxidant activities of supercritical CO2 extracts were determined using phenolic substance determination and flavonoid substance determination methods. According to phenolic substance amount determination, phenolic substance concentrations were found as;

19.19±0.004 µg GAEs/mg for *A. rigida*

65.18±0.15 µg GAEs/mg for *U. flabellum*

34.85±0.019 µg GAEs/mg for *G. barbata.*

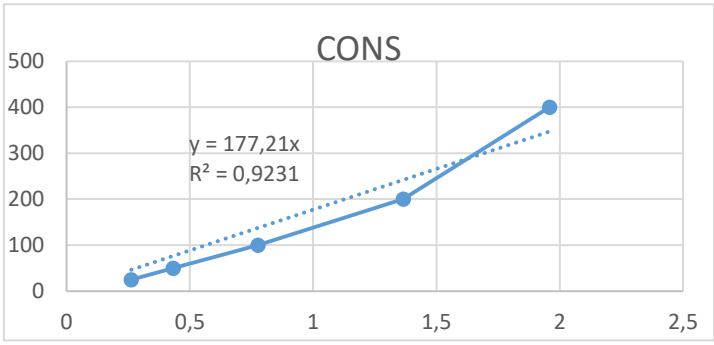

According to flavonoid substance quantity determination, flavonoid substance concentrations were found as;

A. rigida 4.48±0.014 µg QEs/mg

U. flabellum 21.69±0.42 µg QEs/mg

G. barbata 12.97±0.074µg QEs/mg.

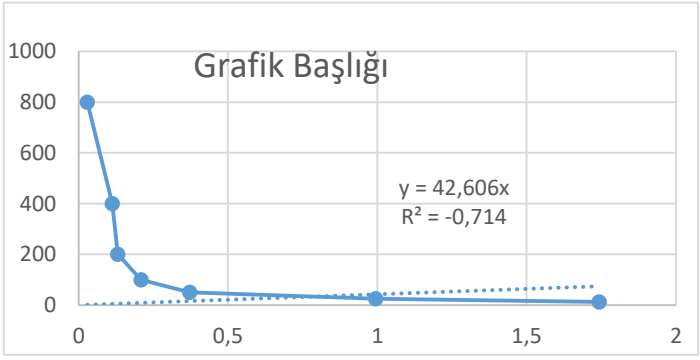

Antimicrobial Test:

Test Microorganisms In the scope of the study, 3gram positive bacteria (*Staphylococcus aureus, Bacillus cereus, Sarcina lutea*) 4 gram negative bacteria (*Escherichia coli, Pseudomonas aeruginosa, Klebsiella pneumoniae, salmonella enteritidis*) 1 fungus was used (*Candida albicans*). A single colony was taken from the bacterial strains incubated at 37 °C for 1 night in Brain Hearth Infusion Agar medium and inoculated into 5 ml Brain Hearth Infusion Broth and the cultures incubated at 37 °C for 18-24 hours were used to determine the antimicrobial effect.

Broth Microdilution Method

In this study, gentamicin was used as a negative control (DMSO) and a positive control in different plates. 100 µl of its 0.1 mg/ml solution was added to the first wells as in the addition of the extract. 0.025 mg/ml-0.02 µg/ml concentrations were obtained between wells 1-12 with dilutions. After these procedures, the lids of the plates were closed and incubated at 37 °C for 18 hours. To indicate the wells with coloration at the end of the incubation period, 20 µl of aqueous 2,3,5-triphenyltetrazolium chloride (ttc) (0.5%) was added to the wells and incubated at 37 °C for another 30 minutes. At the end of the incubation period, the growth in the plates was checked and the lowest extract concentration at which there was no visible growth (non-colored areas), thus inhibiting growth, was evaluated as micro. (M. Albayati 2020).

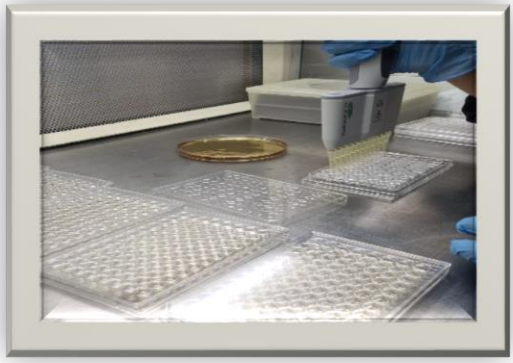

Figure (2) MIC study

Testing Microorganisms	***Amphiroa rigida***	***Gongoloria barbata***	***Udotea felabellum***	***Gentamisin mg/ml***	***Dmso***
Escherichia coli	___	1.56 mg/ml	___	<0.02	3.12
Pseudomonas aeruginosa	1.56 mg/ml	1.56 mg/ml	___	<0.02	3.12
Klebsiella pneumoniae	___	___	___	0.78	3.12
Staphylococcus aureus	3.12 mg/ml	1.56 mg/ml	1.56 mg/ml	<0.02	6.25
Salmonella enteritidis	___	___	___	0.04	3.12
Sarcina lutea	1.56 mg/ml	1.56 mg/ml	1.56 mg/ml	<0.02	3.12
Bacillus cereus	1.56 mg/ml	0.39 mg/ml	0.78 mg/ml	<0.02	3.12
Candida albicans	1.56 mg/ml	0.78 mg/ml	1.56 mg/ml	<0.02	3.12

Table (2)

According to the results of the antimicrobial tests of the supercritical CO2 extracts;

A. rigida was seen against S. aureus strain (MIC: 3.12mg/ml), P. aeruginosa, S. lutea, B. cereus strains (MIC: 1.56mg/ml) were seen. *G. barbata* extract was determined against B. cereus strain (MIC: 0.39mg/ml), *E. coli, P. aeruginosa, S. aureus, S. lutea* (MIC: 1.56mg/ml) were determined. *U. flabellum* extract was determined against B. cereus strain (MIC: 0.78mg/ml), *S. aureus, S. lutea* (MIC: 1.56mg/ml). Antifungal activity against the fungus strain *Candida albicans G. barbata (MIC: 0.78mg/ml).*

Results and Discussion

In the study conducted by Keskinkaya et al. (2023), the total phenolic (TPC) and total flavonoid (TFC) contents of the extracts (OE1 and OE2, respectively) obtained under 150 bar and 300 bar pressures with the supercritical CO2 extraction method (SCFE) of olive leaves belonging to the variety Olea europaea L. Subs. Oleaster (delice olive), which has an important potential, were calculated as 2418.80±102.1 - 3951.46±123.7 µg GAEs/mg extract and 384.61±16.8 - 491.70±27.3 µg QEs/mg extract, respectively. As a result, *O. europaea* subs. It has been observed that oleaster leaf extracts have a very strong richness in phenolic compounds and flavonoids have very interesting antioxidant potential.

In their study, Melis et al. (2021) investigated the antioxidant activities, tpc and tfc contents of algal extracts obtained from *Gongolaria barbata* using different solvents, respectively, ethyl acetate (acoet), water (w) and phosphate buffer (ph). According to the results, etoh, W and PB solvents, The highest total flavonoid content was determined as W (6.91±0.09 mg/g ext.) and PB showed the highest phenolic content (2.29±0.01 mg GAE/g ext.). According to the results of the studies, when the antioxidant contents, total phenolic and flavonoid contents of *Gongolaria barbata* were examined, it was determined that phosphate buffer was a solvent that could be used instead of ethanol.

Keskinkaya et al (2022) aimed to investigate the chemical composition, antimicrobial and antioxidant activities (by 3 methods), (TPC) and (TFC) contents of methanol, ethanol, acetone and water extracts of *Codium fragile* (suringar) hariot 1889. LC-ESI-MS/MS analyses allowed the identification of seven compounds including gallic acid, 4-hydroxybenzaldehyde, 4-hydroxybenzoic acid, p-coumaric acid, salicylic acid, biochanin A and diosgenin. TPC and TFC values of the extracts were calculated as 10.34±0.13-64.67±0.02 µg gaes/mg extract and 12.73±2.68-36.78±1.08 µg qes/mg extract, respectively. methanol, ethanol and acetone extracts showed different levels of activity against gram-negative and gram-positive bacteria (MIC: 3.125-1.562 mg/ml). Water extract showed the highest activity in ABTS•+ (70.43±14.85%) and DPPH• (72.61±11.44%) tests, while acetone extract showed the highest activity in CUPRAC (absorbance: 0.60±0.15) test. In conclusion, *C. fragile* can be used as a natural source of bioactive substances in food preservatives and other industrial and pharmaceutical fields.

Yiğitkurt, S et al, 12 macroalgae species selected from the coasts of Izmir Bay of the Aegean Sea; Green algae Ulva rigida, Ulva lactuca, Ulva compressa, Chaetomorpha linum,Red algae Gracilaria verrucosa, Gracilaria gracilis,

Laurancia papillosa, Laurencia obtusa, Corallina officinalis and Brown algae Cystoseira barbata, Cystoseira crinita, Halopteris scoparia. Pigments (chlorophyll-a and total carotenoids) in the samples were analyzed by spectrophotometric method. The highest total carotene amount was determined as 0.532±0.01 mg/gr in Chaetomorpha linum (Chlorophyta). The lowest total carotene amount was measured as 0.020±0.002 mg/gr in Ulva lactuca. The highest amount of chlorophyll-a was determined as 0.319±0.008 mg/gr in Chaetomorpha linum (Chlorophyta), while the lowest was measured as 0.034±0.0003 mg/gr in Gracilaria verricosa and 0.035±0.004 mg/gr in Laurencia obtusa. macroalgae species have high levels of pigment values. As a result, the economic values of pigment sources of some macroalgae species in Izmir Bay were revealed.

C.Akköz et al (2009), Antioxidant activity of *Enteromorpha intestinalis* was determined by three different methods. Total phenolic concentration of extracts was estimated by Folin-Ciocalteu reagent using gallic acid as standard. Free radical scavenging activities were determined based on 1,1-diphenyl-2-picrylhydrazyl radical (DPPH). Copper (II) ion reducing ability of polyphenols was measured by CUPRAC method. Results were compared with standards butylated hydroxytoluene (BHT) and butylated hydroxyanisole (BHA). Results were obtained in triplicate and data are presented as mean ± standard deviation of three determinations (data not shown). Statistical analyses were performed using one-way analysis of variance.

According to the results obtained in this study on the antioxidant activity and antimicrobial activity of the presence of phenolic compounds such as phenol and flavonoids, steroid structures and pigments such as carotenoids in algae, the highest phenolic and flavonoid amounts were determined in the ethanol extract of *U. flabellum* from green algae (65.18±0.15 µg GAEs/mg), (21.69±0.42µg QEs/mg). The highest antimicrobial activity against the studied test pathogens was seen in the supercritical CO2 extract of *G. barbata* from brown algae and the most effective strain was determined as the gram (+) bacteria strain B. cereus (MIC: 0.39 mg/ml). The antifungal activity of *G. barbata* was measured at the highest level against *C. albicans* strain (MIC: 0.78 mg/ml|). By determining the antioxidant and antimicrobial capacities of the algae samples we studied, we will be able to use these algae as protective and supplementary foods and natural preparations, especially in the field of health. These studies will also lead to drug development.

REFERENCES

König, G. M., Wright, A. D., Stiche, O., Angerhofer, C. K. and Pezzuto, J. M. (1994). Biological activities of selected marine natural products. Planta Medica; 60, 532-537.

Bold, H.C., Wynne, M.J., 1985. Introduction to the algae structure and reproduction, second ed., Prentice-Hall Inc., Englewood Cliffs, NJ, 07632, pp. 1–33.

Hillison, C.I., 1977. Seaweeds, a color-coded, illustrated guide to common marine 1977. Plants of east coast of the United States, Keystone Books. The Pennsylvania State University Press, pp. 1–5.

Goldman, A. 1979. ―What Is Justified Belief? in G. Pappas, ed. Justification and Knowledge (Dordrecht: D. Reidel), 1-23.

Garson, J., 1989. Marine natural products. Nat. Prod. Rep. 6, 143– 170.

Orhan, I., Wisespongpand, P., Aticl, T., ve Sener, B. (2003). Toxicity propensities of some marine and fresh water algae as their chemical defence. Journal of Faculty of Pharmacy of Ankara; 32, 19-29.

Demir, H., 2015, İskenderun Körfezi alglerinin antioksidan ve antimikrobiyal özelliklerinin belirlenmesi, *Hatay Mustafa Kemal Üniversitesi*.

Dominguez, H., 2013, Functional ingredients from algae for foods and nutraceuticals, Elsevier, p.

El Gamal, A. A., 2010, Biological importance of marine algae, *Saudi pharmaceutical journal*, 18 (1), 1-25.

Li, Y.-X., Wijesekara, I., Li, Y. ve Kim, S.-K., 2011, Phlorotannins as bioactive agents from brown algae, *Process biochemistry*, 46 (12), 2219-2224.

Sharma, K., Guleria, S., Razdan, V. K. ve Babu, V., 2020, Synergistic antioxidant and antimicrobial activities of essential oils of some selected medicinal plants in combination and with synthetic compounds, *Industrial Crops and Products*, 154, 112569.

Sharma, K.; Guleria, S.; Razdan, V.K.; Babu, V. Synergistic antioxidant and antimicrobial activities of essential oils of some selected medicinal plants in combination and with synthetic compounds. Ind. Crop. Prod. 2020, 154, 112569. [Google Scholar] [CrossRef].

Abu-Ghannam, N.; Rajauria, G. Antimicrobial activity of compounds isolated from algae. In Functional Ingredients from Algae for Foods and Nutraceuticals; Woodhead Publishing Limited: Shaston, UK, 2013; pp. 287–306. ISBN 9780857095121. [Google Scholar].

Ak, i., 2015, sucul ortamın ekonomik bitkileri; makro algler, *dünya gıda dergisi, 12, 88-97.*

Mchugh, d. J., 2003, A guide to the seaweed industry.

Keskinkaya HB., Üstün Argon Z., Doğu S.,Akdağ T., 2023. Phenolic content and in-vitro antioxidant activity of olea europaea L. Subs. Oleaster leaves by supercritical CO2 extraction, *ereğli tarım bilim. Derg, 3, 75-85.*

Yılmaz, m., Türker, G. Ve ak, İ., 2021, the effect of different solvents on antioxidant properties of gongolaria barbata (phaeophyceae), *çanakkale onsekiz mart university journal of marine sciences and fisheries, 4 (2), 197-201.*

Ak, i., Çankırılıgil, E. C., Türker, G., Sever, O. Ve abomohra, A., 2022, enhancement of antioxidant properties of gongolaria barbata (phaeophyceae) by optimization of combined light intensity and salinity stress, *phycologia, 61 (6), 584-594.*

Suleria, H. A. R., Gobe, G., Masci, P. Ve osborne, S. A., 2016, marine bioactive compounds and health promoting perspectives; innovation pathways for drug discovery, *trends in food science & technology, 50, 44-55.*

Akyıl, s., İlter, I., Koç, M. Ve kaymak-ertekin, F., 2016, alglerden elde edilen yüksek değerlikli bileşiklerin biyoaktif/biyolojik uygulama alanları, *akademik gıda, 14 (4), 418-423.*

Keskinkaya, H. B., Deveci, E., Güneş, E., Okudan, E. Ş., Akköz, C., Gümüş, N. E. Ve karakurt, S., 2022, chemical composition, in vitro antimicrobial and antioxidant activities of marine macroalgae codium fragile (suringar) hariot, *commagene journal of biology, 6 (1), 94-104.*

Slinkard, K. ve singleton, V. L., 1977, total phenol analysis: automation and comparison with manual methods, *american journal of enology and viticulture, 28 (1), 49-55.*

Albayati, m. A. F., 2020, bazı makroalg türlerinin antimikrobiyal aktivitelerinin belirlenmesi. Sü, Fen bilimleri, y.l tezı, 20-36.

Akköz, C., Tekeli, Y. Ve dogan, H. H., 2009, in vitro antioxidant activity of enteromorpha intestinalis (linnaeus) nees, *asian journal of chemistry, 21 (8), 6525.*

Yiğitkurt, S., Kırtık, A., Uğur, S. Ve durmaz, Y., 2020, izmir körfezi kıyılarından toplanan makroalglerin pigment potansiyeli, *menba kastamonu üniversitesi su ürünleri fakültesi dergisi, 6 (2), 45-52.*

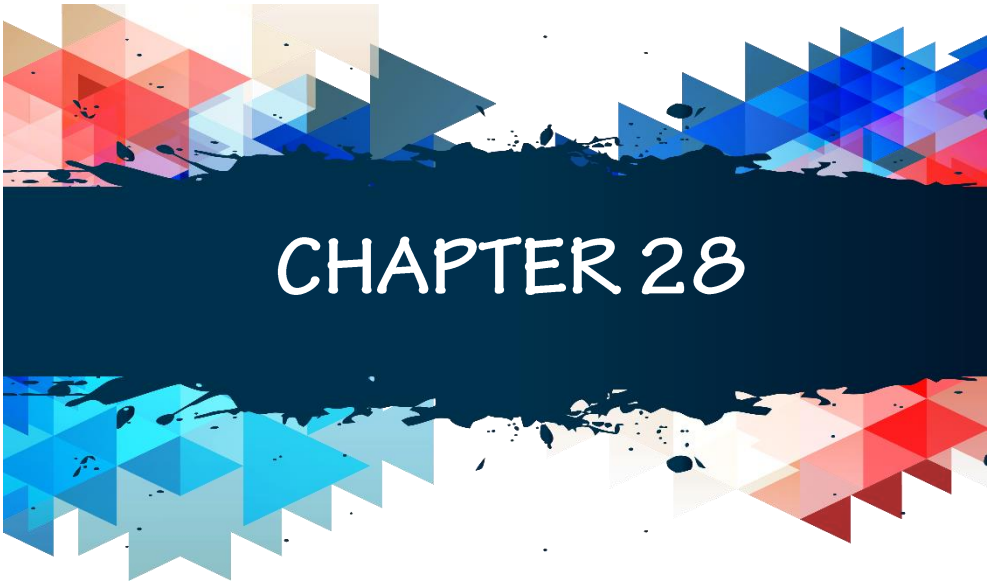

Fertilizers Derived From Marine Plants

***Gözde Hafize Yıldırım*[2]**

[2] Research Assistant Dr., Recep Tayyip Erdoğan University, Faculty of Agriculture, Department of Field Crops, Rize/Turkey, Orcid: 0000-0002-0557-6442

INTRODUCTION

Seaweeds have gained attention as a natural agricultural input in many countries today, both in liquid extract form and through direct soil incorporation. When applied directly to the soil, the aim is to improve soil structure and maintain productivity in the long term. For centuries, some seaweeds carried to shore by natural marine processes have been utilized as fertilizers in agricultural fields (Güner and Aysel, 1996). Seaweed extracts offer numerous advantages in agricultural production, holding a significant place in organic farming. These benefits include reducing post-harvest losses of fruits, increasing crop yields, enhancing the uptake of inorganic nutrients from the soil, accelerating seed germination, and improving plant resistance to stress conditions. As a result, they are widely used, especially in developed countries (Blunden, 1991; Özenç and Şen, 2017).

These natural fertilizers stimulate robust root development in plants, allowing them to absorb more nutrients and water from the soil. Additionally, they support chlorophyll formation, increase the green biomass of plants, and bolster resistance to environmental stresses, diseases, and pests. By ensuring a balanced and consistent intake of macro and microelements, seaweed fertilizers improve yield, enhance quality, and elevate the market and export value of crops (Blunden et al., 1992; Hong et al., 1995; Özenç and Şen, 2017).

The positive effects of seaweeds on plant growth have been demonstrated in various studies, showing significant improvements in parameters such as germination, seedling vigor index, shoot and root length (Layek et al., 2018). Mukherjee and Patel (2020) reported that seaweed promotes plant growth, seedling development, root sheath formation, and secondary root emergence, as well as enhances fruit setting and resistance to pests and diseases, effectively managing stresses such as drought and salinity. These algae are also noted for containing plant growth-regulating phytohormones like auxins, cytokinins, and gibberellins (Maemunah et al., 2019).

Seaweed fertilizers are used via two main methods: soil application and foliar application. In soil applications, they nourish beneficial microorganisms in the rhizosphere and increase the soil's water-holding capacity (Van Oosten et al., 2017). Foliar applications have shown positive results in crops such as grapevine, watermelon, strawberry, apple, tomato, spinach, onion, beans, pepper, carrot, potato, wheat, corn, barley, and rice. These applications have resulted in stronger growth, higher yields, and increased mineral and nutrient content compared to

plants not treated with seaweed (Uppal et al., 2008; Jayaraman et al., 2011; Aroujoa et al., 2012; El Modafar et al., 2012; Shah et al., 2013).

Seaweed applications also enhance flowering and fruiting abilities, improving product quality and yield while increasing resistance to abiotic stress conditions (Jayaraj et al., 2008; Zhang and Ervin, 2008; Çelebi and Ağırağaç, 2022). This review aims to elucidate the fundamental characteristics of seaweed-based fertilizers, the effects of their biological and chemical components, and their positive impacts on plants.

SEAWEED-BASED FERTILIZERS

Seaweeds are categorized into four main types: Rhodophyta (red algae), Phaeophyta (brown algae), Chlorophyta (green algae), and Cyanophyta (blue-green algae). Depending on the type, their compositions vary and include macroelements such as nitrogen, calcium, and magnesium, as well as microelements like iron, zinc, and copper (Hong et al., 1995). Additionally, the presence of betaines and growth-regulating substances enhances plant resilience to environmental stress conditions.

In recent years, microalgae have garnered considerable interest due to their high protein, vitamin, mineral, fatty acid, and pigment content. Nitrogen-fixing species of these organisms, in particular, have been noted for their potential in promoting plant growth in agricultural applications. Blue-green algae, utilizing their photosynthetic mechanisms, produce carbon from carbon dioxide and water and also fix nitrogen. Their energy independence and nitrogen-fixing capacities make them a significant biomass resource in agriculture (Roger and Reynaud, 1982).

Seaweeds are also considered a sustainable resource for enhancing agricultural production. Liquid seaweed extracts, which promote plant growth, are used to improve crop yields. Various studies have shown that dried algal biomass cultivated under anaerobic conditions can be utilized in agricultural products to provide nitrogen (N) and phosphorus (P) distribution. Applying algal biomass as fertilizer has proven to be a more efficient method than conventional fertilizers. In garden systems, specifically, dried algal biomass has been found to outperform traditional fertilizers in supporting plant growth (Mulbry et al., 2005).

Foliar application of seaweed extracts offers significant benefits in agricultural production. It supports root development in plants, enabling them to absorb more nutrients and water from the soil. Additionally, it accelerates chlorophyll production, fostering increased green biomass. These extracts

enhance plant resistance to diseases, pests, and environmental stress factors, while facilitating the uptake of macro and micro nutrients from the soil. Furthermore, they improve yield and quality, enrich the soil's beneficial microorganism population, and exhibit vast potential in agricultural practices (Mancuso et al., 2006; Alam et al., 2013).

In modern agriculture, seaweed-based fertilizers are commonly applied via foliar spraying and have shown effective results in improving product quality (Blunden, 1991). Brown seaweeds, widely used in France for strawberry production, have yielded positive outcomes in greenhouse cultivation (Whapham et al., 1994). Similarly, large thallus algae in the United States and brown algae in Europe are frequently preferred for fertilization purposes. As a natural fertilizer, seaweed-based fertilizers are vital in promoting plant development, particularly by encouraging root growth, enhancing resilience to environmental stresses, and improving product quality.

Research on tomato plants has demonstrated that seaweed accelerates root growth, mitigates root-knot nematode damage, and supports rooting in laboratory conditions (Şen, 2015).

CONTRIBUTIONS OF SEAWEED FERTILIZERS TO PLANT GROWTH

Biostimulants produced from macro and microalgae positively affect plant metabolism, improving numerous processes. Vital functions such as respiration, chlorophyll production, photosynthesis, nucleic acid synthesis, and ion uptake are enhanced by these products. Additionally, these biostimulants increase water retention capacity and support antioxidant formation in plants (Sharma et al., 2014). The effects of seaweed and its derivatives on plant growth have been observed to be more pronounced under favorable environmental conditions, such as optimal temperature, water, and nutrient availability. Under such conditions, the absence of harmful pathogens leads to more robust plant responses (Calvo et al., 2014).

One of the most active components of seaweed extracts is believed to be plant hormones. These hormones are low molecular weight compounds derived from different chemical groups and can significantly impact plant metabolism even at very low concentrations. However, higher doses of these hormones may have adverse effects on plants, potentially disrupting critical biological processes (Tarakhovskaya et al., 2007). Seaweeds also contain phenolic compounds and flavonoids with strong antioxidant properties. The biosynthesis of these compounds increases following plant exposure to stress factors. Particularly in

species like *Fucus vesiculosus*, *Fucus serratus*, and *Ascophyllum nodosum*, the total content of these compounds is notably high. Brown algae contain more phlorotannins than green and red algae, with their dry matter content reaching up to 25-30%, compared to approximately 10% in green and red algae (Singh and Sidana, 2013).

To investigate the effects of seaweeds on plant growth, a greenhouse experiment was conducted using the species *Ascophyllum nodosum*. This study evaluated the effects of foliar application of a seaweed extract (AZAL5) on the growth, nutrient uptake, and yield of winter wheat. Experiments were carried out on soils with water retention capacities of 75% and 45%, with or without additional nitrogen fertilizer. AZAL5, applied at two different concentrations, showed positive effects on all parameters, including growth and nutrient uptake, but only when nitrogen fertilizer was present. This suggests that seaweed extracts help plants utilize soil nutrients more efficiently. In cases where water retention capacity was reduced, doubling the concentration of seaweed extract was required to achieve similar beneficial effects (Stamatiadis et al., 2014).

The agricultural benefits of seaweed-based fertilizers are diverse. These fertilizers support plant growth and yield, as evidenced by their promotion of vegetative growth in Clementine mandarin (Şimşek, 1995). Their biologically active compounds enhance photosynthesis, improving both yield and quality (Ali et al., 2021). Furthermore, they have been reported to accelerate root growth and support seed germination (Demirkaya, 2010).

The impact of these fertilizers on soil is also significant. Seaweed-based fertilizers increase the organic matter content of the soil, improving its water retention capacity (Dede et al., 2011). In the United Kingdom, they are used as soil conditioners in arid and nutrient-poor soils (Güner and Aysel, 1996). Studies on Granny Smith apple varieties have shown that seaweed-based fertilizers improve yield and quality in organic farming systems (Yaman and Özkan, 2009).

Abiotic stress conditions, such as salinity and drought, are significant challenges in agricultural production. Seaweed extracts have been found to improve germination rates in leeks under saline conditions (Yıldırım and Güvenç, 2005). Fertilizers derived from seaweeds like *A. nodosum* and *E. maxima* have demonstrated their ability to enhance plant resilience to stress conditions and improve crop performance (Al-Ghamdi et al., 2018). These effects provide notable advantages for farmers operating in challenging environmental conditions, such as drought.

The effects of seaweed-based fertilizers on fruit and vegetable production are also noteworthy. They have been reported to increase both yield and quality in crops such as tomatoes, strawberries, and carrots (Kasım et al., 2015). In tomato plants, these fertilizers have been observed to enhance flowering rates and provide resistance against fungal diseases (Al-Ghamdi et al., 2018).

CONCLUSION

Seaweed-based fertilizers hold a significant position in modern agriculture in terms of environmental sustainability and crop productivity. As a natural source of fertilizer, seaweeds provide a wide range of benefits, from supporting plant growth to improving soil structure. Thanks to their macro and microelement content, plant hormones, and biologically active compounds, seaweed-based fertilizers promote root development, enhance photosynthesis, and boost resistance to abiotic stress conditions. By applying these fertilizers through foliar or soil methods, plants can achieve more efficient nutrient uptake and exhibit stronger growth. These products, which increase plant resilience in stress conditions like drought and salinity, also visibly enhance yield and quality in agricultural production.

REFERENCES

Alam, M. Z., Braun, G., Norrie, J., & Hodges, D. M. 2013. Effect of Ascophyllum extract application on plant growth, fruit yield and soil microbial communities of strawberry. Can J. Plant Science, 93, 23-36.

Al-Ghamdı, A.A., Elansary, H. O.2018. Synergetic effects of 5-aminolevulinic acid and *Ascophyllum nodosum* seaweed extracts on *Asparagus phenolics* and stress related genes under saline irrigation. Plant Physiol. Biochem, 129:273-284.

Alı, O., Ramsubhag, A., Jayaraman, J. 2021. Biostimulant properties of seaweed extracts in plants: Implications towards sustainable crop production. Plants (Basel). 10:531-558.

Blunden G., Whapham, C., Jenkıns, T., 1992. Seaweed Extracts in Agriculture and Horticulture: Their Origins, Uses and Modes of Action. School of Pharmacy and Biomedical Science and "School of Biological Sciences, University of Portsmouth, King Henry John Street, Portsmouth, Hampshire P01 202, U.K.

Blunden, G., 1991. Agricultural Uses of Seaweeds and Seaweed Extracts. In: Seaweed Resources in Europe: Uses and Potential. Pp.65-81. John Wiley and Sons, Chichester.

Calvo, P., Nelson, L. & Kloepper, J.W. 2014. Agricultural uses of plant biostimulants. Plant and Soil, 383, 3-41.

Çelebi, Ş. Z., & Ağırağaç, Z. (2022). Karasal İklimde Yetiştirilen İkinci Ürün Mısırın Silaj Verimi Üzerine Deniz Yosunu Uygulamasının Etkisi. *ISPEC Journal of Agricultural Sciences, 6*(1), 7-19.

Dede, H. Ö., Dede, G., Özdemir, S. 2011. Toprağa deniz yosunu (Ulva lactuca) karıştırılmasının, toprağın su tutma kapasitesine etkisi ve zaman içindeki değişimi. Sakarya Üniversitesi, Fen Bilimleri Dergisi, Cilt 15, Sayı 1, 30-35.

Demirkaya, M., 2010. Deniz yosunu (*Ascophyllum nodosum*) ekstraktı uygulamalarının biber ve soğan tohumlarının canlılığı ve gücüne etkileri. Erciyes Üniversitesi Fen Bilimleri Enstitüsü Dergisi, 26(3): 217-224.

Güner, H., Aysel, V. 1996. Tohumsuz Bitkiler Sistematiği. 1. Cilt (Algler). Ege Üniversitesi Fen Fakültesi Kitaplar Serisi, No.108, Bornova, İzmir.

Hong, Y.P., Chen, C.C., Cheng, H.L., Lyn, C.H. 1995. Analysis of auxin and cytokinin activity of commercial Aqueous Seaweed Extract. Gartenbauwissenschaft, 60(4), p. 191-194. Verlag Eugen Ulmer GmbH & Co. Stuttgart.

Jayaraman, J., Norrie, J., Punja, Z. K. 2011. Commercial extract from the brown seaweed Ascophyllum nodosum reduces fungal diseases in greenhouse cucumber. Journal of Applied Phycology, 23(3): 353-361.

KASİM, W.A.; HAMADA, E.A.M.; SHAMS EL-DİN, N.G.; ESKANDER, S.K. Influence of Seaweed Extracts on the Growth, Some Metabolic Activities and Yield

of Wheat Grown under Drought Stress. Int. J. Agron. Agric. Res. 2015. 7:173–189.

Layek. J., Das, A., Ramkrushna, G.I., Sarkar, D., Ghosh, A., Zodape, S.T., Lal, R., Yadav, G.S., Panwar, A.S., Ngachan, S., Meena, R.S. 2018. Seaweed extract as organicbiostimulant improves productivity and quality of rice in eastern Himalayas. Journal of Applied Phycology, 30(1): 547-558.

Maimunah, Y., Kilawati, Y. 2019. Profil hemosıt udang vannameı yang dıınfeksı wssv (White Spot Syndrome Virus) dengan ımmunostımulası alga laut. Fish Scientiae, 9(1): 24-34.

Mancuso, S., Azzarello, E., Mugnai, S., Briand, X., 2006. Marine bioactive substances (IPA extract) improve foliar ion uptake and water tolerance in potted Vitis vinifera plants. Advances in Horticultural Science 20,156–161.

Mukherjee, A., Patel, J.S. 2020. Seaweed extract: biostimulator of plant defense and plant productivity. International Journal of Environmental Science and Technology, 17(1): 553-558.

Mulbry, W., Westhead, K., Pizzarro, C. and Sıkora, L. 2005. Recycling of Manure Nutrients: Use of Algal Biomass From Dairy Manure Treatment As a Slow Release Fertilizer. BioresourceTechnology 96, 451–458.

Özenç, D. B., & Şen, O. (2017). Farklı gelişim dönemlerinde uygulanan deniz yosunu gübresinin domates bitkisinin gelişim ve bazı kalite özelliklerine etkisi. *Akademik Ziraat Dergisi*, *6*, 235-242.

Roger, P.A. and Reynaud, P.A. 1982. Free living blue-green algae in tropical soils. Dommergues H. Diem eds. Microbiology of tropical soils and plant productivity. Martinus Nijhoff Publisher La Hague. pp 147-168.

Sharma, H.S.S., Fleming, C., Selby, C., Rao, J.R., Martin, T., 2014. Plant biostimulants: a review on the processing of macroalgae and use of extracts for crop management to reduce abiotic and biotic stresses. J. Appl. Phycol. 26,465–490.

Singh, I. P. & Sidana, J. 2013. Phlorotannins. Functional Ingredients from Algae for Foods and Nutraceuticals

Stamatiadis, S., Evangelou, L., Yvin, J.C., Tsadilas, C., Mina, J.M.G. & Cruz, F. 2014. Responses of winter wheat to Ascophyllum nodosum (L.) Le Jol. extract application under the effect of N fertilization and water supply. Journal of Applied Phycology, 27, 589-600.

Şen, O. (2015). *Aşılı ve aşısız domates çeşitlerinin bitki gelişimi ve bazı kalite özellikleri üzerine deniz yosunu gübresi uygulamalarının etkisi* (Master's thesis, Fen Bilimleri Enstitüsü).

Şimşek, Z. 1995. Klemantin Mandarininde Bilezik Alma, Demir Bileşikleri ve Deniz Yosunu Özü Uygulamalarının Verim ve Kalite Üzerine Etkileri. Yüksek Lisans Tezi. Akdeniz Üniv. Zir. Fak. Bahçe Bitkileri Bölümü, Antalya.

Tarakhovskaya, E.R., Maslov, Y.I. & Shishova, M.F. 2007. Phytohormones in algae. Russian Journal of Plant Physiology, 54, 163-170.

Uppal, A.K., El Hadrami, A., Adam, L.R., Tenuta, M., Daayf, F. 2008. Biological control of potato Verticillium wilt under controlled and field conditions using selected bacterial antagonists and plant extracts. Biological Control, 44(1): 90-100.

Van Oosten, M.J., Pepe, O., De Pascale, S., Silletti, S., Maggio, A. 2017. The role of biostimulants and bioeffectors as alleviators of abiotic stress in crop plants. Chemical and Biological Technologies in Agriculture, 4(1), 1-12.

Whapham, C.A., Blunden, G., Jenkins, T., Hankins, S.D. 1994. The role of seaweed extracts, *ascophyllum nodosum*, in the reduction in fecundity of meloidogyne javanica. Fundam. Appl. Nematol., 17(2): 181-183.

Yaman, F., Özkan. Y., 2009. Farklı organik materyal uygulamalarının Granny Smith elma çeşidinin performansı ve yaprak besin maddesi içeriği üzerine etkileri. Tarım Bilimleri Araştırma Dergisi, 2 (2): 123-132.

Yıldırım, E., Güvenç, İ. 2005. Deniz yosunu özü uygulamalarının tuzlu koşullarda pırasada tohum çimlenmesi üzerine etkisi. Bahçe, 34(2): 83-87.

Zhang, X., Ervin, E.H. 2008. Impact of seaweed extract- based cytokinins and zeatin riboside on creeping bentgrass heat tolerance. Crop Science, 48(1): 364-370.

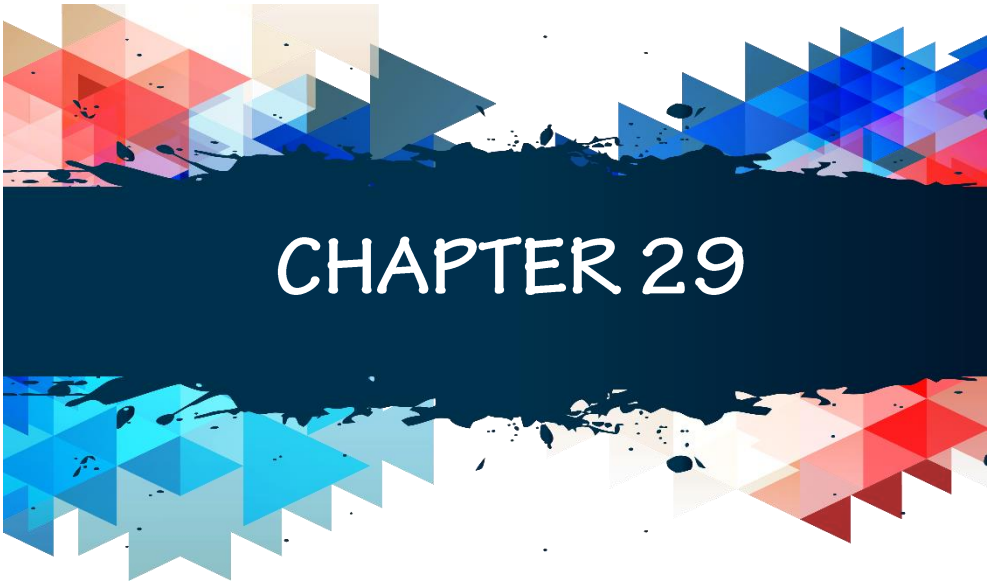

Energy Production From Cereals

***Gözde Hafize Yıldırım*[1]**

[1] Research Assistant Dr., Recep Tayyip Erdoğan University, Faculty of Agriculture, Department of Field Crops, Rize/Turkey, Orcid: 0000-0002-0557-6442

INTRODUCTION

Humankind's energy demand has far exceeded the natural energy resources required by other living organisms and plants, and this demand continues to grow. During the early stages of the industrial revolution, energy needs were met through resources like coal and wood. However, with the development of internal combustion engine technology, fossil fuels, particularly petroleum, became the dominant source of energy. The rapid pace of industrial development, coupled with population growth driven by increased prosperity, has accelerated the consumption of energy resources. Over the past half-century, energy has become one of the most critical topics in global politics.

Today, the desire to possess advanced technology and control global energy resources is a primary driver of international competition. It is widely recognized that primary energy sources such as coal, oil, and natural gas are finite and will eventually be depleted. Given that 81% of global energy production still relies on fossil fuels (Anonymous, 2021), the necessity of transitioning to alternative energy sources becomes increasingly apparent. The environmental damages caused by fossil fuels have highlighted the importance of sustainable and eco-friendly energy sources. Renewable energy sources like bioethanol and biogas play a crucial role in ensuring energy security and contributing to environmental sustainability. Cereals and grasses, with their high carbohydrate and lignocellulosic content, serve as fundamental resources for producing these renewable energy sources.

Bioenergy (BE) refers to energy obtained from organic materials such as plants, forests, animal waste, urban waste, energy crops, and energy forests. This energy can be transformed through traditional or modern technological methods. Many countries have set goals to increase the use of biomass resources to meet the greenhouse gas reduction targets outlined in the Kyoto Protocol (Kyoto Protocol, 1997; Aslantaş, 2018). Cereals such as wheat, corn, barley, and sorghum have significant potential in energy conversion processes. The products and by-products obtained from the agricultural production of these crops can be used to produce bioethanol and biogas. Utilizing cereal waste not only enhances energy production but also contributes to waste management and agricultural development. These processes support the principles of a circular economy in the agricultural sector, offering both economic and environmental benefits. The purpose of this review is to provide an overview of the energy production potential of cereals and highlight their contributions to sustainability.

USE OF CEREALS FOR BIOENERGY

Global energy demand is rapidly increasing due to population growth and accelerated industrial development (Zhu et al., 2005). As of 2006, the average annual per capita energy consumption was measured at approximately 2 tons of oil equivalent (Anonymous, 2010). Today, per capita energy consumption in industrialized countries significantly exceeds the global average, creating severe energy security and supply challenges in developing nations. The limited nature of fossil fuels and their adverse environmental impacts have underscored the importance of renewable energy sources (Shafiee & Topal, 2009; Barbir et al., 1990). International agreements such as the Kyoto Protocol emphasize the need to reduce the environmental impacts of fossil fuels and promote sustainable energy sources (Schlamadinger et al., 2007). Among renewable energy options, biofuels stand out due to their simplicity of production and compatibility with existing infrastructure (Gross et al., 2003).

Among biofuel types, bioethanol holds significant potential for the energy and transportation sectors. Its equivalence to gasoline, ease of transportation, and storability make bioethanol a sustainable alternative to fossil fuels (Demirbas, 2009). Furthermore, its seamless integration with existing oil and natural gas infrastructure enhances its feasibility (Gross et al., 2003). Bioethanol is produced through the fermentation of glucose by yeast, a process similar to beer and wine production methods (Liu et al., 2008; Anonymous, 2010; Harrison & Moselio, 2009).

Cereals and other plants convert solar energy into chemical energy through photosynthesis, producing building blocks like glucose. However, in cereals, glucose is typically stored in polysaccharide forms such as starch or cellulose (Leegood et al., 2004; Bergthaller et al., 2007; Jarvis & Brian, 2009). In bioethanol production, breaking down these complex carbohydrates into glucose is a critical step. This involves milling to break plant tissues and increase active surface area, followed by enzymatic hydrolysis to produce glucose-rich hydrolysate [28]. Enzyme mixtures such as glucoamylase and protease are commonly used in this process and can be sourced from various suppliers or purchased commercially (Melikoğlu & Albostan, 2011).

The starch content in cereals is a crucial resource for bioethanol production. Crops like wheat, barley, and rye, with their high starch content, are effectively utilized in fermentation processes. Notably, corn accounts for approximately 80% of global bioethanol production, underscoring its critical role in this sector (Karimi & Chisti, 2017). In Turkey, molasses derived from sugar beets is widely

used for bioethanol production, yielding 1 ton of ethanol from 100 tons of sugar beets (Oruç, 2008). In recent years, the use of lignocellulosic materials such as straw, hay, and bran for energy production has gained traction. This approach contributes to sustainable energy production by utilizing non-food resources (Karmee, 2016). Additionally, by-products from cereal milling processes, such as fine flour and sub-quality flour, can be utilized for bioethanol production, reducing costs and addressing waste management challenges (Koyuncu, 2014; Neves et al., 2006). Industrial wastes with high carbohydrate and fat content are effective raw materials for biodiesel production. In Turkey, it has been noted that the recovery of cooking oil waste could produce 300,000 tons of biodiesel annually, reducing environmental pollution by 25% (Taşkın et al., 2013). Furthermore, the utilization of organic materials such as biscuit industry waste contributes to this process (Karmee, 2016).

BIOETHANOL PRODUCTION FROM CEREALS

Ethanol is blended with gasoline at specific ratios, such as 10% (E10) and 85% (E85), to reduce fossil fuel consumption and minimize environmental pollution (Yaşar, 2009). Produced through the fermentation of sugar by the yeast species *Saccharomyces cerevisiae*, ethanol is a colorless, flammable, and clear hydrocarbon (Buresova & Hrivna, 2011). Biomass sources used for ethanol production can be categorized into three main groups based on their content and processing methods: sugar-containing feedstocks, starch-containing feedstocks, and lignocellulosic feedstocks. Sugar-containing feedstocks, such as by-products like molasses, are rich in glucose and can be directly fermented without any pretreatment due to their lack of complex structures. Their ease of breakdown by yeast cells makes sugar-based feedstocks highly advantageous for ethanol production (Balat, 2011).

Feedstocks such as corn, wheat, sorghum, and barley contain starch rather than direct sugars. For ethanol production, the starch in these feedstocks must first be converted into glucose, followed by fermentation. This conversion requires the breakdown of starch chains using enzymes such as α-amylase and glucoamylase. Additionally, high-temperature cooking (413–453 K) is applied to gelatinize the starch. Enzymatic hydrolysis is preferred as it prevents the formation of toxic by-products (Aggarwal et al., 2001; Meral & Kamberoğlu, 2012).

Corn is the most widely used cereal crop for bioethanol production globally, owing to its high starch content. Wheat, with its high starch levels and ease of processing, is also an ideal alternative for bioethanol production. Sorghum, which can thrive in water-scarce regions, offers high biomass yields with its energy

sorghum varieties, making it effective for both bioethanol and biogas production. Studies indicate that ethanol production efficiency from wheat can reach up to 90%, with ethanol yields from cereals ranging between 85% and 95% (Wu et al., 2006; Zhao et al., 2009).

Industrial waste presents significant potential as a feedstock for bioethanol production. Biscuit and chocolate industry by-products are among the primary materials that can be utilized for this purpose. Due to their low lignin content, such waste can be used directly in bioethanol production without requiring pretreatment (Pleissner et al., 2014). Ranade et al. (1989) emphasized that these types of waste enhance the efficiency of biogas and bioethanol production.

CONCLUSION

The production of bioethanol from cereals offers great potential for achieving environmental sustainability and enhancing energy security. The limited availability of fossil fuels and their environmental impacts have highlighted the importance of renewable energy sources, with bioethanol emerging as a prominent biofuel. Cereals, with their high carbohydrate content, serve as a suitable resource for bioethanol production, enabling the utilization of non-food agricultural by-products. Cereals such as wheat, corn, and sorghum, with their high starch content, are widely used in bioethanol production. Additionally, the use of lignocellulosic materials and industrial waste in bioethanol production provides economic and environmental benefits. Technological innovations and the optimization of enzymatic processes have the potential to enhance the efficiency of ethanol production from cereals while reducing production costs.

REFERENCES

Aggarwal, N.K., Nigam, P., Singh, D., Yadav, B.S., 2001. Process optimization fort he production of sugar fort he bioethanol industry from sorghum, a non-conventional source of starch. World Journal of Microbiology & Biotechnology, 17: 411-415.

Anonim, Biyoetanol Çalışmaları, Elektrik İşleri Etüt İdaresi Genel Müdürlüğü, http://www.eie.gov.tr/turkce/YEK/biyoenerji/03 -biyoetanol/be_uretim.html, 2010.

Anonim, Energy use per capita, World Bank, http://www.google.com/publicdata?ds=wbwdi&met=eg_use_pcap_kg_oe&tdim=true&dl= en&hl=en&q=world+energy+consumption#met =eg_use_pcap_kg_oe&tdim=true, 2010.

Aslantaş, A. (2018). Dünyada ve Türkiyede biyokütle enerjisinin kullanımı ve potansiyeli (Master's thesis, Sosyal Bilimler Enstitüsü).

Balat, 2011. Production of bioethanol from lignocellulosic materials via the biochemical pathway: A review. Energy Conversion and Management, 52: 858-875.

Barbir, F., Veziroglu, T.N., Plass Jr, H.J., "Environmental damage due to fossil fuels use", International Journal of Hydrogen Energy, 15, 739-749, 1990

Bergthaller, W., Hollmann, J., Johannis, P.K., "Starch", Comprehensive Glycoscience, Elsevier, Oxford, 579-612, 2007

Buresova, I., Hrivna, L., 2011. Effect of wheat gluten proteins on bioethanol yield from grain. Applied Energy, 88: 1205-1210.

Demirbas, A., "Biofuels securing the planet's future energy needs", Energy Conversion and Management, 50, 2239-2249, 2009.

Gross, R., Leach, M., Bauen, A., "Progress in renewable energy", Environment International, 29, 105-122, 2003.

Harrison, M.A., Moselio, S., "Beer/Brewing", Encyclopedia of Microbiology, Academic Press, Oxford, 23-33, 2009.

Jarvis, M.C., Brian, T., "PRIMARY PRODUCTS | Cellulose", Encyclopedia of Applied Plant Sciences, Elsevier, Oxford, 865- 871, 2003.

Karimi, K. and Chisti, Y., 2017. Bioethanol production and technologies. In: Encyclopedia

Karmee, S.K., 2016. Liquid biofuels from food waste: Current trends, prospect and liminitation. Renewable and Sustainable Energy Reviews, 53, 945-953.

Koyuncu, M., 2014. İrmikaltı undan vital gluten ve etanol üretimi üzerine bir araştırma. *Doktora Tezi, Selçuk Üniversitesi Fen Bilimleri Enstitüsü*, Konya.

Leegood, R.C., William, J.L., Lane, M.D., "Photosynthesis", Encyclopedia of Biological Chemistry, Elsevier, New York, 330-335, 2004.

Liu, R., Li, J., Shen, F., "Refining bioethanol from stalk juice of sweet sorghum by immobilized yeast fermentation", Renewable Energy, 33, 1130-1135, 2008.

Melikoğlu, M., & Albostan, A. (2011). Türkiye'de biyoetanol üretimi ve potansiyeli. *Gazi Üniversitesi Mühendislik Mimarlık Fakültesi Dergisi*, *26*(1).

Meral, R., & Kamberoğlu, G. S. (2012). Tahıllardan etanol üretimi. *Journal of the Institute of Science and Technology*, *2*(3), 61-68.

Neves, M.A.D., Kimura, T., Shimizu, N. and Shiiba, K., 2006. Production of alcohol by simultaneous saccharification and fermentation of low-grade wheat flour. Brazilian Archives of Biology and Technology, 49 (3), 481-490.

of Sustainable Technologies. Ed. M.A. Abraham. Elsevier, London, UK, pp. 273-284.

Oruç, N., 2008. Şeker pancarından alternatif yakıt kaynağı olarak biyoetanol üretimi:Eskişehir şeker-alkol fabrika örneği. VII. Ulusal Temiz Enerji Sempozyumu, İstanbul.

Pleissner, D., Kwan, T.H. and Lin, C.S.K., 2014. Fungal hydrolysis in submerged fermentation for food waste treatment and fermentation feedstock preparation. Bioresource Technology, 158, 48-54.

Ranade, D.R., Yeole, Y., Meher, K.K., Gadre, R.V. and Godbole, S.H., 1989. Biogas from solid waste originated during biscuit and chocolate production: A preliminary study. *Biological Wastes*, 28, 157-161.

Schlamadinger, B., Johns, T., Ciccarese, L., Braun, M., Sato, A., Senyaz, A., Stephens, P., Takahashi, M., Zhang, X., "Options for including land use in a climate agreement post2012: improving the Kyoto Protocol approach", Environmental Science & Policy, 10, 295-305, 2007.

Shafiee, S., Topal, E., "When will fossil fuel reserves be diminished?", Energy Policy, 37, 181-189, 2009.

Taşkın, M.F., Yaren, F., Uygun, Ö. ve Alp, A., 2013. Sofradan kaynaklı israfın azaltılmasının çevre ve Türkiye ekonomisi açısından önemi. *Uluslararası Katılımlı Çevre Sempozyumu*, Gümüşhane.

Wu, X., Zhao, R., Wang, D., Bean, S.R., Seib, P.A., Tuinstra, M.R., Campbell, M. And O'Brien, A., 2006. Effects of amylose, corn protein, and corn fiber contents on production of ethanol from starch-rich media. Cereal Chemistry, 83, 569-575.

Yaşar, B., 2009. Alternatif enerji kaynağı olarak biyodizel üretim ve kullanım olanaklarının türkiye tarımı ve ab uyum süreci açısından değerlendirilmesi. Çukuroava Üniversitesi Fen Bilimleri Enstitüsü, Doktora Tezi (Basılmamış), Adana.

Zhao, R., Wu, X., Seabourn, B.W., Bean, S.R., Guan, L., Shi, Y.C., Wilson, J.D., Madl, R. and Wang, D., 2009. Comparison of waxy vs. nonwaxy wheats in fuel ethanol fermentation. Cereal Chemistry, 86, 145-156.

Zhu, S., Wu, Y., Yu, Z., Zhang, X., Wang, C., Yu, F., Jin, S., Zhao, Y., Tu, S., Xue, Y., "Simultaneous Saccharification and Fermentation of Microwave/Alkali Pre-treated Rice Straw to Ethanol", Biosystems Engineering, 92, 229-235, 2005.

Biocompatibility in Energy Harvesting Devices for Healthcare Applications

Sinem Ortaboy Sezer[1] & Melisa Öğretici[2] & Kibar Aras[3]

[1] Doç. Dr., Istanbul University-Cerrahpaşa, Engineering Faculty, Department of Chemistry, 34320, Avcilar, İstanbul, ORCID No: 0000-0003-3152-1637
[2] Yüksek Lisans Öğrencisi, Istanbul University-Cerrahpaşa, Engineering Faculty, Department of Chemistry, 34320, Avcilar, İstanbul, ORCID No: 0009-0003-4141-1009
[3] Arş. Gör., Atatürk University, Faculty of Science, Department of Chemistry, 25240, Yakutiye, Erzurum, ORCID No.: 0000-0002-1736-958X

1. Introduction to Biocompatibility and Energy Harvesting Technologies

Technological developments provide real-time solutions to the current public health challenges and help increase the healthy population. Innovative approaches to healthcare technology have been anticipated to support such solutions through tailored medicines, predictive analytics, and medical devices. The usage of such systems integrated and the knowledge obtained from various scientific and engineering areas can support a better and easier implementation of solutions regarding problems faced by contemporary healthcare. Advanced healthcare approaches require specific solutions to provide medical devices that address patient needs through biocompatibility's required and essential attributes (Singh et al., 2024; Singh et al., 2024; Yang et al., 2022).

The health monitoring devices developed for continuous tracking of physiological signals of living organisms gained significant attention in the medical community. The most important parts of such devices are biocompatible materials that are implanted in the body for a certain period allowing for proper operation without causing harmful effects. These materials play a vital role for the applications of health monitoring systems that can continually harvest energy from the living organisms in the form of thermal, kinetic, electromagnetic, etc. available sources and transform them into electric energy. In addition, biocompatible materials are a kind of material formulations that operate with biomedical entities with good reproducibility, and low side effects. They find extensive usage in medical applications. They assist in regenerating biological tissue in ways that support the body's natural biological processes, similar to conventional materials (Egbo, 2021; Kyriakides et al., 2021; Jurak et al., 2021). The body of living organisms can be equipped with small-scale energy harvesting devices that take vibrational and/or other types of kinetic energy through the physical activities of the organisms to track physiological processes occurring in tissues, organs, and other exterior parts of the body. For example, vibration-based devices can extract vibrational energy from cells and muscles or other components.

1.1. Importance of Biocompatibility

Biocompatibility is by far one of the most important issues about electronic devices that are in close contact with tissues and cells, notably in vivo, for a prolonged period. For a device like a resonant cantilever or piezoelectric bimorph, the main interaction is strain torque energy production by the tissue, which is to be transformed into electricity by the hydro-mechanical-electrical transducing energy process. Lessons learned from health (Wang et al., 2021;

Yang et al., 2021; Gao et al., 2020) care applications of implanted sensors, and also artificial limbs in the clinic, show that tissue around the implant needs to be healthy during the application of mechanical micro-motion and that patient well-being might even increase by this method. The absence of a loss of micro-motion dramatically reduces fibroblast function around the implant, which implies that the implant can keep its function and should live as long as the patient in a healthcare situation. The presence of motion, and its regeneration after trauma, enhances the adaptation of the human body to the foreign material implant (Mobini et al., 2021; Barik & Kirtania, 2023).

There are even favorable effects on the immune defense mechanism. Another factor governing the successful application of micro-implants is the speed of the healing process, which depends upon minimal tissue trauma by the surgical procedure, the stress present in the tissue, and not to be forgotten: the surface area of the implant. By keeping all these factors into account, major progress has been achieved in the design and functionality of such systems, and implants such as cochlear electrodes, intracardiac patches, and sensors for monitoring pressure and blood gases are presently used in a rapidly increasing number of patients around the world (Bucur et al., 2021; Li et al., 2021; Dabbour et al., 2021). Often, biocompatibility is interpreted as the absence of a material-mediated modulation in host response to the device to impact the clinical outcome of the patient.

1.2. Energy Harvesting Technologies in Healthcare Systems

The exploration of energy harvesting technologies in healthcare has gained significant traction, particularly as the demand for sustainable and efficient power sources for biomedical devices increases. The literature presents a comprehensive overview of various energy harvesting methods, highlighting their potential to revolutionize the way healthcare devices are powered.

In their 2014 article, (A Hannan et al., 2014) delve into the concept of Environmental Bio-Energy Harvesting (EEH), which focuses on the utilization of low-grade ambient energy sources to power implantable biomedical devices. The authors emphasize the advantages of EEH as a viable alternative to traditional batteries, particularly in the context of subcutaneous devices that can harness solar energy through innovative technologies such as dye-sensitized solar cells. They also discuss wireless energy transfer methods, including ultrasonic transmission, as promising solutions for powering implantable devices without the drawbacks of battery replacement, thus enhancing the longevity and reliability of these medical technologies.

Building on this foundation, (Srivastava, 2018) introduces a simulation of a spiral-shaped MEMS human energy harvester that employs piezoelectric transduction. This article reflects the growing interest in smart electronics capable of scavenging energy from environmental sources, essentially solar, thermal, and kinetic energy.

(Srivastava, 2018) highlights the efficiency and reliability of energy harvesters as alternatives to conventional batteries, which are often limited by their lifespan and the need for regular replacement. The research underscores the importance of optimizing energy harvester designs to enhance power efficiency and portability, thereby paving the way for wireless autonomous devices that can operate independently of external power sources.

Most recently, (Yahya Alkhalaf et al., 2022) review the advancements in radio frequency (RF) energy harvesting (RFEH) technologies, which have become increasingly relevant in the context of wearable and implantable medical devices. They note that the integration of RFEH can significantly extend the operational lifespan of these devices, mitigating the frequent need for battery changes or recharges. The authors highlight the critical role of IoT-based devices in remote monitoring, particularly in light of the recent global pandemic, where real-time data tracking has become essential for patient care. Despite the promising nature of RFEH systems, they also address the challenges associated with energy supply and power transfer efficiency, which remain important for the widespread adoption of these technologies.

Through this review, it becomes evident that energy harvesting technologies hold transformative potential for healthcare, offering sustainable power solutions that enhance the functionality and reliability of biomedical devices. The combination of various energy harvesting methods not only overcomes the limitations of traditional batteries but also supports the increasing trend towards self-sustaining medical technologies.

2. Biocompatible Materials for Energy Harvesting Devices

The exploration of biocompatible materials for energy harvesting devices has gained significant traction nowadays, particularly in the context of biomedical applications. The literature reveals a progressive understanding of how these materials can be effectively utilized to harness energy from both human activities and environmental sources.

Hannan and his coworkers provide a foundational overview of energy harvesting techniques applicable to implantable biomedical devices. Their review

categorizes energy sources into two main types: those derived from human body movements and those harvested from the environment. They emphasize the potential of kinetic energy, which can be efficiently captured using various transduction methods, including piezoelectric and magnetic induction generators. This work sets the stage for subsequent studies by highlighting the importance of effective energy-harvesting solutions in the development of wireless telemetry bio-devices (Hannan et al., 2014).

Varma et al. (2018) expand on this theme by discussing fiber-type solar cells and nanogenerators tailored for wearable applications. They underscore the significance of material properties and structural design in optimizing energy harvesting capabilities. The authors advocate for the use of biocompatible materials that can withstand the rigors of daily wear and washing, thus enhancing the longevity and functionality of wearable devices. Their insights into the challenges of fabrication, such as achieving flexibility and durability, are critical for advancing the design of energy-harvesting textiles.

The further contribution to the discourse by examining the role of graphene and carbon nanotube (CNT) fibers in energy storage and harvesting systems was provided by Dahiya et al. (2019). Their findings reveal that composite fiber electrodes not only enhance conductivity but also maintain performance under significant mechanical stress. The integration of innovative materials and designs is shown to yield stretchable and flexible energy storage solutions, which are essential for wearable technologies. Another study regarding biomedical technology delves into organic piezoelectric biomaterials, highlighting their biocompatibility and environmental advantages. The authors argue that these materials are pivotal for the next generation of biomedical devices, facilitating efficient energy conversion from mechanical to electrical energy. This review critically evaluates the properties and applications of organic piezoelectric materials, advocating for their broader adoption in energy harvesting technologies (Shin et al., 2020).

In the study performed by Herbert et al., (2020) the importance of soft materials in the context of wearable and implantable electronics were discussed. Their exploration of hydrogels and biodegradable materials emphasizes the need for comfort and seamless integration with biological tissues. The authors present a fascinating case for the use of biocompatible materials to enhance patient experience while advancing the functionality of medical devices.

Focusing on self-powered systems utilizing nanogenerators, Yang et al. (2021) discuss the role of biodegradable materials in enhancing biocompatibility

for implantable applications. They highlight the potential of triboelectric and piezoelectric materials, advocating for their use in applications ranging from health monitoring to therapeutic devices. This review emphasizes the importance of material selection in the development of efficient and safe energy harvesting systems (Yang et al., 2021).

Latif et al. (2021) explore the integration of piezoelectric transducers in fully implanted hearing systems, emphasizing the significance of material compatibility with CMOS processes. Their review addresses the need for flexible and stretchable materials, highlighting the potential of polymer-based piezoelectric devices to meet the demands of modern biomedical applications.

In their recent studies of Lan et al. (2022) the prospects of sustainable natural bio-origin materials for flexible devices were discussed elaborately. They outline strategies for leveraging the unique properties of these materials to create high-performance, eco-friendly devices. Their insights into the sustainability of bio-origin materials contribute to the ongoing discourse on environmentally responsible energy harvesting technologies.

In the literature survey performed by Wang et al. (2022), the necessity for biocompatible components, including encapsulation materials, to ensure long-term safety and efficacy was emphasized to clarify the commercialization challenges of biomedical piezoelectric energy generators. This critical evaluation of material choices underscores the ongoing need for rigorous biocompatibility assessments in the development of implantable energy harvesting devices (Wang et al., 2022).

All these studies illustrate a dynamic and evolving field, where biocompatible materials play a crucial role in advancing energy harvesting technologies for biomedical applications. Integrating innovative materials, coupled with a focus on sustainability and patient safety, is essential for the future of energy-harvesting devices in healthcare technologies.

2.1. Types of Biocompatible Materials

The exploration of biocompatible materials has become increasingly important in the medical field, particularly as advancements in technology and an aging population drive the demand for effective implants. The literature on this subject reveals a multifaceted approach to understanding the properties, applications, and challenges associated with various biocompatible materials.

In 2019, Axinte et al. examined the machining of biocompatible materials, which presents unique challenges due to their specific properties and the stringent

requirements of medical applications. Their review highlighted the importance of surface and structural compatibility, emphasizing that the interaction between implanted materials and human tissues is critical for successful integration. The authors provided insights into the cutting mechanisms involved in machining these materials and discussed the engineering challenges that arise, underscoring the need for high precision in the fabrication of implants (Axinte et al., 2019).

Building upon this foundation, Mastnak et al. addressed the evolving needs of an aging society, focusing on the development of multifunctional bioactive coatings for orthopedic applications. This work emphasized the potential of biocompatible metals enhanced with bioactive coatings to improve surgical outcomes and extend the lifespan of implants. The authors presented a compelling case for the integration of antimicrobial, pain-relieving, and anticoagulant properties into these coatings, thereby enhancing the overall performance of the materials in clinical settings. Their review not only provided a comprehensive overview of available biocompatible materials for coating applications but also discussed the economic and medical rationale for such innovations (Mastnak et al., 2022).

Biocompatible materials are very important in various biomedical applications including tissue engineering, drug delivery, and implantable devices. These materials can be broadly divided into several types based on their origin, properties, and applications. They are very important for healthcare devices to ensure that they interact safely with biological systems. Here are some common types:

2.1.1. Natural Polymers:

Natural polymers such as collagen, chitosan, and silk fibroin, as shown in Fig. 1, are widely recognized for their excellent biocompatibility and biodegradability. Collagen, the primary component of the extracellular matrix (ECM), is widely used in tissue engineering due to its ability to promote cell adhesion and proliferation (Kwon and Han, 2016). Chitosan, derived from chitin, exhibits antimicrobial properties and is used in wound healing and drug delivery systems (Lam et al., 2016). Silk fibroin has attracted attention due to its mechanical strength and biocompatibility, which make it suitable for various biomedical applications including scaffolds for tissue engineering (Kaushik et al., 2020).

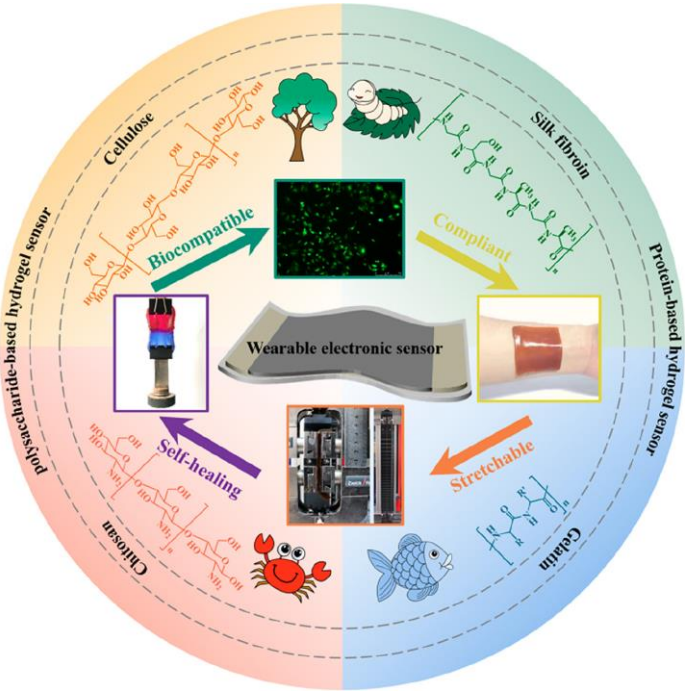

Fig. 1. Natural biopolymers used to manufacture wearable and stretchable sensors. Reproduced with permission from ref. (Cui et. al, 2021). Copyright © 2021, American Chemical Society.

2.1.2. Synthetic Polymers:

Synthetic polymers such as polylactic acid (PLA) and polycaprolactone (PCL) have been designed to have specific mechanical and degradation properties. PLA is biodegradable and has been used in a variety of applications including sutures and scaffolds for bone regeneration (Hlushchenko, 2023). PCL is known for its slow degradation rate and is often used in long-term implants (Sharma et al., 2021). The ability to modify these polymers through copolymerization or blending with natural polymers increases their biocompatibility and functionality (Rossi and Griensven, 2014).

2.1.3. Hydrogels:

Hydrogels, which can be obtained from both natural and synthetic sources, are characterized by their high water content and soft tissue-like properties. They are particularly useful in drug delivery and tissue engineering due to their ability to mimic the ECM (Li et al., 2019). Natural hydrogels such as alginate and gelatin are preferred due to their biocompatibility and ability to support cell growth (Chang et al., 2011). Synthetic hydrogels such as poly(ethylene glycol) (PEG)

can be tailored for specific applications, including controlled drug release (Wang et al., 2022).

Conducting polymers are advantageous materials due to their beneficial features, such as biocompatibility, flexibility, adjustable electrical conductivity, and ease of use. These qualities make them ideal for creating soft, conductive hydrogels for wearable sensors.

Polyaniline (PANI) and Polypyrrole (PPy) are commonly used conducting polymers that can clump together when used alone in hydrogels, leading to brittleness and stiffness that limit their applications. To address this overcome, researchers mix PANI or PPy with natural polymers such as nanocellulose, creating a more evenly distributed structure that improves both strength and conductivity. The resulting hydrogels are highly stretchable (over 600%), strong, and flexible, while also conducting electricity well and sensing strain (Fig. 2).

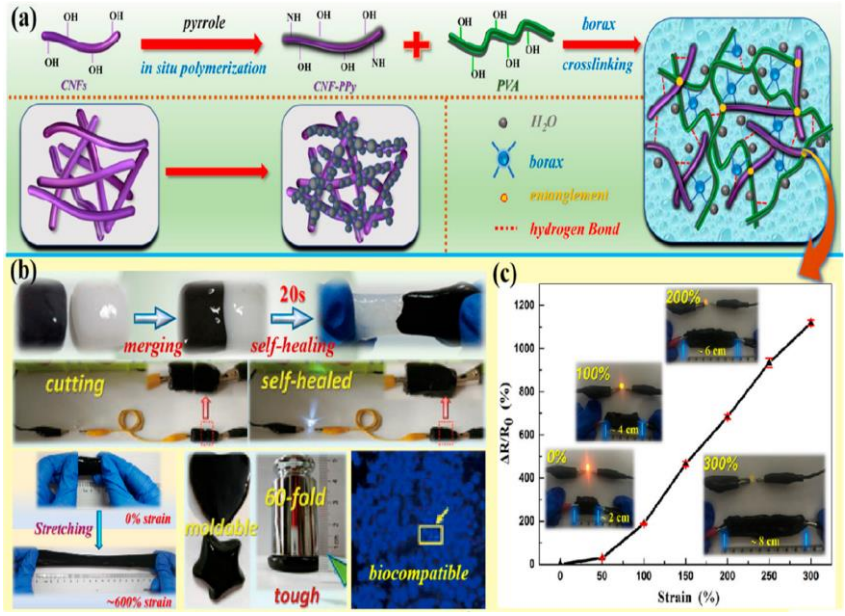

Fig. 2. Hydrogels derived from cellulose-based materials for wearable sensors. (a) The illustration of CNF-PPy/PB hydrogel fabrication processes. (b) Some favorable properties of CNF-PPy/PB hydrogels (i.e. rapid stretchability, plasticity, self-healing ability, toughness, good biocompatibility.) (c) The ratio of electrical resistance (ΔR/R0) of CNF-PPy/PB hydrogels as a function of the applied strain. Reproduced with permission from ref(Cui et. al, 2021). Copyright © 2021, American Chemical Society.)

2.1.4. Bioceramics:

Bioceramics such as hydroxyapatite (HA) and tricalcium phosphate (TCP) are inorganic materials that closely resemble the mineral component of bone. HA is widely used in bone grafts and implant coatings due to its excellent biocompatibility and ability to support osteoconduction (Magni, 2019). TCP is often used in combination with HA to improve the mechanical properties of bone substitutes (Li et al., 2021). These materials are particularly valuable in orthopedic and dental applications.

2.1.5. Composites:

Composite materials that combine natural and synthetic components offer enhanced properties compared to their individual components. For example, chitosan/collagen blends have been developed to improve mechanical strength and biocompatibility for tissue engineering applications (Kaczmarek and Sionkowska, 2017). Similarly, metal-polymer composites have been investigated to create bioactive materials that can support bone regeneration while providing structural integrity (Ryu et al., 2021).

2.1.6. Nanomaterials:

Nanomaterials, including graphene and nanodiamonds, are emerging as promising biocompatible materials due to their unique properties such as high surface area and mechanical strength. Graphene oxide has shown potential in drug delivery and regenerative medicine due to its biocompatibility and ability to enhance cellular responses (Malta et al., 2019). Nanodiamonds have been used for long-term cell tracking and imaging due to their excellent biocompatibility and stability (Hsiao et al., 2016).

Numerous techniques and formulations prepared for biopolymeric nanoparticles (NPs) have shown effective transport properties and remarkable effects on drug carrying systems. Fig. 3 provides insights for different structural properties and their impact on particle size for biomedical applications.

2.1.7. Metals and Alloys:

Bioabsorbable metals, such as magnesium and iron-based alloys, are being investigated for their potential in temporary implants. These materials can provide structural support during healing and gradually dissolve in the body, reducing the need for surgical removal (Ryu et al., 2021). Their biocompatibility and mechanical properties make them suitable for a variety of applications, including orthopedic and cardiovascular devices.

As a result, the landscape of biocompatible materials is diverse and encompasses natural and synthetic polymers, hydrogels, bioceramics, composites, nanomaterials, and bioabsorbable metals. Each type offers unique advantages and is suited for specific biomedical applications, highlighting the importance of material selection in the design of effective medical devices and therapies.

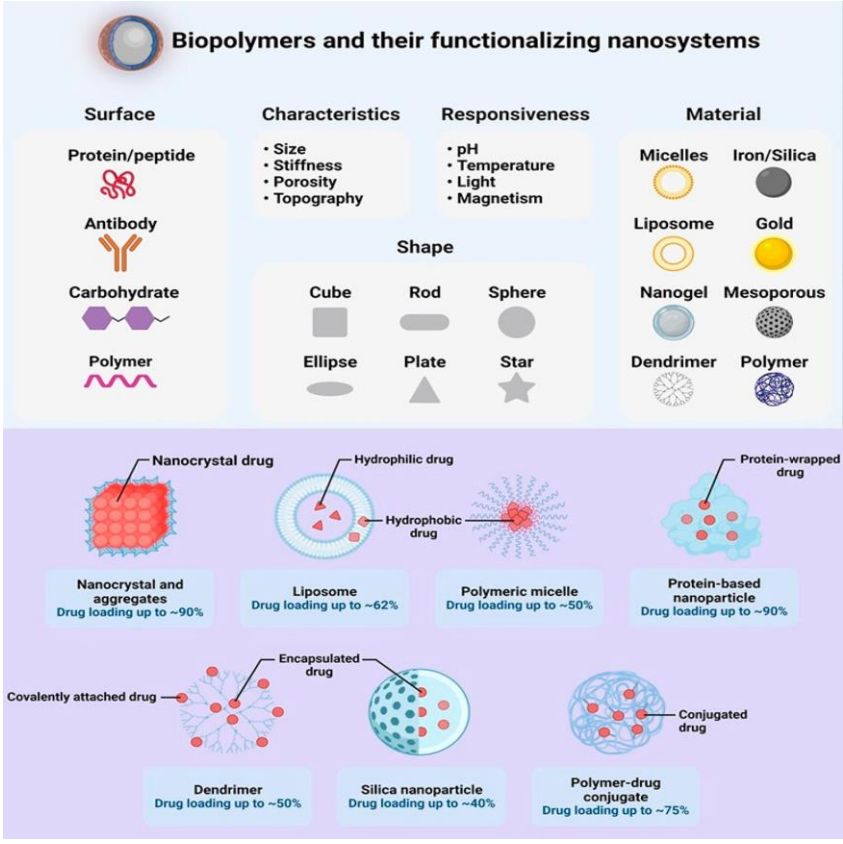

Fig. 3. Graphical illustration of different types of natural polymers and their working performance in drug delivery systems. Reused with permission from ref (Bhattacharya et. al, 2023). Copyright © 2023, American Chemical Society.).

Each of these materials has unique properties suited for specific applications, making biocompatibility a key consideration in device design.

Most recently, Rafikova et al. (2023) explored the interaction of ceramic implant materials with the immune system. Their research highlighted the complex biological responses that occur when implants are recognized as foreign bodies, which can lead to inflammatory reactions and potential implant failure. The authors detailed the varying biological complications associated with

different materials, particularly focusing on the immune response elicited by ceramic implants. They noted that while bioceramics possess beneficial properties such as osteoconductivity and biocompatibility, their mechanical limitations pose challenges for their widespread use in regenerative medicine. This review called attention to the necessity of understanding the cellular and molecular interactions that dictate the success of these materials in clinical applications (Rafikova et al., 2023).

Together, these articles provide a comprehensive overview of the current state of biocompatible materials, illustrating the ongoing challenges and innovations in the field. They underscore the importance of material selection and design in achieving successful integration and functionality of medical implants.

3. Challenges in Biocompatibility of Energy Harvesting Devices

3.1. Common Challenges in Biocompatibility

Biocompatibility is essential for the success of medical devices, but several challenges can arise during development and application. Here are some common challenges:

- *Immune Response:* The body may react negatively to foreign materials, leading to inflammation or rejection. Understanding and mitigating these responses is crucial.
- *Material Degradation*: Biodegradable materials can break down too quickly or not quickly enough, affecting their performance and safety over time.
- *Tissue Integration:* Ensuring proper integration with surrounding tissues can be difficult. Materials must encourage cell attachment and growth without causing adverse effects.
- *Mechanical Properties:* Balancing strength, flexibility, and durability while ensuring biocompatibility can be challenging, especially for load-bearing implants.
- *Biofilm Formation:* Medical devices can become contaminated with bacteria, leading to infections. Designing surfaces that resist biofilm formation is critical.
- *Regulatory Compliance:* Meeting stringent regulatory standards for biocompatibility testing can be time-consuming and costly.

- *Long-term Stability:* Ensuring materials maintain their properties and do not leach harmful substances over time is essential for patient safety.
- *Patient Variability:* Individual patient responses to materials can vary widely due to genetic, environmental, and health factors, complicating predictions of biocompatibility.
- *Sterilization Challenges:* Certain sterilization methods can alter the properties of materials, impacting their biocompatibility and functionality.
- *Complex Manufacturing Processes:* The processes used to create biocompatible devices can introduce contaminants or defects that affect their safety and effectiveness.
- To tackle these challenges effectively, a multidisciplinary approach is essential, integrating materials science, biology, and engineering to create safe and effective healthcare devices.

4. Applications of Biocompatible Energy Harvesting in Healthcare

Biocompatible energy harvesting technologies are essential for the advancement of self-powered medical devices. These innovative devices can capture energy from various biological sources, such as body movements, thermal gradients, and biochemical processes, allowing them to operate independently without needing external batteries. For example, piezoelectric materials can transform the mechanical energy generated by body movements into electrical energy, which can then actuators and power sensors in wearable devices (Algieri et al., 2018; Gao et al., 2018; Smith & Kar-Narayan, 2021). This capability is particularly advantageous for continuous health monitoring, where devices must function autonomously for extended periods.

Moreover, using biocompatible materials in energy harvesting devices ensures their safe integration within the human body. Materials like polyvinylidene fluoride (PVDF) and aluminum nitride (AlN) exhibit outstanding biocompatibility and flexibility, making them well-suited for wearable applications (Zhang et al., 2023; Algieri et al., 2018). These materials can be designed to harvest energy from everyday activities, such as walking or even the subtle movements of internal organs, thereby contributing a sustainable power source for medical devices (Hwang et al., 2015; Zhao et al., 2020).

4.1. Implantable Medical Devices

Implantable devices are surgically inserted into the body to provide various therapeutic and monitoring functions. These devices, which include neurostimulators, pacemakers and drug delivery systems, rely on a reliable power source to function effectively. Traditional batteries used in implantable devices present significant challenges, such as the need for replacement surgeries and the associated risk of infection (Wang et al., 2021).

These devices must be biocompatible and often biodegradable to prevent adverse reactions within the body (Chen et al., 2020; Zhao et al., 2020). Biocompatible energy harvesting technologies offer a promising solution by converting physiological energy into electrical power. This innovation extends the lifespan of these devices and reduces the need for invasive procedures. One notable application of energy harvesting in implantable devices is the development of self-powered pacemakers. Research has shown that piezoelectric nanogenerators can be implanted to harvest energy from heartbeats, creating a sustainable power source for the device (Sun et al., 2018). This advancement not only enhances the longevity of the pacemaker but also minimizes the risks associated with battery replacement surgeries.

Additionally, the use of biodegradable materials in these devices allows them to safely dissolve in the body after their functional life, further reducing the need for additional surgeries to remove non-biodegradable components (Da Silva et al., 2018; Li et al., 2018). The integration of energy harvesting systems in implantable devices also opens up new possibilities for advanced therapeutic applications. For example, energy harvested from the body can be used to stimulate nerve regeneration or promote tissue healing, which is particularly beneficial for neurological disorders and injuries (Guo et al., 2016; Zheng et al., 2016).

Moreover, the encapsulation of energy-harvesting devices is crucial to ensure biocompatibility and prevent immune responses. Materials such as polyimide (Dagdeviren et al., 2014; Zhang et al., 2015) and silicone (Zheng et al., 2016; Laube et al., 2004) are commonly used for encapsulating implantable devices, creating a stable and flexible barrier that minimizes the risk of leakage and adverse reactions.

The integration of energy harvesting technologies into implantable devices holds significant promise. For example, devices can be engineered to harness energy from the human body's natural movements or thermal gradients, thus providing a continuous power supply without the need for battery replacement

(Xu et al., 2023; Hwang et al., 2015; Zhao et al., 2020). This is particularly important for pacemakers, which traditionally depend on batteries that necessitate surgical replacement every few years.

Recent advancements in flexible energy harvesters have enabled the creation of implantable devices that can generate electricity from the cyclic movements of organs like the heart and lungs (Hwang et al., 2015; Kim et al., 2017). These innovations not only extend the longevity of implantable devices but also mitigate the risks associated with surgical interventions for battery replacements. Furthermore, the incorporation of biocompatible materials in the design of these energy harvesting devices ensures that they can safely coexist within the human body. Research indicates that materials such as lead-free piezoceramics and organic piezoelectric biomaterials can be effectively utilized in implantable applications, offering both energy harvesting capabilities and biocompatibility (Jeong et al., 2017; Wang et al., 2021; Shin et al., 2020). This dual functionality is essential for developing self-powered implantable medical devices that can operate autonomously over prolonged periods.

4.2. Wearable Devices

Wearable devices are designed to be worn on the body and are primarily used for monitoring health metrics, facilitating rehabilitation, providing therapeutic interventions, and enhancing physical activity. These devices often incorporate various sensors that track physiological parameters such as heart rate, temperature, and movement. One of the most promising advancements in wearable technology is the integration of energy harvesting systems that can convert body movements or thermal energy into electrical power, thus eliminating the need for frequent battery replacements (Majumder et al., 2017; Liu et al., 2017).

Typically lightweight, flexible, and unnoticeable, these devices enable continuous monitoring without interfering with the user's daily activities. Common examples include fitness trackers, smartwatches, and health monitoring patches (Chen et al., 2020; Nazar, 2023). The incorporation of energy harvesting technologies in wearable devices proves particularly advantageous, as it allows for the collection of energy from body movements or environmental sources. This capability extends the operational lifespan of the device by minimizing the need for frequent recharging (Wang, 2023; Biswas, 2024).

Triboelectric nanogenerators (TENGs) can harvest energy from the mechanical motion of the body, such as walking or even minor movements like wrist bending (Liu et al., 2017). This capability is particularly advantageous in

wearable health monitors that require continuous operation without the inconvenience of recharging. Electricity produced by the conversion of mechanical energy into electrical energy can be used to power sensors that monitor vital physiological parameters, including heart rate, temperature, and sweat composition (Nazar, 2023; Zhao et al., 2023). The ability to generate power independently enhances the practicality of wearable devices, making them increasingly appealing for long-term health monitoring. These devices can be seamlessly integrated into clothing or directly added to the skin, enabling continuous health monitoring without the need for bulky batteries or external power sources.

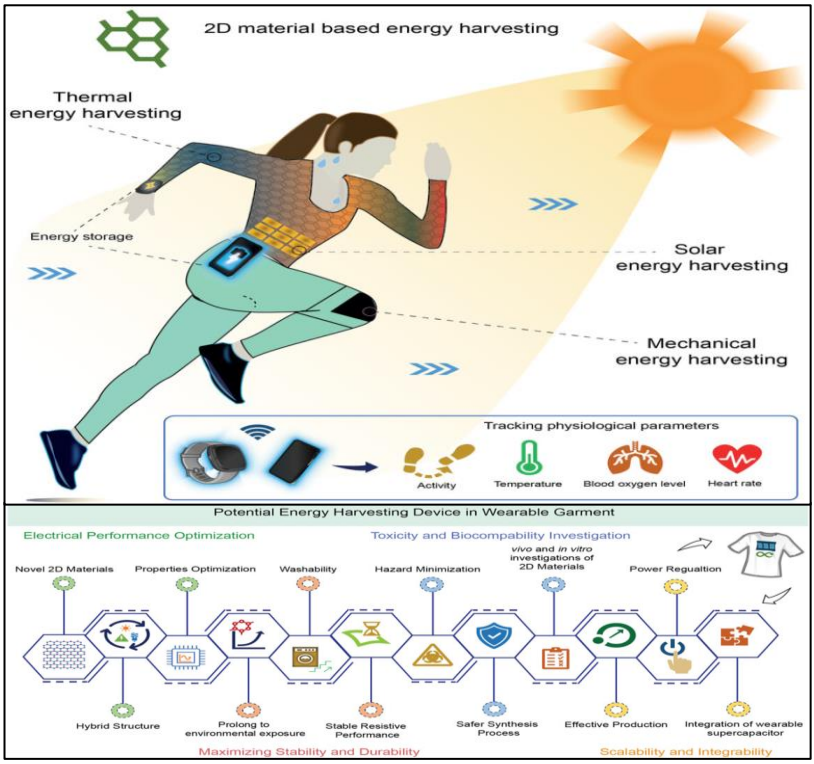

Fig. 4: The schematic illustrations of energy harvesting systems integrated to wearable platforms (top). The preparation steps of energy harvesting devices integrated with wearable garments (bottom). Reused with permission by the ref. (Ali et al., 2024). Copyright © 2023 The Authors. Small Structures published by Wiley-VCH GmbH

These materials not only enhance comfort but also align with sustainability goals by reducing electronic waste through biodegradability. For example, a recent study demonstrated a TENG made from cellulose nanocrystals that could effectively harvest energy while being environmentally friendly (Wang et al.,

2022). Additionally, the incorporation of piezoelectric materials allows for the development of sensors that can detect minute changes in pressure or strain, which can be crucial for applications such as monitoring respiratory patterns or detecting muscle contractions during rehabilitation (Todaro et al., 2018; Peng et al., 2020).

Moreover, the advancement of soft, skin-like materials has led to the creation of wearable devices that can conform to the body's contours, providing more accurate readings and improving user (Gong & Cheng, 2017). The integration of these materials with energy harvesting technologies allows for the development of devices that are not only functional but also aesthetically pleasing and user-friendly. For instance, researchers have developed flexible piezoresistive sensors that can monitor physiological parameters such as pulse and muscle activity, which are essential for rehabilitation and fitness tracking (de Marzo et al., 2024).

In terms of applications, wearable devices are increasingly being utilized in telemedicine and remote patient monitoring. They enable continuous health data collection, which can be transmitted to healthcare beholders for real-time analysis and intervention. This capability is especially valuable for operating chronic conditions, where timely adjustments to treatment plans can significantly impact patient outcomes. Furthermore, the ability to harvest energy from the body means that these devices can operate independently of external power sources, making them more reliable and convenient for users (Fig. 4).

5. Future Trends and Innovations in Biocompatible Energy Harvesting for Healthcare

The healthcare sector is increasingly focused on reducing its environmental impact and transitioning towards more sustainable practices (Jaušovec, 2023). One key area of focus is the development of biocompatible energy harvesting solutions to power healthcare facilities and medical devices (D'Alessandro, 2024).

TENGs have developed as a promising technology for biocompatible energy harvesting, with applications ranging from green energy to healthcare (Zhao et al., 2023). In order to provide wearable and implanted medical devices with a sustainable power supply, TENGs can capture energy from ambient sources such as body heat and human motion (Zhao et al., 2023). Advances in conductive polymers and materials science have been crucial in enabling the integration of TENGs into biomedical applications (Zhao et al., 2023). Beyond TENGs, other innovative biocompatible energy harvesting solutions are also being explored. These include self-powered wearable devices that can generate electricity from

body sweat, movement, or surrounding heat, light, and electromagnetic waves (Gong, 2024). Membrane technology is also being leveraged to improve energy efficiency in healthcare applications such as gas exchange, hemodialysis, and drug delivery (Osman, 2024).

Integrating renewable energy sources, such as wind and solar power, into healthcare facilities is another important trend. Studies have shown that adopting solar energy can significantly reduce healthcare institutions' carbon footprint and energy costs (Balabel et al., 2021; Kapuria, 2024; Albinali, 2024). Efforts are underway to solarize vaccine cold chains and primary healthcare centers, particularly in resource-constrained regions, to enhance sustainability and resilience (Kapuria, 2024).

Sustainable waste management practices in healthcare are also crucial for reducing the sector's environmental impact. If medical waste is properly segregated, the general waste can be harvested for biofuels, creating opportunities for a circular economy (Chisholm et al., 2021). Adopting a reduce-reuse-recycle approach to medical waste can drastically improve sustainability (Chisholm et al., 2021).

Another significant development in environmentally friendly healthcare facilities is the use of smart building technology, such as building management systems (BMS). BMS can optimize energy use, improve operational efficiency, and make it easier to integrate renewable energy sources (Sharma, 2024). Passive energy efficiency measures, like energy-efficient glazing, can also contribute to the sustainability of healthcare buildings (Ismaeil & Sobaih, 2023).

Overarching these technological innovations are the broader trends of corporate sustainability and sustainable business models in healthcare. Healthcare institutions are increasingly recognizing the need to operate in alignment with sustainability principles, fulfilling their environmental and social responsibilities (Ak, 2023; Abaku, 2024). This entails using ethical sourcing to promote social responsibility, cutting waste and carbon emissions, and implementing sustainable procurement methods (Abaku, 2024).

In conclusion, the future of biocompatible energy harvesting for healthcare is characterized by a multifaceted approach that combines technological advancements, renewable energy integration, sustainable waste management, and the adoption of holistic sustainability practices within healthcare institutions. These trends and innovations hold the potential to transform the healthcare sector into a more environmentally responsible and resilient system (Mazzeo, 2023; Ullah, 2023).

REFERENCES

Abaku, E. (2024). Sustainable supply chain management in the medical industry: a theoretical and practical examination. International Medical Science Research Journal, 4(3), 319-340. https://doi.org/10.515 94/imsrj.v4i3.931

Ak, S. (2023). Corporate sustainability in the health sector: a theoretical framework. Journal of Empirical Economics and Social Sciences. https://doi.org/10.46959/jeess.1333490

Albinali, A. (2024). Implementing a solar panel system at king hamad university hospital: a pathway to sustainability and cost efficiency. International Journal of Electrical Engineering and Computer Science, 6, 106-114. https://doi.org/10.3739 4/232027.2024.6.12

Algieri, L., Todaro, M., Guido, F., Mastronardi, V., Desmaële, D., Qualtieri, A., Giannini C., Sibillano T., Vittorio, M. (2018). Flexible piezoelectric energy harvesting exploiting biocompatible aln thin films grown onto spin-coated polyimide layers. ACS Applied Energy Materials. https://doi.org/10.1021/acsaem.8b00820

Ali, I., Dulal, M., Karim, N., Afroj, S. (2024), 2D Material-Based Wearable Energy Harvesting Textiles: A Review. Small Struct., 5: 2300282. https://doi.org/10.1002/sstr.202300282

Axinte, D., Guo, Y., Liao, Z., Shih, A. J., M'Saoubi, R., Sugita, N. (2019). Machining of biocompatible materials — Recent advances. *CIRP Annals*, *68*(2), 629-652. https://doi.org/10.1016/j.cirp.2019.05.003

Balabel, A., Elkalashy, N., Abdelhakeem, M., Issa, U. (2021). Application of solar energy technology in green healthcare camps for fighting covid-19 outbreak in saudi arabia. Journal of Advanced Research in Fluid Mechanics and Thermal Sciences, 81(1), 1-17. https://doi.org/10.37934/arfmts.81.1.117

Barik, A., & Kirtania, M. D. (2023). In-vitro and in-vivo tracking of cell-biomaterial interaction to monitor the process of bone regeneration. *Regenerative Medicine*, 305-329. https://doi.org/10.1007/978-981-19-6008-6_15

Bhattacharya, T., Preetam, S., Ghosh, B., Chakrabarti, T., Chakrabarti, P., Samal, S. K., Thorat, N., (2023). ACS Applied Bio Materials, 6 (10), 3959-3983. https//doi:10.1021/acsabm.3c00458

Biswas, S. (2024). Emerging energy harvesters in flexible bioelectronics: from wearable devices to biomedical innovations. Small Science, 4(3). https://doi.org/10.1002/smsc.202300148

Bucur, S., Vaida, L. L., Olteanu, C. D., Checchi, V. (2021). A brief review on microimplants and their use in orthodontics and Dentofacial orthopaedics. *Applied Sciences*, *11*(22), 10719. https://doi.org/10.3390/app112210719

Chang, C., He, M., Zhou, J., Zhang, L. (2011). Swelling behaviors of ph- and salt-responsive cellulose-based hydrogels. Macromolecules, 44(6), 1642-1648. https://doi.org/10.1021/ma102801f

Chen, X., Xie, X., Liu, Y., Zhao, C., Wen, M., Wen, Z. (2020). Advances in healthcare electronics enabled by triboelectric nanogenerators. Advanced Functional Materials, 30(43). https://doi.org/10.1002/adfm.202004673

Chisholm, J., Zamani, R., Negm, A., Said, N., daiem, M., Dibaj, M., Akrami, M. (2021). Sustainable waste management of medical waste in african developing countries: a narrative review. Waste Management & Research the Journal for a Sustainable Circular Economy, 39(9), 1149-1163. https://doi.org/10.1177/0734242x211029175

Cui, C., Fu, Q., Meng, L., Hao, S., Dai, R., Yang, J., (2021). Recent Progress in Natural Biopolymers Conductive Hydrogels for Flexible Wearable Sensors and Energy Devices: Materials, Structures, and Performance. ACS Applied Bio Materials, 4 (1), 85-121. https://doi.org/10.1021/acsabm.0c0080

D'Alessandro, C. (2024). Exploring circular economy practices in the healthcare sector: a systematic review and bibliometric analysis. Sustainability, 16(1), 401. https://doi.org/10.3390/su16010401

Da Silva, D., Kaduri, M., Poley, M., Adir, O., Krinsky, N., Shainsky-Roitman, J., Schroeder, A. (2018). Biocompatibility, biodegradation and excretion of polylactic acid (PLA) in medical implants and theranostic systems. *Chemical Engineering Journal*, *340*, 9-14, https://doi.org/10.1016/j.cej.2018.01.010

Dabbour, A., Tan, S., Kim, S. H., Guild, S., Heppner, P., McCormick, D., Wright, B. E., Leung, D, Gallichan, R., Budgett, D., Malpas, S. C. (2021). The safety of microimplants for the brain. *Frontiers in Neuroscience*, *15*. https://doi.org/10.3389/fnins.2021.796203

Dagdeviren, C., Yang, B. D., Su, Y., Tran, P. L., Joe, P., Anderson, E., Xia J., Doraiswamy V., Dehdashti B., Feng X., Lu B., Poston R., Khalpey Z., Ghaffari R., Huang Y., Slepian M. J., Rogers, J. A. (2014). Conformal piezoelectric energy harvesting and storage from motions of the heart, lung, and diaphragm. *Proceedings of the National Academy of Sciences*, *111*(5), 1927-1932, https://doi.org/10.1073/pnas.1317233111

Dahiya, A. S., Thireau, J., Boudaden, J., Lal, S., Gulzar, U., Zhang, Y., Gil, T., Azemard, N., Ramm, P., Kiessling, T., O'Murchu, C., Sebelius, F., Tilly, J., Glynn, C., Geary, S., O'Dwyer, C., Razeeb, K. M., Lacampagne, A., Charlot, B., Todri-Sanial, A. (2019). Review—Energy autonomous wearable sensors for smart healthcare: A review. *Journal of The Electrochemical Society*, *167*(3), 037516. https://doi.org/10.1149/2.0162003jes

de Marzo, G., Mastronardi, V. M., Todaro, M. T., Blasi, L., Antonaci, V., Algieri, L., Scaraggi M., De Vittorio, M. (2024). Sustainable electronic biomaterials for body-compliant devices: Challenges and perspectives for wearable bio-mechanical sensors and body energy harvesters. *Nano Energy*, 109336, https://doi.org/10.1016/j.nanoen.2024.109336

Egbo, M. K. (2021). A fundamental review on composite materials and some of their applications in biomedical engineering. *Journal of King Saud University - Engineering Sciences*, *33*(8), 557-568. https://doi.org/10.1016/j.jksues.2020.07.007

Gao, D., Parida, K., Lee, P. S. (2019). Emerging soft conductors for Bioelectronic interfaces. *Advanced Functional Materials*, *30*(29). https://doi.org/10.1002/adfm.201907184

Gao, H., Minh, P., Wang, H., Minko, S., Locklin, J., Nguyen, T., Sharma, S. (2018). High-performance flexible yarn for wearable piezoelectric nanogenerators. Smart Materials and Structures, 27(9), 095018. https://doi.org/10.1088/1361-665x/aad718

Gong, S. (2024). Materials-driven soft wearable bioelectronics for connected healthcare. Chemical Reviews, 124(2), 455-553. https://doi.org/10.1021/acs.chemrev.3c00502

Gong, S. & Cheng, W. (2017). Toward soft skin-like wearable and implantable energy devices. *Advanced Energy Materials*, *7*(23), 1700648, https://doi.org/10.1002/aenm.201700648

Guo, W., Zhang, X., Yu, X., Wang, S., Qiu, J., Tang, W., Li L., Liu H., Wang, Z. L. (2016). Self-powered electrical stimulation for enhancing neural differentiation of mesenchymal stem cells on graphene–poly (3, 4-ethylenedioxythiophene) hybrid microfibers. *ACS nano*, *10*(5), 5086-5095, https://doi.org/10.1021/acsnano.6b00200

Hannan, M. A., Mutashar, S., Samad, S. A., Hussain, A. (2014). Energy harvesting for the implantable biomedical devices: Issues and challenges. *BioMedical Engineering OnLine*, *13*(1). https://doi.org/10.1186/1475-925x-13-79

Herbert, R., Jeong, J., Yeo, W. (2020). Soft material-enabled electronics for medicine, healthcare, and human-machine interfaces. *Materials*, *13*(3), 517. https://doi.org/10.3390/ma13030517

Hlushchenko, V. (2023). Modern approaches and possibilities of application of 3d modeling for tissue engineering and bone regeneration. literature review. Eastern Ukrainian Medical Journal, 11(4), 337-351. https://doi.org/10.21272/eumj.2023;11(4):337-351

Hsiao, W., Hui, Y., Tsai, P., Chang, H. (2016). Fluorescent nanodiamond: a versatile tool for long-term cell tracking, super-resolution imaging, and nanoscale temperature sensing. Accounts of Chemical Research, 49(3), 400-407. https://doi.org/10.1021/acs.accounts.5b00484

Hwang, G., Kim, Y., Lee, J., Oh, S., Jeong, C., Park, D., Ryu J., Kwon H., Lee S., Joung B., Kim D., Lee, K. (2015). Self-powered deep brain stimulation via a flexible pimnt energy harvester. Energy & Environmental Science, 8(9), 2677-2684. https://doi.org/10.1039/c5ee01593f

Ismaeil, E., Sobaih, A. (2023). High-performance glazing for enhancing sustainable environment in arid region's healthcare projects. Buildings, 13(5), 1243. https://doi.org/10.3390/buildings13051243

J. Varma, S., Sambath Kumar, K., Seal, S., Rajaraman, S., Thomas, J. (2018). Fiber-type solar cells, Nanogenerators, batteries, and supercapacitors for wearable applications. *Advanced Science, 5*(9). https://doi.org/10.1002/advs.201800340

Jaušovec, M. (2023). Architectural evaluation of healthcare facilities: a comprehensive review and implications for building design. Buildings, 13(12), 2926. https://doi.org/10.3390/buildings13122926

Jeong, C., Han, J., Palneedi, H., Park, H., Hwang, G., Joung, B., Kim S., Shin H. J., Kang I., Ryu J., Lee, K. (2017). Comprehensive biocompatibility of nontoxic and high-output flexible energy harvester using lead-free piezoceramic thin film. Apl Materials, 5(7). https://doi.org/10.1063/1.4976803

Jurak, M., Wiącek, A. E., Ładniak, A., Przykaza, K.,Szafran, K. (2021). What affects the biocompatibility of polymers? *Advances in Colloid and Interface Science, 294*, https://doi.org/102451. 10.1016/j.cis.2021.102451

Kaczmarek, B. and Sionkowska, A. (2017). Chitosan/collagen blends with inorganic and organic additive—a review. Advances in Polymer Technology, 37(6), 2367-2376. https://doi.org/10.1002/adv.21912

Kapuria, B. (2024). Achieving sustainable, environmentally viable, solarized vaccine cold chain system and vaccination program—an effort to move towards clean and green energy-driven primary healthcare in lebanon. Frontiers in Health Services, 4. https://doi.org/10.3389/frhs.2024.1386432

Kaushik, S., Thungon, P., Goswami, P. (2020). Silk fibroin: an emerging biocompatible material for application of enzymes and whole cells in bioelectronics and bioanalytical sciences. Acs Biomaterials Science & Engineering, 6(8), 4337-4355. https://doi.org/10.1021/acsbiomaterials.9b01971

Kim, D., Shin, H., Lee, H., Jeong, C., Park, H., Hwang, G., Lee, K. (2017). In vivo self-powered wireless transmission using biocompatible flexible energy harvesters. Advanced Functional Materials, 27(25). https://doi.org/10.1002/adfm.201700341

Kwon, H. and Han, Y. (2016). Chondroitin sulfate-based biomaterials for tissue engineering. Turkish Journal of Biology, 40, 290-299. https://doi.org/10.3906/biy-1507-16

Kyriakides, T. R., Raj, A., Tseng, T. H., Xiao, H., Nguyen, R., Mohammed, F. S., Halder, S., Xu, M., Wu, M. J., Sheu, W. C. (2021). Biocompatibility of nanomaterials and their immunological properties. *Biomedical Materials, 16*(4), 042005. https://doi.org/10.1088/1748-605x/abe5fa

Lam, N., Zhang, M., Guo, H., Ho, C., Li, L. (2016). Effect of fiber length and blending method on the tensile properties of ring spun chitosan–cotton blend yarns.

Textile Research Journal, 87(2), 244-257. https://doi.org/10.1177/0040517516629141

Lan, L., Ping, J., Xiong, J., Ying, Y. (2022). Sustainable natural bio-origin materials for future flexible devices. *Advanced Science*, *9*(15). https://doi.org/10.1002/advs.202200560

Latif, R., Noor, M. M., Yunas, J., Hamzah, A. A. (2021). Mechanical energy sensing and harvesting in Micromachined polymer-based piezoelectric transducers for fully implanted hearing systems: A review. *Polymers*, *13*(14), 2276. https://doi.org/10.3390/polym13142276

Laube, T., Brockmann, C., Buß, R., Lau, C., Höck, K., Stawski, N., Stieglitz T., Richter H. A., Schilling, H. (2004). Optical energy transfer for intraocular microsystems studied in rabbits. *Graefe's Archive for Clinical and Experimental Ophthalmology*, *242*, 661-667, https://doi.org/10.1007/s00417-004-0909-8

Li, J., Zhou, P., Attarilar, S., Shi, H. (2021). Innovative surface modification procedures to achieve micro/nano-graded ti-based biomedical alloys and implants. *Coatings*, *11*(6), 647. https://doi.org/10.3390/coatings11060647

Li, L., Yu, F., Zheng, L., Wang, R., Yan, W., Wang, Z., Wang, Z., Xu, J., Wu, J., Shi, D., Zhu, L., Wang, X., Jiang, Q. (2019). Natural hydrogels for cartilage regeneration: modification, preparation and application. Journal of Orthopaedic Translation, 17, 26-41. https://doi.org/10.1016/j.jot.2018.09.003

Li, M., Ma, H., Han, F., Zhai, D., Zhang, B., Sun, Y., Li, T., Chen, L., Wu, C. (2021). Microbially catalyzed biomaterials for bone regeneration. Advanced Materials, 33(49). https://doi.org/10.1002/adma.202104829

Li, Z., Feng, H., Zheng, Q., Li, H., Zhao, C., Ouyang, H., Noreen S., Yu M., Su F., Liu R., Li L., Wang Z. L., Li, Z. (2018). Photothermally tunable biodegradation of implantable triboelectric nanogenerators for tissue repairing. *Nano Energy*, *54*, 390-399. https://doi.org/10.1016/j.nanoen.2018.10.020

Liu, Y., Pharr, M., Salvatore, G. A. (2017). Lab-on-skin: a review of flexible and stretchable electronics for wearable health monitoring. *ACS nano*, *11*(10), 9614-9635, https://doi.org/10.1016/j.nanoen.2018.10.020

Liu, Z., Zhang, S., Jin, Y. M., Ouyang, H., Zou, Y., Wang, X. X., Xie L. X., Li, Z. (2017). Flexible piezoelectric nanogenerator in wearable self-powered active sensor for respiration and healthcare monitoring. *Semiconductor Science and Technology*, *32*(6), 064004, https://doi.org/10.1088/1361-6641/aa68d1

Magni, M. (2019). Hydroxyapatite-based electrodes for metal detection in wastewater. Ecs Meeting Abstracts, MA2019-04(8), 409-409. https://doi.org/10.1149/ma2019-04/8/409

Majumder, S., Mondal, T., Deen, M. J. (2017). Wearable sensors for remote health monitoring. *Sensors*, *17*(1), 130, https://doi.org/10.3390/s17010130

Malta, A., Cortez, D., Romão, D., Pereira, J., Velo, M., Nascimento, T. (2019). Graphene oxide applications in dentistry: integrative literature review. Journal of Health Sciences, 21(4), 376-381. https://doi.org/10.17921/2447-8938.2019v21n4p376-81

Mastnak, T., Maver, U., Finšgar, M. (2022). Addressing the needs of the rapidly aging society through the development of Multifunctional Bioactive coatings for orthopedic applications. *International Journal of Molecular Sciences*, *23*(5), 2786. https://doi.org/10.3390/ijms23052786

Mazzeo, D. (2023). Eco-sustainable energy production in healthcare: trends and challenges in renewable energy systems. Energies, 16(21), 7285. https://doi.org/10.3390/en16217285

Mobini, S., Kuliasha, C. A., Siders, Z. A., Bohmann, N. A., Jamal, S., Judy, J. W., Schmidt, C. E., Brennan, A. B. (2020). Microtopographical patterns promote different responses in fibroblasts and Schwann cells: A possible feature for neural implants. *Journal of Biomedical Materials Research Part A*, *109*(1), 64-76. https://doi.org/10.1002/jbm.a.37007

Nazar, A. (2023). Skin-contact triboelectric nanogenerator for energy harvesting and motion sensing: principles, challenges, and perspectives. Biosensors, 13(9), 872. https://doi.org/10.3390/bios13090872

Osman, A. (2024). Membrane technology for energy saving: principles, techniques, applications, challenges, and prospects. Advanced Energy and Sustainability Research, 5(5). https://doi.org/10.1002/aesr.202400011

Peng, X., Dong, K., Ye, C., Jiang, Y., Zhai, S., Cheng, R., Liu D., Gao X., Wang, Z. L. (2020). A breathable, biodegradable, antibacterial, and self-powered electronic skin based on all-nanofiber triboelectric nanogenerators. *Science Advances*, *6*(26), https://doi.org/10.1126/sciadv.aba9624

Rafikova, G., Piatnitskaia, S., Shapovalova, E., Chugunov, S., Kireev, V., Ialiukhova, D., Bilyalov, A., Pavlov, V., Kzhyshkowska, J. (2023). Interaction of ceramic implant materials with immune system. *International Journal of Molecular Sciences*, *24*(4), 4200. https://doi.org/10.3390/ijms24044200

Rossi, F. and Griensven, M. (2014). Polymer functionalization as a powerful tool to improve scaffold performances. Tissue Engineering Part A, 20(15-16), 2043-2051. https://doi.org/10.1089/ten.tea.2013.0367

Ryu, H., Seo, M., Li, J. (2021). Bioresorbable metals for biomedical applications: from mechanical components to electronic devices. Advanced Healthcare Materials, 10(17). https://doi.org/10.1002/adhm.202002236

Sharma, S., Sudhakara, P., Singh, J., Ilyas, R., Asyraf, M., Razman, M. (2021). Critical review of biodegradable and bioactive polymer composites for bone tissue engineering and drug delivery applications. Polymers, 13(16), 2623. https://doi.org/10.3390/polym13162623

Sharma, V. (2024). Optimizing energy efficiency in healthcare facilities: the pivotal role of building management systems. JAIMLD, 2(1), 209-2013. https://doi.org/10.51219/jaimld/vibhu-sharma/70

Shin, D., Hong, S. W., Hwang, Y. (2020). Recent advances in organic piezoelectric biomaterials for energy and biomedical applications. *Nanomaterials*, *10*(1), 123. https://doi.org/10.3390/nano10010123

Singh, A. B., Khandelwal, C., Dangayach, G. S. (2024). Advancements in healthcare materials: Unraveling the impact of processing techniques on biocompatibility and performance. *Polymer-Plastics Technology and Materials*, *63*(12), 1608-1644. https://doi.org/10.1080/25740881.2024.2350026

Singh, A. B., Khandelwal, C., Dangayach, G. S. (2024). Revolutionizing healthcare materials: Innovations in processing, advancements, and challenges for enhanced medical device integration and performance. *Journal of Micromanufacturing*. https://doi.org/10.1177/25165984241256234

Smith, M. and Kar-Narayan, S. (2021). Piezoelectric polymers: theory, challenges and opportunities. International Materials Reviews, 67(1), 65-88. https://doi.org/10.1080/ 09506608.2021.1915935

Srivastava, T. (2018). *Simulation of Spiral-Shaped MEMS Human Energy Harvester Using Piezoelectric Transduction* (Master's thesis, University of Missouri-Columbia).

Sun, J. G., Yang, T. N., Wang, C. Y., Chen, L. J. (2018). A flexible transparent one-structure tribo-piezo-pyroelectric hybrid energy generator based on bio-inspired silver nanowires network for biomechanical energy harvesting and physiological monitoring. *Nano Energy*, *48*, 383-390, https://doi.org/10.1016/j.nanoen.2018.03.071

Todaro, M. T., Guido, F., Algieri, L., Mastronardi, V. M., Desmaële, D., Epifani, G., De Vittorio, M. (2018). Biocompatible, flexible, and compliant energy harvesters based on piezoelectric thin films. *IEEE Transactions on Nanotechnology*, *17*(2), 220-230.

Ullah, Z. (2023). Life cycle sustainability assessment of healthcare buildings: a policy framework. Buildings, 13(9), 2143. https://doi.org/10.3390/buildings13092143

Wang, L., Jiang, K., Shen, G. (2021). Wearable, Implantable, and interventional medical devices based on smart electronic skins. *Advanced Materials Technologies*, *6*(6). https://doi.org/10.1002/admt.20210010

Wang, S., Qiu, Y., Liu, Q., Wang, Q., Zhou, Q. (2022). Hydrogels for treatment of different degrees of osteoarthritis. Frontiers in Bioengineering and Biotechnology, 10. https://doi.org/10.3389/fbioe.2022.858656

Wang, T., Li, S., Tao, X., Yan, Q., Wang, X., Chen, Y., Huang F., Li H., Chen X., Bian, Z. (2022). Fully biodegradable water-soluble triboelectric nanogenerator for human physiological monitoring. *Nano Energy*, *93*, 106787, https://doi.org/10.1016/j.nanoen.2021.106787

Wang, Y., Hong, M., Venezuela, J., Liu, T., Dargusch, M. (2023). Expedient secondary functions of flexible piezoelectrics for biomedical energy harvesting. *Bioactive Materials*, *22*, 291-311. https://doi.org/10.1016/j.bioactmat.2022.10.003

Wang, Y., Zeng, Q., He, L., Yin, P., Sun, Y., Hu, W., Yang, R. (2021). Fabrication and application of biocompatible nanogenerators. Iscience, 24(4), 102274. https://doi.org/10.1016/j.isci.2021.102274

Wang, Z. (2023). Hydrogel-based energy harvesters and self-powered sensors for wearable applications. Nanoenergy Advances, 3(4), 315-342. https://doi.org/10.3390/nanoenergyadv3040017

Xu, M., Liu, Y., Yang, K., Li, S., Wang, M., Wang, J., Yang D., Shkunov M., Silva S. R. P., Castro F. A., Zhao, Y. (2023). Recent progress in minimally invasive power sources for implantable electronics.. https://doi.or g/10.22541/au.167565791.16406066/v1

Yahya Alkhalaf, H., Yazed Ahmad, M., Ramiah, H. (2022). Self-sustainable biomedical devices powered by RF energy: A review. *Sensors*, *22*(17), 6371. https://doi.org/10.3390/s22176371

Yang, L., Ma, Z., Tian, Y., Meng, B., Peng, Z. (2021). Progress on self-powered wearable and Implantable systems driven by Nanogenerators. *Micromachines*, *12*(6), 666. https://doi.org/10.3390/mi12060666

Yang, Q., Jin, W., Lu, T., Liu, S., Yin, J., Zhou, T., Ren, T. (2022). Biocompatible sensors are revolutionizing healthcare technologies. *Miniaturized Biosensing Devices*, 227-249. https://doi.org/10.1007/978-981-16-9897-2_10

Yang, Q., Wei, T., Yin, R. T., Wu, M., Xu, Y., Koo, J., Choi, Y. S., Xie, Z., Chen, S. W., Kandela, I., Yao, S., Deng, Y., Avila, Y., Liu, T., Bai, W., Yang, Y., Han, M., Zhang, Q., Haney, C. R., Lee, K. B., Aras, K., Wang, T., Seo, M., Luan, H., Lee, S. M., Brikha A., Ghoreishi-Haack, N., Tran, L., Stepien, I., Aird, F., Waters, E. A., Yu, X., Banks, A., Trachiotis, G. D., Torkelson, J. M., Huang, Y., Kozorovitskiy, Y., Efimos, I. R., Rogers, J. A. (2021). Photocurable bioresorbable adhesives as functional interfaces between flexible bioelectronic devices and soft biological tissues. *Nature Materials*, *20*(11), 1559-1570. https://doi.org/10.1038/s41563-021-01051-x

Zhang, H., Zhang, X. S., Cheng, X., Liu, Y., Han, M., Xue, X., Wang S., Yang F., Shankaregowda S. A., Zhang H., Xu, Z. (2015). A flexible and implantable piezoelectric generator harvesting energy from the pulsation of ascending aorta: in vitro and in vivo studies. *Nano Energy*, *12*, 296-304, https://doi.org/10.1016/j.nanoen.2014.12.038

Zhang, W., Wu, G., Zeng, H., Li, Z., Wu, W., Jiang, H., Zhang W., Wu R., Huang Y., Lei, Z. (2023). The preparation, structural design, and application of electroactive poly(vinylidene fluoride)-based materials for wearable sensors and human energy harvesters. Polymers, 15(13), 2766. https://doi.org/10.3390/polym15132766

Zhao, J., Ghannam, R., Htet, K., Liu, Y., Law, M., Roy, V., Michel B., Imran M. A., Heidari, H. (2020). Self-powered implantable medical devices: photovoltaic energy harvesting review. Advanced Healthcare Materials, 9(17). https://doi.org/10.1002/adhm.202000779

Zhao, Z., Mi, Y., Yin, L., Zhu, Q., Cao, X., Wang, N. (2023). From biochemical sensor to wearable device: the key role of the conductive polymer in the triboelectric nanogenerator. Biosensors, 13(6), 604. https://doi.org/10.3390/bios13060604

Zheng, Q., Jin, Y., Liu, Z., Ouyang, H., Li, H., Shi, B., Jiang W., Zhang H., Li Z., Wang, Z. L. (2016). Robust multilayered encapsulation for high-performance triboelectric nanogenerator in harsh environment. *ACS Applied Materials & Interfaces*, *8*(40), 26697-26703, https://doi.org/10.1021/acsami.6b06866

Zheng, Q., Zou, Y., Zhang, Y., Liu, Z., Shi, B., Wang, X., Jin Y., Ouyang H., Li Z., Wang, Z. L. (2016). Biodegradable triboelectric nanogenerator as a life-time designed implantable power source. *Science advances*, *2*(3), e1501478, https://doi.org/10.1126/sciadv.15014